February 2020 Vol. 19 No. 2

ISSN 1582-9596

Environmental Engineering and Management Journal

Founding Editor: Matei Macoveanu
Editor-in-Chief: Maria Gavrilescu

Guest Editors: Irina Volf
Dan Cascaval

Innovative Materials and Processes for Sustainable Development

"Gheorghe Asachi" Technical University of Iasi

February 2020 Vol.19 No. 2 *ISSN 1582 - 9596*

Environmental Engineering and Management Journal

An International Journal

Founding Editor: Matei Macoveanu

Editor-in-Chief: Maria Gavrilescu

Guest Editors: Irina Volf
Dan Cascaval

Innovative Materials and Processes for Sustainable Development

"Gheorghe Asachi" Technical University of Iasi

Environmental Engineering and Management Journal

Environmental Engineering and Management Journal encourages initiatives and actions concerning the improvement of education, research, marketing and management, in order to achieve sustainable development. This journal brings valuable opportunities for those offering products, technologies, services, educational programs or other related activities, creating thus a closer relation with the request of the market in the fields of environmental engineering, management and education. This journal address researchers, designers, academic staff, specialists with responsibilities in the field of environmental protection and management from government organizations (central and local administrations, environmental protection agencies) or from the private or public companies. Also, graduates of specialization courses or of the Environmental Engineering and Management profile, as well as other specialists may find in this journal a direct linkage between the offer and request of the market concerned with the protection of the environment and the administration of natural resources in the national and international context.

The journal was conceived as a means to develop scientific and technical relationships between people who offer and request solutions for environmental protection and conservation of natural resources, creating thus the premises to enhance the transfer of technology and know-how, the confirmation and implementation of ecological products and services.

Taking into consideration these aspects, we gladly welcome any persons or companies which correspond to the above-mentioned purposes and objectives to use our journal to identify potential collaborators.

For subscriptions and orders please contact us at:
OAIMDD (*Academic Organization for Environmental Engineering and Sustainable Development*), 73 Prof. Dimitrie Mangeron Blvd., PO 10, Box 2111, 700050 Iasi, Romania, CIF: 10150285

Phone/Fax: 0040-232-271759
E-mail: brindusa.sluser.at.gmail.com, mgav_eemj.at.yahoo.com

In LEI:
ALPHA BANK ROMANIA (ABR)
SWIFT Code: BUCUROBU
IBAN: RO87BUCU1032235333663RON
Beneficiary: OAIMDD-EEMJ
Address: PO 10, Box 2111, 700050 Iasi, Romania

In EURO:
ALPHA BANK ROMANIA (ABR)
SWIFT Code: BUCUROBU
IBAN: RO79BUCU1031215940036EUR
Beneficiary: OAIMDD-EEMJ
Address: PO 10, Box 2111, 700050 Iasi, Romania

Department of Environmental Engineering and Management and
EcoZone Publishing House - O.A.I.M.D.D.
73 Prof. Dimitrie Mangeron Blvd., 700050, Iasi, Romania
Phone/Fax: 0040-232-271759

***Environmental
Engineering and
Management Journal***

EDITORIAL BOARD

Founding Editor:

Matei Macoveanu, *Gheorghe Asachi* Technical University of Iasi, Romania

Editor-in-Chief:

Maria Gavrilescu, *Gheorghe Asachi* Technical University of Iasi, Romania

SCIENTIFIC ADVISORY BOARD

Maria Madalena dos Santos Alves
University of Minho, Braga
Portugal

Abdeltif Amrane
University of Rennes, ENSCR
France

Ecaterina Andronescu
University *Polytechnica* of Bucharest
Romania

Robert Armon
Technion-Israel Institute of Technology, Haifa
Israel

Adisa Azapagic
The University of Manchester
United Kingdom

Pranas Baltrenas
Vilnius *Gediminas* Technical University
Lithuania

Hans Bressers
University of Twente, Enschede
The Netherlands

Han Brezet
Delft University of Technology
The Netherlands

Dan Cascaval
Gheorghe Asachi Technical University of Iasi
Romania

Yusuf Chisti
Massey University, Palmerston North
New Zealand

Philippe Corvini
University of Applied Sciences Northwestern
Switzerland, Muttenz, Switzerland

Igor Cretescu
Gheorghe Asachi Technical University of Iasi
Romania

Silvia Curteanu
Gheorghe Asachi Technical University of Iasi
Romania

Andrew J. Daugulis
Queen's University Kingston
Canada

Valeriu David
Gheorghe Asachi Technical University of Iasi
Romania

Katerina Demnerova
University of Prague
Czech Republic

Gheorghe Duca
State University of Moldavia, Kishinew
Republic of Moldavia

Emil Dumitriu
Gheorghe Asachi Technical University of Iasi
Romania

Anca Duta Capra
Transilvania University of Brasov
Romania

Jurek Duszczyk
Delft University of Technology
The Netherlands

Francesco Fatone
Marche Polytechnic University, Ancona,
Italy

Fabio Fava
Alma Mater Studiorum University of Bologna
Italy

Eugenio Campos Ferreira
University of Minho, Braga,
Portugal

Cristian Fosalau
Gheorghe Asachi Technical University of Iasi
Romania

Anton Friedl
Vienna University of Technology
Austria

Anne Giroir Fendler
University *Claude Bernard* Lyon 1
France

Silvia Fiore
Polytechnic University of Turin,
Italy

Ion Giurma
Gheorghe Asachi Technical University of Iasi
Romania

Yuh-Shan Ho
Peking University
People's Republic of China

Arjen Y. Hoekstra
University of Twente, Enschede
The Netherlands

Nicolae Hurduc
Gheorghe Asachi Technical University of Iasi
Romania

Ralf Isenmann
Munich University of Applied Sciences
Germany

Marcel Istrate
Gheorghe Asachi Technical University of Iasi
Romania

Ravi Jain
University of Pacific, Baun Hall Stockton
United States of America

Michael Søgaard Jørgensen
Aalborg University
Denmark

Nicolas Kalogerakis
Technical University of Crete, Chania
Greece

Thomas Lindhqvist
International Institute for Industrial Environmental
Economics, Lund University, Sweden

Andreas Paul Loibner
University of Natural Resources and Life Sciences,
Vienna, Austria

Tudor Lupascu
Academy of Sciences, Institute of Chemistry,
Kishinev, Republic of Moldavia

Gerasimos Lyberatos
National Technical University of Athens
Greece

José Mondéjar Jiménez
University Castilla-La Mancha, Cuenca
Spain

Antonio Marzocchella
University of Naples *Federico II*,
Naples, Italy

Mauro Majone
Sapienza University of Rome
Italy

Shin' ichi Nakatsuji
University of Hyogo
Japan

Valentin Nedeff
Vasile Alecsandri University of Bacau
Romania

Alexandru Ozunu
Babes-Bolyai University of Cluj-Napoca
Romania

Yannis A. Phillis
Technical University of Crete, Chania
Greece

Marcel Ionel Popa
Gheorghe Asachi Technical University of Iasi
Romania

Marcel Popa
Gheorghe Asachi Technical University of Iasi
Romania

Valentin I. Popa
Gheorghe Asachi Technical University of Iasi
Romania

Tudor Prisecaru
University *Polytechnica* of Bucharest
Romania

Gabriel-Lucian Radu
Polytechnica University of Bucharest
Romania

Ákos Rédey
Pannon University, Veszprém
Hungary

Maria Angeles Sanromán
University of Vigo,
Spain

Joop Schoonman
Delft University of Technology
The Netherlands

Dan Scutaru
Gheorghe Asachi Technical University of Iasi
Romania

Bogdan C. Simionescu
Gheorghe Asachi Technical University of Iasi
Romania

Florian Statescu
Gheorghe Asachi Technical University of Iasi
Romania

Carmen Teodosiu
Gheorghe Asachi Technical University of Iasi
Romania

Saulius Vasarevicius
Vilnius Gediminas Technical University
Lithuania

Angheluta Vadineanu
The University of Bucharest
Romania

Colin Webb
The University of Manchester
United Kingdom

Peter Wilderer
Technical University Munich
Germany

Environmental Engineering and Management Journal

Environmental Engineering and Management Journal is included and indexed in:
CABI
Chemical Abstracts Service/SciFinder (ACS) (since 2002)
EBSCO Database (since 2002)
EVISA
ICAAP (International Consortium for Advancement of Academic Publications)
Index Copernicus Journal Master List (**ICV/2015=156.46**)
Journal Citation Reports® 2018 Edition (**IF=1.186**), (*Environmental Sciences*, Ranked **211 out of 250**; 5-Year Impact Factor: 0.936; Article Influence® Score: 0.080; Immediacy Index: 0.159; Normalized eigenfactor: 0.19; **Quartile: Q4**)
MedSci
ProQuest (since 2002)
The National University Research Council (RO)
Science Citation Index Expanded™
SJR (SCImago Journal&Country Rank) (*Environmental Sciences*, **SJR index/2018= 0.345**; Ranked **779 out of 1582**, Quartile **Q3**, **H=31,** *Environmental Engineering:* Ranked **72 out of 184, Quartile Q3***; Management, Monitoring, Policy and Law:* Ranked **173 out of 308,** Quartile **Q3***; Pollution*, Ranked **69 out of 148; Quartile: Q3**)
SCOPUS (since 2002), **CiteScore/2018=1.03, SNIP index/2018=0.902**
ISI Master Journal List, Web of Science® (**H=30**)

Home page: *http://www.eemj.icpm.tuiasi.ro;*
http://www.eemj.eu

Full text: *http://www.ecozone.ro, http://www.eemj.eu*

Founding Editor: Matei Macoveanu, Iasi (RO)
Editor-in-Chief: Maria Gavrilescu, Iasi (RO)

Environmental Engineering and Management Journal is edited by
Gheorghe Asachi Technical University of Iasi and _EcoZone_ Publishing House of the _Academic Organization for Environmental Engineering and Sustainable Development_ (O.A.I.M.D.D.)

Editorial and Production Office:
Department of Environmental Engineering and Management – *Cristofor Simionescu* Faculty of Chemical Engineering and Environmental Protection and EcoZone - O.A.I.M.D.D., 73 *Prof. Dimitrie Mangeron* Bd., 700050 Iasi, Romania
Phone: +40-232-278680, ext. 2259, 2137
Fax: +40-232-271759
e-mail: eemjournal.at.yahoo.com, eem_journal.at.yahoo.com, eemjeditor.at.yahoo.com, eemj_editor.at.yahoo.com, eemjournal.at.gmail.com, eemj.editor.at.gmail.com, eemj.office.at.gmail.com

Published 12 issues per year, **under the aegis of the _Gheorghe Asachi_ Technical University of Iasi, Romania**
by *EcoZone* Publishing House of the *Academic Organization for Environmental Engineering and Sustainable Development* (O.A.I.M.D.D.), **http://www.ecozone.ro**

Annual subscription rate 2019 (12 issues)

	Print:	**Electronic full access:**	**Print+Electronic:**
EURO	575 per volume	575 per year	1000 per volume/year
Individual costs			
EURO	55 per issue	45 per issue	

Order directly to the Editorial Office, 73 *Prof. Dimitrie Mangeron* Bd., 700050 Iasi, Romania
Phone/Fax: Fax: +40-232-271759, e-mail: brindusa.sluser.at.gmail.com, eemj.office.at.gmail.com

Electronic, full text: Order or purchase on-line at: **www.eemj.eu, www.ecozone.ro**

Bank account (EURO):
ALPHA BANK ROMANIA (ABR)
SWIFT Code: BUCUROBU,
IBAN: RO79BUCU1031215940036EUR
Beneficiary: OAIMDD-EEMJ, Address: PO 10, Box 2111, 700050 Iasi, Romania

Bank account (LEI):
ALPHA BANK ROMANIA (ABR), IBAN: RO87BUCU1032235333663RON,
Beneficiary: OAIMDD-EEMJ

Environmental Engineering and Management Journal
February, Vol.19, No. 2, 183-368
http://www.eemj.icpm.tuiasi.ro/; http://www.eemj.eu

"Gheorghe Asachi" Technical University of Iasi, Romania

CONTENTS

Environmental Engineering and Management Journal February 2020, Vol. 19, No. 2, 183-194
http://www.eemj.icpm.tuiasi.ro/; http://www.eemj.eu

"Gheorghe Asachi" Technical University of Iasi, Romania

ENVIRONMENTAL PROTECTION IN ROMANIA: PERCEPTIONS VERSUS ACTIVE PARTICIPATION

Simona-Roxana Ulman[1]*, Krisztina-Melinda Dobay[2]

[1]Alexandru Ioan Cuza University of Iasi, CERNESIM Environmental Research Centre,
19 Carol I Boulevard, 700506, Iasi, Romania
[2]Romanian Academy, Iaşi Branch, „Gh. Zane" Institute of Economic and Social Research,
2 Codrescu, 700481, Iasi, Romania

Abstract

This study aims to measure the environmental concern in Romania, to investigate its state of fact at regional and county levels and to provide a better understanding of its determinants. Using data from World Values Survey (2010-2014), there were firstly analyzed the perceptions (care for environment, perspective on environmental pollution, alternative between protecting environment vs. economic growth), then active participation (membership in an environmental organization, financing ecological organization, participation in demonstration for environment) and, lastly, integrating both in one general composite index, we obtained the profiles and the distribution of individuals: (1) with positive perceptions towards environment; (2) with active participation in environmental activities; (3) with a high level of general environmental concern. We found out that the personal position regarding environment concern is influenced by: educational level, post-materialist values, gender and feeling of happiness. Thus, there is a higher probability for a person to be more aware and involved in pro-environmental actions in the conditions of having tertiary education, post-materialist values, feeling happy. More, the probability is higher for men than for women. We also concluded that the environmental concern is very low in all the Romanian regions, but the Northern part of the country registers better levels. Per counties, Harghita and Neamt seem to have the highest levels of concern towards environment. Considering different measuring approaches and a more careful segmentation of population in Romania, our findings represent potential starting points for better targeted national and regional environmental policies.

Key words: environmental concern, environmental policies, general composite index

Received: January, 2019; Revised final: November, 2019; Accepted: November, 2019; Published in final edited form: February, 2020

1. Introduction

Protecting environment has become an important issue, frequently debated in the academic literature devoted to sustainability. The focus was initially on the economic dimension and nowadays greater attention is tending to be put on the environmental one especially because "today's environmental problems are increasingly complex" (Burke et al., 2017) and represent a "threat" to human well-being (Dunlap and Scarce, 1991; Mironiuc and Huian, 2017).

In this process, a fundamental role should be played by what is called co-evolution, i.e. "the constant and active interaction between a living organism and its environment" (Lorenzoni et al., 2000; Norgaard, 1984; Norgaard, 1994), meaning that society with its two dimensions, economic and social, and environment have to be seen as two intimately co-evolving systems (Cappelletto et al., 2018; Lorenzoni et al., 2000). In other words, the environmental aspects have to be integrated within the theory and practices of economic development, meaning the humanization and greening of the economy (Pohoaţă, 2003).

---

* Author to whom all correspondence should be addressed: e-mail: simonaulman@yahoo.com; Phone: +40 23201428

1.1.Literature review

In this context, understanding the general environmental concern, collocation frequently used in the literature (Brieger, 2018; Diekmann and Franzen, 2019; Dunlap and Scarce, 1991; Dunlap and York, 2008; Gatti, 2016; Inglehart, 1995; Kemmelmeier, 2002; Poortinga et al., 2004), represents an initial step in the process of protecting environment because it addresses the changes of people's behaviours (Sneddon et al., 2006), based on opinions and attitudes. Moreover, as Inglehart (1995) mentions, the policies designed to solve environmental problems are unlikely to succeed without broad public support. But, even if the environmental legislation is applied and respected, sometimes the final goal of environmental protection is left unachieved (Ghinea et al., 2017; Marinescu, 2007; Rotaru et al., 2019), its impact and results ultimately depending on the level of awareness and active participation of the individuals.

Although it is not an easy task (Inglehart, 1995), a deep understanding of the environmental concern represented the main challenge in numerous studies (Brieger, 2018; Diekmann and Franzen, 2019; Dunlap and York, 2008; Inglehart, 1995; Kemmelmeier et al., 2002; Poortinga et al., 2004), in which there were developed different measurement approaches, such as: the Environmental Protection Index (Inglehart, 1995), the SACRIFICE Index (Kemmelmeier et al., 2002), the New Environmental Paradigm (NEP) scale (Poortinga et al., 2004) etc.

The environmental concern is influenced by different factors, each determining more or less positive perceptions or active participation in activities related to environmental protection. Although the most evident factors determining a higher level of environmental involvement should be the severe objective problems, as, for example, high levels of air or water pollution, as Inglehart (1995) emphasized, this assumption is a "naive environmental activist" approach, the so-called "challenge-response model". More deepen analyses were made in order to discover different other factors with influence on the level of environmental concern at the individual and national level (Brieger, 2018; Diekmann and Franzen, 2019; Dunlap and York, 2008; Franzen and Vogl, 2013; Inglehart, 1990; Inglehart, 1995; Kemmelmeier et al., 2002; Poortiga et al., 2004; Schultz et al., 2000; Turaga, 2015; Zelezny et al., 2000). Between those determinants, the most common are: education, income, post-materialist values (striving for self-actualization; stressing the aesthetic and the intellectual; cherishing belonging and esteem), gender, employment status etc. Usually, (1) higher levels of education are significantly associated with more pro-environmental attitudes (Kemmelmeier et al., 2002); (2) higher levels of income are related to more favourable attitudes (Diekmann and Franzen, 1999; Kemmelmeier et al., 2002; Lee and Kidd, 1997); (3) persons with post-materialist values give a higher priority to protect the environment than those with materialist values (Bennulf and Holmberg, 1990; Betz, 1990; Hoffmann-Martinot, 1991; Inglehart, 1990; Kemmelmeier et al., 2002; Mueller-Rommel, 1990); (4) females are more disposed to allocate from their time in order to participate in pro-environmental activities than men (Agarwal, 2000).

Some studies highlight the fact that there are differences between perceptions and behaviours, people seeming to be aware and declaratively sustaining a cause, but when it is the case to put this into action, opt to not be implied in pro-environmental activities (Inglehart, 1995). More, the most common theoretical approach is to not differentiate perceptions from active involvement and to generally analyse the environmental concern and its determining factors. Although there are recent studies regarding the environmental concern in the global context (Brieger, 2018; Diekmann and Franzen, 2019; Franzen and Vogl, 2013), the findings show that there is a substantial difference in environmental concern among different countries and that it could be better understood analysing particular contexts in terms of regional and national levels. Moreover, the conclusions of a previous study, focusing on Romania comparatively to other 59 countries from all over the world (Ulman, 2018), showed that this country follows the most common trend of world's undeveloped and developing countries. It became clearly that it is necessary to understand the causes of this situation through a deeper analysis in the national and regional context for finding out the particularities and driving factors towards environmental concern, both in perceptions and active participation.

1.2. Research goals

Taking into consideration the aspects mentioned above and also the facts that: (1) Romania was not enough particularly analysed in terms of environmental concern and (2) its national environmental wellbeing is low (van de Kerk and Manuel, 2017), Romania also registering a low orientation towards environmental problems and a low to medium availability to prioritize environmental protection (Ulman, 2018), our study attempts to:

(1) measure the environmental concern (both perceptions and active participation) in Romania at national, regional and county levels;

(2) identify the profiles of individuals with a high environmental concern (both perceptions and active participation);

(3) analyse and understand the most significant socio-demographic and economic factors of environmental awareness and involvement in the national context.

The paper is structured as follows. Section 2 is dedicated to the methodology and the data used in order to compose the environmental concern indices and to measure their level in Romania. Section 3 illustrates and discusses the main empirical results. Section 4 represents the part dedicated to concluding remarks.

2. Material and methods

2.1. Environmental concern indices

We proposed an analysis in which, initially, we concentrated on environmental perceptions, then observed the active participation in pro-environmental activities and, lastly, integrated both in one index, offering a wider perspective regarding environmental concern. We followed Inglehart's (1995) approach regarding the Environmental Protection Index, with 2 categories (*high* and *low*) according to the answers of the respondents to 4 issues regarding environment. Firstly, we integrated the **declared perceptions** (care for environment, perspective on environmental pollution, alternative between protecting environment vs. economic growth) ($I_{\text{env\_intent-oriented}}$) into a composite index (Table 1). Moving on, the next step was to analyse the **active participation** (membership in an environmental organization, financing ecological organization, participation in demonstration for environment) and we obtained the second composite index ($I_{\text{env\_act-oriented}}$) (Table 1). Then, integrating both perceptions and behaviours in one single measure, we obtained a **general index for environmental concern** (I_{env}) (Table 1).

Table 1. Definition of the variables

Variables	*Description*
Intent oriented to environment Index ($I_{\text{env\_intent-oriented}}$)	Analysing perceptions regarding environment and its problems ($A_{\text{env\_intent-oriented}}$, $B_{\text{env\_intent-oriented}}$, $C_{\text{env\_intent-oriented}}$) (*high*, *low*) = ***high*** (if the respondent gives at least two *high* responses to $A_{\text{env\_intent-oriented}}$, $B_{\text{env\_intent-oriented}}$, $C_{\text{env\_intent-oriented}}$); = ***low*** (if the respondent gives only one or none *high* response to $A_{\text{env\_intent-oriented}}$, $B_{\text{env\_intent-oriented}}$, $C_{\text{env\_intent-oriented}}$)
Care for environment ($A_{\text{env\_intent-oriented}}$)	Looking after the environment is important to this person: to care for nature and save life resources (yes = *high*; no = *low*)
Perspective on environmental pollution ($B_{\text{env\_intent-oriented}}$)	Most serious problem of the world: environmental pollution (yes = *high*; no = *low*)
Protecting environment vs. Economic growth ($C_{\text{env\_intent-oriented}}$)	Protecting the environment should be given priority, even if it causes slower economic growth and some loss of jobs (yes = *high*; no = *low*)
Action oriented to environment Index ($I_{\text{env\_act-oriented}}$)	Analysing active participation of the respondents on diverse activities for improving environmental conditions ($A_{\text{env\_act-oriented}}$, $B_{\text{env\_act-oriented}}$, $C_{\text{env\_act-oriented}}$) (*high*, *low*) = ***high*** (if the respondent gives at least two *high* responses to $A_{\text{env\_act-oriented}}$, $B_{\text{env\_act-oriented}}$, $C_{\text{env\_act-oriented}}$); = ***low*** (if the respondent gives only one or none *high* response to $A_{\text{env\_act-oriented}}$, $B_{\text{env\_act-oriented}}$, $C_{\text{env\_act-oriented}}$)
Member of an environmental organization ($A_{\text{env\_act-oriented}}$)	Active/Inactive membership: environmental organization (yes = *high*; no = *low*)
Given money to ecological organization ($B_{\text{env\_act-oriented}}$)	Past two years: given money to ecological organization (yes = *high*; no = *low*)
Participation in demonstration for environment ($C_{\text{env\_act-oriented}}$)	Past two years: participated in demonstration for environment (yes = *high*; no = *low*)
Environmental concern Index (I_{env})	Integrating the general concern regarding environment comprised both in perceptions and in active participation ($I_{\text{env\_intent-oriented}}$ and $I_{\text{env\_act-oriented}}$) (*high*, *low*) = ***high*** (if the respondent gives at least three *high* responses to $A_{\text{env\_intent-oriented}}$, $B_{\text{env\_intent-oriented}}$, $C_{\text{env\_intent-oriented}}$, $A_{\text{env\_act-oriented}}$, $B_{\text{env\_act-oriented}}$, $C_{\text{env\_act-oriented}}$); = ***low*** (if the respondent registers maximum two *high* from six possible ones)
Age	Age of the respondent
Gender	Gender of the respondent (*female*, *male*)
Marital status	Marital status of the respondent (*single*, *married*, *divorced*)
Number of children	Number of children of the respondent
Educational level	Highest educational level attained (*lower-secondary*, *secondary*, *tertiary*)
Employment status	Employment status (*employed*, *unemployed*, *retired*)
Sector of employment	Where the respondent is employed (*Government* or *public sector*, *private sector*)
Nature of tasks: routine vs. non-routine	If the respondent has on his job mostly *routine task* or mostly *non-routine tasks*
Nature of tasks: manual vs. intellectual	If the respondent has on his job mostly *manual* or mostly *intellectual tasks*
Scale of income	The group of income where the respondent's household is, counting all wages, salaries, pensions and other incomes that come in (*first two steps*, *middle steps*, *last two steps* - meaning the highest incomes)
Post-materialist values	Post-materialist index (*post-materialist*, *mixed*, *materialist*)
Feeling of happiness	Taking all things together, would you say you are: *very or rather happy*; *not very or not at all happy*

Source: Authors' indices and considered factors based on WVS, wave 6, 2010-2014

2.2. Factors determining the environmental concern

One of our aims was to understand the most significant factors of environmental concern in the Romanian context. For doing this, we analysed the data provided by World Values Surveys, wave 6, 2010-2014, a global network of social scientists who surveys the role of values in social and political life, since 1991 in almost 100 countries, conducting national representative surveys (Brieger, 2018). We opted to use this reliable and validated database, with 1019 total observations for Romania, from all counties, which provided us the necessary data to go in in-depth analysis. We mentioned that some of the most relevant studies for the topic of environmental concern also used data from WVS (Inglehart, 1995; Dunlap și York, 2008; Turaga, 2015; Brieger, 2018).

Using 959 entries for Romania, we tested the significant variables that can be correlated to the three different perspectives regarding Romanians' environmental concern. Our ***dependent variables*** were: $I_{env\_intent\text{-}oriented}$, $I_{env\_act\text{-}oriented}$ and I_{env}. Our ***independent variables*** were: (1) *age*; (2) *gender*; (3) *education level*; (4) *marital status*; (5) *number of children*; (6) *employment status*; (7) *sector of employment*; (8) *nature of tasks: routine vs. non-routine*; (9) *nature of tasks: manual vs. intellectual*; (10) *scale of income*; (11) *Post-materialist index*; (12) *feeling of happiness*.

2.3. Statistical methods

Firstly, we descriptively analysed the **regional and county levels of environmental concern**, classifying the percentages of people with a high environmental concern in the following categories: (1) extremely low = <10%; (2) very low = 10%-20%; (3) low = 20%-30%; (4) low to medium = 30%-40%; (5) medium = 40%-50%; (6) medium to high = 50%-60%; (7) high = 60%-70%; (8) very high = 70%-80%; (9) extremely high = >80%, obtaining also some representative maps (Fig. 1-6).

Secondly, based on the test results for independence between the dependent variables and each independent variable, we linked the *high* or *low* environmental concern, with the mentioned independent variables with their categories using a *Joint Correspondence Analysis* (Greenacre and Blasius, 2005; Nenadic and Greenacre, 2007; Pintilescu, 2007), with the aim to describe the associations between them and to identify the **profiles of individuals** in terms of environmental concern. The data was computed into Statistical Package for the Social Sciences (SPSS 25). It represents a preliminary step for the *Logistic Regression Analysis* (Inglehart, 1995; Poortinga et al., 2004; Turaga, 2015), used with the aim of estimating the **probability of an individual to be part of the high level of environmental concern group**, **considering several socio-demographic and economic characteristics**.

Then, since our dependent variables were binary ones, with values of *high* or *low*, we used logistic regression model, having at its base the link between the ***dependent variable*** and ***independent variables***, X_1: *age*, X_2: *gender* (*a. female and b. male*), X_3: *educational level* (*a. primary*, *b. secondary*, *c. tertiary*), X_4: *marital status* (*a. married*, *b. divorced*, *c. single*), X_5: *number of children*, X_6: *employment status* (*a. employed*, *b. retired*, *c. unemployed*), X_7: *sector of employment* (*a. Government and public sector*, *b. private sector*), X_8: *nature of tasks: manual vs intellectual* (*a. mostly manual tasks, b. mostly intellectual tasks*), X_9: *nature of tasks: routine vs creative* (*a. preponderantly non-routine tasks*, *b. preponderantly routine task*), X_{10}: *scale of income* (*a. first two steps*, *b. last two steps*, *c. middle steps*), X_{11}: *post-materialist index* (*a. materialist*, *b. mixed*, *c. post-materialist*), X_{12}: *feeling of happiness* (*a. not very or not at all happy*, *b. rather or very happy*). The logistic regression equation is expressed by Eq. (1), where:

- π_i represents the probability that a member „*i*" to be part of the *high level of environmental concern group* (concern related to perceptions), and $(1-\pi_i)$ indicates the probability that a member „*i*" not to be part of this environmental concern group;
- π_i represents the probability that a member „*i*" to be part of the *high level of environmental concern group* (concern related to actions), and $(1-\pi_i)$ indicates the probability that a member „*i*" not to be part of this environmental concern group;
- π_i represents the probability that a member „*i*" to be part of *the high level of environmental concern group* (general concern), and $(1-\pi_i)$ indicates the probability that a member „*i*" not to be part of this environmental concern group.

The Logistic Regression models are built taking into consideration three dependent variables:

- *Models 1* and *2* have as dependent variable the $I_{env\_intent\text{-}oriented}$;
- *Models 3* and *4* have as dependent variable the $I_{env\_act\text{-}oriented}$;
- *Models 5* and *6* have as dependent variable the I_{env}.

$$ln\left(\frac{\pi_i}{1-\pi_i}\right) = \beta_0 + \beta_1 X_{1i} + \beta_2 X_{2ai} + \beta_{3a} X_{3ai} + \beta_{3b} X_{3bi} + \beta_{4a} X_{4ai} + \beta_{4b} X_{4bi} + \beta_5 X_{5i} + \beta_{6a} X_{6ai} + \beta_{6b} X_{6bi} + \beta_{7a} X_{7ai} + \beta_{8a} X_{8ai} + \beta_{9a} X_{9ai} + \beta_{10a} X_{10ai} + \beta_{10b} X_{10bi} + \beta_{11a} X_{11ai} + \beta_{11b} X_{11bi} + \beta_{12a} X_{12ai} + \varepsilon_i \qquad (1)$$

Interpretation of signs and estimated regression coefficients' significance were made considering the reference group with the following categories: *gender (male)*; *educational level (primary)*; *marital status (single)*, *sector of employment (private sector)*, *nature of tasks (mostly routine)*, *scale of income (middle steps of income)*, *post-materialist index (post-materialist)*, *feeling of happiness (rather or very happy)*. We also determined the Adjusted Odds Ratio for each category of the above mentioned variables in relation to the reference category.

In the case of *Logistic Regression Analysis,* the data was computed into Statistical Analysis System (SAS 9.3).

3. Results and discussions

3.1. Descriptive analysis

Analysing the percentages of people, at national and regional level, that have **positive perceptions**, we observed that: (1) the Centre Region obtains the highest percentages in the country, being integrated into the *medium* category; (2) the North-East, South Muntenia and South-West Oltenia Regions register lower percentages and are part of the *low to medium* category; (3) the West Region integrates into the *low* category; (4) the South-East and North-West Regions into the *very low* category (Fig. 1). Referring to **active participation**, it can be noticed that all the regions register *extremely low* level of personal involvement in environmental activities (Fig. 2). At the general level, the **environmental concern** is not at all notable, but the Northern part of Romania registers better levels (being included in the next category, i.e. *very low*, than the other part of the country that is included in the *extremely low* one) (Fig. 3). At **county level**, related to: (1) environmental positive perceptions, Neamt, Harghita, Brasov and Dolj are the counties with the highest percentages of respondents with a high $I_{\text{env\_intent-oriented}}$, possible to be included in the *medium to high* category (Fig. 4); (2) active participation in environmental activities, Arad and Harghita detain the highest percentages of respondents with a high $I_{\text{env\_act-oriented}}$, still possible to be included only in the *low* category (Fig. 5); (3) general environmental concern, Neamt and Harghita have the highest percentages of a high I_{env} (Fig. 6).

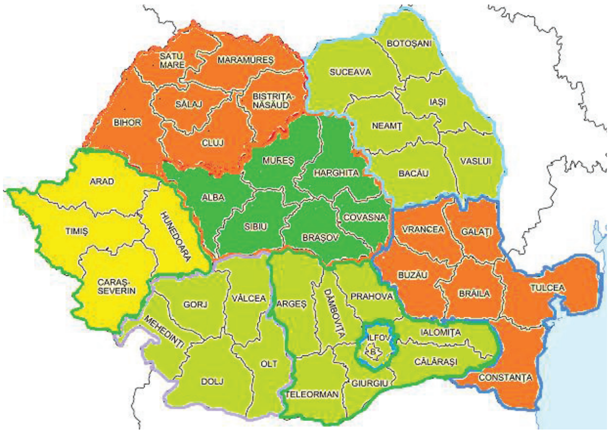

Fig. 1. Intent oriented to environment Index ($I_{\text{env\_intent-oriented}}$) at national level, in different regions of Romania

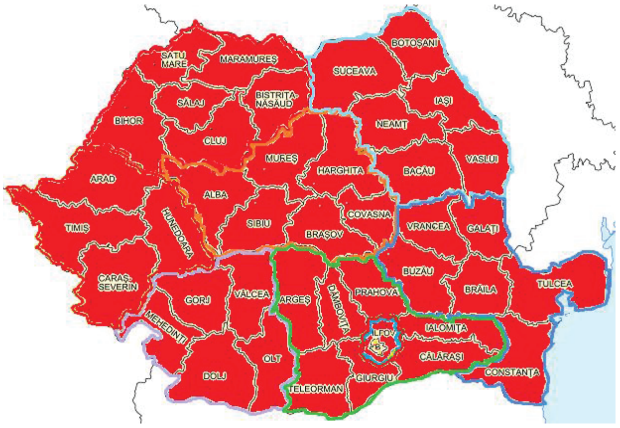

Fig. 2. Action oriented to environment Index ($I_{\text{env\_act-oriented}}$) at national level, in different regions of Romania

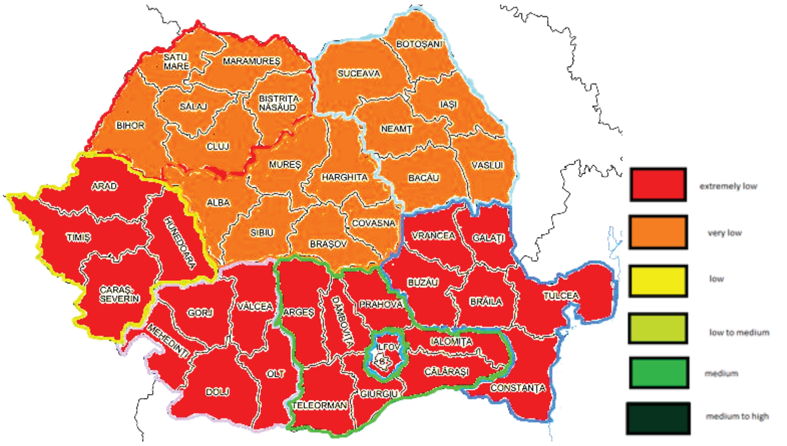

Fig. 3. Environmental concern Index (I_{env}), at national level, in different regions of Romania

Source: Authors' representation based on WVS, wave 6, 2010-2014

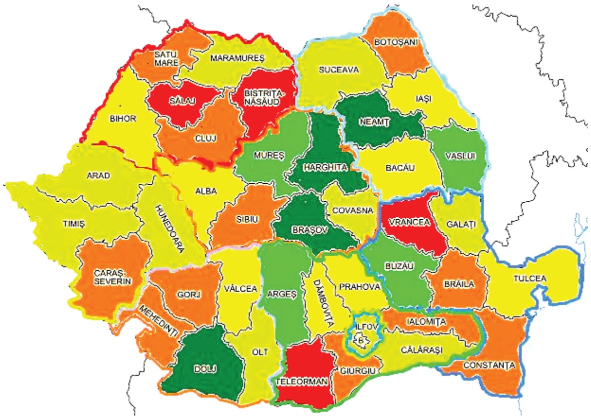

Fig. 4. Intent oriented to environment Index ($I_{env\_intent\text{-}oriented}$) at county level in Romania

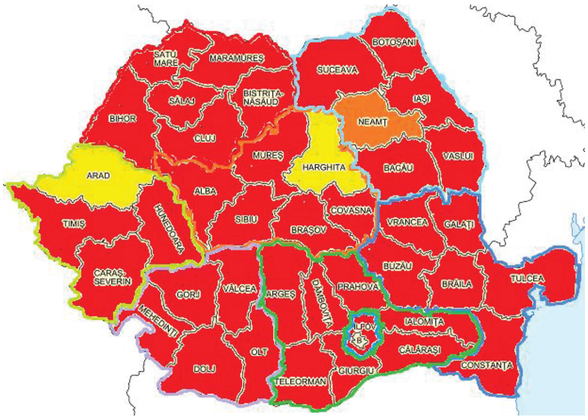

Fig. 5. Action oriented to environment Index ($I_{env\_act\text{-}oriented}$) at county level in Romania

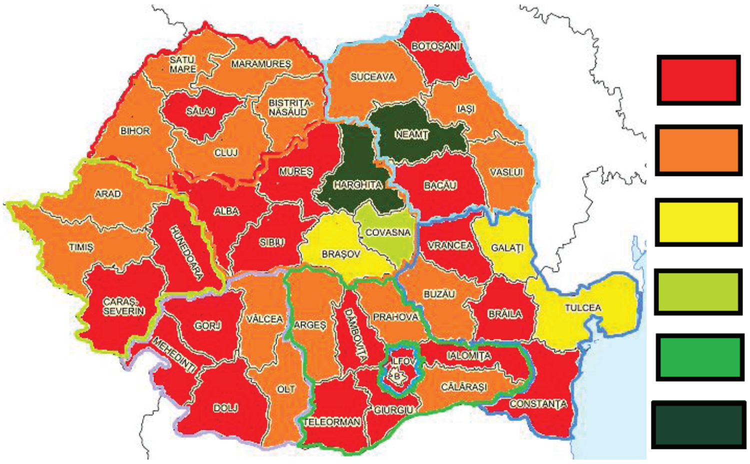

Fig. 6. Environmental concern Index (I_{env}), at county level in Romania
Source: Authors' representation based on WVS, wave 6, 2010-2014

3.2. Identifying the profiles of groups regarding the environmental concern

In this section, we analysed the specific profiles of individuals regarding environmental concern related to **personal characteristics** considered to be representative for the Romanian respondents. We kept for the next analysis only the factors that were significantly correlated to the dependent variables (Table 2).

Table 2. Test results for independence between environmental concern indices and each independent categorical variable

Variables	***Pearson Chi-square***					
	$I_{env\_intent\text{-}oriented}$		$I_{env\_act\text{-}oriented}$		I_{env}	
	Value	Asym. Sig. (2-sided)	Value	Asym. Sig. (2-sided)	Value	Asym. Sig. (2-sided)
(1) Gender	3.16	**0.08***	1.07	0.30.	3.14	**0.08***
(2) Education level	6.55	**0.04****	10.25	**0.01*****	17.75	**0.00*****
(3) Marital status	5.06	**0.08***	1.16	0.56.	0.59	0.74.
(4) Employment status	0.21	0.90.	1.67	0.43.	6.83	**0.03****
(5) Sector of employment	1.81	0.18.	4.14	**0.04****	0.37	0.54.
(6) Nature of tasks: routine vs. non-routine	2.93	**0.09***	9.43	**0.00*****	11.08	**0.00*****
(7) Nature of tasks: manual vs. intellectual	2.58	0.11.	7.54	**0.01*****	6.40	**0.01*****
(8) Scale of income	2.31	0.32.	14.02	**0.00*****	5.06	**0.08***
(9) Post-materialist values	7.69	**0.01*****	8.08	**0.00*****	5.90	**0.02****
(10) Feeling of happiness	8.71	**0.00*****	2.08	0.15.	7.94	**0.02****

Note: (***) indicates the null hypothesis rejection for 1%; (**) indicates the null hypothesis rejection for 5%; (*) indicates the null hypothesis rejection for 10%; (.) indicates the null hypothesis acceptance; the models 1, 3, 5 include all the independent variables taken into consideration and the models 2, 4 and 6 include only the significant ones.

Source: Authors' computation based on WVS, wave 6, 2010-2014, using SAS 9.3

Having the obtained results from the Pearson Chi-square statistic, it can be observed that, in the analysis of the correlations between: (1) $I_{env\_intent-oriented}$ and *employment status*, *sector of employment*, *nature of tasks: manual vs. intellectual*; (2) $I_{env\_act-oriented}$ and *gender, marital status, employment status, feeling of happiness* and (3) I_{env} and *marital status*, *sector of employment*, the calculated value of the statistical test was lower than the theoretical value (or Sig > α=0.10). This result implied the decision of accepting the hypothesis of independence between each index regarding environmental concern and the independent variables.

In the case of the other variables taken into analysis, the calculated values of statistical test indicated the rejection of the null hypothesis with a probability equal to 0.95, observing the fact that, between the three variables related to environment and each other variable, significant associations existed (Table 2).

3.2.1. Joint Correspondence Analysis

After analysing the test results for independence between variables, for identifying the respondents' profiles, the *Joint Correspondence Analysis* was applied. The graphical representation indicated the existence of some associations between the categories of considered variables (Figs. 7-9).

In the investigated sample, it was observed a difference of the respondents' **environmental perceptions** and the categories of the significant independent variables. Thus, on the basis of correspondent point representation for the variables, we obtained the following profiles:

- **the profile of respondents with a high** $I_{env\_intent-oriented}$: (1) educational level: tertiary, (2) nature of tasks: mostly non-routine, (3) Post-materialist index: post-materialist;

- **the profile of respondents with a low** $I_{env\_intent-oriented}$: (1) gender: male and female, (2) educational level: secondary, (3) marital status: married, (4) nature of tasks: mostly routine, (5) Post-materialist index: materialist and mixed.

Differences of the respondents' behaviour in terms of **environmental activities** and the categories of the significant independent variables were recorded and, on the basis of correspondent point representation for these variables, we obtained the following profiles:

- **the profile of respondents with a high** $I_{env\_act-oriented}$: (1) educational level: tertiary, (2) sector of employment: Government or public sector, (3) nature of tasks: mostly intellectual, (4) nature of tasks: mostly non-routine, (5) scale of income: last two steps, (6) Post-materialist index: post-materialist;

- **the profile of respondents with a low** $I_{env\_act-oriented}$: (1) educational level: secondary, (2) sector of employment: private sector, (3) nature of tasks: mostly manual, (4) nature of tasks: mostly routine, (5) scale of income: middle steps, (6) Post-materialist index: materialist and mixed.

In terms of **general environmental concern** and the categories of possible determinants, we defined the following profiles:

- **the profile of respondents with a high** I_{env}: (1) educational level: tertiary, (2) employment status: employed, (3) nature of tasks: mostly intellectual (4) nature of tasks: mostly non-routine, (5) scale of income: last two steps, (6) Post-materialist index: post-materialist, (7) feeling of happiness: very or rather happy;

- **the profile of respondents with a low** I_{env}: (1) educational level: secondary, (2) employment status: retired, (3) nature of tasks: mostly manual, (4) nature of tasks: mostly routine, (5) scale of income: middle steps, (6) Post-materialist index: materialist, (7) feeling of happiness: not very or not at all happy.

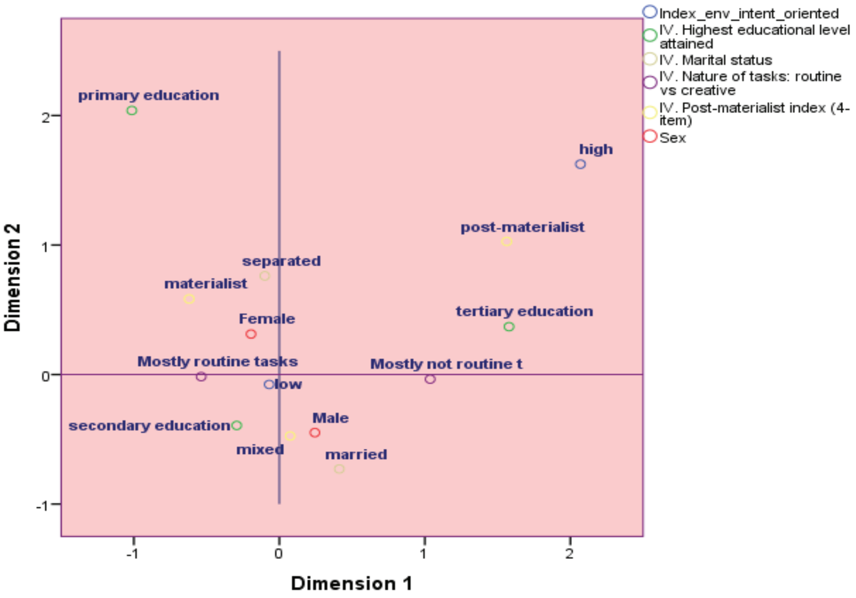

Fig. 7. The values representation on the first two factorial axes
Source: Authors' representation based on WVS, wave 6, 2010-2014, using SPSS 25

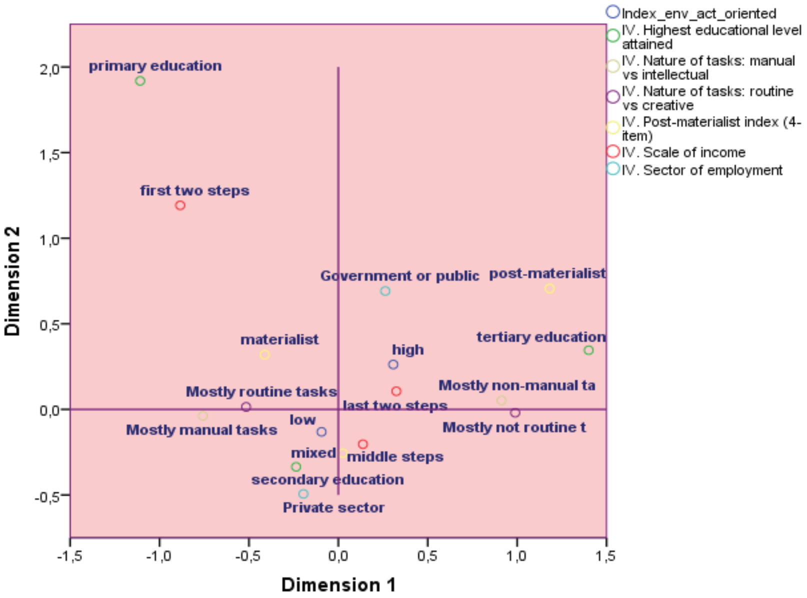

Fig. 8. The values representation on the first two factorial axes

Source: Authors' representation based on WVS, wave 6, 2010-2014, using SPSS 25

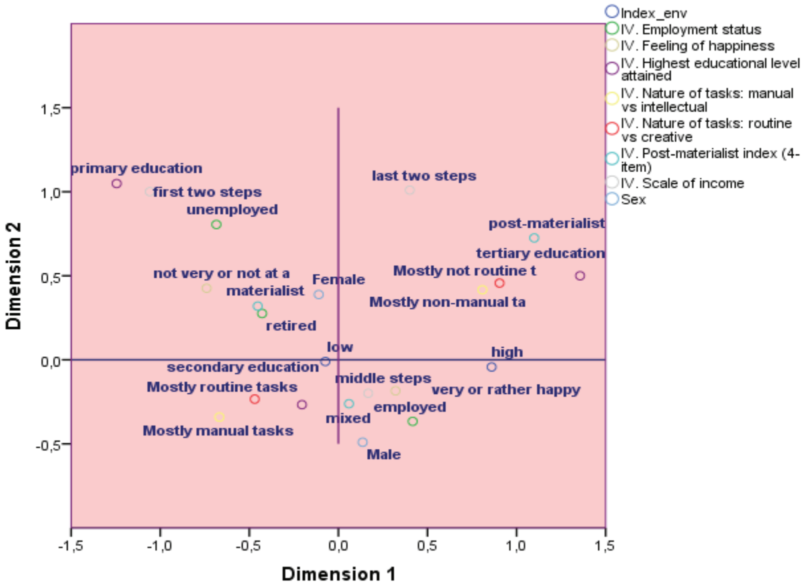

Fig. 9. The values representation on the first two factorial axes

Source: authors' representation based on WVS, wave 6, 2010-2014, using SPSS 25

3.2.2. Binomial Logistic Regression Analysis

As we mentioned in the methodology, the Logistic Regression models were built considering the three dependent variables. The results of testing the influence of independent variables on the probability of belonging to a specific group related to environment, using the Wald statistic test, were summarized in Table 3. The results showed that **gender, marital status, post-materialist values** and **feeling of happiness** had a significant influence on the belonging of the group with a high level of **environmental awareness**. The probability for a high level of **active participation** to environmental activities was significantly explained by s**ector of employment, nature of tasks: routine or creative, scale income** and **values**. Also, the test results indicated a significant impact of **gender, education level, values** and **feeling of happiness** on the probability to be included in the group with a high level of **environmental concern**. The results of estimation test for the three Logistic Regression models that included only the significant variables were presented in Table 4. Applying the Hosmer and Lemenshow Test, the small Chi-squared values (with larger p-value closer to 1) indicated a good logistic regression model fit.

Table 3. Econometrical modelling results

	$I_{env\_intent\text{-}oriented}$		$I_{env\_ act\text{-} oriented}$		I_{env}	
Independent variables	*Model 1*	*Model 2*	*Model 3*	*Model 4*	*Model 5*	*Model 6*
Age	1.03 .	-	2.23 .	-	0.11 .	-
Gender	3.65 **	3.15 *	0.91 .	-	3.23 *	2.55 *
Educational level	2.92 .	-	3.01 .	-	3.88 *	9.81 ***
Marital status	4.46 *	4.68 *	0.51 .	-	0.05 .	-
Number of children	0.01 .	-	2.24 .	-	0.06 .	-
Employment status	2.38 .	-	1.31 .	-	1.25 .	-
sector of employment	0.56 .	-	3.38 *	4.07 **	1.28 .	-
Nature of tasks: manual vs. intellectual	0.21 .	-	0.15 .	-	0.98 .	-
Nature of tasks: routine vs. creative	0.27 .	-	2.94 *	5.83 ***	0.21 .	-
Scale of income	1.85 .	-	4.52 *	11.30 ***	0.56 .	-
Post-materialist values	3.00 .	9.72 ***	3.01 *	7.11 ***	0.57 .	3.05 *
Feeling of happiness	7.74 **	8.02 **	0.11 .	-	6.12 ***	8.97 ***

Note: (***) indicates the null hypothesis rejection for 1%; (**) indicates the null hypothesis rejection for 5%; (*) indicates the null hypothesis rejection for 10%; (.) indicates the null hypothesis acceptance; the models 1, 3, 5 include all the independent variables taken into consideration and the models 2, 4 and 6 include only the significant ones.

Source: Authors' computation based on WVS, wave 6, 2010-2014, using SAS 9.3

For Model 2 and Model 6 (Tabel 4), the results suggestes that the probability of belonging to the group with a high level of environmental orientation was higher for males than for women. For the middle model (Model 4), the gender was no more a significant variable. Again, in the case of orientation put into practice, gender differences were not recorded. Men registered a higher probability to declare that 1) looking after the environment is important for them, caring for nature and saving life resources, 2) most serious problem of the world, in their opinion, is environmental pollution, or 3) protecting the environment should be given priority, even if it causes slower economic growth and some loss of jobs. More than that, our empirical results revealed the fact that the estimated chances for a higher $I_{env\_intent\text{-}oriented}$ in the case of a female, not married or divorced, having preponderantly post-materialist values and declaring rather or very happy was of 0.777 times less than the chances for a male in the same conditions. Contrary, when materializing these opinions into practice, no significant gender differences were met.

Regarding education, in the case of the first two models (Model 2 and 4), non-significant results were obtained. For the third model (Model 6), educational level was a significant variable, indicating that the probability for persons with tertiary education to have a high I_{env} was higher than for the ones with primary education (Tabel 4). Going deeper, we observed that, a male, with a lower-secondary education, with preponderantly post-materialist values and rather or very happy had of 0.489 time lower chances to have a high I_{env} than a man with tertiary education and with the same characteristics. The difference was almost the same (0.479) when comparing secondary education to tertiary one, in the same mentioned conditions. In the case of females, with similar socio-economic characteristics as described above for males, the estimated chances for a high general environmental concern were much more influenced by the level of education, the differences between the ones with lower-secondary education and the ones with secondary or tertiary education were lower than in the case of men (with Odds Ratio equal to 0.978 and 2.044).

Analysing the results of the impact of marital status on the probability to belong to a specific group, non-significant results were observed for the last two models. For the Model 2, the results suggested that the probability for the Romanian respondents to be part of the group with high level of orientation to environment was higher for the divorced ones than for the ones that were single. For the married ones, the differences were not significant.

Going further, a male that was divorced, having preponderantly post-materialist values and declaring rather or very happy had higher chances (equal of 1.889 times) to have a higher $I_{env\_intent\text{-}oriented}$ than the single ones with the same characteristics. Comparing to those that were employed in the private sector, the category working in a Government or public institution was more likely to have a high $I_{env\_act\text{-}oriented}$ and have preponderantly non-routine tasks. In other words, the probability to get more implied in activities related to environment and fighting for resolving its specific problems was higher for the employees from the public sector than for the ones from the private sector.

Table 4. Econometrical modelling results

Variables/Models	***Model 2***		***Model 4***		***Model 6***	
Gender: female	-0.13 (0.07)	*	-		-0.17 (0.11)	***
Education: secondary	-		-		0.23 (0.30)	.
Education: tertiary	-		-		0.25 (0.18)	**
Marital status: married	-0.10 (0.12)	.	-		-	
Marital status: divorced	0.37 (0.18)	**				
Sector of employment: Government or public institution	-		0.38 (0.19)	**	-	
Nature of tasks: mostly non-routine tasks	-		0.45 (0.19)	***	-	
Scale income: first two steps	-		-0.78 (0.44)	*	-	
Scale income: last two steps	-		1.38 (0.43)	***		-
Values: materialist	-0.33 (0.12)	***	-0.50 (0.19)	***	-0.19 (0.11)	*
Values: mixed	-0.12 (0.11)	.	-0.20 (0.12)	***	-0.11 (0.12)	*
Feeling of happiness: not very or not at all happy	-0.21 (0.08)	***		-	-0.47 (0.16)	***
Constant	-0.78 (0.12)	***	-2.80 (0.28)	***	-2.32 (0.20)	***
Hosmer and Lemenshow Test	8.136	.	9.422	.	4.942	.
Note: (***) indicates the null hypothesis rejection for 1%; (**) indicates the null hypothesis rejection for 5%; (*) indicates the null hypothesis rejection for 10%; (.) indicates the null hypothesis acceptance; values in brackets represent estimations of standard errors for the regression coefficients estimators.						

Source: Authors' computation based on WVS, wave 6, 2010-2014, using SAS 9.3

Because the value of Odds Ratio was 2.136, the estimated chances for a person working in the public sector, with mostly routine tasks, with a medium income and with preponderantly post-materialist values were higher than of a person working in the private sector and having the same other conditions. A similar situation was met in the case of a person working in the private sector, with mostly non-routine tasks, from the middle steps of income, and with mostly post-materialist values compared to a person with routine tasks and with the other characteristics being similar (Odds Ratio was equal to 2.479).

The probability for people included in the first two steps from the scale of income to register a high index for active participation in environmental activities was lower than the probability of the ones from the middle steps of income. Contrary, people from the last two steps of income registered a higher probability to have a higher implication in environmental activities than our reference category. We also observed that the estimated chances for a person, employed in the Government or in a public institution, having routine tasks, with preponderantly post-materialist values, feeling happy and being situated in the first steps from the scale of income were of 0.838 lower than the person in the same conditions, but with a middle level of income. In the same time, the ones with similar characteristics as mentioned above, but were positioned on the last steps of income, had more estimated chances (of 7.274 higher) than the ones from the middle steps. It must be mentioned that, among all Odds Ratio, this was the biggest one, meaning that the highest difference between the independent variables was in the case of income, its level being critical in terms of active participation in environmental activities.

Significant differences were also recorded between materialist and post-materialist orientations, regarding all the three indices. The post-materialist people tended to have a higher environmental concern.

The coefficient estimations of the feeling of happiness (Model 2 and Model 6) indicated significant differences between the ones that declare themselves as being very or rather happy than the ones saying that they are not very or not at all happy, the probability for a high level of orientation to environmental problems in terms of opinions, but also of general environmental concern being higher for the ones that considered themselves happy. In the case of Model 4, non-significant results were obtained.

4. Conclusions

Environmental concern is an important point of the policy devoted to environmental protection because it is related to its final recipient that is the human being. This is why the level of public support is essential in the process of putting policies into practice. As a response, we proposed an analysis in which, first, we concentrated on individuals' perceptions regarding environmental problems, then on their active participation in pro-environmental activities and, lastly, we integrated both dimensions in one index offering a wider perspective regarding environmental concern. This study is between the first ones to analyse consecutively the levels of positive perceptions, of active participation and, then, by integrating both, the levels of general environmental concern, in Romania, to our knowledge.

Analysing, at the national and regional levels, the active participation in pro-environmental activities, we concluded that there are no major differences, as the levels were very low. We observed that regarding the positive perceptions, the levels were the highest in the Central Region. Referring to the general environmental concern, we noticed that three regions (North-West, Centre and North-East Regions) had higher levels, even though all the regional levels were very low. At county level, the highest percentages of people with 1) environmental positive perceptions were in Neamt, Harghita, Brasov and Dolj; 2) active participation in environmental activities was in Arad and Harghita; 3) general environmental concern was in Neamt and Harghita.

We also outlined the profile of the individuals concerned with the environment protection in Romania, characterised especially as having tertiary education, a high level of income, post-materialist values, being employed, with mostly non-routine and non-manual tasks, and declaring themselves as being rather or very happy. More, we found out that, the personal position regarding environment, concreted in both perceptions and active participation, is influenced by: gender, educational level, post-materialist values, and feeling of happiness. This means that there is a higher probability for a person to be more aware and get more involved in pro-environmental actions in the conditions of having tertiary education, post-materialist values, feeling happy. Also, the probability is higher for men than for women.

Other findings were related to the personal position in terms of perceptions regarding environment, that is influenced by: gender, marital status, values and feeling of happiness. Thus, the probability for having positive perceptions is higher for a male that is divorced, with post-materialist values, and feeling happy. The active participation on pro-environmental actions is influenced by: sector of employment, nature of personal tasks, scale of income, values. This means that there is a higher possibility for people working in the public sector, with especially creative tasks, high income and post-materialist values to actively participate in environmental activities.

We found that the economic factors are important only in the case of active participation. In other words, the level of income is determinant for the level of involvement in activities such as: active membership in an environmental organization, given money to ecological organization or participating in demonstration for environment.

The state of personal happiness is important for the general environmental concern, but, especially in the phase of forming the opinions in terms of favourable perceptions regarding environment and its specific problems. This confirms the theories that underline the tendency of people to put on the centre of their interests firstly the personal aspects and, only after these are at a satisfactory level, to turn their attention on external problems, such as the environment.

Our findings are consistent with the ones of other studies related to the environmental concern, especially regarding the influence of income, education and post-materialist values on it. It also adds value to the present knowledge regarding the national and regional peculiarities through identifying the profiles and the distribution of individuals with a high environmental concern (both perceptions and active participation) and its main socio-demographic and economic determinants.

These may constitute important foundation elements for the public policies related to environment at national and regional level, helping to target better the population segments with the aim of inducing positive perceptions and appropriate behaviours towards environmental protection in Romania. Yet, there are missing information regarding the differences between the regional profiles of individuals with a high environmental concern, with its main causes, that would be useful for regional and local policies, especially for a better education regarding the necessity of improving the environmental wellbeing that may constitute future directions of research.

References

Agarwal B., (2000), Conceptualising environmental collective action: why gender matters, *Cambridge Journal of Economics*, **24**, 283-310.

Bennulf M., Holmberg S., (1990), The green breakthrough in Sweden, *Scandinavian Political Studies*, **13**, 165-184.

Betz H.G., (1990), Value change in postmaterialist politics: The case of West Germany, *Comparative Political Studies*, **23**, 239-256.

Brieger S.A., (2018), Social identity and environmental concern: The importance of contextual effects, *Environment and Behavior*, 51, 828-855.

Burke T.A., Cascio W.E., Costa D.L., Deener K., Fontaine T.D., Fulk F.A., Jackson L.E., Munns Jr W.R., Orme-Zavaleta J., Slimak M.W., Zartarian V.G., (2017), Rethinking environmental protection: meeting the challenges of a changing world, *Environmental Health*

Perspectives, **125**, A43-49.

Cappelletto M., Fava F., Villanova L.M., Trincardi F., Barbanti A., Bonanno A., Nardelli B.B., Ciappi E., Palama D., d'Alcala M.R., Sarretta A., Sprovieri M., (2018), Codevelop research and innovation for blue jobs and growth in the Mediterranean - the Bluemed initiative, *Environmental Engineering and Management Journal,* **17**, 2313-2327.

Diekmann A., Franzen A., (1999), The wealth of nations and environmental concern, *Environment and Behavior*, **31**, 540-549.

Diekmann A., Franzen A., (2019), *Environmental Concern: A Global Perspective*, In: *Attitudes and Behavior in Empirical Social Research. Analytical Concepts, Applications and Analysis Methods* (in German), Mayerl J., Krause T., Wahl A., Wuketich M. (Eds.), Wiesbaden, Springer VS, 253-272.

Dunlap R.E., Scarce R., (1991), Poll trends: Environmental problems and protection, *The Public Opinion Quarterly*, **55**, 651-672.

Dunlap R.E., York R., (2008), The globalization of environmental concern and the limits of the postmaterialist values explanation: Evidence from four multinational surveys, *The Sociological Quarterly*, **49**, 529-563.

Franzen A., Vogl D., (2013), Time Preferences and Environmental Concern: An Analysis of the Swiss ISSP 2010, *International Journal of Sociology*, **43**, 39-62.

Gatti C.R., (2016), Trends in human development and environmental protection, *International Journal of Environmental Studies*, **73**, 268-276.

Ghinea C., Campean T., Gavrilescu M., (2017), Integrating sustainability indicators for tracking anthropogenic pressure on the earth the footprint family, *Environmental Engineering and Management Journal*, **16**, 935-948.

Greenacre M., Blasius J., (2005), *Correspondence Analysis in the Social Sciences*, Academic Press, London.

Hoffmann-Martinot V., (1991), Gruene and Verts: two faces of European ecologism, *West European Politics*, **14**, 70-95.

Inglehart R., (1990), *Culture Shift in Advanced Industrial Society*, Princeton University Press.

Inglehart R., (1995), Public support for environmental protection: Objective problems and subjective values in 43 societies, *Political Science & Politics*, **28**, 57-72.

Kemmelmeier M., Krol G., Kim Y.H., (2002), Values, economics, and proenvironmental attitudes in 22 societies, *Cross-Cultural Research*, **36**, 256-285.

Lee A-R., Kidd Q., (1997), More on postmaterialist values and environment, *Social Science Quarterly*, **78**, 36-43.

Lorenzoni I., Jordan A., Hulme M., Turner R., Turner R.K., O'Riordan T., (2000), A coevolutionary approach to climate change impact assessment: Part I. Integrating socio-economic and climate change scenarios, *Global Environmental Change*, **10**, 57-68.

Marinescu D., (2007), *Dissertation on Environmental Law*, 2nd Edition, Universul Juridic, Bucharest.

Maslow A. H., (1943), A theory of human motivation, *Psychological Review,* **50**, 370-396.

Mironiuc M., Huian M.C., (2017), Empirical study on the interdependence between environmental wellbeing, financial development and economic growth, *Environmental Engineering and Management Journal,* **16**, 2625-2635.

Mueller-Rommel F., (1990), *New Politics in Western Europe: The Rise and the Success of Green Parties and Alternative Lists*, Westview Press, Boulder.

Nenadic O., Greenacre M., (2007), Correspondence analysis in R, with two-and three dimensional graphics: The ca package, *Journal of Statistical Software*, **20**, 1-13.

Pintilescu C., (2007), *Multivariate Statistical Analysis*, Al. I. Cuza University Press, Iasi, Romania.

Pohoață I., (2003), *Economic Philosophy and the Policies of Sustainable Development*, Economic Print, Bucharest.

Poortinga W., Steg L., Vlek C., (2004), Values, environmental concern, and environmental behavior: A study into household energy use, *Environment and Behavior*, **36**, 70-93.

Rotaru C.S., Manciulea I., Draghici C., (2019), Effect of environmental monitoring on the environmental legislative process, *Environmental Engineering and Management Journal*, **18**, 1843-1847.

Schultz P.W., Zelezny L., Dalrymple N.J., (2000), A multinational perspective on the relation between Judeo-Christian religious beliefs and attitudes of environmental concern, *Environment and Behavior*, **32**, 576-591.

Shobeiri S.M., Omidvar B., Prahallada N.N., (2007), A comparative study of environmental awareness among secondary school students in Iran and India, *International Journal of Environmental Research*, **1**, 28-34.

Sneddon C., Howarth R.B., Norgaard R.B., (2006), Sustainable development in a post-Brundtland world, *Ecological Economics*, **57**, 253-268.

Steg L., de Groot J.I., (2012), *Environmental Values*, In: *The Oxford Handbook of Environmental and Conservation Psychology*, Clayton S.D. (Ed.), Oxford Library of Psychology, Oxford, UK, 81-92.

Turaga R.M.R., (2015), *Does economy matter for public support for environmental protection? Evidence from India*, W.P. No. 2015-03-40, Indian Institute of Management Ahmedabad, India.

Ulman S.R., (2018), Study on general awareness regarding the problem of environmental degradation, *CES Working Papers*, **X**, 1-26.

van de Kerk G., Manuel A., (2017), *Sustainable Society Index - your compass to sustainability*, The Netherlands, Sustainable Society Foundation, On line at: http://www.ssfindex.com/.

World Values Survey Association, (2008), *World Values Survey 2010-2014,* Madrid, ASEP/JDS. Aggregate File Producer: Asep/JDS, Madrid SPAIN, On line at: http://www.worldvaluessurvey.org/wvs.jsp.

Zelezny L.C., Chua P.-P., Aldrich C., (2000), Elaboration on gender differences in environmentalism, *Journal of Social Issues*, **56**, 443-457.

Environmental Engineering and Management Journal February 2020, Vol. 19, No. 2, 195-204
http://www.eemj.icpm.tuiasi.ro/; http://www.eemj.eu

"Gheorghe Asachi" Technical University of Iasi, Romania

MACROSPHERICAL POROUS METALLOSILICATE MATERIALS: CHARACTERIZATION AND APPLICATIONS

Emil Ioan Mureșan[1]*, Teodor Malutan[2], Doina Lutic[3], Adrian Puitel[2], Nicanor Cimpoeșu[4], Bogdan Istrate[5]

[1] "Gheorghe Asachi" Technical University of Iasi, "Cristofor Simionescu" Faculty of Chemical Engineering and Environmental Protection, Department of Organic, Biochemical and Food Engineering, 73 Prof. Dimitrie Mangeron Blvd., 700050, Iasi, Romania
[2] "Gheorghe Asachi" Technical University of Iasi, "Cristofor Simionescu" Faculty of Chemical Engineering and Environmental Protection, Department of Natural and Synthetic Polymers, 73 Prof. Dimitrie Mangeron Blvd., 700050, Iaşi, România
[3] "Alexandru Ioan Cuza" University of Iasi, Faculty of Chemistry, Department of Chemistry, 11 Carol I Blvd., 700506, Iasi, Romania
[4] "Gheorghe Asachi" Technical University of Iasi, Faculty of Materials Science and Engineering, Department of Materials Science, 41A Prof. Dimitrie Mangeron Blvd., 700050, Iasi, Romania
[5] "Gheorghe Asachi" Technical University of Iasi, Faculty of Mechanical Engineering, Department of Mechanical Engineering, Mechatronics and Robotics, 61A Prof. Dimitrie Mangeron Blvd., 700050, Iasi, Romania

Abstract

The main goal of this work was to develop a cheap and easy method for the synthesis of the porous metallosilicate macrospheres. Zirconium silicate macrospheres with diameters in the range 1.5 – 1.6 mm were obtained by the spray gelling technique, using the multi templating method. Tetraethyl orthosilicate was used as silica source. The chitosan played a dual role (pore and shape generating agent), while other inexpensive and easily accessible biomaterials including yeast, sugar and gelatin were used as pore generators. The multi templating technique allowed to obtain spherical form particles with large pores which facilitate the access of the reactants to the active centres located inside the pores. The zirconium silicate beads were characterized by nitrogen sorption technique, XRD, FTIR and SEM/EDAX analyses. The synthesized beads were used as adsorbents for the removal of the Astrazon Blue BG dye from aqueous solutions. The adsorption data were analysed through different adsorption isotherm and kinetic models. The dye removal percentage varied from 92.5% to 88.71% when the initial dye concentration varied from 60 mg/L to 150 mg/L (for an adsorbent concentration of 5 g/L and a temperature of 295 K). Due to their size, hardness and shape these materials can be easy handled, recovered and reused.

Key words: adsorption isotherm, adsorption kinetic model, dye, metallosilicate macrosphere, synthesis

Received: January, 2019; Revised final: November, 2019; Accepted: November, 2019; Published in final edited form: February, 2020

1. Introduction

Dyes are important compounds commonly used in various industries such as textiles, printing ink, ceramics, rubber, paper and pulp, leather, cosmetics. Their presence in water even in concentrations less than 1 ppm exert harmful effects on environmental (Hossein and Foroutan, 2019). The dyes can cause allergies, dermatitis, skin irritation, can inhibit the penetration of the sun into the water stream and to disrupt the aquatic ecosystem. Various physical and chemical methods were used for the removal of the dyes from the wastewaters. These include: coagulation/precipitation (Junxing et al., 2018; Rima et al., 2003; Sizykh et al., 2018), microbial degradation (Forgacs et al., 2004; Znoozi et al., 2018),

---

* Author to whom all correspondence should be addressed: e-mail: eimuresan@yahoo.co.uk, Phone: +40232278683/ 2135; Fax: +40232 271311

chemical oxidation (Cristiana et al., 2009; Nassar et al., 2017) and adsorption (Largitte and Pasquier, 2016; Sohrabnezhad and Pourahmad, 2010). However, the adsorption is the most efficient alternative with a high potential for the removal and the recovery of the dyes from the wastewaters. The most widely used adsorbents include activated carbon (Al-Degs, 2001; Kumar et al., 2017), graphene oxide (Sun et al., 2014; Konicki et al., 2017), lignite (Gurses et al., 2014), mesoporous silica (Chih-Hyng et al., 2011; Peige et al., 2018); zeolites (Briao et al., 2018; Xu et al., 2014); clays (Betega de Paiva, 2008; Huang et al., 2017; Tehrani-Bagha et al., 2011), biowastes (Bellu et al., 2010; Gottipati and Mishra, 2010), ion exchange cellulose monoliths (Yang et al., 2019), polydopamine-modified fibers (Wang et al., 2019). In the last years, the requirement for environmental and more efficient technologies amplified the interest for the use and the development of the hierarchical porous materials (Hammed et al., 2016; Jamwal et al., 2017; Muresan et al., 2015; Rutkowska et al., 2015; Xu et al., 2014).

This type of materials contains at least two types of pores and present the advantages associated with each level of porosity, from selectivity to mass transfer: high surface area (due to the presence of the micro and mesopores) and increased mass transport (due to the presence of large mesopores and macropores). Particularly, hierarchically porous metallosilicates have garnered much attention due to their multiple functionalities: catalysts, adsorbents or supports.

The main limitation of the hierarchical porous materials synthesized via the techniques reported to date in the scientific literature is that they are usually obtained in the form of powder that is difficult to be separarated from the reaction mixture, requiring high speed centrifugation or special filtration.

The aim of this work is to report an easy method for the synthesis of the porous zirconium silicates in the form of macrospheres with good mechanical, thermal and chemical stability, which can be easily separated and recovered by simple filtration. The metallosilicate macrospheres were obtained by the spray gelling technique, using the multi templating method. Tetraethyl orthosilicate was used as silica source. The chitosan played a dual role (structure and shape generating agent), while other inexpensive and easily accessible biomaterials such as yeast, gelatin and sugar were used as pore generators. The synthesized macrospheres were used as adsorbent for the removal of the Basic Blue 3 cationic dye from aqueous solutions.

2. Experimental

2.1. Reagents and materials

$ZrOCl_2 \cdot 8H_2O$, ammonia solution (25%), tetraethylorthosilicate, HCl solution (37%), chitosan with high molecular weight and agar were purchased from Aldrich. Commercial yeast, sugar and gelatin were used into the experiments. The chitosan solution was prepared by dissolving of 4g of chitosan in 96 mL acetic acid solution (92 mL distilled water and 4 mL acetic acid 98%). Commercial basic dye Astrazon Blue BG (C.I. Basic Blue 3) used as adsorbate was obtained from Dye Star Company and was used without any further purification.

2.2. Synthesis of the metallosilicate macrospheres

The zirconium silicate macrospheres were prepared as follows:

(1) Obtaining of the *solution A*: 3 mL of TEOS were poured into a solution containing 11 mL of water, 0.45 mL of HCl 37% and 0.72 g $ZrOCl_2 \cdot 8H_2O$ and the mixture was magnetically stirred for 6 hours at the room temperature.

(2) Preparation of the *templating mixture B*: 2.7 g of yeast were dispersed in 17 ml of distilled water and the suspension was heated at 85ºC for 1.5 hours. 0.36 g of agar, 0.60 g sugar and 0.36 g of gelatine were then added and the stirring continued for 1 hour at the same temperature. The mixture was cooled up to the room temperature and 0.45 mL HCl 37% solution were added and the stirring continued for 15 minutes. Finally, 9 g of 4% chitosan solution were introduced and the resulted gel was mixed for 1 hour.

(3) Homogenization under stirring for 2 hours of the gel resulted by pouring of the solution A over the mixture B.

(4) Dropping of the gel in 25% ammonia solution and keeping of the obtained macrospheres into this solution for 20 minute to harden.

(5) Separation of the hybrid inorganic-organic composite macrospheres by filtration, followed by drying (at 60ºC for 8 hours and subsequently at 160ºC for 12 hours).

(6) Calcination at 625ºC for 12 hours in order to obtain the porous structure by the removal of the organic templating mixture.

2.3. Physicochemical characterization

The FTIR spectra were recorded on a Nexus 470 FTIR spectrometer using the KBr-disk technique. The registrations performed in the wavenumber range 4000 ÷ 400 cm^{-1} were obtained by the co-addition of 32 scans with a resolution of 2 cm^{-1}. The wide angle X-ray diffraction pattern of the sample was recorded on a Philips XPERT MPD diffractometer in the 2θ range of $10^o \div 70^o$, at a scanning speed of 1^o/min, using a nickel-filtered Cu K_α radiation (λ = 0.15418 nm). SEM micrographs and EDX spectra were obtained with an FEI Quanta 200 Scanning Electron Microscope equipped with an EDAX Genesis 400 with Si(Li) detector, type Sapphire. The measurements were carried out at an accelerating voltage of 20 kV, with a Large Field Detector (LFD) in the low Vacuum Mode.

The nitrogen adsorption isotherm was measured at liquid nitrogen temperature (77 K) using a Nova 2200e system (Quantachrome).

2.4. Adsorption studies

The zirconium silicate beads were tested as adsorbent for the removal of the Astrazon Blue BG dye from aqueous solutions. The adsorption experiments were carried out at different initial dye concentrations and various adsorbent concentrations. In all the experiments the temperature was kept at 22°C and the stirring speed was 250 rpm. The unknown dye concentrations from the residual solutions were determined from the calibration curve by using a UV-Vis spectrophotometer.

The percent removal of the dye (R%) and the equilibrium adsorption capacity q_e (mg/g) were calculated using Eqs.1 and 2:

$$R(\%) = \frac{c_0 - c_e}{c_0} \cdot 100 \qquad (1)$$

$$q_e = \frac{(c_0 - c_e) \cdot V}{w} \qquad (2)$$

where c_0 (mg/L) and c_e (mg/L) are the initial and respectively the equilibrium dye concentrations in the liquid-phase, V (L) is the volume of the solution and m (g) is the amount of adsorbent.

2.5. Error analysis

The best fit kinetic/adsorption model was selected based on the linear regression correlation coefficient values R^2, and the average percentage error (APE). The average percentage error (APE) was calculated using the following equation:

$$APE(\%) = \frac{\sum_{i=1}^{n} \left| \left(q_{exp} - q_{calc} \right) / q_{exp} \right|}{n} \cdot 100$$

where, q_{exp} (mg/g) is the experimental adsorbed amount, q_{cal} (mg/g) is the theoretical adsorbed amount and n is the number of experimental data.

3. Results and discussions

The synthesized macrospheres used for the adsorption of the cationic dye from aqueous solutions have diameters comprised in the range 1.5 – 1.6 mm. Due to their size and strength the zirconium silicate spherical beads can be easily handled and recovered from the wastewaters.

3.1. Characterization of the zirconium silicate macrospheres

3.1.1. Energy dispersive X-ray analysis (EDX)

The elemental composition of the zirconium silicate macrospheres was determined by EDX analysis (Fig. 1). The value of the Si/Zr mole ratio (Si: Zr = 1 : 0.162) for the calcined and washed sample is close to the value of the Si/Zr mole ratio (Si: Zr = 1 : 0.17) from the synthesis gel which confirms the efficient incorporation of the metal.

3.1.2. Wide angle X-ray diffraction analysis (WAXD)

The structural characterization by wide angle X-ray diffraction analysis was carried out in order to investigate the amorphous/crystalline structure of the sample. The diffractogram (Fig. 2) contains a single wide peak located between 2θ = 10º ÷ 30º, which indicates that the sample contain a high amount of amorphous zirconium silicate.

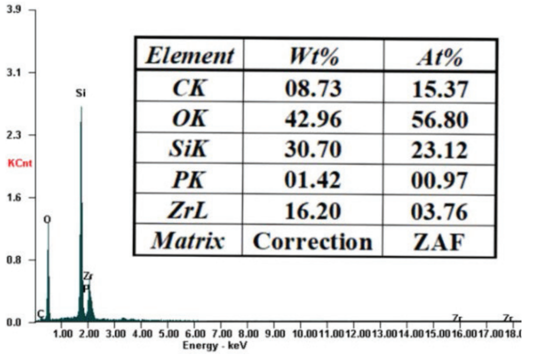

Element	*Wt%*	*At%*
CK	08.73	15.37
OK	42.96	56.80
SiK	30.70	23.12
PK	01.42	00.97
ZrL	16.20	03.76
Matrix	Correction	ZAF

Fig. 1. EDX analysis of the zirconium silicate macrospheres

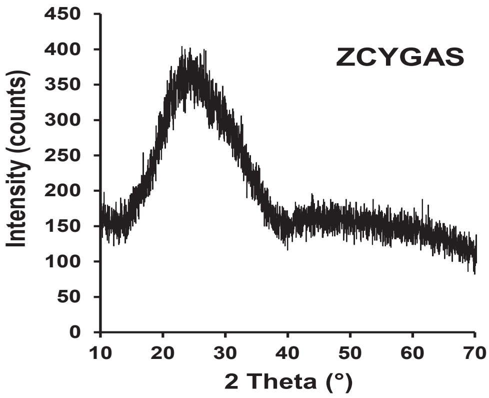

Fig. 2. X-ray diffraction spectrum of the synthesized zirconium silicate

The presence of this wide band and the pronounced background noise recorded during the whole XRD pattern suggests also the existence of some small size particles within the structure of the macrospheres. The absence of the peaks characteristic to zirconium oxide indicates the efficient incorporation of the zirconium into the silica network (or at most the presence of some small size oxide crystallites which are uniformly dispersed on the sample surface and cannot be put into evidence by XRD analysis).

3.1.3. Fourier transformed infrared spectrometry (FTIR)

FTIR analysis (Fig. 3) was performed in order to prove the formation of the Si-O-Zr bonds (incorporation of zirconium within the silica framework) and the Si-O-Si bonds. The spectral data of the zirconium silicate sample and the assignment of the absorption bands to their corresponding types of infrared vibrations are shown in Table 1.

Table 1. FTIR spectral data of the zirconium silicate sample

Peak position (cm^{-1})	***Assignment of the absorption bands***
460	overlap of the rocking bending mode vibrations of the Si-O and Zr-O bonds belonging to the Si-O-Si and Si-O-Fe linkages
801	overlap of the symmetric stretching vibrations of the O-Si-O and O-Zr-O bonds within the polyhedrons
1074	overlap of the asymmetric stretching mode vibrations of the O-Si-O and O-Zr-O bonds within the polyhedrons
1635	bending mode vibrations of the adsorbed water molecules
3461	stretching mode vibrations of the bridging OH groups

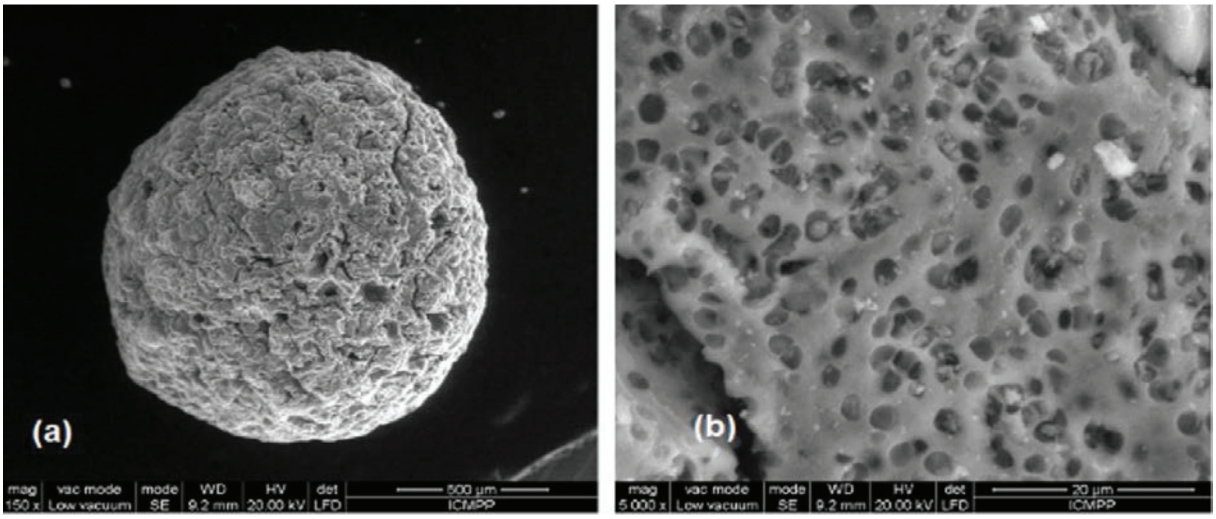

Fig. 4. SEM images of the zirconium silicate macrospheres:
(a) whole spherical bead; (b) detailed surface image

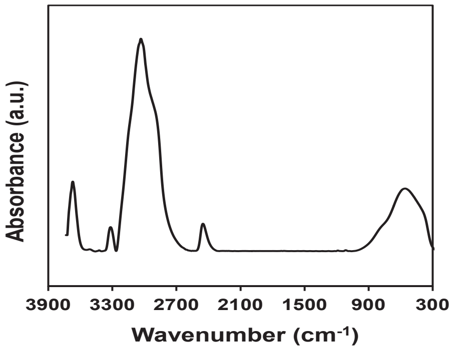

Fig. 3. FTIR spectrum of the zirconium silicate sample

The peaks that occur at 460 cm^{-1}, 801 cm^{-1} and respectively 1074 cm^{-1} prove the incorporation of the zirconium within the silica framework. The absence of the bands at 3757 cm^{-1} and 3780 cm^{-1} attributed to the terminal silanol groups and respectively to the Zr-OH groups show the effectiveness of the condensation reaction and the successful incorporation of the zirconium within the silica matrix (Mureșan et al., 2014, 2015, 2016).

3.1.4. Scanning electron microscope (SEM)

The surface morphology and the pore size of the zirconium silicate macrospheres were investigated by scanning electron microscopy (Fig. 4).

The low magnitude 150x electron microphotograph (Fig. 4a) shows that the zirconium silicate macrospheres look like it would be composed of „aggregates shaped like cereal flakes" and present some cracks in the form of slits on their surface. From the high magnitude 5000x electron microphotograph (Fig. 5b) it is noticed that the sample has a large number of the microns order sized pores which are relatively evenly distributed on its surface.

3.1.5. Determination of the textural properties from the nitrogen physisorption data

The nitrogen sorption experiments were performed in order to determine the textural properties of the synthesized samples. The recorded adsorption-desorption isotherm do not fit very well in the classification given by IUPAC (Fig. 5).

The adsorption branch is similar to the I(b) type isotherm up to the $p/p^0 = 0.72$ value of the relative pressure and looks like the type II isotherm for higher relative pressures (does not reach the final saturation plateau at high values of the relative pressure). The hysteresis loop is a hybrid between H_3 and H_4 types. It resembles better to the H_4 type hysteresis loop which is encountered in the case of the materials containing both micropores and mesopores, but also exhibit some features corresponding to the H_3 type hysteresis loop due to the presence of the large mesopores and macropores (Thommes et al., 2015). The pore size distribution was determined from the adsorption branch of the isotherm using the Barret-Joyner-Halenda (BJH) model. The micropore volume V_μ = 0.053 (cc/g), mesopore volume V_m = 0.099 (cc/g), micropore surface area S_μ = 138.67 (m^2/g) and the external surface area S_{ext} = 132.27 (m^2/g) were calculated using the t-plot method. The BET surface area S_{BET} = 271 (m^2/g) was determined using the adsorption data from the relative pressure range comprised between $p/p^0 = 0.05 \div 0.35$.

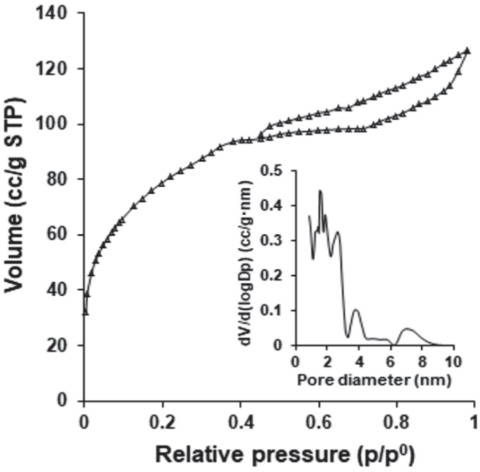

Fig. 5. Nitrogen adsorption-desorption isotherm and the pore size distribution

3.2. Adsorption studies

3.2.1. Effect of the initial dye concentration and contact time

The effect of the initial dye concentration (in the range from 60 to 150 mg/L) and of the contact time on the adsorption capacity of the zirconium silicate beads was investigated (Fig 6).

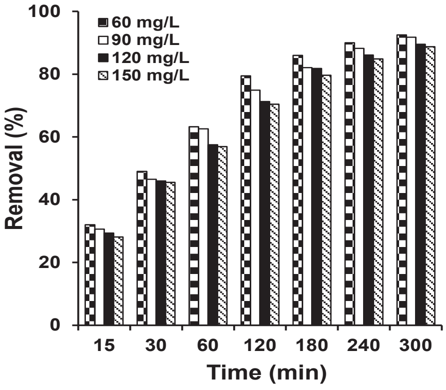

Fig 6. The effect of the initial dye concentration and of the time on the percentage of dye removed from the solution (adsorbent dosage 5 g/L, temperature 295 K, agitation speed 250 rpm)

The adsorption rate of the dye on the zirconium silicate beads is high in the first 60 min due to the availability of a high number of vacant sites. Thereafter, the adsorbed amount increases slowly by the prolonging of the contact time because of the repulsive forces that exhibit between the adsorbed molecules and the ones that exist in the liquid phase. The percentages of dye removed after 180 minutes were 85.9%, 82.1%, 81.8% and 79.6% and reached after 240 minutes at 90%, 88.2%, 86.1% and 84.8% for dye concentrations of 60 mg/L, 90 mg/L, 120 mg/L and 150 mg/L respectively. Given these results it would be advisable to work with dye concentrations between 90 - 120 mg/L and the adsorption time to be 240 minutes.

3.2.2. Effect of the adsorbent concentration on the dye removal

The adsorption capacity of the Astrazon Blue BG dye onto zirconium silicate macrospheres was studied for 2.5, 5, 7.5 and 10 g/L adsorbent dosages (Fig. 7).

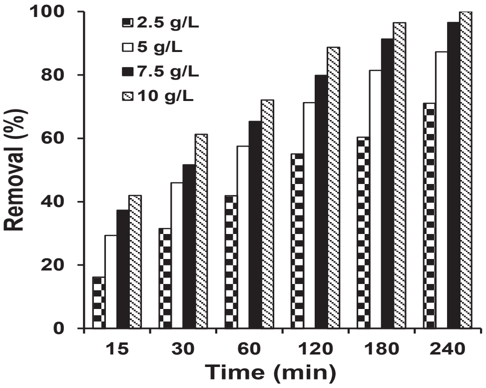

Fig 7. Effect of the adsorbent dosage on the percentage of dye removed from the solution (dye concentration 120 mg/L, temperature 295 K, stirring speed 250 rpm)

The results presented in Fig. 7 show that the percentage of the removed dye increases with the increase of the adsorbent concentration due to the increase of the number of the available adsorption sites.

3.2.3. Adsorption isotherms

Adsorption isotherms describe the relationship between the amount of dye adsorbed onto the adsorbent at equilibrium (q_e) and the equilibrium concentration of the dye remained in solution (C_e) at a given temperature. In order to quantify the affinity of the zirconium silicate macrospheres for the cationic dye the equilibrium adsorption data were analyzed using the Langmuir, Freundlich, Temkin and Dubinin-Radushkevich models (Abshirini et al., 2019; Ahmadi and Esmaeili., 2018; Abbasi et al., 2019; Esmaeili and Foroutan, 2019; Tamjidi and Esmaeili, 2019). The linear equations of the investigated adsorption isotherms are shown in Table 2. The calculated values of the parameters corresponding to the models of the studied adsorption isotherms are listed in the Table 3.

From the data presented in the Table 2 it can be deduced that the adsorption was better defined by the Temkin isotherm model (R^2 = 0.996) followed by the Dubinin-Radushkevich (R^2 = 0.986), Langmuir (R^2 = 0.982) and Freundlich (R^2 = 0.971) isotherm models.

Table 2. Isotherm models

<table>
<tr><th><i>Adsorption isotherm</i></th><th><i>Linear equation</i></th><th><i>Plot</i></th><th><i>Slope</i></th><th><i>Intercept</i></th></tr>
<tr><td><i>Langmuir</i></td><td>$\frac{C_e}{q_e} = \frac{1}{q_m} \cdot C_e + \frac{1}{K_L \cdot q_m}$</td><td>$\frac{C_e}{q_e}$ vs C_e</td><td>$\frac{1}{q_m}$</td><td>$\frac{1}{K_L \cdot q_m}$</td></tr>
<tr><td colspan="5">q_m (mg/g) is the maximum amount of adsorbate per unit weight of adsorbent required to form a saturated monolayer of adsorbate molecules on the adsorbent surface; K_L (L/mg) is the Langmuir isotherm constant which is a measure of the affinity between adsorbate and adsorbent and is related to the free energy of adsorption. The Langmuir model assumes that the adsorption takes place onto homogeneous surfaces with a finite number of sites which have all the same activation energy (Langmuir, 1918).</td></tr>
<tr><td><i>Freundlich</i></td><td>$logq_e = logK_F + \frac{1}{n} \cdot logC_e$</td><td>$logq_e$ vs $logC_e$</td><td>$\frac{1}{n}$</td><td>$logK_F$</td></tr>
<tr><td colspan="5">K_F (mg/g) is a measure of the adsorption capacity (being related to the bonding energy) and 1/n corresponds to the strength of adsorption and to the surface heterogeneity. The value of n describes the adsorption characteristics as follows: if n = 1 the Freundlich expression reduces to a linear adsorption isotherm, which means a homogenous adsorption without interactions between the adsorbed species; n > 1, indicates that the adsorption is a favourable process; n < 1, indicates an unfavourable adsorption process (Freundlich, 1906).</td></tr>
<tr><td><i>Temkin</i></td><td>$q_e = \frac{R \cdot T}{b_T} \cdot lnK_T + \frac{R \cdot T}{b_T} \cdot lnC_e$</td><td>$q_e$ vs lnC_e</td><td>$\frac{R \cdot T}{b_T}$</td><td>$\frac{R \cdot T \cdot lnK_T}{b_T}$</td></tr>
<tr><td colspan="5">b_T is the Temkin constant related to the heat of adsorption (J/mol) which indicates the adsorption intensity of the adsorbent; K_T (mg/L) is the Temkin constant related to the adsorption capacity. The Temkin isotherm assumes that the adsorption heat of the molecules decreases linearly with the surface coverage owing to a decrease of the adsorbent–adsorbate interactions during adsorption (Temkin and Pyzhev, 1940).</td></tr>
<tr><td><i>Dubinin-Radushkevich</i> (<i>D-R</i>)</td><td>$lnq_e = lnq_D - B \cdot \varepsilon^2$</td><td>$lnq_e$ vs ε^2</td><td>B</td><td>lnq_D</td></tr>
<tr><td colspan="5">q_D is the theoretical saturation capacity (mg/g), B is a constant related to the mean free energy of adsorption per mole of adsorbate (mol^2/J^2); $\varepsilon = R \cdot T \cdot ln(1 + 1/C_e)$ is the Polanyi potential; $E = 1/\sqrt{2 \cdot B}$ is the mean sorption energy – based on this energy of activation one can predict whether the adsorption is physisorption or chemisorption. If the value of activation energy is in the range of 8 ÷ 16 kJ/mol is a physisorption process and if the value of activation energy is in the range of 20 ÷ 40 kJ/mol is a chemisorption process (Dubinin, 1960).</td></tr>
</table>

Table 3. Isotherm constants for Astrazon Blue B adsorption onto zirconium silicate

Isotherm	*Parameters*		R^2	*APE*
Temkin	K_T	b	0.996	2.6
	0.507	199.53		
Dubinin-Radushkevich	q_D	B	0.986	3.63
	26.92	4×10^{-6}		
Langmuir	K_L	q_m	0.982	3.84
	0.04563	61.72		
Freundlich	K_F	n	0.971	5.12
	3.53	1.371		

The D-R mean adsorption energy E = 10 kJ/mol indicates an ionic exchange adsorption. The Freundlich constant *n* = 1.371 (*1/n* = 0.729) indicates a favorable adsorption of the Astrazon Blue BG dye onto the zirconium silicate macrospheres.

3.2.4. Adsorption kinetics

The kinetics of the adsorption process was studied in order to provide data concerning the uptake rate of the Astrazon Blue BG dye and the mechanism of adsorption. Four kinetic models (Table 4) were selected and compared in order to find the best fitting model that to describe the sorption of the cationic dye onto the zirconium silicate macrospheres. The calculated values of the parameters corresponding to the adsorption kinetic models (pseudo first order model, pseudo-second order model, Elovich model and modified Freundlich model) are summarized in Table 5. For dye concentrations up to 90 mg/L the adsorption process proceeds fast, since the number of active centers located on the macrospheres surface and on the surface of pores with larger diameters is large enough to retain the dye molecules. For this reason, the adsorption process is better described by a second order kinetic model.

At higher concentrations of adsorbate (greater than 90 mg/L the adsorption process is better described by the Elovich model, which is more suitable for describe slow adsorption processes. Slower adsorption can be explained as follows: dye molecules must reach to the less accessible adsorption centers located in the narrower pores (adsorption times are higher due to the slow internal diffusion). The intraparticle diffusion kinetic model provides information about the mechanisms involved in the adsorption process.

The plot of q_t vs. $t^{0.5}$ for the adsorption of Astrazon Blue BG dye on the zirconium silicate beads (Fig. 8) show three linear sections: the first portion corresponds to the fast uptake of the dye molecules on the external surface area of the adsorbent beads; the second straight portion is attributed to the gradual adsorption stage**;** the third linear portion is attributed to the final equilibrium stage indicating the saturation of the adsorbent surface. The occurrence of the several linear regions is due to the difference between the rate of the mass transfer from the initial stage and the rates of mass transfer that correspond to the other stages of the adsorption process.

3.6. Regeneration and reuse of the adsorbent

In order to investigate the efficency of the zirconium silicate beads, the synthesized macrospheres were reused 10 times. After each use the adsorbent was regenerated by calcination at 600°C for 2 hours to remove the adsorbed dye.

Table 4. Kinetic adsorption models

Kinetic model	Linear equation	Plots	Slope	Intercept
Pseudo first order	$\frac{1}{q_t}=\frac{k_1}{q_e}\cdot\frac{1}{t}+\frac{1}{q_e}$	$\frac{1}{q_t}$ vs $\frac{1}{t}$	$\frac{k_1}{q_e}$	$\frac{1}{q_e}$
k_1 is the pseudo first order rate constant of adsorption (min^{-1}); q_e and q_t (mg/g) are the amounts of adsorbed dye per unit mass of adsorbent at the equilibrium and respectively at time t (min); The model is commonly used for homogeneous sorbents and physical sorption and supposes that the rate of adsorption is influenced by the adsorbate concentration and by the number of free sites for adsorption (Lagergren and Svenska, 1898).				
Pseudo-second order	$\frac{t}{q_t}=\frac{1}{k_2\cdot {q_e}^2}+\frac{1}{q_e}\cdot t$	$\frac{t}{q_t}$ vs t	$\frac{1}{q_e}$	$\frac{1}{k_2\cdot {q_e}^2}$
k_2 is the pseudo second order rate constant of adsorption (g/mg·min); q_t and q_e (mg/g) are the amounts of dye adsorbed at time t and at equilibrium respectively; $k_2\cdot q_e^2$ is the initial adsorption rate (mg/g·min). The pseudo second order model suggests that the adsorption depends both on the adsorbate concentration as well as on the adsorbent concentration. The rate-limiting step is the sorption and the intraparticle diffusion has no role in the mass transfer of the adsorption process (Ho and McKay, 1999).				
Elovich	$q_t=b\cdot ln(a/b)+b\cdot ln(t)$	q_t vs $ln(t)$	b	$b\cdot ln(a/b)$
a = initial adsorption rate (mg/g·min); b = desorption constant related to the extent of surface coverage and to the activation energy for chemisorption (mg/g); q_t = the amount of dye adsorbed at time t (mg/g). This model is usually used in chemisorption on heterogeneous materials and covers a wide range of slow adsorption processes (Elovich, 1962).				
Intra-particle diffusion model	$q_t=k_{id}\cdot t^{0.5}+C_i$	q_t vs $t^{0.5}$	k_{id}	C_i
k_{id} ($mg/g\cdot min^{0.5}$) is the rate constant of stage i (obtained from the slope of the straight-line q_t versus $t^{0.5}$), C_i is proportional with the thickness of the boundary layer. If the intraparticle diffusion is the sole rate-controlling step the plot of q_t vs $t^{0.5}$ is linear over the whole time range and passes through the origin; when the sorption process is controlled by more than one mechanism (the adsorption process proceeds in several steps) the plot of q_t vs $t^{0.5}$ will show multiple linear regions with different slopes (Weber and Morris, 1963).				

Table 5. Kinetic data for Astrazon Blue BG sorption

Kinetic models	***Dye concentration (mg/L)***			
	60	90	120	150
$q_{e,exp}$ (mg/g)	10,60	17.93	25.13	28.83
Pseudo-first order				
k_1 (g/mg·min)	32.416	58.714	28.019	25.066
$q_{e,calc}$ (mg/g)	11.09	21.83	24.04	26.46
R^2	0.972	0.981	0.994	0.99
APE	0.88	6.24	2.94	3.48
Pseudo-second order				
k_2 (g/mg·min)	0.00274	0.00117	0.00114	0.00104
$q_{e,calc}$ (mg/g)	11.14	19.41	25.38	28.41
R^2	0.999 0.996	0.998	0.999	0.998
APE	0.84	3.64	3.66	4.46
Elovich				
a (mg/g·min)	0.811	0.976	1.981	2.4322
b (mg/g)	2.224	4.116	4.844	5.297
$q_{e,calc}$ (mg/g)	11.985	20.409	26.656	29.763
R^2	0.985	0.979	0.997	0.999
APE	3.58	3.71	1.71	0.98
Intraparticle diffusion				
$k_{i,I}$ ($mg/g\cdot min^{0.5}$)	0.9306	1.528	2.1104	2.399
R^2	0.999	0.997	0.987	0.983
$k_{i,II}$ ($mg/g\cdot min^{0.5}$)	0.3391	0.5584	0.8889	0.9788
$C_{i,II}$	4.768	7.840	8.831	10.128
R^2	0.942	0.993	0.984	0.989
$k_{i,III}$ ($mg/g\cdot min^{0.5}$)	0.0918	0.1614	0.3237	0.423
$C_{i,III}$	8.4248	14.04	17.352	18.509
R^2	0.946	0.967	0.987	0.991

Table 6. Adsorption efficiency of different adsorbents for Basic Blue 3

Adsorbent	*Maximum adsorption capacity /Temperature*	*Reference*
Silica	11 mg/g (303 K)	Ahmad and Ram, 1992
CF clay	101 mg/g (298 K)	Bencheqroun et al., 2019
Sphagnum Magellanicum Peat	40.6 mg/g (303 K)	Contreras et al., 2007
Acrylic resin	59.53 mg/g (323 K)	Bârsănescu et al., 2009
Activated carbons from black sapote seeds	58–59.8 mg/g (303 K)	Peláez-Cid et al., 2019
Amberlite XAD-1180	35.7 mg/g (293 K)	Wawrzkiewicz, 2013
Pomelo Peel	23.87 mg/g (293 K)	Liew and Siew, 2014
Fe_3O_4	7.474 mg/g (298 K)	Muhammad et al., 2019
PANI (polyaniline)	8 mg/g (298 K)	Muhammad et al., 2019
PANI/Fe3O4	78.13 mg/g (298 K)	Muhammad et al., 2019
Zirconiumsilicate macrospheres	28.83 mg/g (295 K)	This study

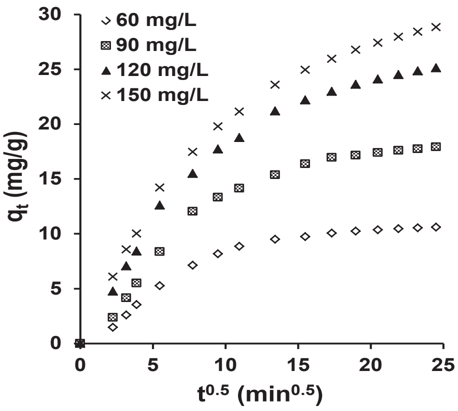

Fig. 8. The plot of the intraparticle diffusion model for adsorption of Astrazon Blue BG dye onto zirconium silicate macrospheres for different initial concentrations of adsorbate

No loss of the adsorptive capacity was noticed which represent an important avantage in view of potential industrial applications.

3.7. Comparison between the adsorption efficiency of different adsorbents for Basic Blue 3

A comparison between the maximum adsorption capacity of Basic Blue 3 dye on porous metallosilicate macrospheres and the maximum adsorption capacities of this dye on other adsorbents is presented in Table 6.

Although the values obtained on the zirconium silicate macrospheres are lower than some of the values previously reported for other adsorbents, the zirconium silicates used in this study have the great advantage that they can be easily separated and reused.

4. Conclusions

In this paper is presented an easy method for the preparation of porous zirconium silicate macrospheres by the spray gelling technique using the multi-templating method. Gelatine, agar, yeast, sugar and chitosan were used as pore generating agents. The multi templating technique allowed to obtain spherical form particles, with large pores, which facilitate the access of the reactants to the active centres located inside the micropores and the narrow mesopores. The wide angle X-ray diffraction, EDX and FTIR analyses proved the good incorporation of the zirconium within the silica framework. The zirconium silicate beads were used as adsorbents for the uptake of the Astrazon Blue BG cationic dye from aqueous solutions.

The adsorption process was found to be dependent on the initial dye concentration, adsorbent dose and contact time. Due to their dimensions (comprised between 1.5 mm and 1.6 mm) the macrospheres can be easily separated from the reaction mixture by simple filtration and reused several times.

Acknowledgements

This work was funded by the TUIASI research grant entitled „Macrospherical hierarchical porous metallosilicate materials obtained by mono or multi-templating technique: synthesis, characterization and application", project number 0199 / 2018, awarded by the "Gheorghe Asachi" Technical University from Iasi.

References

Abshirini Y., Foroutan R., Esmaeili H., (2019), Cr (VI) removal from aqueous solution using activated carbon prepared from *Ziziphus spina-christi* leaf, *Materials Research Express*, **6**, doi.org/10.1088/2053-1591/aafb45.

Ahmadi F., Esmaeili H., (2018), Chemically modified bentonite/Fe3O4 nanocomposite for Pb(II), Cd(II), and Ni(II) removal from synthetic wastewater, *Desalination and Water Treatment*, **110**, 154-167.

Abbasi S., Foroutan R., Esmaeili H., Esmaeilzadeh F., (2019), Preparation of activated carbon from worn tires for removal of Cu(II), Ni(II) and Co(II) ions from synthetic wastewater, *Desalination and Water Treatment*, **141**, 269-278.

Ahmad M.N., Ram R.N., (1992), Removal of basic dye from waste-water using silica as adsorbent, *Environmental Pollution*, **77**, 79-86.

Al-Degs Y., Khraisheh M.A.M., Allen S.J., Ahmad M.N.A., (2001), Sorption behavior of cationic and anionic dyes from aqueous solution on different types of activated carbons, *Separation Science and Technology*, **36**, 91-102.

Atun G., Hisarli G., Kurtoglu A. E., Ayar N., (2011), A comparison of basic dye adsorption onto zeolitic materials synthesized from fly ash, *Journal of Hazardous Materials*, **187**, 562–573.

Bârsănescu A., Buhăceanu R., Dulman V., (2009), Removal of Basic Blue 3 by sorption onto a weak acid acrylic resin, *Journal of Applied Science*, **113**, 607-614.

Bellú S., Sala L., González J., García S., Frascaroli M., Blanes P., García J., Peregrin J. S., Atria A., Ferrón J., Harada M., Cong C., Niwa Y., (2010), Thermodynamic and Dynamic of Chromium Biosorption by Pectic and Lignocellulocic Biowastes, *Journal of Water Resource and Protection*, **2**, 888-897.

Bencheqroun Z., El Mrabet I., Kachabi M., Nawdali M., Neves I., Zaitan H., (2019), Removal of basic dyes from aqueous solutions by adsorption onto Moroccan clay (Fez City), *Mediterranean Journal of Chemistry*, **8**, 158-167.

Betega de Paiva L., Francisco R. V. D., Ana Morales A., (2008), Organoclays: Properties, Preparation and Applications, *Applied Clay Science*, **42**, 8-24.

Brião G.V, Jahn S.L., Foletto E.L., Dotto G.L., (2018), Highly efficient and reusable mesoporous zeolite synthetized from a biopolymer for cationic dyes adsorption, *Colloids and Surfaces A: Physicochemical and Engineering Aspects*, **556**, 43-50.

Chih-Hung H., Chang K.P., Hong D.O., Chiang Y.C., Wang C.F., (2011), Adsorption of cationic dyes onto mesoporous silica, *Microporous and Mesoporous Materials*, **141**, 102-109.

Contreras E., Martinez B., Sepúlveda L., Palma C., (2007), Kinetics of basic dye adsorption onto *Sphagnum magellanicum* Peat**,** *Adsorption Science & Technology*, **25**, 637-646.

Cristiana R., Ionica I., Moater E. I., Stihi C., (2009), Decolourization of textile wastewater containing green cationic dye by AOPs, *Ovidius University Annals of Chemistry*, **20**, 66-71.

Dubinin M. M., (1960), The potential theory of adsorption of gases and vapors for adsorbents with energetically non-uniform surface, *Chemical Reviews*, **60**, 235-266.

Elovich S.Y., Larionov O.G., (1962), Theory of adsorption from solutions of non-electrolytes on solid (I) equation adsorption from solutions and the analysis of its simplest form, (II) verification of the equation of adsorption isotherm from solutions, *Izvestiya Akademii Nauk SSSR, Otdelenie Khimicheskikh Nauk,* **2**, 209-216.

Esmaeili H., Foroutan R., (2019), Adsorptive behavior of methylene blue onto sawdust of sour lemon, date palm, and eucalyptus as agricultural wastes, *Journal of Dispersion Science and Technology*, **40**, 990-999.

Forgacs E., Cserhati T., Oros G, (2004), Removal of synthetic dyes from wastewaters: a review, *Environment International*, **30**, 953–971.

Freundlich H., (1906), Over the Adsorption in Solution, *The Journal of Chemical Physics*, **57**, 385-471.

Gottipati R., Mishra S., (2010), Application of biowaste (waste generated in biodiesel plant) as an adsorbent for the removal of hazardous dye – methylene blue – from aqueous phase, *Brazilian Journal of Chemical Engineering*, **27**, 357-367.

Gurses A., Hassani A., Kıransan M., Acıslı O., Karaca S., (2014), Removal of methylene blue from aqueous solution using by untreated lignite as potential low-cost adsorbent: Kinetic, thermodynamic and equilibrium approach, *Journal of Water Process Engineering*, **2**, 10-21.

Hammed A.K., Dewayanto N., Du D., Abrahim M.H, Nordin M.R., (2016), Novel modified ZSM-5 as an efficient adsorbent for methylene blue removal, *Journal of Environmental Chemical Engineering*, **4**, 2607-2616.

Ho Y.S., McKay G., (1999), Pseudo-second order model for adsorption processes, *Process Biochemistry*, **34**, 451-465.

Huang Z., Li Y., Chen W., Shi J., Zhang N., Wang X., Li Z., Gao L., Zhang Y., (2017), Modified bentonite adsorption of organic pollutants of dye wastewater, *Materials Chemistry and Physics*, **202**, 266-276.

Jamwal H.S., Kumari S., Chauhan G.S., Reddy N.S., Ahn J.H., (2017), Silica-polymer hybrid materials as methylene blue adsorbents, *Journal of Environmental Chemical Engineering*, **5**, 103-113.

Junxing H., Ji L., Li C., Hu C., Wu K., (2018), Show more Rapid, efficient and economic removal of organic dyes and heavy metals from wastewater by zinc-induced in-situ reduction and precipitation of graphene oxide, *Journal of the Taiwan Institute of Chemical Engineers*, **88**, 137-145.

Konicki W., Aleksandrzak M., Mijowska E., (2017), Equilibrium, kinetic and thermodynamic studies on adsorption of cationic dyes from aqueous solutions using graphene oxide, *Chemical Engineering Research and Design*, **123**, 45-49.

Kumar P.S., Ramalingam S., Sathishkumar K., (2011), Removal of methylene blue dye from aqueous solution by activated carbon prepared from cashew nut shell as a new low-cost adsorbent, *Korean Journal of Chemical Engineering*, **28**, 149-155.

Lagergren S., Svenska B. K., (1898), About the theory of so-called adsorption of soluble substance, *Kungliga Svensca Vetenskapsakad. Handling*, **24**, 1-35.

Langmuir I., (1918), The Adsorption of Gases on Plane Surfaces of Glass, Mica and Platinum, *Journal of the American Chemical Society*, **40**, 1361-1403.

Largitte L., Pasquier R., (2016), A review of the kinetics adsorption models and their application to the adsorption of lead by an activated carbon, *Chemical Engineering Research and Design*, **109**, 495-504.

Liew S.W., Siew T.O., (2014), Removal of Basic Blue 3 dye using pomelo peel, *Asian Journal of Chemistry*, **26**, 3808-3814.

Muhammad A., Anwar-ul-Haq A. S., Bilal S., Rahman G., (2019), Basic Blue dye adsorption from water using polyaniline/magnetite (Fe_3O_4) composites: kinetic and thermodynamic aspects, *Materials*, **12**, 1764.

Mureșan E.I., Cimpoeșu N., Bargan A., Istrate B., (2015), Effect of the template on the textural properties of the macrospherical trimodal metallosilicate materials, *Journal of Inorganic and Organometallic Polymers*, **25**, 1060-1068.

Mureșan E.I., Drobota M., Bargan A., Dumitriu C.A.M., (2014), Hard porous chromium containing macrospheres as new catalysts for the esterification reaction of acetic acid with epichlorohydrin, *Central European Journal of Chemistry*, **12**, 528-536.

Muresan E.I., Puitel A., Pui A., Radu C. D., Tampu D., Cimpoesu N., Sandu I., (2016), Hierarchically bimodal porous metallosilicate catalysts for acetolysis of epichlorohydrin, *Revista de Chimie*, **67**, 659-664.

Nassar M.Y., Abdelrahman E.A., (2017), Hydrothermal tuning of the morphology and crystallite size of zeolite nanostructures for simultaneous adsorption and photocatalytic degradation of Methylene blue dye, *Journal of Molecular Liquids*, **242**, 364-374.

Peige Q., Yixin Y., Xiaoting Z., Jiahua N., Yang H., Shufang T., Jinhua Z., Minghua L., (2018), highly efficient, rapid, and simultaneous removal of cationic dyes from aqueous solution using monodispersed mesoporous silica nanoparticles as the adsorbent, *Nanomaterials*, **8**, 1-14.

Peláez-Cid A.A., Hernández V.R., Herrera-González A. M., Bautista-Hernández A., Coreño-Alonso O., (2019), Synthesis of activated carbons from black sapote seeds, characterization and application in the elimination of heavy metals and textile dye*, Chinese Journal of Chemical Engineering,* doi.org/10.1016/j.cjche.2019.04.021.

Rima J.Z., Egidija Z., Rima K., Algirdas Z., (2003), The role of anionic substances in removal of textile dyes from solutions using cationic flocculants, *Colloids and Surfaces A: Physicochemical and Engineering Aspects, Engineering Aspects*, **214**, 37-47.

Rutkowska M., Piwowarska Z., Micek E., Chmielarz L., (2015), Hierarchical Fe-, Cu- and Co-Beta zeolites obtained by mesotemplate-free method. Part I: Synthesis and catalytic activity in N_2O decomposition, *Microporous and Mesoporous Materials*, **209**, 54-65.

Sohrabnezhad S., Pourahmad A., (2010), Comparison absorption of new methylene blue dye in zeolite and nanocrystal, *Desalination*, **256**, 84-89.

Sun J., Li Y., Liu T., Du Q., Xia Y., Xia L., Wang Z., Wang K., Zhu H., Wu D., (2014), Equilibrium, kinetic and thermodynamic studies of cationic red X-GRL adsorption on graphene oxide, *Environmental Engineering and Management Journal*, **13**, 2551-2559.

Sizykh M.R., Batoeva A.A., Khandarkhayeva M.S., (2018), Removal of dyes from water by galvanocoagulation, *Environmental Engineering and Management Journal*, **17**, 27-34.

Tamjidi S., Esmaeili H., (2019), Chemically modified CaO/Fe3O4 nanocomposite by sodium dodecyl sulfate for Cr (III) removal from water, *Chemical Engineering & Technology*, **42**, 607-616.

Tehrani-Bagha A.R., Nikkar H., Mahmoodi N.M., Markazi M., Menger F.M., (2011), The sorption of cationic dyes onto kaolin: Kinetic, isotherm and thermodynamic studies, *Desalination*, **266**, 274-280.

Temkin M.I., (1941), Adsorption equilibrium and the kinetics of processes on non-homogeneous surfaces and in the interaction between adsorbed molecules, *Zhurnal fizicheskoi Khimii*, **15**, 296-332.

Temkin M.J., Pyzhev V., (1940), Recent modifications to Langmuir isotherms, *Acta Physicochimica USSR*, **12**, 217-225.

Thommes M., Kaneko K., Neimark A.V., Olivier J.P., Rodriguez-Reinoso F., Rougerol J., Sing K.S.W., (2015), Physisorption of gases, with special reference of surface area and pore size distribution (IUPAC Technical Report), *Pure and Applied Chemistry*, **87**, 1051-1069.

Wang C., Yin J., Wang R., Jiao T., Huang H., Zhou J., Zhang L., Peng Q., Facile preparation of self-assembled polydopamine-modified electrospun fibers for highly effective removal of organic dyes, *Nanomaterials*, **9**, 116-133.

Wawrzkiewicz M., (2013), Removal of C.I. Basic Blue 3 dye by sorption onto cation exchange resin, functionalized and non-functionalized polymeric sorbents from aqueous solutions and wastewaters, *Chemical Engineering Journal*, **217**, 414-425.

Weber W.J.Jr., Morris J.C., (1963), Kinetics of Adsorption of Carbon from Solution, *Journal of the Sanitary Engineering Division*, *American Society of Civil Engineering*, **89**, 31-60.

Weber W.J., Morris, J.C., (1963), Kinetics of adsorption on carbon from solution, *Journal of the Sanitary Engineering Division ASCE*, **89**, 31-60.

Xu H.Y., Wu L.C., Shi T.N., Liu W.C., Qi S.Y., (2014), Adsorption of acid fuchsin onto LTA-type zeolite derived from fly ash, *Science China Technological Sciences*, **57**, 1127-1134.

Yang Z, Asoh T.A., Uyama H., (2019), Removal of cationic or anionic dyes from water using ion exchange cellulose monoliths as adsorbents, *Bulletin of the Chemical Society of Japan*, **92**, 1453-1461.

Zonoozi M.H., Moghaddam M.R.A., Maknoon R., (2018), Treatment of an azo dye - containing wastewater in integrated anaerobic-aerobic membrane sequencing batch reactor (MSBR) at different hydraulic retention times (HRTS), *Environmental Engineering and Management Journal*, **17**, 2667-2676.

Environmental Engineering and Management Journal
February 2020, Vol. 19, No. 2, 205-217
http://www.eemj.icpm.tuiasi.ro/; http://www.eemj.eu

"Gheorghe Asachi" Technical University of Iasi, Romania

MODELING OF A RECTANGULAR CHANNEL MONOLITH REACTOR FOR SORPTION-ENHANCED WATER-GAS SHIFT

Vlad-Cristian Sandu[1], Ionela-Dorina Dumbrava[1], Ana-Maria Cormos[1], Arpad Imre-Lucaci[1], Calin-Cristian Cormos[1*], Paul Cobden[2], Robert de Boer[3]

[1]*Faculty of Chemistry and Chemical Engineering, Babes-Bolyai University, Arany Janos 11, Cluj-Napoca, RO-400028, Romania*
[2]*Swerim AB, Box 812, SE971 25 Lulea, Sweden*
[3]*TNO Energy Transition, PO Box 15, 1755 ZG, Petten, The Netherlands*

Abstract

As CO_2 concentration levels in the atmosphere are steadily reaching a point of no return, it is paramount that actions are taken towards mitigating emissions by improving the efficiency of existing processes. Sorption-enhanced water-gas shift (SEWGS) combines the water-gas shift reaction with in-situ adsorption of CO_2 on potassium-promoted hydrotalcite (K-HTC). This enables a direct conversion of syngas into separate hot streams of H_2 at feed pressure and CO_2 at regeneration pressure, making the process attractive for pre-combustion carbon capture and storage (CCS) and reduction of greenhouse gas emissions. The current work is evaluating the high-temperature, high-pressure adsorption step of the SEWGS process enhanced by a novel technology which replaces common packed bed reactors with 3D-printed monolithic structures. This approach would enable an overall increase in process productivity. To this extent, innovative dynamic models based on validated competitive adsorption isotherms were developed in this work. COMSOL Multiphysics was used to develop a 1D computational fluid dynamics (CFD) model of adsorption for a fixed bed reactor in order to verify the model accuracy against existing studies. Subsequently, 2D CFD simulations were developed to describe adsorption inside monolith structures, both free and porous regions. The multi-component adsorption isotherm used in the simulations was validated with published breakthrough capacities for CO_2 and H_2O at different pressures. Model predictions are in agreement with expected behavior, as monolith reactors provide a more efficient mass transfer, and will be used to enhance the performance of experimental monolith structures used in SEWGS.

Key words: adsorption isotherm, carbon capture and storage, computational fluid dynamics, sorption-enhanced water-gas shift

Received: January, 2019; Revised final: November, 2019; Accepted: November, 2019; Published in final edited form: February, 2020

1. Introduction

Since the beginning of the Industrial Revolution in eighteenth century Britain, when the increased use of steam power led to thriving metallurgical and chemical industries human activities have continued to negatively impact Earth's climate through the emission of greenhouse gases (GHG). The major anthropogenic GHG is CO_2, which causes the absorption of energy of specific wavelengths that would normally leave the atmosphere to radiate back towards the surface, warming it (Le Treut et al., 2007). Levels of CO_2 emissions in the atmosphere had reached an all-time high in 2010 with a value of almost 400 ppm, accounting for 76% of total anthropogenic GHG emissions. Most CO_2 emissions come from fossil fuel combustion and industrial processes, with electricity and heat production being the leading causes for pollution (IPCC, 2014; Zivkovic et al., 2018). Measures to improve the energy sector and reduce greenhouse gas emissions have been assessed by the Intergovernmental Panel on Climate Change (IPCC). One option for mitigating CO_2 involves a technology known as carbon capture and storage

---

[*] Author to whom all correspondence should be addressed: e-mail: cormos@chem.ubbcluj.ro; Phone: +40264 593833

(CCS), which refers to separating CO_2 from industrial point sources and transporting it to storage sites to be deposited. The IPCC outlines three different types of CCS: post-combustion, in which CO_2 is separated from the exhaust of industrial processes, oxyfuel combustion, based on high purity oxygen use, and pre-combustion, a process in which, through water-gas shift, separated carbon dioxide and hydrogen are obtained to be used in combustion or for other purposes (IPCC, 2005).

Hydrogen is valuable due to its role in industrial processes, such as obtaining ammonia and methanol, and shows promise as an efficient, clean source of energy. However, an issue that needs to be addressed is the connection between industrial scale H_2 production and CO_2 emissions (Winter, 2009). A way to achieve both carbon dioxide emissions reduction and hydrogen production is a high potential pre-combustion technology called sorption-enhanced water-gas shift (SEWGS) (Voldsund et al., 2016).

SEWGS is a process that combines the water-gas shift (WGS) reaction (Eq. 1) with in-situ adsorption of CO_2 (Eq. 2) at high-temperatures between 300-500 °C and high-pressure levels between 10-40 bar. Steam adsorption (Eq. 3) is possible based on process conditions (Hufton et al., 1999).

$$CO + H_2O \leftrightarrow CO_2 + H_2 \quad (1)$$

$$CO_2 + \bullet \leftrightarrow CO_2 - \bullet \quad (2)$$

$$H_2O + \bullet \leftrightarrow H_2O - \bullet \quad (3)$$

Conventional WGS technology requires two consecutive reactors to obtain high conversion of CO, followed by pressure swing gas adsorption (PSA) to separate the CO_2 from the pure H_2, whereas with SEWGS, the second reactor and PSA can be combined into a SEWGS unit, leading to less process steps and less equipment needed. Moreover, in the case of a steam methane reformer without carbon capture, the CO_2 is released into the atmosphere, while SEWGS enables high CO_2 capture ratios at a higher energy efficiency and lower cost in comparison with more mature technologies (van Selow et al., 2011).

Considerable efforts were made in testing different sorbents to be used in a SEWGS process, however, most proved to be less desirable for various reasons. Hydrotalcite based adsorbents seem to outclass other types of adsorbents, as they demonstrate high thermal stability, fast sorption kinetics and high CO_2 selectivity (Ebner et al., 2006; Walspurger et al., 2010). The most commonly known hydrotalcite is Mg-Al hydrotalcite (Sikander et al., 2017). The impregnation of the hydrotalcite with alkaline metals, such as K_2CO_3, has been observed to increase the sorbent's capability to adsorb basic species (Lee et al., 2008). The potassium-promoted hydrotalcite (K-HTC) has two roles: acting as catalyst for the WGS reaction and sorbent for reversibly adsorbing CO_2 (Jang et al., 2012; Zheng, et al., 2014). After adsorption, the CO_2 that is released during K-HTC regeneration is sufficiently pure to be stored (Hufton et al., 1999; Lee et al., 2010; Yong et al., 2002).

The SEWGS process (Fig. 1) involves a series of traditional packed bed reactors which run in pressure cycles, enabling the periodic loading and regeneration of the sorbent. Since multiple reactors are being used, the process acts as if continuous and leads to a constant production of separate streams of CO_2 and H_2. In the first cycle step, syngas enters the column in which CO reacts with steam to obtain CO_2 and H_2. CO_2 is taken up by adsorption and a H_2 rich stream is obtained. Once the sorbent is saturated, a medium-pressure steam rinse takes place pushing the syngas into another reactor. After the rinse, a number of pressure equalizations are performed. During this step, the rinse gas in the high-pressure reactor expands and pushes the remaining syngas into a lower pressure reactor. Gas pressure is conserved since the high-pressure reactor that required depressurization will connect to a lower pressure one that needs to be pressurized. In the blowdown step, the pressure in the reactor is rapidly decreased to 1 bar and some CO_2 is released from the sorbent, exiting the reactor with the steam and allowing particle regeneration. By purging the reactor with low-pressure steam, additional CO_2 is released and sorbent regeneration is enhanced. Following pressure equalization with a high-pressure reactor and re-pressurization, the reactor will be ready to undergo the SEWGS process from the beginning. SEWGS is an attractive process for both pre-combustion CCS and GHG emissions reduction since it directly converts syngas into a hot H_2 stream at feed pressure and a separate CO_2 stream at regeneration pressure (Boon et al., 2015). SEWGS appears to be a promising CCS technology, as discussed by Riboldi and Bolland (2017), who highlight the good potential of PSA in pre-combustion applications with hot gas separation processes, especially when considering sorption-enhanced processes.

One bottleneck for traditional fixed bed solutions for sorbent-based CCS technologies is the trade-off between flow-rate through the reactor, pressure drop and kinetics of the adsorption process. A monolith reactor has a honeycomb structure made of thin-walled supports. Many straight parallel channels in micron- and millimeter-scale combine to create the entire structure. These channels can have various shapes, such as square, triangular, circular, hexagonal or others, depending on purpose. In the case of sorption, monolithic structures provide an attractive alternative to regular fixed bed reactors due to the high active surface area of the channels (Govender and Friedrich, 2017). Several fixed bed processes are believed to be able to benefit from the use of monolith configurations, due to pressure drop or mass transfer constraints, as monolithic structures exhibit an outstanding pressure drop to mass transfer ratio (Boger and Sorensen, 2004).

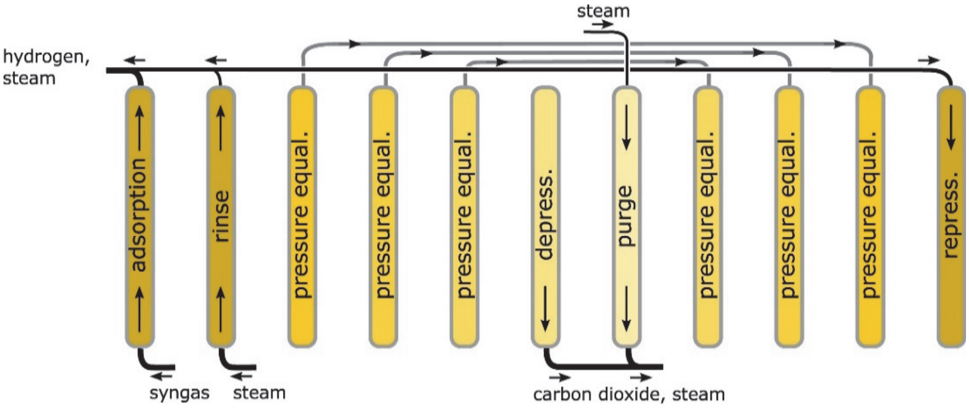

Fig. 1. Eleven step SEWGS cycle with concurrent steam rinse (Boon et al., 2015)

In the last years, the idea of replacing packed bed reactors with monoliths has received more and more attention. The applications that have been proposed include two categories: automobile applications (Dhanushkodi et al., 2008; Sadeghi et al., 2017; Tischer and Deutschmann, 2005) and industrial applications: syngas combustion (Pramanik and Ravikrishna, 2017), benzene alkylation (Dai et al., 2013), PSA (Pahinkar and Garimella, 2018), catalytic oxidation of volatile organic compounds (Rodríguez et al., 2016), Natural Gas Reforming (Heidebrecht et al., 2011), etc. The majority of modeling and simulation research has been focused on gas phase in the monolith, with a small number of papers published on multi-phase monolith reactors (Bertrand et al., 2012; Durán Martínez et al., 2016; Lei et al., 2016).

Depending on the objectives, applications and numerical computational limitations, these models can be classified as 1D, 2D or 3D models (Chen et al., 2008). Based on the monolith structure, there are different modeling scales: single channel (majority of the developed models), multi-channel (Dai et al., 2013; Lupše et al., 2016) or an entire reactor (Bauer et al., 2005).

In order to compare various modeling approaches, the effect of channel geometry (i.e. circle, hexagon, square, rectangle, and regular triangle) on the reactor performance was investigated (Dai et al., 2013, Sadeghi et al., 2017). For monolith catalysts, a regular triangular or rectangular channel shape is favorable when considering pressure drop and process selectivity/conversion. Furthermore, the effect of the most important operating parameters, such as temperature, porosity and wall/wash-coat thickness, inlet velocities, residence time on the conversion in the reactor were investigated by Lupše et al. (2016), Pramanik and Ravikrishna (2017) and Sadeghi et al. (2017).

This paper studies the adsorption step of SEWGS, in which the traditional fixed bed configuration is replaced with monolith structures made of K-HTC adsorbent material. To date, there are few articles published regarding SEWGS modeling and even less on monolith computational fluid dynamics (CFD) simulations for hydrogen production. Reijers et al. (2009a, 2009b) developed a 1D model to study a sorption-enhanced reaction process for CO_2 capture with steam methane reforming (SMR) and WGS reactions taking place in the packed bed reactor, then validated the model based on experimental data. A SEWGS model on packed bed reactors was developed for IGCC by Wright et al. (2011) to investigate the effects of using different feedstocks and discovered that steam amount needed to operate SEWGS units was similar when using syngas from either natural gas or coal. Boon et al. (2014) developed a SEWGS reactor model which uses the linear driving force (LDF) approximation and double component isotherm to accurately predict breakthrough performance and highlight competitive adsorption between CO_2 and H_2O in SEWGS. Irani et al. (2011) developed a CFD model of SMR and WGS in monolith reactors for hydrogen production, but their model was steady state with the purpose of investigating efficiency of surface or volume-based reaction models in terms of better predictions.

In this work, CFD models were developed in COMSOL Multiphysics to simulate adsorption of CO_2 and H_2O, the first step of SEWGS, in space-time. For validation purposes, a 1D model of a fixed bed reactor was developed to enable comparison to existing published data. Subsequently, a 2D model considering mass, heat and momentum transfer was built to simulate adsorption inside a single channel of a monolith reactor. As no experimental data was available on such configurations, pre-validation was done through analytical methods. The key target was using CFD for assessment of adsorption kinetics in structured bed configurations for SEWGS.

2. Model development

2.1. Breakthrough measurements

Boon et al. (2014) performed breakthrough experiments in a multi-column SEWGS test rig, which was accurately described by van Selow et al. (2009). H_2O breakthrough capacity was measured at three total pressure levels: 8, 17.5 and 27 bar(a). At each of the pressure levels, breakthrough measurements were carried out with 11, 43 and 78 volume percentage of steam in argon-nitrogen gas mixture. Subsequently,

CO_2 breakthrough experiments were performed at 7, 12, 17, 22 and 27 bar(a) total pressure. The volume percentages of CO_2 in argon-nitrogen mixture were 3, 33 and 71 for every pressure setting. The CO_2-H_2O mixture breakthrough experiments were aimed at measuring excess adsorption of CO_2 and H_2O at 400 °C and 27 bar(a). In total, 32 conditions were tested with CO_2 partial pressures ranging between 0.5-24 bar and H_2O partial pressures ranging between 4-24 bar.

2.2. Adsorption isotherm

Boon et al. (2014) managed to fit a multi-component adsorption isotherm to the SEWGS system. A model based on two double isotherms was derived to take into account surface contributions and nanopores contributions for CO_2 and H_2O adsorption at high pressures. The regressed parameters are shown in Table 1. Although the surface sites are specific, either adsorbing CO_2 or H_2O, competitive adsorption in nanopores is likely to take place. The surface adsorption of CO_2 was described by a Langmuir isotherm (first term on right side in Eq. 4), in agreement with most other studies found in literature. For the surface contribution of H_2O, a Freundlich isotherm was used (first term on right side in Eq. 5), as to reflect the heterogenous character of the sites for H_2O. Nanopore contribution of both CO_2 and H_2O was described through a Dubinin-Astakhov equation (second term on right side in Eqs. (4-5)) based on volume filling theory, where the assumption of no lateral interactions between adsorbed species enabled the amount of gas adsorbed to be determined by the limiting nanopore volume V_0, pore-size distribution parameter m and the nanopore-sorbate interaction energy E (Do, 1998; Coenen et al., 2017). As such, in the case of CO_2 (Eq. 4):

$$q^*_{CO_2} = \frac{q^S_{CO_2} K_{CO_2} p_{CO_2}}{1+K_{CO_2} p_{CO_2}} + \frac{A_{CO_2}(V_0 - V_0 A_{H_2O})}{v_{m,CO_2}(1 - A_{CO_2} A_{H_2O})} \tag{4}$$

$$q^*_{H_2O} = K_{H_2O} p_{H_2O}^{1/n} + \frac{A_{H_2O}(V_0 - V_0 A_{CO_2})}{v_{m,H_2O}(1 - A_{CO_2} A_{H_2O})} \tag{5}$$

where:

$$A_i = exp\left(-\left[\left(\frac{RT}{E_i}\right) ln\left(\frac{p_{0,i}}{p_i}\right)\right]^{m_i}\right) \tag{6}$$

$$p_{0,i} = p_{c,i}\left(\frac{T}{T_{c,i}}\right)^2 \tag{7}$$

$$v_{m,i} = \frac{RT_{c,i}}{8p_{c,i}}\left(\frac{T}{Tc_{,i}}\right)^{0.6} \tag{8}$$

The values presented in Table 1 were in agreement with values published by other groups. For CO_2 adsorption on K-HTC, Lee et al. (2007) reported similar a monolayer capacity $q^S_{CO_2}$ between 0.25-0.45 mol kg^{-1}, but much higher gas-solid interaction parameter K_{CO_2} at 400 °C in the range of 167 - 369 MPa^{-1}. However, in a study by van Selow et al. (2013), the value reported was 44.5 MPa^{-1}. For H_2O adsorption, the Freundlich exponent n, quantifying the nonlinearity of the isotherm, has been reported to be within the range of 1.7-5.1 on various clays (Hatch, Wiese, Crane, Harris, Kloss, & Baltrusaitis, 2012). Maroño et al. (2013, 2014) found nanopore volumes in the range of 50-60 cm^3 kg^{-1}. The parameter m, which characterizes nanopore heterogeneity, has been found to usually vary between 1-6 (Do, 1998). The characteristic energy E values for CO_2 and H_2O are regular values for nanopore-sorbate energies using the Dubinin-Astakhov model (Do, 1998).

Table 1. Regressed multi-component isotherm parameters used in Eqs. (4-8) (Boon et al., 2014)

Parameter	***Estimate***
$q^S_{CO_2}$[mol kg^{-1}]	0.45 ± 0.13
K_{CO_2} [MPa^{-1}]	28 ± 26
E_{CO_2} [kJ mol^{-1}]	23 ± 1
m_{CO_2} [-]	5.2 ± 1.5
K_{H_2O} [mol kg^{-1} MPa$^{-1/n}$]	0.37 ± 0.07
n [-]	1.9 ± 0.5
E_{H_2O} [kJ mol^{-1}]	12 ± 1
m_{H_2O} [-]	3.6 ± 0.8
V_0 [cm^3 kg^{-1}]	74 ± 17

2.3. Reactor models

2.3.1. Fixed bed reactor model

To investigate the kinetics of adsorption, Boon et al. (2014) developed a reactor model based on a previous reactor model for low-pressure sorption-enhanced reforming published by Reijers et al. (2009). With the purpose of validation, a 1D model simulating adsorption in a fixed bed reactor with sorbent pellets was carried out in the current work. The model was built with COMSOL Multiphysics, using the Chemical Reactions and Engineering Module, which enabled simulation of transport in porous media. Discretization of the porous domain was done using a custom made extremely fine mesh, calibrated for fluid dynamics. Since the model was one dimensional, only the x-coordinate was taken into account. The transport equation in the bulk (Eq. 9) accounted for the combined effects of convection and diffusion:

$$\frac{\partial c_i}{\partial t} + \nabla \cdot (-D_i \nabla c_i) + u \cdot \nabla c_i = R_i \tag{9}$$

where, the first term described the rate of change in concentration with respect to time, the second was the diffusive term and the third the convective term. The reaction rate term R_i was 0.

The transport equations in the porous domain (10) accounted for effective diffusion and convection: where the first and second terms describe the rate of change in concentration and bed porosity, respectively, with respect to time, the third term was the effective diffusivity and the fourth was the convective term. Again, the value for the reaction rate term R_i was 0. Eqs. (11-14) used for the intraparticle model are based on the common LDF assumption for porous spherical particles (Table 2) (Reijers et al., 2009a). Eq. 11 shows the rate of change in loading amount with respect to time, proportional with the mass transfer coefficient k_{LDF} (Eq. 12), with two components accounting for pore diffusion (Eq. 13) and surface diffusion (Eq. 14). Model dimensions and process conditions are presented in Table 3.

2.3.2. Structured bed reactor model

A graphical representation of the monolith structure with square channels considered in this work is presented in Fig. 2a and a single channel is shown in Fig. 2b. The monolith reactor's axial section was considered circular. The number of possible channels was based on the channel dimensions and reactor surface. By assuming that the flow was evenly distributed within the monolith structure and that each channel was identical, it was possible to characterize the entire monolith by studying just one channel (Chen et al., 2008; Sharma and Birgersson, 2016). The channel's axial section was considered square. The transition from 3D to 2D was decided based on having less model complexity, which translates into less computation time and hardware requirements needed to run the simulations. Model dimensions are shown in Table 4.

The wall thickness corresponding to each channel was obtained by assuming that the entire surface of adsorbent is equally active, including near the edges of the reactor where diffusion effects might be weaker, thus dividing the surface available of adsorbent by the number of channels.

The high length-width ratio between the reactor length of 1 m and channel width of 1 mm led to a complicated meshing process. However, the mesh was finely discretized with special focus on the transition zone between the inlet section with slip wall condition and free channel, the boundaries between free channel and the porous domain itself. Error tolerances were also tightened accordingly to obtain accurate predictions. Relative error values were below 10^{-4} for all solved variables.

The following assumptions were considered for the 2D monolith reactor simulation:

1. Uniform distribution of sorbent activity;
2. Dynamic mixture, thermodynamic and transport properties;
3. Convection and diffusion in the bulk and porous media (Fick's Law);
4. Compressible laminar fluid flow;
5. Heat transfer in the fluid and porous media;
6. WGS was not considered;
7. Adsorption of CO_2 and H_2O were taken into account (surface and nanopore contributions);
8. Porous mass transfer resistance calculated with LDF approximation.

The equations used in the mathematical model are presented in Table 5. The fluid was considered as being compressible with a time dependent density, which led to the continuity equation (Eq. 15).

$$\left(\boldsymbol{\varepsilon_b} + \boldsymbol{\rho_b k_{p,i}}\right)\frac{\partial \boldsymbol{c_i}}{\partial \boldsymbol{t}} + \left(\boldsymbol{c_i} - \frac{\rho}{(1-\varepsilon_b)}\boldsymbol{c_{p,i}}\right)\frac{\partial \boldsymbol{\varepsilon_b}}{\partial \boldsymbol{t}} + \boldsymbol{\nabla}\cdot\left(-\boldsymbol{D_{e,i}}\boldsymbol{\nabla c_i}\right) + \boldsymbol{u}\cdot\boldsymbol{\nabla c_i} = \boldsymbol{R_i} \qquad (10)$$

Table 2. Intraparticle equations (Eqs. 11-14)

Species i adsorption reaction rate	$\frac{\partial q_i}{\partial t} = k_{LDF}\cdot(q_i^* - q_i)$	(11)
LDF mass transfer coefficient	$k_{LDF} = k_{LDF}^{pore} + k_{LDF}^{surf}$	(12)
k_{LDF} for pore diffusion	$k_{LDF}^{pore} = \frac{15D_s}{(d_p/2)^2}\frac{\varepsilon_p}{\varepsilon_p + (1-\varepsilon_p)\rho_p RT(\partial q_i^*/\partial p_i)}$	(13)
k_{LDF} for surface diffusion	$k_{LDF}^{surf} = \frac{15D_s}{(d_p/2)^2}\frac{\rho_p RT(\partial q_i^*/\partial p_i)}{\varepsilon_p + (1-\varepsilon_p)\rho_p RT(\partial q_i^*/\partial p_i)}$	(14)

Table 3. Fixed bed model dimensions and process conditions (Reijers et al., 2009a)

Parameter	*Value*	*Parameter*	*Value*
L [m]	0.2	d_p [m]	3.15e-4
h [m]	0.02	ε_b [-]	0.4
d [m]	0.016	ε_p [-]	0.07
u_f [m s^{-1}]	0.0056	ρ_b [kg m^{-3}]	553
p_f[Pa]	101325	ρ_p [kg m^{-3}]	922
T_f [K]	673.15	y_{CO_2} [-]	0.05
D_m [m^2 s^1]	7.4e-5	y_{H_2O} [-]	0.29
D_p [m^2 s^{-1}]	1.2e-6	y_{N_2} [-]	0.66
D_s^0 [m^2 s^{-1}]	1.5e-10	k_{LDF} [-]	0.1

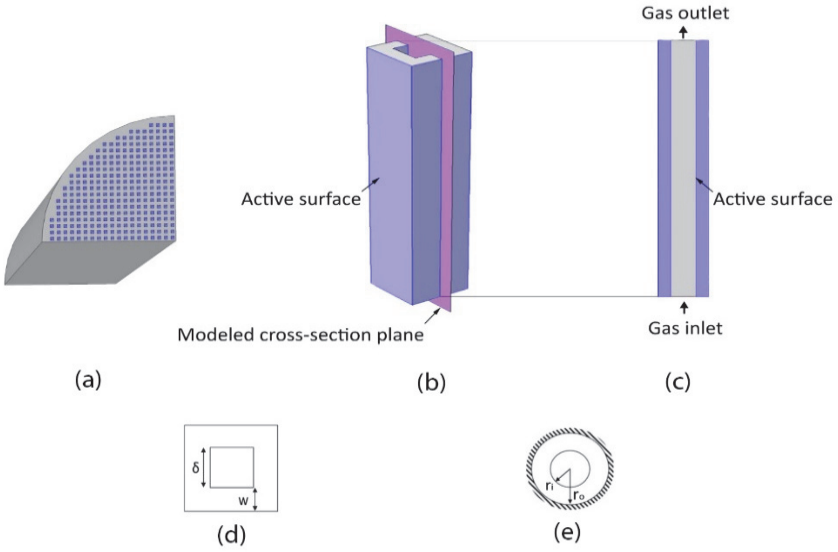

Fig. 2. 3D schematic representation of a monolith reactor with straight square channels (a), 3D representation of a single channel (b), 2D geometry used in models (c), channel axial section (d), hollow cylinder with insulated external surface (e) (Patton et al., 2004)

Table 4. Structured bed model dimensions and process parameters

Parameter	*Value*	*Parameter*	*Value*
L [m]	1	ε [-]	0.57
d_R [m]	0.038	ρ_m [kg m^{-3}]	1848
d [m]	0.001	$\Delta H_{CO_2}^{ads}$ [J mol^{-1}]	-65000
wt [m]	0.000573	$\Delta H_{H_2O}^{ads}$ [J mol^{-1}]	-50000
nc [-]	457	C_p [J kg^{-1} K^{-1}]	1048
L_{inlet} [m]	0.25	K [m^2]	1e-12
Q_V [SL/min]	20	y_{CO} [-]	0.03
u_f [m s^{-1}]	0.029	y_{H_2} [-]	0.6
p_f[Pa]	25e5	y_{CO_2} [-]	0.13
T_f [K]	673.15	y_{H_2O} [-]	0.21
D_m [m^2 s^1]	3.85e-6	y_{N_2} [-]	0.03

The vector fields were considered only for directions x and y. Mass transport in the bulk was solved by using a convection-diffusion equation (Eq. 16), while mass transport inside the porous domain was modeled with a porous media transport equation (Eq. 17). Adsorption of CO_2 and H_2O took into account the double-component isotherm (Eqs. (4-5)) and was solved by Eq. 18, using a dynamic k_{LDF}, considered a sink in the mass transport equation inside the porous media (Eq. 17).

Fluid flow was modeled with the Navier-Stokes equations for laminar flow in the bulk (Eq. 19), which accounted for fluid velocity, fluid pressure, fluid density and fluid dynamic viscosity. The term on the left-hand side corresponded to momentum transferred by convection in free flow, while the term on the right-hand side corresponded to pressure and viscous forces. The Forchheimer corrected Brinkman equations (Eq. 20) were used for flow inside the porous domain, which also accounted for the permeability of the porous medium, the porosity and a friction coefficient C_f (Eq. 21). The term on the left-hand side represented a contribution associated with the drag force experienced by the fluid flowing through a porous medium. Additionally, the last term on the right-hand side presented the Forchheimer correction (Eq. 22) to account for turbulent drag contributions to the resistance to flow in the porous domain. Boundary conditions are a flat inlet velocity at the channel entrance based on the channel area and desired flow rate, no slip condition at the walls and a pressure condition with suppressed backflow at the channel exit. In order to avoid inconsistent boundary conditions, an inlet section with assumed symmetry prescribing no penetration and vanishing shear stresses was added to the geometry.

Heat transfer in the fluid was modeled by Eq. 23, while heat transfer in the porous domain was calculated with Eq. 24. Due to fluid motion, convective and conductive contributions were included in the heat transfer equations (Eqs. (23-24)). The conductive heat flux, describing gas-solid heat transfer, was proportional to the temperature gradient (Eq. 25). Heat transfer in porous media had an additional term for adsorption related heat source Q (Eq. 24). The SEWGS process took place after a SMR reactor, followed by a pre-shift process, which can be noticed in the inflow gas composition (Table 4). Based on the compositions, the WGS reaction was considered negligible. The main focus of the simulation was investigating the adsorption process and without the WGS reaction, the calculation of a stoichiometric breakthrough time to verify adsorption was possible.

Another key difference separating the monolith structure from the fixed bed reactor was the LDF mass transfer coefficient. A different expression (Eq. 26) was used to calculate the mass transfer coefficient k as a function the monolith wall thickness w and channel width *δ*. Since the shape of the monolith channels in this work was considered square (Fig. 2d), it was possible to transform the geometry into an equivalent cylinder, such as a hollow cylinder with insulated external surface (Fig. 2e), the surface representing halfway inside the monolith wall where internal loading was zero. The transformation allowed the use of the LDF approximation for cylinders (Eq. 31) (Patton et al., 2004).

3. Results and discussions

3.1. Breakthrough capacities for CO_2 and H_2O

The adsorption capacities for CO_2 and H_2O have been derived from the breakthrough experiments. The data points in Fig. 3 show CO_2-H_2O mixture breakthrough capacities. The lines are drawn based on the isotherm developed from the full dataset, described earlier in detail in the paper, while the diamonds mark experimental data.

Pure CO_2 capacities can be explained by a two-step adsorption mechanism. Adsorption of up to 0.4 mol kg-1 is attributed to surface sites, while the rest at pressures above 3 bar is due to nanopores.

Table 5. Structured bed model equations

Continuity	$\frac{\partial \rho}{\partial t} \nabla \cdot (\rho u) = 0$	(15)
Mass transfer in bulk	$\frac{\partial c_i}{\partial t} + \nabla \cdot (-D_i \nabla c_i) + u \cdot \nabla c_i = 0$	(16)
Mass transfer in solid	$(\varepsilon + \rho_m k_{p,i}) \cdot \frac{\partial c_i}{\partial t} + \left(c_i - \frac{\rho}{(1-\varepsilon)} \cdot c_{p,i}\right) \frac{\partial \varepsilon}{\partial t} + \nabla \cdot (-D_{e,i} \nabla c_i) +$ $+ u \cdot \nabla c_i = R_{ADS,i}$	(17)
Adsorption rate	$R_{ADS,i} = \frac{dq_i}{dt} = k_{LDF} \cdot (q_i^* - q_i)$	(18)
Momentum in bulk	$\rho \frac{\partial u}{\partial t} + \rho (u \cdot \nabla) u = \nabla \cdot \left[-pI + \mu \left(\nabla u + (\nabla u)^T - \frac{2}{3} \mu (\nabla \cdot u)\right) I\right]$	(19)
Momentum in solid	$\frac{1}{\varepsilon} \rho \frac{\partial u}{\partial t} + \frac{1}{\varepsilon} \rho (u \cdot \nabla) u \frac{1}{\varepsilon} = \nabla \cdot [-pI + \mu \frac{1}{3} (\nabla u + (\nabla u)^T -$ $- \frac{2}{3} \mu \frac{1}{\varepsilon} (\nabla \cdot u) I] - \left(\mu K^{-1} + \beta_F \lvert u \rvert + \frac{\nabla \cdot (\rho u)}{\varepsilon^2}\right) u$	(20)
Friction coefficient	$C_F = \frac{1.75}{\sqrt{150 \varepsilon^3}}$	(21)
Forchheimer coefficient	$\beta_F = \frac{\rho \varepsilon C_f}{\sqrt{K}}$	(22)
Heat transfer in fluids	$d_z \rho C_p \frac{\partial T}{\partial t} + d_z \rho C_p u \cdot \nabla T + \nabla \cdot q = q_0$	(23)
Heat transfer in solids	$d_z (\rho_m C_{p,m})_{eff} \frac{\partial T}{\partial t} + d_z \rho_m C_{p,m} u \cdot \nabla T + \nabla \cdot q = d_z Q + q_0$	(24)
Conductive heat flux	$q = -d_z k \nabla T$	(25)

$$k = \frac{4}{k_1 - k_2} \tag{26}$$

where:

$$k_1 = \left(\frac{r_o}{r_i} - 1\right) \cdot (r_o^2 - r_i^2) \tag{27}$$

$$k_2 = \left(\frac{1}{r_i \cdot (r_o - r_i)}\right) \cdot \frac{1}{2} (r_o^4 - r_i^4) - \left(\frac{4}{3} r_o\right) \cdot (r_o^3 - r_i^3) + r_o^2 \cdot (r_o^2 - r_i^2) \tag{28}$$

$$r_i = \frac{2\delta}{\pi} \tag{29}$$

$$r_o = \sqrt{\frac{4w}{\pi}(w + \delta) + r_i^2} \tag{30}$$

$$k_{LDF} = k \cdot D_s \cdot \frac{\varepsilon_p}{\varepsilon_p + (1 - \varepsilon_p) \rho_p RT (\partial q_i^* / \partial p_i)} \tag{31}$$

A similar behavior is seen for pure H_2O capacities. At pressures below 12 bar, experimental data shows the surface contribution around 0.3 mol kg^{-1}. The one point around 20 bar can be attributed to nanopore contribution. Overall, considering the full partial pressure range, the trend in steam adsorption matches the trend observed by Hatch et al. (2012) and supports the idea of a binary adsorption mechanism.**Error! Reference source not found.** demonstrates the importance of the sorbent's nanostructure, especially at higher partial pressures. An indicator towards this is how the impact of CO_2 on the capacity of H_2O is much stronger than the reverse. The larger molar volume of CO_2 in comparison to that of H_2O ensures that the available nanopore volume is more strongly taken up by CO_2 than by H_2O.

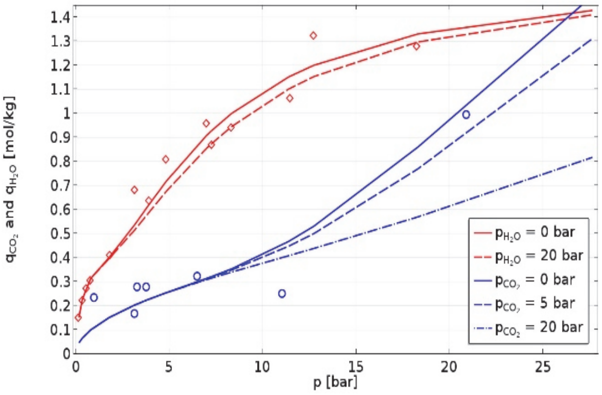

Fig. 3. CO_2-H_2O breakthrough capacities for CO_2 (red diamonds) and H_2O (blue circles) versus partial pressure, predicted pure component capacities (line) and mixture capacities (dashed lines). The experimental dataset obtained by Boon et al. (2014) was used to plot the breakthrough capacities in COMSOL Multiphysics

3.2. Fixed bed reactor model describing CO_2 adsorption

The 1D fixed bed model simulated the adsorption of CO_2 during SEWGS with process conditions shown in Table 3. Fig. 4 presents the comparison between the breakthrough curve published by Reijers et al. (2009a) and the CFD model predicted breakthrough. The CFD model predictions were in accordance with expected behavior, as when compared to the published data, the breakthrough times are within close range, of around 500 s, and the breakthrough curves show nearly identical profiles. The fixed bed model is considered successfully validated.

3.3. Structured bed reactor model describing CO_2 and H_2O adsorption in a single channel

The geometry of the channel used in the 2D model, which had a square cross section and a rectangular longitudinal section, can be seen in Fig. 2c with the addition of an inlet section in order to avoid inconsistent boundary conditions. The dimensions and process conditions can be found in Table 4. The breakthrough curve obtained by the model is presented in Fig. 5a and a summary of results in Table 6.

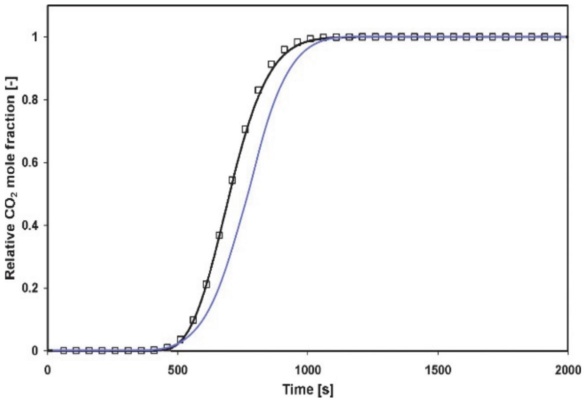

Fig. 4. CO_2 mole fraction at the reactor outlet relative to CO_2 mole fraction of the feed gas. Black – published by Reijers et al. (2009a), line - MATLAB model, symbols - analytical solution; Blue – calculated by the CFD model for a constant k_{LDF} = 0.1 s^{-1}

The total simulated breakthrough time taken at a relative CO_2 mole fraction of 0.95 (Fig. 5a) was 150 s, but the simulation included flow through the inlet section where no adsorption took place. Accounting for the time needed to travel the 250 mm slip wall conditioned inlet section of 8.62 s, the actual CFD model predicted breakthrough time was 141.38. Since the only sink or source of CO_2 was the adsorption process, it was possible to verify accuracy of the predicted loading amount by calculating the stoichiometric breakthrough time:

$$t^* = \frac{q_{CO_2} \cdot m_{ads}}{Q_M} \tag{32}$$

where, q_{CO_2} was the loading amount at breakthrough for $C_{out}/C_{in} = 0.95$ predicted by the CFD simulation (Wood, 2002).

Based on the values of the predicted breakthrough time and analytically calculated stoichiometric breakthrough time (Table 6), the predicted loading amount of CO_2 and accuracy of the model were verified successfully.

The laminar profile of CO_2 flow in the free flow region and the diffusion dominating porous media flow can be seen in Fig. 5b. While convective flow is present in the porous media, its contribution with values of 10^{-6} m/s was negligible. As a result, diffusion dominated porous media flow.

The CFD model predicted a relative CO_2 mole fraction at breakthrough of 0.95 instead of an expected value of 1. This can be explained by the effects related to heat transfer. While breakthrough was achieved, the adsorption process was not entirely completed. As the CFD model simulated the adsorption process over a longer time period (Fig. 6), the relative CO_2 mole fraction reached a value of 1, at which point the adsorbent was completely saturated.

The interdependency of all simulated phenomena is highlighted in Fig. 7 where surface graphs for temperature T K, CO_2 loading amount qCO_2 mol kg^{-1} and H_2O loading amount qH_2O mol kg^{-1} are represented at different time values. The strong impact of heat transfer over the adsorption process can also be observed. As the fluid traveled the channel and diffused into the porous material, the adsorption of CO_2 led to a rise in temperature since the adsorption process was exothermic. At some point, as adsorption took place further into the reactor channel, the continuous inflow of fluid at initial temperature influenced the system closer to the inlet by cooling it. The lower temperature of the adsorbent material increased the adsorption capacity and triggered additional adsorption of CO_2 and desorption of H_2O, highlighting the competitive nature of adsorption in this process.

These effects are in agreement with predictions by the adsorption isotherms (Fig. 3). An isothermal model was developed to verify the predictions of the CFD model regarding heat transfer effects. The breakthrough curve is presented in Fig. 8. The relative CO_2 mole fraction reached a value of 1 during the initial breakthrough because, without heat transfer, no additional adsorption is triggered.

Breakthrough occurred at around 200 s, much later when compared to the non-isothermal model. Without the temperature increase due to exothermic effects, the adsorption capacity was at its highest capacity during the entire process, meaning more CO_2 to be adsorbed and a longer time until breakthrough. Mass transfer efficiency can be investigated by studying the mass transfer zone (MTZ) behavior and length. MTZ graphs at different simulation times are seen in Fig. 9.

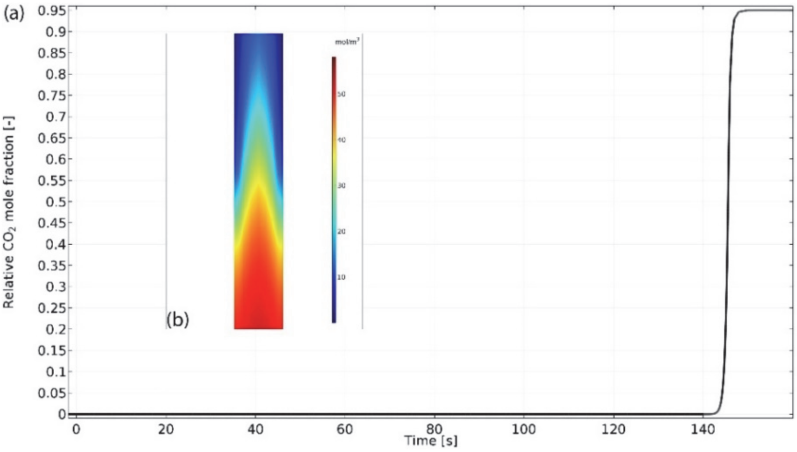

Fig. 5. CO_2 mole fraction at the reactor outlet relative to CO_2 mole fraction of the feed gas calculated by the CFD model with a dynamic k_{LDF} (a) and CO_2 surface flow profile (b)

Table 6. Structured bed model predictions

Total adsorbent mass [kg]	***Breakthrough time [s]***	***Loading at breakthrough [kg/mol]***	***CO_2 molar flow rate [mol s^{-1}]***	***Stoichiometric breakthrough time [s]***	***Pressure drops [Pa]***
0.765	141.38	0.36	0.00195	141.37	17.04

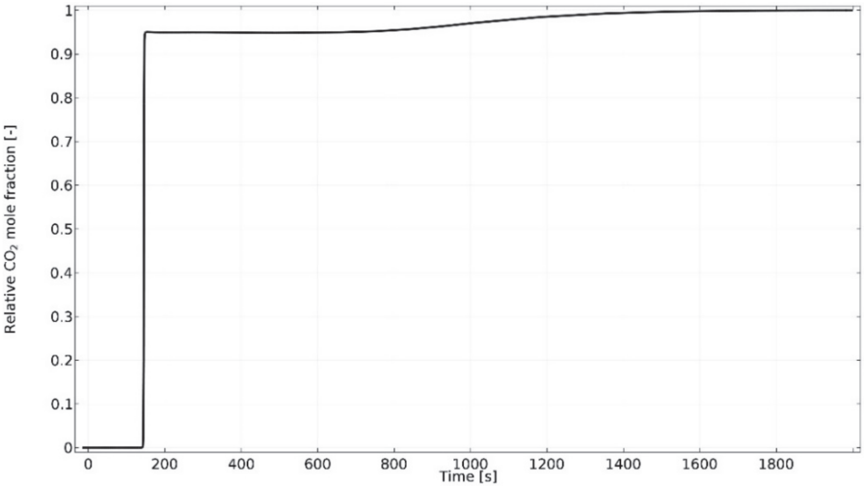

Fig. 6. CO_2 mole fraction at the reactor outlet relative to CO_2 mole fraction of the feed gas calculated by the CFD model with a dynamic k_{LDF} over a time period of 2000 s

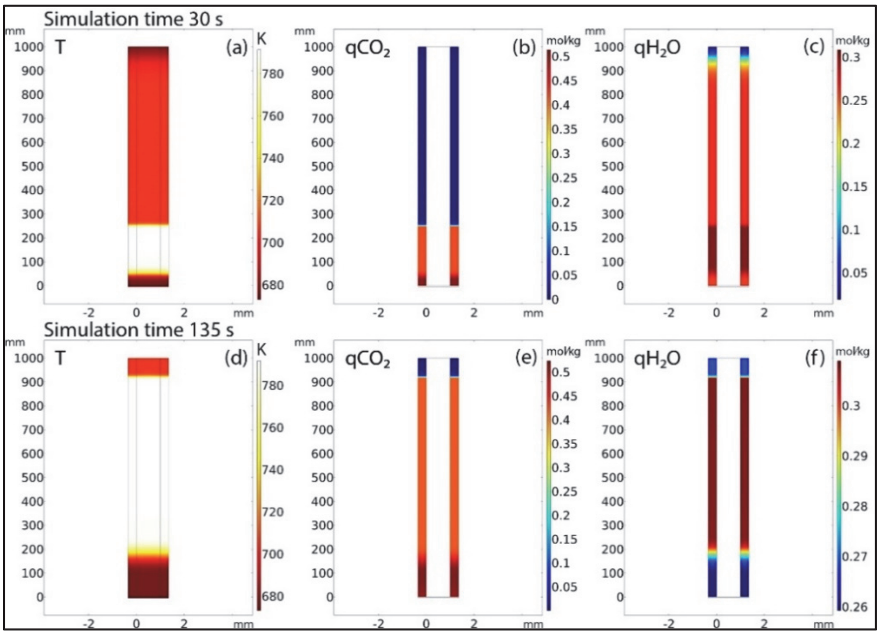

Fig. 7. Surface graphs at 30 s simulation time, before H_2O breakthrough, for temperature K (a), CO_2 loading mol kg^{-1} (b), H_2O loading mol kg^{-1} (c) and at 135 s, before CO_2 breakthrough, for temperature K (d), CO_2 loading mol kg^{-1} (e), H_2O loading mol kg^{-1} (f)

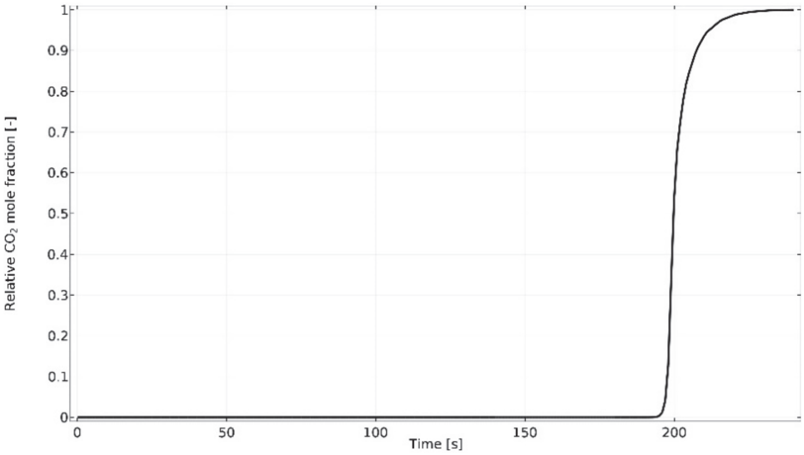

Fig. 8. CO_2 mole fraction at the reactor outlet relative to CO_2 mole fraction of the feed gas calculated by the isothermal CFD model with a dynamic *k_{LDF}*

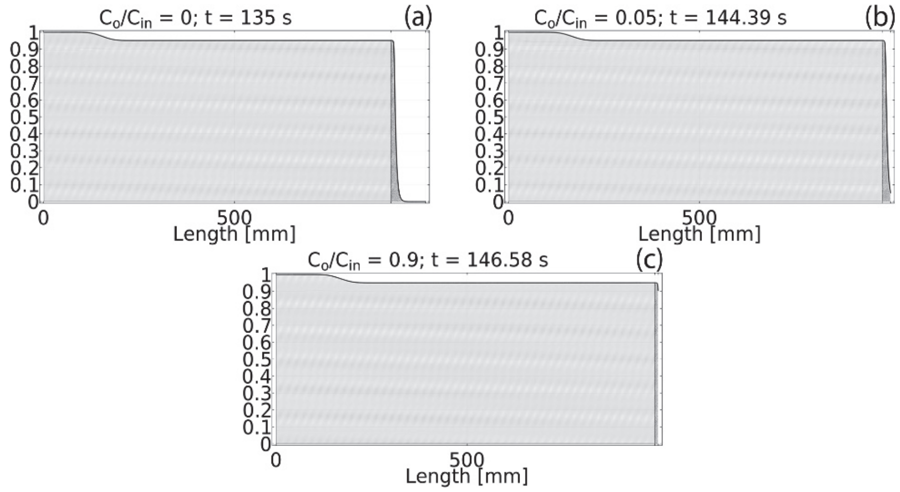

Fig. 9. MTZ behavior before breakthrough (a), at the beginning of breakthrough (b) and near the end of breakthrough (c); Grey area - saturated zone, dark grey area - adsorption zone (MTZ), white area - fresh adsorbent

It can be seen that the MTZs at different times are relatively short, evidence of high mass transfer rates and low mass transfer resistance. The breakthrough curve profile (Fig. 5a) can also be used for mass transfer assessment. The predicted breakthrough curve profile was steep, which is an indication of low transfer resistance and a very efficient utilization of the adsorbent bed (McCabe et al., 2004; Seader et al., 2011).

4. Conclusions

A multi-component competitive isotherm for CO_2 and H_2O was implemented in COMSOL Multiphysics and successfully validated using experimental data found in literature. The adsorption isotherm is composed of a first term that describes surface adsorption at lower pressures and a second term that reflects nanopore adsorption at higher pressures. The interaction seen at higher pressure values leads to the assumption of a competitive mechanism.

COMSOL Multiphysics was used to develop a 1D fixed bed model of adsorption of CO_2 in the SEWGS process. The model used the multi-component isotherm and the LDF approximation to describe adsorption. The model was successfully validated as breakthrough predictions were in agreement with predictions available in literature.

A novel approach to enhance SEWGS productivity, by replacing standard packed bed reactors with monolithic 3D-printed structures, was studied. To that end, a 2D CFD model of CO_2 and H_2O adsorption inside a single monolith reactor channel during the SEWGS process was developed. The developed dynamic model accounted for mass, heat and momentum transfer. The mesh density was sufficiently increased and error tolerance tightened until a favorable trade-off between computation time and accuracy of solution was reached. Predictions showed that heat transfer had a strong impact over adsorption capacity and reinforced the existence of a competitive adsorption mechanism highlighted by the isotherms. The development of an isothermal model confirmed the heat transfer effects. Although experimental validation was not possible due to the lack of any data available in literature, an analytical verification of the predicted loading amount was successfully carried out. Based on pressure drop values, steepness of the breakthrough curve profile and short size of the mass transfer zones, a preliminary assessment can be made that a structured bed configuration for SEWGS would provide more efficient mass transfer than traditional configurations.

Future work involves model transition from 2D to 3D, simulations of different channel geometries to study effects on mass transfer, development of a CFD fixed bed model for proper comparisons and experimental validation.

Acknowledgements

This work was supported by a grant of the Romanian National Authority for Scientific Research and Innovation, CCCDI - UEFISCDI, project number COFUND-ACT ERANET–3D-CAPS (contract number: 87/2017): "*3D Printed Capture Materials for Productivity Step-Change*", within PNCDI III.

Nomenclature

A	nanopore-sorbate interaction parameter, -
c	bulk concentration, mol m^{-3}
c_p	adsorbed concentration, mol kg^{-1}
C_p	specific heat capacity, J kg^{-1} K^{-1}
d	channel diameter, m
d_p	particle diameter, m
d_R	reactor diameter, m
D_m	molecular diffusion coefficient, m^2 s^{-1}
D_p	intraparticle diffusion coefficient, m^2 s^{-1}
D_s	surface diffusion coefficient, m^2 s^{-1}
D_s^0	surface diffusion coefficient at zero coverage, m^2 s^{-1}
E	nanopore-sorbate interaction energy, J mol^{-1}
h	bed height, m
ΔH	adsorption enthalpy, J mol^{-1}
i	species index, -
k_{LDF}	LDF intraparticle mass transfer coefficient, s^{-1}
k_p	adsorption isotherm, m^3 kg^{-1}
K	surface-sorbate interaction parameter, MPa^{-1}
K_m	porous material permeability, m^2
L	reactor length, m
L_{inlet}	inlet section length, m
m	pore-size distribution parameter, -
n	Freundlich isotherm parameter, -
nc	monolith channels number, -
p	pressure, Pa
p_c	critical pressure, Pa
p_f	feed pressure, Pa
p_0	saturation pressure, Pa
q_i	species excess amount adsorbed, mol kg^{-1}
q^*	equilibrium amount adsorbed, mol kg^{-1}
q^s	maximum (monolayer) amount adsorbed, mol kg^{-1}
q	conductive heat flux, W m^{-2}
q_0	convective heat flux, W m^{-2}
Q_V	volumetric flow rate, SL min^{-1}
r_i	inner radius of hollow cylinder, m
r_o	outer radius of hollow cylinder, m
R	gas constant, J mol^{-1} K^{-1}
R_{ADS}	adsorption rate expression, mol m^{-3} s^{-1}
t	time, s
t^*	stoichiometric breakthrough time, s
T	temperature*, K*
T_f	feed temperature, K
T_c	critical temperature, K
u	velocity, m s^{-1}
u_f	feed velocity, m s^{-1}
V_0	limiting nanopore volume per mass of sorbent, cm^3 kg^{-1}
w	half of total wall thickness, m
wt	wall thickness per channel, m
y	mole fraction, -

Greek symbols

q	conductive heat flux, W m^{-2}
q_0	convective heat flux, W m^{-2}

Q_V	volumetric flow rate, SL min^{-1}
r_i	inner radius of hollow cylinder, m
r_o	outer radius of hollow cylinder, m
R	gas constant, J mol^{-1} K^{-1}
R_{ADS}	adsorption rate expression, mol m^{-3} s^{-1}
t	time, s
t^*	stoichiometric breakthrough time, s

Abbreviations

CCS	carbon capture and storage
CFD	computational fluid dynamics
GHG	greenhouse gas
K-HTC	potassium promoted hydrotalcite
LDF	linear driving force
MTZ	mass transfer zone
PSA	pressure swing adsorption
SEWGS	sorption-enhanced water-gas shift
SMR	steam methane reforming

References

Bauer T., Guettel R., Roy S., Schubert M., Al-Dahhan M., Lange R., (2005), Modelling and simulation of the monolithic reactor for gas-liquid-solid reactions, *Chemical Engineering Research and Design*, **83**, 811-819.

Bertrand F., Devals C., Vidal D., Préval C.S. de, Hayes R.E., (2012), Towards the simulation of the catalytic monolith converter using discrete channel-scale models, *Catalysis Today*, **188**, 80-86.

Boger T., Heibel A.K., Sorensen C.M., (2004), Monolithic catalysts for the chemical industry, *Industrial & Engineering Chemistry Research*, **43**, 4602-4611.

Boon J., Cobden P.D., van Dijk H.A.J., Hoogland C., van Selow E.R., van Sint Annaland M., (2014), Isotherm model for high-temperature, high-pressure adsorption of CO_2 and H_2O on K-promoted hydrotalcite, *Chemical Engineering Journal*, **248**, 406-414.

Boon J., Cobden P.D., van Dijk H.A.J., van Sint Annaland M., (2015), High-temperature pressure swing adsorption cycle design for sorption-enhanced water-gas shift, *Chemical Engineering Science*, **122**, 219-231.

Chen J., Yang H., Wang N., Ring Z., Dabros T., (2008), Mathematical modeling of monolith catalysts and reactors for gas phase reactions, *Applied Catalysis A: General*, **345**, 1-11.

Coenen K., Gallucci F., Pio G., Cobden P., van Dijk E., Hensen E., van Sint Annaland M., (2017), On the influence of steam on the CO_2 chemisorption capacity of a hydrotalcite-based adsorbent for SEWGS applications, *Chemical Engineering Journal*, **314**, 554-569.

Dai C., Lei Z., Zhang J., Li Y., Chen B., (2013), Monolith catalysts for the alkylation of benzene with propylene, *Chemical Engineering Science*, **100**, 342–351.

Dhanushkodi S.R., Mahinpey N., Wilson M., (2008), Kinetic and 2D reactor modeling for simulation of the catalytic reduction of NO_x in the monolith honeycomb reactor, *Process Safety and Environmental Protection*, **86**, 303–309.

Do D.D., (1998), *Adsorption Analysis: Equilibria and Kinetics*, vol. 2, Imperial College Press, London, UK.

Durán Martínez F.L., Julcour C., Billet A.-M., Larachi F., (2016), Modelling and simulations of a monolith reactor for three-phase hydrogenation reactions - Rules and recommendations for mass transfer analysis, *Catalysis Today*, **273**, 121–130.

Ebner A.D., Reynolds S.P., Ritter J.A., (2006), Understanding the adsorption and desorption behavior of CO_2 on a K-promoted hydrotalcite-like compound (HTlc) through nonequilibrium dynamic isotherms, *Industrial & Engineering Chemistry Research*, **45**, 6387-6392.

Govender S., Friedrich H., (2017), Monoliths: a review of the basics, preparation methods and their relevance to oxidation, *Catalysts*, **7**, 1-29.

Hatch C.D., Wiese J.S., Crane C.C., Harris K.J., Kloss H.G., Baltrusaitis J., (2012), Water adsorption on clay minerals as a function of relative humidity: application of BET and Freundlich adsorption models, *Langmuir*, **28**, 1790-1803.

Heidebrecht P., Pfafferodt M., Sundmacher K., (2011), Multiscale modelling strategy for structured catalytic reactors, *Chemical Engineering Science*, **66**, 4389-4402.

Hufton J.R., Mayorga S., Sircar S., (1999), Sorption-enhanced reaction process for hydrogen production, *AIChE Journal*, **45**, 248-256.

IPCC, (2005), *Carbon Dioxide Capture and Storage*, report, Prepared by Working Group III of the Intergovernmental Panel on Climate Change, Cambridge, England.

IPCC, (2014), *Climate Change 2014: Synthesis Report*, report, Contribution of Working Groups I, II and III to the Fifth Assessment Report of the Intergovernmental Panel on Climate Change, Geneva, Switzerland.

Irani M., Alizadehdakhel A., Pour A.N., Hoseini N., Adinehnia M., (2011), CFD modeling of hydrogen production using steam reforming of methane in monolith reactors: Surface or volume-base reaction model? *International Journal of Hydrogen Energy*, **36**, 15602–15610.

Jang H.M., Lee K.B., Caram H.S., Sircar S., (2012), High-purity hydrogen production through sorption enhanced water gas shift reaction using K_2CO_3-promoted hydrotalcite, *Chemical Engineering Science*, **73**, 431-438.

Le Treut H., Sommerville R., Cubasch U., Ding Y., Mauritzen C., Mokssit A., Peterson T., Prather M., (2007), *Historical Overview of Climate Change Science*, In: *Climate change 2007: the physical science basis. Contribution of Working Group I to the Fourth Assessment Report of the Intergovernmental Panel on Climate Change*, Cambridge University Press, Cambridge, UK and New York, USA, 95-122.

Lee J.M., Min Y.J., Lee K.B., Jeon S.G., Na J.G., Ryu H.J., (2010), Enhancement of CO_2 sorption uptake on hydrotalcite by impregnation with K_2CO_3, *Langmuir*, **26**, 18788-18797.

Lee K.B., Beaver M.G., Caram H.S., Sircar S., (2008), Reversible chemisorbents for carbon dioxide and their potential applications, *Industrial & Engineering Chemistry Research*, **47**, 8048-8062.

Lee K.B., Verdooren A., Caram H.S., Sircar S., (2007), Chemisorption of carbon dioxide on potassium-carbonate-promoted hydrotalcite, *Journal of Colloid and Interface Science*, **308**, 30-39.

Lei Z., Guo Y., Dai C., Zi L., Chen B., (2016), Simulation of hydrodynamic and mass transfer performances in monolith channel, *Catalysis Today*, **276**, 150-160.

Lupše J., Campolo M., Soldati A., (2016), Modelling soot deposition and monolith regeneration for optimal design of automotive DPFs, *Chemical Engineering Science*, **151**, 36-50.

Maroño M., Torreiro Y., Gutierrez L., (2013), Influence of steam partial pressures in the CO_2 capture capacity of K-doped hydrotalcite-based sorbents for their application to SEWGS processes, *International Journal of Greenhouse Gas Control*, **14**, 183-192.

Maroño M., Torreiro Y., Montenegro L., Sánchez J., (2014), Lab-scale tests of different materials for the selection of suitable sorbents for CO_2 capture with H_2 production in IGCC processes, *Fuel*, **116**, 861-870.

McCabe W.L., Smith J.C., Harriott P., (2004), *Unit Operations of Chemical Engineering*, 7th Edition, McGraw-Hill Education, New York, NY.

Pahinkar D.G., Garimella S., (2018), A novel temperature swing adsorption process for natural gas purification: Part I, model development, *Separation and Purification Technology*, **203**, 124-142.

Patton A., Crittenden B.D., Perera S.P., (2004), Use of the linear driving force approximation to guide the design of monolithic adsorbents, *Chemical Engineering Research and Design*, **82**, 999-1009.

Pramanik S., Ravikrishna R.V., (2017), Numerical study of rich catalytic combustion of syngas, *International Journal of Hydrogen Energy*, **42**, 16514-16528.

Reijers H.T.J., Boon J., Elzinga G.D., Cobden P.D., Haije W.G., van den Brink R.W., (2009), Modeling study of the sorption-enhanced reaction process for CO_2 capture. I. Model development and validation, *Industrial & Engineering Chemistry Research*, **48**, 6966-6974.

Reijers H.T.J., Boon J., Elzinga G.D., Cobden P.D., Haije W.G., Van Den Brink R.W., (2009), Modeling study of the sorption-enhanced reaction process for CO_2 capture. II. Application to steam-methane reforming, *Industrial and Engineering Chemistry Research*, **48**, 6975-6982.

Riboldi L., Bolland O., (2017), Overview on pressure swing adsorption (PSA) as CO_2 capture technology: state-of-the-art, limits and potentials, *Energy Procedia*, **114**, 2390-2400.

Rodríguez M.L., Cadús L.E., Borio D.O., (2016), VOCs abatement in adiabatic monolithic reactors: Heat effects, transport limitations and design considerations, *Chemical Engineering Journal*, **306**, 86-98.

Sadeghi F., Tirandazi B., Khalili-Garakani A., Nasseri S., Nabizadeh Nodehi R., Mostoufi N., (2017), Investigating the effect of channel geometry on selective catalytic reduction of NO_x in monolith reactors, *Chemical Engineering Research and Design*, **118**, 21-30.

Seader J.D., Henley E.J., Roper D.K., (2011), *Separation Process Principles. Chemical and Biochemical Operations*, 3rd Edition, Wiley, Hoboken, NJ.

Sharma A.K., Birgersson E., (2016), Validity and scalability of an asymptotically reduced single-channel model for full-size catalytic monolith converters, *Applied Mathematics and Computation*, **281**, 186-198.

Sikander U., Sufian S., Salam M.A., (2017), A review of hydrotalcite based catalysts for hydrogen production systems, *International Journal of Hydrogen Energy*, **42**, 19851-19868.

Tischer S., Deutschmann O., (2005), Recent advances in numerical modeling of catalytic monolith reactors, *Catalysis Today*, **105**, 407-413.

van Selow E.R., Cobden P.D., van den Brink R.W., Hufton J.R., Wright A., (2009), Performance of sorption-enhanced water-gas shift as a pre-combustion CO_2 capture technology, *Energy Procedia*, **1**, 689-696.

van Selow E.R., Cobden P.D., van Dijk H.A.J., Walspurger S., Verbraeken P.A., Jansen D., (2013), Qualification of the ALKASORB sorbent for the sorption-enhanced water-gas shift process, *Energy Procedia*, **37**, 180-189.

van Selow E.R., Cobden P.D., Wright A.D., van den Brink R.W., Jansen D., (2011), Improved sorbent for the sorption-enhanced water-gas shift process, *Energy Procedia*, **4**, 1090-1095.

Voldsund M., Jordal K., Anantharaman R., (2016), Hydrogen production with CO_2 capture, *International Journal of Hydrogen Energy*, **41**, 4969-4992.

Walspurger S., Cobden P.D., Safonova O.V., Wu Y., Anthony E.J., (2010), High CO_2 storage capacity in alkali-promoted hydrotalcite-based material: In situ detection of reversible formation of magnesium carbonate, *Chemistry – A European Journal*, **16**, 12694-12700.

Winter C.J., (2009), Hydrogen energy — abundant, efficient, clean: A debate over the energy-system-of-change, *International Journal of Hydrogen Energy*, **34**, S1-S52.

Wood G.O., (2002), Quantification and application of skew of breakthrough curves for gases and vapors eluting from activated carbon beds, *Carbon*, **40**, 1883–1890.

Wright A.D., White V., Hufton J.R., Quinn R., Cobden P.D., van Selow E.R., (2011), CAESAR: Development of a SEWGS model for IGCC, *Energy Procedia*, **4**, 1147-1154.

Yong Z., Mata V., Rodrigues A.E., (2002), Adsorption of carbon dioxide at high temperature - a review, *Separation and Purification Technology*, **26**, 195-205.

Zheng Y., Shi Y., Li S., Yang Y., Cai N., (2014), Elevated temperature hydrogen/carbon dioxide separation process simulation by integrating elementary reaction model of hydrotalcite adsorbent, *International Journal of Hydrogen Energy*, **39**, 3771-3779.

Zivkovic S., Vukadinovic B., Veljkovic M., (2018), Cleaner and energy efficient production: a case study, *Environmental Engineering and Management Journal*, **17**, 175-188.

Environmental Engineering and Management Journal
February 2020, Vol. 19, No. 2, 219-227
http://www.eemj.icpm.tuiasi.ro/; http://www.eemj.eu

"Gheorghe Asachi" Technical University of Iasi, Romania

PHYSICAL AND CHEMICAL CHARACTERIZATION AND FLORISTIC PECULIARITIES OF A SOIL AFFECTED BY ANTHROPIC ACTIVITIES

Teodora Alexandra Zotica[1], Simona Dumitrița Chirilă[2], Cătălin Bălan[1], Irina Volf[1]*

[1] *"Gheorghe Asachi" Technical University of Iasi, "Cristofor Simionescu" Faculty of Chemical Engineering and Environmental Protection, 73 Prof. D. Mangeron Blvd., 700050, Iasi, Romania*
[2] *"Alexandru Ioan Cuza" University of Iaşi, Faculty of Biology, 20A, Carol I. Blvd., 700505, Iaşi, Romania*

Abstract

In last years, a significant decline in soil quality has occurred due to contamination caused by anthropic activities. These lead to adverse changes in soil physical, chemical and biological attributes and drastically reduce soil fertility. There currently are no generally accepted criteria to evaluate changes in soil quality. This lack impedes the design and evaluation of meaningful soil management programs. This paper examines the principal physical, chemical and biological characteristics that can serve as indicators of a change in soil quality under particular anthropic pollution. The proposed indicators include bulk density/penetration resistance, pH, soil organic matter, nutrient availability, heavy metal concentration and floristic peculiarities in terms of number of species, subspecies and varieties, the presence of different families of vascular plants and categories of life forms. We also discuss the justification for selecting these key attributes and critical concentrations for changes in soil quality. All these data represent inputs for a diagnostic analysis of a polluted area.

Key words: soil quality, pollution, physical and chemical characteristics, floristic elements

Received: February, 2019; Revised final: November, 2019; Accepted: November, 2019; Published in final edited form: February, 2020

1. Introduction

Soil is a natural resource, a basic medium for plant growing and a part of matter and energy circulation in terrestrial ecological systems (Alloway, 2013; Chen et al., 2015; Dedeke et al., 2016; Sobolev and Begonia, 2008; Zhang et al., 2018). Being a largely non-renewable component of ecosystem, soil is very sensitive to industrial pollutants (Tzovolou and Tsakiroglou, 2018). As a component of ecosystem soil might be considered as filter, buffer and transformational component (Palavan-Unsal et al., 2011). Due to the strong internal connectedness in the ecosystem, soil could be a source for pollutants to migrate to atmosphere, water bodies, and organisms (Caeiro et al., 2005; Gay and Korre, 2006; Serafimovski et al., 2018; Silva et al., 2014).

Cause to continuous industrialization and urbanization, the content of soil pollutants has increased rapidly (Liu et al., 2018). Thus, a significant decline in soil quality has occurred through adverse changes in its physical, chemical and biological attributes. Soil monitoring and remediation is therefore a very important component in ecosystems managing (Tănase et al., 2014).

The area of study has a length of 385 m and a width of 202 m and is affected by some anthropic activities such as the proximity of transport infrastructure, accidentally waste disposal and more important by industrial activities. The area is located in the proximity of a thermal power plant operating since 1986 and covering 1.387.574 square meters of land. The power plant converts the chemical energy of solid fuels into thermal and electrical energy by

---

* Author to whom all correspondence should be addressed: e-mail: iwolf@tuiasi.ro

exploiting two 420 t/h steam boilers. Also, intensive but unauthorized grazing was reported in the area.

There currently are no generally accepted criteria to evaluate the soil quality. This lack impedes the design and evaluation of meaningful soil bioremediation programs (Arshad and Coen, 1992).

This paper examines some physical and chemical attributes that can serve as indicators of soil quality. Proposed indicators include soil depth to a root restricting layer, bulk density/penetration resistance, soil organic matter, nutrient availability/retention capacity, pH, heavy metal concentration and floristic peculiarities in terms of number of species, subspecies and varieties, the presence of different families of vascular plants, categories of life forms, floristic elements, ecological preferences and economic value of species. We also discuss the justification for selecting these key attributes, critical concentrations for changes in soil quality. All these data represent inputs for a diagnostic analysis of the polluted area in order to design an ecological restoration plan.

2. Material and methods

2.1. The study area

The selected study area is located in Holboca village (47°09'02.6" N - 27°42'51.5" E), at approximately 10 km outside Iasi district, Romania (Fig. 1).

The inventory at the operation site covers the inputs and outputs for the generation of steam energy in the entire life of the boiler. The data of inputs, i.e. boiler, water, electricity and wood chips are obtained from the textile manufacturer in Thailand and calculated from boiler efficiency. The transportation of wood chips and boiler to the operation plant are also included. The installation and maintenance of the boiler are excluded because the detailed data of these steps are not available and their burdens are insignificant compared to the total burden of whole life time of the boiler (Beccali et al., 2012). The emissions from biomass combustion are calculated using emission factors reported by IPCC (2006) and EEA (2013).

Emission of CO_2 from the combustion process is excluded according to a carbon neutral rule. The functional unit of 1 MJ of steam energy is used at the operation stage. The input and output for 1 MJ of steam energy production, shown in Table 2, are calculated based on the total energy produced, the input used and the output released through the entire life of the boiler. While the energy of 43,441,110 MJ is produced through the entire life of the new boilers, the energy of 24,815,700 and 28,960,740 MJ is produced through the entire life of the recycled boilers, having the efficiency 60 and 70%, respectively. Since the recycled boiler generates less steam energy in its entire life, the amount of boiler needed is larger per unit of steam.

The inventories for the production of raw materials, water and waste management are obtained from the database in SimaPro 7.3.3 software, such as the database of Ecoinvent 2.0, ELCD 2.0. For example, “steel hot rolled coil” in ELCD 2.0 database is used for the steel plate, grade ss400 applied in the boiler construction.

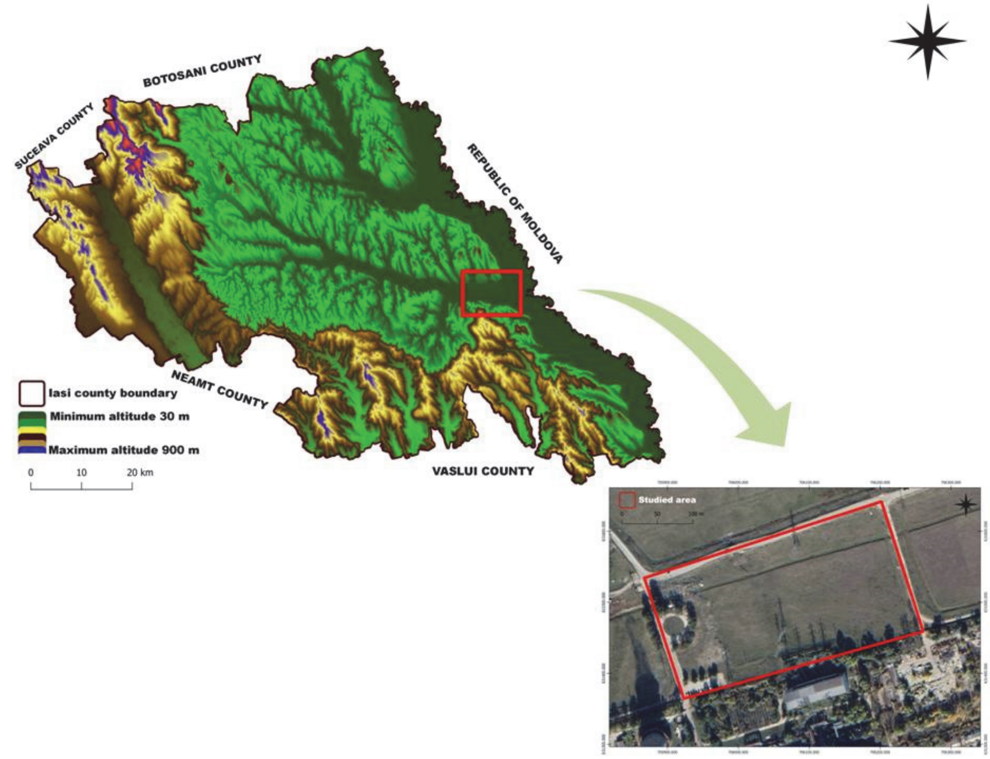

Fig. 1. Location of study area

2.2. Sampling, processing and analysis

The sampling points were set taking into account the pollution sources and were chosen at different distances from the thermal power plant, in all directions of wind. The study focused on 15 sampling points and the samples were collected within an 80 m grid (Fig. 2). The raster method was used as a research tool for soil sampling. A raster contains data points equally spaced from each other (Goodchild, 1992) and is commonly used in digital soil mapping (McBratney and Minasny, 2003). All the maps in this work were realized using ArcGis 10.2.1 (Geographic Information System).

Soil samples were collected in 2018 on March 30, and for each sampling point two samples were taken: one surface sample (after eliminating the vegetation) - 0 cm and one depth sample - 25 cm. For all physical and chemical tests soil samples were pre-treated according SR ISO 11464 (1998) standard. The samples have undergone certain steps of cleaning, drying, grinding, sieving and homogenization and were subsequently stored at 20°C, in a room free of dampness, solar radiation and airflow.

Soil pH was measured according to SR ISO 10390 (2015) and volumetric density determinations were followed the SR ISO 39231 (2008) standard. For soil humus determinations the Walkley-Black (Tiurin) method was used (Abraham, 2013) and soil organic carbon was calculated based on the percentage average carbon content in humus (Lăcătuşu et al., 2011).

To evaluate the concentration of heavy metals such Cd, Cu, Fe, Pb and Zn, the soil samples were digested by a mixture of HNO_3 (65 %, analytical grade, Merck), HCl (35% analytical grade, Merck) and deionized water (4/12/5) (v/v/v) at 150ºC for 7 hours. Samples and blank digestions were performed in triplicate. After digestion, solutions were filtered, using cellulose acetate membranes (Sartorius Stedim, porosity 0.45 mm), and metal concentrations were measured using a GBS Avanta atomic absorption spectrometer, following SR ISO 11047:1999 method.

2.3. Vascular flora analysis

The vascular flora of the area was studied during the optimal vegetation period in 2018, from March to November, using the line transect method (Buckland et al., 2007). The voucher collected served as a study material and subsequently determined in laboratory conditions. In order to organise the information and to establish the floral elements bio-forms the comparative-morphological methods were used (Ciocârlan, 2000; Ellenberg, 1974; Sanda et al., 1983; Sârbu et al., 2001). Regarding the systematic classification of taxa, the phylogenetic system implemented by Pop and collaborators (1983) was adopted.

3. Results and discussions

3.1. *Study area characterization*

The climate area is continental, with a mean annual temperature of 9ºC. The multi-annual average cold season temperature is around -1ºC and during the warm season the average is approximately 21ºC. The average temperature during the vegetation season is 14-15° C. Multiannual average rainfall is around 500-550 mm per year. The most frequent winds blow in the north-west and south-east directions, generally winds of low intensity, with an average annual speed of 6 m/s.

Fig. 2. Distribution of the sampling points in the study area

3.2. Characterization of soil: physical and chemical attributes

The type of soil identified in area is Solonthes, on recent fluvial and fluvial-lake deposits. This type of soil is part of the Salsodisols class (SAL), the Solonite (SN) type having a loamy texture, and a strong to very strong casting. These types of soils are formed under the influence of salts such as $NaHCO_3$, Na_2CO_3, Na_2SiO_3 and $MgCO_3$, but also neutral salts (Na_2SO_4, NaCl) and they are conditioned by the groundwater and poor drainage conditions. Specific to this type of soil is halophilous vegetation and the presence of the nitric horizon, often associated with a humus-rich surface horizon and underlying salinized horizons.

The color of the soil is from brown to black and the structure is large, prismatic or even massive. The dominant physical characteristics of this type of soil are the weak structure stability, waterproofing under wet conditions and the strengthening of the matric dry horizon. For chemical characterization the proposed indicators include pH, bulk density/penetration resistance, total soil organic matter, nutrient availability/retention capacity, and heavy metal concentration.

Soil pH is one of the main soil properties to maintain an active concentration of hydrogen ions in soil solutions. It is determined by the nature of soil, by biological and chemical processes occurring in soil such decomposition (Bååth et al., 1980), mineralization (Aciego Pietri and Brokes, 2008) and respiration (Högberg et al., 2007). Likewise, metal availability and speciation, physiological and ecological pH thresholds and tolerance ranges, availability of nutrients and metal toxicity/availability are influenced by pH (Nielsen et al., 2017; Sauve et al., 2000).

In the study area the pH values decreased with depth increasing. In most of the sampling points the pH are over 8 describing an alkalinized soil (Fig. 3 and Fig. 4). In the charts, each column corresponds to the sampling points identified in Fig. 2. The bulk density values are closely correlated with penetration resistance or degree of soil compaction. These values can oscillate frequently between 1-2 g/cm³, being smaller in humus-rich and well-structured soils.

For all soil samples the bulk density values were between 0.954 and 1.104 g/cm^3 for higher horizons and between 0.966 and 1.140 g/cm^3 for depth ones (Fig. 5 and Fig. 6). Lower densities were recorded in higher horizons where the compression is lower. The concentration of heavy metal ions was assessed in surface samples in P3, P8 and P13 sampling point at different distances from the thermal power plant (Table 1). The results reported represent the average values of triplicate determinations (Table 2). The normal content of cadmium in soils is 1 mg/kg, the alert limit for sensitive uses is 3 mg/kg, and the intervention one is 5 mg/kg (Order 756, 1997). For P13 and P8 sampling point (located at the nearest distance from slag and ash storage yard and from the flue gas stack) the cadmium concentration average values are 1 mg/kg or exceed the normal concentration.

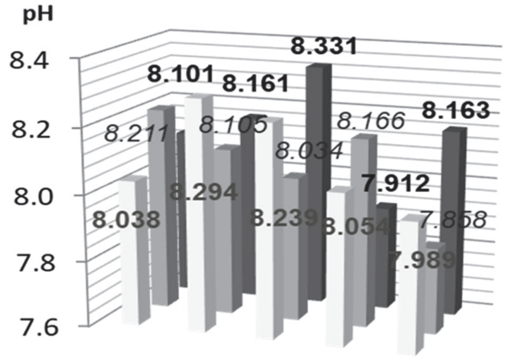

Fig. 3. pH values - Surface samples (0 cm)

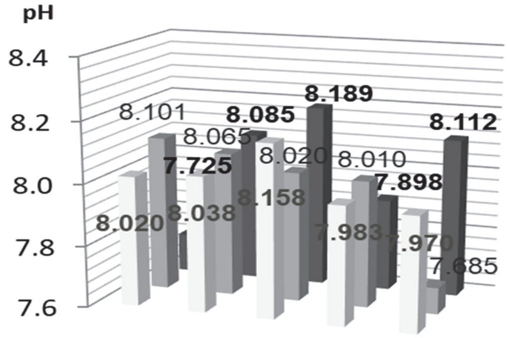

Fig. 4. pH values – Depth samples (25 cm)

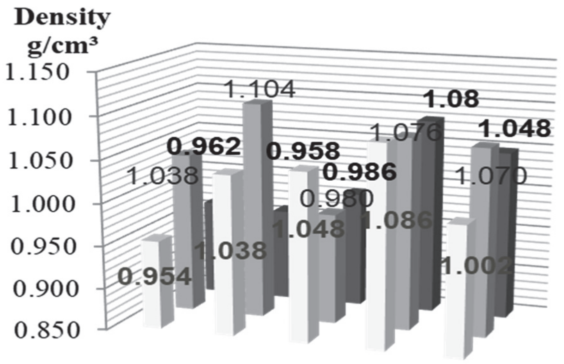

Fig. 5. Volumetric density (g/cm³) –
Surface samples (0 cm)

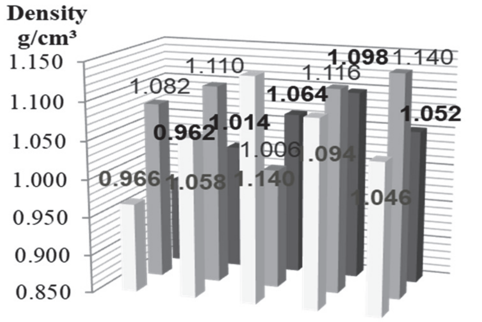

Fig. 6. Volumetric density (g/cm³) - Depth samples (25cm)

Table 1. Location of soil sampling points

Soil sample	*Location of soil sampling points*
P3	360m from the flue gas stack and 760 m from the slag and ash disposal
P8	280m from the flue gas stack and 680 m from the slag and ash disposal
P13	200m from the flue gas stack and 600 m from the slag and ash disposal

Table 2. Concentration of heavy metals in soil samples (mg/kg dry substance)

Sample	*Cadmium ions concentration (mg/kg)*	*Copper ions concentration (mg/kg)*	*Iron ions concentration (mg/kg)*	*Lead ions concentration (mg/kg)*	*Zinc ions concentration (mg/kg)*
P3	0.75	38.875	24834	68	83.75
P8	1	42.75	31904	89.25	92.125
P13	1.125	37.125	25582	94.61	81.75

Copper has an average content in soils of 20 mg/kg, an alert limit for sensitive uses of 100 mg/kg and an intervention limit of 200 mg/kg. Therefore, on all sampling points there were excesses of the average value. The highest concentration for copper recorded was 42.75 mg/kg.

The concentrations of lead ions in soil have an average of 20 mg/kg, an alert limit of 50 mg/g and an intervention limit of 100 mg/kg. The content of lead ions has decreased with the distance to the flue gas stack. However, the concentrations exceed the limit alert being very close to the intervention limit. High concentration of potentially mobile Pb(II) and Cu(II) in soil run the risk of their downward migration and possible contamination of groundwater (Tănase, 2014). Iron concentration for all soil samples was appeared to be higher than Fe(III) critical level.

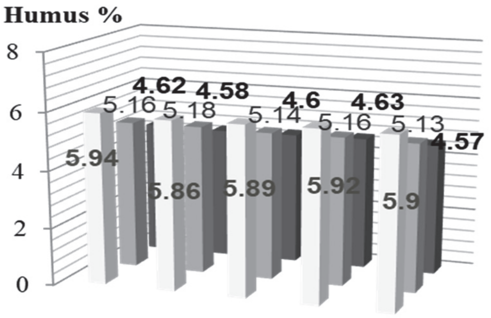

Fig. 7. Soil humus content

Humus and soil organic carbon content are excellent indicators for evaluating ecosystem's functioning efficiency. The soils, which have under 2% humus content, are the arable land. The water erosion has in this case a major negative impact where the first shifting material is the organic matter. On the arable land the values of humus % do not show considerable fluctuation contrary the grassland. On the grassland the humus content shows high heterogenity, having higher humus content values as a result of the smaller disturbance and the persistence of the vegetal ground cover (Fehér et al., 2016). The soil organic carbon and humus content in the study area fits into the limits of high and medium textured soils, with values of SOC % in the range 2.596 - 3.56 and humus % between 4.57 – 5.94 (Fig.7 and Fig. 8).

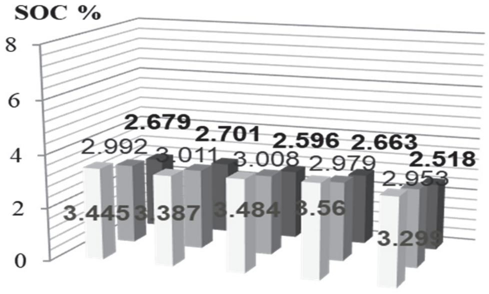

Fig. 8. Soil organic carbon content

3.3. Vascular flora assessment

The list of the vascular flora identified in studied area contains 123 taxa, who belong to 78 genres and 28 botanical families. The largest share belongs to the families: Compositae (18 species), Poaceae (14 species), Fabaceae (9 species), Lamiaceae (6 species), Rosaceae (5 species), Brassicaceae, Cyperaceae (4 species). These 7 families comprise 60 species, totalizing for 65.21% of all species reported. The other 21 families identified in our study area are represented by 1-3 plant species (Table 3). The spatial distribution of botanical families in the study area are highlighted in Fig. 9. The largest majority of the plants are distributed as far away as possible from the anthropic activities.

Life forms analysis

The analysis of bioforms reveal the high share of the hemicryptophytes (H) (44 species), which represents 47.82% of the total (Table 4). The next category is represented by the terophytes (T) 14.13%. The relatively high percentage of annual or biennial therophytes reflects a high degree of anthropization of vegetation in the area. Hemitherophytes (Ht) represent 13.04% of the total number of species in the area. The significant percentage of hemiterophites could be explained by the milder winters in this area.

Geophytes (G) have also an important representation. These mainly gather the prevernal and vernal species and less aestival species, all of these having different resistance and propagation underground organs, as an adaptation of short vegetation periods or to maintain optimal ecological conditions for a limited period of time (hibernal season). Very low percentage have the hydrohelophytes (HH) represented by only one species (1.08%). In order to assess the anthropic influence the flora altitudinal index (Pop and Drăgulescu, 1983) was calculated and additional information about the climate, the vegetation layers, and the intensity of the anthropic pressure were obtained. This index can be calculated by Eq. (1):

$$K = T / H \times 100 \qquad (1)$$

where: K – is flora altitudinal index, T – therophytes percentage, H – hemicryptophytes number.

For the studied area the K index is 70,83%. The value is included in 51-90% range highlighting a significant anthropic impact in the area.

Table 3. Numeric distribution of vascular flora in study area

Magnoliophyta/Magnoliatae						
No. crt.	***Family***	***Genus***	***Species***	***Subspecies***	***Variety***	**Total**
1.	**Apiaceae lindl.**	2	2	-	-	2
2.	**Boraginaceae juss.**	3	3	-	-	3
3.	**Brassicaceae burnett**	4	4	1	-	5
4.	**Caryophyllaceae juss.**	1	1		-	1
5.	**Chenopodiaceae vent.**	1	1	1	1	3
6.	**Compositae giseke**	15	18	7	-	25
7.	**Convolvulaceae juss.**	1	1	-	-	1
8.	**Dipsacaceae juss.**	1	1	-	-	1
9.	**Euphorbiaceae juss.**	1	1	-	-	1
10.	**Fabaceae lindl.**	7	9	4	1	14
11.	**Geraniaceae juss.**	1	1	-	-	1
12.	**Lamiaceae lindl.**	5	6	2	-	8
13.	**Lythraceae j. St.-hil.**	1	1	-	-	1
14.	**Malvaceae juss.**	1	1	1	-	2
15.	**Plantaginaceae juss.**	3	3	1	-	4
16.	**Polygonaceae juss.**	3	3	-	-	3
17.	**Ranunculaceae juss.**	2	3	2	-	5
18.	**Rosaceae**	3	5	2	-	7
19	**Scrophulariaceae juss.**	1	1	-	-	1
20.	**Rubiaceae juss.**	1	2	-	-	2
21.	**Ulmaceae mirb.**	1	1	-	-	1
22.	**Urticaceae juss.**	1	1	1	-	2
23.	**Verbenaceae**	1	1	-	-	1
Total	**23**	**60**	**70**	**22**	**2**	**94**
Magnoliophyta/Liliatae						
No. crt.	***Family***	***Genus***	***Species***	***Subspecies***	***Variety***	**Total**
1.	**Alismaceae vent.**	1	1	-	-	1
2.	**Cyperaceae juss.**	3	4	1	-	5
3.	**Juncaceae**	1	1	-	-	1
4.	**Poaceae barnhart**	12	14	6	1	21
5.	**Typhaceae juss.**	1	1	-	-	1
Total	**5**	**18**	**21**	**7**	**1**	**29**

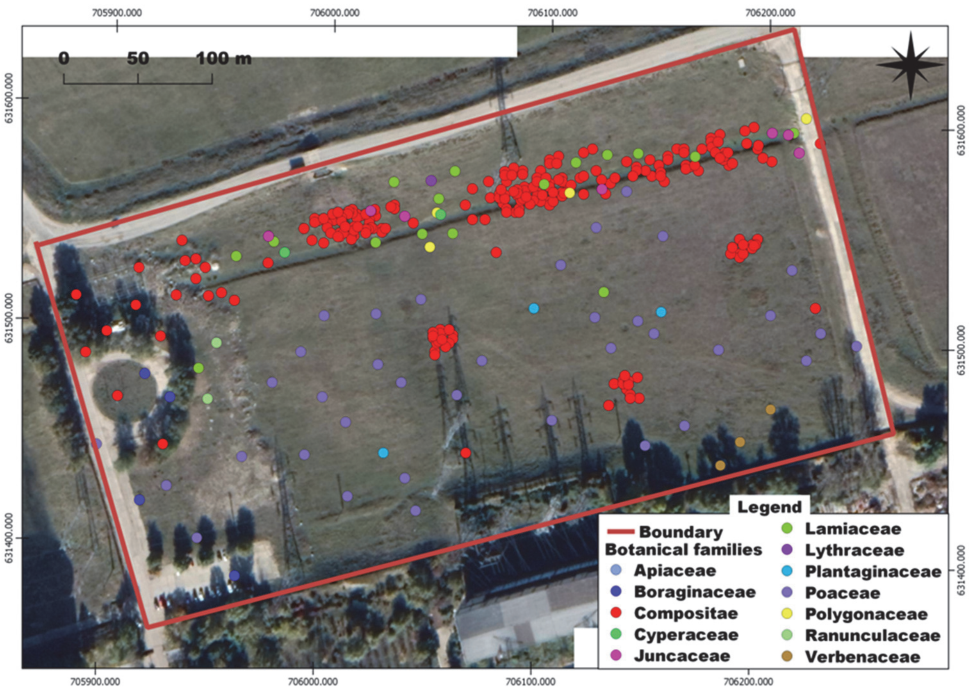

Fig. 9. Spatial distribution of botanical families in study area

Table 4. Statistical analysis of the life forms

Life form		*No. of. species*	*% per categories*	*% from total*
H.	Hemicryptophytes	44	91.66	47.82
	Hemicryptophytes (Geophytes)	3	6.25	3.26
	Hemicryptophytes (Hydrohelophytes)	1	2.08	1.08
	Total H	48	100	52.16
HH.	Hydrohelophytes	1	100	1.08
Ht.	Hemitherophytes	12	80	13.04
	Hemiterophites – Hemicryptophytes	3	20	3.26
	Total Ht	15	100	16.30
G.	Geophytes	2	33.33	2.17
	Geophytes (Hydrohelophytes)	3	50	3.26
	(Geophytes) Hemicryptophytes	1	16.66	1.08
	Total G	6	100	6.51
Ph.	Phanerophytes	3	100	3.26
T.	Therophytes	13	68.42	14.13
	Therophytes - TH.	1	5.26	1.08
	Therophytes – Hemitherophytes	5	26.31	5.43
	Total T	19	100	20.64

4. Conclusions

A soil affected by anthropic activities was chose for a diagnostic analysis and the following effects were observed:

The climate area is continental, with a mean annual temperature of 9ºC. The type of soil identified in area is Solonthes, on recent fluvial and fluvial-lake deposits.

The high pH values, in most of the cases over 8, describe an alkalinized soil; pH values decreased with depth increasing. Volumetric density values are a little higher on the depth samples than the surface ones but still in normal limits. The soil organic carbon and humus contents set out the soil fits into the limits of high and medium textured soils. Concerning the heavy metal ions concentration, the soil exceeded the average for cadmium and copper.

For lead, the concentrations exceeded the limit alert, being very close to the intervention limit and the iron content was higher than the critical level.

The vegetation is composed of halophilous plants; the spatial distribution of botanical families is dominated by *Compositae, Fabaceae, Lamiaceae* and *Rosaceae*. Regarding the statistical analysis of the life forms, the study area belongs to the hemicryptophytes (H) with (44 species), which has the highest dominance and generally characterizes a high degree of anthropization.

All data conclude in the studied area an ecological restoration plan have to be design and implemented in order to mitigate the anthropic effects on ecosystem.

Acknowledgements
This work was supported by a grant of the Romanian National Authority for Scientific Research, CNCS – UEFISCDI, project number PN-III-P4-ID-PCE-2016-0683, Contract no. 65/2017.

References

Abraham J., (2013), Organic carbon estimations in soils: analytical protocols and their implications, *Rubber Science,* **26**, 45-54.

Aciego Pietri J.C., Brokes P.C., (2008), Nitrogen mineralisation along a pH gradient of a silty loam UK soil, *Soil Biology & Biochemistry*, **40**, 797-802.

Alloway B.J., (2013), *Sources of Heavy Metals and Metalloids in Soils. Heavy Metals in Soils*, Springer, Netherlands, 11-50.

Arshad M.A., Coen G.M., (1992), Characterization of soil quality: Physical and chemical criteria, *American Journal of Alternative Agriculture*, **7**, 25-31.

Bååth E., Berg B., Lohm U., Lundgren B., Lundkvist H., Rosswall T., Sodermstorm B., Wiren A., (1980), Effects of experimental acidification and liming on soil organisms and decomposition in a Scots pine forest, *Pedobiologia*, **20**, 85-100.

Buckland S.T., Borchers D.L., Johnston A., Henrys P.A., Marques T.A., (2007), Line transect methods for plant surveys, *Biometrics*, **63**, 989-998.

Caeiro S., Costa M.N., Ramos T.B., Fernandes S., Silveira N., (2005), Assessing heavy metal contamination in Sado Estuarysediment: an index analysis approach, *Ecological Indicators*, **5**, 151-169.

Chen H., Teng Y., Lu S., Wang Y., Wang J., (2015), Contamination features and health risk of soil heavy metals in China, *Science of the Total Environment*, **512**, 143-153.

Ciocârlan V., (2000), *The Illustrated Flora of Romania. Pteridophyta et Spermatophyta* (in Romanian), Ceres Publishing House, Bucharest, Romania.

Dedeke G.A., Owagboriaye F.O., Adebambo A.O., Ademolu K. O., (2016), Earthworm metallothionein production as biomarker of heavy metal pollution in abattoir soil, *Applied Soil Ecology*, **104**, 42-47.

Ellenberg H., (1974), Indicator values of vascular plants in Central Europe, *Scripta Geobotanica*, **9**, Verlag Erich Goltze KG, Göttingen.

Fehér Á., Szabó B., Katona K., Pósa P., Centeri C., (2016), *Effects of Soil Structure, Nutrient Availability and Humus Content on Vegetation Dynamics in a Turkey Oak-Sessile Oak Forest*, 15th Alps-Adria Scientific Workshop Hungary, 231-234.

Gay J.R., Korre A., (2006), A spatially evaluated-methodology for assessing risk to a population from contaminated land, *Environmental Pollution*, **142**, 227-234.

Goodchild M., (1992), Geographical data modelling, *Computers and Geosciences*, **18**, 401-408.

Högberg M.N., Högberg P., Myrold D.D., (2007), Is microbial community composition in boreal forest soils determined by pH, C-to-N ratio, the trees, or all three? *Oecologia*, **150**, 590-601.

Lăcătuşu R., Rizea N., Ştefănescu D., Tănase V., Vrînceanu N., Preda M., Lăcătuşu A., Matei M., Matei S., (2011), *Methods of Chemical and Microbiological Analysis*, Sitech Press, Craiova.

Liu J., Zhang Y., Wang H., Du Y., (2018), Study on prediction of soil heavy metal elements content based on visible near-infrared spectroscopy, *Spectrochimica Acta Part A: Molecular and Biomolecular Spectroscopy*, **199**, 42-49.

McBratney A.B., Mendonça Santos M.L., Minasny B., (2003), On digital soil mapping, *Geoderma*, **117**, 3-52.

Nielsen K.E., Irizar A., Nielsen L.P., Kristiansen S.M., Damgaard C., Holmstrup M., Petersen A.R., Strandberg M., (2017), In situ measurements reveal extremely low pH in soil, *Soil Biology & Biochemistry*, **115**, 63-65.

Order 756, (1997), Order MAPPM no. 756 of November 3, 1997 for the approval of the regulation regarding the assessment of environmental pollution, *Romanian Official Monitor*, no. 303 bis, 6 November 1997.

Palavan-Unsal N., Kefeli V., Blum W., (2011), *Mechanisms of Landscape Rehabilitation and Sustainability*, Bentham Press, DOI: 10.2174/97816080516871110101.

Pop I., Drăgulescu C., (1983), Altitude distribution of cormophytes on the Valea Sadului (Cindrel Mountains), *Studia Universitatis Babeş-Bolyai*, **28**, 3-8.

Sanda V., Popescu A., Dolţu M.I., Doiniţă N., (1983), Ecological and phytocenological characterization of spontaneous species in Romanian flora, *Studies and Communications, Brukenthal National Museum*, Sibiu, Romania.

Sauve S., Hendershot W., Allen H.E., (2000), Solid-solution partitioning of metals in contamined soils: dependence on pH, total metal burden, and organic matter, *Environmental Science and Technology*, **34**, 1125-1131.

Sârbu D., Ivănescu L., Ştefan N., (2001), *Illustrated Flora of Vascular Plants from Eastern Romania: Determinator,* (in Romanian), vol. I., Alexandru Ioan Cuza University Publishing House, Iasi, Romania.

Serafimovski T., Stafilov T., Tasev G., (2018), Soil metal pollution related to active Buchim copper mine, Republic of Macedonia, *Environmental Engineering and Management Journal*, **17**, 2597-2608.

Silva V., Loredo J., Fernandez-Martinez R., Larios R., Ordonez A., Gomez B., Rucandio I., (2014), Arsenic partitioning among particle-size fractions of mine wastes and stream sediments from cinnabar mining districts, *Environmental Geochemistry and Health*, **36**, 831-843.

Sobolev D., Begonia M., (2008), Effects of heavy metal contamination upon soil microbes: lead-induced changes in general and denitrifying microbial communities as evidenced by molecular markers, *International Journal of Environmental Research and Public Health,* **5**, 450-456.

SR ISO 10390, (2015), *Soil quality - Determination of pH.*

SR ISO 11047, (1999), *Soil quality - Determination of cadmium, chromium, cobalt, copper, lead, manganese, nickel and zinc*, Flame and electrothermal atomic absorption spectrometric methods.

SR ISO 11464, (1998), *Soil quality - Pretreatment of samples for physico-chemical analyses*.

SR ISO 39231, (2008), *Soil quality – Determination of density*.

Tănase C., Volf I., Popa V.I., (2014), Enhancing copper and lead bioaccumulation in rapeseed by adding hemp shives as soil natural amendments, *Journal of Environmental Engineering and Landscape Management*, **22**, 245–253.

Tzovolou D.N., Tsakiroglou C.D., (2018), Experimental study of in situ remediation of low permeability soils by bioventing, *Environmental Engineering and Management Journal*, **17**, 2645-2656.

Zhang P., Qin C., Hong X., Kang G., Qin M., Yang D., Pang B., Li Y., He J., Dick R.P., (2018), Risk assessment and source analysis of soil heavy metal pollution from lower reaches of Yellow River irrigation in China, *Science of the Total Environment*, **633**, 1136-1147.

Environmental Engineering and Management Journal
February 2020, Vol. 19, No.2, 229-234
http://www.eemj.icpm.tuiasi.ro/; http://www.eemj.eu

"Gheorghe Asachi" Technical University of Iasi, Romania

STUDY OF VOLATILE COMPOUNDS OF ROMANIAN RED WINES AGED WITH OAK CHIPS

Georgiana-Diana Dumitriu Gabur[1], Carmen Teodosiu[1]*, Valeriu V. Cotea[2], Rafael Andres Peinado[3], Iulian Gabur[4], Nieves Lopez de Lerma[3]

[1]"Gheorghe Asachi" Technical University of Iasi, Romania, "Cristofor Simionescu" Faculty of Chemical Engineering and Environmental Protection, Department of Environmental Engineering and Management, 73 Prof. D. Mangeron Blvd., 700050 Iasi, Romania
[2]University of Agricultural Sciences and Veterinary Medicine "Ion Ionescu de la Brad" Iasi, Romania Department of Viticulture and Oenology, 3 Mihail Sadoveanu Alley, 700490, Iași, Romania
[3]University of Córdoba, Spain, Department of Agricultural Chemistry, Agrifood Campus of International Excellence ceiA3, Campus de Rabanales, Edificio Marie Curie, 14071, Córdoba, Spain
[4]University of Agricultural Sciences and Veterinary Medicine "Ion Ionescu de la Brad" Iasi, Romania Department of Plant Sciences, 3 Mihail Sadoveanu Alley, 700490, Iași, Romania

Abstract

Wine aroma plays an essential role and can be considered one of the most important attributes of the overall wine quality. Generally, aroma is a remarkable complex chemical matrix comprising compounds from various chemical classes (alcohols, esters, acids, aldehydes, lactones, phenols, terpenes, ketones, norisoprenoids, etc.). Although some studies tackle wine aroma in general, the chemical changes attributed to wine aroma during the ageing process are still poorly understood.

In this study, the profiles of minor volatile compounds of wine obtained from *Fetească neagră* grape variety, aged for 1.5 and 3 months by using stir bars sorptive extraction and gas chromatography coupled to mass spectrometry (SBSE-GS-MS) were investigated. Red wines were aged using medium toast oak wood chips with the following dimension 0.5 × 1.5 × 0.2 cm (width × length × thickness). The analysis identified 20 minor volatile compounds in samples. These compounds belong to four major chemical groups, namely esters, volatile phenols, carbonilics and oak compounds. Samples aged for 3 months registered an increase, when compared to 1.5 months samples, for all identified and quantified compounds. However, heptanal and octanal concentrations decreased. Principal components analysis of the minor volatile compounds differentiated wines according to their ageing time. The first principal components (PC1) explained 78.80% and PC2 14.03% of the total variance. Sensory profile of Fetească neagră aged with oak chips was characterized by high notes of woody, toasty, vanilla, smoky and cacao and an attenuation of ripe fruit and herbaceous attributes.

Key words: oak chips, red wines, SBSE-GC-MS analysis, volatile compounds

Received: January, 2019; Revised final: November, 2019; Accepted: November, 2019; Published in final edited form: February, 2020

1. Introduction

Since the end of last century, innovation in winemaking allowed the development of alternative methods as ageing by using oak wood, especially in red wine production. Traditionally, wine ageing was performed in oak barrels. This represents an essential stage to produce high quality wines. However, the use of barrels requires long periods of wood-wine contact time, is not cost efficient, and is limited by their lifetime (5-6 years). Moreover, barrels cleaning is particularly challenging as undesirable microorganism such as *Brettanomyces* and *Dekkera* may cause severe contaminations and negative environmental impacts.

---

* Author to whom all correspondence should be addressed: e-mail: cteo@tuiasi.ro

The combined effect of the mentioned drawbacks makes traditional ageing systems very laborious, costly and environmental unfriendly due to the enormous volume of trees required for the barrels (Garde-Cerdán and Ancín Azpilicueta, 2006).

Alternative techniques, such as oak wood chips, offer a promising solution to traditional barrel ageing. Nowadays, oak chips have become a common winemaking practice in the world. Oak chips are cost efficient and produce chemical and sensory properties similar to wines produced in barrels (Dumitriu et al., 2016, 2017, 2019; García Carpintero et al., 2014; Wilker and Gallander, 1988). Wines aged with oak chips are known to present a deeper colour and higher levels of volatile oak extraction (Del Álamo Sanza et al., 2004).

The ageing process may cause losses of fruit and floral aromas characteristic to young wines and produce new “ageing” aromas (Petrozziello et al., 2018). Aged young red wines are described to contain notes attributed to “red fruit”- red and black currant, cherry, “floral” - rose, violet, “nutty” - almond, hazelnut, “sweet” - caramel, honey, “balsamic” and “resinous” - pine, eucalyptus aromas (Rogerson et al., 2001). Additionally, wines have rich flavors of blackcurrants and intense aromas of dried prunes. At the end of the ageing period, wines could be described as having deep flavors of intense fruit and mellow spices, with just a hint of pepper and cloves from the oak chips. Overall, wine aroma can be considered a crucial attribute of wine quality, playing a vital role in consumer selection and preferences. Generally, wine aroma is a remarkable complex chemical matrix where compounds from all chemical classes interact and provides to wine specificity and typicity. Nevertheless, the effect of the ageing process on wine aroma is poorly understood and needs comprehensive studies to be elucidated.

Fetească neagră vine variety is one of the oldest Romanian varieties, whose origin is indisputable. This variety appeared through popular selection made in time by local winemakers, from the wild forest vine (*Vitis silvestris*) which was cultivated by the Dacian peoples in the area between the Carpathians and the Nistru River. According to OIV, in Romania, in 2015, *Fetească neagră* was cultivated only in Romania on 2845 ha (OIV, 2015).

In this study we investigated the profiles of minor volatile compounds of *Fetească neagră* wines, aged for 1.5 and 3 months, with medium toast degree by using stir bars sorptive extraction and gas chromatography coupled to mass spectrometry (SBSE-GS-MS).

2. Material and methods

2.1. Winemaking protocol

Wine was obtained from a red single-variety (cv. *Fetească neagră, V. vinifera*) processed on a pilot scale in a cellar of Department of Viticulture and Oenology, University of Agricultural Sciences and Veterinary Medicine “Ion Ionescu de la Brad” Iași, Romania.

The maceration-fermentation process was made at 10-12°C for 7 days. Then, the grape skins were pressed to extract the remaining juice. The pressed wine was blended with the free run wine, and the mixture was pumped off into stainless steel tanks to complete alcoholic and malolactic fermentations. The wine obtained was divided and placed in glass vessels. The wines were aged with oak wood chips for 1.5 and 3 months. Wood species used in this experiment are *Quercus petraea*, from France. The dimension chips in centimeters were 0.5 × 1.5 × 0.2 (width × length × thickness). The chemical parameters of the initial wines were: total acidity, as tartaric acid, 5.82 g/L, pH 3.69, volatile acidity, as acetic acid, 0.52 g/L, and alcoholic strength by volume, 14.95 % v/v.

2.2. Minor volatile compounds

Aroma extraction was determined according to Tredoux et al. (2008) with minor changes. Stir bars (0.5 - mm film thickness, 10 - mm length, Gerstel GmbH, Mülheim an der Ruhr, Germany) coated with PDMS were used. The wine samples were diluted tenfold with a hydroethanolic solution (12% ethanol (v/v) and pH 3.5).

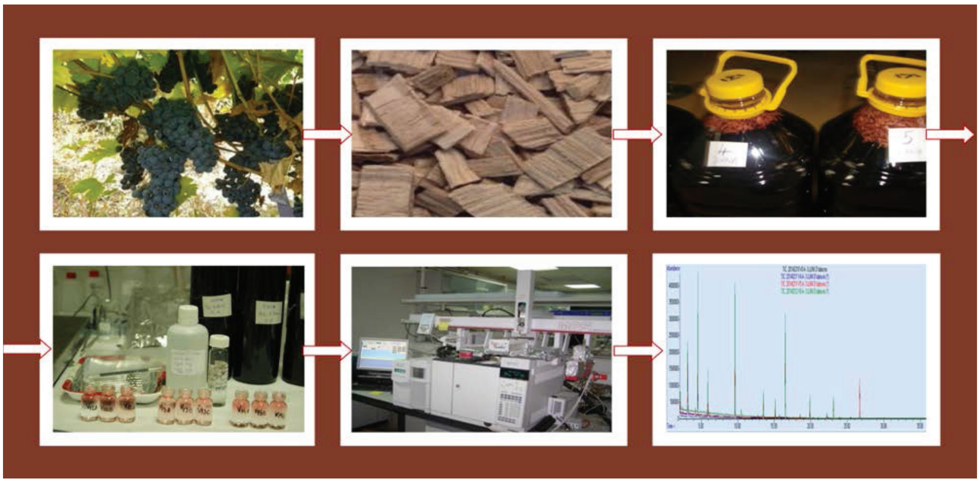

Fig. 1. Experimental design of identification and quantification of minor aroma compounds

The stir bars were placed in a 10 mL glass headspace vials containing 10 mL of the diluted sample and 0.1 mL of ethyl nonanoate (0.4464 mg/L) as internal standard. The vials were sealed with a Teflon-coated crimp cap and they were stirred at 1500 rpm at 25 ºC for 100 min. After removal from the wine samples, the stir bars were softly dried with lint-free tissues and then transferred into the glass thermal desorption tubes for GC/MS analysis.

The glass thermal desorption tubes were introduced into a GC/MS equipped with a Gerstel TDS 2 thermo desorption system. The stir bars were heated to release and transfer the extracts into a cooled injection system/programmed temperature vaporizer (CIS 4 PTV) containing a tenax adsorption tube. Retention times, spectral libraries supplied by Wiley (version 7 N) and pure chemical compounds from Merck, Sigma-Aldrich, Riedel de Haen, and Fluka were used for identification, confirmation and preparation of standard solutions of the volatile compounds.

Each compound was quantified from its calibration curve, which was obtained by using standard solutions of known concentrations previously subjected to the same treatment as the samples in conjunction with the target and qualifier ions selected for each compound by the Hewlett Packard Chemstation (Palo Alto, CA).

2.3. Sensory analysis

Wine samples underwent a panel sensory analysis in order to determine the influence of ageing with oak chips on the organoleptic characteristics. The samples were in cold storage for a period of time and transferred to room temperature (20ºC) two hours before the sensory analysis.

Nine wide and well-defined tasting places were set up. Sensory testing panel was composed of 15 tasters. Before starting the analysis, the test objective and methodology were explained in details. Samples were coded by using a key consisting of three randomly select letters, keys being different for each sample.

Analysis targeted the following specific aroma descriptors: ripe fruit, woody, toasty, smoky, vanilla, cacao and licorice. Tasters were instructed to give a score of 1 to 5 (1-detectable, 2-weak perceptible, 3-moderate perceptible, 4-strong perceptible and 5-very perceptible) in increasing order of perceived intensity to each aroma descriptor.

2.4. Statistical analysis

Statistical data analyses were performed by using Statgraphics Centurion XVI of StatPoint Technologies Inc. (Warrenton, Virginia). Principal Component Analysis was carried out to analyze the relationship between the parameters analyzed and the different time periods used in the ageing of wine.

3. Results and discussions

3.1. Volatile compounds and sensory analysis

Medium toasted oak wood chips are able to change wine aroma by adding of compounds such as aldehydes (furfural and syringaldehyde), phenols (vanillin, eugenol and guaiacol), lactones (*cis* and *trans* whiskey lactone), furanic compounds (García-Carpintero et al., 2014), and therefore these compounds confer aromas of wood, smoky, spice vanilla and clove (Cano-López et al., 2008; Schumacher et al., 2013). Moreover, Cano López et al., (2008) found that the oak chip addition improves the aroma profile and modify the sensory descriptors as compared to the samples without chips.

Results on the volatile compounds found in wine samples subjected to the ageing indicate clear differences between samples aged with oak chips after 1.5 and 3 months (Fig. 2). These compounds were classified into four chemical groups, namely esters, volatile phenols, carbonilics and oak compounds (Fig. 2). As expected, increased amounts were observed for all identified and quantified compounds for samples aged 3 months, in comparison to 1.5 months samples.

Esters are known as essential compounds for the overall complex sensory properties of wines. Their content depends on several factors, such as yeast strain, fermentation temperature and aeration (Perestrelo et al., 2006). In this study we observed that, in general, esters contribute with positive aromas, exhibiting with fruity and floral notes (Fig 2A). The concentrations of ethyl octanoate (322.62 µg/L at 1.5 months and 564.36 µg/L at 3 months), ethyl butanoate (251.89 µg/L at 1.5 months and 384.28 µg/L at 3 months) and ethyl propanoate (292.72 µg/L at 1.5 months and 326.86 µg/L at 3 months) were higher as compared with those of other esters such as: ethyl decanoate (69.48 µg/L at 1.5 months and 111.65 µg/L at 3 months) and 2-phenylethyl acetate (79.17 µg/L at 1.5 months and 126.92 µg/L at 3 months).

Within the volatile phenols group, differences of guaiacol and 4-vinylguaiacol amounts were observed, especially with higher values in samples aged 3 months than in those aged 1.5 months (Fig. 2B). Guaiacol concentration varied from 16.67 µg/L at 1.5 months to 21 µg/L at 3 months, while for 4-vinylguaiacol values of 50.33 µg/L at 1.5 months and 63.01 µg/L at 3 months were observed.

Similarly to previously describes compounds, the class of carbonilics compounds registered differences among the two ageing methods (1.5 or 3 months). Increased amounts were detected form furfural (slightly ‘toasty’, ‘woody’, ‘caramel’, ‘burned almonds’ odor), 5-methylfurfural (‘caramel’, ‘butterscotch’ aroma), heptanal (‘herbal’, ‘rancid’, ‘nut’), octanal (‘citrus’, ‘green’, ‘fresh’) and benzaldehyde (‘almond’, ‘smoked’, ‘cherry’ odour, ‘pistachio’ flavor) (López de Lerma et al., 2012; Peinado et al., 2004) within the category of Port wines with ‘indication of age’.

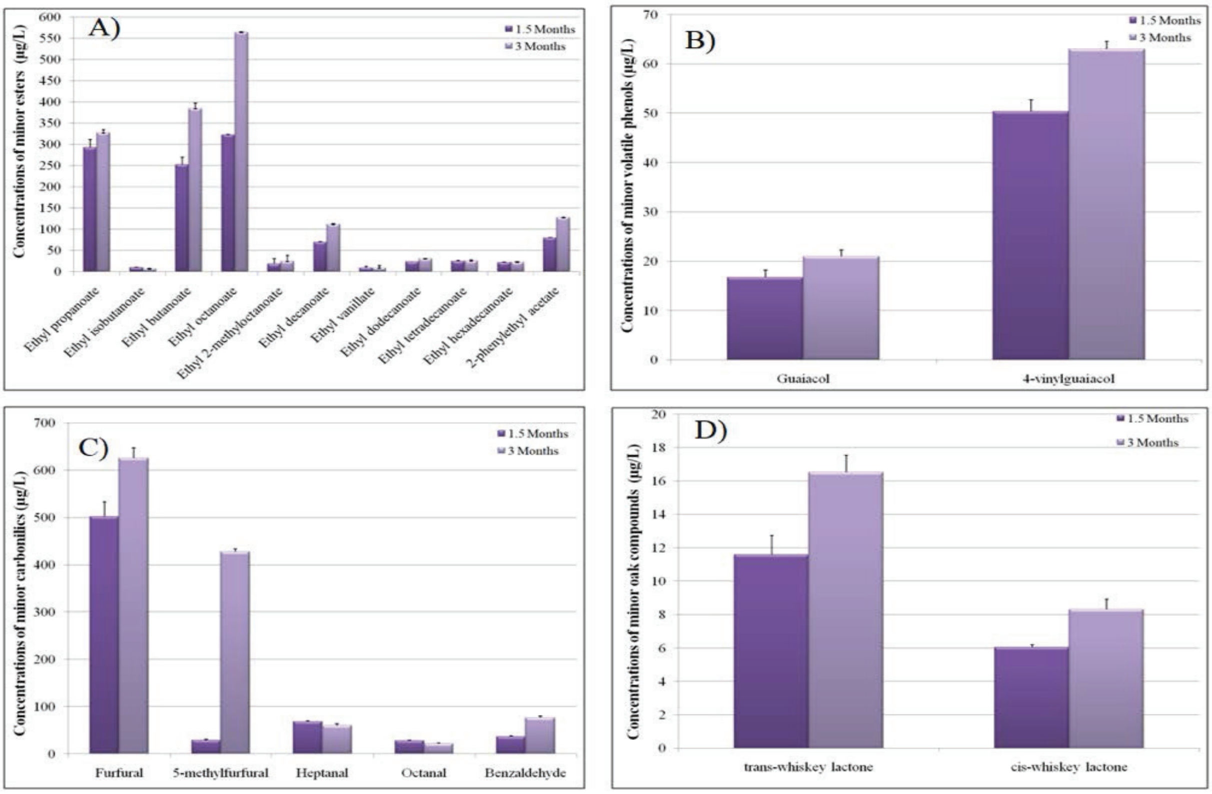

Fig. 2. Concentrations of minor volatile compounds grouped in four chemical families – A) esters, B) volatile phenols, C) carbonilics, D) oak compounds

This increase seems to be linked to the oxidative process during ageing. Furfural and 5-methylfurfural are derived from carbohydrate dehydration followed by cyclization in Maillard-type systems and are linked to wine browning during ageing. Furfural is produced from pentoses (xylose) and 5-methylfurfural arises from rhamnose (Câmara et al., 2006). Furfural and 5-methylfurfural registered the highest concentration among the two ageing methods, varying between 29 and 626 µg/L. According to Câmara et al. (2006) and in other studies, the furan compounds can be used as wine age indicators of wines. However, heptanal and octanal concentrations decreased in the same time frame (Fig. 2C).

The oak compounds, *cis* and *trans*-whiskey lactone presented higher values after 3 months of ageing (Fig. 2D). Concentrations for *cis*-whiskey lactone varied from 6.04 µg/L at 1.5 months to 8.32 µg/L at 3 months, while for *trans*-whiskey lactone from 11.59 µg/L at 1.5 months to 16.51 µg/L at 3 months. Generally, *cis*-whiskey lactone is correlated with the woody character of wines (Chatonnet et al., 1990), while the *trans* isomer has a higher sensory threshold.

Sensory evaluation is a scientific discipline used to evoke, measure, analyze, and interpret reactions to stimuli perceived through the senses (ASTM 2005)" (Lesschaeve, 2007). Giacalone (2018) defines sensory methods as a heterogeneous set of tools aimed at understanding "how different ingredients, formulations, and processing parameters are reflected in the sensory profile of the products".

The sensory analysis of the red wines obtained by adding oak chips at 2 periods of time was performed by evaluating the overall organoleptic quality to observe differences among the samples. The sensory profile of *Fetească neagră* aged with oak chips was characterized by high scores assigned to woody, toasty, vanilla, smoky and cacao notes and an attenuation of ripe fruit and herbaceous attributes (Fig. 3).

3.2. Principal component analysis (PCA)

Principal components analysis (PCA) was realized to observe a reduced number of linear combinations of the variables that explain the greater variability in the data. The graphical representation of the variables analyzed in the principal components (PCs) is associated with the values of volatile compounds. Minor volatile compounds differentiated wines according to the ageing time as presented in Fig. 4. PCA results show that the first two components explain 92.83% of the variability of the data. PC1 explains 78.80% of the variance and is negatively related to the octanal and ethyl isobutanoate and positively associated to the 5-methylfurfural, ethyl decanoate, furfural and *trans*-whiskey lactone.

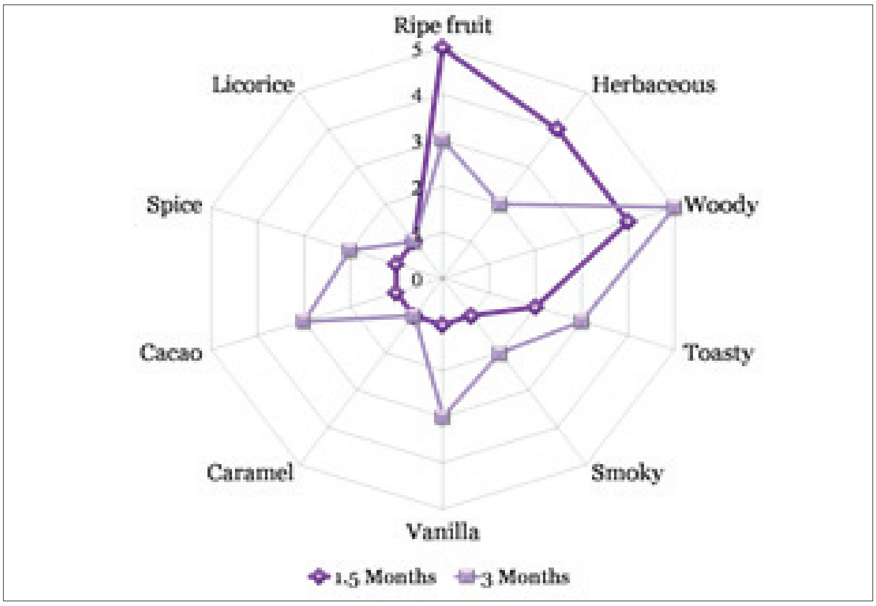

Fig. 3. The sensory profile of *Feteascǎ neagrǎ* aged with oak chips

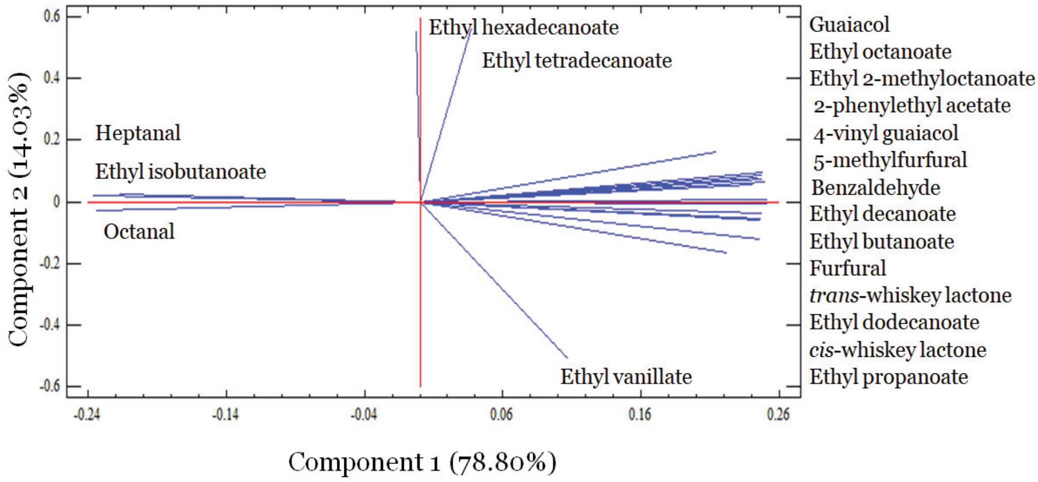

Fig. 4. PCA of wines aged 1.5 and 3 months with oak chips

The compounds that contribute highly to this differentiation were ethyl octanoate, ethyl decanoate, ethyl butanoate, furfural and ethyl dodecanoate. While PC2 explaining 14.03% of the variance is defined by ethyl hexadecanoate and ethyl tetradecanoate in the positive axis and with the ethyl vanillate in the negative axis. In the second component, it was observed that compounds with the highest weight are ethyl hexadecanoate, ethyl tetradecanoate, ethyl vanillate, ethyl propanoate and guaiacol.

4. Conclusions

The SBSE-GC-MS hyphenated techniques, combined with chemometric methods applied to the analysis of volatile compounds allows the differentiation of wines aged during 1.5 and 3 months with oak chips. The addition of oak chips has a significant influence on the aroma composition and sensory profile of *Feteascǎ neagrǎ* red wines. Red wines aged for 3 months showed the highest concentration of aroma compounds when comparative with aged wines for 1.5 months. Woody, vanilla, cacao, smoky and toast notes had a higher intensity in wines made in contact with oak chips for 3 months.

The ageing process with oak chips of *Feteascǎ neagrǎ* red wines could be a useful tool to obtain wines through cost-efficient, environmental friendly and feasible alternatives to the traditional, barrique based winemaking methods.

Acknowledgements

This study was supported by a grant of Ministry of Research and Innovation, CNCS - UEFISCDI, project number **PN-III-P1-1.1-PD-2016-0325**, "Environmental and human related impacts and risks of toxic compounds in the winemaking process" within PNCDI III". Additional funding was provided by the University of Córdoba Research Plan, call 2018, modality synergy, Córdoba, Spain.

We are also grateful to the Oenological Research Center-Romanian Academy, Iasi Branch.

References

Camara J.S., Alves M.A., Marques J.C., (2006), Changes in volatile composition of Madeira wines during their oxidative ageing, *Analytica Chimica Acta*, **563**, 188-197.

Cano-López M., Bautista-Ortín A.B., Pardo-Mínguez F., López-Roca J.M., Gómez Plaza E., (2008), Sensory descriptive analysis of a red wine aged with oak chips in stainless steel tanks or used barrels: effect of the contact time and size of the oak chips, *Journal of Food Quality*, **31**, 645-660.

Chatonnet P., Boidron J.N., Pons M., (1990), The aging of red wines in oak barrels: the formation of specific volatile components and their impact on aroma, *Science des Aliments*, **10**, 565–587.

Del Álamo-Sanza M., Nevares-Dominguez I., Cárcel-Cárcel L.M., Navas-Gracia L., (2004), Analysis for low molecular weight phenolic compounds in a red wine aged in oak chips, *Analytica Chimica Acta*, **513**, 229-237.

Dumitriu G.D., Lopez De Lerma N., Cotea V.V., Zamfir C.I., Peinado R.A., (2016), Effect of ageing time, dosage and toasting level of oak chips on the color parameters, phenolic compounds and antioxidant activity of red wines (var. 'Fetească neagră'), *European Food Research and Technology*, **242**, 2171-2180.

Dumitriu G.-D., López de Lerma N., Zamfir C.-I., Cotea V.V., Peinado R.A., (2017), Volatile and phenolic composition of red wines subjected to aging in oak cask of different toast degree during two periods of time. *LWT - Food Science and Technology*, **86**, 643–651.

Dumitriu (Gabur) G.-D., Peinado R.A., Cotea V.V., López de Lerma N., (2019), Volatilome fingerprint of red wines aged with chips or staves: influence of the aging time and toasting degree, *Food Chemistry*, **310**, 125801.

Garde-Cerdán T., Ancín-Azpilicueta C., (2006), Effect of oak barrel type on the volatile composition of wine, Storage time optimisation, *LWT-Food Science and Technology*, **39**, 199–205.

Giacalone D., (2018), *Sensory and Consumer Approaches for Targeted Product Development in the Agro-Food Sector*, In: *Case Studies in the Traditional Food Sector*, Cavicchi A., Santini C. (Eds.), Elsevier Ltd., Cambridge, MA, 91-128.

García-Carpintero G.E., Sánchez-Palomo E., González Viñas M.A., (2014), Volatile composition of Bobal red wines subjected to alcoholic/malolactic fermentation with oak chips, *LWT - Food Science and Technology*, **55**, 586-594.

Lesschaeve I., (2007), Sensory evaluation of wine and commercial realities: review of current practices and perspectives, *The American Journal of Enology and Viticulture*, **58**, 252-258.

López de Lerma N., Bellicontro A., Mencarelli F., Moreno J., Peinado R.A., (2012), Use of electronic nose, validated by GC–MS, to establish the optimum off-vine dehydration time of wine grapes, *Food Chemistry,* **130***,* 447–452.

OIV, (2015), *Grapevine varieties' area by country, International Organization of Vine and Wine*, On line at: http://www.oiv.int/public/medias/5882/grapevine-varieties-area-by-country-2015.pdf.

Peinado R.A., Moreno J., Bueno J.E., Moreno J.A., Mauricio J.C., (2004), Comparative study of aromatic compounds in two young white wines subjected to pre-fermentative cryomaceration, *Food Chemistry,* **84,** 585–590.

Perestrelo R., Fernandes A., Albuquerque F.F., Marques J.C., Câmara J.S., (2006), Analytical characterization of the aroma of Tinta Negra Mole red wine: Identification of the main odorants compounds, *Analytica Chimica Acta*, **563**, 154-164.

Petrozziello M., Torchio F., Piano F., Giacosa S., Ugliano M., Bosso A., Rolle L., (2018), Impact of increasing levels of oxygen consumption on the evolution of color, phenolic, and volatile compounds of nebbiolo wines, *Frontiers in Chemistry*, **6**, doi: 10.3389/fchem.2018.00137.

Rogerson F.H., Castro N., Fortunato Z., Azevedo A., Freitas V., (2001), Chemicals with sweet aroma descriptors found in Portuguese wines from the Douro region: 2,6,6-Trimethylcyclohex-2-ene-1,4-dione and diacetyl, *Journal of Agriculture and Food Chemistry*, **49**, 263-269.

Schumacher R., Alañón M.E., Castro-Vázquez L., Pérez-Coello M.S., Díaz-Maroto M.C., (2013), Evaluation of oak chips treatment on volatile composition and sensory characteristics of Merlot wine, *Journal of Food Quality*, **36**, 1-9.

Tredoux A., de Villiers A., Májek P., Lynen F., Crouch A., Sandra P., (2008), Stir bar sorptive extraction combined with GC-MS analysis and chemometric methods for the classification of South African wines according to the volatile composition, *Journal of Agricultural and Food Chemistry*, **56**, 4286-4296.

Wilker K.L., Gallander J.F., (1988), Comparison of Seyval blanc wine aged in barrels and stainless steel tanks with oak chips, *American Journal of Enology and Viticulture,* **39**, 38-43.

Environmental Engineering and Management Journal

February 2020, Vol. 19, No. 2, 235-245
http://www.eemj.icpm.tuiasi.ro/; http://www.eemj.eu

“Gheorghe Asachi” Technical University of Iasi, Romania

COMPARATIVE STUDIES REGARDING MOLYBDATE ADSORPTION ONTO Mg_nFe LAYERED DOUBLE HYDROXIDES OBTAINED FROM REAGENT AND WASTE SLUDGE

Alin Golban, Lavinia Lupa, Laura Cocheci, Rodica Pode*

Politehnica University Timisoara, Faculty of Industrial Chemistry and Environmental Engineering,
6 Vasile Parvan Blvd., 300223, Timisoara, Romania

Abstract

Molybdate anions are used in a lot of fields and represent an essential trace element for plant and animal life; however, excessive amounts can cause adverse effect on various organism and environment. Therefore, in the present paper the adsorption performance of Mg_nFe- layered double hydroxides in the removal process of molybdate from aqueous solutions was studied. The layered double hydroxide (LDH) was synthesized by co-precipitation at low oversaturation method. Different ratio between Mg and Fe ions was used (Mg:Fe = 2:1; 3:1 and 4:1). The studied Mg_nFe- layered double hydroxides were synthesized starting from reagent and from iron waste sludge resulted from hot-dip galvanizing industry. In the removal process of molybdate from aqueous solutions were used the as-obtained and calcined at 450 °C adsorbents. The structural and morphological characterization of the obtained samples were made using BET (Brunauer-Emmett-Teller) analysis method, X-ray diffraction (XRD) and Scanning electron microscopy (SEM). The LDH materials obtained from an industrial waste have structural characteristics and similar or even higher adsorptive performance, as compared to those obtained from analytical grade reagents. Therefore, the approached LDH synthesis method, starting from secondary resources, represents a viable, affordable, and green route. This can successfully replace the expensive and resource-intensive traditional synthesis method, leading to cost reduction and valuable benefits in terms of environmental protection.

Key words: adsorption, layered double hydroxide, molybdate

Received: January, 2019; Revised final: January, 2020; Accepted: January, 2020; Published in final edited form: February, 2020

1. Introduction

Layered double hydroxides (LDH) with the general formula $[M(II)_{1-x}M(III)_x(OH)_2]^{x+}$ $(A^{n-}_{x/n})$ mH_2O, are synthetic anionic clays, which attracted a lot of interest due to their specific properties (Cavani et al., 1991). Their structure is formed from divalent ionic metals (e.g. Mg^{2+}, Zn^{2+}, Fe^{2+}) placed in the form of brucite-type layers, part of them being substitute by trivalent ions (e.g. Al^{3+}, Fe^{3+}) leading to positively charged layers. In the interlayers are found organic or inorganic anions which assure the molecules electroneutrality, conjugated with water molecules. Their layered structure confers best applies of these materials as ion exchangers, molecular sieves, catalysts or catalyst supports, biosenzors and sorbents (Benselka-Hadj Abdelkader et al., 2011; Kamiyama et al., 2016; Fahami and Beall, 2016; Zhang et al., 2014, Gilea et al., 2019). Due to their manageability interlayer region and due to their fluffy structure, these types of compounds are intensively used in the removal process of different pollutants from various environment samples (Turk et al., 2009). In general, for synthesizing LDHs compounds the most commonly used method is co-precipitation at a constant or variable pH by using pure chemical reagents that are rather expensive, or by using secondary sources of waste from different types of industries (Meng et al., 2016). A potential industry, which produces a significant amount of waste that

---

* Author to whom all correspondence should be addressed: e-mail: rodica.pode@upt.ro

could be used as secondary sources for LDHs obtaining is represented by the hot-dip galvanizing industry. One efficient method for using this waste is chemical extraction of valuable materials by using different organic or inorganic acid (acetic or citric acid, H_2NO_3, HCl, H_2SO_4) (Chou et al., 2010; Gheju et al., 2011; Shin et al., 2009; Xie et al., 2009). Therefore, in this study the iron sludge resulted from hot-dip galvanizing industry was used as secondary source of iron for the obtaining of Mg_nFe- layered double hydroxides (n = 2, 3 and 4). The aim of this work is to compare the structural properties of the obtained LDHs from secondary sources with those of the similar samples obtained from reagents. Besides structural properties, also the adsorption performance of the synthesised samples was also compared. In this aim as target pollutant, which to be retained by the studied materials, was chosen to be molybdenum (Mo). Molybdenum has many applications such as: micronutrient, corrosion inhibitors and alloying element. (Ardau al., 2012; Paikaray et al., 2013). At the same time, if it is present at higher concentration than it is recommended it can be harmful for human life (World Health Organization (Namasivayam and Sengeetha, 2006; WHO, 2011;). From this reason the development of new, efficient and less expensive method for molybdenum removal or recover from various aqueous solution always represent a challenge.

2. Experimental

2.1. Adsorbent obtaining and characterization

The synthesis method for Mg_nFe - layered double hydroxides consist in co-precipitation at low oversaturation, as described by Cavani et al., 1991. The sludge used for obtaining of iron precursor was received from a local hot-dip galvanizing plant. The dissolution of iron sludge was detailed in our previous published work (Goban et. al., 2018) the optimum condition of iron ions extraction from sludge being: 20% sulfuric acid solution, solid:liquid ratio 1:1.2 and a contact time between the two phases of 60 minutes. In the resulted iron precursor solution, the iron concentration is of 84 g/L and the Zn ions have a concentration of 2.38 g/L. The other ions present in the sludge were extracted in a smaller amount due to the formation of calcium and lead sulphates, which are hardly soluble.

A calculated amount of solution, obtained from acid dissolution of sludge, was used as precursor of the trivalent cation (iron) for, Mg_nFe -S synthesis or $Fe(NO_3)_3 \cdot 9H_2O$ analytical grade reagent for preparation of a blank sample - Mg_nFe -R. A measured amount of $Mg(NO_3) \cdot 6H_2O$ analytical grade reagent was also used, in order to obtain different molar ratio of Mg/Fe (n = 2, 3 and 4). This solution was added dropwise to a 1 M solution of Na_2CO_3, under vigorous magnetic stirring and keeping the pH value to 11.5 by means of 2 M NaOH solution. The brown-red precipitate was maintained under stirring for 2 h in order to finish the incorporation of cations solution, and then aged at 70 °C for 18 h, washed several times with distilled water in order to remove the unreacted substances, filtered and dried at 70°C over night. The obtained samples were crushed to powders and sieved. The calcined samples were heated at 450 °C using a rate of 10 °C/min. A Nabertherm oven was used for the sample calcination.

The structural and morphological characterization of the Mg_nFe layered double hydroxides, obtained from both sources: iron sludge and also analytical grate reagents, were made using X-ray diffraction (XRD), scanning electron microscopy (SEM) and BET (Brunauer-Emmett-Teller) analysis.

A Rigaku Ultima IV X-ray diffractometer was used for the XRD analyse. SEM images were register with a Quanta FEG 250 microscope. The BET analysis method used to determine the specific surface area and pore volume were determined by N_2 adsorption-desorption at 77 K, using, with a Micromeritics ASAP 2020 instrument.

2.2. Sensitivity analysis Mo(VI) adsorption

For the adsorption of Mo(VI) on the studied samples, a stock solution of 1 g/L Mo(VI) was prepared using ammonium molybdate tetrahydrate $(NH_4)_6Mo_7O_{24} \cdot 4H_2O$. All adsorption experiments were performed by contacting 25 mL of solutions containing Mo(VI) with the adsorbents samples corresponding to a solid:liquid ratio of 1g/L. The Mo(VI) removal was conducted in a batch shaker model Julabo, to reach the adsorption equilibrium. At equilibrium, the solid was separated by filtration and the residual concentration of Mo(VI) ions was analysed by atomic adsorption spectrophotometer (Varian SpectrAA 280 FS).

Different initial pH values (4, 6, 8, 10) of a 30 mg/L Mo(VI) solution were used to determine the pH effect upon the adsorption efficiency. The pH value was modified by using 1 mol/L NaOH or 1 mol/L HCl, and the pH was determined with a Mettler Toledo pH-meter. To determine the effect of sorption time, different time intervals have been set (15-240 min).

Adsorption isotherm was conducted in the optimum conditions of pH and contact time established before, using solutions containing different initial concentrations of Mo(VI) (5, 10, 30, 50, 100 and 150 mg/L). The quantity of molybdate retained by the studied materials was calculated using the following Eq (1):

$$q_e = (C_0 - C_e)\ V/m \qquad (1)$$

where: q_e is the adsorption capacity of sorbent material at equilibrium (mg/g), V the volume of solution (L), C_0 (mg/L) and C_e (mg/L) the initial and equilibrium concentrations of Mo(VI), and m is the mass of adsorbent (g).

3. Results and discussions

3.1. Adsorbent characterization

The XRD patterns of the as-synthesised sample and calcined at 450°C are presented in Fig. 1 and can be observed that both the Mg_nFe - layered double hydroxides obtained from reagents and obtained from secondary sources correspond to the formula of pyroaurite: $Mg_6Fe_2CO_3(OH)_{16}\cdot 4H_2O$ (DB card number 9009439). The use of solution obtained from acid dissolution of iron sludge as iron precursor doesn't lead to the obtaining of second phases or impurities in the synthesized samples. In case of the samples calcined at 450°C the layered structure collapses and the RX spectrum are specific for amorphous phases. From this reason it is expected that the samples calcined at 450 °C to develop higher adsorption capacity than the as-synthesized samples.

For the basal planes (0 0 3) and (0 0 6) the corresponding reflexions are found at low 2θ angles, while for the non-basal planes (0 1 2), (0 1 5), (0 1 8), (1 1 0) and (1 1 3), the corresponding reflexions are found at high 2θ angles. The values of 2θ angles corresponding to the basal and non-basal planes of the as-synthetized samples, and the calculated basal spacing are presented in Table 1. The values of the basal spacing $d_{(0\,0\,3)}$ are close to each other and correspond to carbonate interlayer pyroaurites. Also, the values of $d_{(1\,1\,0)}$ spacing are typical for Mg-Fe layered double hydroxides, as presented in literature data (Ahmed and Gasser, 2012; Vucelic et. al, 1997)

Fig. 2. shows the SEM images of the synthesised LDH both from reagents and secondary sources. It can be observed that both the materials obtained from secondary sources and from reagent present similar morphology as fluffy particles staked in overlaid layers. This aerated structure is more evident with the increasing of the Mg/Fe molar ratio. Through calcination at 450 °C the samples are more amorphous presenting a cotton appearance (Fig. 2).

The values resulted from the BET analysis regarding the specific surface area and the pore volume of the studied sample are listed in Table 2.

For all the samples (obtained from reagents or from secondary sources) it can be observed that by increasing the molar ratio Mg/Fe lead to a slide increasing of the specific surface area. The calcinated samples present almost a double surface area than their precursors.

Considering the morphological structure of the sample it is expected that the adsorption capacity developed in the removal process of Mo(VI) from aqueous solutions to increase with the Mg/Fe molar ratio increasing and to be much higher for the calcinated samples.

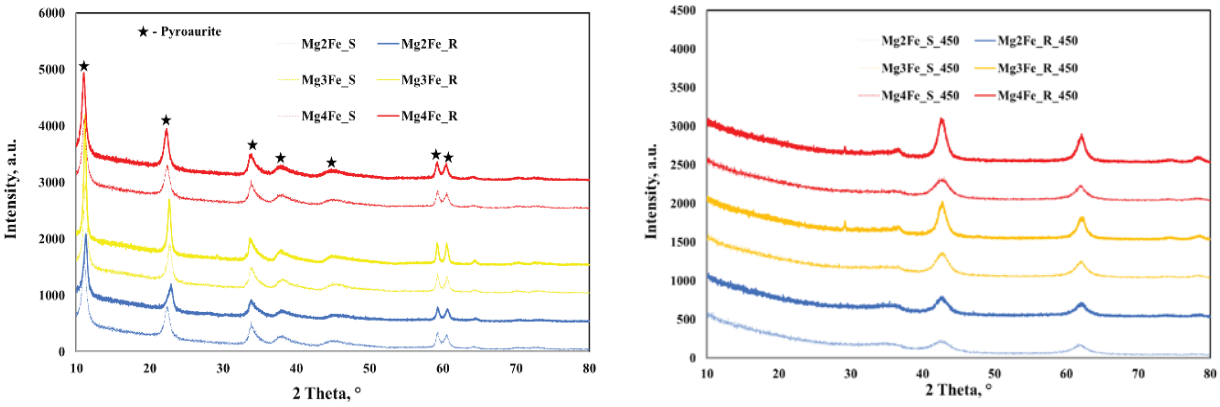

(a) (b)

Fig. 1. XRD pattern of: a) Mg_nFe as-synthesised and b) Mg_nFe - calcinated at 450 °C

Table 1. Values of 2θ angles for the basal and non-basal planes of as-synthetized samples

	Mg_2Fe-R	*Mg_2Fe-S*	*Mg_3Fe-R*	*Mg_3Fe-S*	*Mg_4Fe-R*	*Mg_4Fe-S*
$d_{(0\,0\,3)}$ (Å)	7.90	7.81	7.82	7.83	8.02	7.98
$d_{(1\,1\,0)}$ (Å)	1.56	1.57	1.56	1.56	1.57	1.56
(h k l) plane	**2θ (°)**					
(0 0 3)	11.04	11.30	11.17	11.21	11.00	11.05
(0 0 6)	23.04	22.92	22.64	22.71	22.24	22.33
(0 1 2)	38.42	38.52	37.68	38.30	37.58	37.64
(0 1 5)	45.10	45.08	44.78	44.89	44.40	44.52
(0 1 8)	59.28	59.30	59.20	59.25	59.10	59.20
(1 1 0)	60.61	60.66	60.50	60.57	60.35	60.48
(1 1 3)	72.77	72.84	72.51	72.96	72.66	72.58

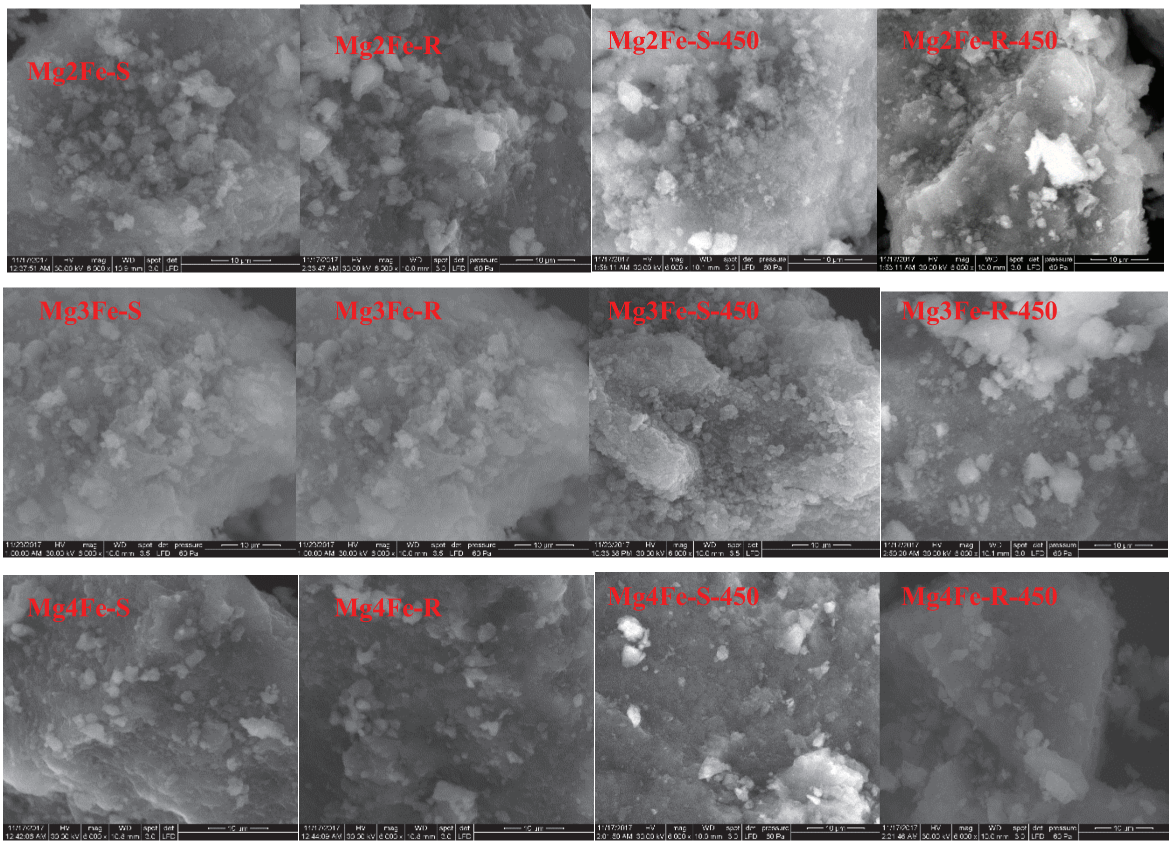

Fig. 2. SEM images of the Mg_nFe - LDH as-synthesised and calcinated at 450 °C

Table 2. Specific surface area and pore volume

Adsorbent material	*S_{BET} (m^2/g)*	*V_p (cm^3/g)*
Mg2Fe-S	64.2	0.64
Mg2Fe-R	44.2	0.41
Mg3Fe-S	73.4	0.56
Mg3Fe-R	50.7	0.50
Mg4Fe-S	98.9	0.53
Mg4Fe-R	83.3	0.44
Mg2Fe-S-450	130	0.75
Mg2Fe-R-450	121	0.60
Mg3Fe-S-450	144	0.78
Mg3Fe-R-450	132	0.64
Mg4Fe-S-450	189	0.82
Mg4Fe-R-450	170	0.66

3.2. Effect of pH upon the adsorption efficiency

The effect of the initial pH of the sample upon the adsorption capacity developed by the studied materials in the removal process of Mo(VI) from aqueous solutions are presented in Fig. 3. It can be observed that through increasing of the initial pH from 4 to 6 the adsorption capacity increase obtaining a maximum at pH 6. At this pH value the Mo(VI) are present in solution only as molybdate anion (MoO_4^{2-}) (Tkac and Paulenova 2008). At higher pH there is a competition between the molybdate anion (MoO_4^{2-}) and the hydroxyl anions (HO^-) present in solution, which lead to a decreasing of the obtained adsorption capacities. Therefore, for the subsequent experiments a pH value of 6 was selected.

3.3. Effect of contact time on the adsorption efficiency

The behaviour of adsorption capacity of the studied materials in the removal process of Mo(VI) from aqueous solutions function of time is presented in Fig. 4. It can be observed that the equilibrium between the adsorbent and molybdate anion is achieved in 60 minutes for all the studied materials, this being considered the work time for the following experiments.

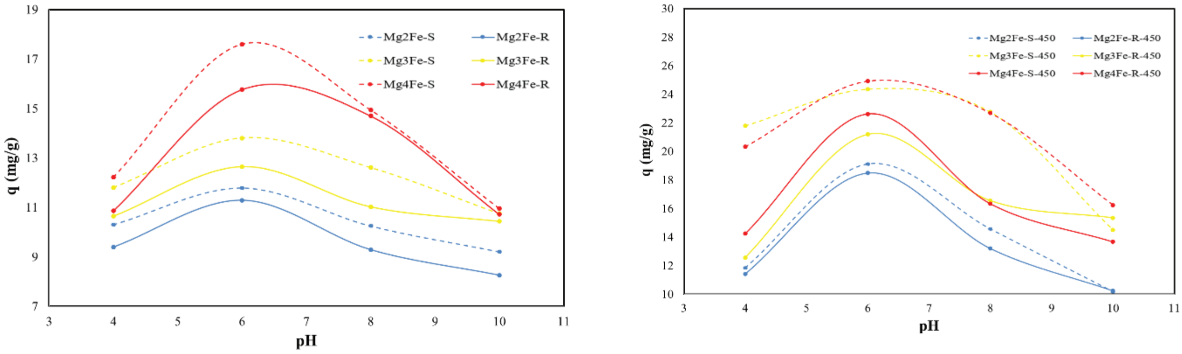

a) Mg_nFe as-synthesised b) Mg_nFe - calcined at 450 °C

Fig. 3. Effect of initial pH on the adsorption capacity of the studied materials in the removal process of Mo(VI) ions from aqueous solutions

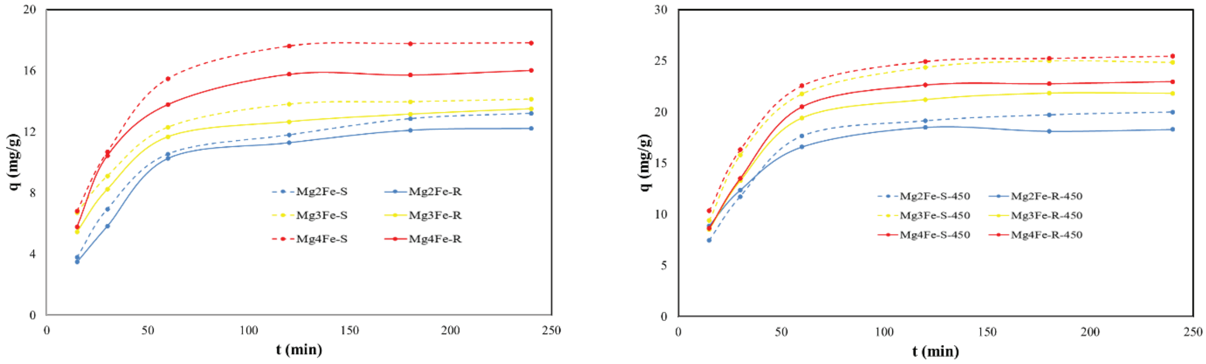

a) Mg_nFe as-synthesised b) Mg_nFe - calcined at 450 °C

Fig. 4. Effect of contact time on the adsorption capacity of the studied materials in the removal process of Mo(VI) ions from aqueous solutions

The experimental data regarding the dependence of the adsorption capacity of the studied materials function of contact time were used for kinetic modelling. In this way three kinetic models: pseudo-first-order equation, pseudo-second-order reaction model and intra-particle diffusion model, were discussed. The pseudo-first-order kinetic model is defined by the Equation: (Ardau et al. 2012; Haro et al. 2017; Namasivayam and Sengeetha 2006).

$$\ln(q_e - q_t) = \ln q_t - k_1 \cdot t \qquad (2)$$

where: q_e and q_t are the amount of the Mo(VI) adsorbed onto the studied materials (mg/g) at equilibrium and after time *t*, respectively. *t* is the contact time (min), k_1 is the specific sorption rate constant (min^{-1}).

The values of the adsorption rate constant (k_1) were determined from the plot of *ln* ($q_e - q_t$) versus *t* (Fig. 5). The linear form of the pseudo-second order model based on the solid phase adsorption and implying that the chemisorption is the rate controlling step is defined by: (Ardau et al., 2012; Namasivayam and Sengeetha, 2006; Haro et al., 2017).

$$\frac{t}{q_t} = \frac{1}{k_2 \cdot q_e^2} + \frac{t}{q_e} \qquad (3)$$

where: q_e and q_t are the amount of the Mo(VI) adsorbed onto the studied materials (mg/g) at equilibrium and at time *t*, respectively. *t* is the contact time (min), k_2 is the pseudo-second-order adsorption rate constant (g/(mg·min)). The value q_e and k_2 are determined from the slope and intercept of (t/q_t) versus *t* (Fig. 6.).

In order to determine the rate-limiting step in the process of molybdate adsorption onto the studied materials, intra-particle diffusion model was studied. This step could be controlled by boundary layer dispersion or intra-particle (pore) dispersion of solute towards the solid surface. The Weber-Morris ecuation was used to identify the possibility of intra-particle diffusion resistance:

$$q_t = k_{int} \cdot t^{1/2} + C \qquad (4)$$

where: k_{int} is the intra-particle diffusion rate constant ($mg/g \cdot min^{1/2}$) and *C* is the intercept. The values of q_t versus $t^{1/2}$ and the rate constant k_{int} are directly evaluated from the slope of the regression line (Fig. 7).

The values of the constants, together with the regression coefficients (R^2) obtained in all cases are summarized in Table 3.

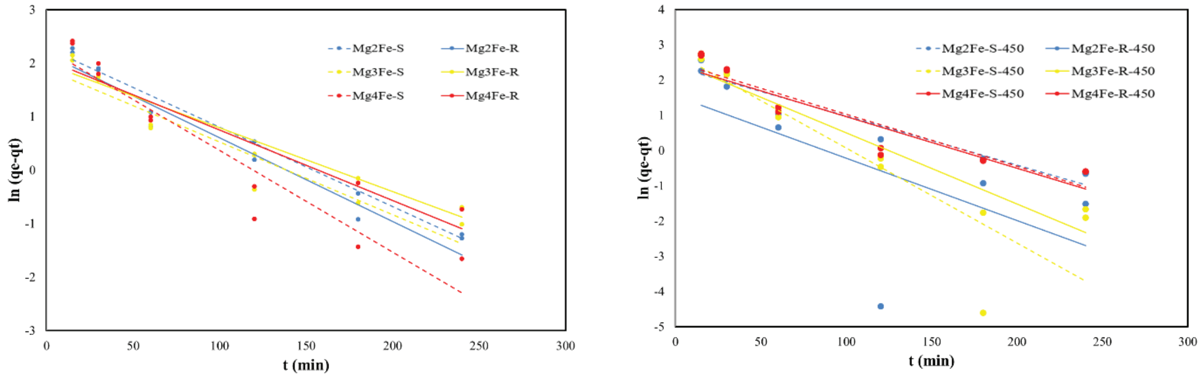

Fig. 5. Pseudo-first order kinetic models for Mo(VI) adsorption onto the studied materials

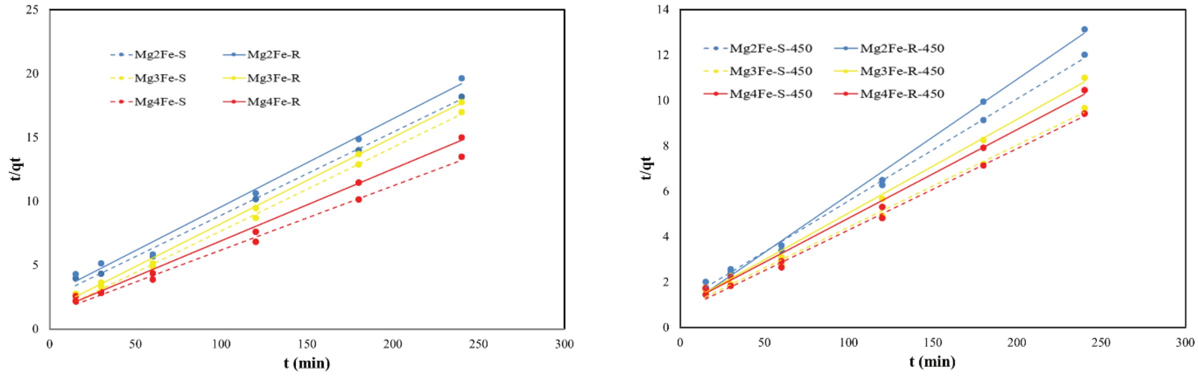

Fig. 6. Pseudo-second order kinetic model for Mo(VI) adsorption onto the studied materials

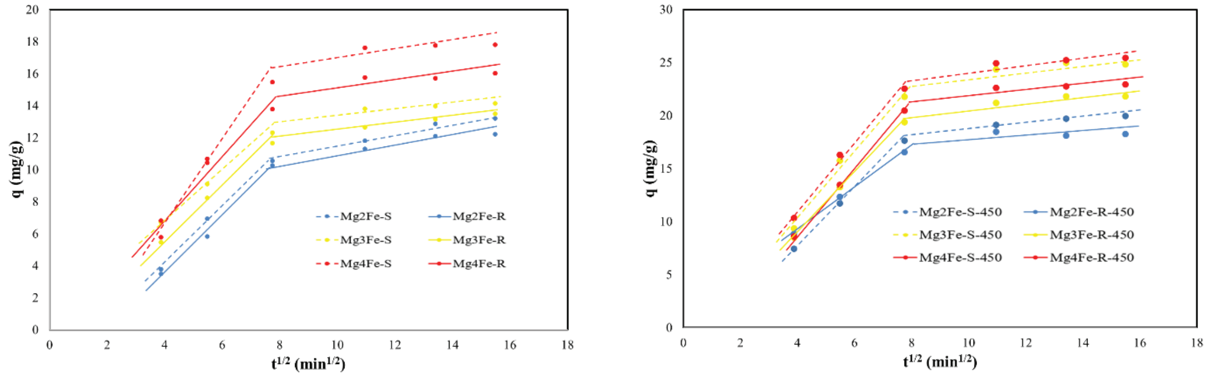

Fig. 7. Intraparticle diffusion of Mo(VI) onto the studied materials

Table 3. Kinetic parameters for Mo(VI) sorption onto the studied materials

Adsorbent material	$q_{e,exp}$ *mg Mo(VI) /g*	*Pseudo-first-order model*			*Pseudo-second-order model*			*Intraparticle diffusion*	
		$q_{e,calc}$, *mg/g*	k_1, *min*$^{-1}$	R^2	$q_{e,calc}$, *mg/g*	k_2, *min/(mg/g)*	R^2	k_{int}	R^2
Mg$_2$Fe-S	13.5	9.86	0.0142	0.9831	15.6	0.00172	0.9952	1.73	0.9952
Mg$_2$Fe-R	12.5	8.71	0.0156	0.9538	14.5	0.00182	0.9907	1.76	0.9941
Mg$_3$Fe-S	14.5	6.59	0.0132	0.9041	15.4	0.00376	0.9982	1.44	0.9984
Mg$_3$Fe-R	14.0	7.24	0.0108	0.9318	14.8	0.00314	0.9986	1.60	0.9974
Mg$_4$Fe-S	18.0	9.63	0.0189	0.8995	20.0	0.00221	0.9957	2.23	0.9976
Mg$_4$Fe-R	16.5	7.90	0.0132	0.8623	17.8	0.00258	0.9958	2.03	0.9632
Mg$_2$Fe-S-450	20.5	10.7	0.0126	0.9168	22.7	0.00183	0.9958	2.63	0.9997
Mg$_2$Fe-R-450	18.5	4.72	0.0169	0.4048	20.0	0.00346	0.9968	1.98	0.9982
Mg$_3$Fe-S-450	25.0	15.8	0.0268	0.8904	27.8	0.00163	0.9957	3.16	0.9863
Mg$_3$Fe-R-450	22.0	12.4	0.0192	0.9254	24.4	0.00195	0.9959	2.80	0.9986
Mg$_4$Fe-S-450	26.0	12.1	0.0136	0.8892	28.6	0.00174	0.9967	3.13	0.9924
Mg$_4$Fe-R-450	23.5	11.3	0.0138	0.8563	25.6	0.00176	0.9949	3.07	0.9995

Due to the fact that in case of the pseudo-first-order equation the experimental data are far apart from the linearity, obtaining poor regression coefficients and because there is a discrepancy between the q_e values experimentally obtained and the values obtained directly from the kinetic plot (Fig. 5.) can be mentioned that this kinetic model does not describe the Mo(VI) adsorption onto the studied materials. In all the cases the correlation coefficients for the linear plot of the pseudo-second-order kinetic plot is excellent, greater than 0.99. In the same time the values obtained for the adsorption capacity obtained experimentally and from the kinetic plot are very close. Therefore, can be concluded that the Mo(VI) adsorption onto the studied materials is best described by the pseudo-second order kinetic model. As respect for the intra particle diffusion, it can be observed that the Mo(VI) adsorption onto the studied materials present a complex mechanism which take place in two steps: the first linearity represents the distribution of adsorbate through the solution to the external surface of adsorbent, and the second one could be attributed to the gradual adsorption stage, where intraparticle diffusion is rate limiting (Cong and Jianping, 2018).

3.4. Effect of Mo(VI) initial concentration on the adsorption efficiency

The equilibrium isotherm of the Mo(VI) adsorption onto the studied materials are presented in Fig. 8. The adsorption capacities developed by the studied materials increase with the increasing of the equilibrium concentration, until it reaches a constant value which represent the saturation of the adsorbent with the molybdate anions.

In order to determine the maximum adsorption capacities of the studied materials the experimental data were fitted with the following isotherms: Langmuir, Freundlich, Temkin and Dubinin-Radushkevich (Abubeah et al., 2018). The Langmuir isotherm is described by the following equation in its linear form: (Xiaoliang et al., 2017)

$$\frac{C_e}{q_e} = \frac{1}{K_L \cdot q_m} + \frac{C_e}{q_m} \qquad (5)$$

where: q_e is the amount of Mo(VI) uptake per gram of adsorbent (mg/g), and C_e is the equilibrium concentration of adsorbate in the bulk solution after adsorption (mg/L). q_m is the measure of the monolayer sorption capacity (mg/g) and K_L denotes the Langmuir isotherm constant related to the affinity between adsorbent and the adsorbate (L/mg). From the plot of C_e/q_e versus C_e presented in Fig. 9 there were determined the Langmuir parameters which are showed in Table 2. Eq. (6) is the linear form of the Freundlich equation (Wang et al., 2018),

$$ln\, q_e = ln\, K_F + \frac{1}{n} ln\, C_e \qquad (6)$$

where: K and $1/n$ are characteristic constants that can be related to the relative adsorption capacity of the adsorbent (mg/g) and the intensity of the adsorption, respectively. These parameters listed in Table 4 were determined from the slope and intercept of the linear plot of lnq_e against C_e (Fig. 10).

The interactions between adsorbent-adsorbate could be described by the linear equation of Temkin isotherm: (Johnson and Arnold, 1995)

$$q_e = \frac{RT}{b} \ln k_T + \frac{RT}{b} \ln C_e \qquad (7)$$

where: T is the absolute temperature (K), R is the gas constant, K_T (L/mg) is the equilibrium binding constant corresponding to the maximum binding energy, b (kJ/mol) is Temkin isotherm constant, RT/b (dimensionless) is related to the heat adsorption. K_t and b can be calculated from the slope and intercept of the linear plot of q_e versus lnC_e (Fig. 11.) and the results together with the regression coefficient are listed in Table 4.

The D-R isotherm model in its linear form was tested to establish the mechanism type of Mo(VI) adsorption (physical or chemical) onto the studied materials: (Hu and Zhang, 2019).

$$\ln q_e = \ln q_s - K_{ad} \cdot \varepsilon^2 \qquad (8)$$

where: q_e = amount of adsorbate in the adsorbent at equilibrium(mg/g); q_s = theoretical isotherm saturation capacity (mg/g); K_{ad} = Dubinin–Radushkevich isotherm constant (mol^2/kJ^2). ε can be correlated as given by Eq. (9):

$$\varepsilon = RT \ln\left[1 + \frac{1}{C_e}\right] \qquad (9)$$

where: R, T and are the gas constant (8.314 J/mol.K), absolute temperature (K) and adsorbate equilibrium concentration (mg/L) respectively. The parameters specific for D–R isotherm were determined from the linear plot of lnq_e function of ε^2 (Fig. 12.) and were listed in Table 4.

The Langmuir isotherm showed a better design of the experimental data resulted during the adsorption of molybdenum onto the studied materials, than the rest of the isotherms. The fact that the Langmuir isotherm fits the experimental data well may be due to homogeneous distribution of active sites on the studied samples since the Langmuir equation estimates that the adsorbent outer is uniform charge. The maximum adsorption capacity developed by the studied materials increase with the molar ratio increasing between Mg and Fe from the synthesised LDH. The LDH synthesised from secondary sources present even slightly higher maximum adsorption capacity than the LDH obtained from reagents. The maximum adsorption capacities developed by the calcinated samples at 450°C are with 50% higher than those of their precursors.

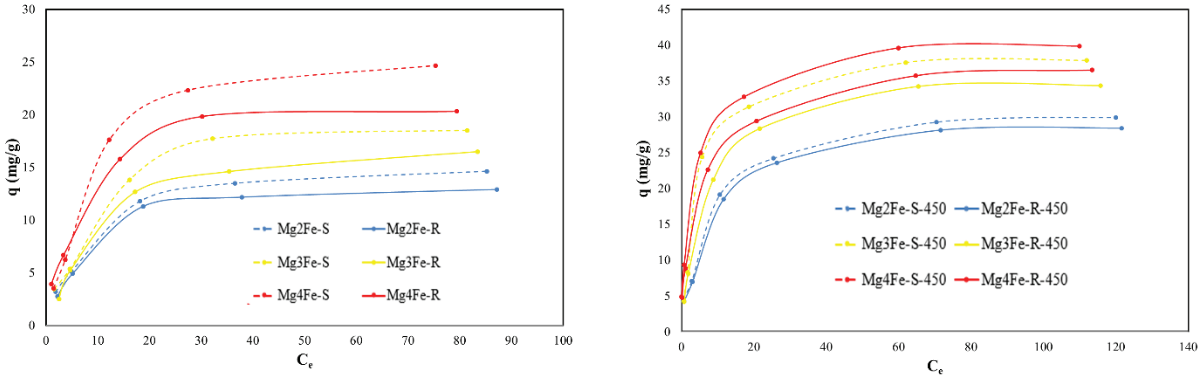

Fig. 8. Equilibrium isotherm of Mo(VI) adsorption onto the studied materials

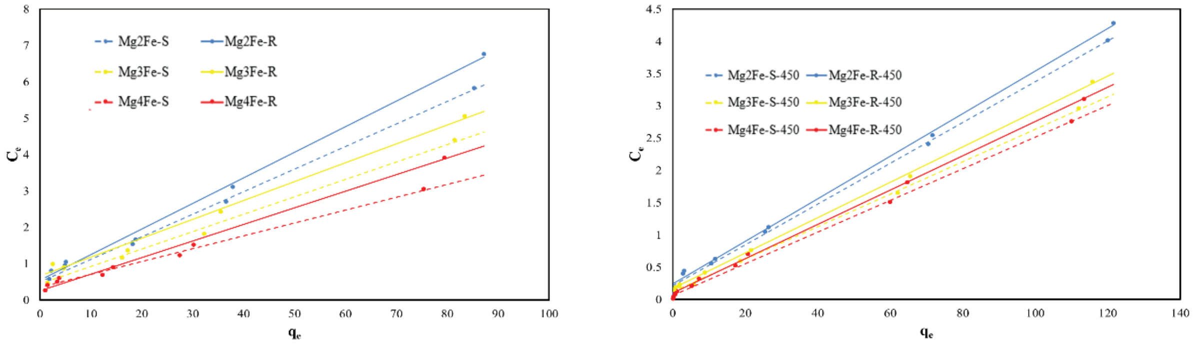

Fig. 9. Langmuir isotherm for Mo(VI) adsorption onto the studied materials

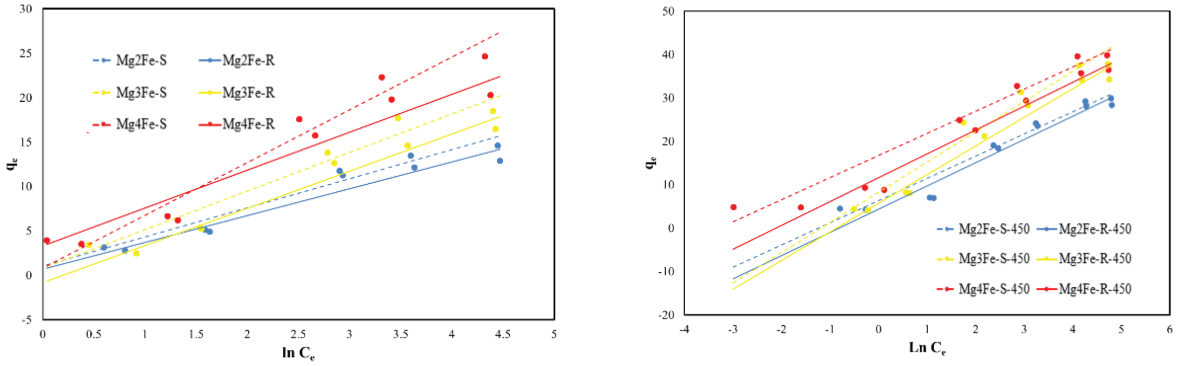

Fig. 10. Freundlich isotherm for Mo(VI) adsorption onto the studied materials

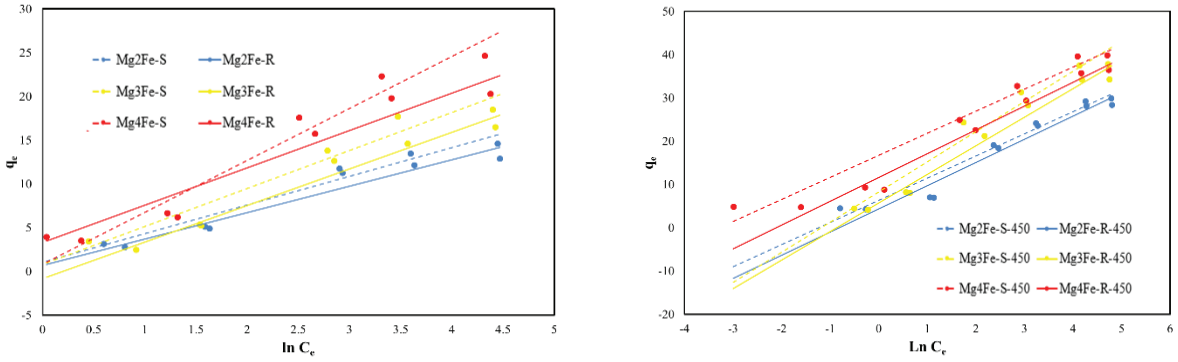

Fig. 11. Temkin isotherm for Mo(VI) adsorption onto the studied materials

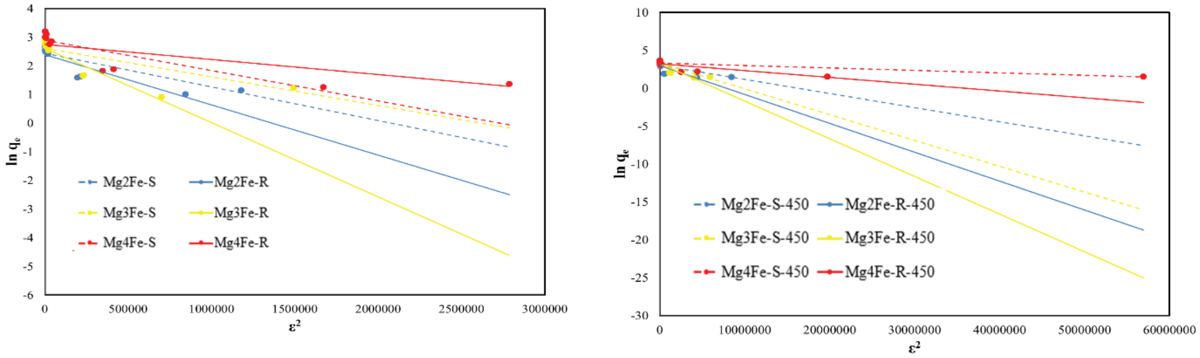

Fig. 12. Dubinin- Radushkevich isotherm for Mo(VI) adsorption onto the studied materials

Table 4. Equilibrium sorption isotherm parameters for Mo(VI) adsorption onto the studied materials

Studied materials	***$q_{m\ exp}$, mg/g***	***Langmuir***			***Freundlich***			***Temkin***			***Dubinin- Radushkevich***		
		K_L, L/mg	***$q_{m\ calc}$, mg/g***	***R^2***	***K_F, mg/g***	***1/n***	***R^2***	***K_T, L/g***	***b_T, J/mol***	***R^2***	***K_{ad}, mol^2/kJ^2***	***q_s, mg/g***	***R^2***
Mg_2Fe-S	14.6	0.124	16.1	0.9979	2.69	0.426	0.9379	24.8	755	0.9603	$1.24*10^{-6}$	12.1	0.7768
Mg_2Fe-R	12.9	0.127	14.2	0.9964	2.31	0.438	0.9019	99.5	820	0.9350	$2.53*10^{-6}$	10.9	0.8582
Mg_3Fe-S	18.5	0.109	20.9	0.9920	2.92	0.472	0.9337	290	570	0.9428	$1.34*10^{-6}$	13.7	0.7112
Mg_3Fe-R	16.5	0.0787	19.2	0.9926	2.01	0.534	0.8995	157	593	0.9695	$3.48*10^{-6}$	13.6	0.9259
Mg_4Fe-S	24.7	0.102	28.2	0.9931	3.33	0.528	0.9179	1863	417	0.9545	$1.46*10^{-6}$	18.0	0.7791
Mg_4Fe-R	20.3	0.181	21.9	0.9972	4.21	0.413	0.9385	3.67	579	0.9497	$5.27*10^{-7}$	15.6	0.7499
Mg_2Fe-S-450	30.0	0.151	31.5	0.9975	6.10	0.371	0.9391	2.25	485	0.9486	$2.28*10^{-7}$	20.2	0.6170
Mg_2Fe-R-450	28.5	0.137	30.3	0.9983	5.15	0.403	0.9362	3.42	463	0.9619	$4.18*10^{-7}$	20.1	0.6773
Mg_3Fe-S-450	37.9	0.206	39.7	0.9993	7.25	0.414	0.8800	2.34	355	0.9536	$3.49*10^{-7}$	28.1	0.7896
Mg_3Fe-R-450	34.5	0.163	36.5	0.9995	6.02	0.426	0.9151	3.19	376	0.9785	$5.47*10^{-7}$	26.2	0.8424
Mg_4Fe-S-450	39.9	0.422	39.4	0.9991	12.0	0.295	0.9611	1.35	487	0.9528	$3.26*10^{-8}$	27.2	0.6845
Mg_4Fe-R-450	36.6	0.265	338	0.9989	9.07	0.337	0.9605	1.60	451	0.9788	$9.05*10^{-8}$	25.5	0.7218

In the Langmuir equation K_L is used to classify the equilibrium parameter (R_L) using Eq. 10:

$$R_L = \frac{1}{1 + K_L C_0} \qquad (10)$$

where: K_L is the Langmuir constant and C_o is the initial concentration of Mo(VI) ions. The value of separation parameter R_L provides important information about the nature of adsorption. The value of R_L indicated the type of Langmuir isotherm to be irreversible (R_L =0), favourable (0< R_L< 1), linear (R_L=1), or unfavourable (R_L> 1) (Meroufel et al., 2013) The R_L was found to be between 0 and 1 for the entire concentration range, and for all the studied material which indicates the favourable adsorption of Mo(VI) onto the studied materials.

The Freundlich plots have a lower correlation coefficient. This suggests that the use of the Freundlich isotherm is limited. The 1/n parameter from the Freundlich plot point out also the attraction of the studied samples for Mo(VI) ions. If it is bellow one the affinity between these two is strong.

Temkin and D-R isotherms developed lower regression coefficient, therefore these two isotherms should be restrictively used for fitting the experimental data. The samples resulted after Mo(VI) adsorption were subjected to the XRD analysis in order to identify the adsorption mechanism of the Mo(VI) onto the studied samples.

The results are presented in Fig. 13, where from it is evident that, after Mo(VI) adsorption, the diffractograms of the studied materials did not suffer any changes, all the XRD patterns being characteristics for the pyroaurite group of layered double hydroxides. The calcined materials regained their layered structure after contacting the molybdate solution, the specific peaks of pyroaurite being present, with no evidence of molybdate anion presence in the interlayer space (the position of peaks and their intensities did not suffer substantial modifications).

This indicates that the molybdate anion didn`t displaced the carbonate anion from the interlayer space. It is well known that the displacement of carbonate anion from the layered double hydroxides structure is very difficult to achieve. Therefore, it is supposed that the retained mechanism of Mo(VI) onto the surface of the studied materials is its adsorption on the surface, due to the electrostatic interections between the positively charged brucite type layers and molybdate anions. The calcinated samples due tio the contacted with the molybdate solutions firstly regained their layered structure and then adsorbed the target anions. They developed a higher adsorption capacity due to their higher specific surface area.

Table 5 presents the maximum adsorption capacity, reported in literature, developed by different adsorbents in the removal process of Mo(VI) from aqueous solutions.

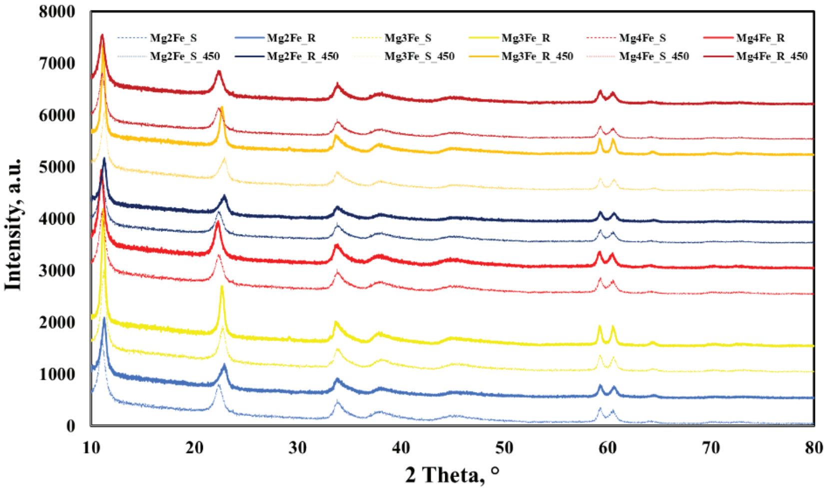

Fig. 13. XRD pattern of the studied samples after Mo(VI) adsorption

Table 5. The adsorption capacities of different adsorbents developed in the removal processes of MoO_4^{2-} ions from aqueous solutions

Adsorbent	*q_m (mg/g)*	*References*
Maghemite (γ-Fe_2O_3)	33.4	Afkhami and Norooz-Asl, 2009
$MgFeSO_4$-type HT-LDH	15.5	Paikaray et al., 2013
$ZnCl_2$ activated coir pitch carbon	18.9	Namasivayam and Sengeetha, 2006
Mg4Fe-S	24.7	Present paper
Mg4Fe-S-450	39.9	

It can be observed that the studied LDH structures present close or even higher efficiency than similar adsorbents reported in the literature.

4. Conclusions

This paper aimed the structural and adsorptive properties characterization of a Mg_nFe layered double hydroxide and its calcined product, to be used for molybdate Mo(VI) retention from waters.

The structural analysis by X-ray diffraction confirmed that the as-synthesized sample was a Mg_nFe - layered double hydroxides. The calcined LDH shows higher specific surface area and total pore volume than its LDH precursor.

The kinetic study of the adsorption showed that the process accurately obeyed pseudo-second order kinetics (correlation coefficients > 0.99). The results concerning the equilibrium of the process showed that the calcinated samples at 450°C exhibited better efficiency (maximum adsorption capacity 39.9 mg/g) in the adsorption process of Mo(VI) from aqueous solutions, than its precursor LDH (24.7 mg/g), in accordance with their specific surface area.

The correlation of the techniques used for the characterization of the obtained LDH, before and after molybdate adsorption, lead to the conclusion that the LDH materials obtained from an industrial waste have structural characteristics and similar or even higher adsorptive performance, as compared to other materials obtained from expensive analytical grade reagents reported in the literature. Therefore, the approached LDH synthesis method, starting from secondary resources, represents a viable, affordable, and green route. This can successfully replace the expensive and resource-intensive traditional synthesis method, leading to cost reduction and valuable benefits in terms of environmental protection.

The use of iron sludge as an alternative sources of iron ions for the synthesis of Mg_nFe – LDH represent an advantage for both economic and environmental protection point of view.

Acknowledgements

The studies were done during the PhD program from the Doctoral School of the University Politehnica Timisoara.

References

Abubeah R., Altaher H., Khalil T.E., (2018), Removal of hexavalent chromium using two innovative adsorbents, *Environmental Engineering and Management Journal,* **17,** 1621-1634.

Afkhami, A., Norooz-Asl, R., (2009), Removal, preconcentration and determination of Mo(VI) from water and wastewater samples using maghemite nanoparticles, *Colloids and Surfaces A: Physicochemical and Engineering Aspects*, **346**, 52-57.

Ahmed, I.M., Gasser, M.S., (2012), Adsorption study of anionic reactive dye from aqueous solution to Mg–Fe–CO_3 layered double hydroxide (LDH), *Applied Surface Science*, **259**, 650-656.

Ardau C., Frau F., Dore E., Lattanzi P., (2012), Molybdate sorption by Zn-Al sulphate layered double hydroxides, *Applied Clay Science*, **65-66**, 128-133.

Benselka-Hadj Abdelkadera N., Bentouami A., Derrichea Z., Bettahara N., de Menorval L.-C, (2011), Synthesis and characterization of Mg–Fe layer double hydroxides and its application on adsorption of Orange G from aqueous solution, *Chemical Engineering Journal*, **169**, 231-238.

Cavani F., Trifiro F., Vaccari A., (1991), Hydrotalcite-type anionic clays: preparation, properties and applications, *Catalysis Today*, **11**, 173-301.

Chou J.D., Lin C.L., Wey M.Y., Chang S.H., (2010), Effect of Cu species on leaching behavior of simulated copper sludge after thermal treatment: ESCA analysis, *Journal of Hazardous Materials*, **179**, 1106-1110.

Cong L., Jianping C., (2018), Potential role of intraparticle diffusion in dynamic partitioning of secondary organic aerosols, *Atmospheric Pollution Research*, **9**, 1131-1136.

Fahami A., Beall G., (2016), Structural and morphological characterization of $Mg_{0.8}Al_{0.2}(OH)_2Cl_{0.2}$ hydrotalcite produced by mechanochemistry method, *Journal of Solid State Chemistry*, **233**, 422–427.

Gheju M., Pode R., Manea F., (2011), Comparative heavy metal chemical extraction from anaerobically digested biosolids, *Hydrometallurgy,* **108**, 115-121.

Gilea D., Lutic D., Carja G., (2019), Heterostructures of silver and zinc based layered double hydroxides for pollutant removal under simulated solar light, *Environmental Engineering and Management Journal,* **18**, 1765-1772.

Golban A., Cocheci L., Lazau R., Lupa L., Pode R., (2018), Iron ions reclaiming from sludge resulted from hot-dip galvanizing process, as Mg3 Fe-layered double hydroxide used in the degradation process of organic dyes, *Desalination and Water Treatment,* **131**, 317-327.

Haro N.K., Del Vecchio P., Marcilio N.R., Feris L.A., (2017), Removal of atenolol by adsorption - Study of kinetics and equilibrium, *Journal of Cleaner Production*, **154**, 214-219.

Hu Q., Zhang Z., (2019), Application of Dubinin-Radushkevich isotherm model at the solid/solution interface: A theoretical analysis, *Journal of Molecular Liquids*, **227**, 646-648

Johnson R. D., Arnold F. H., (1995), The Temkin isotherm describes heterogeneous protein adsorption, *Biochimica et Biophysica Acta (BBA)-Protein Structure and Molecular Enzymology*, **1247**, 293-297.

Kamiyama N., Panomsuwan G., Yamamoto E., Sudare T., Saito N., Ishizaki T., (2016), Effect of treatment time in the Mg(OH)2/Mg-Al LDH composite film formed on Mg alloy AZ31 by steam coating on the corrosion resistance, *Surface & Coatings Technology*, **286**, 172–177.

Meroufel B., Benali O., Benyahia M., Benmussa Y., Zenasni M.A., (2013), Adsorptive removal of anionic dye from aqueous solutions by Algerian kaolin: Characteristics, isotherm, kinetic and thermodynamic studies, *Journal of Materials and Environmental Science*, **4**, 482-491.

Namasivayam C., Sengeetha D., (2006), Removal of molybdate from water by adsorption onto $ZnCl_2$ activated coir pith carbon, *Bioresource Technology*, **97**, 1194-1200.

Paikaray S.M., Hendry J., Essilfie-Dughan J., (2013), Controls on arsenate, molybdate, and selenate uptake by hydrotalcite-like layered double hydroxides, *Chemical Geology*, **345**, 130–138.

Shin S.M., Senanayake G., Sohn J.-S., Kang J.-G., Yang D.-H., Kim T.-H., (2009), Separation of zinc from spent zinc-carbon batteries by selective leaching with sodium hydroxide, *Hydrometallurgy,* **96**, 349-353.

Tkac P., Paulenova A., (2008), Speciation of molybdenum (VI) in aqueous and organic phases of selected extraction systems, *Separation Science and Technology*, **43**, 2641-2657.

Turk T., Alp I., Deveci H., (2009), Adsorption of As(V) from water using Mg–Fe-based hydrotalcite (FeHT), *Journal of Hazardous Materials*, **171**, 665–670.

Vucelic M., Jones W., Moggridge, G.D., (1997), Cation ordering in synthetic layered double hydroxides, *Clays and Clay Minerals*, **45**, 803-813.

Wang J., Xu J., Xia J., Wu F., Zhang Y., (2018), A kinetic study of concurrent arsenic adsorption and phosphorus release during sediment resuspension, *Chemical Geology*, **495**, 67-75.

WHO, (2011), *Guidelines for drinking water quality*, Fourth edition, World Health Organization, On line at: https://www.who.int/water_sanitation_health/publications/drinking-water-quality-guidelines-4-including-1st-addendum/en/

Xiaoliang L., Gaoling W., Juan X., Fuding T., Hongping H., Chenchen Q., Hui Y., Jianxi Z., Runliang Z., Zonghua Q., Jing Z., (2017), Adsorption isotherm, mechanism, and geometry of Pb(II) on magnetites substituted with transition metals, *Chemical Geology*, **470**, 132-140.

Xie F., Cai T., Ma Y., Li H., Li C., (2009), Recovery of Cu and Fe from Printed Circuit Board waste sludge by ultrasound: Evaluation of industrial application, *Journal of Cleaner Production*, **17**, 1494-1498.

Yang Y., Yan X., Hu X., Feng R., Zhou M., Cui W., (2018), Development of zeolitic imidazolate framework-67 functionalized Co-Al LDH for CO_2 adsorption, *Colloids and Surfaces A: Physicochemical and Engineering Aspects*, **552**, 16-23.

Zhang X., Zhou L., Pi H., Guo S., Fu J., (2014), Performance of layered double hydroxides intercalated by a UV stabilizer in accelerated weathering and thermal stabilization of PVC, *Polymer Degradation and Stability*, **102**, 204–211.

Environmental Engineering and Management Journal
February 2020, Vol. 19, No. 2, 247-254
http://www.eemj.icpm.tuiasi.ro/; http://www.eemj.eu

“Gheorghe Asachi” Technical University of Iasi, Romania

CONGO RED REMOVAL FROM AQUEOUS EFFLUENTS BY ADSORPTION ON CHERRY STONES ACTIVATED CARBON

Cristina-Gabriela Grigoraș[1], Andrei-Ionuț Simion[1], Lidia Favier[2], Lucian Gavrilă[1*]

[1] ”Vasile Alecsandri” University of Bacău, Faculty of Engineering, Department of Food and Chemical Engineering,
Calea Mărășești 157, 600115, Bacău, România
[2] University Rennes, Ecole Nationale Supérieure de Chimie de Rennes, CNRS, UMR 6226; 11 Allée de Beaulieu,
CS 50837, 35708 Rennes Cedex 7, France

Abstract

Soluble dyes are intensively used in various industrial activities. They represent an important class of water pollutants from which they are rather difficult to remove. This paper focusses on the elimination of Congo Red (CR) ionic azo dye by adsorption on a low cost material. Cherry stones were used for activated carbon preparation by carbonization method. A temperature of 600 °C and a time of 4 h were found as adequate parameters for the physical activation and led to a final white powder with fine particles. The obtained product was put in contact with CR aqueous solutions having concentrations ranging between 200 mg/L and 1000 mg/L and pH values between 2 and 12 and the mixtures were magnetically agitated for periods of 10 to 180 minutes. The best results were recorded at acidic and neutral pH where the CR removal percentage was over 99 % while in alkaline environment the adsorption was negligible. The applied tests revealed that the process is well described by a pseudo-second-order kinetic model (with correlation coefficients close or equal to unity) and that Freundlich isotherm is suitable to insure a very good fit with the experimental data (with correlation coefficients values higher than 0.99).

The acquired results proved that cherry stones (a rarely used waste from food industry) can constitute an interesting and adequate alternative for manufacturing inexpensive materials possessing adsorption properties with high capacity for dye removal from aqueous solutions.

Key words: adsorption kinetics, cherry stones activated carbon, Congo Red dye, Freundlich isotherm

Received: January, 2019; Revised final: January, 2020; Accepted: January, 2020; Published in final edited form: February, 2020

---

1. Introduction

Soluble dyes coming from a wide variety of industrial activities (textile, paint, tanning, paper, cosmetic, food etc.) constitute an important class of pollutants (Basheer and Ali, 2018; Basheer, 2018) which is known as being difficult to remove from wastewater due to the high registered values of alkalinity, biological oxidation demand, chemical oxidation demand, total dissolved solids (Basheer, 2018; Srinivasan and Viraraghavan, 2010;) etc.

Biological, chemical and physical methods going from enzymatic degradation (Chacko and Subramaniam, 2011) or anaerobic-aerobic treatments (Manavi et al., 2017) to electrochemical destruction (Liang et al., 2018), electrocoagulation (Ali et al., 2013; Madi et al., 2019), ozonation (Mehrjouei et al., 2015), oxidation (Gagol et al., 2018; Kitinya et al., 2017), coagulation-flocculation (Gil Pavas et al., 2017; Sizykh et al., 2018), membrane filtration (Hosseini et al., 2019) or irradiation (He et al., 2016; Martin de Vidales et al., 2017) are applied for wastewater purification.

These methods are proved to be efficient in removing different dyes from aqueous effluents but they present also specific disadvantages. The biological treatments are not sufficient alone since they may not completely eliminate all dye particles.

---

[*] Author to whom all correspondence should be addressed: e-mail: lgavrila@ub.ro

Moreover, they necessitate living microorganisms with length growth phase requiring particular conditions (nitrogen confined area, large reactors etc.) and their use can lead to undesirable by-products formation (methane, sludge, colorless toxic by-products). In terms of chemical dye removal methods, drawbacks such as high electrical energy demand, chemical reagents consumption, and generation of toxic secondary pollution can be cited (Katheresan et al., 2018).

As for the physical techniques, even though they can imply high financial costs and generate important quantities of sludge, due to their simplicity, efficiency and predictability (Yagub et al., 2014) and to the fact that they require the least amount of chemicals, they are the most commonly used methods for dye elimination adsorption being, by far, the best alternative among them (Ali et al., 2013; Ali et al., 2016). The process implies a mass transfer of a substance (called adsorbate) at the interface between a liquid and a solid phase (called adsorbent). It frequently takes place through physical sorption and, in rare cases, by chemical sorption. The materials employed for dye adsorption must possess a high surface area (Ali et al., 2018a; Ali et al. 2018b; Ali et al., 2019a; Nodeh et al., 2016) and an important porosity in order to insure a high diminishment of dye concentration from treated aqueous effluents. Adsorbents such as industrially obtained activated carbon, silica gel, zeolites, clay, alumina or nanomaterials (Ali, 2018; Ali et al., 2017; Ali et al., 2018c; Ali et al., 2019b; Natarajan et al., 2018) are often used to this purpose but, in the last years, low cost materials intensively replace them.

There are researches showing, for example, that Psyllium stalks (Periyaraman et al., 2019) coffee wastes (Kyzas et al., 2012), orange peel (Annadurai et al., 2002), rice husk (Vadivelan and Kumar, 2005), *Pistia stratiote* aquatic macrophyte (Modenes et al., 2018) sewage sludge (Dhouadi and M'Henni, 2009), red mud (Gupta et al., 2004) or activated clay (Ho et al., 2001) can successfully adsorb dyes as Coomassie Brilliant Blue, Black Krom KJR, Basic Blue 30, Methylene Blue, Vat Red 10, Rhodamine B, Fast Green etc.

In this paper we report on the possibility to use by-products from food industry to adsorb dyes from liquid solutions. The experimental program was conducted on three different steps. The first one was focused on the preparation of low-cost activated carbon from dried, grounded cherry stones by physical process of carbonization at different temperatures and time periods. In the second step of the study, the obtained porous material was used as adsorbent for Congo Red (an anionic azo dye) elimination from aqueous solutions and the effect of pH, dye concentration and contact time was examined. At the end, adsorption kinetics and equilibrium sorption behavior of the adsorbents have been studied.

2. Material and methods

2.1. Reagents

Sodium chloride 0.1 N and hydrochloric acid 0.1 N used for the experiments were purchased from Chemical Company (Iasi, Romania).

2.2. Activated carbon preparation

The cherry stones, manually separated from fruits bought from a local market, were intensively washed with tap water to eliminate any residue or strange material, dried for one week at room temperature and crushed to powder with a coffee grinder. Aliquots of 10 g of this powder were placed in porcelain capsules which were introduced in a Caloris L1003 laboratory furnace (Caloris Group, Romania) at temperatures between 500 °C and 900 °C for periods between 4 h and 6 h. After calcination, the capsules were cooled in a desiccator. The obtained product (abbreviated as CS) was weighed and stored in closed recipients at room temperature. The process yield was calculated by multiplying with 100 the ratio between the quantity of the final product and the amount of grounded cherry stones.

2.3. Congo Red (CR)

The analytical purity CR dye powder (molecular structure in Fig. 1) was supplied by Sigma Aldrich (Merk, France). A stock solution (1 g/L) was prepared with distilled wat r. Dilutions to 20 mg/L were adjusted at five pH values (2, 4, 7, 10 and 12) by adding small volumes of hydrochloric acid 0.1 N or sodium chloride 0.1 N. pH measurements were made with a portable pH-meter (Hanna Instruments Service, Romania). The solutions were introduced in quartz cuvettes (pathlength 10 mm) and scanned in a Zuzi 4201 UV-VIS spectrophotometer (Auxilab, Spain). The recorded UV-VIS spectra are given in Fig. 2 and served for determination of maximum absorbance wavelengths which were: 570 nm for pH 2; 530 nm for pH 4 and 500 nm for pH 7, 10 and 12.

2.4. Adsorption experiments

In order to evaluate the adsorption of CR on the prepared cherry stones low cost adsorbent material, 0.1 g CS were put in contact with 20 mL of CR solutions having concentrations of 200, 400, 600, 800 and 1000 mg/L and different pH values (2, 4, 7, 10 and 12). The mixtures were magnetically stirred on a Nahita Blue 692 heating plate (Auxilab, Spain) at room temperature for 10, 20, 30, 40, 50, 60, 90, 120, 150 and 180 minutes. The adsorbent was than separated from the aqueous dye solution in a Nahita 2615/1 digital centrifuge (Auxilab, Spain) set at 3000 rpm for 5 minutes.

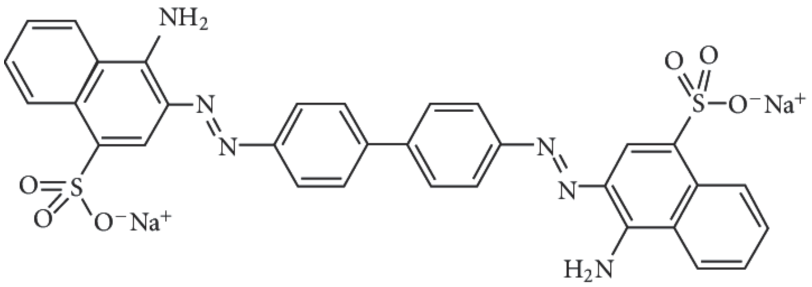

Fig. 1. Congo Red structure

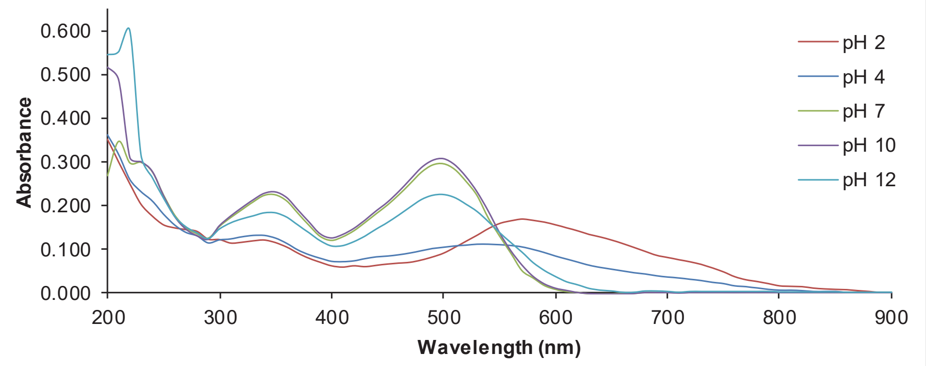

Fig. 2. Congo Red UV-VIS spectra at different pH values

The final residual concentration of each resulting supernatant was determined based on pH specific calibration curves.

2.5. Adsorption kinetics

The adsorption process mechanisms and dynamics were evaluated by calculating the dye uptake. Eq. (1) was employed to this purpose.

$$q_t = \frac{C_0 - C_t}{M} \cdot V \quad \text{(mg/g)} \tag{1}$$

where q_t (mg/g, mg of CR per g of CS) is the sorption capacity at time *t*; C_0 and C_t are dye initial and time *t* concentrations (mg/L); *V* (L) is the CR solution volume and *M* (g) is the mass of CS adsorbent used in the experiment.

2.6. Adsorption isotherm determination

CR efficiency removal ($R_{\%}$) from tested solutions was calculated using the Eq. (2):

$$R_{\%} = \frac{C_0 - C}{C_0} \cdot 100 \tag{2}$$

where C_0 (mg/L) and *C* (mg/L) are the CR initial and final concentrations respectively.

The amounts of CR adsorbed on CS were calculated using the following equation:

$$q_e = \frac{C_0 - C_e}{M} \cdot V \quad \text{(mg/g)} \tag{3}$$

where q_e (mg of CR per g of CS) is the equilibrium adsorption capacity; C_0 and C_e are the initial and equilibrium dye solutions concentrations (mg/L); *V* (L) is the CR solution volume and *M* (g) is the adsorbent mass.

3. Results and discussions

3.1. Cherry stones activated carbon preparation

Cherry stones are a food waste with wide availability and high mechanical strength but in general abandoned or incinerated. Different researchers analyzed the possibility of using this waste to produce activated carbon by chemical or physical methods. For example, Angin (2014) studied the chemical activation process, which implies the presence of a reagent influencing the pyrolysis, and revealed as optimum conditions an impregnation ratio with zinc chloride of 3:1 and a carbonization temperature of 700 °C. Olivares-Marin et al. (2005, 2012) focused on the use of potassium hydroxide or of sulfuric acid as dehydration agents and of a temperature of 400 °C to 900 °C. Their resulted carbons possessed high specific surface area and porosity. Despite its good results, these methods generate undesirable wastes. That is why an increasing interest is accorded to the possibility of using the easiest available and the most environmental friendly technological processes of activated carbon production. Duran-Valle et al. (2006) evaluated the physical activation which consists in submitting CS to oxidizing gases (air, nitrogen, carbon dioxide etc.) at temperatures of 350 °C to 1000 °C. They applied heat treatments going from 400 °C to 900 °C in nitrogen atmosphere and they concluded that the obtained products are characterized by a low ash content and an important fixed carbon amount being essentially porous materials. Nowicki et al. (2015) submitted the cherry stones to pyrolysis at 500 °C and 800 °C and, after a cooling down period in argon, to a physical activation step at 800 °C under carbon dioxide. Good adsorption properties towards organic (methylene blue, iodine) and inorganic (nitrogen dioxide, hydrogen sulfide) pollutants were registered.

In view of the above, our experiments were directed on the preparation of activated carbon by direct calcination without any preliminary treatment. 600 °C and 240 minutes were considered as adequate and used afterwards. In this case the process yield was of 1.2 %. At a temperature of 500 °C applied for 5 h, the product contained black particles of residual unburned organic material. When higher temperatures (*e. g.* 900 °C) and longer periods (*e. g.* 6 h) were employed the yield was substantially reduced. The evolution from the initial cherry stones to the activated carbon is illustrated in Fig. 3.

3.2. Effect of adsorption parameters

One of the most important parameters affecting the CR adsorption is represented by the pH of dye aqueous solutions. The process has good results at low values (Fig. 4). The color removal is over 99 % at pH 2, 4 and 7 (for a starting concentration of 1000 mg/L). At pH 10 and 12 the removal percentage decreases drastically being of only 14.95 % and 5.99 % respectively. The observations recorded are explained by the fact that at alkaline pH, the HSO_3^- groups of CR turn into $-SO_3^-Na^+$ radicals while the CS has more negative charges which has undesirable effects on the adsorption process due to electrostatic repulsion.

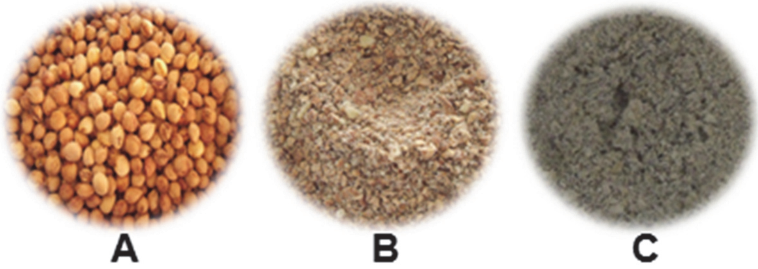

Fig. 3. Cherry stones activated carbon (A – dried cherry stones; B – grounded cherry stones; C – activated carbon)

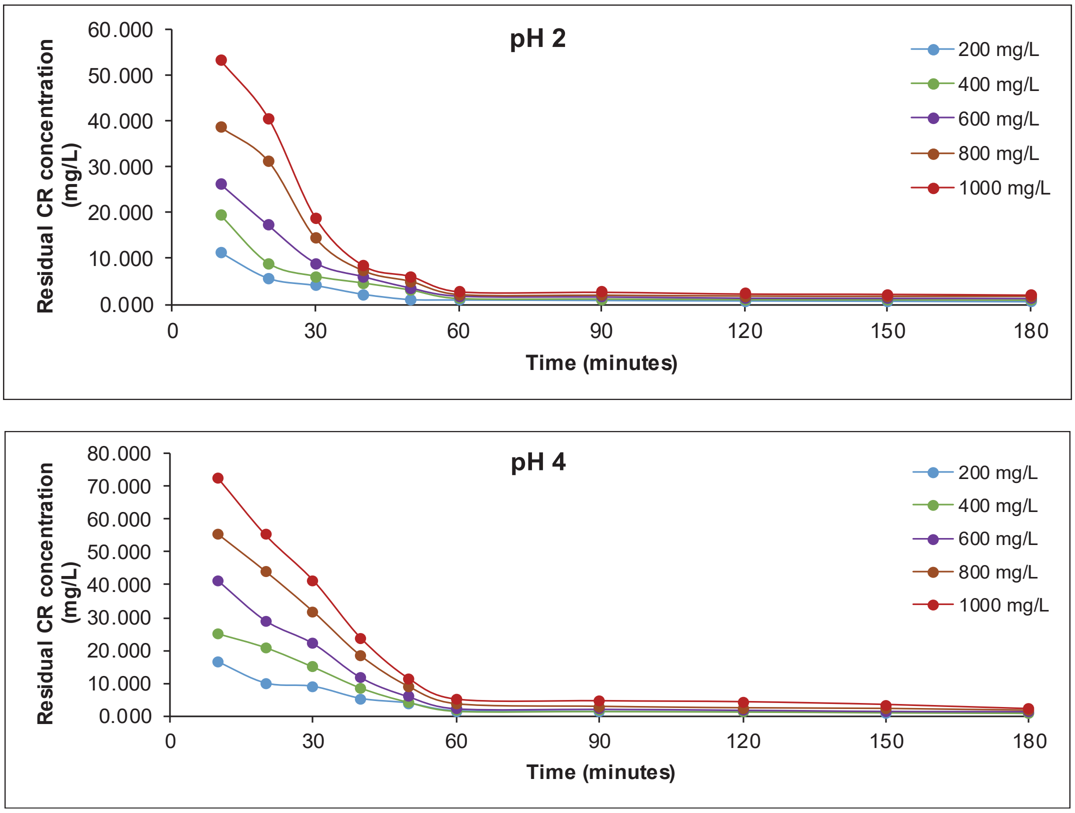

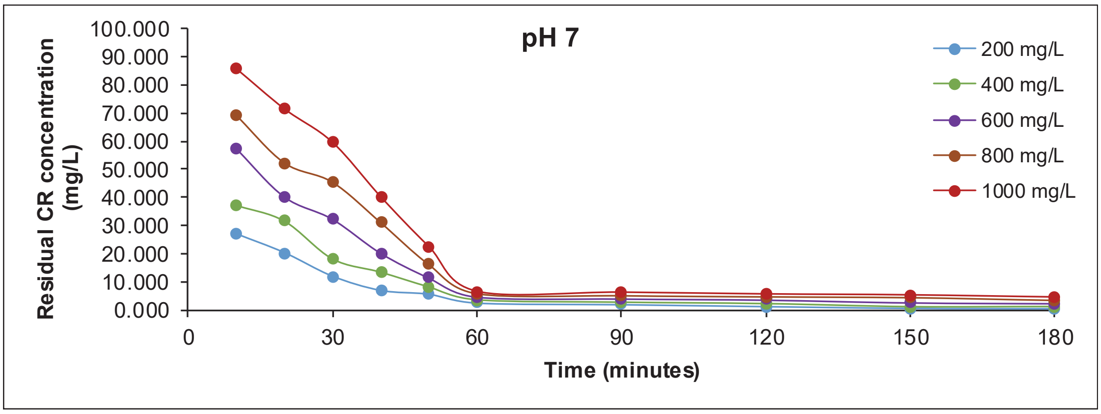

Fig. 4. Residual CR concentration depending at studied adsorption parameters

Moreover, in this case, a CR high concentration increases the ion strength reducing also the CS adsorption capacity. At acidic pH, CR is dissociated to polar groups and the adsorbent has an increased protonation at its surface which favors the interactions between the CS and HSO_3^- groups and enhances the adsorption. These findings are similar with those reported by other studies focused on CR elimination from aqueous effluents by using various adsorbents such as carbonized leonardite (Ausavasukhi et al., 2016), biowaste materials (Kaur et al., 2013), or activated carbon obtained from wood sawdust (Cheng et al., 2015) or with electropositive amine modification (Tian et al., 2018).

Dye initial concentration is another parameter which influences the adsorption. The removal percentage decreased with the increase of CR initial concentration. This indicates that the available active sites of CS are not abundant enough for the adsorption of all the amount of CR existing in the treated aqueous solutions. The process is even more difficult in alkaline environment and high CR concentrations the registered results being far from satisfactory.

In terms of contact time, one can note (also from Fig. 4) that the adsorption takes place systematically in the first 60 minutes after that the CR retained on the adsorbent surface being rather insignificant. Taking into consideration the obtained results, in the experienced conditions, it is recommended to conduct the removal of CR by adsorption on cherry stones activated carbon at pH values between 2 and 7, for at least 1 h.

3.3. Adsorption kinetics

As specified earlier, the contact time has a great impact on CR adsorption. Two recurrently employed kinetic models (pseudo 1st order and pseudo 2nd order) were tested to establish which is more appropriate to describe the studied process. If the pseudo 1st order kinetic was not capable to define the acquired data, very good results were recorded for the pseudo 2nd order kinetic model. Its equation is illustrated by the Eq. (4):

$$\frac{t}{q_t} = \frac{1}{k \cdot q_e^2} + \frac{t}{q_e} \tag{4}$$

where: k (g/mg·min) is the pseudo-2nd order rate constant, q_e is CR quantity retained by CS at equilibrium and q_t is CR amount adsorbed at time t.

k and q_e values were established from the slopes and intercepts obtained by figuring t/q_t against t at different CR concentrations and are shown in Table 1. The correlation coefficients which are very close or even equal to unity reveal that there were no significant differences between the experimental collected q_e and those determined from the obtained equations. Therefore, it can be considered that the pseudo-2nd order kinetic model successfully describes the adsorption process. This conclusion is sustained also by Li et al. (2016) which concentrated their studies on the CR retention on an activated carbon prepared from a Mexican herb.

3.4. Adsorption isotherms

The adsorption equilibrium can be defined by numerous isotherm models providing information on adsorbent – adsorbate relation. Among them, Langmuir and Freundlich ones are regularly employed. The first is based on the assumption that there are no conjoint interactions between the adsorbed molecules the process occurring only as monolayer adsorption on the active sites of the adsorbent material (Azizian et al., 2018; Hu et al., 2018). The hypothesis of the second mentioned model sustains that the sorption happens initially on the stronger binding sites existing on the adsorbent heterogeneous surface and that the retention diminishes gradually until all the sites are occupied by the adsorbed molecules (Brizi Neris et al., 2019; Putro et al., 2017; Syafiuddin et al., 2018).

Table 1. The pseudo-second-order kinetic parameters for CR removal by CS

Concentration [mg/L]	***Linear equation coefficients***		***Calculated q_e [mg/g]***	***k [g/mg min]***	***R^2***
	a	***b***			
pH 2					
200	0.02498	0.01223	40.032	0.051	1.00000
400	0.01249	0.00542	80.064	0.029	1.00000
600	0.00832	0.00354	120.192	0.020	1.00000
800	0.00624	0.00315	160.256	0.012	0.99999
1000	0.00499	0.00264	200.401	0.009	0.99999
pH 4					
200	0.02492	0.02671	40.128	0.023	0.99998
400	0.01246	0.01092	80.257	0.014	0.99998
600	0.00830	0.00708	120.482	0.010	0.99998
800	0.00622	0.00595	160.772	0.007	0.99998
1000	0.00498	0.00492	200.803	0.005	0.99998
pH 7					
200	0.02477	0.04714	40.371	0.013	0.99997
400	0.01243	0.01734	80.451	0.009	0.99997
600	0.00830	0.01093	120.482	0.006	0.99997
800	0.00622	0.00827	160.772	0.005	0.99996
1000	0.00498	0.00700	200.803	0.004	0.99994

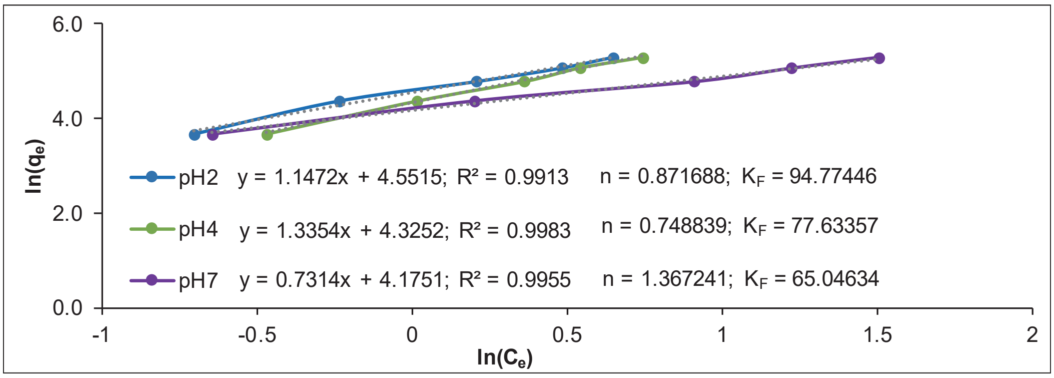

Fig. 5. Freundlich isotherm model of CR adsorption on CS

Our experimental data do not follow the Langmuir model even though there are studies such as that published by Belhachemi and Addoun (2012) showing this type of isotherm along with that of Redlich-Peterson as being highly adequate. Instead, they accurately fit the Freundlich isotherm in which equation's (Eq. 5) q_e is the amount of CR (mg) adsorbed on CS (g), C_e (mg/L) is the dye equilibrium concentration and K_F and n are constants.

$$\log q_e = \log K_F + \frac{1}{n} \log C_e \tag{5}$$

Linear graphical representation of log(qe) versus log(Ce) (Fig. 5) served to calculate K_F and n constants their registered values indicating an encouraging adsorption. Comparable conclusions were emphasized also by other researches (Mane and Vijay Babu, 2013; Kannan and Meenakshisundaram, 2002).

4. Conclusions

The possibility of using cherry stones for activated carbon preparation by carbonization method was investigated in this study. The obtained product possesses good adsorption properties its abilities to retain pollutants being tested for the removal of Congo Red from aqueous solutions.

The experiments carried out show that, in acidic and neutral media, over 99 % of the existing dye was eliminated after 180 minutes and that a pH above 7 it is not recommended. The conducted research allowed us to conclude that the adsorption process follows a pseudo-second-order kinetics and that it fits with a very high confidence degree the Freundlich isotherm model.

References

Ali I., (2018), Microwave assisted economic synthesis of multi walled carbon nanotubes for arsenic species removal in water: Batch and column operations, *Journal of Molecular Liquids*, **271**, 377-384.

Ali I., Al-Harbi O.M.L., Al-Othman Z.A., Al-Warthan A., (2018a), Facile and eco-friendly synthesis of functionalized iron nanoparticles for cyanazine removal in water, *Colloids and Surfaces B: Biointerfaces*, **171**, 606-613.

Ali I., Al-Harbi O.M.L., Al-Othman Z.A., Al-Warthan Z.A., Al-Mohaimeed A.M., (2019a), Preparation of a carboxymethylcellulose-iron composite for uptake of atorvastatin in water, *International Journal of Biological Macromolecules*, **132**, 244-253.

Ali I., Al-Harbi O.M.L., Al-Othman Z.A., Badjah A.Y., (2018b), Kinetics, thermodynamics, and modeling of Amino Black dye photodegradation in water using Co/TiO_2 nanoparticles, *Photochemistry and Photobiology*, **94**, 935-941.

Ali I., Al-Harbi O.M.L., Al-Othman Z.A., Badjah A.Y., Al-Warthan A., Basheer A. A., (2018c), Artificial neural network modelling of amido black dye sorption on iron composite nano material: Kinetics and thermodynamics studies, *Journal of Molecular Liquids*, **250**, 1-8.

Ali I., Al-Othman Z. A., Al-Warthan A., (2015), Removal of secbumeton herbicide from water on composite nanoadsorbent, *Desalination and Water Treatment*, **57**, 10409-10421.

Ali I., Al-Othman Z.A., Al-Warthan A., (2016), Sorption, kinetics and thermodynamics studies of atrazine herbicide removal from water using iron nano-composite material, *International Journal of Environmental Science and Technology*, **13**, 733-742.

Ali I., Al-Othman Z.A., Al-Warthan A., (2017), Uptake of propranolol on ionic iron nanocomposite adsorbent: Kinetic, thermodynamics and mechanism of adsorption, *Journal of Molecular Liquids*, **236**, 205-213.

Ali I., Asim M., Khan T.A., (2013), Arsenite removal from water by electro-coagulation on zinc-zinc and copper-copper electrodes, *International Journal of Environmental Science and Technology*, **10**, 377-384.

Ali I., Basheer A.A., Mbianda X.Y., Burakov A., Galunin E., Burakova I., Mkrtchyan E., Tkachev A., Grachex V., (2019b), Graphene based adsorbents for remediation of noxious pollutants from wastewater, *Environmental International*, **127**, 160-180.

Angin D., (2014), Production and characterization of activated carbon from sour cherry stones by zinc chloride, *Fuel*, **115**, 804-811.

Annadurai G., Juang R. S., Lee D.J. (2011), Use of cellulose-based wastes for adsorption of dyes from aqueous solutions, *Journal of Hazardous Materials*, **92**, 363-374.

Ausavasukhi A., Kampoosaen C., Kengnok O., (2016), Adsorption characteristics of Congo Red on carbonized leonardite, *Journal of Cleaner Production*, **134**, 506-514.

Azizian S., Eris S., Wilson L.D., (2018), Re-evaluation of the century-old Langmuir isotherm for modeling adsorption phenomena in solution, *Chemical Physics*, **513**, 99-104.

Basheer A.A., (2018), Chemical chiral pollution: Impact on the society and science and need of the regulations in the 21st century, *Chyrality*, **30**, 402-406.

Basheer A.A., (2018), New generation nano-adsorbents for the removal of emerging contaminants in water, *Journal of Molecular Liquids*, **261**, 583-593.

Basheer A.A., Ali I., (2018), Stereoselective uptake and degradation of (±)-*o,p*-DDD pesticide steromers in water-sediment system, *Chyrality*, **30**, 1088-1095.

Belhachemi M., Addoun F., (2012), Adsorption of Congo Red onto activated carbons having different surface properties: studies of kinetics and adsorption equilibrium, *Desalination and Water Treatment*, **37**, 122-129.

Brizi Neris J.B., Martinez Luzardo F.H., Galvao Paranhos da Silva E., Garcia Velasco F., (2019), Evaluation of adsorption processes of metal ions in multi-element aqueous systems by lignocellulosic adsorbents applying different isotherms: A critical review, *Chemical Engineering Journal*, **357**, 404-420.

Chacko J.T., Subramaniam K., (2011), Enzymatic degradation of azo dyes – A review, *International Journal of Environmental Sciences*, **6**, 1250-1260.

Cheng Z., Zhang L., Guo X., Jiang X., Li T., (2015), Adsorption behavior of direct red 80 and congo red onto activated carbon/surfactant: Process optimization, kinetics and equilibrium, *Spectrochimica Acta Part A: Molecular and Biomolecular Spectroscopy*, **137**, 1126-1143.

Dhaouadi H., M'Henni F., (2009), Vat dye sorption onto crude dehydrated sewage sludge, *Journal of Hazardous Materials*, **164**, 448-458.

Duran-Valle C.J., Gomez-Corso M., Gomez-Serrano V., Pastor-Villegaas J., Rojas-Cervantes M.L., (2006), Preparation of charcoal from cherry stones, *Applied Surface Science*, **252**, 5957-5960.

Gagol M., Przyjazny A., Boczkaj G., (2018), Wastewater treatment by means of advanced oxidation processes based on cavitation, *Chemical Engineering Journal*, **338**, 599-627.

Gil Pavas E., Dobrosz-Gomez I., Gomez-Garcia M.A., (2017), Coagulation-flocculation sequantial with Fenton of Photo-Fenton processes as an alternative for the industrial textile wastewater treatment, *Journal of Environmental Management*, **191**, 189-197.

Gupta V.K., Li I., Saini V.K., (2004), Removal of Rhodamine B, Fast Green and Methylene Blue from wastewater using red mud, an aluminum industry waste, *Industrial and Engineering Chemistry Research*, **43**, 1740-1747.

He S., Sun W., Wang J., Chen L., Zhang Y., Yu J., (2016), Enhanced of biodegradability of real textile and dyeing wastewater by electron beam irradiation, *Radiation Physics and Chemistry*, **124**, 203-207.

Ho Y. S., Chiang C. C., Hsu Y. C., (2001), Sorption kinetics for dye removal from aqueous solution using activated clay, *Separation Science Technology*, **36**, 2473-2488.

Hosseini S.A., Vossoughi M., Mahmoodi N.M., (2019), Clay-based electrospun nanofibrous membranes for colored wastewater treatment, *Applied Clay Science*, **168**, 77-86.

Hu Q., Liu Y., Feng C., Zhang Z., Lei Z., Shimizu K., Predicting equilibrium time by adsorption kinetic equations and modifying Langmuir isotherm by fractal-like approach, *Journal of Molecular Liquids*, **268**, 728-733.

Kannan N., Meenakshisundaram M., (2002), Adsorption of Congo Red on various activated carbons, *Water, Air, and Soil Pollution*, **138**, 289-305.

Katheresan V., Kasendo J., Lau S.Y., (2018), Efficiency of various recent wastewater dye removal methods: A review, *Journal of Environmental Chemical Engineering*, **6**, 4676-7697.

Kaur S., Rani S., Mahajan K., (2013), Adsorption kinetics for the removal of hazardous dye Congo Red by biowaste materials as adsorbents, *Journal of Chemistry*, On line at: http://dx.doi.org/10.1155/2013/628582.

Kitinya J., Onyango M., Ochieng A., (2017), Removal of Multilan Red and multi-active blue dyes from aqueous solution by adsorption and oxidation techniques: Equilibrium, kinetics and thermodynamic studies, *Environmental Engineering and Management Journal*, **16**, 2731-2743.

Kyzas G.Z., Lazaridis N.K., Mitropoulos A.C., (2012), Removal of dyes from aqueous solutions with untreated coffee residues as potential low-cost adsorbents: equilibrium, reuse and thermodynamic approach, *Chemical Engineering Journal*, **189-190**, 148-159.

Li C., Zhang L., Xia H., Peng J., Zhang S., Cheng S., Shu J., (2016), Kinetics and isotherms studies for Congo Red adsorption on mesoporous *Eupatorium adenopborum*-based activated carbon via microwave-induced H_3PO_4 activation, *Journal of Molecular Liquids*, **224**, 737-744.

Liang S., Zhang B., Shi J., Wang T., Zhang L., Wang Z., Chen C., (2018), Improved decolorization of dye wastewater in an electrochemical system powered by microbial fuel cells and intensified by micro-electrolysis, *Bioelectrochemistry*, **124**, 112-118.

Madi K., Yahiaoui I., Aissani-Benissad F., Vial C., Audonnet F., Favier L., (2019), Basic Red Dye removal by coupling electrocoagulation process with biological treatment, *Environmental Engineering and Management Journal*, **18**, 563-573.

Manavi N., Kazemi A. S., Bonakdarpour B., (2017), The development of aerobic granules from conventional activated sludge under anaerobic-aerobic cycles and their adaptation for treatment of dyeing wastewater, *Chemical Engineering Journal*, **312**, 375-384.

Mane V.S., Vijay Babu P.V., (2013), Kinetic and equilibrium studies on the removal of Congo Red from aqueous solution using Eucalyptus wood (*Eucalyptus globulus*) saw dust, *Journal of the Taiwan Institute of Chemical Engineers*, **44**, 81-88.

Martin de Vidales M.J., Millan M., Saez C., Canizares P., Rodrigo M.A., (2017), Irradiated-assisted electrochemical processes for the removal of persistent pollutants from real wastewater, *Separation and Purification Technology*, **175**, 428-434.

Mehrjouei M., Muller S., Moller D., (2015), A review on photocatalytic ozonation used for the treatment of water and wastewater, *Chemical Engineering Journal*, **263**, 209-2019.

Modenes A.N., Bisinella Scheufele F.B., Barbosa J.C., Colombo A., Goes Trigueros D.E., Espinoza-Quinones F.R., Hinterholz C.L., Kroumov A.D., (2018), Assessment of kinetics, equilibrium and thermodynamics of Black Krom KJR dye adsorption onto aquatic macrophyte *Pistia stratiote*, *Environmental Engineering and Management Journal* **17**, 2587-2595.

Natarajan S., Bajaj H.C., Tayade R.J., Recent advances on the synergetic effect of adsorption for removal of dyes from waste water using photocatalytic process, *Journal of Environmental Sciences*, **65**, 201-222.

Nodeh H.R., Ibrahim W.A.W., Ali I., Sanagi M.M., (2016), Development of magnetic graphene oxide adsorbent for the removal and preconcentration of As (III) and As (IV) species from environmental water samples, *Environmental Science and Pollution Research*, **23**, 9759-9773.

Nowicki P., Kazmierczak J., Pietrzak R., (2015), Comparison of physicochemical and sorption properties of activated carbons prepared by physical and chemical activation of cherry stones, *Powder Technology*, **269**, 312-319.

Olivares-Martin M., Fernandez-Gonzales C., Macias-Garcia A., Gomez-Serrano V., (2005), Preparation of activated carbons from cherry stones by activation with potassium hydroxide, *Applied Surface Science*, **252**, 5980-5983.

Olivares-Martin M., Fernandez-Gonzales C., Macias-Garcia A., Gomez-Serrano V., (2012), Preparation of activated carbon from cherry stones by physical activation in air. Influence of the chemical carbonization with H_2SO_4, *Journal of Analytical and Applied Pyrolysis*, **94**, 131-137.

Periyaraman P.M., Karan S., Ponnusamy S.K., Vaidyanathan V., Vasanthakumar S., Dhanasekaran A., Subramanian S., (2019), Adsorption of an anionic dye onto native and chemically modified agricultural waste, *Environmental Engineering and Management Journal*, **18**, 257-270.

Putro J.N., Kurniawan A., Ismadji S., Ju Y.-H., (2017), Nanocellulose based biosorbents for wastewater treatment: Study of isotherm, kinetic, thermodynamic and reusability, *Environmental Nanotehcnology, Monitoring & Management*, **8**, 134-149.

Sizykh M.R., Batoeva A.A., Khandarkhayeva M.S., (2018), Removal of dyes from water by galvanocoagulation, *Environmental Engineering and Management Journal*, **17**, 27-34.

Srinivasan A., Viraraghavan T., (2010), Decolorization of dye by wastewaters by biosorbents: A review, *Journal of Environmental Management,* **91**, 1915-1929.

Syafiuddin A., Salmiati S., Jonbi J., Fulazzaky M.A., (2018), Application of the kinetic and isotherm models for better understanding of the behaviors of silver nanoparticles adsorption onto different adsorbents, *Journal of Environmental Management*, **218**, 59-70.

Tian C., Feng C., Wei M., Wu Y., (2018), Enhanced adsorption of anionic toxic contaminant Congo Red by activated carbon with electropositive amine modification, *Chemosphere*, **208**, 476-783.

Vadivelan V., Kumar K.V., (2005), Equilibrium, kinetics, mechanism, and process design for the sorption of methylene blue onto rice husk, *Journal of Colloid Interface Science*, **286**, 90-100.

Yagub M.T., Sen T.K., Afroze S., Ang H.M., (2014), Dye and its removal from aqueous solution by adsorption: A review, *Advances in Colloid and Interface Science*, **209**, 172-184.

Environmental Engineering and Management Journal
February 2020, Vol.19, No. 2, 255-267
http://www.eemj.icpm.tuiasi.ro/; http://www.eemj.eu

"Gheorghe Asachi" Technical University of Iasi, Romania

PROCESS WATER TREATMENT IN A THERMAL POWER PLANT: CHARACTERISTICS AND SEDIMENT/SLUDGE DISPOSAL

Dorina Stănciulescu[1], Carmen Zaharia[2]*

[1]Veolia Energie Iasi Co., 23 Chişinău Street, Iaşi, Romania
[2]Gheorghe Asachi Technical University of Iasi, "Cristofor Simionescu" Faculty of Chemical Engineering and Environmental Protection, Department of Environmental Engineering and Management, 73 Prof. Dr. docent D. Mangeron Street, Iasi, 700050, Romania

Abstract

The industrial water quality of a thermal power plant is of high importance, and a process water treatment station being always required. Whatever the adopted treatment system is, it is accompanied by the production of different amounts of sediment and sludge, which must be disposed and valorized. This paper presents in detail, the physical-chemical treatment system applied for the industrial water production in a Romanian thermal power plant (Veolia Energy Iasi Co.), referring to its installations, performance achieved, and also the quality characteristics of the treated industrial process water and certain types of produced sludges (i.e. primary and desulfurization ones).

The industrial water treatment performance is very good (85-100%) in terms of suspended solids, turbidity, organics (expressed by COD), fixed residues, heavy metals content, total hardness and microbiological inhibitors. The water and total iron contents were high in the primary sludge and, for the desulfurization sludge, low water and moderate calcium contents were found to be present.

Information on the applied treatment and valorization possibilities of primary sediment and sludge are recommended, all being dependent on the operational and maintenance costs of used conditioning and dehydration installations. The final result can be a newly added-value byproduct which would be used as raw or auxiliary material (uniform compact plates), but also the minimization of produced sludge amounts in association with the environment protection and the control of environmental pollution due to industrial water treatment station functioning.

Key words: ferrous salts-based coagulation, industrial water softening, process water treatment, sediment/sludge thickening, thermal power plant

Received: January, 2019; Revised final: January, 2020; Accepted: January, 2020; Published in final edited form: February, 2020

1. Introduction

Any thermal power generation is not a fully effective process in terms of environmental impact due to its by-products and wastes produced (gaseous, liquid-gas and solid ones), among others. In the energy sector, a conventional thermal power plant is based on the combustion of a 'clean' fossil fuel to produce steam and/or hot water for different industrial and domestic utilizations by using different installations/systems, e.g. transport/transfer installations, fuel preparation and storage systems, combustion installations, water supply systems, process water treatment stations, wastewater treatment systems, or neutralization systems, sewage systems, disposal platforms of slag, ashes and by-products of neutralization processes etc.

Process water, depending on its origin, can contain a wide range of dissolved substances or/and suspended solids, being well known that water is commonly a very good solvent. Therefore, as one of important raw matter, industrial water is usually

---

* Author to whom all correspondence should be addressed: e-mail: czah@ch.tuiasi.ro, czaharia2003@yahoo.com; Phone: +40 232 278683 ext 2175; Fax: +40 232 271311

treated in a station to obtain the quality required as process water in a thermal power plant, considering its principal scope of useful and safe thermal energy production and its efficient distribution, conversion and consumption by all interconnected industrial, public and domestic consumers.

The treated water will be used as process water or industrial water in the water-steam and/or water-water circuits of the thermal power plant where can be impurified due to the dissolved chemicals, formed precipitates and agglomerates, as well as residual chemicals caused of evaporation, cooling and heating processes in different thermal installations, etc.

Process water can be used as *additional process water* (with very low content of salts and gases), requiring pre-treatment by mechanical (filtration, sedimentation), chemical (carbonation by absorption with lime, coagulation, ionic exchange) and physical (thermal degasifying, vaporization, boiler stripping) methods, and as *cooling water* (with as low as possible temperature) after a corresponding treatment (especially water softening or demineralization).

Therefore, the main aim of a process water treatment station in a thermal power plant consists in the production of industrial water with adequate characteristics for specific use in order to ensure a safe and long time period exploitation of thermo-energetic installations and connected systems from the water-steam, or water-water circuits, meaning those used in:

(i) The chemical degasifying station (i.e. carbonation and desulfurization processes by absorption of CO_2 and SO_2 gases in alkaline/lime solution followed by mechanical filtration);

(ii) The primary process water treatment station (coagulation-sedimentation);

(iii) The industrial water softening station (hardness reduction by ionic exchange process), but also the treatment, disposal and valorisation (when is possible) of primary and desulfurization sludges separated from the industrial water treatment stations in association or not with other technological process steps.

The implementation of 'circular economy' concept in the thermal power plant implies an increasing interest for individual, or even 'in mixture' treatment and valorization of its by-products and wastes for new raw matter or auxiliary/conditioning material preparation with certain added-value, chemical reagents solution preparation, or uses of hybrid thermal power systems (conventionally associated with renewable ones) which will minimize and control the environmental impact and potential risks, among others (Bangviwat and Sakda, 2018; Fabian et al., 2016; Grigore et al., 2016; Sposato et al., 2017; Zivkovic et al., 2018). Therefore, the process water treatment system would be continuously improved and its produced sediment and sludge treated and completely valorized (Ahmadi et al., 2013; http://purebalticsea.eu; http://veoliawatertechnologies.co.za).

That is why this work is focused on the in-detail presentation, for the first time, of the case study of Veolia Energie Iasi Company, a Romanian thermal power plant, especially considering the following important key elements of the industrial water treatment system:

- The principle characteristics of the existing industrial water treatment stations, discussed mainly considering (i) the required process water quality; (ii) the industrial water treatment system and its performance, and (iii) the existing facilities and its required improvements;
- The primary sludge characterisation produced in the primary water treatment station and also the characteristics of the sludge formed in other technological steps (Zaharia, 2015; Zaharia, 2018; Zaharia and Suteu, 2013), mainly in the flue gas desulfurization step, referring to some physical-chemical quality indicators of the primary and desulfuration sludges;
- The disposal and valorization possibilities of the primary sludge and other sludges separated from the industrial water treatment steps, individually and in mixture with different solid waste produced in the technological process of solid fossil fuel combustion in the studied thermal power plant (e.g., slag, bottom and fly ashes, neutralization waste), as raw materials or auxiliary/conditioning materials with new added-value, possible to be used in the preparation/synthesis of new adsorbents, coagulants, geotextiles, synthetic fibers or stabilized composite products) (Harja et al., 2009; Niculita et al., 2017; Singh et al., 2016; Serbanoiu et al., 2017; Sua-Iam and Makul, 2017; Yuyou et al., 2016; Wang et al., 2017).

2. Experimental

2. 1. Short presentation and location of the studied Romanian thermal power plant

The investigated Romanian thermal power plant is owned by Veolia Energie Iasi Company and is located on the platform of a former heat and power co-generation plant (CET Electrica Iasi Co.), and composed actually of two thermal energy stations: (*1*) *a thermal power station* (named CET 2), working based on a 'clean' solid fossil fuel i.e. processed superior coal - huile (washed and treated with specific chemicals for impurities removal) which is oxidized rapidly (exothermic steps, its chemical potential energy is transformed into thermal energy – 140 Gcal produced by combustion of 140,000 tons of huile for six months) by the oxidant (O_2/air) and uses significantly high quantity of industrial process water which must be permanently treated and added in the closed water-steam or water-water circuits (two boiling systems CPG-42 steam boilers of 420 t/h), normally operating only in the cold season (*November – April*), and (*2*) *a process water boiling station* (named CET 1), working with an ecological gaseous fossil fuel, i.e. methane gas, used only for hot water production (one boiler of 80 Gcal/h) in the hot season

(*May – September*), meaning around 20 Gcal of thermal energy produced by using 9 million Nm^3 of methane gas during 6 months, which requires also significant quantity of industrial water which must be continuously treated and added in the closed thermal circuits.

The fresh industrial water for CET 1 and CET 2 thermal power stations is supplied by ApaVital Iasi Company, as *industrial* and/or *potable water*, and a huge amount of recyclable industrial water (after a corresponding mechanical – physical-chemical treatment) is used, too (recycles up to 80-90% of water used in the company, the rest being lost in the technological process of thermal energy production).

This Romanian thermal power plant is located in the industrial area of one of the most important historical, economic and cultural centers of Moldavia region, one of the oldest cities in Romania, Iasi municipality (371,889 inhabitants). A few residential zones are nearly the company site and separated by permanent surface water (i.e. Bahlui River, having a mean flowrate of 0.189 m/s, a mean shape of 5.3 %, and an annual flow of 2.16 m^3/s in Iasi county area) (Zaharia and Surpateanu, 2006), that is why the prevention, reduction and control of environmental pollution produced by all activities onto emplacement of this studied Romanian power plant is one of significant company concerns/issues and also imposed legal obligation.

The most important facilities of this studied thermal power plant are divided as follows: an industrial water supply system, a solid and gaseous combustion fuel station, a steam and hot water generation system (with certain important principal and secondary thermal circuits), and an electric energy transformation and transmission system to/from the National Energy System (NES) (Stanciulescu, 2004; Zaharia and Surpateanu, 2006). The thermal power plant is an important consumer of water (i.e. industrial process water as demineralized, or soft water, or cooling water, but also drinking water for its employee’s needs) (Zaharia, 2006), that must be permanently treated for adequate use as process water in the thermal energy production, distribution and consumption by local population and all institutes and companies connected to the municipality heating system.

2.2. Industrial water treatment stations: materials, chemical reagents, analysis methods used and schematic treatment flux description

The principal materials and chemicals used in the industrial water treatment stations are grouped as follows (Stanciulescu, 2004; Zaharia, 2006):

(i) Lime and ferrous sulfate-based coagulants, used in the industrial water treatment step, as:

- *Lime*, in hydrated powder form, corresponding to SR EN 459-1:2003 standard (EN 459-I CL 90-s) with the following characteristics: min. 80–90% total sum of CaO and MgO; 3-5% MnO; 4-7% CO_2; 2% SO_3; apparent density of 0.3–0.6 kg/dm^3; max.7% R009; max. 2% R020; 2% free water; the stability test is adequate. It is stocked in three cylindrical metallic tins fixed with 4 arms on the industrial cement concrete platform (each one possesing a superior lid with three covered adapters and a conic bottom with a discharging hole on which is mounted the dosing installation of powder lime). It is used as lime solution for the industrial water treatment station, prepared by dosing of a specific lime amount and dissolved it with water till a homogeneous lime solution preparation in each consumption tank (cylindrical tank of 2 m^3, diameter of 2.2 m, and useful height of 2.2 m) using a dosing pump (Rotosole, flowrate of 10 m^3/h, 10 m CA, 2.2 kW, 3,000 rot/min, for 0-300 kg of powder lime/h) and ejecting pump (flowrate of 20 m^3/h, 4.5-5 kgf/cm^2, 55 m CA, 17 kW, 2,950 rot/min) for gravity settling tank supply.

- *Ferrous sulfate,* in hydrated solid form of $FeSO_4 \cdot 7H_2O$*,* as residual product from iron (and steel) works (Galati), resulting by dissolution of steel rests from different mechanical processing, with the following characteristics: microcrystals of greenish color, purity of 97.5% for Ist class and 95% for IInd class, and solubility of 99.8 %. It is stocked in specific deposit with two discharging holes and a supplying source for coagulated water in which is dissolved ferrous sulfate in two preparation-dissolution tanks and after introduced in the underground consumption tanks. These consumption tanks dispose of mechanical agitation system, being supplied from four dosing pumps (*two* of PVC type, with flowrate of 0-0.6 m^3/h, 25 m CA, 2.2 kW, 1,425 rot/min, and *two* of Dorel 320 type, ICPEET Cluj, with flowrate of 0-0.6 m^3/h, 50 m CA, 2.2 kW, 1,425 rot/min) and discharged in the primary settling tank. Ferrous sulfate is the *coagulation agent* and reacts in the primary settler with the lime solution forming the ferrous and ferric hydroxide as precipitates in high volume which agglomerate and retain in settling, the fine solids in colloidal range as well as specific adsorbed organics and not used / remanent microbiological inhibitors. The ferrous sulfate consumption tank is a cylindrical metallic tank with internal protection by surface rubbering (4 m^3, diameter of 2 m, liquid height of 1.4 m and total height of 2.2 m) equipped with three steel holes at inferior bottom for emptying, outlet of ferrous sulfate solution (Dn 80) and inlet of compressed air (Dn 50) and a lateral hole (Dn 50) for recycling of ferrous sulfate solution.

(ii) Compressed air – the compressed air system (EC10, 6 kgf/cm^2, temperature range of -25 ÷ 40°C, 2 compressing steps, 4 cylinders, 10 L-oil bath, regulatory rotation of 900 rot/min, minimal operating rotation of 400 rot/min, (10 atm)-flowrate of 5 m^3/min, 52 kW) is composed of a recipient of 1 m^3 (or 16 m^3) capacity, a drops separator and a dryer with silicagel, which continues in a distribution unit with 4 holes with valves and a gas gauge. It is required in the mechanical filtration, pneumatic discharging of powder lime from transport machines in tins and also lime solution preparation and supplying of primary settling tank for normal operation and fluidization, when is necessary.

(iii) Sulfuric acid, hydrochloric acid and sodium hydroxide – for the neutralization processes (concentrated and diluted working solutions) and *salt solution* (7-10 % NaCl, flowrate of 25 m^3/h, 9000 L-total consumption of 25% NaCl solution for an active cycle) for regeneration of ion exchange materials;

(iv)Ammonia, hydrazine and *sodium phosphate solution*– for water conditioning in water-steam circuit, used when is required;

(v) Silting and erosion inhibitors, chlorine and sulphuric acid – for cooling water conditioning, and

(vi) Polymer (mixed anionic and *cationic polyelectrolyes)*, as commercial product (concentrated solution, 35-40 %) (only when is required, for no significant supplementary added cost) – for primary and 'in mixture' sludge concentration and its valorization after mechanical dehydration (by simple gravity thickening or gravity belt thickening).

A number of other chemicals, e.g. acids, alkalis and organic compounds, are used for maintenance of existing installations and equipments, and others are required in the permanent analysis of the most significant physical-chemical quality indicators of industrial water (suspended solids, dissolved oxygen, chlorides, COD, or COT, total hardness, content of calcium, magnesium, sodium, carbonates, ammonia, phosphates, extractible substances, certain specific anions, etc.) using international approved analysis standard methods (Zaharia and Surpateanu, 2006; Zaharia, 2014, 2018). From the whole industrial process water treatment station, it is produced the predominant inorganic primary sludge which is pumped and separated in a simple gravity thickening basin (4 compartments-based basins for sludge concentration and separation (iron-based hydroxide precipitates or co-precipitates associated with other separated aggregates or colloids) and, in a few cases, in a gravity belt thickener which uses a polymer to make sludge particles larger to be well separated.

The general scheme of the industrial water technological treatment plant is illustrated in Fig. 1, in the form received from the company responsible staff (in Romanian).

3. Results and discussions

3. 1. Industrial water treatment processes and specific systems: mechanisms and performance

The industrial water treatment involves the removal from raw or loaded industrial water of constituents detrimental to specific use (addition or cooling water, hot water). Industrial water supplies must be nearly sterile and turbidity-free and should have a very low total dissolved solids concentration (as total dissolved salts, or fixed residues at 105°C) (Haller, 1977; Zaharia, 2006, 2014). Specific chemical species such as hardness ions (calcium and magnesium ions), or specific metal ions such as iron species, and organics must be removed in the majority of cases.

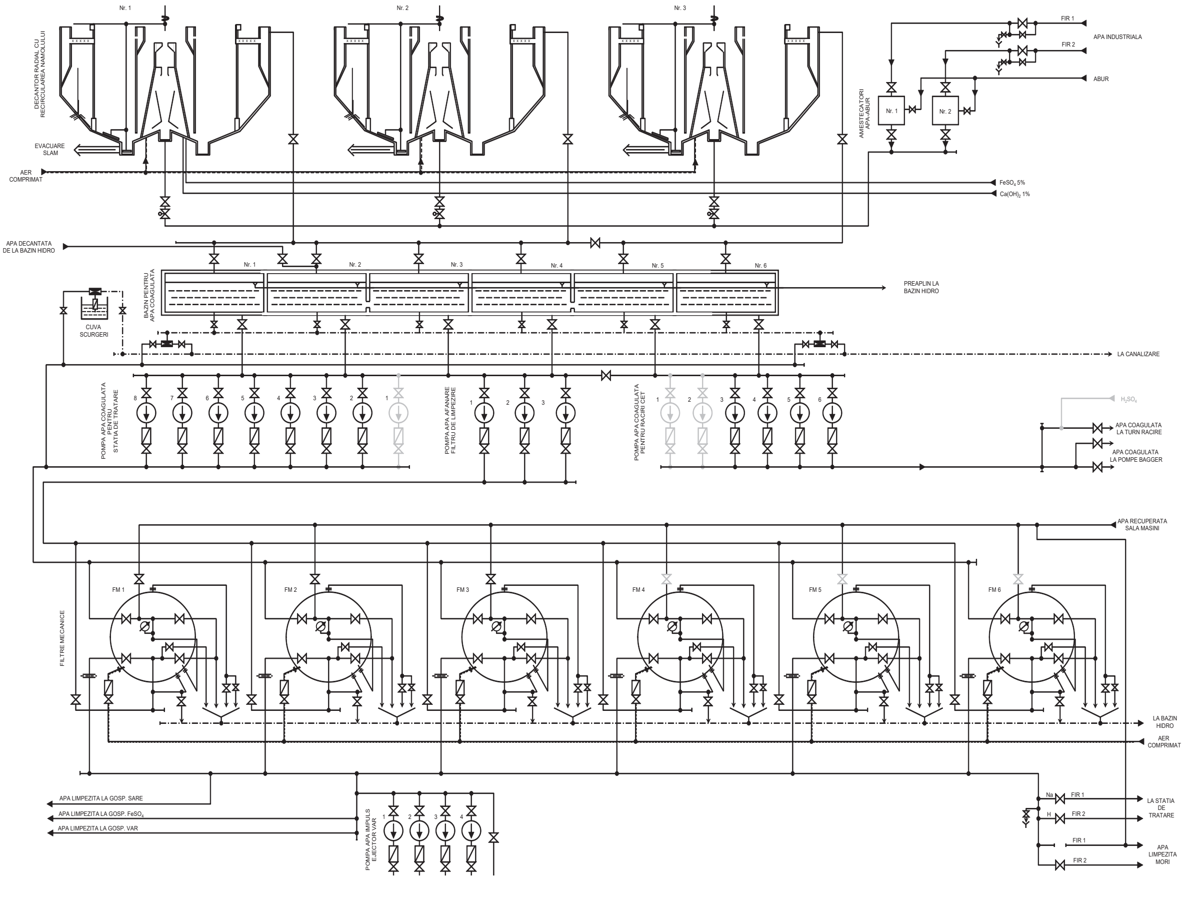

Fig. 1. Schematic representation of the industrial water treatment plant (Veolia Energie Iasi Co.)

Requirements for industrial uses of water vary widely, from *(i)cooling* which has a relatively loose requirements (corrosion, scale formation, bacterial growth in pipes and cooling towers as primary concerns) to *(ii) boiler feed water supply* (working at high temperature and pressure) which has a major problem with scale formation, and a particular one with silica, that is why boiler feed water must be very low in turbidity (no more than 0.05-0.1 FTU), dissolved oxygen (< 2 mg O_2/L; the imposed ISCIR norm (ISCIR – State Inspection for Boilers, Under Pressure Recipients and Lifting Installations (www.iscir.ro) is of 0.02 mg O_2/L), total iron content (<0.1 mg/L) and total hardness (zero value is recommended).

Consequently, industrial water quality is a significant concern in such cases, and requires mechanical-physical and chemical treatment by specific common processes and operations such as *coagulation-sedimentation* for turbidity removal, *precipitation and ion exchange* for dissolved solids and total hardness removals (i.e. hardness removal by precipitation and ion exchange, and also iron removal by oxidation and precipitation to insoluble trivalent form), or *disinfection* by *chlorination* (easy operation and low cost) in cooling towers, pipes and mechanical systems for prevention or control of slime growth. Thus, the industrial water treatment should be organized on well-defined treatment steps, such as *pretreatment* (with lime for the elimination of CO_2 and SO_2) followed by *primary treatment* and *softening* which are characterized as mechanism, specific installations and performance in further sections.

3.1.1. Primary industrial water treatment processes and specific systems

The primary industrial water treatment step consists in coagulation of fine suspended particles of colloidal range normally carried out prior to sedimentation and filtration steps, associated or not with the chemical degasifying process (CO_2 and SO_2 elimination with lime by carbonation and desulfurization followed by mechanical filtration) and reduction of total hardness (reduction of Ca^{2+} and Mg^{2+} ions in treated industrial water by precipitation as carbonates in gas-water-solid equilibrium situations, or by lime-soda softening process closed to the atmosphere but open to the solid precipitation/scale formation). Usually coagulants (lime and ferrous sulfate) are added to industrial water and rapidly agitated for a few minutes to disperse, and after gently mixed for 15-30 min for flocs' formation (precipitated agglomerates as flocs). When only slower mixing rates are used, higher coagulant dosages may be necessary due to the range of metal-complex species produced. At high mixing rates, the increased surface area produced by particle disintegration increases coagulant dosage requirements. Data on suspended solids, residual turbidity, total hardness, permanent acidity and alkalinity should be measured as a function of coagulant dosage, pH, Reynolds number and temperature.

When ferrous sulfate is used in water treatment devoid of oxygen, the pH must be higher than 9.5, effect achieved by the addition of lime solution (Eq. 1). However, when oxygen is present, the ferrous sulfate is oxidized to ferric hydroxide (Eq. 2), which is more insoluble than ferrous hydroxide (Haller, 1977; Yen, 2007).

Ferrous sulfate is transformed in precipitate which will coagulate all suspensions. In this manner, ferrous sulfate is used as a coagulant when oxygen is sufficient (Eqs. 1-2).

$$FeSO_4 + Ca(OH)_2 \rightarrow Fe(OH)_2\downarrow + CaSO_4\downarrow \quad (1)$$

$$2Fe(OH)_2 + \tfrac{1}{2}O_2 + H_2O \rightarrow 2Fe(OH)_3\downarrow \quad (2)$$

It can be also performed the partial reduction of water hardness, silica and CO_2 (even SO_2) elimination as in Eqs. (3-9).

$$Ca^{2+} + 2HCO_3^- + Ca(OH)_2 \rightarrow 2CaCO_3\downarrow + 2H_2O \quad (3)$$

$$Mg^{2+} + 2HCO_3^- + 2Ca(OH)_2 \rightarrow Mg(OH)_2\downarrow + 2CaCO_3\downarrow + \\ + 2H_2O \quad (4)$$

$$CO_2 + Ca(OH)_2 \rightarrow CaCO_3\downarrow + H_2O \quad (5)$$

$$2SO_2 + 1/2O_2 + Ca(OH)_2 \rightarrow CaSO_4\downarrow + H_2O \quad (6)$$

$$Mg^{2+} + 2Cl^- + Ca(OH)_2 \rightarrow Mg(OH)_2\downarrow + Ca^{2+} + 2Cl^- \quad (7)$$

$$Mg^{2+} + SO_4^{2-} + Ca(OH)_2 \rightarrow Mg(OH)_2\downarrow + Ca^{2+} + SO_4^{2} \quad (8)$$

$$H_2SiO_3 + Ca(OH)_2 \rightarrow CaSiO_3\downarrow + 2H_2O \quad (9)$$

The permanent *Mg*-hardness is usually transformed in permanent *Ca*-hardness (Eq. 10) as

$$Mg^{2+} + Ca(OH)_2 \rightarrow Mg(OH)_2\downarrow + Ca^{2+} \quad (10)$$

For the complete $Mg(OH)_2$ forming reaction (as stable precipitate) (Eqs. 7-8), a high concentration of hydroxyl ions (OH^-) must be present. This requires frequently a pH of 10.8 which is practically achieved by adding an excess of 35 mg/L lime (as CaO). The excess of added lime can be removed by carbonation with CO_2 (Eq. 5) or desulfurization (Eq. 6). In addition, some calcium ions are not precipitated or settled out in the primary treatment, and $Mg(OH)_2$ is soluble to about 9 mg/L which corresponds to 15 mg/L hardness as $CaCO_3$. With the additional $CaCO_3$ in solution and allowing incomplete precipitation, the final hardness can be over 50 mg/L (as $CaCO_3$).

Because pH must be above 9.5, recarbonation must be used to generate a product in an acceptable pH range. The most important reason for this pH reduction (till no more than 8.6) is to prevent downstream precipitation of $CaCO_3$ (at this pH value, $CaCO_3$ solubility-S_{CaCO3} is higher than that of its solubility product-P_{CaCO3}) (Zaharia, 2014). Many ions can be precipitated by modifying the water pH, but the interaction of constituents is also important.

The required coagulant dose (i.e. critical coagulant concentration) is verified in practice by the calculation of '2*p* – *m*' for lime dose, or 'p/m' and '*m*' for ferrous sulfate dose, where '*m*' is the acidity of coagulated water (as HCO_3^- equivalent), and '*p*' is the alkalinity of coagulated water (as $CaCO_3$ equivalent).

Because of high flow rates associated with industrial water supplies, there are economic constraints on the capital and operating costs which can be incurred. These constraints limit solids removal and separation methods to gravity sedimentation and thickening, in most cases. In some cases, filtration is necessary because of residual, unsettled precipitate in the industrial water. Operating cost is considerably higher because of the required amount of chemicals addition and the increased sludge-disposal problem.

Finally, concentration and separation of primary sludge (a watery mixture of solids), or conditioning of final sludge produced from this industrial water treatment plant is sometimes required prior to the final disposal. Therefore, a gravity sludge thickening basin (multi-compartments), or, in certain cases, a gravity belt thickener (requiring polymer for sludge conditioning) is needed for primary sludge concentration and separation. The installations and types of equipment used in the primary industrial water treatment station are as follows:

- the dosing installation of lime (from 3 bins with powder lime) and ferrous sulfate (solid form, from specific deposit) (Fig. 2), equipped with specific dosing units and pumps for prepared working solutions;
- 1 primary radial settling tank (D=20 m, H=5 m, v_S=0.3 m/min, and around t_S=1.5-2 hs) (Fig. 1);
- 6 pumps for coagulated water (*Sigma* type);
- 6 mechanical filters (D=3.4 m, H_t=5.5 m, V_t =45.3 m^3) (Fig. 1) for preliminary step;
- 2 basins with coagulated water (300 m^3);
- 1 installation of compressed air (2 compression pumps of *EC10* type);
- 1 gravity (4-compartments) thickening basin (or a gravity belt thickener, only if this option is selected, requiring polymer for sludge conditioning/concentration).

A few analyzed values of some quality indicators of coagulated water permanently controlled after the primary treatment station are summarized in Table 1, as average or mean value for 2018. Each analysis was performed in triplicate, in each month at least 10 times per week, especially in summer season (when operating at CET 1 thermal power station was activated) but also in cold season (when was worked the CET 2 thermal power station), and the standard deviation was in acceptable limit of ± 10%, in range of (-6.34 – 5.32) %.

The performance of primary industrial water treatment station is very good due to more than 90% permanent removal of suspended solids in colloidal ranges (e.g., admissible limits of turbidity under 0.5-1 FTU, with reduction or treatment degree greater than 85-90%, respecting the norms imposed in the best available techniques (BAT) for water and wastewater treatment), organics expressed as COD (removal higher than 80.00 - 87.50%) and certain analyzed dissolved substances (i.e. different cations and anions, conductivity, fixed residues, hardness etc.) as shown in Table 1. Unfortunately, the content of disolved salts and metal ionic species is still high for use as process water in the energy sector and requires reduction in the further industrial water softening station (i.e. total hardness reduction till zero value; total iron concentration lower than 0.1 mg/l and pH of 8.5-9.5).

Majority values of analyzed quality indicators for coagulated water are in agreement with the imposed limits by the local environmental regulation authority (as shown in Table 1), but, in energy sector, the industrial process water used in the principal and secondary thermal circuits must take into account the ISCIR norms (www.iscir.ro) which impose complete elimination of a few ionic species, especially of the cations responsible for the total hardness (e.g., Ca^{2+} and Mg^{2+} cations). Therefore, in the further industrial water treatment station will be eliminated the total content of cations, especially in the form of calcium and magnesium ionic species (Ca^{2+} and Mg^{2+}) by using specific ionic exchange processes.

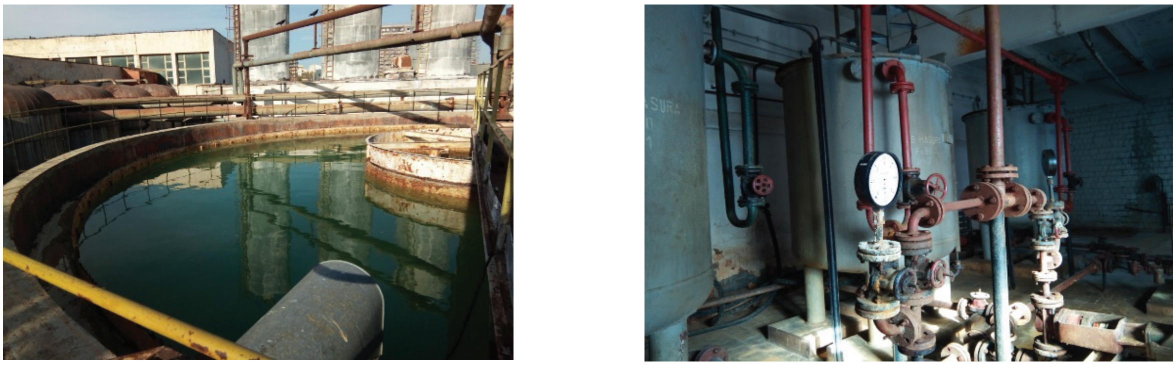

(a) View with lime tins, mechanical filters and primary radial settling tank

(b) $FeSO_4$ solution pumping units and dosing installations

Fig. 2. Views with a few installations and units used in primary industrial water treatment station

Table 1. Characteristics of analyzed industrial water in the primary treatment station (after the coagulation-sedimentation step) (inlet, outlet and maximum admissible limits)

Indicator	***Measured units***	***Inlet (In)***	***Outlet (Out)***	***M.A.C.****	***Indicator***	***Measured units***	***Inlet (In)***	***Outlet (Out)***	***M.A.C.****
pH	-	8.5-9.5	8	7.0-9.5	COD	mg O_2/L	8-10	1-2	2
TSS (or turbidity)***	mg/L (FTU)	18-22 (17-15)	1-2 (0.5-1)	5 (0.02)	Fixed residues	mg/L	880-900	260-285	300
Total iron	mg/L	5	0.084	1.0	Conductivity	□S/cm	426	500	300
Alkalinity (m) (as $CaCO_3$)**	mg/L mmol/L	185 3.7	145 2.9	150 3.0	Total hardness (as $CaCO_3$)	mg/L mmol/L	300 3	8.68 (°G)	min. 5°G
Ca^{2+}	mmol/L	2.5	1.0	5.0	HCO_3^-	mmolL	5.80	3.40	3.5
Mg^{2+}	mmol/L	0.5	0.54	2.0	Cl^-	mmol/L	1.0	0.985	7.0
Na^+	mmol/L	4.5	4.2	4.35	SO_4^{2-}	mmol/L	2.7	0.575	2.6
Σ(cations)	*mmol/L*	*7.5*	*5.74*	*11.35*	*Σ (anions)*	*mmol/L*	*7.5*	*4.96*	*13.1*

** M.A.C.- maximum admissible concentration for treated industrial water after primary treatment station; ** The relative alkalinity (p/m) was around the value of 0 / 2.9; *** the turbidity and other cations and anions concentrations will be minimized or even completely eliminated in the further softening step.*

3.1.2. Industrial water softening processes and specific units

The industrial water softening station has an important role caused by requirements imposed for total hardness reduction and control of coagulated water coming from the primary treatment station (zero hardness, that means $\Sigma(Ca^{2+}+Mg^{2+})=0$), and sometimes complete demineralization (Σ (cations+anions)=0).

The major anions associated with dications as Ca^{2+}, Mg^{2+}, Si^{2+}, Fe^{2+} are HCO_3^-, SO_4^{2-}, SiO_3^{2-}, Cl^-, NO_3^-, and they are transformed in adherent precipitated particles (t ≥80°C) in the technological process of thermal energy generation (heating). Other fraction of anions is transformed in precipitated solids in the preliminary and primary water treatment stations, and the rest is present in coagulated water and will be completely eliminated by demineralization in the industrial water softening station, if is required.

Therefore, the coagulated industrial water is introduced in five Na-cationic-exchange units (Na-cationic filters) with ion-exchange materials of Vionit CS3 type (high acid exchanger) characterized as solid mass (granules of 0.3–1.2 mm), insoluble in water, with macroporous structure and low affinity towards hydrogen ions (H^+); increasing cationic affinity order as $H^+< Na^+< K^+< Mg^{2+}< Ca^{2+}< Al^{3+} < Fe^{3+}$.

The general cationic exchange reaction corresponds to Eq. (11).

$$2R\text{-}SO_3Na + Ca^{2+} \ (\mathit{or}\ Mg^{2+}) \rightarrow (RSO_3)_2Ca \ (\mathit{or}\ (RSO_3)_2Mg) + 2Na^+ \qquad (11)$$

Regeneration of ion-exchange material is performed with salt solution of 7-10% NaCl. The calcium and magnesium ions presented in coagulated water, which is further used as an industrial process water in the thermal power station, can lead to boiler scale formation (on surface of heat exchangers) resulting from the decomposition of bicarbonate in steam line (e.g., $CaCO_3$) at high temperature, according to Eq. (12).

$$Ca^{2+} + 2HCO_3^- \leftrightarrow CaCO_3\downarrow + H_2O + CO_2 \qquad (12)$$

Therefore, all calcium and magnesium ionic species must be eliminated by ion exchange processes in the Na-cationic exchange filters before further used as industrial water in the thermal circuits of the thermal power plant based on characteristic chemical reactions as

$$2R\text{-}Na + CaCl_2 \rightarrow R_2Ca + 2\ NaCl \qquad (13)$$

$$2R\text{-}Na + MgCl_2 \rightarrow R_2Mg + 2\ NaCl \qquad (14)$$

$$2R\text{-}Na + CaSO_4 \rightarrow R_2Ca + 2\ NaSO_4 \qquad (15)$$

$$2R\text{-}Na + MgSO_4 \rightarrow R_2Mg + 2\ NaSO_4 \qquad (16)$$

The Na-cationic exchange filters are functioning in two steps (in series) assuring in this way the required industrial water quality according with imposed ISCIR norms (www.iscir.ro) (a two steps cycle consisting of cation exchanges followed by regeneration of exhausted exchanger material).

The basic installations and specific units used consists of:

- 5 Na-cationic exchange units/filters (D= 2.8 m, H_t= 5.1 m) (Fig. 3);
- 2 Basins with salt solution (V= 100 m^3) constructed with concrete plated with anti-acid bricks;
- 4 Steel pumps for salt solution (Q=40 m^3/h, 25 mCA) of DN 80-50-200 type.

The industrial water softening station achieves 100%-removal of total hardness during the entire working period of time of a year. Consequently, for the whole industrial water treatment plant, the treatment performance (i.e. pretreatment with lime followed by mechanical filtration→coagulation-sedimentation→softening, and sometimes disinfection by chlorination) is very good, being higher than 85-90% in terms of total suspended solids (TSS), turbidity, organics (expressed by COD), fixed residues, total iron content and 100% in terms of total hardness, other cations and even anions and no slime growth on cooling system, pipes and other mechanical systems.

Fig. 3. View with ion-exchange filters

Engineering responsibility for industrial water treatment must have in view performing of required water treatment degree (> 75÷85 % till 100%), correct system design and treatment operation (complete or high efficiency in each industrial water treatment station for all required pollutants removal), industrial water quality standards (both qualitative and quantitative aspects; e.g., consistent production of industrial water with low COD (<2 mg O_2/L), dissolved oxygen (around 0.02 mg O_2/L), alkalinity (m) (0.03 mg/L), total iron content (< 0.02 mg/L), conductivity (<0.3 mS/cm) and suspended solids concentrations (less than 8 mg/L regardless of influent concentrations, and pH of 8.5-9.0) and also concentration, conditioning and disposal/valorization facilities of its produced sludge (primary and desulfurization sludges), and also production wastes as slag and bottom/fly ashes).

3.3. Primary and desulfurization sludge: main characteristics, separation and valorisation possibilities

3.3.1. Primary sludge characteristics

The solids that settle to the bottom of the primary settling tank (PST) is scraped to a sump and removed by a pump. This watery mixture of solids is named primary sludge and removes between 85-90% of suspended solids, 90-95 % of settleable solids and 25-40% organics. For increasing sludge thickening and valorisation possibilities as raw material source in manufacturing of added value product (e.g. iron-based coagulant, iron-based catalyst and adsorbent material), or as conditioning/auxiliary agents (in new composites), the primary sludge must be characterized mainly by a few principal physical-chemical quality indicators, recommended by the environmental norms and homologation standards, or requirements of different industrial products. Preliminary analysis and some analysed physical-chemical quality indicators were presented in Tables 2 and 3. Each analysis was performed in triplicate, and the standard deviation value was in acceptable limit of ± 10%, exactly in the range of (-2.86 – 3.85) %.

The prelevated sludge samples were analyzed in period of 2017-2018, especially in the cold season, during 6 months (November-April) when was operated the CET 2 thermal power station, the values presented in tables must be considered as the average/mean value of all analysed samples in this period of time. These preliminary characteristics are indicated no possibility to energetically valorize these preliminary sludges for useful thermal energy extraction due to their very low organic content, being predominantly inorganic in nature.

Therefore, some mineral constituents of this primary sludge can be valorized individually or in mixture for synthesis of new added-value products, e.g., new coagulants, or auxiliary/conditioning agents for composite products with metals in their basic matrix which can be used also as catalyst in advanced oxidation treatment of different industrial effluents.

This primary sludge has a common high water content (72.33%), very low organic content (1.25 % COD in dried substance), relative normal content of sulphates (207.5 mg/kg of dried substance) and also very low content of extractable substances in organic solvents (< 5 mg/kg) and total hydrocarbons (<5 mg/kg).

As it was mentioned above its chemical composition is predominantly inorganic with a lot of metal species (as precipitated/co-precipitated hydroxides, carbonates, sulphates, other chloride-based complexes, or oxides-hydroxides-carbonates agglomerates) in its primary sludge matrix, the dominant metals being iron (total iron content of 2,152 mg/kg of dried substance) and calcium (239.081 mg/kg of dried substance). Low toxicity can be also noted due to arsenic (1.72 mg/kg of dried substance) and tin (< 5 mg/kg of dried substance), but these values are still not critical for obligatory intervention and are considered as in approved alert level.

Table 2. Preliminary analysis of primary sludge produced

Characteristics	*Results / Mean value*	*Analysis standard*
Aspect	Solid as soft paste, yellow-brown color	Visual
Reactivity	No reactivity in water, or alkalis (1N NaOH); very strong reactivity in acid medium (1N HCl) with effervescence	Internal methodology
Behavior in contact with an ignition source	It is not burning in contact with an ignition source	Internal methodology
pH (at 25° C)	9.16	ISO 10390: 2005
Caloric power, [kcal/kg]	Not burning in the calorimetric bomb	ISO 1928: 2009

Table 3. The mean values of some physical-chemical quality indicators of primary sludge

Indicator	*Measurement units*	*Mean value*	*Analysis standard used*
Water content	%	72.33	SR EN 12880: 2007
Dried residue	%	26.67	SR EN 14346: 2007
Total organic carbon (TOC)	% of dried substance	1.25	SR ISO 14235
Extractible substances in organic solvents	mg/kg	<5.0	IR spectrometry
Total hydrocarbons content (TPH)	mg/kg of dried substance	<5.0	IR spectrometry
Sulfates from aqueous extract (1:5)	mg/kg of dried substance	207.4	SR ISO 11048/1999
Cadmium (Cd)	mg/kg of dried substance	<0.03	SR ISO 11047/1999
Chrome (VI)	mg/kg of dried substance	<0.005	SR ISO 11083/1998
Copper (Cu)	mg/kg of dried substance	<0.2	SR ISO 11047/1999
Nickel (Ni)	mg/kg of dried substance	<0.2	SR ISO 11047/1999
Lead (Pb)	mg/kg of dried substance	<0.3	SR ISO 11047/1999
Arsenic (As)	mg/kg of dried substance	1.72	AAS –hydride technique
Selenium (Se)	mg/kg of dried substance	<0.015	AAS-hydride technique
Mercury (Hg)	mg/kg of dried substance	<<0.003	AAS-hydride technique
Antimony (Sb)	mg/kg of dried substance	<0.5	EPA 7000B/2007
Tin (Sn)	mg/kg of dried substance	<5.0	EPA 7000B/2007
Calcium (Ca)	mg/kg of dried substance	239.081	EPA 7000B/2007
Total Iron (Fe)	mg/kg of dried substance	2152	EPA 7000B/2007

Moreover, this primary sludge was accumulated all three toxic heavy metals (Cd, Pb, Hg) but their contents are very low being considered as ‘in traces’ (<0.003 mg/kg of dried substance) for Cd and Hg, and more than 100 times higher but not critical (in approved admissible limits) for Pb content (<0.5 mg/kg of dried substance).

Finally, the characteristics of this primary sludge are corresponding to those of inorganic wastes grouped in 19 09 02 coded categories (sludges from water clarifying) that can be easily stabilized by inertness in cement concrete matrix (or other composite matrices) and vitrifying.

3.3.2. Characteristics of the desulfurization sludge

For degasifying, or control and reduction of polluting species from gaseous combustion flux it is used commonly chemical degasifying with lime for the elimination of CO_2 and SO_2 by carbonation and desulfurization processes when are formed precipitates/co-precipitates of calcium carbonate and calcium sulphate or sulphite. The solubility of these precipitates is strongly influenced by pH, stable precipitates being formed in strong alkaline pH range (pH>10.6) (in excess lime solution). A preliminary analysis and some physical-chemical quality indicators were presented in Tables 4 and 5.

The preliminary analysis confirms the high stability of desulfurization sludge caused of its very high pH range (pH>10.6), and utilization of significant amount of ‘in excess’ lime (due to very high pH value of 12.69). It must be also mentioned that each analysis was performed in triplicate, and the standard deviation value was in acceptable limit of ± 10% (in range of -3.32 – 4.92) %.

The prelevated desulfurization sludge samples were analysed in period of 2017-2018, in the cold season (November-April, 6 months) when was operated the CET 2 thermal power station, all values presented in tables must be considered as the average/mean value of all analysed samples in this period of time.

Table 4. Preliminary analysis of desulfurization sludge

Characteristics	*Results / Value*	*Analysis standard*
Aspect	Solid as powder, grey-black	Visual
pH (at 25° C)	12.69	ISO 10390: 2005

Table 5. The mean values of some physical-chemical quality indicators of desulfurization sludge

Indicator	*Measurement units*	*Mean values*	*Analysis standard*
Water content	%	72.33	SR EN 12880: 2002
Dried residue	%	27.67	SR EN 14346: 2002
Calcium	%	18.19	EPA 7000B/2007
Sulphates	%	3.68	STAS 11048/1999
Sulphites	mg/kg	50.50	Spectroquant Merck

The physical-chemical analysis results indicate a high water content (72.33%) which is a relative common content in a separated sludge, and high calcium content (27.67%) in the dried residue predominantly as sulphite (50.50%) but also low sulphate (3.68%) forms, being evidently its normal production in a desulfurization step, meaning SO_2 elimination by absorption in alkaline solution such as only lime solution, or mixed soda (Na_2CO_3)/lime solution system. This desulfurization sludge is stable in very alkaline conditions and can be valorised in neutralisation treatment processes of very acidic media for minimization of corrosion problems and also to control and reduce the acidification in different aqueous environments and/or soils.

3.4. Disposal and valorization possibilities of primary and desulfurization sludge (individually or in mixture with other solid production wastes generated in the thermal power plant)

The primary sludge from industrial water treatment plant must be separated and disposed of, usually by thickening using two ways chosen based on company economic situations in a certain period of times, or strict imposed environmental managerial initiatives, each one with its merits, as:

(i) A first open *gravity thickening basin* with four compartments receiving the incoming sludge in each compartment (fresh or diluted ones), the sludge having only a certain odor and settleability problem in summer (evaporation and gravity separation being the predominant active forces). Usually, after one or two months, the concentrated sludge is transferred with the help of a vacuum system onto the disposal platform (CET II Holboca, Iasi) of the production wastes (ashes, slag, neutralization wastes, among others), in a specially designed location place. The resulted sludge quantity is of 15 – 20 t/month and has the pH of 9-10.

(ii) A secondary closed *gravity belt thickener* (Fig. 4) in which polymer (polyelectrolyte) is required, recommended with centrifuge, having a certain problem with chemicals and electricity, when centrifuging and belt is working. Mechanical dehydration operates when the mixture of polymer and sludge is spread across a horizontal porous belt allowing water to drain down by gravity and solid concentrated plates (blocks) to be formed and transferred with trucks to company depositing/disposal platform of production wastes (CET II Holboca, Iasi). Polymer feed is important; the amount of polymer as well as agitation regime must be determined by experimental study for each specific sludge. The recommended polymer concentration is in the range of 50-150 mg of polymer/L of sludge in two agitation steps (a rapid one of 250-300 rpm for 3-10 minutes, and a second slow one of 30-50 rpm for 15-30 minutes).

Also the belt speed must be set properly, a belt slowly operated is recomendable. In this context, the gravity belt thickener operates as follows: the sludge is pumped into the conditioning thickening unit with centrifuge by a delivery pump (a centrifugal sludge trap, in fact a rotating drum, consisting of a helical rotor with an independent rotation movement related to that of rotating drum).

(**a**) Ready-to-use polymer injection system

(**b**) Installation for polymer preparation

(**c**) Conveyor belt for sludge dehydration

(**d**) Collecting unit of concentrated solid plates

Fig. 4. Views with gravity sludge belt thickener (polymer required, and centrifuge recommended)

The ready-to-use polymer is continuously introduced in the conditioning unit and added to sludge proportional to the solid amount. While the sludge is gently conveyed on a slowly operating conveyor belt, the filtrate (separated water) is collected and used for polymer preparation. The conditioning tank and ready-to-use polymer preparation system is controlled by a process computer and visualized on a control panel (Fig. 4b).

The dehydrated sludge is discharged directly into a container. After filling, the container is transported with a truck and cleared to the company disposal platform of slag and ash (CET II Holboca, Iasi). The resulted sludge quantity is of 16 – 22 t/month and has the pH of 7.5-9. This second sludge belt thickener offers benefits as (i) reduced size of dehydrated sludge; (ii) low washing water demand and relative low energy demand; (iii) odor-free station; (iv) wear is reduced to a minimum and noise eliminated due to the slow speed of the conveyor belt, and (v) high operational reliability.

For the company actual economic situation it is enough the gravity thickening basin used. Other solid wastes produced in the thermal power station (slag, bottom/fly ash, neutralization wastes, havinglow price, low polluting effects, continuous processing possibilities, high hydrophilia) are usually storaged onto the company disposal platform (CET II Holboca, Iasi) and properly valorised, when is possible. A few cert possibilities of sludge valorisation, individually and, in mixture with other production wastes, is summarized in Table 6.

Conclusions

The industrial process water of Veolia Energy Iasi Company requires continuous and efficient treatment in its mechanical-physical-chemical treatment plant, which is presented in detail, for the first time, in this work, this treatment plant being adapted to operate in different extreme economic situations and also to be in agreement with all consumers' requirements.

Therefore, three industrial water treatment stations, i.e. the preliminary (degasifying by absorption in lime solution), primary (coagulation-sedimentation) and softening (ion exchange process) treatment stations, were described referring to its unitary processes/operations, mechanisms, installations, performance achieved, and also the quality characterization of its treated industrial process water and certain types of produced sediment and sludge. A few valorization directions of solid sludges and production wastes were recommended in association with the already performed scientific researches and reported data sources. Moreover, Veolia Energie Iasi Company is still considering the industrial water quality as a key factor in ensuring of good and efficient operating conditions of its thermal power station in association with the good quality products/byproducts offered on the free market of products/services.

Table 6. Certain valorisation directions of individual and ‚in mixture' sludge with certain production wastes of Veolia Energie Iasi Company (slag, ashes and neutralization by-products)

Valorisation direction	*Possible application*	*Reference*
Added-value product preparation/ synthesis (e.g., utilisation as -binding material, -auxiliary material, -conditioning agent, -raw matter, etc.)	- manufacturing of ceramic composites (bricks, Ceramica Iasi Co., RO), or other composite types	Ponkarthikeyan et al., 2016; Zaharia, 2018
	- preparation of construction materials, after stabilisation by inertness in cement concrete matrix, or vitrifying, - production of cement/consolidated concrete used in eco-industrial parks, - synthesis of polypropylene fiber/high calcium fly ash geopolymers, geotextiles, or derived sawdust as specific mixture of sawdust-ash	Chindaprasirt and Rattanasak, 2017; Guo et al., 2017; Ciocan et al., 2017; Harja et al., 2009; Kong et al., 2017; Lepadatu et al., 2018; Niculita et al., 2017; Rattanasak, 2017; Serbanoiu et al., 2017; Sua-Ian and Makul, 2017
	- preparation of magnetic zeolitic materials obtained from coal fly ash in mixture with magnetic zeolites	Shoumkova and Stoyanova, 2017
	- new iron (metal)-based catalysts in effluent treatments, - new coagulants in water/wastewater treatment	Zhang et al., 2012; Wang et al., 2017
	- new adsorbent material for persistent organic and heavy metal species removal, discoloration purposes, different hazardous organics removals from industrial effluents	Harja et al., 2010, 2011; Willett et al., 2019; Zaharia, 2015, 2018; Zaharia and Suteu, 2013; Zhao et al., 2016
Neutralization / soil remediation	- aggressive reduction of industrial effluents, or aqueous environments due to sulfates or acidic species; - reduction of soil acidity (use as soil conditioning agent) or other soil remediate actions and improvements in agricultural cropping	Abdelhadi et al., 2018; Cocarta et al., 2017; Masu et al., 2016; Singh et al., 2016; Yuyou et al., 2016; Yu et al., 2017

The company is continuously interested in maintenance of high performances of all industrial water treatment stations and also its efficiency improvement and/or technical modernization.

This addresses especially the automatic control of involved production processes and operations by investments in new advanced high-tech systems, and also initiating of preventive, treatment and valorization actions of its produced sludge/waste for possible homologation of new added-value products, or useful substance recovery for different industrial purposes.

References

Abdelhadi M., Rotaru A., Gavrilescu M., Ţăranu N., (2018), Compressive strength analysis on problematic soils stabilized with fly ash in Jordan, *Environmental Engineering and Management Journal*, **17**, 1855-1861.

Ahmadi M., Bayati N., Babaei A., Teymouri P., (2013), Sludge characterization of an industrial wastewater treatment plant, Iran, *Iran Journal of Health Sciences,* **1**, 10-18.

Bangviwat A., Sittikruear S., (2018), Application of Analytical Hierarchy Process (AHP) in evaluating measures for mitigation of emission impact on communities near lignite-fired power plant at Mae Moh, Thailand, *Environmental Engineering and Management Journal*, **17**, 1457-1466.

Chindaprasirt P., Rattanasak U., (2017), Synthesis of polypropylene fiber/high-calcium fly ash geopolymer with outdoor heat exposure, *Clean Technologies and Environmental Policy*, **19**, 1985-1992.

Serbanoiu A.A., Barbuta M., Burlacu A., Gradinaru C.M., (2017), Fly ash cement concrete with steel fibers – comparative study, *Environmental Engineering and Management Journal*, **16**, 1123-1128.

Cocarta D.M., Subtirelu V.R., Badea A., (2017), Effect of sewage sludge application on wheat crop productivity and heavy metal accumulation in soil and wheat grain, *Environmental Engineering and Management Journal*, **16**, 1093-1100.

Fabian F., Fiore S., Genon G., Panepinto D., Nedeff V., Panaite M., (2016), Preliminary evaluation of the environmental impact of water treatment process, *Environmental Engineering and Management Journal*, **15**, 1867-1872.

Grigore R., Capat C., Hazi A., Hazi G., (2016), Eco-efficiency indicators in the evaluation of environmental performance of thermal power plants, *Environmental Engineering and Management Journal*, **15**, 143-149.

Guo Y., Liu W., Tian J., He R., Chen L., (2017), Eco-efficiency assessment of coal-fired combined heat and power plants in Chinese eco-industrial parks, *Journal of Cleaner Production*, **168**, 963-972.

Haller E.J., (1995), *Simplified Wastewater Treatment Plant Operations*, Technomic Publishing Co. Inc., Lancaster-Basel, U.S.A.-Switzerland.

Harja M., Barbuta M., Gavrilescu M., (2009), Utilization of coal fly ash from power plants II. Geopolymer obtaining, *Environmental Engineering and Management Journal*, **8**, 513-520.

Harja M., Barbuta M., Carja G., Ciobanu G., (2010), Synthesis of new adsorbents for desulphurization on the base of ash and lime, *Bulletin of the Petroleum-Gas University of Ploiesti (Technical series)*, **62**, 51-56.

Harja M., Barbuta M., Rusu L., Munteanu C., Buema G., Doniga E., (2011), Simultaneous removal of Astrazone Blue and lead onto low cost adsorbents based on power plant ash, *Environmental Engineering and Management Journal*, **10**, 341-347.

Kong L., Su M., Peng V., Hon L., Liu J., Li H., Diao Z., Shih K., Xiong Y., Chen D., (2017), Producing sawdust derived activated carbon by co-calcinations with limestone for enhanced Acid Orange II adsorption, *Journal of Cleaner Production*, **168**, 22-29.

Lepadatu D., Barbuta M., Rujanu M., Judele L., Mitroi R., (2018), Fly ash concrete with fibers: comparison of tensile strength using neural network and design of experiments methods, *Environmental Engineering and Management Journal*, **17**, 1321-1328.

Masu S., Jurj N.L., Lixandru B., Burtica G., (2016), Application of fly ash as amendment in agricultural field of *Arena sativa*, *Environmental Engineering and Management Journal*, **15**, 2681-2688.

Niculita L., Chirica R.I., (2017), Study on the use of geotextiles for ensuring drainage within industrial fly ash ponds, *Environmental Engineering and Management Journal*, **16**, 2525-2536.

Ponkarthikeyan P., Ganesh R., Sheerin Farzana A., (2016), Experimental study on bricks using water treatment sludge, *International Journal for Research in Applied Science & Engineering Technology*, **4**, 485-493.

Shoumkova A., Stoyanova V., (2017), Preparation and SEM-EDX-XRD characterization of magnetic zeolitic materials obtained from coal fly ash, *Environmental Engineering and Management Journal*, **16**, 2553-2559.

Singh K., Pandey V.C., Singh B., Patra D.D., Singh R.P., (2016), Effect of fly ash on crop yield and physico-chemical, microbial and enzyme activities of sodic soils, *Environmental Engineering and Management Journal*, **15**, 2433-2440.

Sposato P., Preka R., Cappellaro F., Cutaia L., (2017), Sharing economy and circular economy. How technology and collaborative consumption innovations boost closing the loop strategies, *Environmental Engineering and Management Journal*, **16,** 1797-1806.

Stanciulescu D., (2004), *Environmental impact assessment generated by C.E.T.1 Company, Iasi* (in Romanian), Master Thesis, Gheorghe Asachi Technical University of Iasi, Romania

Sua-Iam G., Makul N., (2017), Incorporation of high-volume fly ash waste and high-volume recycled alumins waste in the production of self-consolidating concrete, *Journal of Cleaner Production*, **159**, 194-206.

Wang N.N., Zhao Q., Zhang A.L., (2017), Catalytic oxidation of organic pollutants in wastewater via a Fenton-like process under the catalysis of HNO_3-modified coal fly ash, *RSC Advances*, **7**, 27619-27628.

Willett C., Fu G.Y., Jackson N.M., (2019), Color removal from pulp mill effluents using coal ash produced from Georgia coal combustion plants, *Environmental Engineering and Management Journal*, **18,** 945-956.

Yen T.F., (2007), *Chemical Processes for Environmental Engineering*, Imperial College Press, London, United Kingdom.

Yu R., Xu J., Hu G., (2017), Application of fly ash-stabilized municipal sewage sludge on growth of *Brassica chinensis* and heavy metal transfer in pot experiment with a barren soil, *Environmental Engineering and Management Journal*, **16**, 2803-2812.

Yuyou Y., Zengdi C., Xiangqian L., Haijun D., (2016), Development and materials characteristics of fly ash-slag-based grout for use in sulfate-rich environments, *Clean Technologies and Environmental Policy*, **18**, 946-956.

Zaharia C., (2006), *Energy and the Environment,* 2nd Edition (in Romanian), Ecozone Publishing House, Iasi, Romania.

Zaharia C., (2014), *Environmental Chemistry. Laboratory tests and problems* (in Romanian), Performantica Publishing House, Iasi, Romania.

Zaharia C., (2015), Application of waste materials as 'low cost' sorbents for industrial effluent treatment: a comparative overview, *International Journal of Materials and Product Technology*, **50**, 196-220.

Zaharia C., (2018), Discoloration of industrial effluents by adsorption-based treatment onto coal fly ash activated with lime, *Desalination and Water Treatment*, **127**, 364-376.

Zaharia C., Surpateanu M., (2006), Environmental impact assessment using the method of global pollution index applied for a heat and power cogeneration plant, *Environmental Engineering and Management Journal*, **5**, 1141-1152.

Zaharia C., Suteu D., (2013), Coal fly ash as adsorptive material for treatment of a real textile effluent: operating parameters and treatment performance, *Environmental Science and Pollution Research*, **20**, 2226-2235.

Zhang A.L., Wang N.N., Zhou J.T., Jiang P., Liu G.F., (2012), Heterogeneous Fenton-like catalytic removal of p-nitrophenol in water using acid-activated fly ash, *Journal of Hazardous Materials,* **201-202**, 68-73.

Zhao D., Qui Q., Wang Y., Huang M., Wu Y., Liu X., Jiang T., (2016), Efficient removal of acid dye from aqueous solutions via adsorption using low cost blast-furnance slag, *Desalination and Water Treatment*, **57**, 28486-28495.

Zivkovic S., Vukadinovic B., Veljkovic M., (2018), Cleaner and energy efficient production: A case study, *Environmental Engineering and Management Journal,* **17**, 175-188.

Web sites

http://purebalticsea.eu/index.php/gpsm:good_practices PURE Project on urban reduction of eutrophication, Part_financed by EU, Programme 2007-2013, Baltic Sea Region websites: Good practices in sludge management.

http://veoliawatertechnologies.co.za/water-technologies-sludge treatment handling - Water Tech Websites, Veolia Water Technologies from South Africa - Sludge Treatment and Handling.

http://www.iscir.ro

Environmental Engineering and Management Journal
February 2020, Vol.19, No. 2, 269-279
http://www.eemj.icpm.tuiasi.ro/; http://www.eemj.eu

"Gheorghe Asachi" TechnicalUniversity of Iasi, Romania

FIXED-BED-COLUMN STUDIES FOR METHYLENE BLUE REMOVAL BY CELLULOSE CELLETS

Iulia Nica[1], Gabriela Biliuta[2], Carmen Zaharia[1], Lacramioara Rusu[3],
Sergiu Coseri[2], Daniela Suteu[1]*

[1]"Cristofor Simionescu" Faculty of Chemical Engineering and Environmental Protection, "Gheorghe Asachi" Technical University of Iaşi, 73 Prof .Dr. Docent D.Mangeron Blvd, 700050-Iasi, Romania
[2]"Petru Poni" Institute of Macromolecular Chemistry of Romanian Academy, 41A Gr. GhicaVoda Alley, 700487, Iasi, Romania
[3]"Vasile Alecsandri" University of Bacau, Faculty of Engineering, 157 Calea Mărăşeşti, 600115 Bacau, Romania

Abstract

The *Cellets* product represents a cellulose material, which combines different properties such as the perfect sphericity, fine particle size distribution, low friability and solubility, and inertness. The experiments were carried out with *Cellets 200* granulated celluloses used as a filling material for a laboratory glass column, using diluted dye solution (9-10 mg of dye /L of solution) at adequate initial pH (4.7). The effect of flow rate was investigated, and the modeling of experimental data for dynamic adsorption of Methylene Blue organic dye from aqueous solution in a fixed bed column was studied based on Thomas, and Yoon-Nelson models. The optimal volume of working dye solution per adsorbent mass was determined as higher than 0.01368 m^3/day and the adsorption capacity of *Cellets 200* celluloses in fixed-bed column study for Methylene Blue dye removal was in the range of 1.375-3.303 mg/g. The obtained results confirm that the tested granulated cellulose can be considered as a good adsorbent into dynamic operating systems, which can be used in the treatment of wastewater containing organic dyes.

Key words: cellulosic adsorbent, cationic dye, dynamic adsorption, flow rate effect, Thomas and Yoon-Nelson model

Received: January, 2019; Revised final: January, 2020; Accepted: January, 2020; Published in final edited form: February, 2020

1. Introduction

Although a wide variety of strategies have been developed for removal of colored species, dyes are an inevitable presence in all areas of everyday life, being still considered as major pollutants in the water resources. They are generally present in the effluents of different industries, highlighting the textile, paper and pharmaceutical industries.

The aesthetic aspect but also the toxic effects (possible carcinogenicity) of dyes and their degradation products (i.e. benzidine), as well as damage to aquatic life by blocking the light penetration and aeration, have determined that their removal be a subject of increasing attention and concern for the environmental specialists (Zaharia and Şuteu, 2012).

Nowadays, a large number and various types of methods for dyes removal, such as chemical oxidation, ion exchange, electrochemical reduction, ozonation, reverse osmosis, membrane technologies, adsorption, photocatalytic degradation have certain efficiency (but their initial and operational costs are too high) (Gupta et al., 2015; Madi et al., 2019; Muthusaravananet al., 2019; Sivarajasekar et al., 2017; Subashini et al., 2020; Zaharia and Şuteu, 2012). It is worth noting that there is a continuous diversification of these simple but especially combined treatment methods, which ensure an increased efficiency of the wastewater cleaning treatments with adequate cost-efficient investments.

One method of interest in the industrial practice is *adsorption*, but using innovative materials as adsorbents, along with improved and/or optimized

---

* Author to whom all correspondence should be addressed: e-mail: danasuteu67@yahoo.com; czah@ch.tuiasi.ro

operating techniques (Adeyemo et al., 2017; Anastopoulos et al., 2018; Chiucholi et al., 2014; Dawood and Sen, 2014; Kharat, 2015; Nacu et al., 2019; Panic et al., 2013; Salahshoor and Shahbazi, 2014; Seow and Lim, 2016; Tomczak and Tosik, 2017; Vital et al., 2016).

Being a renewable resource, cellulose still remains a serious candidate for obtaining various biomaterials, such as numerous materials for water and/or wastewater depollution due to their good adsorptive properties, availability and easiness of use in different forms as granules, fibers, filters etc. (Wang, 2019). Among its advantages are noticed: the possibility of processing in different forms, the large specific surface, the ease of physical and chemical functionalization and regeneration, the tolerance to biological structures, and the relative fast adsorption (Lazzari et al., 2019). One of such material is the *Cellets* product, which combines different properties, for instance the perfect sphericity, the narrow particle size distribution, the low friability, the low solubility and inertness (Șuteu et al., 2019). The satisfactory results obtained with this cellulosic material, as an adsorbent for retaining dyes (Methylene Blue) in terms of static retrieval (Șuteu et al., 2015) and its regeneration (Mazouz et al., 2016; Șuteu et al., 2019), have led us to expand our works to the dynamic adsorption studies for establishing the optimal operating parameters as one of the finishing cleaning step in the study of real systems, *i.e.* wastewaters with variable contents of dyes, associated with its adequate modeling and specific corresponding design.

The study of adsorption into dynamic regime has permitted the establishing of a few correlations between the adsorbent properties, the characteristics of pollutant (Methylene Blue cationic dye), and the profile of flowing regime through the fixed bed of adsorbent, information which will permit to identify the optimal operating conditions for the implementation of such system at the industrial scale setup.

The paper presents our results on the adsorption study into a fixed-bed column for the removal of Methylene Blue (MB) cationic dye from aqueous solutions (low concentration of cationic dye, < 10 mg of dye/L of solution). The experiments were carried out using granulated *Cellets 200* celluloses. The adsorption modeling of experimental data in dynamic regime was based on Thomas and Yoon-Nelson models. For complete description of dye-cellulose adsorption system behavior and performance, all findings in this fixed bed column study were compared with our results performed in the batch adsorption studies which were carried out for description of mechanism, especially from the equilibrium isotherms and estimated adsorption capacity of *Cellets 200* cellulose for MB cationic dye. The information from only batch adsorption studies was not enough to design an effluent treatment system in continuous operating regime.

The obtained results reconfirmed that the studied celluloses can be considered as a good candidate as adsorbent in static but also dynamic operating system in order to be applied in the treatment of effluents containing organic dyes.

2. Material and methods

2.1. Materials

Adsorbent. The Cellets 200 cellulose is used in this experimental work, being purchased from Synthafarm Company from Germany, and some of its main physical-chemical characteristics are shown in Table 1 (Șuteu et al., 2015).

Dye. It was selected *Methylene Blue* dye (Basic Blue 9; C.I. 52015 – MB, chemical formula: $C_{16}H_{18}ClN_3S$), used as commercial salts. This is a cationic phenothiazine dye, with molecular weight of 319.85 g/mol and maximum wavelength (λ_{max}) at 660 nm considered as the most commonly used reference material for dyeing cotton, wool and silk. The dye stock solution was of about 468 mg of dye /L of solution concentration, and the working solutions were prepared by appropriate dilution, such as to be ranged in the concentration domain of 9-10 mg of dye/L of solution.

2.2. Analytical methods for physicochemical and quantitative characterization of dye removal

The residual dye concentration in the aqueous samples periodically collected was determined spectrophotometrically by measuring the absorbance at the maximum dye wavelength of 660 nm (MB dye) with a JK-VS-721N VIS spectrophotometer, using a calibration curve method (range of working concentrations selected in the Lambert-Beer region). The solution pH value was measured directly on a Hanna high precision KL-009(I) pH-meter, the pH adjustment being performed specifically with 0.1N NaOH or 0.1N HCl solution. Usually, the initial pH of the dye solution is a key factor in all reported adsorption studies, but if the adequate pH was found for the system of adsorbent (*Cellets 200*) - adsorbate (MB dye), all experiments can be focused on other different operating factors, or designing parameters and norms at the known pH value for dye adsorption. For this adsorption study in dynamic regime, it was selected the corresponding pH from the batch adsorption study for this system, meaning pH of 4.7 which permitted to estimate an adsorption capacity of 81.968 mg of MB dye/g of *Cellets 200* adsorbent (Suteu et al., 2019). The adsorption capacities of this cellulosic adsorbent (q_e) were evaluated by means of the amount of adsorbeddye (Eq 1):

$$q_e = \frac{C_0 - C_e}{G} \cdot V \qquad (1)$$

where: C_0 and C_e are the initial and equilibrium concentration of dye in solution (mg of dye/L of solution); G is the amount of cellulose (g), and V is the volume of treated solution (L).

The *Cellets 200* cellulose behavior in the MB dye adsorption (dynamic regime) was analyzed considering the shape of its breakthrough curve for each selected flowrate which represents the plotting of dye concentration in effluent (C_t), or normalized dye concentration in effluent (C_t/C_0) as a function dependent of time (t), or treated volume (V). These breakthrough curves are significant in evaluation of operation performance and dynamic response of a fixed bed in an adsorption column (Tofan et al., 2013). Usually, when C_t approaches 90% of its initial concentration (C_0), the adsorbent is closed to its exhausted form, and can be considered as essentially exhausted (C_{exh}) (Mazouz et al., 2016). The breakthrough concentration (C_b) is chosen arbitrarily beginning with a low value (e.g., the C_t value when approaches 10% of its initial concentration, or a legislative norm for the dye concentration in water resource, i.e. the maximum admissible concentration of MB dye in treated effluent (M.A.C.=1 mg of dye/L of effluent), or other imposed value). The total adsorption time (t_{ads}) is considered as the adsorption time after which the adsorbent is exhausted (C_t=C_0), meaning that the analyzed samples has the dye concentration value equal or a little bit (no more than 10%) higher than the initial dye concentration.

2.3. Characterization of adsorbent

FT-IR analysis: Infrared spectra were recorded on a Fourier transform infrared spectroscopy (FTIR) Bruker Vertex 70 Spectrophotometer (Bruker, Ettlingen, Germany) in the transmission mode, using KBr pellets, and the spectra were acquired by accumulation of 32 scans with a resolution of 2 cm^{-1}, recorded in the range of 400–4000 cm^{-1}.

Polarized Light Microscopy (PLM): PLM observations were carried out with an Olympus BH-2 polarized light microscope (Olympus, Hamburg, Germany), under crossed polarizers with a Linkam THMS 600/HSF9I heating stage and a TMS91 control unit (Desy, Hamburg, Germany). The sample was prepared by pressing around 1 mg of adsorbent between two lamellae.

2.4. Dynamic adsorption procedure

Dynamic adsorption working methodology. Dynamic adsorption studies were performed in a glass column of 1.5 cm in inner diameter and 21 cm in length. The column was filled with a known varying amounts of *Cellets 200* cellulose (4 - 8 g) providing a packed bed height of adsorbent between 3 - 7 cm. A dye solution of known concentration (commonly 9.04 mg of dye/L of solution) was introduced on the top of the column by means of a feeding funnel to ensure uniform continuous flow. The passing of the dye solution through the column was done freely, gravitationally, and the effluent was collected from the bottom for further analyzing and control. At specified time intervals (5, or 10 min depending on the selected flowrate), samples of 5 mL of effluent were taken from outlet (the bottom of the column) at different time intervals and analyzed with the UV-VIS Digital Spectrophotometer, model S 104D /WPA, especially for the residual dye concentration in the treated effluent.

In order to evaluate the proposed adsorption model, all experiments had to be performed considering the following operating parameters: (1) the feed temperature and pH were stabilized at 25°C and 4.7 (normal pH of aqueous dye solution), based on the best results performed in the batch adsorption study (Şuteu et al., 2019); (2) three different flowrates (F_{vi}, i=1…3) of dye-containing solutions with the same dye concentration were passed through the fixed adsorbent bed in the column: 5.5, 9.5 and 13.0 mL/min, corresponding to the mass of celluloses (m) equal to 7.63, 4.06 and 5.14 g, respectively. All experiments were stopped when saturation was achieved and further control (at least three samplings after the saturation point establishment, meaning the point where the final dye concentration had equal or higher value than the initial dye concentration in the collected treated samples).

Adsorption designing in the fixed bed column. Some operating parameters necessary to design the fixed bed column adsorption were determined, i.e. (i) the mean flowrate per adsorbent mass (b_i) for establishment of the optimal volume of treated dye solution (V_{opt}); (ii) the adsorption time (t_{ri}) till attaining of a maximum admissible dye concentration in the treated effluent, and also (iii) the sizes of a proposed adsorption tank, or reactor (H_{ads}, D_R, H_R), working with granulated *Cellets 200* celluloses. Thus, the optimal volume of treated dye solution per adsorbent mass (V_{opt}) was determined experimentally by using a number (i) of identical columns with fixed bed of adsorbent inside, working at different flowrates (F_v= 5.5, 9.5 or 13.0 mL/min). In each column, it was stabilized the mean flowrate of dye-containing solution per adsorbent mass (b_i, mL/g.min) as follows (Eq. 2):

$$b_i = \frac{V_n + n_i \cdot v}{m \cdot t_{ni}} \tag{2}$$

where, $V_n$is the volume of dye solution passed through the fixed adsorbent bed, collected at the bottom of the column (mL); n_i- the number of samples periodically analyzed for the dye content; v - the volume of each analyzed sample (v=5 mL); m - the mass of adsorbent (g) and $t_{ni}$is the total adsorption time till attaining the maximum residual dye concentration in the treated effluent (min).

Moreover, it was determined for each treatment experiment, the adsorption time (t_{ri}) after which the solution passing through each fixed bed in the column attained the maximum admissible limit (M.A.C.) of dye concentration (1 mg of dye/L of solution). Accordingly, there were obtained three values for t_{r1}, t_{r2} and t_{r3} for each tested flowrate (F_{v1}, F_{v2} and F_{v3}).

After that, it was calculated the volume of solution treated per adsorbent mass till attaining of the maximum admissible concentration of dye in the treated effluent (V_i, mL/g) (Eq. 3) as:

$$V_i = b_i \cdot t_{ri} \qquad (3)$$

There were calculated three values (V_1, V_2 and V_3) which were interpreted considering the graphical representation, $V_i = f(b_i)$, in order to determine the optimal volume of dye solution (V_{opt}) passed through the fixed bed of adsorbent in the column till the maximum admissible concentration of MB dye in the treated effluent (dynamic regime) attained. The V_{opt} value corresponds to the inflexion point of the above mentioned graphical representation. Further, the main sizes of an adsorption tank or column reactor are calculated based on adsorbent mass (M_{ads}) and corresponding adsorbent volume in the fixed bed column (V_{ads}), bulk density of adsorbent (ρ_{ads}), estimated flowrate (F_{Vi}), estimated adsorption time (t_{ni}), uniformity distribution coefficient (β) of adsorbent in the fixed bed (β=1-3), and free space above the fixed bed of adsorbent (λ corresponds to (0.3−1)·V_{ads}, or (1-3)·H_{ads}), mainly considering the correlations presented in Table 2 (Musteret et al., 2014).

2.5. Modeling of adsorption experimental data into dynamic regime

For determination of the characteristic adsorption parameters in the dynamic adsorption system, a few well-organized experimental data must be processed using a few of the most known models from the scientific literature, i.e. Thomas and Yoon-Nelson models. These selected models are briefly described in table 3 (Bulgariu and Bulgariu, 2013; Gopal et al., 2016; Smaranda et al., 2017; Tofan et al., 2015), and applied specifically for the investigated adsorption system retaining the MB dye onto the fixed bed of adsorbent in continuous dynamic regime. The specific parameters are determined from the slope and intercepts of the graphical representation of the linearized form of these two kinetic models, considering the specific theoretical assumptions for each one.

Table 1. The main characteristics of microcrystalline *Cellets 200* cellulose spheres

Physical-chemical characteristic	***Value***
Particle size distribution (μm) (size fraction %)	200 – 355 (≥ 85 %)
Loss on drying (%)	≤ 7.0
Bulk density (g/cm^3)	0.80 ± 0.05
Sphericity degree (average)	0.90 ± 0.05
Degree of polymerization	≤ 350
pH value	5.0 – 7.0
Conductivity (μS /cm)	≤ 75

Table 2. Correlations for the experimental design of an adsorption tank (column reactor)

Adsorbent mass (kg)	***Adsorbent volume, (m³)***	***Internal diameter of adsorption tank, (m)***	***Height of fixed bed, (m)***	***Height of adsorption tank, (m)***
$M_{ads} = \frac{F_{Vi} \cdot t_{ni}}{V_{opt}}$	$V_{ads} = \frac{M_{ads}}{\rho_{ads}}$	$D_R = \sqrt[3]{\frac{4 \cdot M_{ads}}{\beta \cdot \pi \cdot \rho_{ads}}}$	$H_{ads} = \beta \cdot D$	$H_R = \lambda \cdot H_{ads}$

Table 3. Adsorption models in dynamic regime applied for fixed-bed column reactor

Model	***Characteristic model, linearized form***	***Observations***
Thomas	$\ln(\frac{C_0}{C_t} - 1) = \frac{k_T \cdot q_{0(T)} \cdot m}{F_V} - \frac{K_T \cdot C_0}{F_V} \cdot V_t \qquad (4)$ where: C_0 and C_t - the dye concentration at initial moment (t=0) and time t (mg/L); k_T - the Thomas constant (L/min mg); F_V - the volumetric flowrate (L/min); $q_{0(T)}$ - the maximum adsorptive capacity (mg/g), m – the weighted adsorbent mass (g) and V_t - the treated volume at time t (L). The linear model corresponds to the graphical representation of $ln(C_0/C_t-1)$ versus V_t.	The model does not rely on the internal and external mass transfer resistance and omits the axial dispersion phenomenon (Tomczak and Tosik, 2017).
Yoon-Nelson	$ln(\frac{C_t}{C_0 - C_t}) = k_{YN} \cdot t - t_{1/2} \cdot k_{YN}$ …………………… (5) where, k_{YN} - the Yoon-Nelson rate constant (min^{-1}); $t_{1/2}$ - the time required for 50% dye breakthrough; t - the adsorption time (min). The linear model corresponds to the graphical representation of $ln\ [C_t/(C_0-C_t)]$ versus t.	The model stated on the assumption that the decrease of adsorption rate for each adsorbate molecule is proportional with probability of adsorbate breakthrough onto adsorbent bed (Chowdhury et al., 2013).

The most general and widely used adsorption model in fixed bed column studies is considered to be the Thomas model which is based on the assumption of Langmuir kinetics of adsorption-desorption without axial dispersion, and the hypothesis of rate driving force corresponding to second-order reversible reaction kinetics (Tofan et al, 2013).

A less complicated model is proposed by the Yoon-Nelson model based on the assumption that the dye amount adsorbed in a fixed bed is half of the total initial dye amount entering the fixed bed within $t_{1/2}$ period (Gupta et al., 2000).To compare the models with experimental data, it was used the linear regression method, where the linear regression coefficients (R^2) must be as closed as possible to unity for best accordance of calculated model values with the experimental ones.

3. Results and discussions

3.1. Characterization of the Cellets cellulose

Characterization of the Cellets 200 before and after adsorption. For completing the already known physicochemical characteristics of *Cellets 200* cellulose adsorbent, before and after adsorption (Şuteu et al., 2019), it was used the new data resulted from IR spectrometry (FT-IR) and Polarized Light Microscopy (PLM) of the *Cellets* 200. Fig. 1a shows the FTIR spectra of *Cellets* samples before and after adsorption of MB dye. The spectra of *Cellets* and *Cellets* with MB dyeshows similar chemical composition, with representative peaks located at around 4000 – 2995 cm^{-1} (hydrogen-bonded OH stretching), 2891 cm^{-1} (CH stretching mode). The other two typical peaks for cellulose are present at 1430 cm^{-1} (“crystalline” adsorption band) and 900 cm^{-1} (“amorphous” adsorption band). The band from 1645 cm^{-1} is attributed to the OH bending of absorbed water, since the region between 1200 - 1000 cm^{-1} summarizes the totality of the C-O-C symmetric stretching, OH plane deformation, C-O-C asymmetrical stretching, and as well as the C-C, C-OH, C-H ring and side group vibrations.

The PLM of the *Cellets 200* samples are presented in Fig. 1b. Cellulose samples have a uniform aspect, after adsorption the sample reveals also a homogeneous aspect, which are explained by a good incorporation of MB dye into the cellulose matrix.

3.2. Fixed bed column adsorption study in dynamic regime

3.2.1. Breakthrough curves

The breakthrough curve for retaining of MB dye onto a column filled with granulated*Cellets200* adsorptive cellulose, represented in coordinates: dye concentration at t time (C_t, mg of dye/L of solution) versus profile of adsorption time (t, min), is illustrated in Fig. 2. Its shape offers preliminary information on the nature of the studied adsorption process and the loading behavior of the dye in the continuous column. Also, there are calculated a series of characteristic parameters of adsorption models presented in Table 4, from the slope and intercepts of the breakthrough curves.

From Fig. 2, it can be observed that the breakthrough curves had a shape assimilated to “S” type, being the result of some competitive interactions between the adsorbed dye molecules, in which the significant role is possessed by the mass transfer processes (Chowdhury et al., 2013; Tofan et al., 2013).

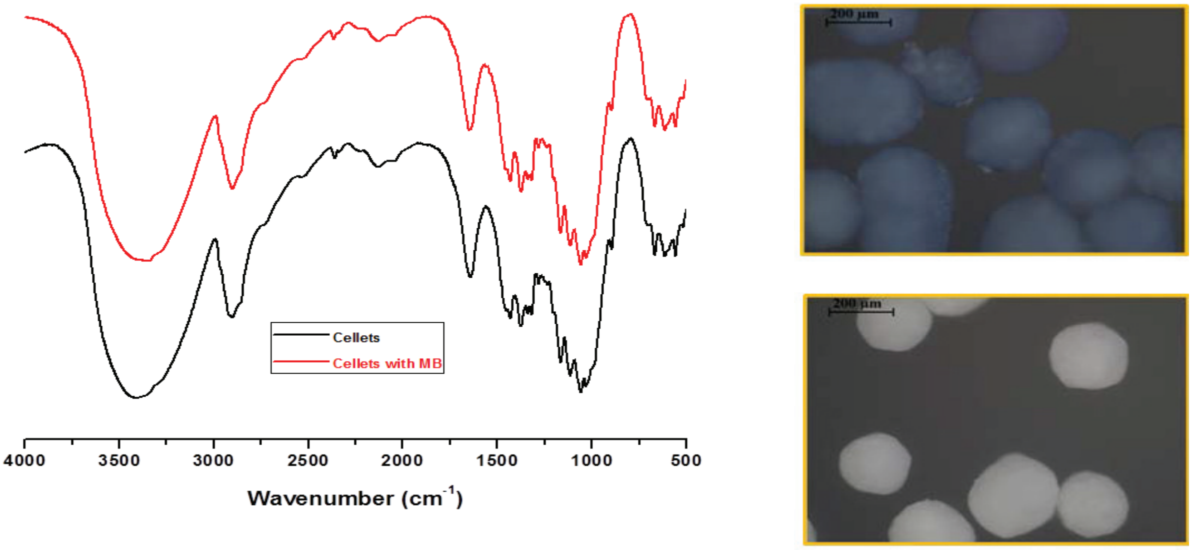

(a) **(b)**

Fig. 1. FTIR spectra (a)and PLM microphotographs(b) of *Cellets 200* before and after adsorption

In case of “S” type breakthrough curve, these interactions usually cause the stabilization for adsorbate species onto the fixed adsorbent bed and thus is produced a surface affinity for adsorbate species such as the surface excess withadsorbate species increases. Moreover, at low initial dye concentration, the breakthrough curve is commonly dispersed. This finding was noting in the same line of conclusions resulted from the adsorption study in static regime (Şuteu et al., 2019). Also, it is shown that the increase of flowrate (F_V) leads to the decrease of breakthrough time (t_b), fact that induces the idea that the cellulose saturation achieves much faster. This fact is confirmed also by the value of breakthrough time (t_b) (Table 4) that is reduced with the increase of working solution flowrate, and also the volume of treated solution till breakthrough point (V_b) that is decreased from 786 mL (F_v= 5.5 mL/min) to 299 mL ($\mathrm{F_v}$=13 mL/min). A similar behavior is registered for the saturation time (t_s)and the saturation volume ($\mathrm{V_S}$), i.e. the saturation time (t_s) reduced from 143 min (F_v=5.5 mL/min) to 111 min (F_v= 13 mL/min), as well as the breakthrough volume (V_b) decreases from 1,619 mL (F_v=5.5 mL/min) to 1,443 mL ($\mathrm{F_v}$= 13 mL/min).

The calculated data suggest that the adsorption of MB dye onto *Cellets 200* celluloses placed in a vertical column depends of the flowrate of working dye solution through the filled column. The highest volume of working dye solution (V_t) and adsorption time till the maximum admissible concentration of MB dye in treated solution ($\mathrm{t_{ri}}$) was performed for the lowest flowrate (F_v=5.5 mL/min). Caused lower adsorption time till a residual dye concentration in treated effluent equal with the recommendedmaximum admissible dye content in water resources (from environmental legislation)was performed in case of higher flowrate, and also a lower volume of working dye solution is passed through the fixed adsorbent bed in the column, a compromise between the volume of working dye solution and adsorption time in dynamic regime must be proposed, and the optimal volume of treated working solution per adsorbent mass must be determined (V_{opt}).

The plotting of b_i values (mL/gmin) versus V_i (mL/g) permits to determine the corresponding value of optimal volume per adsorbent mass as V_{opt}= 150.384 mL/g =150.384·10^{-3} m^3/kg, in accordance with Fig. 3. The optimal volume of working solution per adsorbent mass (V_{opt}=150.384 m^3/kg) is corresponding to a flow rate of 0.01368 m^3/day (9.5 mL/min). In further experiments, it is indicated to work in all adsorptive treatments in dynamic regime for MB dye - *Cellets 200* system with a flowrate of 13.68 L/day, or higher (but no more than 100 L/day).

For a common flowrate of 50 m^3/day (2.083 m^3/h) in the fixed bed column reactor and an adsorption time corresponding to a day (24 h) (or to a working shift, 8 h), considered as the reference for the textile wastewater treatment by adsorption in dynamic regime, the sizes/ dimensions of a column reactor (adsorption tank) filled with a packed bed of *Cellets 200* cellulose (ρ_{ads}=800 kg/m^3)used for MB dye removal from working influent solution, considering the determined optimal value of $\mathrm{V_{opt}}$= 150.384·10^{-3} m^3 kg^{-1}, and also β=1.5, λ= 2, are estimated as in Table 5.

3.2.2. Modeling the experimental column data

In order to determine the characteristic parameters in dynamic adsorption system, the experimental data were processed using a few of the most known models from the literature: Thomas and Yoon-Nelson models (Table 6). The experimental data are plotted considering the linearized form of the two models selected for adsorption study in dynamic regime as in Fig. 4 for the Thomas model and Fig. 5 for the Yoon-Nelson model, respectively.

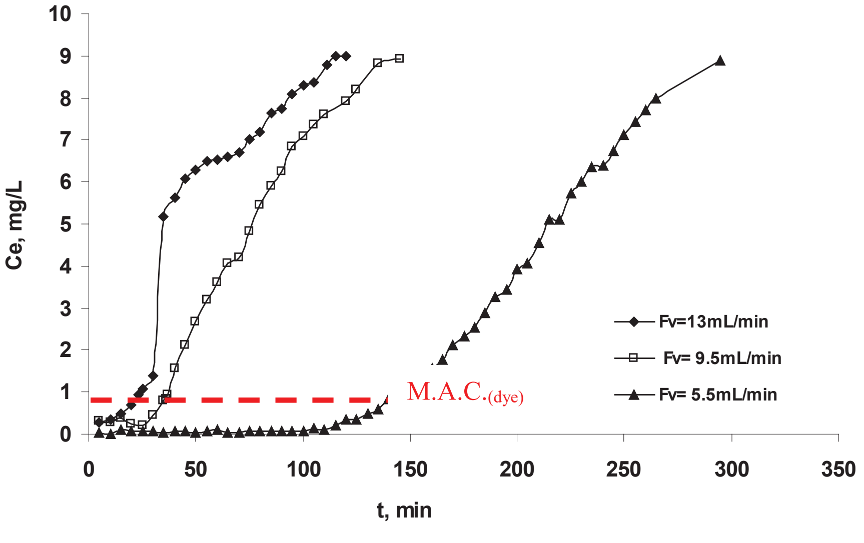

Fig. 2. Breakthrough curve of Methylene Blue dye adsorption in a fixed-bed column filled with granulated *Cellets 200* cellulose. Operating conditions: T = 20^0C, C_0 = 9.04 mg/L

Table 4. Characteristic parameters of the breakthrough curves

Parameter	***Significance and characteristics***	***Experimental values for each studied flowrate (F_V), (mL/min)***		
		5.5	***9.5***	***13***
Adsorbent bed height – h (cm)	Height in column of each added adsorbent amount	7.0	3.0	4.0
Breakthrough time - t_b(min)	Time required for attaining the breakthrough point, when the dye concentration has the value of $0.1C_0$ (C_b)	142.4	36.5	22.6
Saturation time - t_s (min)	Time required for attaining the saturation point, where dye concentration has a value of $0.9C_0$ (C_S)	294.4	135	111
The length of mass transfer zone – L(MTZ) (cm)	$L(MTZ) = h \cdot \left(1 - \frac{t_b}{t_s}\right)$ where, h - the heigth of adsorbent bed (cm)	3.609	2.189	3.185
Breakthrough volume – V_b (L)	Volume of working solution at breakthrough point, calculated as $V_b = F_V \cdot t_b$, where Fvis the volumetric flowrate (L/min).	0.78	0.347	0.294
Saturation volume – V_s (L)	Volume of working solution at saturation point, calculated as $V_S = F_V \cdot t_S$, where Fvis the flowrate (L/min)	1.617	1.282	1.443
Breakthrough capacity - q_b (mg/g)	Amount of MB dye retained per adsorbent mass at breakthrough point. $q_b = \frac{(C_0 - C_b) \cdot V_b}{m}$ where, m - adsorbent mass, g.	0.8015	0.602	0.467
Saturation capacity - qs (mg/g)	Amount of MB dye retained per adsorbent mass at saturation point. $q_S = \frac{(C_0 - C_S) \cdot V_S}{m}$ where, m - adsorbent mass, g.	0.0322	0.072	0.073
Rate of exhaustion - R_{AE} (g/L)	Amount of exhausted adsorbent (g) per volume of working solution at the breakthrough point. $R_{AE}\ (g/L) = \frac{\text{mass of exhaused adsorbent}}{\text{volume of working solution}}$	2.47	1.351	1.392

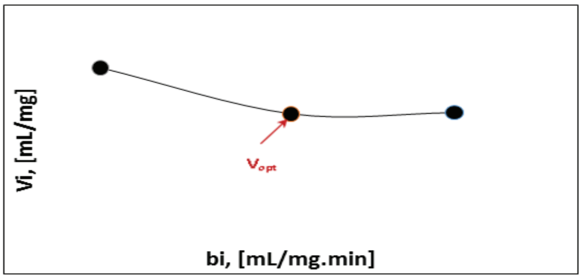

Fig. 3. Graphical representation of b_i versus V_i

Table 5. The estimated characteristic operating dimensions of packed bed column reactor

Characteristic operating dimensions	*Notation*	*Measured units*	*Value*
Adsorbent mass	M_{ads}	(kg)	332.482
Adsorbent volume	V_{ads}	(m^3)	0.416
Internal diameter of reactor, or adsorbent bed diameter ($D_R = D_{bed}$)	D_R	(m)	0.707
Height of fixed bed	H_{ads}	(m)	1.060
Height of adsorption reactor (H_R= 2 H_{ads})	H_R	(m)	2.120

Table 6. Thomas and Yoon-Nelson model applied for dynamic MB dye – *Cellets 20* adsorption system

Model	***F_v, Initial flowrate (mL/min)***	***k_T (L/min.mg)***	***$q_{0(T)}$ (mg/g)***	***R^2***	***k_{YN} (min^{-1})***	***$t_{1/2}$ (min)***	***$q_{0(YN)}$ (mg/g)***	***R^2***
Thomas	5.5	1.82×10^{-3}	2.7552	0.9589				
	9.5	2.86×10^{-3}	3.2442	0.9567				
	13.0	2.25×10^{-3}	3.3034	0.9604				
Yoon-Nelson	5.5				0.0340	211.065	1.375	0.9645
	9.5				0.0490	74.900	1.585	0.9730
	13.0				0.0407	73.852	1.688	0.9604
$q_{0\ (Langmuir)*}$(mg/g)	81.968*							

[*] *(Suteu et al., 2019)*

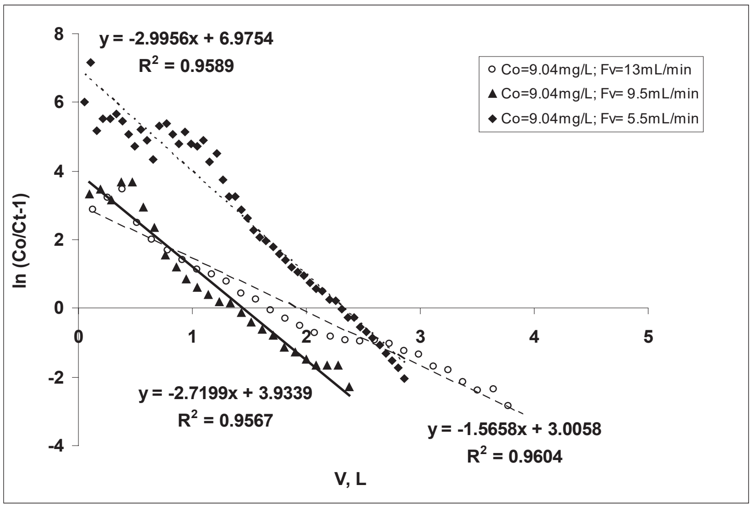

Fig. 4. Graphical representation of linearized form of dynamic Thomas adsorption model/min to 3.303 mg/g at 13.0 mL/min

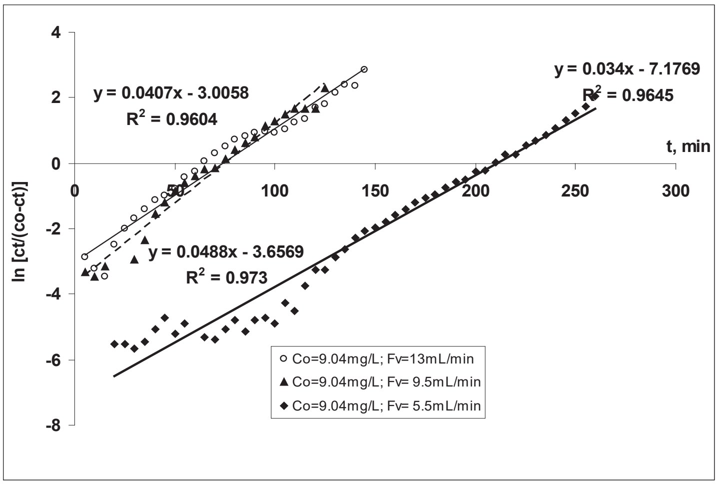

Fig. 5. Graphical representation of linearized form of dynamic Yoon-Nelson adsorption model

After the analysis of the processed experimental adsorption data from Table 6, and also the linear regression coefficient (R^2) values, it seems that the experimental data provided by the dynamic fixed bed column adsorption of MB dye from aqueous solution (low concentration) were verified better the Yoon-Nelson model due to its higher R^2 value referring to Thomas model. This finding complies with the results of batch study which pointed that the MB dye adsorption onto *Cellets 200* cellulose is very well described by the Langmuir isotherm model and follows a pseudo-second order kinetics (Şuteu et al., 2019). For the same concentration of the working dye solution passing through the adsorbent bed in the column (dynamic regime), the breakthrough time (t_b) and adsorption removal capacity (q_0) depends on the adsorbent amount fixed in the packed bed of the column (m) and the flowrate (F_V).

The values of Thomas rate constant (k_T) are varied in the range of (1.825 – 2.837) x 10^{-3} L/min.mg, and the *Cellets 200* maximum adsorption capacity ($q_{0(T)}$) is increasing as the flowrate increases from 2.755 mg/g at 5.5 mL/min to 3.303 mg/g at 13.0 mL/min.

It is clear shown in Table 5 that the values of the Yoon-Nelson rate constant (k_{YN}) are ranged of 0.0340-0.0407 min^{-1}, and the *Cellets 200* maximum adsorption capacity ($q_{0(YN)}$) increases as the flowrate increases from 1.375 mg/g at 5.5 mL/min to 1.688 mg/g at 13.0 mL/min.

Moreover, the *Cellets 200* maximum adsorption capacity (q_0) for MB cationic dye in this fixed-bed column study is higher when it was applied Thomas model than Yoon-Nelson model by more than 1.957-2.004 times in the selected flowrate range (5.5-13.0 mL/min). For the same dye concentration (9.04 mg/L) and adsorption pH (4.7), the adsorption capacity of *Cellets 200* cellulose for MB dye was highest in all batch adsorption study (81.968 mg/g) than in this dynamic fixed bed column adsorption study (1.375-3.303 mg/g), more than 24.813-59.613 times.

3.2.3. Column regeneration and comparison of Cellets 200 adsorption capacity with other adsorbents

The column with fixed adsorbent bed of 3 - 7 cm in depth and flowrate in range of 5.5 – 13.0 mL/min saturated with 9.04 mg of MB dye /L of solution was regenerated by successive desorption carried out with deionized water, acetic acid (CH_3COOH 1N) or sulphuric acid (H_2SO_4 4 N) till a constant pH value of washing/regeneration solution. It was observed that the 1st desorption cycle was almost finished after at least 24 h, after which further desorption was not significant. The adsorption efficiency of regenerated cellulose adsorbent in the fixed bed column study for MB dye removal working with diluted dye solution (9.04 mg of dye/L of solution) at a flowrate of 5.5-13.0 mL/min decreases with more than 30-50%, and also the breakthrough time (t_b) and saturation time (t_s). The values of dye adsorption capacities in batch and fixed bed column systems are compared in Table 7. It was found that the adsorption capacity of batch system performed better than that of fixed bed column system. The increased capacity of batch adsorption system may be attributed to a long continuous contact between the two phases (adsorbent-dye solution), high specific surface of adsorbent, while the gradient concentration decreases with time.

It is well known that a direct comparison between different absorbents is difficult to be performed due to the utilization of different experimental conditions for maximum adsorption capacity establishment. Data from Table 7 shows that dye adsorption capacity of cellulose adsorbent is significant and comparable, the *Cellets 200* celluloses being considered as a valuable adsorbent for treatment of industrial effluents containing organic dyes.

4. Conclusions

The dynamic adsorption system, Methylene Blue cationic dye – *Cellets 200* cellulose, was studied in fixed bed column, and the main working parameters were established in terms of adequate flowrate and adsorption time (breakthrough and saturation time) for dye removal till its maximum admissible concentration (1 mg of dye/L of solution) in water resources. It was worked with diluted dye solution (9-10 mg of dye/L ofsolution) at adequate initial pH (4.7) for highest MB dye adsorption onto Cellets celluloses. The optimal volume of working dye solution per adsorbent mass was determined as higher than 0.01368 m^3/day.

The adsorption kinetics for dye removal from aqueous solution were described by Thomas and Yoon-Nelson models, being associated with their characteristic parameters and coefficients, the best fitting corresponding to Yoon-Nelson model for packed bed adsorption column. The slope of the obtained breakthrough curves is deeper as influent flowrate decreases.

Table 7. Dye adsorption capacities of cellulose-based adsorbents in fixed bed column study

Adsorbent	*Type of adsorbed dye*	*q_{exp}, mg/g*	*Reference*
Chitosan impregnated with cetyl tri-methyl ammonium bromide (CTAB)	Brilliant Black (BBN) azo dye	0.16 - 1.89 (4-8 cm bed height, 0.8-1.5 mL/min, 20-100 mg/L of dye)	Rouf and Nagapadma, 2015
Rubber leaf powder	MB cationic dye	85.0 - 96.0 (5-10 cm bed height, 20 mL/min, 50-100 mg/L of dye)	Chowdhury et al., 2016
Granulated slag *Arcelor-Mittal, Algeria)	MB cationic dye	0.296 (15 cm bed height, 2 mL/min, 10 mg/L of dye)	Mazouz et al., 2016
Coffee residues	MB basic dye	104.5 (15 cm bed height, 20 mL/min, 800 mg/L of dye)	Kopsidas, 2016
Can Papyrus	MB cationic dye	0.0213 - 0.2044 (1-3 cm bed height, 12.5 mL/min, 5-15 mg/L of dye)	Saed et al., 2014
Carbon-alumina composite pellet	Acid fuchsin	2.185 - 3.89 (2.5-7 cm bed height, 5-15 mL/min, 20 mg/L of dye)	Dutta and Basu, 2014
Acid activated sawdust	Malachite Green dye	4.5 - 10.06 (7.5-15 cm bed height, 100 mL/min, 500 mg/L of dye)	Singh et al., 2015
TES fixed-bed (NaOH Treated Eggshell)	AO7 azo dye	0.567 - 17.111 (5-15 cm bed height, 2-6 mL/min, 5-30 mg/L of dye)	Chafi et al., 2015
Chitosan-glutaraldehyde	Direct Blue 7lAzo dye	343.59 (3-12 cm bed height, 1-3 mL/min, 50 mg/L of dye)	Lopez-Cervantes et al., 2018
Cellets 200 cellulose	MB cationic dye	1.375 - 3.3037 (3-7 cm bed height, 5-13.5 mL/min, 9.04 mg/L of dye)	This study

The adsorption capacity of Cellets 200 celluloses in fixed-bed column study for MB dye removal (1.375-3.3034 mg/g) was much lower than that of dye-cellulose batch system (81.968 mg/g).

References

Adeyemo A.A., Adeoye I.O., Bello O.S., (2017), Adsorption of dyes using different types of clay: a review, *Applied Water Science*, **7**, 543-568.

Anastopoulos I., Hosseini-Bandegharaei A., Fu J., Mitropoulos A.C., Kyzas G.Z., (2018), Use of nanoparticles for dye adsorption: review, *Journal of Dispersion Science and Technology*, **39**, 836-847.

Bulgariu D., Bulgariu L., (2013), Sorption of Pb(II) onto a mixture of algae waste biomass and anion exchanger resin in a packed-bed column, *Bioresource Technology*, **129**, 374-380.

Chafi M., Akazdam S., Asrir C., Sebbahi L., Gourich B., Barka N., Essahli M., (2015), Continuous fixed bed reactor application for decolourization of textile effluent by adsorption on NaOH treated eggshell, *World International Journal of Materials and Textile Engineering*, **9**,1242-1248.

Chiucholi M., Sagwekar P., Nagaria C., Kulkarni S., Dhokpaude S., (2014), Removal of dye by adsorption on various adsorbents: A review, *International Journal of Science, Engineering and Technology Research*, **3**, 835-840.

Chowdhury Z.Z., Zain S.M., Rashid A.K., Rafique R.F., Khalid K., (2013), Breakthrough curve analysis for column dynamica sorption of Mn (II) ions from wastewater by using *Mangostana garcinia* peel-based geanular activated carbon, *Journal of Chemistry*, On line at: http://dx.doi.org/10.1155/2013/959761.

Chowdhury S., Yasin M., Uddin M.T., Islam M.A., (2016), Batch and continuous (fixed bed column) adsorption of Methylene Blue by rubber leaf powder, *International Journal of Integrated Sciences & Technology*, **2**, 24-28.

Dawood S., Sen T.K., (2014), Review on dye removal from its aqueous solution into alternative cost effective and non-conventional adsorbents, *Journal of Chemical and Process Engineering*, **1**, 1-11.

Dutta M., Basu J.K., (2014), Fixed-bed column study for the adsorptive removal of acid fuchsin using carbon-alumina composite pellet, *International Journal of Environmental Science and Technology*, **11**, 87-96.

Gopal N., Asaithambi M., Sivakumar P., Sivakumar V., (2016), Continuous fixed bed adsorption studies of Rhodamine-B dye using polymer bound adsorbent, *Indian Journal of Chemical Technology*, **23**, 53-58.

Gupta V.K., Srivastava S.K., Tyagi R., (2000), Design parameters for the treatment of phenolic wastes by carbon columns (obtained from fertilizer waste material), *Water Research*, **34**, 1543-1550.

Gupta V.K., Khamparia S., Tyagi I., Jospal D., Malviya A., (2015), Decolorization of mixture of dyes: A critical review, *Global Journal of Environmental Science and Management*, **1**, 71-94.

Kharat D.S., (2015), Preparing agricultural residue based adsorbents for removal of dyes from effluents - a review, *Brazilian Society of Chemical Engineering,* **32**, 1-12.

Kopsidas O., (2016), Fixed-bed-column studies for Methylene Blue removal and recovery by untreated coffee residues, *Journal of Environmental Science and Engineering*, **B5**, 412-418.

Lazzari L.K., Zampieri V.B., Neves R.M., Zanini M., Zattera A.J., Baldasso C., (2019), A study on adsorption isotherm and kinetics of petroleum by cellulose cryogels, *Cellulose*, **26**, 1231-1246.

Lopez-Cervantes J., Sachez-Machado D.I., Sanchez-Duarte R.G., Correa-Murrieta M.A., (2018), Study of a fixed column in the adsorption of an azo dye from aqueous medium using a chitosan-glutaraldehyde biosorbent, *Adsorption Science & Technology*, **36**, 215-232.

Madi K., Yahiaoui I., Aissani-Benissad F., Vial C., Audonnet F., Favier L., (2019), Basic red dye removal by coupling electrocoagulation process with biological treatment, *Environmental Engineering and Management Journal*, **18**, 563-573.

Mazouz R., Filali N., Hattab Z., Guerfi K., (2016), Valorization of granulated slag of Arcelor-Mittal (Algeria) in cationic dye adsorption from aqueous solution: column studies, *Journal of Water Reuse and Desalination*, **6**, 204-213.

Muthusaravanan S., Vivek J.S., Deenadayalan K.G.N, Yogesan M., Bala S.D., Sivarajasekar N., Ram K., Kumaravel K., (2019), Green synthesized silver nanoparticles using aqueous leaf extracts of *Leucasaspera* exhibits antimicrobial and catalytic dye degradation properties, *SN Applied Sciences*, **1**, 208-218.

Musteret C., Fighir D., Gavrilescu D., Zaharia C., Teodosiu C., (2014), *Treatment of Waters and Wastewaters: Practical Applications* (in Romanian), Politehnium Press, Iasi, Romania.

Nacu G., Suteu D., Tofan L., Paduraru C., Bulgariu L., (2019), Removal of Zn(II) ions from aqueous solution by sorption using cellulose functionalized with reactive dyes as sorbent, *Environmental Engineering and Management Journal*, **18**, 321-327.

Panic V.V., Seslija S.I., Nesic A.R., Velickovic S.J., (2013), Adsorption of azo dyes on polymer materials, *HemijskaIndustrija*, **67**, 881-900.

Rouf S., Nagapadma M., (2015), Modeling of fixed bed column studies for adsorption of azo dye on chitosan impregnated with a cationic surfactant, *International Journal of Scientific & Engineering Research*, **6**, 538-544.

Saed A.U., Nahrain M.H.A., Atshan A.A., (2014), Adsorption of Methylene Blue dye from aqueous solution using can papyrus, *Journal of Babylon University, Engineering Sciences*, **22**, 218-229.

Salahshoor Z., Shahbazi A., (2014), Review of the use of mesoporous silicas for removing dye from textile wastewaters, *European Journal of Environmental Sciences*, **4**, 116-130.

Seow T.W.,Lim C.K., (2016), Removal of dye by adsorption: a review, *International Journal of Applied Engineering Research*, **11**, 2675-2679.

Singh S.K., Katoria D., Nehta D., Sehgal D., (2015), Fixed bed column study and adsorption modelling on the adsorption of Malachite Green dye from wastewater using acid activated sawdust, *International Journal of Advanced Research*, **3**, 521-529.

Sivarajasekar N., Balasubramani K., Mohanraj N., Prakash Maran J., Sivamani S., Ajmal K.P., Karthik V., (2017), Fixed-bed adsorption of atrazine onto microwave irradiated *Aeglemarmelos Correa* fruit shell: Statistical optimization, process design and breakthrough modeling, *Journal of Molecular Liquids*, **241**, 823-830.

Smaranda C., Popescu M.C., Bulgariu D., Malutan T., Gavrilescu M., (2017), Adsorption of organic pollutants onto a Romanian soil: Column dynamics and transport, *Process Safety and Environmental Protection*, **108**, 108-120.

Subashini R., Sirarajasekar N., Balasubramani K., Prakashmaran J., (2020), *Saponin-Aided Reverse Micellar Extraction of Malachite Green Dye from Aqueous Solutions*, Global Challenges in Energy and Environment, Springer, Singapore, 89-97.

Șuteu D., Biliuta G., Rusu L., Coseri S., Nacu G., (2015), Cellulose CELLETS as new type of adsorbent for the removal of dyes from aqueous media, *Environmental Engineering and Management Journal*, **14**, 525-532.

Șuteu D., Biliuta G., Rusu L., Coseri S., Vial C., Nica I., (2019), A regenerable microporous adsorbent based on microcrystalline cellulose for organic pollutants adsorption, *Desalination and Water Treatment*, **146**, 176-187.

Tofan L., Teodosiu C., Paduraru C., Wenkert R., (2013), Cobalt (II) removal from aqueous solutions by natural hemp fibers: Batch and fixed-bed column studies, *Applied Surface Science*, **285P**, 33-39.

Tofan L., Paduraru C., Teodosiu C., Toma O., (2015), Fixed bed column study on the removal of chromium (III) ions from aqueous solutions by using hemp fibers with improved sorption performance, *Cellulose Chemistry and Technology*, **49**, 219-229.

Tomczak E., Tosik P., (2017), Waste plant materials as a potential adsorbent of a selected dye, *Chemical and Process Engineering*, **38**, 283-294.

Vital R.K., Saibaba K.V.N., Shaik K.B., Gopinath R., (2016), Dye removal by adsorption: a review, *Journal of Bioremediation & Biodegradation*, **7**, 371- 374.

Zaharia C., Suteu D., (2012), *Textile Organic Dyes – Characteristics, Polluting Effects and Separation/Elimination Procedures from Industrial Effluents – A Critical Overview*, In: *Organic Pollutants Ten Years After the Stockholm Convention – Environmental and Analytical Update*, Puzyn T. (Ed.), INTECH Publisher, Rijeka, Croatia, 55-86.

Wang D., (2019), A critical review of cellulose-based nanomaterials for water purification in industrial processes, *Cellulose*, **26**, 687-701.

Environmental Engineering and Management Journal February 2020, Vol. 19, No. 2, 281-288
http://www.eemj.icpm.tuiasi.ro/; http://www.eemj.eu

"Gheorghe Asachi" Technical University of Iasi, Romania

THERMODYNAMIC ANALYSIS OF HEAVY METALS PRECIPITATION FOR THEIR RECOVERY FROM INDUSTRIAL WASTEWATERS

Igor Povar[1,2*], Inga Zinicovscaia[1,2,3], Stefano Ubaldini[4], Oxana Spinu[1], Boris Pintilie[1], Tudor Lupascu[1], Gheorghe Duca[1]

[1]The Institute of Chemistry, 3 Academiei Str., 2028 Chisinau, Republic of Moldova
[2]Joint Institute for Nuclear Research, 6 Joliot-Curie Street, 1419890 Dubna, Russia
[3]Horia Hulubei National Institute for R&D in Physics and Nuclear Engineering, 30 Reactorului Street, MG-6, Bucharest - Magurele, Romania
[4]Institute of Environmental Geology and Geoengineering, Italian National Research Council, Research Area of Rome 1, 00015 Monterotondo, Italy

Abstract

This work seeks to develop a suitable heavy metals precipitation modeling approach that could give reasonable results in mainstream use with industrial wastewater treatment. This paper is devoted to the thermodynamic analysis of the degree of precipitation of slightly soluble hydroxides and salts in industrial wastewaters in order to optimize the technological schemes of extraction and reuse of heavy metals from industrial waste. Based on the notion of the solubility product, the equations describing the dependence of the precipitation degree of the metal ion γ in the form of slightly soluble salts and hydroxides on the initial concentrations of the components, including complexing agents, and the pH of the solution, have been deduced. The thermodynamic meaning of the quantity γ has been revealed. Possibility of forming stable complexes between the metal ion and complexing agents in galvanic wastewater is taking into account**.** Degree of precipitation (in parentheses, %) and distribution of chemical species of metal ions (*Al* (43)*, Cr* (0)*, Fe* (100)*, Zn* (0)*, Sr* (100) and *Ba* (100)) from the multicomponent industrial effluents of an engineering company (electroplating units of the Tactical Missiles Corporation, Dubna, Russia) were analyzed at pH 6.

Key words: complex formation reaction, degree of precipitation, industrial wastewater, ion metal hydrolysis, slightly soluble compounds

Received: January, 2019; Revised final: January, 2020; Accepted: January, 2020; Published in final edited form: February, 2020

1. Introduction

The pollution of the environment with heavy metals ions pose a serious danger to the biosphere. One of the main sources of the environment pollution with heavy metals are industrial wastewater, which enter surface water courses (Ayangbenro and Babalola, 2017; Duca and Covaliova, 2017; Malschi et al., 2018; Marzougui et al., 2017; Wu et al., 2018; Zinicovscaia et al., 2015). The greater part of heavy metals enters the environment with wastewater from machine-building enterprises, galvanic units, mining enterprises and non-ferrous metallurgy (Khalturina and Bobric, 2018). In addition to pollution of natural and artificial water ecosystems with heavy metals, these industrial processes are characterized high water consumption (Makisha and Yunchina, 2017; Sofińska-Chmiel and Kolodynska, 2017).

In most cases, metal-containing wastewater are purified by conventional techniques, using chemical reagents, the effectiveness of which cannot be considered always satisfactory (Fu and Wang, 2011; Gunatilake, 2015). The reagent method of galvanic wastewater treatment is relatively common due to

---

[*] Author to whom all correspondence should be addressed: e-mail: ipovar@yahoo.ca

several advantages: relative simplicity, reliability, ease of automatic pH control (Luptáková et al., 2012; Ubaldini et al., 2013). However, complex chemical composition of the wastewater makes unattainable the reduction of metal concentration till maximum admissible levels, since it is almost impossible to define such pH range in which all ions of heavy metals could precipitate simultaneously (Kanamarlapudi et al., 2018). In addition, the presence in solution of complexing agents complicates the task (Gogina and Makisha, 2014). In this regard, the scientific development and improvement of both reagent and non-reagent methods for the neutralization of metal-containing wastewater from machine-building enterprises and mining, is an actual problem (Gaikwad and Gupta, 2008; Nancucheo, 2017). Review on removal of heavy metals from acid mine drainage.

Therefore, a new approach for evaluation of this method, based on the physicochemical analysis of not previously considered factors is needed.

The main objective of the paper is to derive the equations for the evaluation of the effectiveness of the reagent method used in the wastewater treatment, based on the calculations of the residual concentrations and degree of precipitation of heavy metal hydroxides and salts in an aqueous medium. The obtained expressions allow the determination of the pH range of hydroxides precipitation in the presence of complexing agents (organic or inorganic ligands), which ensures a minimum residual concentration of heavy metal ions in the wastewater (Aljerf, 2018). On other hand, it becomes possible to find the optimal conditions for the deep and complete extraction of metals, achieving high purity of the final products due to the joint and selective extraction and separation of elements with close properties, which is a main object for the next paper.

2. Theoretical considerations

For quantitative estimation of the precipitation process of compounds from aqueous solutions different characteristics are used, the most commonly used being the solubility S. Solving the problem of this kind is related to certain difficulties, because under real conditions, the ions of the solid phase participate in conjugated reactions with both the solvent (water) dissociation products and other substances present in the solution (as impurities), which leads to the reduction of the precipitated metal fraction in the form of slightly soluble compounds (Povar, 1994; Povar and Spinu, 2014a; Povar and Spinu, 2015; Povar and Spinu, 2016). At the same time, in many technological schemes and analytical procedures, a pre-estimation of the fraction or metal ion part precipitated as slightly soluble compounds, which depends on a series of parameters (the ratio of the initial concentrations of the components, the pH of the solution etc.) is strictly necessary. As a characteristic of the precipitated metal ion fraction, the degree of precipitation was introduced in (Povar and Spinu, 2016) study:

$$\gamma = \frac{C_M^0 - C_M^r}{C_M^0}, \tag{1}$$

where: C_M^0 and C_M^r are the total concentration of the metal ion in the mixture and its residual concentration in solution. In the cited above paper the following set of reactions in the "*$M_mA_{n(S)}$ - saturated aqueous solution*" system were considered:

$$M_mA_{n(S)} = mM + nA, \qquad K_S = [M]^m[A]^n \cdot \tag{2}$$

$$iM + jH_2O = M_i(OH)_j + jH, \quad K_{ij} = [M_i(OH)_j][H]^j/[M]^i \tag{3}$$

$$A + kH = H_kA, \quad \beta_k = [H_kA]/([H]^k[A]). \tag{4}$$

In Eqs. (2 - 4), the corresponding expressions of the law of the mass action are included next to the reaction equations. For the evidence of metal ion hydrolysis and anion protonation the α coefficients are used:

$$\alpha_M = C_M^r/[M] = 1 + \sum_{i=1}\sum_{j=1} iK_{ij}[M]^{i-1}[H]^{-j}$$

$$\alpha_A = C_A^r/[A] = 1 + \sum_{k=1}\beta_k[H]^k.$$

As it was mentioned, in paper (Povar and Spinu, 2016) only the equilibria (2 - 4) were taken into account. But multicomponent wastewater contains beside many inorganic ions and many organic compounds, which can act as complexing agents forming thermodynamically stable complexes with heavy metal ions. Their presence could transform essentially the whole picture of complex chemical equilibria and distribution of soluble and insoluble metal ion species. If the complexing agents, capable to form polydentate *ML* or stepwise complexes of the *ML_i* type are present in the system, the polynuclear complexes practically cannot be formed. Consequently, in addition to the hydrolysis of the metal ion to form *$M(OH)_j$* mononuclear complexes, dependent on the pH and the total concentrations of the ligands C_L^0 or /and C_Y^0, the following side reactions are possible (for simplicity the charges of species are omitted):

$$M + kL = ML_k, \qquad \beta_k = [ML_k]/([M][L]^k) \tag{5}$$

$$M + sY = MY_s, \qquad \beta_s = [MY_s]/([M]Y]^s) \tag{6}$$

$$L + qH = H_qL, \qquad \beta_q = [H_qL]/([L][H]^q) \tag{7}$$

$$Y + rH = H_rY, \qquad \beta_r = [H_rY]/([Y][H]^r) \tag{8}$$

The last two Eqs. (7-8) take into account the possibility of protonation of corresponding ligand. Here just two complexing agents (ligands) will be considered, *L* and *Y*, but our thermodynamic analysis proves that the form of deduced equations remains the same for any numbers of ligands. For the system considered, the mass balance conditions take the form:

$$C_M^r = [M] + \sum_{i=1} [M(OH)_i) + \sum_{k=1} [ML_k] + \sum_{s=1} [MY_s] + ... = [M]\alpha_M \tag{9}$$

where the coefficient α_M is defined by the expression:

$$\alpha_M = 1 + \sum_{i=1} K_i [H]^{-i} + \sum_{k=1} \beta_k [L]^k + \sum_{s=1} \beta_s [Y]^s + ... \tag{10}$$

$$C_L^0 = [L] + \sum_{q=1} [H_q L] + \sum_{k=1} k[ML_k] = [L]\left(1 + \sum_{q=1} \beta_q [H]^q + \sum_{k=1} k\beta_k [L]^k\right) \tag{11}$$

$$C_Y^0 = [Y] + \sum_{r=1} [H_r Y] + \sum_{s=1} s[MY_s] = [L]\left(1 + \sum_{r=1} \beta_r [H]^r + \sum_{k=1} s\beta_s [L]^s\right) \tag{12}$$

When $C_L^0 >> C_M^0$ and $C_Y^0 >> C_M^0$ (condition *A*), in the Eq. (10) instead of the equilibrium concentrations of ligands *L* and *Y* can be used their total (analytical) concentrations C_L^0 and C_Y^0. Furthermore, under the condition *A,* in the Eqs. (11 - 12) the terms, associated with complex formation reactions, may be neglected.

Between the total concentration of the metal ion C_M^0 and its residual concentration in the solution C_M^r there is a mutuality relationship

$$C_i^0 = \Delta C_i + C_i^r, \tag{13}$$

where ΔC_i is the amount of precipitated metal ion (in moles) in a volume unit of the solution.

Consequently, the expression for the conditional solubility product can be presented as follows (Fishtik et al., 1986; Fishtik et al., 1987; Povar and Spinu, 2014a):

$$K_S^{cond} = \left(C_M^r\right)^m \left(C_A^r\right)^n = K_s \alpha_M^m \alpha_A^n. \tag{14}$$

By marking through *P* the amount of precipitated salt in a volume unit of the solution, with the evidence of precipitate stoichiometry, the mass balance conditions can be rewritten as follows:

$$C_M^0 = mP + C_M^r, \qquad C_A^0 = nP + C_A^r \cdot \tag{15}$$

Joint solution of relations (1) and (15) with respect to *γ* gives:

$$\gamma = \frac{mP}{C_M^0} \cdot \tag{16}$$

From Eqs. (15 - 16), it follows:

$$\gamma = \frac{m}{n}\left(\frac{C_A^0 - C_A^r}{C_M^r}\right), \qquad C_A^r = C_A^0 - \frac{n}{m}\gamma C_M^0 \cdot \tag{17}$$

Finally, by combining Eqs. (1, 14, 17), the following expression is obtained:

$$K_S^{cond} = \left(C_M^0 (1-\gamma)\right)^m \left(C_A^0 - \frac{n}{m}\gamma C_M^0\right)^n. \tag{18}$$

Eq. (18) is a non-explicit equation of the function *γ* of the total concentration of ions in the mixture C_M^0, C_A^0, C_L^0 and the pH of the environment. Taking into account the relation (14), the last equation can be converted in relation to *γ*:

$$\gamma = 1 - \frac{\left(K_S^{cond}\right)^{1/m}}{C_M^0 \left(C_A^r\right)^{n/m}}. \tag{19}$$

By solving the system of Eqs. (16 - 18), the calculation formula of function *γ = f(pH)* for fixed values C_M^0, C_A^0 and C_L^0 is derived. For example, *for m = 1, n = 2* and $C_A^0 = 2C_M^0$, it is obtained:

$$\gamma^3 - 3\gamma^2 + 3\gamma + \frac{K_S \alpha_M \alpha_A^2}{2\left(C_M^0\right)^2} - 1 = 0$$

In the case of the stoichiometric ratio of the total concentrations of the solid phase components in the mixture, i.e. $nC_M^0 = mC_A^0$ (condition *B*), Eq. (18) takes the form:

$$\gamma = 1 - \frac{1}{C_M^0}\left(\frac{K_S^{cond} m^n}{n^n}\right)^{\frac{1}{m+n}} \tag{20}$$

Thus, if condition *B* is met, the degree of precipitation of the metal ion is calculated using a single Eq. (20). It should be mentioned that Eqs. (19 - 20) are applicable only when, from a thermodynamic point of view, it is impossible to convert the salt precipitate into a less soluble hydroxide $M(OH)_{n(S)}$, which usually takes place in the alkaline medium at high metal ion concentrations in solution.

In a series of papers (Povar and Spinu, 2014a; Povar and Spinu, 2016) the thermodynamic relationship between the expression for the Gibbs energy change of the summary process (2 - 4) ΔG_S^{tot}

and the residual concentrations C_M^r and C_A^r was revealed (Eq. 21):

$$\Delta G_S^{tot} = -mRT\ln\frac{C_M^r}{C_M^0} - nRT\ln\frac{C_A^r}{C_A^0}. \qquad (21)$$

Our thermodynamic analysis shows that the expression (21) is valid for the summary process (2 - 8), when the metal ion forms stable complexes with ligands present in the studied systems. Therefore, taking into account the above mentioned expressions between residual concentrations and the degree of precipitation, one can be concluded - the quantity γ has a rigorously thermodynamic meaning.

Table 1 gives the values for slightly soluble salts $M_mA_{n(S)}$ of different composition in case of condition *B* satisfactory, obtained from Eq. (20). The last equation also allows an explicit determination of the γ dependence on the stoichiometric $M_mA_{n(S)}$ salt composition. Thus, with the increase of the coefficient *n*, according to Eq. (20), the degree of precipitation will increase under the conditions of invariance of the other parameters. In some analogous considerations, the increase in *m* will result in the precipitation diminution. Analogously, the relationship for calculating the degree of precipitation of the metal ion in the form of slightly soluble hydroxide with the formation of the hydroxocomplexes Eq. (3) and stable complexes Eqs. (5 - 6), has been deduced

$$M(OH)_{n(S)} + nH^+ = M^{n+} + nH_2O, \qquad K_{Sh} = [M][H]^{-n},$$

$$\gamma = 1 - \frac{K_{Sh}\alpha_M[H]^n}{C_M^0} \qquad (22)$$

where α_M is described by the Eq. (10).

Previously (Povar and Spinu, 2014a), it was deduced the expression (23) for the Gibbs energy change of the summary process (2 - 8):

$$\Delta G_S^{sum} = -RT\ln K_S\alpha_M + RT\ln\left(C_M^0\right)[H]^{-n}. \qquad (23)$$

Using the Eqs. (21 - 22) and taking into account the relationship between C_M^0, C_M^r and γ it is easy to found the expression (24):

$$\Delta G_S^{tot} = -RT\ln\frac{C_M^r}{C_M^0} = -RT\ln(1-\gamma) \qquad (24)$$

For both Eqs. (21 - 23) or Eq. (24), the solid-phase is stable if $\Delta G_S^{tot} > 0$. Depending on the ΔG_S^{tot} value, precipitation conditions and the plenitude of the precipitate can be determined. The condition $\Delta G_S^{tot} = 0$ corresponds to the beginning of its dissolution and (or) sedimentation.

For metal ions, which form stable anionic soluble hydroxyl complexes, the function γ (pH) passes through the maximum as the precipitation degree decreases in the range of alkaline solutions.

3. Materials and methods

Industrial effluents

The chemically complex wastewater with pH 6.0 was obtained from electroplating units of the Tactical Missiles Corporation (Dubna, Russia). The composition of wastewater was determined using atomic absorption spectrometry (AAC-spectrometer, Russia). Measurements were done in triplicate and obtained values ± SD are given in Table 2.

Table 1. Equations for the degree of precipitation γ for different composition salts $M_mA_{n(S)}$, $nC_M^0 = mC_A^0$

m/n	*1*	*2*	*3*
1	$1-\left(K_S^{cond}\right)^{1/2}/C_M^0$	$1-\left(K_S^{cond}/4\right)^{1/3}/C_M^0$	$1-\left(K_S^{cond}/27\right)^{1/4}/C_M^0$
2	$1-\left(2K_S^{cond}\right)^{1/3}/C_M^0$	$1-\left(K_S^{cond}\right)^{1/4}/C_M^0$	$1-\left(8K_S^{cond}/27\right)^{1/5}/C_M^0$
3	$1-\left(3K_S^{cond}\right)^{1/4}/C_M^0$	$1-\left(9K_S^{cond}\right)^{1/5}/C_M^0$	$1-\left(K_S^{cond}\right)^{1/6}/C_M^0$

Table 2. Industrial effluent chemical composition at pH = 6 and MPC values

Metal	*Concentration in wastewater, mg/L*	*MPC for Russia, mg/L*	*MPC established by WHO, mg/L*
Al	0.2±0.006	0.2	0.2
Cr	0.1±0.0025	0.5 (Cr^{3+}) 0.05 (Cr^{6+})	0.05
Fe	3.0±0.075	0.3	0.2
Zn	0.2±0.006	1.0	3.0
Ba	0.1±0.005	0.7	0.7
Sr	0.5±0.015	7.0	-
SO_4^{2-}	10000±500	-	-
NH_4^+	3000±270	-	-

4. Results and discussions

Using atomic absorption spectrometry, six elements were determined in analysed wastewater. In Table 2, the chemical composition of the studied effluent along with values of maximum permissible concentration (MPC) for elements in effluent established in Russia (Anonymous, 2003) and by World Health Organization (Anonymous, 2011) are given. The concentrations of Al, Ba, Sr and Zn in the effluent are lower than MPC, while Cr and Fe concentrations exceed MPC values.

In order to determine the quantities of of soluble and insoluble firstly, the function ΔG_S^{tot} was computed. For this purpose, the Gibbs energy values for this complex process, where the reactions (2 - 8) proceed concomitantly, was calculated by the Eq. (21) for slightly soluble salts and Eq. (24) for slightly soluble hydroxides. Then the partial molar fractions (γ_i) of all the heavy metal species containing the metal ion were calculated taking into consideration the obvious relation:

$$\gamma + \gamma^{tot} = 1$$

where γ^{tot} is the sum of the partial molar fractions of all metal soluble species, calculated from the system of Eqs. (9 - 12), taking the restriction (13), by the well-known expressions (Butler and Cogley, 1998). The total (analytical) experimental concentrations of heavy metal, C_M^0, were taken from Table 2. All the equilibrium constants needed for calculation were taken from (Ball and Nordstrom, 2001).

4.1. Chemical species of iron in wastewater

The hydroxide of iron as ferrihydrite $Fe(OH)_{3(S)}$ is stable in the region of pH 4.4 – 12.0, ΔG_S^{tot}.> 0. The degree of precipitation has been calculated by the Eq. (22). At the experimental pH = 6 all iron precipitates. The complexes $FeSO_4^+$ and $Fe(SO_4)_2^+$ diminishes the stability of the solid phase in the region of pH 4.4 – 5.2, while in alkaline media the anionic hydroxocomplex $Fe(OH)_4^-$ competes with ferrihydrite (Fig. 1). Other iron hydroxomplexes, including polynuclear complexes $Fe_2(OH)_2^{4+}$ and $Fe_3(OH)_4^{5+}$ have a insignificant influence on the stability of solid phase (Smith et al., 2004).

4.2. Chemical species of chromium in wastewater

At the pH 6.0 all chromium (III) is present in wastewater in form of soluble complex $CrSO_4^+$. The pH of the beginning of precipitation of $Cr(OH)_{3(S)}$ is 7.4, while when pH is > 7.8 the solid phase is a predominant species. The hydroxocomplexes of *Cr(III)* practically do not contribute under studied conditions on the weakening of the thermodynamic stability of the chromium (III) hydroxide (Fig. 2).

4.3. Chemical species of aluminium in wastewater

The slightly soluble hydroxide of aluminium (as Gibbsite) is found to be thermodynamically stable in the region of pH 6.0 (experimental value) – 8.4 (Fig. 3). At the experimental pH 6 the following aluminium-containing species exist (in terms of their partial molar fractions): $\gamma\left(Al(OH)_2^+\right) = 0.04$, $\gamma\left(AlSO_4^+\right) = 0.12$, $\gamma\left(Al(SO_4)_2^-\right) = 0.41$, e.g. $\gamma^{tot} = 0.57$ and $\gamma\left(Al(OH)_{3(S)}\right) = 0.43$. Then the contribution of soluble species decreases with increasing pH. In the alkaline media the solid phase dissolves due to formation of thermodynamically more stable anionic hydroxocomplex $Al(OH)_4^-$ (Povar and Spinu, 2014b). This result correlates with the finding of authors that aluminum precipitated best at pH 7.0 with aluminum recovery 97.2% (Wei et al., 2005).

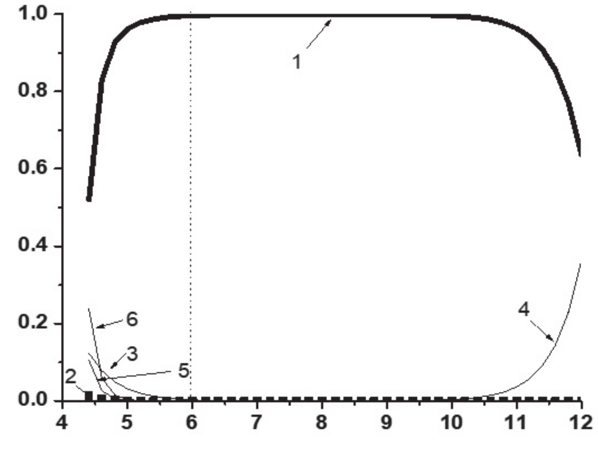

Fig. 1. Distribution curves of the soluble species and solid phase in the wastewater contaning 3 mg/L of iron and 10000 mg/L SO_4^{2-} : 1 – $Fe(OH)_{3(S)}$, 2 - $Fe(OH)^{2+}$, 3 - $Fe(OH)_2^+$, 4 - $Fe(OH)_4^-$, 5 - $FeSO_4^+$, 6 - $Fe(SO_4)_2^+$

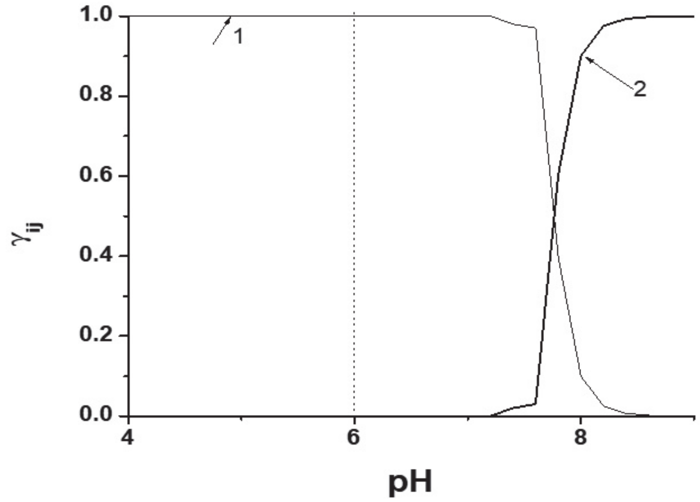

Fig. 2. Distribution curves of the soluble $CrSO_4^+$ chrome species (1) and insoluble chrome species $Cr(OH)_{3(S)}$ (2) in the wastewater contaning 0.1 mg/L of chrome and 10000 mg/L SO_4^{2-}

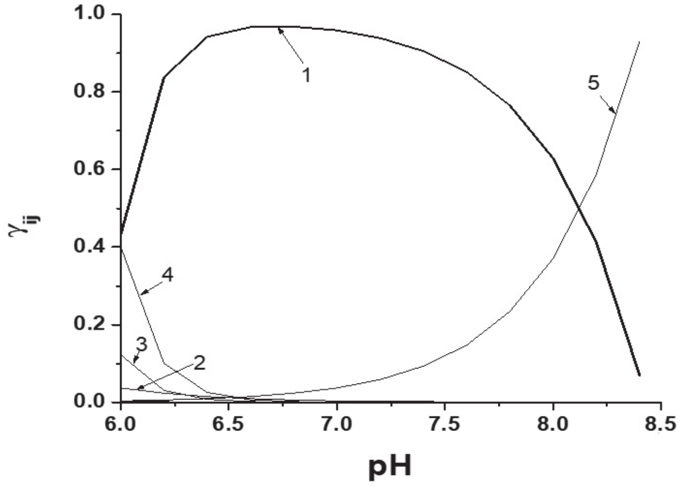

Fig. 3. Distribution curves of the soluble and insoluble aluminium species in the wastewater contaning 0.3 mg/L of chrome and 10000 mg/L SO_4^{2-} : 1 - $Al(OH)_{3(S)}$, 2 - $Al(OH)_2^+$, 3 - $AlSO_4^+$, 4 - $Al(SO_4)_2^+$, 5 - $Al(OH)_4^-$.

4.4. Chemical species of zinc in wastewater

Our thermodynamic analysis shows that for the wastewater of given composition within the pH range 2.0 – 9.0, under the excess of sulfate ions, the quantity ΔG_S^{tot}, calculated by Eq. (23), takes the negative values over all pH range. For this homogeneous solution, the partial molar fractions are computed by the usual equations used for the construction of distribution diagrams (Butler and Cogley, 1998). In this case, under conditions of only mononuclear complex species formation, the partial molar fraction values do not depend on the initial concentration of the components. Therefore, all the containing zinc species are soluble due to formation of stable complexes $ZnSO_4^0$ and $Zn(SO_4)_2^{2-}$, which prevent the formation of the precipitate of $Zn(OH)_{2(S)}$, γ^{tot} = 1 and γ = 0 (Fig. 4). At the experimental pH 6 there is a following distribution of soluble zinc-containing species (in terms of partial molar fraction): $\gamma(Zn^{2+})$=0.02, $\gamma(ZnSO_4)$ = 0.53 and $\gamma(Zn(SO_4)_2^{2-}$= 0.45. Zinc ammonia complexes practically do no influence the chemical equilibria due the formation of NH_4^+ stable ion and therefore instable complex formation under the studied conditions.

4.5. Chemical species of barium and strontium in wastewater

Due to the large amounts of sulfate ions in wastewater, all the barium and strontium precipitated in the form of $BaSO_{4(S)}$ and $SrSO_{4(S).}$, respectively. The Gibbs energy of the process (2 - 6), calculated by the Eq. (21), gives constant positive value over all the pH range. The quantity γ has been calculated from the formula taken from the Table 1. For all the pH range, γ = 1 and γ^{tot} = 0.

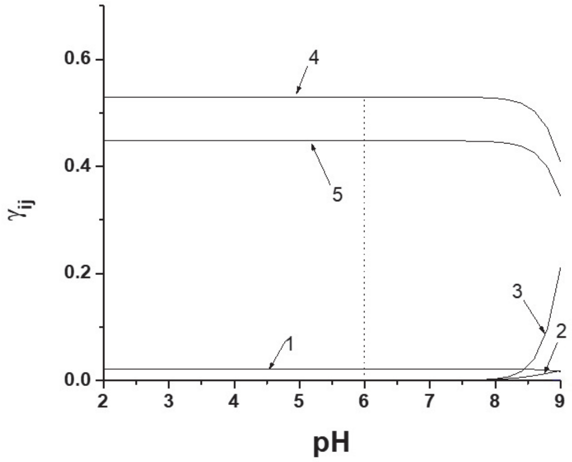

Fig. 4. Diagram of distribution of the soluble zinc species in the wastewater contaning 0.3 mg/L of chrome and 10000 mg/L SO_4^{2-} : 1 - Zn^{2+}, 2 - $ZnOH^+$, 3 - $Zn(OH)_2^0$, 4 - $ZnSO_4^0$, 5 - $Zn(SO_4)_2^{2-}$

5. Conclusions

The expressions of the dependence of the precipitation degree of the metal ion in the form of slightly soluble salts and hydroxides on the initial concentrations of the components and solution pH, including complexing agents have been deduced. The possibility of forming stable complexes between the metal ion and complexing agents in galvanic wastewater is taking into account. The thermodynamic meaning of the degree of precipitation for slightly soluble hydroxides and salts has been revealed.

The degree of precipitation and distribution of chemical species of metal ions (*Al, Cr, Fe, Zn, Sr* and *Ba*) in the complex industrial effluents of an engineering company (electroplating units of the Tactical Missiles Corporation, Dubna, Russia), under large amounts of sulfate ions, were analyzed. It has been shown that pH values, which ensure minimum solubility of metal hydroxides are very different from each other and are within the pH range from 5 to 11, which in principle does not allow optimizing the process of precipitation of hydroxides at simultaneous presence of various metals in solution. At pH 6.5-8.5, allowed for discharge of sewage into water bodies, only iron hydroxide can be precipitated to the maximum extent.

The efficiency of the method of precipitation depends on the chemical composition of wastewater that contains complexing agents, capable to bind the heavy metals in thermodynamically stable complexes. Additionally, it is necessary to take into account the co-precipitation and competitive processes. The iron hydroxide precipitated can act as sorbent and remove other heavy metals present in wastewater.

Acknowledgments

Authors are thankful for the financial support accorded by the National Research Council of Italy and Academy of Sciences of Moldova of their project “Thermodynamic optimization of innovative processes developed to valorize industrial wastes containing valuable metals” during the 2018-2019 years.

References

Aljerf L., (2018), High-efficiency extraction of bromocresol purple dye and heavy metals as chromium from industrial effluent by adsorption onto a modified surface of zeolite: kinetics and equilibrium study, *Journal of Environmental Management*, **225**, 120-132.

Ayangbenro A., Babalola O., (2017), A new strategy for heavy metal polluted environments: a review of microbial biosorbents, *International Journal of Environmental Research and Public Health,* **14**, 94.

Ball J., Nordstrom D., (2001), *User's manual for WATEQ4F, with revised thermodynamic data base and test cases for calculating speciation of major, trace, and redox elements in natural waters*, Menlo Park, California.

Butler J., Cogley D., (1998), *Ionic Equilibrium: Solubility and pH Calculations*, John Wiley and Sons, New York.

Duca G., Covaliova O., (2017), *Intensified Water Treatment Methods*, 10th Int. Conf. on Management Science and Engineering Management, Springer, Singapore, 1041-1051.

Fu F., Wang Q., (2011), Removal of heavy metal ions from wastewaters: a review, *Journal of Environmental Management,* **92**, 407-418.

Gaikwad R.W., Gupta D.V., (2008), Review on removal of heavy metals from acid mine drainage, *Applied Ecology and Environmental Research*, **6**, 81-98.

Gogina E., Makisha N., (2014), Information technologies in view of complex solution of waste water problems, *Applied Mechanics and Materials*, **587**, 636-639.

Gunatilake S., (2015), Methods of removing heavy metals from industrial wastewater, *Journal of Multidisciplinary Engineering Science Studies*, **1**, 12-18.

Kanamarlapudi S.L.R.K., Chintalpudi V.K., Muddada S., (2018), Application of biosorption for removal of heavy metals from wastewater, *Biosorption*, **18**, 69.

Khalturina T.I., Bobric A.G., (2018), Intensification of purification of sewage water-generation manufacturing enterprises of metallurgy enterprises and machine-building complex containing ions of chrome, copper, nickel and zinc, *Urban Construction and Architecture*, **8**, 27-34.

Luptáková A., Ubaldini S., Mačingová E., Kotuličová I., (2012), Study of precipitating methods for elimination of heavy metals from acid mine drainage, *Nova Biotechnologica et Chimica*, **11**, 133-138.

Malschi D., Muntean L., Oprea I., Roba C., Popiţa G., Ştefănescu L., Rinba E., (2018), Research on wastewaters bioremediation with aquatic species for constructed wetlands, *Environmental Engineering & Management Journal*, **17**, 1753-1764.

Makisha N., Yunchina M., (2017), *Methods and Solutions for Galvanic Waste Water Treatment*, MATEC Web of Conferences, **106**, 07016.

Marzougui Z., Damak M., Elleuch B., Elaissari A., (2017), *Occurrence and Enhanced Removal of Heavy Metals in Industrial Wastewater Treatment Plant Using Coagulation-Flocculation Process*, Euro-Mediterranean Conf. for Environmental Integration, Springer, Cham, 535-538.

Nancucheo I., Bitencourt J.A., Sahoo P.K., Alves J.O., Siqueira J.O., Oliveira G., (2017), Recent developments for remediating acidic mine waters using sulfidogenic bacteria, *BioMed Research International*, **2017**, 1-17.

Povar I., (1994), Thermodynamic calculation of pH of minimum solubility of poorly soluble oxides and hydroxides under polynuclear hydrolysis of metal ions, (In Russian), *Ukrainian Chemistry Journal,* **60**, 371-376.

Povar I., Spinu O., (2014a), *The Thermodynamics of Complex Chemical Equilibria in Multicomponent Heterogeneous Systems* (in Romanian), Printing House ASM, Chisinau, Republic of Moldavia.

Povar I., Spinu O., (2014b), The role of hydroxy aluminium sulfate minerals in controlling Al^{3+} concentration and speciation in acidic soils, *Open Chemistry*, **12**, 877-885.

Povar I., Spinu O., (2015), Application of the buffer theory for evaluating attenuation and natural remediation of ionic pollutants in aquatic ecosystems, *Ecological Processes,* **4**, 17.

Povar I., Spinu O., (2016), Correlation between global thermodynamic functions and experimental data in multicomponent heterogeneous systems, *Canadian Journal of Chemistry*, **94**, 113-119.

Smith A.A., Coxall R.A., Harrison A., Helliwell M., Parsons S., Winpenny R.E., (2004), High-temperature synthesis of polynuclear iron oxo-hydroxy complexes, *Polyhedron*, **23**, 1557-1565.

Sofińska-Chmiel W., Kołodyńska D., (2018), Application of ion exchangers for the purification of galvanic wastewater from heavy metals, *Separation Science and Technology*, **53**, 1097-1106.

Ubaldini S., Luptakova A., Fornari P., Yoplac E., (2013), *Application of Innovative Remediation Processes to Mining Effluents Contaminated by Heavy Metals*, Proc. 16th Int. Conf. on Heavy Metals in the Environment, **1**, 25001.

Wei X., Viadero Jr R.C., Buzby K.M., (2005), Recovery of iron and aluminum from acid mine drainage by selective precipitation, *Environmental Engineering Science*, **22**, 745-755.

Wu P., Li K., Xu L., Peng Q., Huang Z., Zhang J., Shen Y., (2018), Simultaneous treatment of sulfate wastewater and domestic sewage with micro-aeration, *Environmental Engineering and Management Journal*, **17** , 2561-2568.

Zinicovscaia I., Duca G., Cepoi L., Chiriac T., Rudi L., Mitina T., Frontasyeva M., Pavlov S., Gundorina S., (2015), Biotechnology of metal removal from industrial wastewater: zinc case study, *CLEAN–Soil, Air, Water,* **43**, 112-117.

Environmental Engineering and Management Journal

February 2020, Vol. 19, No. 2, 289-301
http://www.eemj.icpm.tuiasi.ro/; http://www.eemj.eu

"Gheorghe Asachi" Technical University of Iasi, Romania

REMOVAL OF METHYL ORANGE AND CADMIUM FROM SOLUTION USING MODIFIED ACTIVATED CHARCOAL

Nicoleta Popa[1,2], Maria Visa[1]*

[1] *Transilvania University of Brasov, R&D Centre of Renewable Energy Systems and Recycling,*
Eroilor 29, 500036 Brasov, Romania
[1,2] *Department of Forest District Teliu, National Directorate of Forests Romsilva, Romania*

Abstract

In this work, the removal of methyl orange (MO) and Cd^{2+} by simultaneous adsorption on adsorbent obtained from modified charcoal (BCBH) coated with TiO_2 has been studied. The synthesized materials obtained from wood branches were characterized using atomic force microscopy (AFM) for the roughness and SEM to determine the morphology of the surface. EDX spectroscopy indicates the presence of C, N, O, Na, K, P and Ti on the surface of the adsorbent materials. The micro-porosity and BET specific surface were carried out by N_2 adsorption. Additionally, the FT-IR spectroscopy illustrates that hydroxyl, carboxyl groups developed on the adsorbent surface are able to adsorb MO and Cd^{2+}. The effect of the experimental conditions on the adsorption behavior was studied by varying the contact time, amount of adsorbent and initial MO concentration. The adsorption data were modeled using the Langmuir and Freundlich adsorption isotherms equations. The kinetic studies showed that the adsorption followed pseudo-second-order kinetic model. The maximum adsorption capacity ($q_{\max}$) was found to be 5.06 mg/g MO for the adsorbent in hydrothermal activated with NaOH. In case of adsorption from bicomponent systems under mechanical stirring the $q_{\max}$ for MO was 5.1 mg/g and for Cd^{2+} cations was 294.11 mg/g for BCBHD1 adsorbent.

Key words: adsorption, cadmium, hydrothermal charcoal, methyl-orange

Received: January, 2019; Revised final: January, 2020; Accepted: January, 2020; Published in final edited form: February, 2020

1. Introduction

The generation and disposal of huge amounts of the industrial waste and other pollutants have heavily contaminated our environment and waters. The synthetic dyes and heavy metals are becoming increasingly prevalent as the most dangerous pollutants in soil and in surface waters. Every year $7*10^5$ tones and over 10,000 different types of dyes and pigments are produced in the World (Kolodynska et al., 2017) and are presented in the effluents of the textile, leather, paper and dye industries. The recent estimates have indicated that, approximately 12% of synthetic textile dyes used each year is lost during manufacturing and processing operation and major amounts of these dyes go in the environment through effluents (Hema and Arivoli, 2007; Pattnaik and Dangayach, 2019). They are causing great concern worldwide due to their toxicity to many life forms. Even if the concentration of the dyes is lower than 1 mg/L this can give undesirable color to water surface. The health effects of the methyl orange are: irritation in case of skin, of eye by contact, of ingestion and of inhalation. Cadmium is a heavy metal and toxic environmental pollutant, classified as a human carcinogen which is mainly coming from electroplating and battery industries.

Many processes have been applied to remove the harmful pollutants, including adsorption (Visa and Duta, 2008; Visa et al., 2011), biosorption (Guerrero-Coronilla et al., 2019; Kumar and Ahmad, 2011; Pholosi et al., 2013), electrochemical coagulation,

---

* Author to whom all correspondence should be addressed: e-mail: maria.visa@unitbv.ro; Phone: +40-729109355

photodegradation (Matos et al., 2017), membrane filtration (Yang and Garrahan, 2005), electro flocculation and ozonation (Ciardelli and Ranieri, 2001), photo-Fenton (Visa and Duta, 2013), and simultaneous methods (Visa and Nacu, 2011). The adsorption method is intensely used for removing soluble and insoluble pollutants from surface water and from wastewater without the generation of hazardous by-products (Popa and Visa, 2017) being inexpensive, with simple equipment, easy to operate and with highly effective treatment.

The adsorbents materials produced from biomass of the forest, agricultural by-products have been used, such as: raw wood (Yagmur et al., 2013), pine biomass (Ofomaja et al., 2015), waste from grape industrial processing (Sayğili et al., 2015), wheat straw (Robinson et al., 2002; Zhang et al., 2014;), rice husk (Chakraborty et al., 2011), orange peel (Sivaraj et al., 2001), oak leaves, palm leafs (El-Shafey et al., 2016), Korean cabbage waste (Sewu et al., 2017). The biocharcoal obtained from them follows to be chemical or physical activated. Environmentally friendly utilization of agricultural by-products/waste materials for removal the pollutants from the wastewater is an opportunity to solve a waste by other waste. The preparation of the charcoal from tree branches (forest waste/biomass) using the built “Bocsa” may appear a valuable path. Because, its burning is slow, takes approximately 2-3 weeks, depending on the size of the Bocsa. The oxygen intake is controlled therefore; combustion should be slow which may offer a good carbonization of this biomass.

The aim of this work is to obtain the mesoporous charcoal by hydrothermal method modified in alkali environmental and impregnated with TiO_2 (Degussa P25), used as an adsorbent for simultaneous removal of methyl orange (MO) dye and cadmium cations (Cd^{2+}) from aqueous solution.

2. Experimental

2.1. Preparation of materials and substrate

The precursor material was the tree branches collected from deciduous forest of Brasov, Romania. The branches were carbonized with an insufficient amount of air up to 400-550 °C and then the channel was blocked and left few days to cool. The process of obtaining biocharcoal (BC) from wood waste can be divided into three steps:

1. Drying: in this phase water is eliminated from branches, virtually drying occurs between 0-110°C;
2. Dry distillation: occurs between 150- 350°C. At 180°C hemicelluloses and 1/3 of cellulose usually begin decomposition, and the wood resistance drops significantly when the temperature reaches 260°C;
3. Charcoal formation: the beginning of this stage is at 350 - 400°C, ending at 400 - 550°C, depending on the production conditions. This stage is characterized by removing large amounts of incondensable gases resulting from breakdown of cellulose and lignin (Li et al., 2001; Suhas et al., 2016; Yang et al., 2007). This biocharcoal was activated with NaOH in hydrothermal conditions, at 100 °C, stirred 24 h and, then was washed with ultra-distillate water and dried at 105 - 115°C till constant mass. This adsorbent material was noted (BCBH).

2.2. Modification of BCBH with TiO_2

To improve the adsorbent and photocatalytic properties of the BCBH substrate, three composites noted as BCBHD1, BCBHD2 and BCBHD3 were developed by adding the TiO_2 (Degussa P25, 80% anatase and 20% rutile) to BCBH substrate in ratio 1:1; 1:2; 1:3 under ultrasounds for 10 h.

These composites were tested as adsorbents for removal of the MO and Cd^{2+} cations from aqueous solution. It is expected that, due to the synergistic effect of the exposed functional groups (-OH) and TiO_2 on the charcoal surface, the new composites will exhibit a good adsorption and photocatalytic ability in the wastewater treatment process.

2.3. Materials characterization

The surface morphology of the substrates was observed using Scanning Electron Microscopy (SEM, model S-3400N-Hitachi) at 20 -30 kV. The surface elemental composition was evaluated using Energy Dispersive X-ray (EDX) measurements. The surface roughness and macro-pores size distribution was evaluated using AFM (Ntegra Spectra, NT-MDT model BL222RNTE). The FT-IR spectra of the samples were recorded with Spectrum BX Perkin Elmer BX II 75548, λ=400 – 4000 nm to analyze the surface functional groups. The XRD patterns of the samples were recorded using an X-ray diffractometer (XRD Bruker D8 Discover Diffractometer) operating at 40 kW and 20 mA, 2θ range from 10 -70° and scan speed 2s/step).

2.4. Adsorption experiments

2.4.1. Experimental conditions

The pollutant systems were synthetically prepared using ultrapure water with resistivity of 18.23 MΩ cm^{-1}, $CdCl_2 \cdot 2.5H_2O$ (Scharlau Chemie S.A., c<98 %) and MO($C_{14}H_{14}N_3NaO_3S$) (Fluka AG., with molecular weight (327.33 g/mol). The experiments were done using solutions in the concentrations of C_{Cd}= 0.01 N, C_{MO}= 0.03125 mM. A series of the experiments on adsorption were done: - adsorption under mechanical stirring with: (a) MO and (b) MO+Cd^{2+} on BCBH, BCBHD1, BCBHD2 and BCBHD3. In order to demonstrate the adsorbent capacity of the adsorbents, the methodology followed the steps below: adsorption parameters determination - *contact time* (t), *ratio of solution volume, adsorbent dose ($V_{sol.}/m_s$), initial concentration of pollutants;* kinetic models investigation - pseudo-first-order, pseudo second-order, intra particle diffusion, to establish the adsorption mechanisms; the adsorption isotherms Langmuir and Freundlich were investigated.

2.4.2. Effect of contact time and adsorbent dose on adsorption efficiency

In order to optimize the contact time, 0.1 g of the adsorbent at the temperature range 20 - 23 °C, were dispersed in MO and MO+Cd^{2+} solutions with C_{MO}= 0.03125 mM and C_{Cd}=0.01N, initial concentration. The suspension was stirred at 100 rpm. for 10, 20, 30, 45, 60, 90, 120, 150, 180 min, then the substrate was removed by filtration on 0.45 μm filter. After adsorption, the residual dye concentration (MO) in supernatant solution was analyzed by UV-VIS spectrometry (Perkin Elmer Lambda 25) on the calibration curve registered at the maximum absorption peak of MO (λ=464nm). The Cd^{2+} cations concentration was analyzed by AAS (Analytic Jena, ZEEnit 700) at λ_{Cd} = 228.8 nm. The losses due to adsorption onto the flask walls and filter paper were negligible. The removal efficiency of the pollutants, [%], were calculated by Eq. (1):

$$\eta = (c_0 - c_t) * 100 / c_0 \ [\%] \qquad (1)$$

where: c_0 is the initial concentration (mg/L); c_t is the concentration at moment *t* (min).

The amount of MO or Cd^{2+} cations adsorbed at any time, q_t (mg.g $^{-1}$), was calculated by Eq. (2):

$$q_t = (c_0 - c_t) \times V_{sol} / m_s \qquad (2)$$

The results of pollutants, MO and Cd^{2+} removal from solutions on substrates are presented in Fig. 1.

Fig. 1 shows a rapid adsorption of MO dye at the initial stages of the adsorption and the equilibrium was attained within 30-45 min. The adsorption efficiency of the MO on each substrate in present of cadmium cations is higher with 10-20 % than in absences of Cd^{2+} cations. Such uptake indicates a high degree of affinity towards the MO molecules via chemisorption or more active sites are developed in present of TiO_2.

The best performance was obtained for substrates BCBHD1 and BCBHD2, which showed adsorption of Cd^{2+} cations than 69.62 % and 60.42 % respectively at 60 min. comparing with 13.82 % of the BCBHD3. In this case a higher amount of TiO_2 added to charcoal would favor photocatalyst over adsorption.

At optimal contact time, 45 min, the percentages removal of MO and of the Cd^{2+} cations increased with the increase in dose of the adsorbent (Fig. 2). This may be due to the increase in availability of surface-active sites resulting from increased dose and conglomeration of the adsorbent particles.

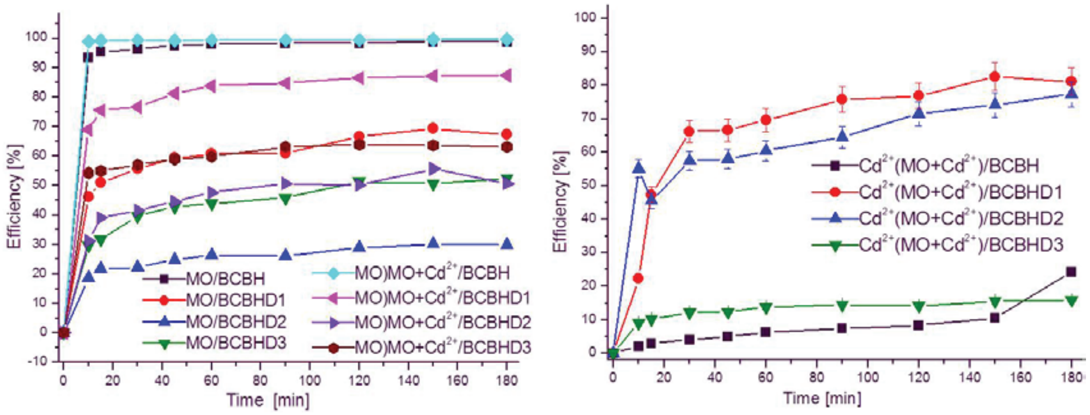

Fig. 1. Removal efficiency vs. time of MO dye, MO dye in present of Cd^{2+} cations; and of Cd^{2+} cations from di-solute aqueous solutions

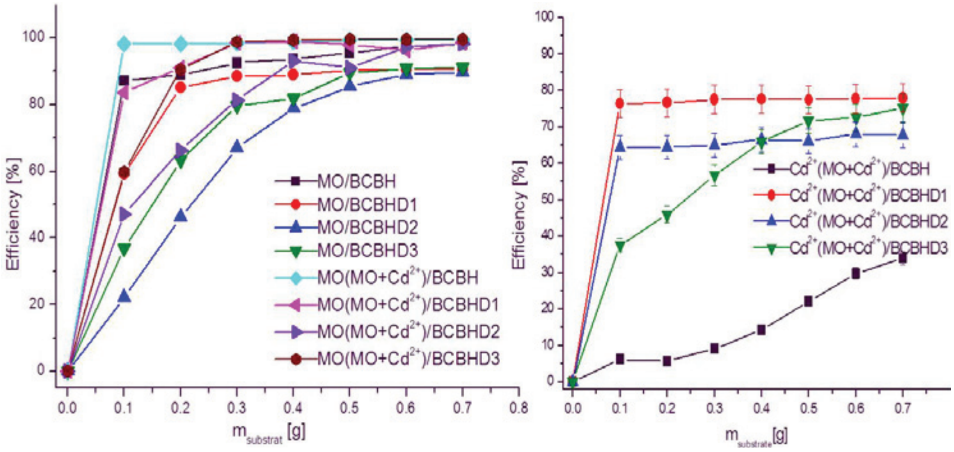

Fig. 2. Adsorption efficiency of MO and of Cd^{2+} cations on different amounts of adsorbent

As it can be seen in Fig. 3.b, at the equal concentrations, q_t adsorbate/g adsorbent changed the hierarchy of adsorbed species, while that of adsorbent maintain the same trend. This aspect shows that a higher number of Cd^{2+} cations are adsorbed by comparing to the number of MO dye, due to the dimensional reasons.

3. Results and discussions

3.1. Crystalline structure of substrate

The phase's composition of BCBH, BCBHD1, BCBHD2 and BCBHD3 were evaluated with XRD analysis and the XRD patterns are presents in Fig. 4.

The modified charcoal (BCBHD1; BCBHD2; BCBHD3) composition is confirmed by the XRD analysis and the results are presented in Table 1. The predominant crystalline components of BCBH are: (SiO_2), Nitratine, syn($NaNO_3$) and $Mg_3Fe_2(SO_3)6H_2O$ while anatase and rutile are prevalence in substrates BCBHD1, BCBHD2 and BCBHD3. The XRD data show that the new modified biocharcoal has well embedded titanium oxide with crystallite sizes from 145 to 277.8 Å. The crystallites size, τ, was calculated using the Scherrer relationship (Eq. 3).

$$\tau = K\lambda / \beta \cos\theta \tag{3}$$

where: *K* is the shape factor with a typical value 0.94; λ is the X-ray wavelength (1.541 Å); *β*-is the line broadening at half the maximum intensity (of a peak); *θ*- is the diffraction angle.

Also, traces of K, Na and P species were identified as impurities of the BCBHD substrate.

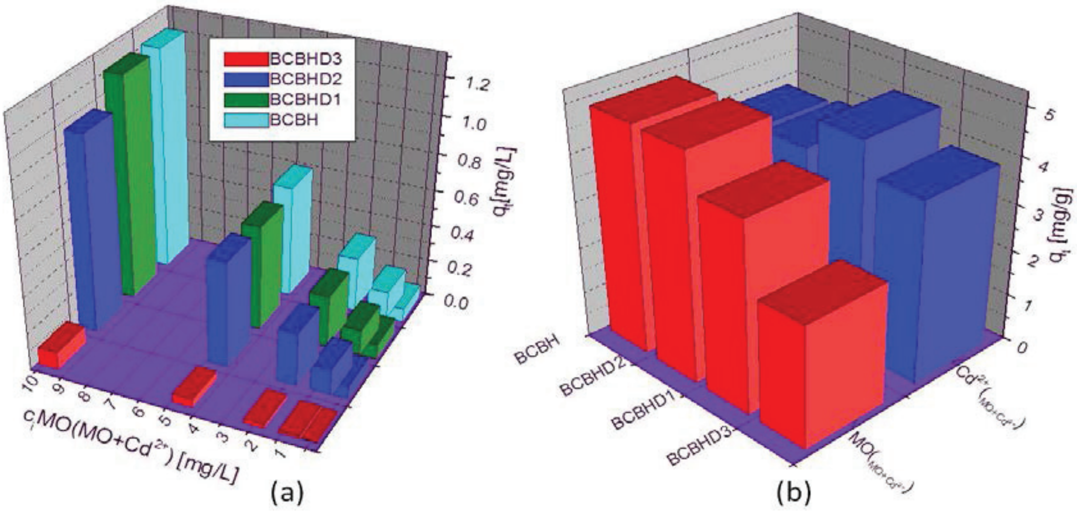

Fig. 3. Adsorption capacity (a); at different concentrations; (b) for MO and Cd^{2+} cations at the equal concentrations (10 mg/L)

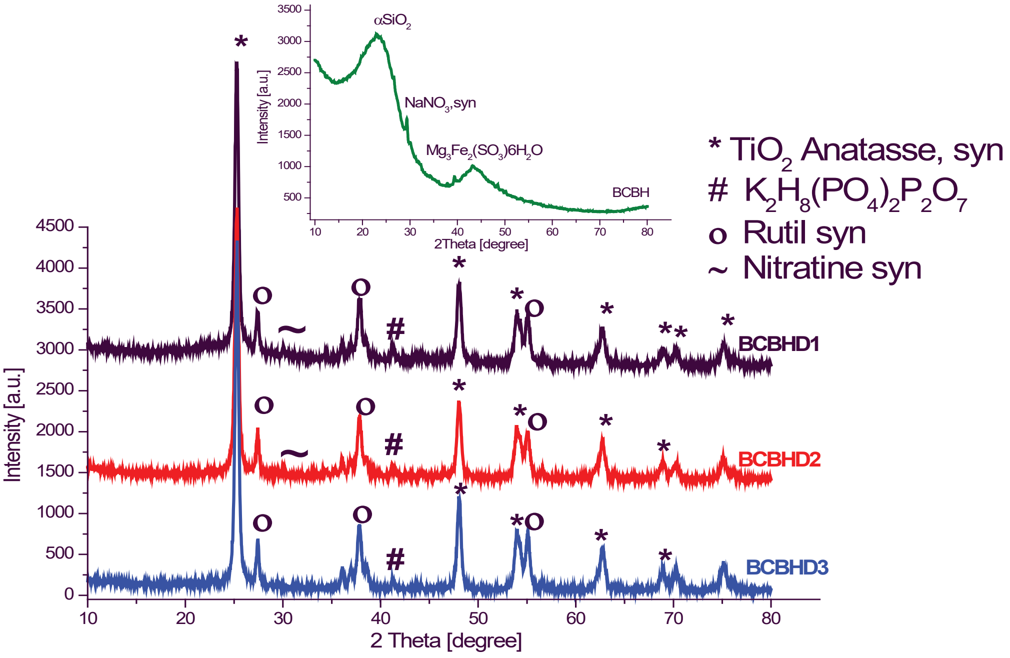

Fig. 4. XRD patterns of the samples: (a) BCBH; (b) BCBHD1; BCBHD2; BCBHD3

Table 1. The composition of the crystalline phases

2Θ	*COD/PDF*	*Crystalline phases*	*Structures of the crystallite*	*Crystallite size (Å)*	*Crystallinity [%]*
		BCBH			
23.26	00-028-0790	αSiO_2 Silicon Oxide	triclinic	343.2	51.60
29.36	00-022-0841	$Na(NO_3)$ Nitratine, syn	rombo.H.axe	426.6	
43.36	01-088-0537	$Mg_3Fe_2(SO_3)6(H_2O)$	triclinic	271.6	
		BCBHD			
25.309	00-064-0863	TiO_2 Anatase, nano	tetragonal	211.7	BCBHD1 73.6 BCBHD2: 90.9 BCBHD3: 81.6
29.383	01-070-1518	$NaNO_3$ Nitratine, syn	rhombo.H	604.2	
36.996	00-064-0863	TiO_2 Anatase, nano	tetragonal	212.9	
48.032	00-004-0477	TiO_2 Anatase, syn	tetragonal	184.9	
53.985	00-064-0863	TiO_2 Anatase, nano	tetragonal	145	
62.739	00-064-0863	TiO_2 Anatase, nano	tetragonal	165.5	
56.683	00-004-0478	TiO_2 Rutile	monoclinic	252.3	
	00-025-0638	TiO_2 Rutile	monoclinic	276.1	
41.207	00-021-0385	$K_2H_8(PO_4)_2P_2O_7$	orthorhombic	277.8	

3.2. Morphology and surface tension of the substrates

The AFM images (Figs. 5a, b, c) and pore size distributions (Fig. 5d) show the different granular shape in the size range of 0 -200 nm, also give information about the distribution of TiO_2 on charcoal that is very important in adsorption process.

The AFM images give information about the rough surface with larger pores/voids heterogeneously distributed that is confirmed by the pores/voids distribution curve in Fig. 5 (d). Thus, low roughness value (9.621 nm; 11.332 nm) of the BCBHD2 and BCBHD3 displays a higher number of aggregates differently in shaped (almost round) and stable.

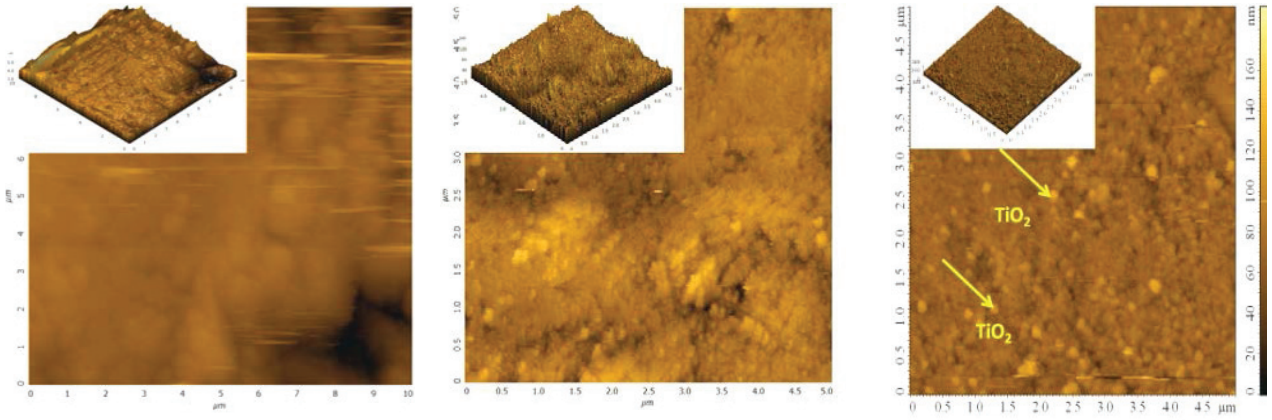

(a) Average roughness:173.927nm

(b) Average roughness: 9.621 nm

(c) Average roughness:11.332 nm

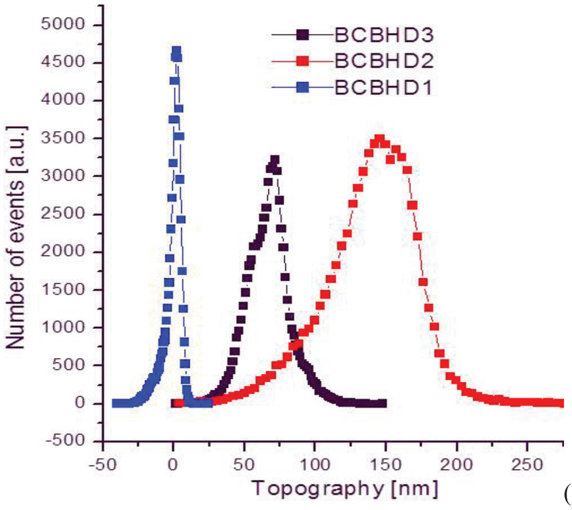

(d)

Fig. 5. The AFM topography (a) BCBHD1 (b) BCBHD2, (c) BCBHD3; (d) Pore histogram

The porosity parameters of these adsorbents such as S_{BET}, pore volume and micropores volume are presented in Table 2. The surface increases after hydrothermal treatment with NaOH and decreases by adding TiO_2 with S_{BET} of 50 m^2/g.

Table 2. The S_{BET} and pores structures

Sample	***S_{BET} [m^2/g]***	***V_t [cm^3/g]***	***$V_{micro\ pores}$ [cm^3/g]***
BCBH	387.882	0.217	0.126
BCBHD1	241.388	0.271	0.062
BCBHD2	128.405	0.243	0.049
BCBHD3	74.267	0.228	0.018

The morphology/topography of the substrates was obtained from the SEM micrographs (Fig. 6a). The SEM images of the surface and the surface composition of the hydrothermal charcoal (BCBH) and of BCBHD with Degussa P25 are shown in Figs. 6a, a`, b, b`, c, c`, d, d`. Many honeycomb- shape gaps with diameters over 4.0 μm appear on the surface of BCBH. These irregular gaps are surrounded by contracted twisted walls. The walls are thick and smooth without any structure. Based on the SEM images, when the charcoal particles are in contact with NaOH, a thin film of NaOH should cover their surface and the interior of chars should be covered with Na^+ and HO^- that are displayed in XRD spectra. However, the watering of NaOH to the gap interior favors the micropore development that results in an increase of the micropore number (Ho et al., 2000; Tseng and Tseng, 2005). The cavities are very irregular indicating that, during activation, the alkaline reagent (NaOH) caused a higher porosity in the adsorbent materials. The high density of the precursor has an importance contribution to enhance of amount of the carbon from 52.47 to 100 wt.% in BCBH or from 15.12 to 100 wt.% in substrates with TiO_2, respectively.

The SEM images confirm that the charcoal particles were cracked and micro-restructuring occurred with significant modification of the surface aspect, as results of/imbedded of nano-sized TiO_2 in the micro BCBH grains. The hydrothermal process promotes the surface interactions, including dissolution, re-crystallization, re-precipitation of the charcoal raw components and new components are developed.

From SEM, AFM and BET isotherm resulted that MBCBH is characterized by the high porosity, high BET surface, high micro-pores volume, and all these explain the best adsorptive capacity of the BCBH substrate. The titanium oxide added at BCBH substrate favors the adsorption of Cd^{2+} or another species of cadmium which exist in system.

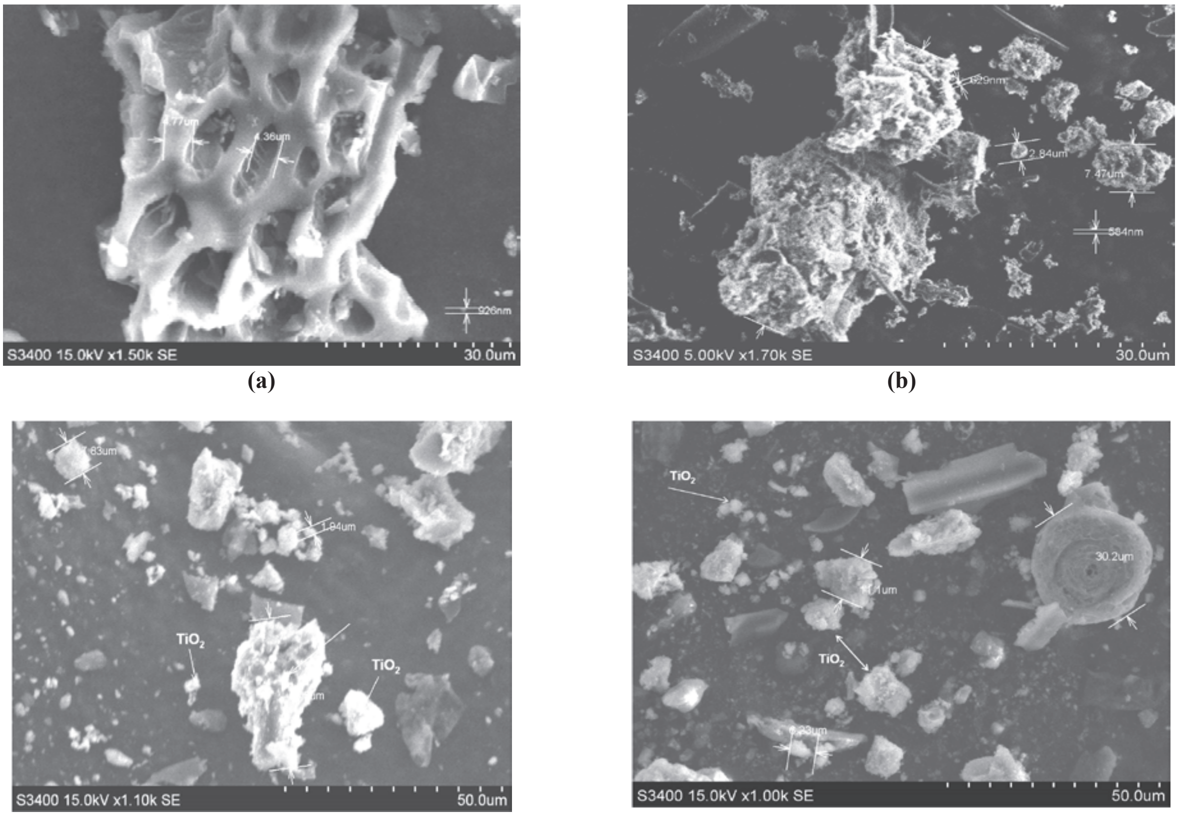

(a) (b)

(c) (d)

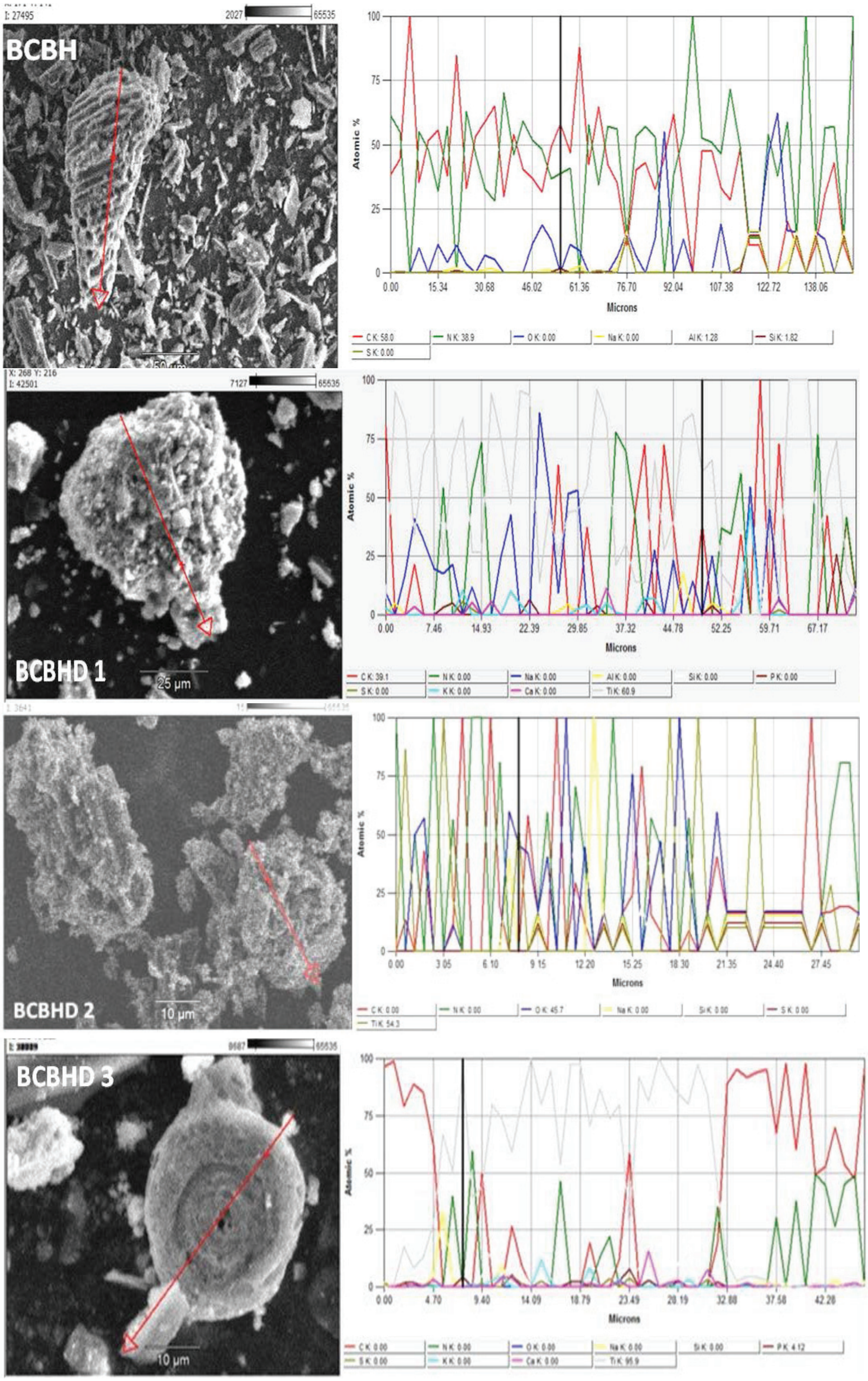

C:52.47-100Wt.%
N:52-100wt%
and:
O; Na; Al; Si.

(a`)

C:32.47-100Wt.%
N:52–75wt%
Ti:16.8– 98.2wt%
and:
O; Na; Al; Si.

(b`)

C:30.25-100Wt.%
N:52-100wt% Ti:22.4–100Wt%
and:
O; Na; Al; Si

(c`)

C:15.12-100Wt.%
N:32-53.3wt%
Ti:70.4–100Wt%
and:
O; Na; Al; Si.

(d`)

Fig. 6. (a) SEM micrographs of BCBH; (b) SEM micrographs of BCBHD1; (c) SEM micrographs of BCBHD2; (d) SEM micrographs of BCBHD3; (a`) EDX image of BCBH on the agglomerate; (b`), (c`), (d`) EDX images of BCBHD1, BCBHD2, BCBHD3 on the agglomerate with TiO_2

3.3. FT-IR analysis of the adsorbent substrates

The infrared spectrum of the adsorbent materials BCBHD1, BCBHD2 and BCBHD3 was performed to identify chemical bounds as well as functional groups. Each sample was scanned from 400 to 4000 cm^{-1} and the peaks were examined (Fig.7). Strong absorption in the frequency region of 410-1000 cm^{-1} corresponds to Ti–O–Ti bonding. The mixture of polymorphic phases of anatase and rutile was observed from 400–820 cm^{-1} in the composites. The absorption peaks at 595 and 600 cm^{-1} shows the rutile phase on surface of the composites. The characteristic peaks at 1450 and 1630 cm^{-1} revealed the existence of ketone or aldehydes carbonyl stretching, while latter conjugated with aromatic rings. The peaks around 2355cm^{-1} were assigned to the asymmetric or symmetric deformation of C–H in methyl and methylene (Li et al., 2001; Yang et al., 2007)

Adsorption as surface process is influenced not only on the crystallinity and morphology, but also by surface charge. Surface charge depends on the pH of the solution and must be discussed based on the value(s) of the point of zero charge (PZC). The pH $_{PZC}$ of BCBH and BCBHD substrates depends on the alkali-acid character of surface hydroxyl, carboxyl lactone groups.

The pH in the aqueous solution is lower than pH_{PZC}, the surface is positively charged, and when pH in the aqueous solution is higher than pH_{PZC}, the surface is negatively charged. The calculated pH_{PZC} for BCBH, BCBHD1, BCBHD2 and BCBHD3 are from 7.77 to 8.96, 9.67, 9.97 that explains well the high adsorption efficiency of MO and of cadmium on new substrates. The working pH is over 7.8 value and as results the adsorbent surface is negative and Cd^{2+} cations and other hydrated species or precipitate can be adsorbed.

4. Adsorption kinetics modeling

The kinetic data of the adsorption studies were processed to understand the adsorption mechanism of the MO on substrates with TiO_2 embedded onto hydrothermal charcoal and the adsorption mechanism of MO with Cd^{2+} cations. In the present study, the applicability of the pseudo-first-order (Eq.4), pseudo-second-order and intraparticle diffusion models (Eqs. 5, 6 and 7) were tested. These models have been fitted with experimental data at various physico-chemical conditions for which all fitting plots are not presented here. The plot t/qt versus t, should give a straight line with higher linear correlation coefficients if pseudo-second-order kinetics is applicable, and qe, k_2 can be determined from the slope and intercept, Fig. 8.

The pseudo-first order equation of Lagergren is generally expressed as follows (Mahmood et al., 2017) Eq. (4)

$$log(q_e - q_t) = log(q_e) - K_L t / 2.303 \qquad (4)$$

where: K_L (min^{-1}) is the Lagergren constant (the adsorption rate constant); q_t and respectively q_e ($mg \cdot g^{-1}$) are the amount of adsorbed pollutants by adsorbent at time *t* (min) and respectively at the equilibrium.

The second kinetic model applied was the pseudo-second order. The rate expression is based on the adsorption capacity of the solid phases, which has been investigated using the kinetics of the chemisorption processes. It is calculated by means of the equation developed by Ho and Mc Kay, Eq. (5), (Ho and Mc-Kay, 1998; Mahmoud et al., 2016;).

$$t / q_t = 1 / k_2 q_e^2 + t / q_e \qquad (5)$$

where: k_2 is the equilibrium rate constant for the pseudo-second order adsorption (g mg^{-1} min^{-1}). The adsorption capacity at equilibrium (q_e) and adsorption rate constant (k_2) are determined from the slope and intercept of linear plot of t/q_t against *t* for Eq. (5) This model is based on the assumption that the rate limiting step may be a chemisorption involving the valence forces through sharing or exchange of electrons between the adsorbent and the adsorbate (Duman et al., 2009). The pseudo-second order kinetic (Eq. 5) is the model which best describes the adsorption of the pollutants on the new adsorbent materials.

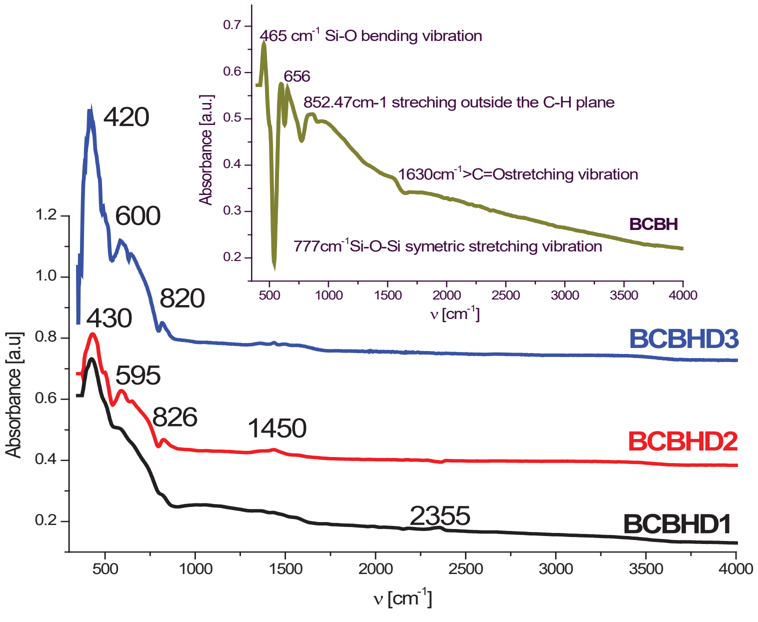

Fig. 7. FT-IR spectrum of substrates

Intra-particle diffusion model developed by Weber and Morriss is used to identify the rate controlling step in the adsorption process and the mechanism of adsorption. The mechanism of adsorption involves multiple steps: the MO molecules or Cd^{2+} cations migrant from the bulk solution to the surface of the adsorbent diffuse through the boundary layer to the surface of adsorbent and followed by intra-particle diffusion into the interior of the adsorbent. The amount of MO or Cd^{2+} cations can be calculated by Eq. (6).

$$q_t = K_{id} t^{1/2} + C \qquad (6)$$

where: k_{id} is the intra-particle diffusion rate constant ($mg \cdot g^{-1} \cdot min^{-0.5}$) and it can be calculated from the slope of the linear Eq. (6) of the linear plot q_t against $t^{1/2}$. The constant C ($mg \cdot g^{-1}$) indicates the thickness of the boundary layer. Higher C values are indicative of higher boundary layer effect and thus are descriptive of the inapplicability of pore diffusion as the sole rate-determining step in describing the dynamics of the adsorption process (Alijeboree et al., 2017). The kinetic parameters are presented in Table 3. A linear relationship between t/q_t against t and almost identical values between q_e and q_t indicate the applicability of this model. The linearization proved that the pseudo-second kinetic order describes fairly well the adsorption mechanism for MO and for the Cd^{2+} cations in all cases (Fig. 8).

The correlation coefficient of the second order kinetic model (1) is greater than for the first order kinetic model (0.906), while the MO adsorption on BCBH proved also to be faster (k_2= 0.1115 g $mg^{-1}min^{-1}$) as (k_1=0.0223 min^{-1}). This confirms that the rate limiting step is chemisorption (Hsu et al., 2011).

Kinetic experiments clearly indicated that adsorption of methyl orange on substrate obtained from wood biomass is a two-step process: a rapid adsorption of dye onto the external surface followed by intra-particle diffusion into the interior of adsorbent which has also been confirmed by intra-particle diffusion model.

5. Adsorption isotherms modeling

At contact time optimal by 45 min, determined from the adsorption efficiency in time (Fig. 1 and Fig. 2) and m_{ss}/V_{sol} ratio (0.2 g/50 mL for adsorption of MO), the adsorption isotherms were ploted at different MO concentration (10.228-0.639 mg/L). Based on optimised parameters, the adsorption isotherm q = f(Ce) was plotted.

The adsorption isotherm models investigated were based on Langmuir and Freundlich equations, Eqs. (7, 8) and (9):

- *the Langmuir isotherm (linear form):*

$$C_{eq} / q_{eq} = 1 / q_{\max} K_a + C_{eq} / q_{\max} \qquad (7)$$

where: q_{max} represents the maximum monolayer adsorption capacity (mg g^{-1}); K_a is Langmuir constant (L mg^{-1}) related to the adsorption free energy, q_{eq} is the amount of dye adsorbed from the solution at the equilibrium time; C_{eq} is equilibrium concentration of dye in solution ((mg g^{-1}). From the slop and intercept of the plot between C_{eq}/q_{eq} vs. C_{eq} the values of K_a and q_{max} respectively, are calculated. The isotherm model was expressed in terms of the dimensionless constant separation factor R_L, Eq. (8).

$$R_L = 1/1 + K_a C_0 \qquad (8)$$

where: C_0 is the initial dye concentration (mg g^{-1}); R_L- the separation factor and can be determined from Langmuir plot with the Eq. (7) and indicates the type of adsorption. For the values of R_L= 0 adsorption can be irreversible, for 0.00<R_L<1, adsorption is favorable, for R_L =1 the adsorption is linear, while R_L >1 is the indicative of unfavorable adsorption (Bhatti et al., 2017).

Table 3. Kinetic parameters of the adsorption processes

Adsorbent	*Pseudo-first order*			*Pseudo-second order*			*Intra-particle diffusion*		
	K_L (min^{-1})	$q_{e(exp)}$ (mg/g)	R^2	k_2(g/mg·min)	$q_{e(cal)}$ (mg/g)	R^2	K_{id} (mg/g $min^{0.5}$	C (mg/g)	R^2
MO from monopollutant system									
BCBH	0.0223	5.059	0.906	0.1115	5.066	1.00	0.017	4.845	0.842
BCBHD1	0.0161	3.547	0.907	2.1439	3.605	0.997	0.103	2.215	0.918
BCBHD2	0.0226	1.539	0.908	5.004	1.574	0.995	0.054	0.862	0.938
BCBHD3	0.0205	2.688	0.905	4.3152	2.831	0.997	0.111	1.306	0.929
MO from ($MO+Cd^{2+}$) system									
BCBH	0.0154	5.092	0.821	0.0161	5.092	1.00	0.001	5.078	0.821
BCBHD1	-	4.466	0.461	0.6587	4.490	0.997	0.064	3.515	0.516
BCBHD2	0.0089	28.00	0.981	2.1882	2.755	0.994	2.444	8.56	0.952
BCBHD3	0.0239	3.225	0.961	0.8115	3.304	0.999	0.051	2.642	0.945
Cd^{2+} from ($MO+Cd^{2+}$) system									
BCBH	0.0032	29.00	0.983	1.82	38.61	0.938	1.959	2.4	0.997
BCBHD1	0.0193	237.5	0.870	0.070	294.12	0.991	8.929	125.5	0.849
BCBHD2	0.0145	222.6	0.929	0.044	227.27	0.989	7.655	118.1	0.901
BCBHD3	0.01727	45.35	0.892	0.187	46.083	0.994	1.751	23.03	0.919

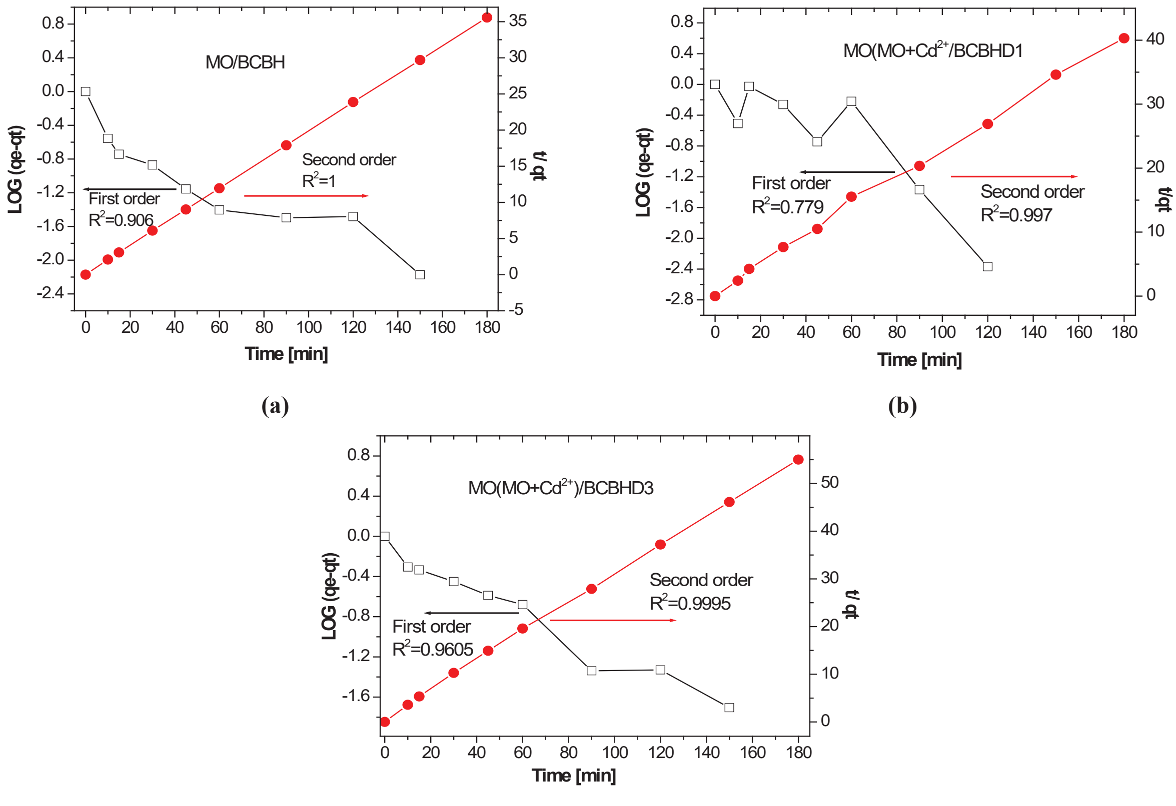

(a) **(b)**

(c)

Fig. 8. The pseudo first order and the second order kinetic plot for MO adsorption on BCBH (a), BCBHD1 (b) and BCBHD3 (c)

- *the Freundlich isotherm (linear form):*

$$\ln q_{eq} = \ln k_F + 1/n \ln c_{eq} \qquad (9)$$

where: k_F is Freundlich constant indicating the adsorption capacity; *1/n* is a dimensionless parameter indicating the adsorption density.

The parameters of both models are presented in Table 4 and outline that chemisorption is as described by the Langmuir model. The results show a significantly higher adsorption capacity of the substrate during adsorption. Generally, the value of the linear regression correlation coefficient R^2 gives the indication which model to choose to give best-fit. The values of R^2 (0.998; 0.946) and q_{max} = 6.165 mg/g; 2.926 mg/g indicate that the Langmuir adsorption model can well discribe the removal of the MO by using BCBH adsorbent, and BCBHD3, respectively. For the values of R_L ($0.00<R_L<1$), adsorption can be favorable. The Freundlich adsorption isotherm model yields a heterogeneous adsorption surface with unequal available sites and different adsorption energies. All the substrates on methyl orange adsorption also can be described by Freundlich isotherm (R^2 = 0.990; 0.979; 0. 950). The value of 1/n closer zero (0.565 -1.245) indicates more surface heterogeneity on certain areas. The adsorption of Cd^{2+} cations is fitted on Langmuir model isotherm on BCBH, BCBHD1 and BCBHD3 with q_{max} = 45.456 mg/g. Generally, the best isotherm model is chosen based on a high linear regression coefficient (R^2) value. Table 5 show a comparison with the maximum adsorption capacities of several adsorbents found in literature. The results obtained in this work are in same order of magnitude as the reported materials.

Two parallel adsorption mechanisms occurs, one involving electrostatic interactions and a second one involving dispersive interactions. In aqueous solutions at pH> pH_{PZC} the present of TiO_2 may have a positive effect in adsorption of Cd^{2+} cations, according to the Eqs. (10, 11), (Janusz and Matysek, 2006; Visa and Duta, 2013).

$$\equiv\equiv Ti{-}OH + HO^- \rightarrow \equiv\equiv Ti{-}O^- + H_2O \qquad (10)$$

$$2\equiv\equiv Ti{-}O^- + Cd^{2+} \rightarrow (\equiv\equiv Ti{-}O^-)_2Cd^{2+} \text{electrostatic interaction} \qquad (11)$$

The charcoal (BCBH) is adsorbent with acidic and basic groups (- COOH; - HO) that can interact with Cd^{2+} cations (Pyrzynska, 2019).

6. Regeneration and reuse of the adsorbent

Moreover, the subsequent regeneration and reuse of the adsorbent are important attributes of the adsorption process from economic and environmental viewpoint. In this paper, the reusability of BCBHD3 adsorbent is presented. This adsorbent loaded with MO and cadmium was regenerated using absolute ethanol, bidistilated water and drying at 115 ^{0}C. The adsorption studies were done in the same conditions that in the first cycle: 0.1 g BCBHD3 regenerated, $C_{0/MO}$ = 0.03125 mM, $C_{0/Cd}$ =0.01 N. The results are presented in Fig. 9.

Table 4. Adsorption isotherm parameters for MO and Cd^{2+} removal on adsorbents

Adsorbent		***Langmuir Isotherm***			***Freundlich Isotherm***		
	q_{max} [mg g^{-1}]	K_a [L mg^{-1}]	R^2	R_L	*n*	K_F	R^2
MO from monopollutant system							
BCBH	6.165	0.0383	0.823	0.7186	0.803	0.3334	0.998
BCBHD1	-	-	0.408	-	0.933	0.1258	0.994
BCBHD2	1.423	0.6088	0.903	0.1382	1.590	1.2E-05	0.969
BCBHD3	2.926	0.0996	0.946	0.4952	1.767	2.2E-12	0.979
MO from ($MO+Cd^{2+}$) system							
BCBH	-	-	0.055	-	0.878	0.0036	0.948
BCBHD1	-	-	0.349	-	0.763	0.0051	0.932
BCBHD2	2.238	0.3471	0.873	0.2196	1.200	1.5E-11	0.970
BCBHD3	-	-	0.776	-	-	3.5E-09	0.805
Cd^{2+} from ($MO+Cd^{2+}$) system							
BCBH	9.823	0.0930	0.995	0.0191	1.934	0.0022	0.950
BCBHD1	43.49	0.004	0.975	0.3051	3.648	1.5381	0.713
BCBHD2	-	-	0.049	-	1.052	0.9E-08	0.938
BCBHD3	45.46	0.0138	0.963	0.6396	-	-	0.475

Table 5. Comparative adsorption capacities of Cd $^{2+}$ cations and of MO on different adsorbents (Pyrzynska, 2019)

Adsorbent	$Q_{max/Cd}$ *[mg/g]*	$Q_{max/MO}$ *[mg/g]*	*References*
Alginate–calcium carbonate	10.20	-	(Mahmood et al., 2017)
Chitosan-AC	52.63	-	(Hydari et al., 2012)
Na-magadiite	57.00	-	(Attara et al., 2018)
Chitosan derivative	98.04	-	(Boamah et al., 2015)
Apple peels	0.80	-	(Abdolali et al., 2016)
Mandarin peels	3.33	-	
Coffee grounds	16.20	-	(Dutta et al., 2015)
Orange peel	40.00		(Gupta and Nayak, 2012)
Orange peeland Fe2O3 nanoparticles	76.02	-	
Orange peel modified with KCl	125.60	-	(Liu et al., 2010)
Banana peels	5.91	-	(Deshmukh et al., 2017)
Sun flower plant	35.97	-	(Pyrzynska K, 2019)
Aguaje stones	26.33	-	(Hydari et al., 2012)
Camel Thorn Plant	-	19.61	(Mogaddasi et al., 2010)
Moringa peregrine	-	15.43	(Bazrafshan et al., 2014)
BCBH	9.82	6.16	This study
BCBHD1	43.49	4.49	This study
BCBHD3	45.35	3.22	This study

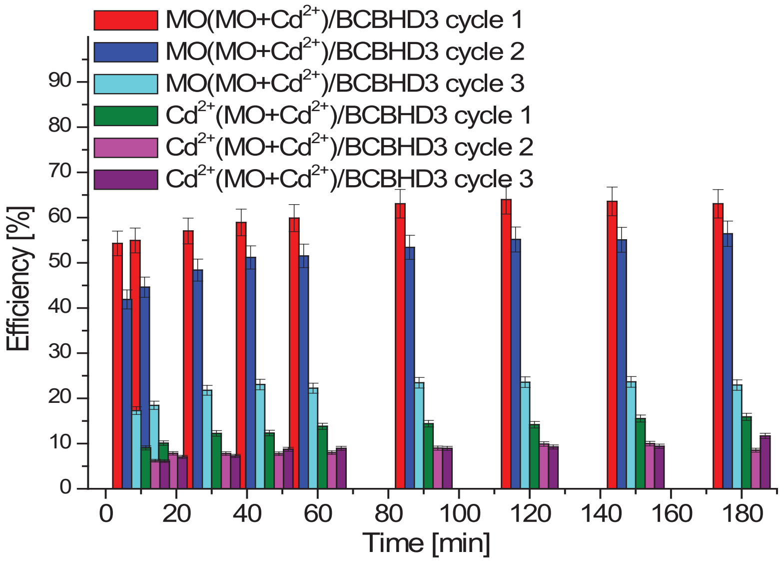

Fig. 9. Efficiency simultaneous removal of MO and Cd^{2+} cations from aqueous solutions by reusing the BCBHD3 adsorbent

The adsorption efficiency of reusability of BCBHD3 adsorbent decreased with increasing desorption cycles. Almost with 15.62 % decreased the adsorption efficiency of MO in the second cycle and with 56.20 % in the third cycle. Adsorption efficiency of Cd^{2+} cations decreased in the second cycle with 35.27% and in the third cycle almost is constant.

7. Conclusions

The charcoal from wood branches activated with NaOH by hydrothermal method (BCBH) with 387.88 m^2/g surface area can explain the higher adsorption efficiency of MO (98.14 %) and (97.55 %) from mono respectively, di-solute aqueous solutions.

The best adsorbents for uptake the Cd^{2+} cations are BCBHD1 and BCBHD2 which evidenced the high BET surface (241.388 m^2/g and 128.405 m^2/g respective), and the highest crystalline (73.6 % and 90.9 % respectively). On these adsorbents the efficiency removal of Cd^{2+} cations are 69.62 %/BCBHD1 and 60.42 %/BCBHD2. The charcoal (BCBH) can be a good support for TiO_2 for to obtain the composites for adsorption of dye (MO) and heavy metals (Cd^{2+} cations), but a large amount of TiO_2 embedded into charcoal (BCBHD3) decrees the BET surface (74.267 m^2/g) and don't favor de adsorption of MO or of Cd^{2+} cations.

The adsorption efficiency of MO is increased in present of the Cd^{2+} cations, which are adsorbed in pores of the substrate and MO adsorption happen on the heterogeneous composite BCBH: TiO_2 surface. The kinetic studies showed that MO and Cd^{2+} cations adsorption process followed pseudo-second-order kinetics models (R^2> 0.94 even 1). Langmuir and Freundlich equations both are applicable to describe the adsorption of MO on charcoal and composites within this initial dye concentration range. The constant value, R_L (low separation factor), in Langmuir isotherm and Freundlich constant, n, both give an indication of favourable adsorption.

The results show that the adsorption mechanism for removing MO and MO + Cd^{2+} cations from wastewater by means of the above presented composites BCBH, BCBHD1, BCBHD2, and BCBHD3 is a viable, low cost, up-scalable and sustainable for the adsorption technology.

Acknowledgements

This paper is supported by the Doctorat Program from Transylvania University of Brasov.

References

Abdolali A., Ngo H.H., Guo W., Lu S., Chen S.S., Nguyen N.C., Zhang X., Wang J., Wu Y., (2016), A break through biosorbents in removing heavy metals: equilibrium, kinetic, thermodinamic and mechanism analyses in a lab-scale study, *Science of the Total Environment*, **542**, 603-611.

Alijeboree A.M., Alshirifi A.N., Alkaim A.F., (2017), Kinetics and equilibrium study for the adsorption of textile dyes on coconut shell activated carbon, *Arabian Journal of Chemistry*, **10**, 3381-3393.

Attara K., Bouazza D., Miloudi H., Tayeb A., Boos A., Sastre A.M., Demey H., (2018), Cadmium removal by a low-cost magadiite-based material: Characterization and sorption applications, *Journal of Environmental Chemical Engineering*, **6**, 5351-5360.

Bazrafshan E., Zarei A.A., Nadi H., Mohammad A.Z., (2014), Adsorptive removal of methyl Orange and Reactive Red 198 dyes by *Moringa peregrine* ash, *Indian Journal of Chemical Technology*, **21,** 105-113.

Bhatti H.N, Jabeen A., Iqbal M., Noreen S., Naseem Z., (2017), Adsorptive behavior of rice bran-based composites for malachite green dye: Isotherm, kinetic and thermodynamic studies*, Molecular Liquids*, **237**, 322-333.

Boamah P.O., Huang Y., Hua M., Zhang Q., Liu Y., Onumah J., Wang W., Song Y., (2015), Removal of cadmium from aqueous solution using low molecular weight chitosan derivative, *Carbohydrate Polymers*, **122**, 255-264.

Ciardelli G., Ranieri N., (2001), The treatment and reuse of wastewater in the textile industry by means of ozonation and electroflocculation, *Water Resources*, **35**, 567-572.

Chakraborty S., Chowdhury S., Saha P.D., (2011), Adsorption of Crystal Violet from aqueous solution onto NaOH-modified rice husk, *Carbohydrates Polymers*, **86**, 1533-1541.

Guerrero-Coronilla I., Aranda-Garcia E., Cristiani-Urbina E., (2019), Biosorption of metanil yellow dye from aqueous solutions by the entire water hyacinth plant (*Eichhornia crassipes*) and its vegetative organs, *Environmental Engineering and Management Journal,* **18**, 1671-1682.

Deshmukh P.D., Khadse G.K., Shinde V.S., Labhasetwar P., (2017), Cadmium removal from aqueous solutions using dried banana peels as an adsorbent: kinetics and equilibrium modeling, *Journal of Bioremediation & Biodegradation*, **8**, 395, doi: 10.4172/2155-6199.1000395.

Duman G., Onal Y., Okutucu C., Onenc S., Yanik J., (2009), Production of activated carbon from pine cone and evaluation of its physical chemical and adsorption properties, *Energy & Fuels*, **23**, 2197-2204.

Dutta A., Diao Y., Jain R., Rene E.R., Dutta S., (2015), Adsorption of cadmium from aqueous solutions onto coffee grounds and wheat straw: equilibrium and kinetic study, *Journal of Environmental Engineering,* **142,** 9.

El-Shafey E.I., Ali S.N.F., Al-Busafi S., Al-Lawati H.A.J., (2016), Preparation and characterization of surface functionalized activated carbons from date palm leaflets and application for methylene blue removal, *Journal of Environmental Chemical Engineering*, **4**, 2713-2724.

Gupta V.K., Nayak A., (2012), Cadmium removal and recovery from aqueous solutions by novel adsorbents prepared from orange peel and Fe_2O_3 nanoparticles, *Chemical Engineering Journal*, **180**, 81-90.

Hema M., Arivoli S., (2007), Comparative study on the adsorption kinetics and thermodinamics of dyes onto acid activated low cost carbon, *International Journal of Physical Science*, **2**, 010-017.

Ho Y.S., Mc-Kay G., (1998), The kinetic of sorption of basic dyes from aqueous solution by sphagnum Moss peat, *The Canadian Journal of Chemical Engineering*, **76**, 822-827.

Ho Y.S., Mc-Kay G., Wase D.A.J., Foster C.F., (2000), Study of the sorption of divalent metal ions on to peat, *Adsorption Science &. Technology*, **18,** 639-650.

Hsu L.J., Lee L.T., Lin C.C., (2011), Adsorption and photocatalytic degradation of polyvinyl alcohol in aqueous solution using P-25 TiO_2, *Chemical Engineering Journal*, **173**, 698-705.

Hydari S., Sharififard H., Nabavinia M., Parvizi M.R., (2012), A comparative investigation on removal performances of commercial activated carbon, chitosan biosorbent and chitosan/activated carbon composite for cadmium, *Chemical Engineering Journal*, **193-194**, 276-282.

Janusz W., Matysek M., (2006), Coadsorption of Cd (II) and oxalate ions at the TiO_2/electrolyte solution interface, *Journal of Colloid and Interface Science,* **296**, 22-29.

Kolodynska D., Halas P., Franus M., Hubicki Z., (2017), Zeolite properties improvement by chitosan modification - Sorption studies, *Journal of Industrial and Engineering Chemistry*, **52**, 187-196.

Kumar R., Ahmad R., (2011), Biosorption of hazardous crystal violet dye from aqueous solution onto treated ginger waste (TGW), *Desalination*, **265**, 112-118.

Mahmoud H.R, Ibrahim S.M., El-Molla S.A, (2016), Textile dye removal from aqueous solutions sing cheap MgO nanomaterials: Adsorption Kinetics studies and thermodynamics, *Advanced Powder Technology*, **27**, 223-231.

Mogaddasi F., Momen Heravi M., Bozorgmehr M.R., Ardalan P., Ardalan T., (2010), Kinetic and thermodynamic study on the removal of methyl orange from aqueous solution by adsorption onto camel thorn plant, *Asian Journal of Chemistry,* **22,** 5093-5100.

Li S., Lyons-Hart J., Banyasz J., Shafer K., (2001), Real-time evolved gas analysis by FTIR method: an experimental study of cellulose pyrolysis, *Fuel*, **80**, 1809-1817.

Liu Y., Sun X., Li B.U., (2010), Adsorption of Hg (II) and Cd (II) by ethylenediamine modified peanut shells, *Carbohydrate Polymers*, **81**, 335-339.

Mahmood T., Ali R., Naeem A.N., Hamayun M., Aslam M., (2017), Potential of used *Camellia sinensis* leaves as precursor for activated carbon preparation by chemical activation with H_3PO_4; optimization using response surface methodology, *Process Safety and Environmental Protection*, **109,** 548-563.

Matos J., Cuevas S.M., Ruiz-Delgado A., Oller I., Malato S., (2017), Development of TiO_2-C photocatalysts for solar treatment of polluted water, *Carbo,* **122**, 361-373.

Ofomaja A.E., Pholosi A., Naidoo E.B., (2015), Application of raw and modified pine biomass material for cesium removal from aqueous solutions, *Ecological Engineering*, **82**, 258-266.

Pattnaik P., Dangayach G.S., (2019), Sustainability of wastewater management in textile sectors: a conceptual framework, *Environmental Engineering and Management Journal,* **18**, 1947-1965.

Popa N., Visa M., (2017), The synthesis, activation and characterization of charcoal powder for the removal of methlene blue and cadmium from wastewater, *Advanced Powder Technology,* **28**, 1886-1876.

Pholosi A., Ofomaja A.E, Naidoo E.B., (2013), Effect of chemical extract ants on the biosorptive properties of pine cone power: Influence on lead (II) removal mechanism, *Journal of Saudi Chemical Society*, **17**, 77-86.

Pyrzynska K., (2019), Removal of cadmium from wastewaters with low-cost adsorbents, *Journal of Environmental Chemical Engineering*, **7**, 102795.

Robinson T., Chandran B., Nigam P., (2002), Effect of pretreatments of three waste residues, wheat straw, corncobs and barley husks on dye adsorption, *Bioresource Technology*, **85**, 119-124.

Sayğili H., Güzel F., Önal Y., (2015), Conversion of grape industrial processing waste to activated carbon sorbent and its performance in cationic and anionic dyes adsorption, *Cleaner Production,* **93**, 84-93.

Sewu D.D., Boakye P., Woo S.H., (2017), Highly efficient adsorption of cationic dye by biochar produced with Korean cabbage waste, *Bioresource Technology*, **224**, 206-213.

Sivaraj R., Namasivayam C., Kadirvelu K., (2001), Orange peel as an addorbent in the removal of acid violet 17 (acid dye) from aqueous solutions, *Waste Management*, **21**, 105-110.

Suhas G., Gupta V.K., Carrott P.J.M., Singh R., Chaudhary M., Kushwaha S., (2016), Cellulose: A review as natural, modified and activated carbon adsorbent, *Bioresource Technology,* **216**, 1066-1076.

Tseng R-L., Tseng S-K., (2005), Pore structure and adsorption performance of the KOH-activated carbons prepared from corncob, *Journal of Colloid and Interface Science,* **287**, 428-437.

Visa M., Duta A., (2008), Advanced Cd^{2+} removal on dispersed TiO_2 –fly ash, *Environmental Engineering and Management Journal,* **7**, 373-378.

Visa M., Nacu M., (2011), Comparative heavy metals and dyes removal efficiency on fly ash and wood ash, E*nvironmental Engineering and Management Journal,* **10**, 1407-1413.

Visa M., Andronic L., Lucaci D., Duta A., (2011), Concurrent dyes adsorption and photo-degradation on fly ash based substrates, *Adsorption Journal*, **17**, 102-108.

Visa M., Duta A., (2013), Methyl-orange and cadmium simultaneous removal using fly ash and photo-Fenton systems, *Journal of Hazardous Materials*, **244**, 773-779.

Yang C.L., Garrahan J.Mc, (2005), Electrochemical coagulation for textile effluent decolorization, *Journal of Hazardous Materials*, **B127**, 40-47.

Yang H., Yan R., Chen H., Lee D.H, Zheng C., (2007), Characteristics of hemicelluloses, cellulose and lignin pyrolysis, *Fuel*, **86,** 1781-1788.

Yagmur E, Tun M. S., Banford A., Aktas Z., (2013), Preparation of activated carbon from auto hydrolysed mixed southern hard wood, *Journal of Analytical and Applied Pyrolysis*, **104**, 470-478.

Zhang R., Zhang J., Zhang X., Dou C., Han R., (2014), Adsorption of Congo red from aqueous solutions using cationic surfactant modified wheat straw in batch mode: kinetic and equilibrium study, *Journal of the Taiwan Institute of Chemical Engineers,* **45**, 2578-2583.

Environmental Engineering and Management Journal

February 2020, Vol. 19, No. 2, 303-310
http://www.eemj.icpm.tuiasi.ro/; http://www.eemj.eu

"Gheorghe Asachi" Technical University of Iasi, Romania

STRUVITE PRECIPITATION FROM SEWAGE SLUDGE ASH

Bogdan Adrian Militaru, Rodica Pode*, Lavinia Lupa, Florica Manea

Politehnica University of Timisoara, Faculty of Industrial Chemistry and Environmental Engineering, Timisoara, Romania

Abstract

The recovery of nutrients from sewage sludge ash, especial phosphorus, is one of the most important alternative in sewage sludge management. Phosphorus is an essential element for all living organisms and very important for agriculture and industry, as well as. Because the phosphorus is a non-regenerative resource, its recovery plays an important role for society. Phosphorus capitalization as struvite ($NH_4MgPO_4 \cdot 6H_2O$) from sewage sludge has attracted considerable attention due to its potential to be re-used as fertilizer through phosphorus recovery.

The aim of this paper is the recovery of phosphorus as struvite from the ash resulted after the sewage sludge incineration. The optimal conditions chosen were: L:S=5:1 and 5% sulfuric acid solution, obtaining in this case a phosphorus extraction eficieny of 92% and having a phosphorus content in of 8.2 g/L. The precipitation process was studied for two values of the Mg:P ratio of 1.5 and 1.2 for pH ranging between 8.5 and 10. For struvite precipitation, magnesium sulfate heptahydrate ($MgSO_4 \cdot 7H_2O$) and ammonium chloride (NH_4Cl) were used as the magnesium and nitrogen sources in alkaline media using 4M NaOH solution. The precipitates were characterized chemically and morpho-structurally. The optimum pH for the struvite formation is pH=9. The XRD pattern for the sample precipitated at pH of 9 shows the struvite as the only detectable crystalline phase with the highest intensity compared with other precipitates.

The proposed method for struvite obtaining represents a green and less expensive technology presenting advantages from both economic and environmental point of view.

Key words: phosphorus recovery; sewage sludge ash management; fertilizer

Received: January, 2019; Revised final: January, 2020; Accepted: February, 2020; Published in final edited form: February, 2020

1. Introduction

Phosphorus is one of the most important elements for biological growth (Jalali and Jalali, 2016; Metaxa et al., 2019; Yuanyao et al., 2017). The global population will grow from 7.2 billion individuals to 9.6 billion by the year 2050 (UN, 2014). Also, the food consumption rate will increase at a rate of 3.1% every year (Heffer and Prud'homme, 2014) and therefore the sustainable intensification of agricultural production will need to be implemented globally with the agricultural production growing by 60% (Kataki et al., 2016). Fertile soils play an important role for the intensification of agriculture production, which are highly dependent of commercial fertilizer. Commercial fertilizers also depend upon the availability of phosphorus (Kataki et al., 2016). On the other hand, it is predicted that the rock phosphate reserves will run out in the next 70-100 years (Łukawska, 2014). From this reasons the recovery of phosphorus from secondary sources is a global concern and is in agreement with the sustainable development and the "principle of natural sources protection".

The European Parliament has reviewed the list of critical raw material (CRM) for the European Union, which phosphate is an important rock due to the risks of a shortage of supply (COM, 2014). Europe has no important P mines and depends on the import of ore. Therefore, it is really important to implement at the level of the European Union a sustainable method for recycling and conserving the phosphorus

---

* Author to whom all correspondence should be addressed: e-mail: rodica.pode@upt.ro

resource (Lederer et al., 2014). Recovery of phosphorus through efficient and economically viable processes from waste and resides sources rich in phosphorus is a priority for sustainable development (Kataki et al., 2016).

In the European Union there is only one country where phosphates are produced from apatite deposits: Finland. Most of the countries which own large deposits of phosphate rock use these resource for their own needs or are politically unstable (Adam et al., 2009). Thus, there is a high potential in European Union to recover phosphorus from secondary source: waste streams, such as: wastewater (Zhang et al., 2013), sludge (Jeyakumar et al., 2019; Millier and Hooda, 2011), meat and bone meal (Darwish et al., 2016) and biomass.

Struvite precipitation ($MgNH_4PO_4{\cdot}6H_2O$) is one of the best ways to recover phosphorus from different types of wastewaters: swine wastewater (Rahman et al., 2011), calf manure wasterwater (Schuiling and Andrade, 1999), leather tanning wastewater (Tunay et al., 1997), sewage sludge (Munch and Barr, 2001), wasted sludge (Jaffer et al., 2002), digested supernatant (Pastor et al., 2010), industrial wastewater (Diwani et al., 2007), agro-industrial wastewater (Barreto dos Santos et al., 2016; Hidalgo et al., 2014; Moerman et al., 2009), and fertilizer plant wastewater (Yu et al., 2013). Precipitation of struvite has also been studied experimental using chemical reagents (Huang et al., 2019; Le Corre et al., 2005; Li et al., 2016; Polat and Sayan, 2019; Yan and Shih, 2016; Wei et al., 2019).

Sewage sludge ash also represents an important phosphorus source due to the high concentration of phosphorus. In this work is presented the recovery of phosphorus from a natural material (sewage sludge ash) using sulfuric acid as leaching solution studying the influence of different concentration of acid and different liquid: solid ratios upon the extraction efficiency. Struvite is obtained from the resulted extracted solution via chemical precipitation. Xu et al. (2012) investigated the possibilities of using the sewage sludge as secondary source for phosphorus precursor in order to obtain struvite precipitation. In this case they compared the phosphorus leaching efficiency using hydrochloric acid or sodium hydroxide solutions. The conclusion was that the acid was more effective than the alkaline solutions, but in their case the extraction of heavy metals (present in sewage sludge) was an inconvenient. In our case, using the sulfuric acid, the extraction of the heavy metals present in the sewage sludge is reduced due to the fact that the obtained metals sulfates have lower solubility. In other studies, phosphorus was extracted using sulfuric acid or citric acid, but in this cases, the phosphorus was recovered as iron phosphates, thus a further purification step using ion exchange to remove iron was required to increase the degree of P release (Shiba and Ntuli, 2017). Also, Franz and his co-workers (2007) used two methods to extract heavy metals from the extracted solution: ion exchange and sulfide precipitation. Another study presented a pretreatment method for heavy metals extraction using thermochemical treatment (Mattenberger et al., 2008). Therefore, the present study presents an efficient method of phosphorus recovery using sulfuric acid as leaching solution unlike the methods presented until now in the specialty literature. The direct precipitation of phosphorus from the resulted solution after the acid leaching process eliminate the need of extra purification, which minimize the production cost.

2. Experimental

2.1. Materials

The sewage sludge used throughout the present study was collected from a municipal wastewater treatment plant from Timis county, Romania. The sewage sludge ash was obtained after drying the sewage sludge at 105°C for 20 hours and then calcinated at 850°C for 3 hours using Nabertherm B180 oven.

Sulfuric acid (H_2SO_4, 98%) of analytical reagent grade used for the extraction experiments was provided by Merck, Darmstadt, Germany. Magnesium sulfate heptahydrate and ammonium chloride of analytical reagent grade used for the precipitation process were supplied also by Merck, Darmstadt, Germany. Ultrapure water was used for the analytical method.

2.2. Sewage sludge ash characterization

The sewage sludge ash was digested with aqua regia in order to determine its composition. The initial phosphorus content was determined using a Hach Lange DR 3900 spectrometer in accordance with Standard Method EPA 4500-P C (American Public Health Association, 2005) and metal content was analyzed by atomic absorption spectroscopy.

The structural characteristics of the sewage sludge ash were determined by transmission electron microscopy. A Titan G2 80-200 electron microscope (FEI Company, Netherlands) was used to analyze sewage sludge ash samples deposited from ethanol on 200 mesh copper grids (3 mm) coated with holey carbon film at an acceleration voltage of 200kV. TEM images were recorded using Digital Micrograph software and elemental distribution maps were obtained using Esprit software.

2.3. Phosphorus extraction from sewage sludge ash

The phosphorus extraction from sewage sludge ash was carried out in batch mode batch at room temperature using sulfuric acid as extraction agent. The influence of acid concentration and of the liquid: solid (L:S) ratio upon the extraction efficiency were studied.

Therefore, a measured amount of sewage sludge ash sample was mixed with a measured volume of sulfuric acid to reach the values of liquid: solid ratios ranged from 5:1 to 20:1. The stirring rate was

400 rpm. In order to determine the influence of the acid concentration upon the extraction efficiency different sulfuric acid concentrations ranged from 5% to 15%, were used.

The samples were stirred magnetically at constant speed for 15 minutes and then the slurry was centrifuged at 3500 rpm for 10 minutes, analyzing the phosphorus content from supernatant.

The extraction efficiency was calculated based on the equation bellow (1):

$$\eta(\%) = \frac{C}{C_0} \cdot 100 \tag{1}$$

where: η represents the extraction efficiency (%), C is phosphorus concentration from extraction acidic sample (g/L), and C_0 is initial phosphorus concentration (g/L).

2.4. Phosphorus recovery as struvite

The phosphorus extracted from the sewage sludge ash was recovered and capitalized as struvite. For struvite precipitation, ammonium chloride (NH_4Cl) and magnesium sulfate heptahydrate ($MgSO_4 \cdot 7H_2O$) were used as the nitrogen and magnesium source. The pH adjustment was achieved by a 4M NaOH solution. The magnesium source was firstly poured into the optimal acidic extracted solution, followed by the addition of NaOH solution for pH adjustment (8.5, 9, 9.5, 10). Finally, the nitrogen source for struvite precipitation was added. The magnesium and nitrogen source were introduced in order to obtain a Mg: P ratio of 1.5 and a N: P ratio of 1.2. Afterwards, the mixture was stirred at constant speed for 15 minutes, the suspension was filtered, and the precipitate was dried at 35°C.

2.5. Characterization of the obtained struvite

In order to determine if the extracted phosphorus from the sewage sludge ash was recovered as struvite the precipitates obtained at various pH values were subjected to the chemical analysis, X-ray diffraction (XRD) analysis, scanning electron microscopy (SEM and EDAX).

The obtained precipitates were digested using hydrochloride acid (HCl, 37%) in order to determine the total amount of phosphorus, magnesium, nitrogen and other metals. The phosphorus and iron concentrations were determined through molecular absorption spectrometry using a Hach Lange DR 3900 and DR 2800 spectrometers. The phosphorus concentrations were determined in accordance with ISO 6878:2004 (ISO, 2004). The nitrogen and calcium concentrations were performed using an automated wet chemistry analyzer known as continuous flow analyzer San++ from Skalar. The magnesium, sodium and potassium were determined through atomic absorption spectrometry using a Perkin Elmer Analyst 800 spectrometer. The other elements (Al, Pb, Cr, Ni, Cu, Cd, Se, Mn) were determined through inductively coupled plasma mass spectrometry (ICP-MS) using a Perkin Elmer NexION 350X spectrometer.

The obtained precipitates were ground into powder and examined by XRD to determine their crystalline phase compositions. The X-ray diffraction patterns were recorded by using a Rigaku Ultima IV X-ray diffractometer (40 kV, 40 mA) with CuKα radiation (λ = 0.15406 nm) to identify the crystalline phases using PDF 4+ databases.

The morphology of the synthetized samples (SEM images) were observed using a Quanta FEG 250 microscope, equipped with an EDAX/ZAF quantifier. The thermal behavior of the struvite obtained in optimum conditions was determined through thermogravimetric analysis using a Derivatograph TG 209 F1 Libra, DSC 204 F1 Phoenix NETZSCH in static air atmosphere between 25 °C and 1000 °C with the heating rate of 5°C/min.

3. Results and discussions

3.1. Sewage sludge ash characterization

From the chemical composition of the sewage sludge (Militaru et al., 2019), can be observed that Ca, Fe, P and Al are the main elements contained in the ash. The phosphorus content was 4.3% P (42991 ppm) and respective, 9.86% P_2O_5.

The mapping technique was used as a structural characterization method, which highlighted by different colorations the presence of phosphorus, oxygen, calcium, magnesium, iron and aluminum, and the results are presented in Fig. 1, which illustrates a STEM image acquired on chosen area of the ash sample. It can be observed that the main elements, resulted also from the chemical analysis, are uniform distributed in the structure of the sewage sludge ash. Due to its high present and uniform distribution in the sewage sludge ash, the purpose of this study is to capitalize the phosphorus ions under struvite form.

Table 1. Chemical composition of the resulted extracted solution

Parameter	*Concentration of the resulted extracted solution (g/L)*
P	8.12
Ca	1.09
Al	2.32
Fe	0.650
K	0.959
Cu	0.051
Mn	0.142
Zn	0.108
Pb	UDL*
Cr	0.002
Ni	0.002
Cd	UDL*
Na	1.16
Mg	2.08

**UDL - under detection limit*

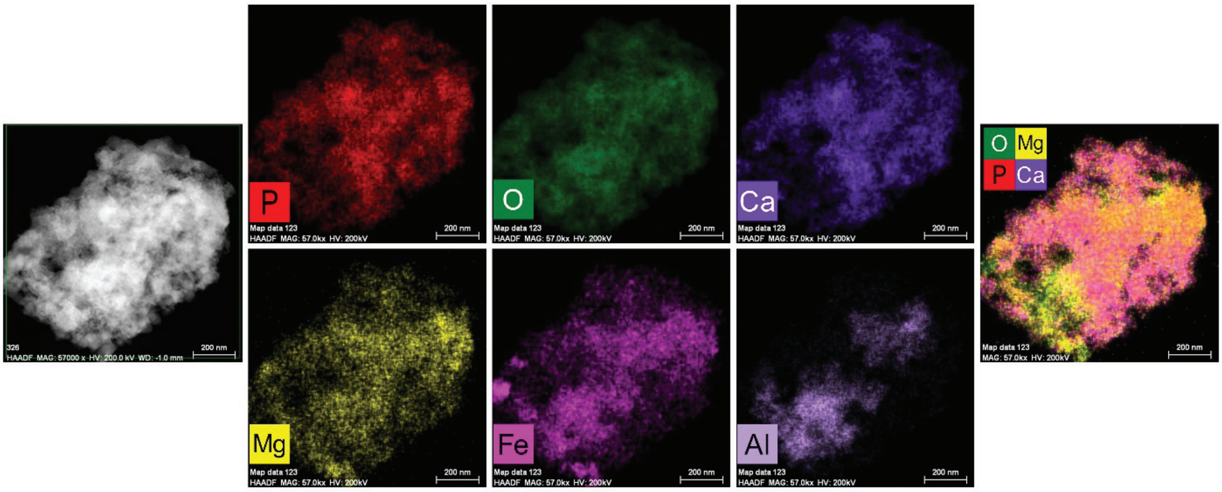

Fig. 1. STEM image of the studied sewage sludge ash

3.2. Extraction studies

In order to find the easiest way for phosphorus valorification as struvite, this study was conducted to find optimum conditions for its extraction in sulfuric acid as an intermediar step of the phosphorus recycling process. Fig. 2a shows the influence of liquid: solid (L:S) ratio upon the phosphorus extraction efficiency using three different concentration of sulfuric acid solution (5, 10 and 15%). Fig. 2b shows the evolution of the phosphorus concentration in the obtained exctracted solution.

It can be noticed that the phosphorus extraction efficiencies present a slow increasing with the L:S ratio increasing and with the increasing of the sulfuric acid concentration. For all the cases the obtained extraction efficiens were above 90%. In the same time, the increasing of the L:S ratio lead to a decreasing of the phosphorus concentration from the extracted solution. Therefore, from this reason and from economical point of view is not recomanded to use a higher L:S ratio and is not justified to use a higher concentration of sulfuric acid solution.

Based on these arguments the optimal conditions chosen in order to obtain the struvite were: L:S=5:1 and 5% sulfuric acid solution, obtaining in this case a phosphorus extraction eficieny of 92% and having a phosphorus content in the extracted solution of 8.12 g/L. In this case a higher extraction degree is obtained than the extraction degree reported in other reported studies (Ali and Kim, 2016, Sano et al., 2012, Shiba and Ntuli, 2017). Another important aspect is the presence of other impurities in the resulted extracted solution such as: heavy metals and other elements. In table 1 is presented the chemical composition of the resulted extracted solution parameters. It can be observed that the major elements extracted are P, Al, Mg, Mn, Na, K, Ca and Fe.

These elements are also used as micro and macro elements in different fertilizers, so their presence in the struvite will not be a problem. The heavy metals present in the sewage sludge which could raise a concern if will be present in the struvite were extracted in a very small quantity < 3 ppm, being in the range of the maximum admited levels (GD, 2004). Due to the fact that as leaching solutions is used the sulfuric acid, the extraction of the impurities is minimised compared with the resultes reported in literature when hydrocloric acid solution is used for extraction (Xu et al., 2012). Due to the highest content of phosphorus ion in the resulted extracted solutions, this could be capitalized as struvite.

These elements are also used as micro and macro elements in different fertilizers, so their presence in the struvite will not be a problem. The heavy metals present in the sewage sludge which could raise a concern if will be present in the struvite were extracted in a very small quantity < 3 ppm, being in the range of the maximum admited levels (GD, 2004). Due to the highest content of phosphorus ion in the resulted extracted solutions, this could be capitalized as struvite.

3.3. Recovery of phosphorus as struvite

Compared with other fertilizers, struvite ($MgNH_4PO_4{\cdot}6H_2O$) is an excellent slow release fertilizer with a high content in P (Xu et al., 2012). Struvite precipitation is a promising solution for P recovery technology (Jalali and Jalali, 2016).

The formation of struvite highly depends on the pH and the molar ratio of Mg:N:P. Previous studies also reported the influence of these factors (Xu et al., 2012). It was demonstrated that the struvite formation was highly pH dependent. The optimal parameters were observed at pH = 10, Mg: P = 1.6 and N: P = 1.6.

In the present study, for struvite obtaining the chosen parameters were: Mg: P = 1.5, N: P = 1.2 and pH ranged from 8.5 to 10. Struvite crystallization also depends by other factors such as the presence of impurities and the mixing speed (Bouropoulos and Koutsoukos, 2000, Li et al., 2016).

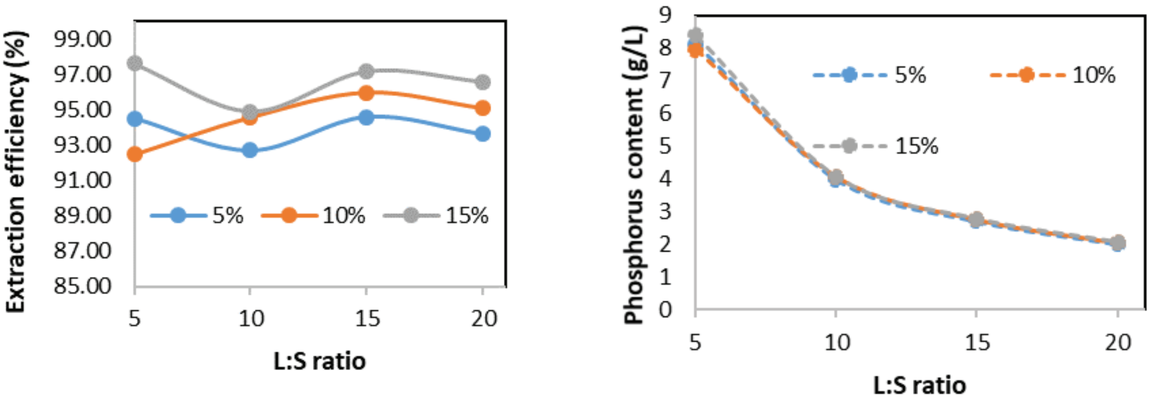

(a) (b)

Fig 2. Influence of L:S ratio upon the extraction efficiency (a) and the phosphorus content in the extracted solution (b)

The presence of impurities from the acid extraction solution affects struvite product morphology and purity. In Table 2 is presented the chemical composition for each precipitate obtained from the resulted extracted solution. It can be noticed that the concentration of P, N, Al, Mn, Cu, Zn, Fe, K and Ca decreases as the pH increases. On the other hand, the concentration of Mg and Na increases as the pH increases. The concentration of other elements remains almost constant during the precipitation. During phosphorus precipitation from resulted extracted solution heavy metals inevitably co-precipitated and further contaminated the precipitates. Even if, in the obtained struvite are present a lot of impurities from the sewage sludge ash (Table 3), these do not exceed the limits of fertilizer ordinance (GD, 2004). Table 3 shows the theoretical molar ratio in order to obtain the struvite and the molar ratios calculated for each precipitate.

It can be concluded that the optimum pH for struvite obtaining through precipitation is pH=9. At this pH the experimental molar ratio is closed to the theoretical one, and in this case are obtained the smallest quantity of impurities from the resulted struvite.

Table 3. Theoretical and experimental molar ratio

Element	*P*	*Mg*	*N*
Theoretical molar ratio	1	1	1
Molar ratio pH 8.5	1	0.76	0.76
Molar ratio pH 9	1	0.97	0.83
Molar ratio pH 9.5	1	1.10	0.83
Molar ratio pH 10	1	1.14	0.86

SEM pictures of the precipitates for each pH value (8.5, 9, 9.5, 10) are shown in Fig. 3. It can be observed the struvite crystalline rectangular particles formed during the precipitation. On the other hand, the surfaces of the struvite particles were covered with small amorphous particles. Li and co-workers observed similar SEM pictures for struvite obtained from pure reagents (Li et al., 2016).

Table 2. Chemical composition for precipitates

Element (%)	*pH = 8.5*	*pH = 9.0*	*pH = 9.5*	*pH = 10.0*
P	10.4	9.44	9.17	8.69
N	3.05	2.96	2.99	2.83
Mg	6.14	7.02	7.93	7.75
Ca	0.494	0.491	0.197	0.266
Al	3.21	3.20	2.84	2.46
Fe	1.31	1.21	1.07	0.885
K	0.203	0.417	0.171	0.129
Cu	0.061	0.058	0.055	0.048
Mn	0.138	0.155	0.135	0.117
Zn	0.121	0.195	0.113	0.098
Pb	0.002	0.005	0.007	0.001
Cr	0.003	0.012	0.005	0.003
Ni	0.002	0.002	0.003	0.002
Cd	UDL	UDL	UDL	UDL
Na	6.20	6.41	7.16	7.24

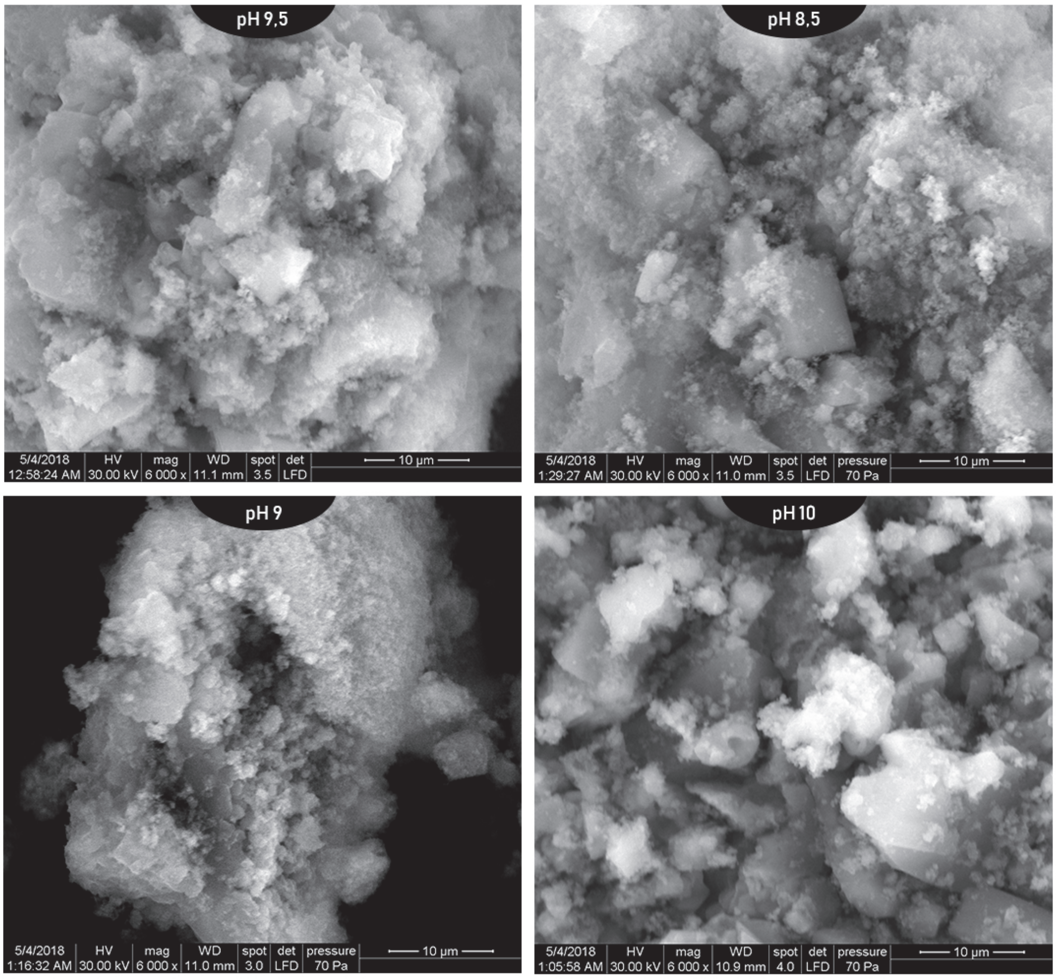

Fig. 3. SEM images of the precipitates for different pH values

The XRD pattern of the obtained struvite at different pH are presented in Fig. 4. The XRD pattern for the sample precipitated at pH of 9 shows the struvite as the only detectable crystalline phase with the highest intensity compared with other precipitates. The obtained RX in this case is similar with other RX difractograms presented for struvite in the specialty literature (Le Corre et al., 2005, Li et al., 2016, Xu et al., 2012). At pH=8.5 the P:Mg:N molar ratio is 1:0.76:0.76, which indicates an excess of P with the possible formation of other chemical compounds. The XRD pattern revealed the presence of the secondary crystalline phase: apatite.

As the pH increases, besides the presence of the struvite as the main phase, the XRD pattern reveals two more crystalline phases: sodium sulfate and magnesium sulfate. P:Mg molar ratio is 1:1.10 and 1:1.14 for pH=9.5 and pH=10, respectively, which indicates an excess of Mg and therefore formation of magnesium sulfate can take place. Correlating the results from the chemical analysis with the XRD patterns of samples it can be concluded that the optimum precipitation pH is 9. The best P:Mg:N molar ratio is for pH=9 (1:0.97:0.83) which indicates the formation of struvite as only crystalline phase.

The plot of thermogravimetric analysis (TG) and differential scanning calorimetry (DSC) of the obtained struvite in optimum conditions are presented in Fig. 5.

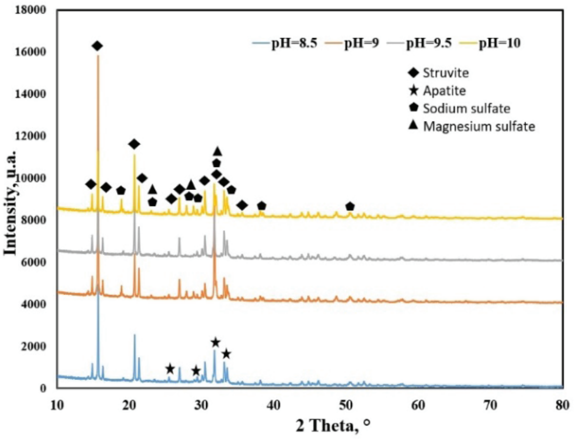

Fig. 4. RX spectrum of the precipitates obtained at pH=8.5,9, 9.5 10: ◆ $Mg(NH_4)(PO_4)(H_2O)_6$ – COD ID: 2106462, ★ $Ca_5(PO_4)_3(OH)$ – COD ID: 9010051, ⬟ Na_2SO_4 – COD ID: 9004092, ▲ $MgSO_4$ – COD ID: 9015317.

From the DSC curve can be observed an endothermic pic (at 112°C) corresponding to the main mass loss (~36%), which correspond to the ammonium decomposition and the loss of 5 molecules of water of crystallization (Chetan and Mihirkumar, 20140; Heraldy et al., 2017; Iovi et al., 2004).

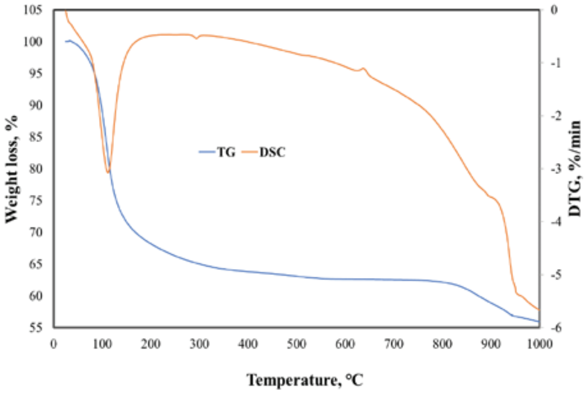

Fig. 5. Thermal analysis of the precipitate obtained at pH=9

At 294°C can be observed another endothermic effect due to the decomposition of the last moll of water (Iovi et al., 2004). The release of ammonium take place gradually (Frost et al., 2004). At 637°C can be observed an exothermic effect which correspond to the transformation of struvite in pyrophosphate (Paul et al., 2002). The water resulted in this reaction is loss at higher temperature, as can be seen the two-endothermic effect at 875°C and 950°C.

4. Conclusions

The sewage sludge ash resulted from the calcination of sewage sludge can be used as a phosphorus source due to the content of phosphorus (4.3% P, 9.86% P_2O_5). The presence of phosphorus was also confirmed by the STEM image using mapping technique.

The phosphorus extraction was performed using sulfuric acid as an extraction agent at high concentrations and lower liquid: solid ratios. The phosphorus extraction efficiencies present a slow increasing with the L:S ratio increasing and with the increasing of the sulfuric acid concentration. The optimal conditions chosen were: L:S=5:1 and 5% sulfuric acid solution, obtaining in this case a phosphorus extraction eficieny of 92% and having a phosphorus content in of 8.2 g/L.

To obtain the struvite, the chosen parameters were: Mg: P = 1.5, N: P = 1.2 and pH ranged from 8.5 to 10. The optimum pH for the struvite formation is pH=9. At this pH, the experimental molar ratio is closed to the theoretical one, are obtained the smallest quantity of impurities from the resulted struvite and also The XRD pattern for the sample precipitated at pH of 9 shows the struvite as the only detectable crystalline phase with the highest intensity compared with other precipitates.

The proposed method for struvite obtaining represents a green and less expensive technology presenting advantages from both economic and environmental point of view.

Acknowledgements

The studies were done during the PhD program from the Doctoral School of the University Politehnica Timisoara.

References

Adam C., Peplinski B., Michaelis M., Kley G., Simon F.G., (2009), Thermochemical treatment of sewage sludge ashes for phosphorus recovery, *Waste Management*, **29**, 1122-1128.

Ali U.T., Kim D.J., (2016), Phosphorus extraction and sludge dissolution by acid and alkali treatments of polyaluminum chloride (PAC) treated wastewater sludge, *Bioresource Technology*, **217**, 233-238.

American Public Health Association, (2005), *Standard methods for the examination of water and wastewater*, 21st Edition, American Public Health Association/American Water Works Association, Water Environment Federation, Washington DC.

Barreto dos Santos W.R., Foletto E.L., Mazutti M.A., Cancelier A., Jahn S.L., (2016), Removal of phosphorus from waste of a beverage industry by struvite precipitation, *Environmental Engineering and Management Journal*, **15**, 2505-2509.

Bouropoulos N.C., Koutsoukos P.G., (2000), Spontaneous precipitation of struvite from aqueous solutions, *Journal of Crystal Growth*, **213**, 381–388.

Chetan K.C., Mihirkumar J.J., (2014), Growth and characterization of struvite-Na crystals, *Journal of Crystal Growth*, **401**, 221-226.

COM 297, (2014), Communication from the Commission to the European Parliament, the Council, the European Economic and Social Committee and the Committee of the Regions on the Review of the List of Critical Raw Materials for the EU and the Implementation of the Raw Materials Initiative, European Commission, Brussels, On line at: https://ec.europa.eu/transparency/regdoc/rep/1/2014/EN/1-2014-297-EN-F1-1.Pdf

Darwish M., Aris A., Puteh M.H., Jusoh M.N.H., Kadir A.A., (2016), Waste bones ash as an alternative source of P for struvite precipitation, *Journal of Environmental Management,* **203**, 861-866.

Diwani G.E., Rafie S.E., Ibiari N.N.E., El-Aila H.I., (2007), Recovery of ammonia nitrogen from industrial wastewater treatment as struvite slow releasing fertilizer, *Desalination*, **214**, 200–214.

Franz M., (2008), Phosphate fertilizer from sewage sludge ash (SSA), *Waste Management*, **28**, 1809-1818.

Frost R.L., Weier M.L., Erickson K.L., (2004), Thermal decomposition of struvite, *Journal of Thermal Analysis and Calorimetry*, **76**, 1025-1033.

GD, (2004), Governmental Decision No.344/708 regarding the approval of technical standards on environmental protection and especially of soils when sewage sludge is used in agriculture, published in *Romanian Official Monitor*, No. 344 from 16th of August 2004, Bucharest, Romania.

Heffer P., Prud'homme M., (2014), *Fertilizer Outlook 2014–2018*. 82nd Annual Conf. Int. Fertilizer Industry Association, Sydney, Australia May 2014, 1-9.

Heraldy E., Rahmawatui F., Heyyanto H., Poernama P., (2017), Preparation of Struvite from desalination waste, *Journal of Environmental Chemical Engineering*, **5**, 1666-1675.

Hidalgo D., Corona F., Gomez M., Aguado A., Antolin G., (2014), Integrated and sustainable system for multi-waste valorization, *Environmental Engineering and Management Journal*, **13**, 2467-2475.

Huang H., Li B., Li J., Zhang P., Yu W., Zhao N., Guo G., Young B., (2019), Influence of process parameters on the heavy metal (Zn^{2+}, Cu^{2+} and Cr^{3+}) content of struvite obtained from synthetic swine wastewater, *Environmental Pollution*, **245**, 658-665.

Iovi A., Iovi C., (2004), *Ecological Technologies. Chemistry and Technology of Technique Phosphates*, Politehnica Publishing House, Bucharest, Romania.

ISO 6878, (2004), Water quality. Determination of phosphorus. Ammonium molybdate spectrometric method, On line at: https://www.iso.org/standard/36917.html

Jaffer Y., Clark T.A., Pearce P., Parsons S.A., (2002), Potential phosphorus recovery by struvite formation, *Water Research,* **36**, 1834– 1842.

Jalali M., Jalali M., (2016), Relation between various soil phosphorus extraction methods and sorption parameters in calcareous soils with different texture*, Science of the Total Environment*, **566**, 1080-1093.

Jeyakumar L., Zhao Y.Q., Hu Y.S., Babatunde A., Zhao X.H., (2019), Modelling high rate p-removal in a two-stage pilot scale alum sludge based constructed wetland system, *Environmental Engineering and Management Journal*, **18**, 359-366.

Kataki S., West H., Clarke M., Baruah D., (2016), Phosphorus recovery as struvite from farm, municipal and industrial waste: Feedstock suitability, methods and pre-treatments, *Waste Management*, **49**, 437–454

Le Corre K., Jones E., Hobbs P., Parsons S.A., (2005), Impact of calcium on struvite crystal size, shape and purity, *Journal of Crystal Growth*, **283**, 514-522.

Lederer J., Laner D., Fellner J., (2014), A framework for the evaluation of anthropogenic resources: the case study of phosphorus stocks in Austria, *Journal of Cleaner Production*, **84**, 368-381.

Li B., Boiarkina I., Young B., Yu W., (2016), Quantification and mitigation of the negative impact of calcium on struvite purity, *Advanced Powder Technology*, **27**, 2354-2362.

Łukawska M., (2014), Speciation analysis of phosphorus in sewage sludge after thermal utilization of sludge, *Inzynieria i Ochrona Srodowiska*, **17**, 433-439.

Mattenberger H., Fraissler G., Brunner T., Herk P., Hermann L., Obernberger I., (2008), Sewage sludge ash to phosphorus fertiliser: Variables influencing heavy metal removal during thermochemical treatment, *Waste Management*, **28**, 2709-2722.

Metaxa I., Petrea S.M., Mogodan A., (2019), Balance of phosphorus in two different types of cyprinids polyculture ponds, *Environmental Engineering and Management Journal*, **18**, 1821-1832.

Militaru B.A., Pode R., Manea F., Linul P.A., (2019), Simple and combined acidic extraction of phosphorus from sewage sludge ash, *Revista de Chimie (București)*, **70**, 133-139.

Millier H.K., Hooda P.S., (2011), Phosphorus species and fractionation. Why sewage derived phosphorus is a problem, *Journal of Environmental Management*, **92**, 1210-1214.

Moerman W., Carballa M., Wandekerckhove A., Derycke D., Werstraete W., (2009), Phosphate removal in agro-industry: pilot and full-scale operational considerations of struvite crystallization, *Water Research,* **43**, 1887-1892.

Munch E.V., Barr K., (2001), Controlled struvite crystallization for removing phosphorus from anaerobic digester side streams, *Water Research*, **35**, 151-159.

Pastor L., Mangin D., Ferrer J., Seco A., (2010), Struvite formation from the supernatants of an anaerobic digestion pilot plant, *Bioresource Technology,* **101**, 118-125.

Paul I., Varghese G., Ittyachem M.A., (2002), Thermal decomposition studies of struvite, *Indian Journal of Pure and Applied Physics*, **40**, 664-669.

Polat S., Sayan P., (2019), Application of response surface methodology with a Box–Behnken design for struvite precipitation, *Advanced Powder Technology,* **30**, 2396-2407.

Rahman M.M., Liu Y.H., Kwag, J.H., Ra C.S., (2011), Recovery of struvite from animal wastewater and its nutrient leaching loss in soil, *Journal of Hazardous Materials*, **186**, 2026–2030.

Ryu H.D., Kim D., Lee S.I., (2008), Application of struvite precipitation in treating ammonium nitrogen from semiconductor wastewater, *Journal of Hazardous Materials*, **156**, 163–169.

Sano A., Kanomata M., Inoue H., Sugiura N., Xu K., Inamori Y., (2012), Extraction of raw sewage sludge containing iron phosphate for phosphorus recovery, *Chemosphere*, **89**, 1243-1247.

Shiba N.C., Ntuli F., (2017), Extraction and precipitation of phosphorus from sewage sludge, *Waste Management*, **60**, 191-200.

Smol M., Kulczycka J., Kowalski Z., (2016), Sewage sludge ash (SSA) from large and small incineration plants as a potential source of phosphorus - Polish case study, *Journal of Environmental Management*, **184**, 617-628.

Schuiling R.D., Andrade A., (1999), Recovery of struvite from calf manure*, Environmental Technology*, **20**, 765-768.

Tunay O., Kabdasli, I., Orhon, D., Kolcak, S., (1997), Ammonia removal by magnesium ammonium phosphate precipitation in industrial wastewaters, *Water Science Technology*, **36**, 225-228.

UN, (2014), Concise Report on the World Population Situation in 2014, Department of Economic and Social Affairs, Population Division, United Nations.

Wei L., Hong T., Cui K., Chen T., Zhou Y., Zhao Y., Yin Y., Wang J., Zhang Q., (2019), Probing the effect of humic acid on the nucleation and growth kinetics of struvite by constant composition technique, *Chemical Engineering Journal*, **378**, 122-130.

Xu H., He P., Gu W., Wang G., Shao L., (2012), Recovery of phosphorus as struvite from sewage sludge ash, *Journal of Environmental Sciences*, **24**, 1533-1538.

Yan H., Shih K., (2016), Effects of calcium and ferric ions on struvite precipitation: A new assesment based on quantitative X-ray diffraction analysis, *Water Research*, **95**, 310-318.

Yu R., Geng J., Ren H., Wang Y., Xu K., (2013), Struvite pyrolysate recycling combined with dry pyrolysis for ammonium removal from wastewater, *Bioresource Technology,* **132**, 154–159.

Yuanyao Y., Huu Hao N., Wenshan G., Yiwen L., Jixiang L., Yi L., Xinbo Z., Hui J., (2017), Insight into chemical phosphate recovery from municipal wastewater, *Science of the Total Environment*, **576**, 159-171.

Zhang, X., Spanjers H., van Lier J.B., (2013), Potentials and limitations of biomethane and phosphorus recovery from sludges of brackish/marine aquaculture recirculation systems: a review, *Journal of Environmental Management*, **131**, 44-54.

Environmental Engineering and Management Journal

February 2020, Vol. 19, No. 2, 311-323
http://www.eemj.icpm.tuiasi.ro/; http://www.eemj.eu

"Gheorghe Asachi" Technical University of Iasi, Romania

OPTIMIZATION OF *CHLOROPHYLL A* REMOVAL FROM WASTEWATERS USING BIO-INSPIRED ALGORITHMS

Elena Niculina Dragoi[1,2], Silvia Curteanu[1*], Florin Leon[2], Ghasem Azarian[3], Kazem Godini[4], Lucian Eva[5], Vlad Dafinescu[5], Mihaela Dana Turliuc[5]

[1]"Gheorghe Asachi" Technical University of Iasi, Faculty of Chemical Engineering and Environmental Protection "Cristofor Simionescu", 73 Prof. D. Mangeron Blvd., 700050, Iasi, Romania
[2]"Gheorghe Asachi" Technical University of Iasi, Faculty of Automatic Control and Computer Engineering, 27 Prof. D. Mangeron Blvd., 700050, Iasi, Romania
[3]Hamadan University of Medical Sciences, Faculty of Health and Research Center for Health Sciences, Department of Environmental Health Engineering, Hamadan, Iran
[4]Kurdistan University of Medical Sciences, Research Institute for Health Development, Environmental Health Research Center, Sanandaj, Iran
[5]Emergency Clinical Hospital "Prof. Dr. Nicolae Oblu", Str. Ateneului, No. 2, 700309, Iasi, Romania

Abstract

The bio-inspired algorithms are versatile approaches that can be applied to a variety of problems. However, their efficiency is influenced by a multitude of characteristics such as quality of final solution, consumed computational resources, diversity management, convergence, complexity of the problem being solved. Consequently, the issue of choosing the best approach for a particular problem is a difficult task. In this work, the performance of two bio-inspired algorithms, Differential Evolution (an improved version) and Differential Search, is tested on an electro-coagulation process applied for removing *chlorophyll a* from the final effluent of aerated lagoons in a wastewater treatment plant. Based on a set of experimental data, a regression model was generated to determine the correlations between the process characteristics and the remained *chlorophyll a*. After that, a set of simulations using the two algorithms were performed with the goal of determining the optimal conditions leading to a minimization of *chlorophyll a* in two different cases: i) when the interval for the process parameters is the same with the experimental data and ii) when limits on the process parameters were imposed (as a mean to reduce the resources consumed). The results obtained indicated that the two algorithms are able to provide acceptable results.

Key words: electro-coagulation, chlorophyll a, differential evolution, differential search

Received: January, 2019; Revised final: February, 2020; Accepted: February, 2020; Published in final edited form: February, 2020

1. Introduction

One of the biggest challenges of the last century with regard to issues such as population growth, deforestation, rapid urbanization, industrialization and warming global climate change is water resources preservation. Nowadays, due to these factors, the access to safe drinking water is limited. Therefore, in order to maintain quality and improve quantity while also ensuring environmental protection and sustainability, there is a stringent need to develop efficient technologies for treating and managing all types of wastewaters (urban, industrial and agricultural wastewaters). Also, more robust and efficient drinking water treatments are required when dealing with risks posed by environmental contamination. Electrocoagulation (EC) is a process that combines the benefits of coagulation, flotation

---

[*] Author to whom all correspondence should be addressed: e-mail: silvia_curteanu@yahoo.com

and electrochemistry and it can be efficiently used for the treatment of drinking water and wastewater (Hakizimana et al., 2017; Lofrano and Meric, 2019; Moussa et al., 2017). EC is a green and eco-friendly process; besides, its reactions occur in a short time and investment costs are low (Ighilahriz et al., 2018; Mollah et al., 2001). The presence of algae in drinking water resources leads to change in taste, odour, and production of toxic materials. Moreover, the growth of algae in wastewater treatment plants causes suspended solid concentration to increase and exceed its standard (Fast et al., 2014). In the recent years, the EC method has been applied to remove algae from aqueous solutions (Fast et al., 2014; Uduman et al., 2011). However, the main downside of this way is the difficulty of optimizing the operating parameters as two or several parameters may react together and/or the relationship between response and one or a few factors is nonlinear.

In this work, an approach combining an improved version of Differential Evolution (DE) (that includes the opposition based principle, self-adaptation and a Local Search procedure), Differential Search (DS) and a statistical regression model is applied on an electro-coagulation process for the removal of *chlorophyll a* (as indicator of algae) from the final effluent of aerated lagoons in a wastewater treatment plant.

Because DE and DS are flexible and do not require special conditions for the properties of constraints and objective functions (Feoktistov, 2006), it can be effectively applied to solve the optimization of the electro-coagulation process. The objective is twofold: i) to efficiently optimize the considered process; and ii) to identify which of the two selected approaches is better suited for the problem at hand. As methodology, a regression model is first generated to determine the correlations between the process characteristics and the remained chlorophyll. Then, it was included into the optimization procedure in order to minimize the amount of *chlorophyll a*. Both optimizers provided a multitude of combinations leading to minimum values for *chlorophyll a.* However, DE tended to provide slightly better results (in term of the minimum: 1.16E-05 vs 8.97E-04) but DS had a higher exploration capability and generated solutions containing a higher variation in the process conditions.

2. State of the art

2.1. The electro-coagulation process

As it combines the benefits of coagulation, flotation and electrochemistry, EC is an emerging technology in water and wastewater treatment. EC is designed to work for any treatment capacity and has a series of advantages that leads to a good removal performance. For example, compared with chemical coagulation, the EC process generates lower quantity and more stable of sludge (Song et al., 2017).

In this process, since the electron is the primary reagent, there is no need for additional chemicals. Therefore, EC is considered as an environmentally friendly technology and many researchers studied the fundamentals and emerging applications of the EC technique in water and waste water treatment (Bazrafshan et al., 2012, Emamjomeh and Sivakumar, 2009, Garcia-Segura et al., 2017, Hakizimana et al., 2017, Kabdaşlı et al., 2012, Moussa et al., 2017, Song et al., 2017). This process has extensively been used to treat water and different kinds of wastewater. Most studies optimize parameters like electrode type, current density and other parameters effective in the process (Hakizimana et al., 2017). However, studies focusing on modelling the input and output variables of the system are still limited. Furthermore, microalgae harvesting by the EC process has attracted great attention of researchers across the world. An example of modelling is the study (Curteanu et al., 2011), where algal removal by the EC process is approached using different types of neural networks. Good results for the removal efficiency and other system parameters were reported proving that the neural modelling is an adequate modelling tool.

The theory behind coagulation/ flocculation and EC is basically the same. Both methods target the removal of particles from wastewater through destabilizing/ neutralizing the repulsive forces that keep the particles suspended in water. When the repulsive forces are neutralized, the suspended particles will form larger particles that can settle down for easier separation from water (Moussa et al., 2017). EC combines various mechanisms that can be electrochemical (metal dissolution and water reduction, pollutant electro-oxidation or electro-reduction), chemical (acid/base equilibria with pH change, hydroxide precipitation, redox reaction in the bulk) and physical (physical adsorption, coagulation, flotation). These can be sequential and/or parallel (Hakizimana et al., 2017). The EC process is based on the formation and aggregation of a colloidal system and its further coagulation enhanced by the use of the coagulating agents. Metallic and organic pollutants are separated from the aqueous phase by their precipitation with the coagulants and subsequently removed from the treated water. The aggregates formation is explained by the Derjaguin-Landau-Verwey-Overbeek theory where it is assumed that the formation of an aggregate depends on the interaction forces by the sum of Van der Waals and double layer forces (Garcia-Segura et al., 2017).

Although this process is utilized in many industries to remove different pollutants, the basis of contamination removal is nearly alike, which can be divided into five main mechanisms as follows:

(1) Metal ions (mainly aluminium and iron) are released from the sacrificed anode's surface with the exertion of electricity current to an electrochemical reactor.

(2) OH^- and H_2 ions are formed simultaneously on the cathode's surface.

(3) Polymeric species of aluminium and iron ions are formed in the solution.

(4) Pollutants and particles become unstable and accumulate and, in turn, flocks are formed via the mechanisms of electrostatic attraction and physical entrapment.

(5) Finally, the formed flocks are separated from the aquatic solution through two mechanisms: electro-flotation and sedimentation (Azarian et al., 2018, Mollah et al., 2001, Yavuz and Ögütveren, 2018).

The possible reactions over the process using the aluminium electrode are as follows:

Anode:

$$Al_{(s)} \rightarrow Al^{3+}_{(ag)} + 3e^{-} \quad (1)$$

$$2H_2O_{(L)} \rightarrow O_{2(g)} + 4H^{+}_{(L)} + 4e^{-} \quad (2)$$

Cathode:

$$2H_2O_{(L)} + 2e^{-} \rightarrow H_{2(g)} + 2OH^{-}_{(ag)} \quad (3)$$

Solution bulk:

$$2Al + 6H_2O + 2OH^{-} \rightarrow 2Al(OH_4^{-}) + 3H \quad (4)$$

$$nAl(OH)_3 \rightarrow Al_n(OH)_{3n} \quad (5)$$

Chlorophyll a reaction:

$Fe(OH)n$ or $Al_n(OH)_{3n}$ + *chlorophyll a* → removal by using sedimentation or flotation (6)

2.2. Optimization

In case of real-world processes, due to the complex interactions and high number of parameters (that not always can be correctly measured), the optimization problem is much difficult. Therefore, efficient approaches able to cope with all these aspects must be applied. Generally speaking, there are two main classes of optimizers: exact (deterministic) techniques and stochastic algorithms (Weise and Chiong, 2015). The majority of the exact optimizers are based on gradients (eq. Steepest Descent. Quasi-Newton etc.) and always find the same solution if they start from the same point (Mirjalili et al., 2017). On the other hand, the stochastic optimizers use stochastic operators and do not require derivatives. As a result, even if they start from the same point, stochastic optimizers provide different solutions, making them less reliable.

However, due to the randomness behaviour, they can avoid the local optima, this being one of the main advantages of stochastic algorithms (Mirjalili et al., 2017). For this type of algorithms, different classifications can be applied, the most encountered variants being based on: i) source of inspiration (biological, environment, human behaviour, physics, chemistry, etc.); and ii) number of random solutions generated at each step (individual based and population based). The majority of algorithms are population based and, in the latest years, a raising trend of developing new stochastic optimizers was observed. The majority of these algorithms are meta-heuristics, in the sense that they provide a general framework with a heuristic strategy for exploring the solution space (Sörensen, 2015).

The list of meta-heuristics optimizers is quite long, in the last ten years, more than 200 new algorithms being proposed. Table 1 presents some examples of algorithms, organized based on their source of inspiration. As it can be observed from Table 1, there are many meta-heuristics that can be chosen to solve the current problem.

Table 1. Example of meta-heuristic optimizers

Source		***Examples of algorithms***
Animals	Birds	Hummingbird Optimization Algorithm (Zhuoran et al., 2018); Emperor Penguin Optimization (Dhiman and Kumar, 2018); Seagull Optimization Algorithm (Dhiman and Kumar, 2019); Owl Search Algorithm (Jain et al., 2018)
	Mammals	Spotted Hyena Optimization (Dhiman and Kumar, 2017); Binary Artificial Sheep Algorithm (Wang et al., 2017); Rhino Heard (Wang et al., 2018); Squirrel Search Algorithm (Jain et al., 2019)
	Insects	Butterfly Optimization (Arora and Singh, 2018); Grasshopper Optimization Algorithm (Saremi et al., 2017); Pity beetle algorithm (Kallioras et al., 2018)
Simple cell	Viruses	Virus Optimization Algorithm (Liang and Cuevas Juarez, 2015); Virus Colony Search (Li et al., 2016)
	Eukaryote	Physarum Optimization (Liang et al., 2015);
	Prokaryote	Bacterial Gene Recombination Algorithm (Hsieh, 2014)
Plants		Artificial Algae Algorithm (Uymaz et al., 2015); Hybrid Artificial Root Foraging Optimization (Liu et al., 2017); Tree Growth Algorithm (Cheraghalipour et al., 2018)
Environment		Rain-fall Optimization Algorithm (Aghay Kaboli et al., 2017); Lightning Attachment Procedure Optimization (Nematollahi et al., 2017); Farmland Fertility (Shayanfar and Gharehchopogh, 2018)
Human behaviour	Social behaviour	Queuing Search Algorithm (Zhang et al., 2018); Future Search Algorithm (Elsisi, 2019); Team Arrangement Heuristic Algorithm (Babayan and Tahani, 2019); Poor and Rich optimization algorithm (Moosavi and Bardsiri, 2019)
	Services	Market Competition Behaviour (Qiu and Liu, 2016)
	Music and sports	World Competitive Contests (Masoudi-Sobhanzadeh and Motieghader, 2016); Volleyball Premier League (Moghdani and Salimifard, 2018);
Physics		Optics Inspired Optimization (Husseinzadeh Kashan, 2015); Electro-Search algorithm (Tabari and Ahmad, 2017); Henry Gas solubility optimization (Hashim et al., 2019)

However, identifying the appropriate metaheuristic for optimizing a complex problem is not always an easy task as there are multiple traits that can be considered: quality of the final solution, efficiency, diversity management, convergence. In addition, the performance is also influenced by the characteristics of the problem being solved: convexity, derivability, non-linearity.

From the multitude of bio-inspired optimization metaheuristics the literature presents, in this work, two population based algorithms were selected: DE (Storn and Price, 1995) and DS (Civicioglu, 2012) and applied comparatively. The main reason for choosing these two algorithms consists in the fact that they proved efficient for a variety of problems. In addition, DE is well known and can be considered as a reference for the newer approaches (such as DS).

DE is inspired from the Darwinian principle of evolution and is one of the most popular algorithms from its class (Wu et al., 2018) because it has a simple structure, it is efficient and simple to use. Over the years, different strategies to improve its performance were proposed: i) use of adaptation and self-adaptation for the control parameters (Peñuñuri et al., 2016); ii) steps alteration (Sallam et al., 2017; Vaishali et al., 2018; Zhang and Zhang, 2017); iii) hybridization with other approaches (Ahandani, 2016; Cai et al., 2016; Nama et al., 2016). Two observations are worth mentioning regarding DE: i) although it is not a recent algorithm, it still proves its efficiency, exceeding many other algorithms; ii) as the mentioned literature shows, a lot of work is being done on DE, respectively, different techniques are applied for its improvement, thus obtaining new variants, with higher performances. As a result, in its simple form or combined with other approaches, DE was successfully used to solve a variety of problems from different domains.

In the area of environmental protection and wastewater treatment, examples of applications include: i) support for environmental decision making (Cortes et al., 2002); ii) design of a continuous ion exchange process for the wastewater treatment (Bochenek et al., 2011); iii) depollution of gaseous streams (Curteanu et al., 2014); iv) soil remediation (Sobariu et al., 2017); v) removal of heavy metals (Bleotu et al., 2018); vi) water quality monitoring (Yazdi, 2018). Compared with DE, DS is a newer algorithm. It is inspired from the Brownian motion of migrating organisms and shows a good potential for being better than the state-of-the-art approaches. As it is still in its infancy, its effectiveness was not fully tested on a variety of cases and only a few improvements and adaptations were proposed (Kumar et al., 2015; Liu, 2014; Liu et al., 2016). Similar to the other metaheuristics, DS is a flexible algorithm and can be used for various applications like: solar photovoltaic panels (Paital et al., 2018), image processing (Gunen et al., 2016; Kotte et al., 2018), reactive power dispatch (Abaci and Yamaçli, 2017), identification of the 2-Chlorophenol oxidation model (Chen et al., 2015)

3. Case study

3. 1. Wastewater properties and analysis

Bu Ali Industrial Town, Hamedan, Iran, has a waste water treatment plant (WWTP) containing an aerated lagoon system without sludge return. It receives the sewage of different industries (600 m^3/day) and its daily capacity is 800 m^3. The main treatment processes of this plant include preliminary treatment (screening), two aerated lagoons (complete mix reactors), and a sedimentation lagoon. At the end of the process, the effluent is chlorinated and used for agricultural usages. One of the problems with this plant is that it cannot meet the out standard levels because of algae growth, particularly in warm seasons. The properties of the effluent have been indicated in Table 2.

Table 2. Physicochemical characteristics of the Bu Ali Industrial Town WWTP effluent

Parameters	*Value*
Chlorophyll a/(mg/m^3)	*739±687*
COD /(mg/L)	*197±66*
TSS /(mg/L)	*150±63*
pH	*6.9±1.1*
Salinity /(mg/L)	*2323±1840*
TDS /(mg/L)	*2400±1900*

In order to detect the concentration of algae, a spectrophotometric method was used, according to the Standard Methods for *chlorophyll a* determination (Association and Association, 1989). Also, for measurement of COD and TSS, open reflex and gravimetric methods were applied, respectively. TDS and pH were determined using a lab pH-meter (from Hach Co).

3.2. Experimental setup

In this study, a 6-compartment pilot-scale reactor with continuous flow was used (Fig. 1). It should be noted that, since the concentration of algae changes during different hours a day because of sunlight, an equalization basin was used prior to the electrochemical reactor. The main reactions (Eqs. 1-5) take place in the first chamber (8 L) and sedimentation and separation occur in the second chamber (12 L). So as to study the variables, current density (0.7-12 A/L), hydraulic contact time (5 - 60 min), different distances between electrodes (1-3.5 cm), and electrode type (stainless steel and aluminium) with monopolar arrangement were operated. Moreover, the size and effective surface of the electrodes and flow rate were as follows: 14 x 24 cm, 3300 cm^2 and 10 - 100 L/h, respectively. In order to provide electricity, a DC power supply with the range of 0 - 100 A for current and 0 - 50 V for voltage (Adak, ps_405, Hamadan Kit CO, Iran) was used.

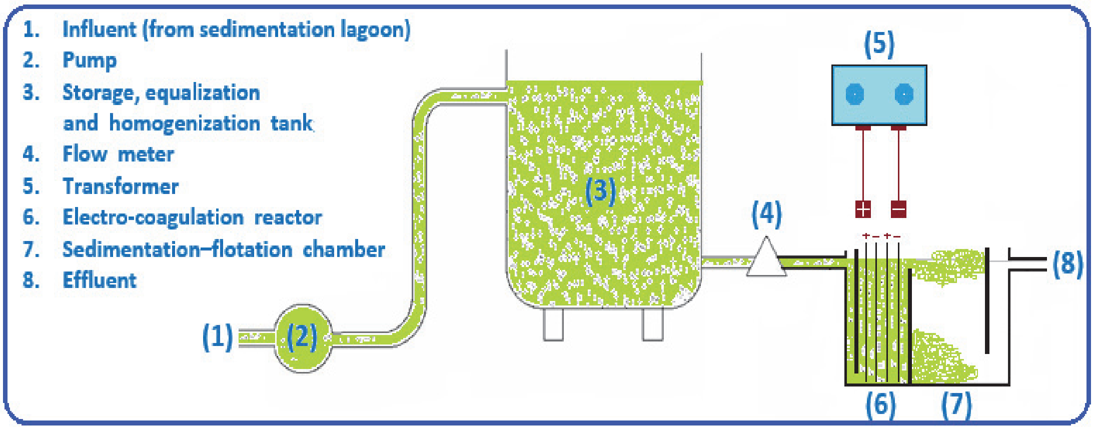

Fig. 1. A schematic diagram of the electrochemical reactor used in this study

A very important point here is that hydrogen micro-bulbs are generated on the surface of any cathode. In contrast, the mechanisms governing algae removal depend on the kind of anode. For instance, in the case of the stainless-steel electrode, oxygen gas is released from water electrolysis and, in turn, the main mechanism is electro-flotation by the generation of oxygen and hydrogen micro-bulb on the anode and cathode surface, respectively. When the aluminium electrode is used, aluminium ions are released and metal hydroxides, as well as different species of monomer and polymeric aluminium are formed, which are the main reason for electrocoagulation (Eqs. 1-6) (Azarian et al., 2018; Curteanu et al., 2011; Yavuz and Ögütveren, 2018).

The process analysis was done in different conditions of retention time (5-50 min) and using two types of electrodes based on aluminium and stainless steel, with different distances between electrodes (from 1.0 to 3.5 cm)

4. Process optimization

The complexity of the mechanism involved in the electrochemical process makes difficult the development of a phenomenological model, and, consequently, a regression model was determined. After that, a series of simulations were performed with DE and DS by varying the algorithms settings (various combinations of control parameters and a self-adaptive procedure) and the results were analysed and compared.

4.1. Differential search

In the DS algorithm, the population represents an artificial super-organism that migrates (Civicioglu, 2012). During the migration process, the members of the population (also known as artificial organisms) change their position, the decision to stay in a new position (stopover site) being determined based on the fitness function (Guney et al., 2014). This movement is repeated until a stop criterion is reached.

A simplified schema of the DS algorithm is presented in Fig. 2.

(1) In the first step, the DS parameters (population size and individual length) are initialized. If the size of the population (*N*) is user defined and can be changed at every run, the individual length is in close correlation with the problem dimensionality (*D*). For the initial DS algorithm, the length of the individual is equal to *D*.

(2) After that, based on a random number generator, the initial population is generated:

$$x_{i,j} = rand * \left(up_j - low_j\right) + low_j \qquad (7)$$

where *rand* is a randomly generated number in the interval (0,1), *up* and *low* represent the upper and the lower limits, i=1..N and j=1..D.

The evaluation of the individuals in the population is realized based on a fitness function. For the problem considered in this case, the fitness is represented by the mean squared error between the regression model predictions and the experimental data.

(3) In the donor selection step, a random shuffling procedure is applied in order to discover the stopover site and then the donor is randomly selected: $donor = x_{r1}$, where r1=1..N.

(4) In order to determine the stopover site, a set of parameters need to be reset: *scale*, p_1 and p_2. Scale controls the change occurring in the position of the individuals and is determined according to Eq. (8). The DS control parameters (p_1 and p_2) influence the degree of trial pattern mutation in comparison with the target patterns (Alkan and Balkaya, 2018) and their most suitable values are p_1=0.3*rand and p_2=0.3*rand.

$$scale = randg * (2 * rand1) * (rand2 - rand3) \qquad (8)$$

where *randg* is a random number generated with the gamma distribution and *rand1, rand2* and *rand3* are generated with a normal distribution.

(5) The stopover site is determined with Eq. (9):

$$s_i = x_i + scale * (donor - x_i) \qquad (9)$$

(6) If the fitness of the stopover site is better than the current position, the individual moves to the new position.

4.2. Differential Evolution

Similar to the DS algorithm, DE works with a population of potential solutions. The optimum is found by evolving the solutions (through mutation, crossover and selection) until a stop criterion is reached. Various studies (Al-Dabbagh et al., 2018; Dragoi and Dafinescu, 2015; Sallam et al., 2017; Vaishali et al., 2018; Zhu et al., 2016) showed that although the initial DE version proposed in (Storn and Price, 1995) is powerful enough to solve complex problems, its performance can be improved through the application of different approaches such as Opposition based Learning (OBL) (Tizhoosh, 2005), local search and/or self-adaptive control parameters. Therefore, in this work, an improved DE approach is used (Fig. 3).

(1) In the first step, the parameters (population size and individual length) of the algorithm are initialized. As this is an improved DE version, the control parameters (*F*, *Cr*) are automatically selected based on a self-adaptive procedure. This implies that the individuals forming the population contain these variables and they are modified using the same mechanism used for the other characteristic of the individual.

(2) Then, the initial solutions are generated using the same mechanisms as in DS case (Eq. 7). In order to improve this initial set of solutions, the OBL approach is applied. The individuals with the best fitness function are kept in the population, while the others are discarded.

(3) In the mutation step, a set of new individuals are generated based on the existing ones. The approach considered is called differentiation and, in this work, has the following form:

$$x_i^{mutated} = x_{base} + F(x_{r1} - x_{r2}) + F(x_{r3} - x_{r4}) \tag{10}$$

where: x_{base} is the base vector (which in this work is randomly selected from the population) and *r1*, *r2*, *r3*, *r4* are randomly selected from the population ($base \neq r1 \neq r2 \neq r3 \neq r4$) and ordered based on the corresponding individual's fitness function from the best to worst.

(4) After that, the characteristic of the individuals from the mutated population and from the current population are combined using a binomial crossover. The resulting trial population is then evaluated to determine the fitness of its individuals.

(5) In the selection step, the current and the trial population are competing one to one, the winners forming the new generation.

(6) In the last step, the best solution found so far is identified and improved using the Local Search algorithm.

5. Results and discussion

Based on the experimental setup, a set of 44 points were gathered. The measured parameters and their statistical information are presented in Table 3, where, for the electrode type, 0 indicates aluminium and 1 stainless steel.

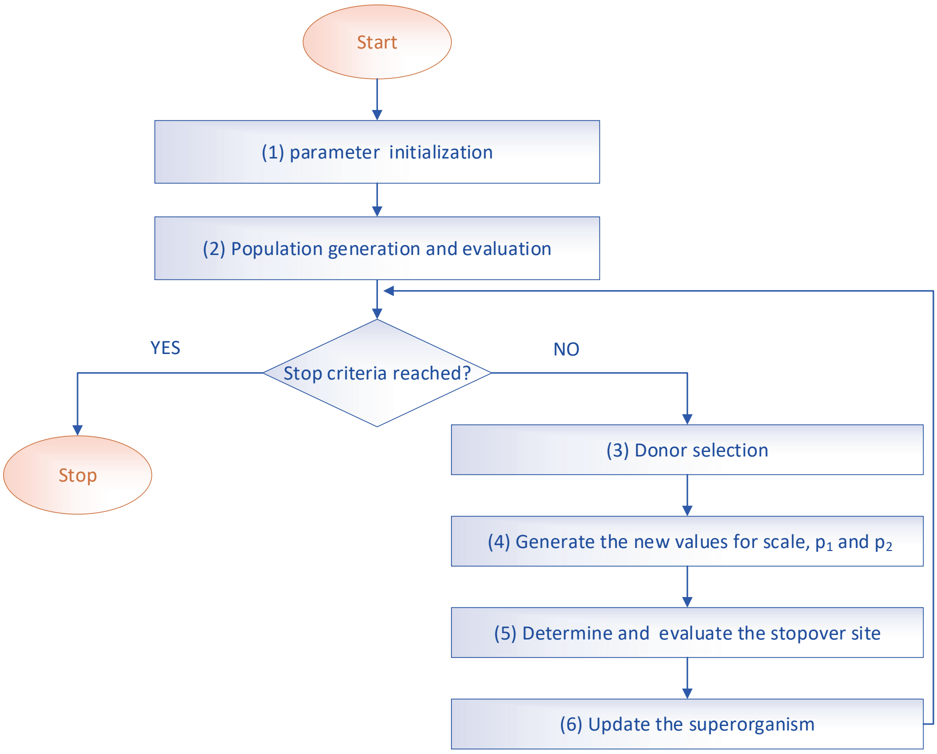

Fig. 2. DS general schema

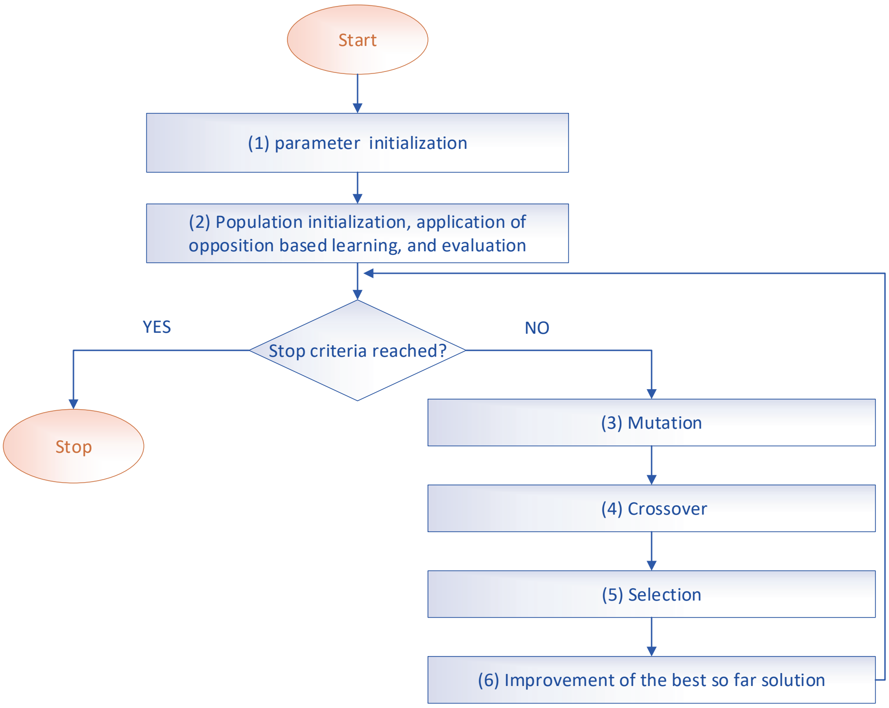

Fig. 3. General schema of the DE algorithm

5.1. Regression model

The regression model was determined based on the experimental data using Minitab 17 software. The objective was to generate predictions of the final amount of *chlorophyll a*, determined as function of initial values of *chlorophyll a* and operation conditions (electric power, time, electrode distance and electrode type). Initially, all order two interactions were considered. For this combination of process characteristics, the F-test (that displays the results based on the normal distribution and that is better than Bonett's test and Levene's test for normal distributions) indicates that the null hypothesis can be rejected and that the model provides a better fit than the intercept-only approach (Table 4). However, the p-value (the probability of making a Type 1 error) is higher than the significance value (0.05) for a multitude of sources. Consequently, these sources must be removed one by one until all sources have a p-value < 0.05. Table 5 presents the final combination that respects this condition (Eq. 11).

$$Final\_cholorophyll\ a = 397.9 - 1.659*Power - 16.57*Time + 0.0661*Initial\_chlorophyll\ \underline{a} + 0.001251*Power*Power + 0.3065*Time*Time + 41.22*Electrode\_distance*Electrode\_distance - 8.45*Time*Electrode\_distance - 3.97*Time*Electrode\_type + 0.6421*Electrode\_type*Initial\_cholorophyll\ a \tag{11}$$

Table 3. Characteristics of the experimental dataset

	***Power* (*W dm*$^{-3}$)**	***Time* (*min*)**	***Electrode Distance (cm)***	***Electrode type***	***Initial Chlorophylla (mg/m*^{3}*)***	***Final Chlorophylla (mg/m*^{3}*)***
Minimum	50	5	1	0	550	0
Maximum	600	40	3.5	1	1415	1220
Standard deviation	117.9953	9.319231	0.4702	0.5	352.9903	389.0013

Table 4. Analysis of variance for all the order two combination of process parameters

Source	***DF***	***Adj SS***	***Adj MS***	***F-Value***	***P-Value***
Regression	14	6299331	449952	216.19	0
Power	1	21279	21279	10.22	0.004
Time	1	25911	25911	12.45	0.002
Electrode_distance	1	3835	3835	1.84	0.186
Electrode_type	1	2297	2297	1.1	0.303
Cholorophylla_i	1	13277	13277	6.38	0.018
Power*Power	1	31982	31982	15.37	0.001

Source	***DF***	***Adj SS***	***Adj MS***	***F-Value***	***P-Value***
Time*Time	1	19811	19811	9.52	0.005
Electrode_distance*Electrode_distance	1	12326	12326	5.92	0.022
cholorophylla_i*cholorophylla_i	1	12063	12063	5.8	0.023
Power*Electrode_type	1	1196	1196	0.57	0.455
Power*cholorophylla_i	1	3146	3146	1.51	0.23
Time*Electrode_type	1	19231	19231	9.24	0.005
Electrode_distance*Electrode_type	1	0	0	0	0.988
Electrode_type*cholorophylla_i	1	295782	295782	142.12	0
Error	27	56194	2081	-	-
Total	41	6355525	-	-	-

Table 5. Analysis of variance for the final regression model

Source	***DF***	***Adj SS***	***Adj MS***	***F-Value***	***P-Value***
Regression	8	6284417	785552	364.56	0
Power	1	89108	89108	41.35	0
Cholorophylla_i	1	10922	10922	5.07	0.031
Power*Power	1	22271	22271	10.34	0.003
Time*Time	1	21622	21622	10.03	0.003
Electrode_distance*Electrode_distance	1	121069	121069	56.19	0
Time*Electrode_distance	1	33200	33200	15.41	0
Time*Electrode_type	1	14704	14704	6.82	0.013
Electrode_type*cholorophylla_i	1	1749235	1749235	811.78	0
Error	33	71108	2155	-	-
Total	41	6355525	-	-	-

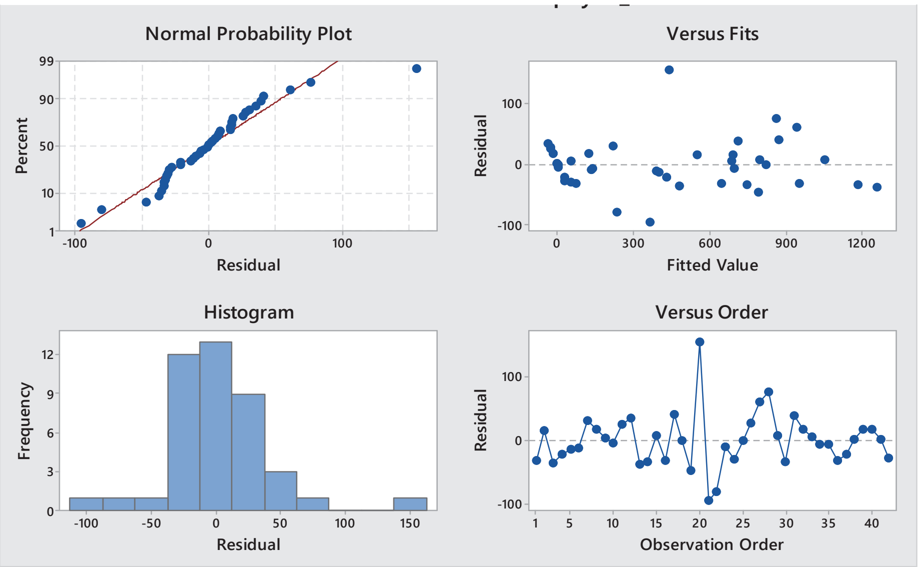

Fig. 4. Residual plots for the regression model

For the model represented by Eq. (11), the R^2 is 98.88% and R^2 predicted is 97.8%. In addition, the residual plots show that there is a good fit between predictions and experimental data (Fig. 4).

5.2. Process optimization

In order to determine the best conditions leading to the minimization of the *chlorophyll a* amount, the regression model (Eq. 11) was introduced in two optimization procedures and then the process was optimized considering two distinct situations: i) when no limits were imposed on the values of the process variables (free optimization) and ii) when limits were imposed to the power and time (as means to reduce the consumed resources). For the population based optimizers (such as DS and DE), a high diversity greatly contributes to the algorithm performance (Črepinšek et al., 2013). There are many types of diversity measures (that can be applied at phenotypic, genotypic or of combination of the two levels). In this work, the Euclidian distance for both the phenotype and the genotype was computed. Fig. 5 presents the evolution of population diversity during one run of DS and DE algorithms when population size = 20 and number of generations = 50.

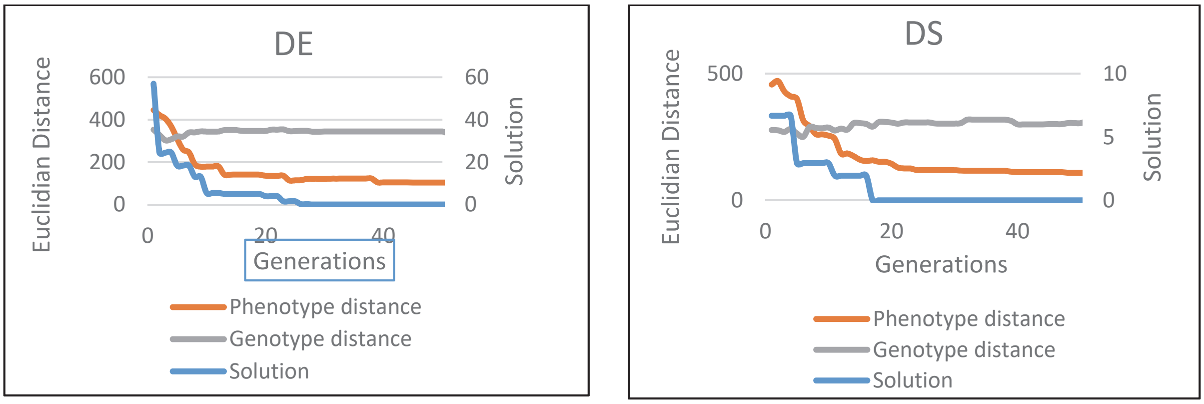

Fig. 5. The variation of genotype and phenotype Euclidian distance of population for a run of DE and DS algorithms

Table 6. Optimization results when no limits are imposed to the process parameters

Algorithm	***Power***	***Time***	***Electrode distance***	***Electrode type***	***Initial chlorophyll a***	***Final chlorophyll a***
DE	439.0825	17.10557	1.658527	1	674.05	1.16E-05
	273.1378	25.7525	2.955883	1	805.8041	3.32E-05
	113.0527	14.43881	1.736773	0	553.4427	4.88E-05
	181.1513	23.83266	2.464719	1	597.2389	6.65E-05
	56.75889	20.52621	2.311446	0	1269.269	0.000131889
	181.1439	23.83296	2.464157	1	597.2393	0.000191438
	63.41612	18.02164	1.750245	0	629.5137	0.000209039
	81.75216	18.12765	2.165013	0	1020.361	0.000273067
	66.4293	19.34524	1.913533	0	1127.098	0.000278022
	269.2604	34.54132	2.384222	1	1078.049	0.000328435
DS	569.0366	38.48206	1.829056	1	1319.474	0.000897
	441.9285	22.51206	1.631638	1	845.3106	0.001279
	82.3452	16.86449	1.638057	0	685.7981	0.002221
	249.9485	22.38937	3.342996	1	588.3224	0.003566
	357.9998	26.02614	2.215163	1	914.3702	0.006044
	157.6763	30.67182	1.957816	1	739.4357	0.006905
	145.191	14.16615	1.773388	0	1096.574	0.009847
	494.1183	15.86036	2.865394	1	579.8832	0.010892
	583.1663	23.74353	2.268303	1	991.3192	0.011091
	204.0818	13.50792	2.667839	0	1022.926	0.011521

As it can be observed, as the best solution found so far tends to go to the known optimum, the diversity of the genotype slightly varies (but tends not to decrease), while the diversity of the phenotype decreases (fact which indicates that the all solutions corresponding to the algorithm population are closer to each other – thus indicating convergence).

For each case, simulations with the two algorithms were performed with the same parameters as previously mentioned for diversity measurement. The results obtained are listed in Table 6 (when no limits are imposed), Table 7 (when the power is reduced to half) and Table 8 (when both power and time are reduced to half). In all cases, the optimization results obtained with DS tend to be higher than the ones provided by DE. This indicates that DE has a better ability to determine solutions in the vicinity of the optimum.

However, DE has a series of improvements which were not included in the DS. Consequently, using the same computational resources, DS is able to provide solutions that are very close to the ones provided by state-of-the-art approaches. By analysing the results from Table 7, it can be observed that for DE, the best solutions include a single type of electrode, while DS provides good solutions with both types of electrodes.

Table 7. Optimization results when power is max 300 (W dm^{-3})

Algorithm	***Power***	***Time***	***Electrode distance***	***Electrode type***	***Initial Chlorophyll a***	***Final Chlorophyll a***
DE	173.978	23.90775	2.162471	1	582.952	0.000020
	240.2209	8.534644	1.014559	0	1184.092	0.000024
	154.8637	13.52497	1.339635	0	1152.587	0.000039
	121.7448	14.9971	1.947845	0	840.3587	0.000172
	103.0692	16.99657	1.547172	0	1156.265	0.00018
	240.2348	8.528611	1.005121	0	1184.096	0.0002
	86.9473	38.15249	2.017428	1	786.5364	0.000306
	58.76761	39.61623	2.788856	1	905.0404	0.000314
	184.2887	27.95771	3.405659	1	743.4344	0.000353
	207.8778	14.50962	3.153631	0	688.5527	0.00038
DS	244.6455	27.60734	2.589079	1	839.0545	0.000156
	269.001	25.89906	1.701132	1	758.5855	0.000403
	126.915	14.39722	1.657018	0	846.318	0.000453
	270.8095	28.1681	1.496425	1	789.1706	0.00402
	195.7066	33.6045	2.728779	1	975.5855	0.004628
	296.8384	25.96891	2.331379	1	845.2135	0.004756
	200.3242	39.16004	2.578027	1	1126.356	0.005049
	247.9442	38.62538	1.111742	1	825.386	0.005292
	195.1983	12.60131	2.245067	0	1054.5	0.006194
	286.7926	34.11249	1.647067	1	962.9404	0.006812

Table 8. Optimization results when power is maximum 300 (W dm^{-3}) and time is maximum 20 (min)

Algorithm	***Power***	***Time***	***Electrode distance***	***Electrode type***	***Initial Chlorophyll a***	***Final Chlorophyll a***
DE	266.2541	8.643512	1.719983	0	1197.21	0.000003
	121.8393	14.70286	1.427637	0	853.0357	0.000004
	181.7065	11.71665	1.855785	0	848.5507	0.000010
	122.3597	16.40069	1.458446	0	1363.444	0.000011
	88.114	18.34693	2.147467	0	1244.182	0.000025
	191.8063	10.08559	1.072846	0	820.1439	0.000046
	235.4215	9.468854	1.124013	0	1370.725	0.000064
	169.6223	13.08194	1.467117	0	1290.162	0.000078
	128.2034	19.30973	3.312592	0	1332.756	0.000102
	250.1725	7.305586	1.300235	0	818.6908	0.000172
DS	203.4231	12.66206	2.484784	0	905.309	0.000206
	265.8488	11.86848	2.637116	0	1301.496	0.000663
	198.3828	13.58535	2.492489	0	1218.969	0.000918
	266.9814	8.022167	1.99729	0	605.34	0.00106
	273.2927	10.61477	2.54385	0	980.921	0.001385
	276.7541	19.22381	2.508266	1	557.9237	0.001457
	212.4807	11.18528	1.96101	0	1088.547	0.001726
	230.5229	8.928798	1.765343	0	700.5778	0.00223
	299.0072	18.31621	2.265906	1	563.0647	0.004593
	226.3156	10.38376	2.043597	0	902.6361	0.005762

This indicates that, for the considered case study, DS has a tendency to capture different characteristics of the search space and thus locate more variations of the parameters that lead to good solutions.

6. Conclusions

In this work, the performance of two bio-inspired optimizers, DE and DS, was performed and analysed when applied to determine the optimal conditions leading to the minimization of the *chlorophyll a* (as an indicator of algae) from the final effluent of aerated lagoons in a waste treatment plant of Bu-Ali Industrial Estate. The method employed for the removal of *chlorophyll a* is indirect electrolysis and the experiments were performed varying different conditions: retention time, power, type of electrodes (aluminium and stainless steel) and distance between the electrodes.

In order to optimize the process, a model describing the relation between parameters is required. As there are complex mechanisms involved in the electrochemical process and the development of a phenomenological model is difficult, in this work, a two-order regression model was determined. After that, the two algorithms (DE and DS) were applied to determine the conditions for which the highest percent of *chlorophyll a* is removed.

Two distinct cases were considered: i) when no limits on the parameters were imposed (and they vary within the experimental interval) and ii) when limits on some of the parameters were imposed: a) limited power and b) limited power and time.

Using the same settings for number of iterations and population size, a multitude of parameter combinations were identified. In all the optimization cases, both algorithms were able to provide good results. Overall, DS tends to provide slightly worst solution, but had a better capability of providing more combination of parameters leading to acceptable results.

Acknowledgements

This work was supported by "Program 1. Development of the national system for research and development. Postdoctoral research projects" financed by UEFISCDI, project no. 23/2018.

References

Abaci K., Yamaçli V., (2017), Optimal reactive-power dispatch using differential search algorithm, *Electrical Engineering,* **99,** 213-225.

Aghay Kaboli S.H., Selvaraj J., Rahim N.A., (2017), Rain-fall optimization algorithm: A population based algorithm for solving constrained optimization problems, *Journal of Computational Science,* **19**, 31-42.

Ahandani M.A., (2016), Opposition-based learning in the shuffled bidirectional differential evolution algorithm, *Swarm and Evolutionary Computation,* **26**, 64-85.

Al-Dabbagh R.D., Neri F., Idris N., Baba M.S., (2018), Algorithmic design issues in adaptive differential evolution schemes: Review and taxonomy, *Swarm and Evolutionary Computation,* **43**, 284-311.

Alkan H., Balkaya Ç., (2018), Parameter estimation by Differential Search Algorithm from horizontal loop electromagnetic (HLEM) data, *Journal of Applied Geophysics,* **149**, 77-94.

Arora S., Singh S., (2018), Butterfly optimization algorithm: a novel approach for global optimization, *Soft Computing,* **23**, 715-734.

Azarian G., Miri M., Nematollahi D., (2018), Combined electrocoagulation/electrooxidation process for the COD removal and recovery of tannery industry wastewater, *Environmental Progress & Sustainable Energy,* **37**, 637-644.

Babayan N., Tahani M., (2019), Team Arrangement Heuristic Algorithm (TAHA): Theory and application, *Mathematics and Computers in Simulation,* **166**, 155-176.

Bazrafshan E., Moein H., Kord Mostafapour F., Nakhaie S., (2012), Application of electrocoagulation process for dairy wastewater treatment, *Journal of Chemistry,* **2013**, 1-8.

Bleotu I., Dragoi E.N., Mureşeanu M., Dorneanu S.-A., (2018), Removal of Cu(II) ions from aqueous solutions by an ion-exchange process: Modeling and optimization, *Environmental Progress & Sustainable Energy,* **37**, 605-612.

Bochenek R., Sitarz R., Antos D., (2011), Design of continuous ion exchange process for the wastewater treatment, *Chemical Engineering Science,* **66**, 6209-6219.

Cai Y., Zhao M., Liao J., Wang T., Tian H., Chen Y., (2016), Neighborhood guided differential evolution, *Soft Computing,* **21**, 4769-4812.

Chen G.Z., Wang J.Q., Li R.Z., (2015), Parameter Identification of the 2-chlorophenol oxidation model using improved differential search algorithm, *Journal of Chemistry,* **2015**, 1-10.

Cheraghalipour A., Hajiaghaei-Keshteli M., Paydar M.M., (2018), Tree growth algorithm (TGA): A novel approach for solving optimization problems, *Engineering Applications of Artificial Intelligence,* **72**, 393-414.

Civicioglu P., (2012), Transforming geocentric cartesian coordinates to geodetic coordinates by using differential search algorithm, *Computers & Geosciences,* **46**, 229-247.

Cortes U., Rodriguez-Roda I., Sanchez-Marre M., Comas J., Cortes C., Poch M., (2002), *DAI-DEPUR: An Environmental Decision Support System for the control and supervison of Municipal WasteWater Treatment Plants,* Proc. of the 15th European Conf. on Artificial Intelligence, IOS Press, Amsterdam.

Črepinšek M., Liu S.-H., Mernik M., (2013), Exploration and exploitation in evolutionary algorithms: A survey, *ACM Computing Surveys (CSUR),* **43**, 1-33.

Curteanu S., Piuleac C.G., Godini K., Azaryan G., (2011), Modeling of electrolysis process in wastewater treatment using different types of neural networks, *Chemical Engineering Journal,* **172**, 267-276.

Curteanu S., Suditu G.D., Buburuzan A.M., Dragoi E.N., (2014), Neural networks and differential evolution algorithm applied for modelling the depollution process of some gaseous streams, *Environmental Science and Pollution Research,* **21**, 12856-67.

Dhiman G., Kumar V., (2017), Spotted hyena optimizer: A novel bio-inspired based metaheuristic technique for engineering applications, *Advances in Engineering Software,* **114**, 48-70.

Dhiman G., Kumar V., (2018), Emperor penguin optimizer: A bio-inspired algorithm for engineering problems, *Knowledge-Based Systems,* **159**, 20-50.

Dhiman G., Kumar V., (2019), Seagull optimization algorithm: Theory and its applications for large-scale industrial engineering problems, *Knowledge-Based Systems,* **165**, 169-196.

Dragoi E.-N., Dafinescu V., (2015), Parameter control and hybridization techniques in differential evolution: a survey, *Artificial Intelligence Review,* **45**, 447-470.

Elsisi M., (2019), Future search algorithm for optimization, *Evolutionary Intelligence,* **12**, 21-31.

Emamjomeh M.M., Sivakumar M., (2009), Review of pollutants removed by electrocoagulation and electrocoagulation/flotation processes, *Journal of Environmental Management,* **90**, 1663-1679.

Fast S.A., Kokabian B., Gude V.G., (2014), Chitosan enhanced coagulation of algal turbid waters– Comparison between rapid mix and ultrasound coagulation methods, *Chemical Engineering Journal,* **244**, 403-410.

Feoktistov V. (2006), *Differential Evolution: in Search of Solutions,* Berlin, Springer.

Garcia-Segura S., Eiband M.M.S., De Melo J.V., Martínez-Huitle C.A., (2017), Electrocoagulation and advanced electrocoagulation processes: A general review about the fundamentals, emerging applications and its association with other technologies, *Journal of Electroanalytical Chemistry,* **801**, 267-299.

Gunen M.A., Civicioglu P., Beşdok E., (2016), *Differential Search Algorithm Based Edge Detection. International Archives of the Photogrammetry*, Remote Sensing and Spatial Information Sciences - ISPRS Archives, 667-670.

Guney K., Durmus A., Basbug S., (2014), Antenna array synthesis and failure correction using differential search algorithm, *International Journal of Antennas and Propagation,* **2014,** 1-8.

Hakizimana J.N., Gourich B., Chafi M., Stiriba Y., Vial C., Drogui P., Naja J., (2017), Electrocoagulation process in water treatment: A review of electrocoagulation modeling approaches, *Desalination,* **404**, 1-21.

Hashim F.A., Houssein E.H., Mabrouk M.S., Al-Atabany W., Mirjalili S., (2019), Henry gas solubility optimization: A novel physics-based algorithm, *Future Generation Computer Systems,* **101**, 646-667.

Hsieh T.-J., (2014), A bacterial gene recombination algorithm for solving constrained optimization problems, *Applied Mathematics and Computation,* **231**, 187-204.

Husseinzadeh Kashan A., (2015), A new metaheuristic for optimization: Optics inspired optimization (OIO), *Computers & Operations Research,* **55**, 99-125.

Ighilahriz K., Ahmed M.T., Djelal H., Maachi R., (2018), Efficiency of an electrocoagulation treatment of water contaminated by hydrocarbons in a continuous mode powered by photovoltaic solar modules, *Environmental Engineering and Mnagement Journal*, **17**, 1521-1529.

Jain M., Maurya S., Rani A., Singh V., (2018), Owl search algorithm: a novel nature-inspired heuristic paradigm for global optimization, *Journal of Intelligent & Fuzzy Systems,* **34,** 1573-1582.

Jain M., Singh V., Rani A., (2019), A novel nature-inspired algorithm for optimization: Squirrel search algorithm, *Swarm and Evolutionary Computation,* **44**, 148-175.

Kabdaşlı I., Arslan-Alaton I., Ölmez-Hancı T., Tünay O., (2012), Electrocoagulation applications for industrial wastewaters: a critical review, *Environmental Technology Reviews,* **1**, 2-45.

Kallioras N.A., Lagaros N.D., Avtzis D.N., (2018), Pity beetle algorithm – A new metaheuristic inspired by the behavior of bark beetles, *Advances in Engineering Software,* **121**, 147-166.

Kotte S., Rajesh Kumar P., Injeti S.K., (2018), An efficient approach for optimal multilevel thresholding selection for gray scale images based on improved differential search algorithm, *Ain Shams Engineering Journal,* **9**, 1043-1067.

Kumar V., Chhabra J.K., Kumar D., (2015), Differential search algorithm for multiobjective problems, *Int. Conf. on Computer, Communication and Convergence (ICCC 2015),* **48**, 22-28.

Li M.D., Zhao H., Weng X.W., Han T., (2016), A novel nature-inspired algorithm for optimization: Virus colony search, *Advances in Engineering Software,* **92**, 65-88.

Liang L., Yuning S., Haiyang Z., Huadong M., Vasilakos A.V., (2015), Physarum optimization: A biology-inspired algorithm for the steiner tree problem in networks, *IEEE Transactions on Computers,* **64**, 818-831.

Liang Y.-C., Cuevas Juarez J.R., (2015), A novel metaheuristic for continuous optimization problems: Virus optimization algorithm, *Engineering Optimization,* **48**, 73-93.

Liu B., (2014), Composite differential search algorithm, *Journal of Applied Mathematics,* **2014**, 1-15.

Liu J., Teo K.L., Wang X., Wu C., (2016), An exact penalty function-based differential search algorithm for constrained global optimization, *Soft Computing,* **20**, 1305-1313.

Liu Y., Liu J., Ma L., Tian L., (2017), Artificial root foraging optimizer algorithm with hybrid strategies, *Saudi Journal of Biological Sciences,* **24**, 268-275.

Lofrano G., Meric S., (2019), A review on occurrence, measurement, toxicity and tannin removal processes from wastewaters, *Environmental Engineering and Management Journal*, **17**, 109-123.

Masoudi-Sobhanzadeh Y., Motieghader H., (2016), World Competitive Contests (WCC) algorithm: A novel intelligent optimization algorithm for biological and non-biological problems, *Informatics in Medicine Unlocked,* **3**, 15-28.

Mirjalili S., Gandomi A.H., Mirjalili S.Z., Saremi S., Faris H., Mirjalili S.M., (2017), Salp Swarm Algorithm: A bio-inspired optimizer for engineering design problems, *Advances in Engineering Software,* **114**, 163-191.

Moghdani R., Salimifard K., (2018), Volleyball premier league algorithm, *Applied Soft Computing,* **64**, 161-185.

Mollah M.Y.A., Schennach R., Parga J.R., Cocke D.L., (2001), Electrocoagulation - science and applications, *Journal of Hazardous Materials,* **84**, 29-41.

Moosavi S.H.S., Bardsiri V.K., (2019), Poor and rich optimization algorithm: A new human-based and multi populations algorithm, *Engineering Applications of Artificial Intelligence,* **86**, 165-181.

Moussa D.T., El-Naas M.H., Nasser M., Al-Marri M.J., (2017), A comprehensive review of electrocoagulation for water treatment: Potentials and challenges, *Journal of Environmental Management,* **186**, 24-41.

Nama S., Saha A.K., Ghosh S., (2016), A new ensemble algorithm of differential evolution and backtracking s algorithm with adaptive control parameter for function optimization, *International Journal of Industrial Engineering Computations,* **7**, 323-338.

Nematollahi A.F., Rahiminejad A., Vahidi B., (2017), A novel physical based meta-heuristic optimization method known as lightning attachment procedure optimization, *Applied Soft Computing,* **59**, 596-621.

Paital S.R., Ray P.K., Mohanty A., Dash S., (2018), Stability improvement in solar PV integrated power system using quasi-differential search optimized SVC controller, *Optik,* **170**, 420-430.

Peñuñuri F., Cab C., Carvente O., Zambrano-Arjona M.A., Tapia J.A., (2016), A study of the Classical Differential Evolution control parameters, *Swarm and Evolutionary Computation,* **26**, 86-96.

Qiu H., Liu Y., (2016), Novel heuristic algorithm for large-scale complex optimization, *Procedia Computer Science,* **80**, 744-751.

Sallam K.M., Elsayed S.M., Sarker R.A., Essam D.L., (2017), Landscape-based adaptive operator selection mechanism for differential evolution, *Information Sciences,* **418-419**, 383-404.

Saremi S., Mirjalili S., Lewis A., (2017), Grasshopper optimisation algorithm: Theory and application, *Advances in Engineering Software,* **105**, 30-47.

Shayanfar H., Gharehchopogh F.S., (2018), Farmland fertility: A new metaheuristic algorithm for solving continuous optimization problems, *Applied Soft Computing,* **71**, 728-746.

Sobariu D.L., Fertu D.I.T., Diaconu M., Pavel L.V., Hlihor R.M., Dragoi E.N., Curteanu S., Lenz M., Corvini P.F., Gavrilescu M., (2017), Rhizobacteria and plant symbiosis in heavy metal uptake and its implications for soil bioremediation, *New Biotechnology,* **39**, 125-134.

Song P., Yang Z., Zeng G., Yang X., Xu H., Wang L., Xu R., Xiong W., Ahmad K., (2017), Electrocoagulation treatment of arsenic in wastewaters: a comprehensive review, *Chemical Engineering Journal,* **317**, 707-725.

Sörensen K., (2015), Metaheuristics the metaphor exposed, *International Transactions in Operational Research,* **22**, 3-18.

Storn R., Price K., (1995), Differential evolution - a simple and efficient adaptive scheme for global optimization over continuous spaces. Berkley.

Tabari A., Ahmad A., (2017), A new optimization method: Electro-Search algorithm, *Computers & Chemical Engineering,* **103**, 1-11.

Tizhoosh H.R., (2005), *Opposition-Based Learning: A New Scheme for Machine Intelligence,* Int. Conf. on Computational Intelligence for Modeling, Control and Int. Conf. on Intelligent Agents,Web technologies and Internet Commerce, 2005/11/28/ Vienna, 695-701.

Uduman N., Bourniquel V., Danquah M.K., Hoadley A.F., (2011), A parametric study of electrocoagulation as a recovery process of marine microalgae for biodiesel production, *Chemical Engineering Journal,* **174**, 249-257.

Uymaz S.A., Tezel G., Yel E., (2015), Artificial algae algorithm (AAA) for nonlinear global optimization, *Applied Soft Computing,* **31**, 153-171.

Vaishali Y., Sharma T.K., Abraham A., Rajpurohit J., (2018), Enhanced asynchronous differential evolution using trigonometric mutation, *Advances in Intelligent Systems and Computing,* doi:10.1007/978-3-319-60618-7_38.

Wang G.-G., Gao X.-Z., Zenger K., Coelho L.D.S., *A novel metaheuristic algorithm inspired by rhino herd behavior*, Proc. of the 9th EUROSIM Congress on Modelling and Simulation, EUROSIM 2016, The 57th SIMS Conf. on Simulation and Modelling SIMS 2016, 2018, Linköping University Electronic Press, 1026-1033.

Wang W., Li C., Liao X., Qin H., (2017), Study on unit commitment problem considering pumped storage and renewable energy via a novel binary artificial sheep algorithm, *Applied Energy,* **187**, 612-626.

Weise T., Chiong R., (2015), An alternative way of presenting statistical test results when evaluating the performance of stochastic approaches, *Neurocomputing,* **147**, 235-238.

Wu G., Shen X., Li H., Chen H., Lin A., Suganthan P.N., (2018), Ensemble of differential evolution variants, *Information Sciences,* **423**, 172-186.

Yavuz Y., Ögütveren Ü., (2018), Treatment of industrial estate wastewater by the application of electrocoagulation process using iron electrodes, *Journal of Environmental Management,* **207**, 151-158.

Yazdi J., (2018), Water quality monitoring network design for urban drainage systems, an entropy method, *Urban Water Journal,* **15**, 227-233.

Zhang J., Xiao M., Gao L., Pan Q., (2018), Queuing search algorithm: A novel metaheuristic algorithm for solving engineering optimization problems, *Applied Mathematical Modelling,* **63**, 464-490.

Zhang X., Zhang X., (2017), Improving differential evolution by differential vector archive and hybrid repair method for global optimization, *Soft Computing,* **21**, 7107-7116.

Zhu Q., Lin Q., Du Z., Liang Z., Wang W., Zhu Z., Chen J., Huang P., Ming Z., (2016), A novel adaptive hybrid crossover operator for multiobjective evolutionary algorithm, *Information Sciences,* **345**, 177-198.

Zhuoran Z., Changqiang H., Hanqiao H., Shangqin T., Kangsheng D., (2018), An optimization method: hummingbirds optimization algorithm, *Journal of Systems Engineering and Electronics,* **29**, 386-404.

Environmental Engineering and Management Journal February 2020, Vol. 19, No. 2, 325-333
http://www.eemj.icpm.tuiasi.ro/; http://www.eemj.eu

"Gheorghe Asachi" Technical University of Iasi, Romania

PACKED COLUMN SIMULATION FOR CO_2 CHEMISORPTION IN ACTIVATED SOLUTIONS

Elisabeta Droniuc Hultuana[1], **Lidia Favier**[2], **Lacramioara Rusu**[3],
Igor Cretescu[4*], **Gabriela Ciobanu**[1], **Maria Harja**[1*]

[1] *"Gheorghe Asachi" Technical University of Iasi, Faculty of Chemical Engineering and Environmental Protection, Chemical Engineering Department, 73 Prof.dr.doc. Dimitrie Mangeron Blvd., 700050 Iasi, Romania*
[2] *University Rennes, Ecole Nationale Supérieure de Chimie de Rennes, CNRS, ISCR – UMR6226, F-35000 Rennes, France*
[3] *"Vasile Alecsandri" University of Bacau, Faculty of Engineering, 157 Mărăşeşti Blvd., 600115, Bacau, Romania*
[4] *"Gheorghe Asachi" Technical University of Iasi, Faculty of Chemical Engineering and Environmental Protection, Department of Environmental Engineering and Management, 73 Prof.dr.doc. Dimitrie Mangeron Blvd., 700050 Iasi, Romania*

Abstract

Apart of new equipment's development such as absorption columns with higher efficiency, for chemical industry, there is a strong need for greenhouse gases reduction in order to assure the environmental protection and, consequently, many studies regarding the purification methods of exhausted gases have been performed. There are several types of reactors used for gases purification, such as: bubbling jet reactor, combined packed and spray tower absorber, cable wet scrubber and packed column. Among these, chemisorption in packed column was considered and analysed in this paper because of its increased absorption rate achieved by adding of activators and providing a good contact between liquid and gas phases.

Using a validated model at industrial scale, the performance of a packed column under various conditions was assessed, aiming to establish the effects of several parameters as temperature, pressure, activator concentration, transformation degree, initial solution concentration, etc. on the purification process performance. Based on the obtained results, new reactors for purification of the exhausted gases generated from burning process of fossil fuels, can be designed.

Key words: activated solution, chemisorption, influence of parameters, packed column

Received: January, 2019; Revised final: February, 2020; Accepted: February, 2020; Published in final edited form: February, 2020

1. Introduction

Important chemical processes such as carbon dioxide (CO_2) capture, flue gas desulphurization, synthesis gas purification, sulphonation, carbonatation, ammonization, nitric acid synthesis, chlorination, hydrogenation, etc. involve an absorption process when they are used either for treatment purposes or manufacture of new products. These processes are commonly applied in organic and inorganic industries, as well as in environmental protection but the reactor modeling still have to be extensively studied (Harja et al., 2019).

Carbon dioxide (CO_2) is considered an important greenhouse gas that influences the climate change. The global warming caused by increasing emission of carbon dioxide is one of the most serious environmental problems (Berechet et al., 2019; Cai et al., 2019; Chisalita et al., 2019; Rotaru et al., 2019). Carbon dioxide constitutes the largest segment of the greenhouse gases that contribute to global warming and climate change. CO_2 is usually used as a reference for global warming potential (Aaron and Tsouris 2005; Năstase and Șerban, 2019).

Emissions of CO_2 result from waste incinerations, burning fossil fuel and wood, industrial

---

[*] Author to whom all correspondence should be addressed: e-mail: icre@tuiasi.ro; mharja@tuiasi.ro

processes such as cement, brick and glass manufacture, metallurgical plant, human activities etc. (EPA, 2019). Global emissions of carbon dioxide increased with an average of 2.0% per year. Based on estimation done by International Energy Agency (IEA), the global CO_2 emission has increased from approximately 21,000 Mt in 1990 to 28,000 Mt in 2006 (IEA, 2019). The CO_2 emission rate resulting from only fuel combustion was 32,000 Mt in 2014 and is predicted that this amount will be double in the next 50 years). Carbon dioxide resulted through burning of fossil fuel in thermoelectric plant, constitutes nearly 80% of the amount of all CO_2 discharged. This is the reason why the environmental effects of carbon dioxide are of great concern worldwide. The global warming caused by increasing emission of carbon dioxide is one of the most serious environmental problems. In the last years, researchers tried hard to control and reduce the CO_2 emissions into the atmosphere. Removal of carbon dioxide from flue gases is a key measure for reducing the CO_2 emission (Aroonwilas et al., 2003; Dincă and Badea, 2019; Zeng et al., 2013).

There are different industrial processes for gas treatment including the absorption into a physical or chemical liquid phase, absorption into ionic liquids; adsorption onto solids (zeolites, molecular sieves, activated carbon); membranes separation; cryogenic separation; biological fixation; chemical conversion in other compounds, etc. (Akinola et al., 2019a; Cowan et al., 2011; Harja, 1999; Yildirim et al., 2012). Among them, the absorption is the process recommended for removal of acidic contaminants, especially for removal of CO_2 from flue gases as a result of the fact that the solution can be regenerated with recovery of CO_2, or capitalization of final compounds as new products.

The absorption accompanied by chemical reaction (chemisorption) can be considered as a viable method for reducing CO_2 emission from exhaust gases. Chemically reactive solvents have to exhibit higher absorption capacity and higher mass transfer rates (Devries, 2014).

The possibilities to recover the reaction products, the financial investments (solvent, activators and equipment cost), CO_2 capitalization in other industrial area, energy requirements for regeneration process are the most important factors, decisive in selecting process (Fărmuș and Harja, 2017). The most widely used chemical solvents employed for removal of acid gases (CO_2, H_2S and COS) are:

- potassium carbonate solution with addition of amines (Hagiu and Harja, 1997; Harja et al., 2018; Hultuana et al., 2018; Ramazani et al., 2016),
- aqueous solution of amines such as: monoethanolamine (MEA), diethanolamine (DEA), trithanolamine (TEA), monoethylenediamine (MDEA), piperazine (PZ), diisopropanolamine (DIPA) etc. (Akinola et al., 2019b; Das et al., 2017; Ma'mun and Svendsen, 2018),
- ammonia solution with different additives (Zeng et al., 2013).

The potassium carbonate solutions promoted by amines was investigated by several research groups for implementation of new amines as additives for CO_2 absorption (Hu et al., 2017; Khan et al., 2017; Sivtsova et al., 2017). The promoted potassium carbonate solution at a temperature of 70-80°C has several advantage over an aqueous solution of amines consisting in lower cost, better suitability for regeneration process, no toxicity, noncorrosive behavior etc. (Behr et al., 2011; Harja and Siminiceanu, 2000; Qin et al., 2016). On the other hand, it presents also disadvantages, such as: low CO_2 loading capacity, high equipment corrosion, degradation of amines by SO_2, NO_2, HCl and O_2 from the flue gas, high energy consumption for regeneration, toxicity, negative impact over environment etc. (Tay et al., 2017).

The ammonia solution can be an alternative absorbent for removing CO_2 from flue gas, because it has high absorption capacity and fast absorption rate. Moreover, the salts formed from reaction with CO_2 can be used as liquid fertilizer. Aqueous ammonia is not easy to be degraded and the solution does not have a corrosion related problem. However, the process has disadvantages considering that the: temperature in absorber must be lower than 60°C in order to prevent decomposition of ammonium bicarbonate, fact that involves a supplementary cooling process. Other disadvantages are the high volatility and ammonia presence into the outlet gas (Tan et al., 2012).

There are several types of reactors for flue gas treatment as: bubbling jet, spray tower, cable bundle wet scrubber, packed column, perforated plates etc. (Altway et al., 2015; Petrescu and Harja, 2006; Xu et al., 2000; Yasari, 2017). Packed column is taken for analysis within this work, due to its increased absorption rate, as well as to the fact that it provides a good contact with liquid and gas phases.

In this paper the performance of a packed column (reactor) was assessed experimentally under various conditions aiming at finding the effects of process parameters, including temperature, pressure, activator concentration, decarbonation degree, concentration of potassium carbonate on the absorption efficiency for CO_2 capture. The data obtained can be used successfully for the design of industrial CO_2 capture reactors when low temperature and pressure conditions are used in order to ensure energy savings.

2. Data for simulation

The simulation is performed in order to determine the operating conditions of the column that would result in high productivity at low prices. For this purpose, the influence of the main parameters of the process was studied, including: temperature, pressure, amine concentration, initial solution concentration, degree of regeneration, etc. The absorption is carried out in a solution of K_2CO_3 and $KHCO_3$. The initial solution used within the studied process, has the following composition: 25-28%

K_2CO_3, 4-7% K $KHCO_3$, 1.9% DEA and 0.4% V_2O_5 at the inlet of the column, the combustion gases contain 20% CO_2 (Harja and Siminceanu, 2000).

The quantitative criterion considered was the CO_2 fraction at the outlet of the absorption column. A low CO_2 content at the column outlet involves an advanced purification of the combustion gases. Also extreme cases, impossible to be carried out in practice have been considered for the process simulation, including the use of all possible compositions for the regenerated solution, absorption in totally regenerated solutions etc. (Harja, 1999; Harja et al., 2019; Koronaki et al., 2015).

The mathematical model of the packed column consists of Eqs. (1 - 7) and was broadly described and validated in a previous work (Harja et al., 2019).

The data required for the simulation were obtained for an industrial column used in the ammonia industry (Bui et al., 2014; Choi et al., 2017; Harja et al., 2019; Wang et al., 2005). The simulation of the column aims at identifying the parameters that influence the process.

$$\frac{dy_{CO_2}}{dz} = -\frac{1}{\dot{n}_{A''}} v_{CO_2} AS_v \tag{1}$$

$$\frac{dy_{H_2O}}{dz} = -\frac{1}{\dot{n}_{A''}} (\pm N_{H_2O}) AS_v \tag{2}$$

$$\frac{d\dot{n}_g}{dz} = \dot{n}_{A''} \left(\frac{dy_{CO_2}}{dz} + \frac{dy_{H_2O}}{dz} \right) \tag{3}$$

$$\frac{d\dot{n}_L}{dz} = \frac{\dot{M}_L}{M_g} \left(\frac{d\dot{n}_g}{dz} \right) \tag{4}$$

$$\frac{dC_{Cb}}{dz} = \frac{\rho_L}{M_L \dot{n}_L} \left(-\frac{M_L}{\rho_L} C_{Cb} \frac{d\dot{n}_L}{dz} + v_{CO_2} AS_v \right) \tag{5}$$

$$\frac{dC_{Bc}}{dz} = \frac{\rho_L}{M_L \dot{n}_L} \left(-\frac{M_L}{\rho_L} C_{Cb} \frac{d\dot{n}_L}{dz} + 2v_{CO_2} AS_v \right) \tag{6}$$

$$M_g = \frac{8.6 + 44 \cdot y_{CO_2} + 18 \cdot y_{H_2O}}{1 + y_{CO_2} + y_{H_2O}} \tag{7}$$

The data required for the simulation were obtained for an industrial column used in the ammonia industry (Bui et al., 2014; Choi et al., 2017; Harja et al., 2019; Wang et al., 2005). The simulation of the column aims at identifying the parameters that influence the process.

3. Results and discussions

The mathematical model of the packed column with counter flow phase circulation under isobar-isothermal conditions, with a 4% error, has been considered for the simulation of the process (Harja et al., 2019; Harja et al., 2008; Petrescu et al., 1998).

3.1. Influence of temperature

Temperature is an important parameter in the CO_2 absorption process. The parameters used in process modeling, whose values vary with the temperature are: potassium bicarbonate solubility, Henry's constant, interface concentration, hydroxyl ion content, reaction rate constants, CO_2 diffusion coefficient through liquid phase, transfer mass partial coefficients, density and viscosity of the liquid phase (Harja et al., 2008; Todinca et al., 2007). Considering that the temperature has an important effect upon the process, the influence of the temperature on the absorption rate of carbon dioxide in water, in potassium carbonate-bicarbonate solutions as well as in potassium carbonate-bicarbonate solutions activated with DEA has been investigated first. The temperature range studied was 273-373 K.

Fig. 1 shows the variation of the carbon dioxide absorption rate with temperature.

The temperature exponentially influences the rate of carbon dioxide absorption, as shown in Fig. 1. At the same time, it is obviously that the rate is strongly enhanced by adding the activator. Curves 1 and 2 of Fig. 1 correspond to an initial solution with the following composition: C_{K2CO} = 2.50 mol/L and C_{KHCO3}= 1.38 mol/L. The absorption rate at 350 K is nearly 10 folds higher in activated carbonate solutions compared to inactivated ones.

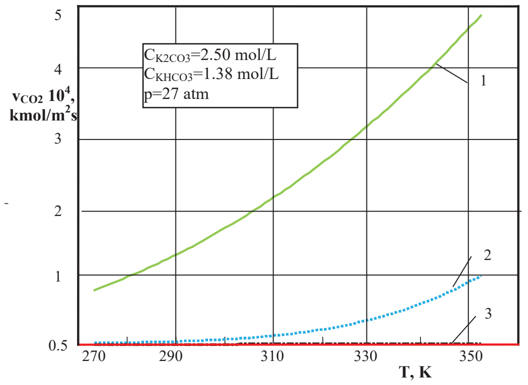

Fig. 1. The influence of temperature on CO_2 absorption rate: 1– C_{DEA}=0.01818 mol/L; 2 – C_{DEA}=0 mol/L; 3 – distilled water

In Fig. 2, the variation of the carbon dioxide fraction in gas, as function of the temperature is presented

For simulation, three temperatures, ranged between 353 and 373 K, were considered. The calculation was performed for the composition corresponding to the semi-generated solution. By increasing the temperature from 368 K to 378 K, the CO_2 fraction of 0.0084 in the gas phase at the column outlet, was obtained for a packing material height of

16 m. For these reasons, it is advisable to work at temperatures above 370 K avoiding thus, an advanced evaporation of the solvent. This is an advantage of the method since the combustion gas exhibits temperatures above 373 K after the economizer, thus saving energy also in the removal stage.

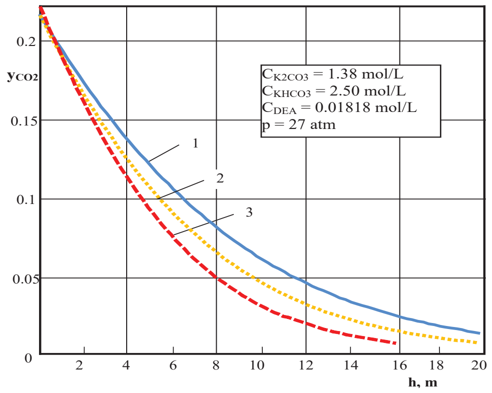

Fig. 2. The influence of temperature on CO_2, fraction profile: 1– 353 K, 2 – 368 K, 3 – 378 K

3.2. Influence of pressure

The pressure directly influences the absorption process rate. Increasing the pressure leads to an increase in the driving force of the process. The pressure values studied were ranged between 15 and 80 atm (Isa et al., 2016). According to Fig. 3, increase of absorption process rate with the pressure is higher at increased temperatures.

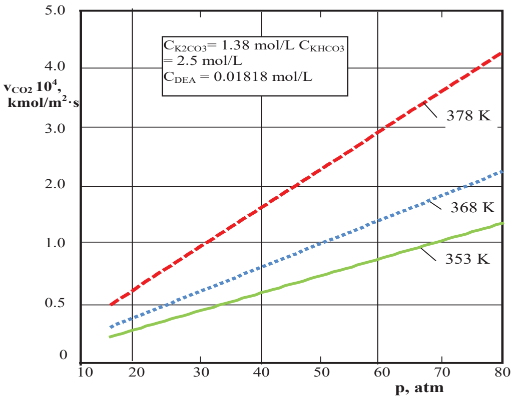

Fig. 3. The influence of pressure on the CO_2 absorption rate

By increasing the pressure from 20 atm to 80 atm, at a temperature of 378 K, the absorption process rate increases more than eight fold. The fact that the pressure has a strong positive influence on the absorption process suggests the necessity to increase the working pressure. However, the increasing of pressure lead to additional costs for process operation, and therefore an optimum should be established in order to assure a medium rate of the absorption process, corresponding to a reasonable operation costs. Fig. 4 depicts the variation of the CO_2 fraction from the gas phase with the pressure. The analysis was performed for pressures ranged between 15 atm and 40 atm.

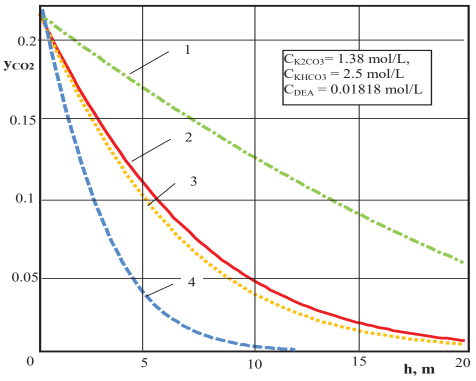

Fig. 4. The variation in y_{CO2} with the pressure: 1 – 15 atm, 2 – 27 atm, 3 – 30 atm, 4 – 40 atm

It has been found that, when pressure increases, the concentration of carbon dioxide in the column gas phase decreases more rapidly, as shown in Fig. 4, so that the volume of packing material required for reaching the same final concentration is much lower. By increasing the pressure from 30 atm to 40 atm, the height of the packing material necessary to achieve the same quality of the gas phase is lower. Although the increase in pressure results in a positive influence, there is no question of increasing the pressure over the value of the boiler, due to economic and safety related reasons. Working at constant pressure leads to energetic and financial savings.

3.3. Influence of amine concentration

As shown in Fig. 1, by adding the activator, the reaction rate increases with a factor depending on the amount of activator. Simulations for amine concentrations (DEA) ranging from 0.01818 mol/L to 0.025 mol/L were performed. In Fig. 5, the variation in the absorption rate with the amine concentration at different temperatures is described. Fig. 5 shows that at 360 K, the absorption rate is 1.5 10^{-4} kmol/m^2s K within the inactivated solution, whereas for the composition corresponding to the semi-generated solution with 0.01818 mol/L DEA, the absorption rate is 4.7 10^{-4} kmol/m^2s, hence, three fold higher.

Fig. 6 shows the variation in the CO_2 absorption rate with amine concentration, at 355 and 367 K. The amine concentration was considered in the range 0.01-0.18 mol/L, while the composition for which the calculations were performed is that of the semi-generated solution. From Fig. 6, one may see that at an amine concentration of 0.02 mol/L, the absorption rate has a value of 5.8, 10^{-4} kmol/m^2s, and the increase of the amine concentration to 0.1 mol/L results in an absorption rate of 12.1 10-4 kmol/m^2s. Consequently, a five-fold increase in the amine concentration results in the twofold increase in the absorption rate. Since, by increasing the amine concentration above a certain limit, the absorption rate increases insignificantly, it is not feasible from economic point of view to work with concentrations higher than 5 %.

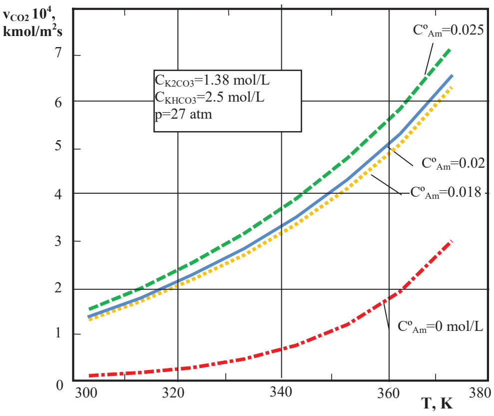

Fig. 5. Influence of amine concentration on CO_2 absorption rate

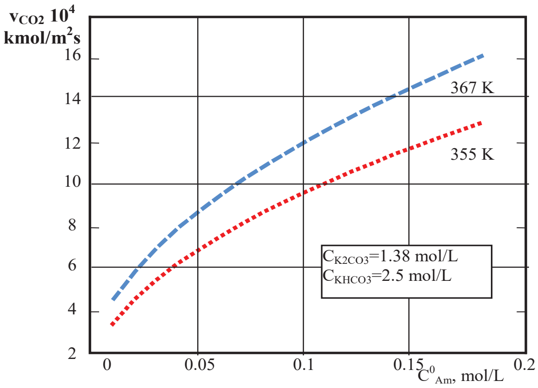

Fig. 6. The variation in CO_2 absorption rate with DEA concentration

In Fig. 7, the variation of the carbon dioxide fraction profile depending on the activator concentration is presented. In order to describe these dependencies, amine (DEA) concentrations ranging from 1.9% to 6% (0.018-0.05 mol/L) were used for calculation.

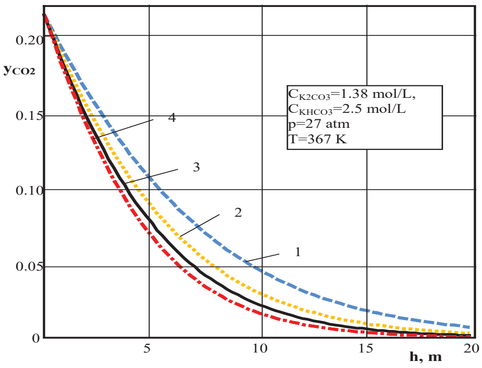

Fig. 7. Influence of amine concentration on CO_2 fraction: 1 – 0.018 mol/L; 2 – 0.03mol/L; 3 – 0.04 mol/L; 4 – 0.05 mol/L

Increasing the concentration of the activator leads to a faster decrease of the carbon dioxide fraction in the gas phase. However, by increasing the amine concentration from 0.04 mol/L to 0.05 mol/L, the decrease in carbon dioxide content in the gas phase is not significant. Due to this, as well as to high price and toxicity, it is not justified to increase the amine concentration above a certain limit.

The data presented in Fig. 6 and Fig. 7 leads to the conclusion that an optimal compromise is achieved by using an amine concentration of 0.05 mol/L

3.4. Influence of initial solution composition

If an increase in temperature requires high energy consumption and the pressure cannot be changed within very large limits, the composition of the liquid phase should be modified in order to obtain higher possible absorption rates (Wu et al., 2017). The composition of the initial solution has a significant influence on the CO_2 fraction in the gas phase. Fig. 8 shows the data obtained by simulating the column.

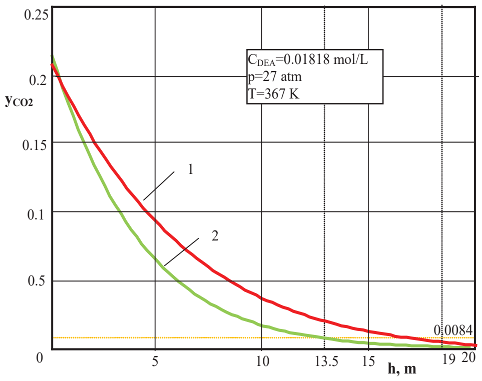

Fig. 8. The CO_2 fraction profile as function of initial solution concentration: 1 – C_{K2CO3}=1.7156, C_{KHCO3}=3.438; 2 – C_{K2CO3}=2.678, C_{KHCO3}=1.512 mol/L

Analyzing the data in Fig. 8 one may notice that, by regenerating the spent solution at the established value, the y_{CO2} fraction has the value of 0.0084 at a height of packing material equal to 5 m. The same value of the fraction, considering the actual composition, was obtained at a height of packing material of 19 m.

Since a significant influence of the initial solution composition on the carbon dioxide fraction was observed, the simulation of the packed column was performed under the conditions of several established initial solution compositions.

3.4.1. Absorption in potassium carbonate solutions

At the moment the plant started to work, the absorption column was fed with a potassium carbonate solution containing the activator in the established amount.

It has been analyzed the way how the potassium carbonate concentration in the initial solution in influences the carbon dioxide fraction profile. It was considered that the initial solution had a content of 20, 25, 30, 35, and 40% K_2CO_3, whereas the content in $KHCO_3$ was that corresponding to hydrolysis. The results achieved by simulation are shown in Fig. 9. Fig. 9 reveals that the increase in the potassium carbonate concentration into the initial solution does not involve the increasing in the degree of purity of the gas at the column outlet.

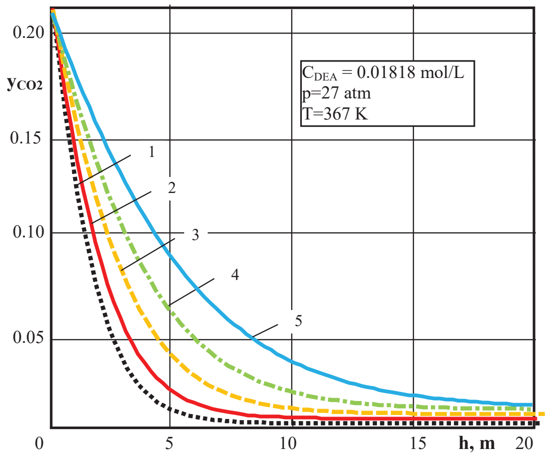

Fig. 9. The influence of potassium carbonate concentration in initial solution: 1 – 20% K_2CO_3; 2 – 25% K_2CO_3; 3 – 30% K_2CO_3; 4 – 35% K_2CO_3; 5 – 40% K_2CO_3

This can be explained by the fact that in diluted potassium carbonate solutions, the salting-out effect of potassium bicarbonate resulting from the chemical reaction does not appear very strongly. Increasing the potassium carbonate concentration in the solution has a significant influence on the Henry's constant. When working with 25% solutions at high temperatures, the negative influence of the potassium bicarbonate salting-out is avoided. Balance data analysis indicates a potassium carbonate concentration ranged between 2.3 and 2.5 mol/L. The results obtained by simulation are consistent with the equilibrium data.

3.4.2. Variable carbonate and constant bicarbonate contents

The solution used for absorption, will also contain potassium bicarbonate in amounts depending on the degree of regeneration of the spent solution, due to its recirculation. It was considered the case where the spent solution was regenerated to a potassium bicarbonate content equal to 0.64 mol/L. The concentration of potassium carbonate in the initial solution was assumed to be in the range 1.8-2.6 mol/L, while the potassium bicarbonate content was equal to 0.64 mol/L.

The variation of the carbon dioxide fraction from the gas phase along the first part of the column is shown in Fig. 10. Increasing the potassium carbonate content in the liquid phase, due to the occurrence of the salting-out, does not increase the absorption process performance, as shown in Fig. 10. When the bicarbonate content was considered to be 2 mol/L, the CO_2 absorption rate was influenced by the potassium carbonate content according to the dependencies depicted in Fig. 11. The highest absorption rate was obtained for the lowest concentration in potassium carbonate due to the above-mentioned salting-out effect. Fig. 12 shows the y_{CO2} profile in the gas phase for the concentration of 2 mol/L $KHCO_3$.

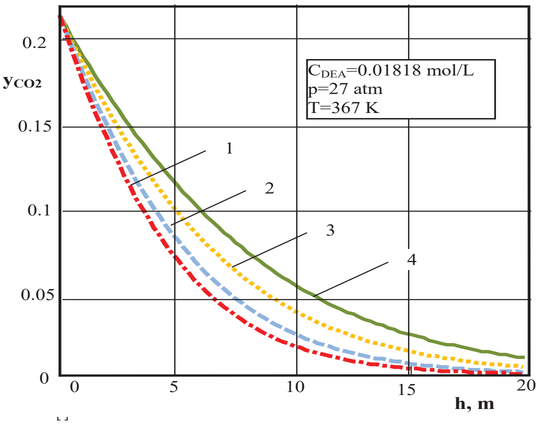

Fig. 10. The CO_2 fraction profile: 1– 1.8 mol/L K_2CO_3, 2 – 2.0 mol/L K_2CO_3, 3 – 2.3 mol/L K_2CO_3, 4 – 2.6 mol/L K_2CO_3

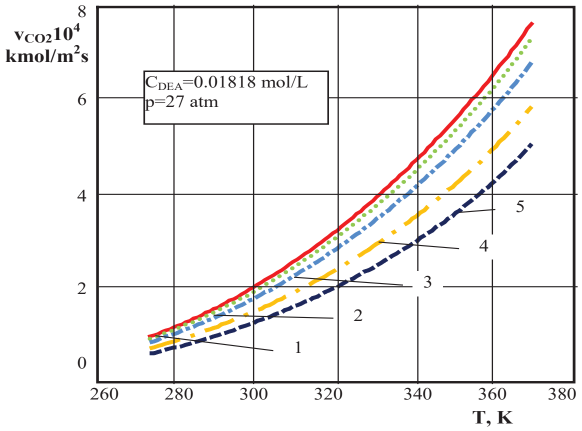

Fig. 11. The variation in the absorption rate with the initial solution concentration: 1 – 1.31 mol/L K_2CO_3, 2 – 1.38 mol/L K_2CO_3, 3 – 1.50 mol/L K_2CO_3, 4 – 1.75 mol/L K_2CO_3, 5 – 2 mol/L K_2CO_3

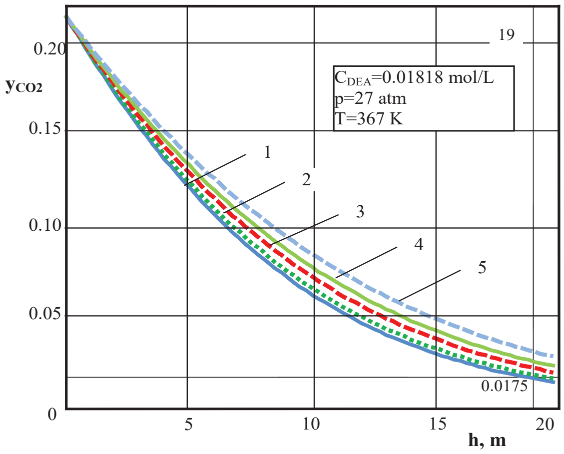

Fig. 12. The variation in CO_2fraction for 2 mol/L $KHCO_3$ solution: 1 – 1.31 mol/L K_2CO_3, 2 – 1.38 mol/L K_2CO_3, 3 – 1.50 mol/L K_2CO_3, 4 – 1.75 mol/L K_2CO_3, 5 – 2 mol/L K_2CO_3

From Fig. 12 it is found that the carbon dioxide fraction in the gas phase is not positively influenced by the increase of the carbonate concentration in the liquid phase. Given that the potassium bicarbonate content in the liquid phase was 2 mol/L, it was observed that the gas phase at the reactor outlet, at 19 m height, had a fraction of y_{CO2} = 0.0175. The calculated CO_2 fraction has a double value compared to the value of 0.0084, obtained in the previous cases.

3.4.3. Constant carbonate and variable bicarbonate contents

For potassium bicarbonate content in the range o1.8-2.5 mol/L and carbonation degrees in the range 27.2-37.5%, the potassium carbonate concentration was set to a value of 1.5 mol/L (Table 1). The y_{CO2} variation was shown in Fig. 13.

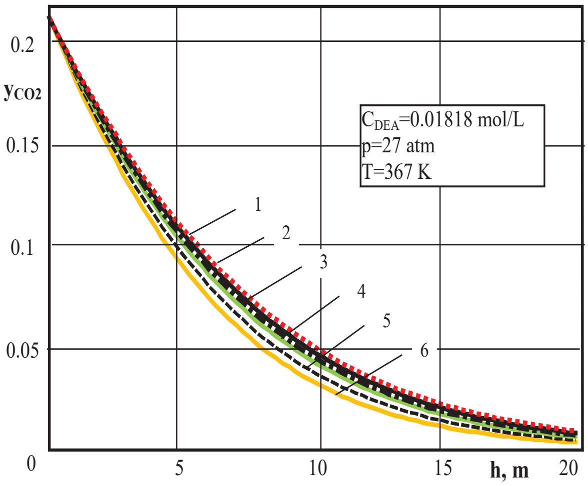

Fig. 13. The CO_2 fraction profile for K_2CO_3 constant concentrations

At the same potassium carbonate content, the increase in potassium bicarbonate concentration results in decreasing the absorption capacity of the solution. Fig.13 reveals that for a composition of C_{K2CO3} = 1.5 mol/L and C_{KHCO3} = 1.8 mol/L solution, a molar fraction of carbon dioxide in the gas phase of 0.0084 was obtained at a reactor height of 18 m. If the initial solution of potassium carbonate used for the absorption exhibits a concentration of 25% (2.31 mol/L), a regeneration up to 1.5 mol / L K_2CO_3 leads to good absorption results.

The data obtained from the mathematical model of the column show that the solution should exhibit a $KHCO_3$ content ranged between 1.5-1.75 mol/L (max. 2 mol/L). By using these concentrations for the feed solutions, a carbon dioxide content of the gas phase at the column outlet below 0.1% is ensured.

Table 1. The corresponding concentration of absorption solutions used in different experimental conditions

	1	*2*	*3*	*4*	*5*	*6*
C_{K2CO3}	1.5	1.5	1.5	1.5	1.5	1.5
C_{KHCO3}	2.5	2.4	2.3	2.2	2	1.8

4. Conclusions

The simulation presented in this paper aimed at establishing the operating conditions of a packed column. In this respect, the influence of the main parameters of the process was studied. Particular attention was paid to the establishment of concentrations in potassium carbonate, potassium bicarbonate and DEA that would lead to achieving of the desired quality for the gas phase. The influence of temperature, pressure and amine content on the CO_2 absorption rate was investigated. Given that high working pressures are not highly recommended for economic reasons, the possibilities to improve the process are related in particular to changing the temperature and composition of the initial liquid phase.

Temperature has a complex influence on absorption. At low temperatures, the solubility of potassium bicarbonate is low, fact that would lead to its crystallization. The rate of CO_2 absorption at 350 K is almost 10 times higher in activated solutions compared to inactivated ones.

Increasing pressure will increase the driving force of the process. Thus, at 378 K by increasing the pressure from 20 atm to 80 atm, an eight-fold increase in the absorption rate is observed.

By adding DEA as an activator, the reaction rate increases function of the amount added. The five-fold increase in amine concentration results in twofold increase in the rate of CO_2 absorption. Concentrations of around 5% are recommended in order to achieve the beneficial effect of increasing DEA concentration without affecting the economic aspects.

The composition of the initial solution has a significant influence on the CO_2 fraction profile in the final gas phase. The increase in the potassium carbonate concentration in the initial solution does not involve the increase in the degree of purity of the gas at the column outlet. This owe to fact that in the potassium carbonate diluted solutions, the $KHCO_3$ salting-out is not very strong. In order to avoid the occurrence of solid phase, 25% potassium carbonate solutions are recommended.

The analysis of the equilibrium data indicates a liquid phase composition in potassium carbonate within the range of 2.3-2.5 mol/L, according to the results obtained by simulation; The absorption process is not improved by the increase in potassium carbonate content in the liquid phase as a result of the appearance of the salting-out effect. At the same content in K_2CO_3, the increase in concentration of the solution in $KHCO_3$ causes the decrease in the absorption capacity. Increasing the carbonate level of the initial solution adversely affects the CO_2 fraction in the gas phase.

The data obtained leads to the conclusion that a total regeneration of the depleted/spent solution results in an advanced purity of the gas, but this also results into high costs in the desorption process. A compromise solution is recommended in the sense of partial regeneration of the solution supplied to the column. According to the obtained results, the semi-generated solution must have a $KHCO_3$ content within 1.5-1.75 mol/L (maximum 2 mol/L). The proposed column can be successfully used to absorb CO_2 from combustion gases.

Acknowledgements
We would like to thank "Gheorghe Asachi" Technical University Doctoral School of Iasi for financial support.

References

Aaron D., Tsouris C., (2005), Separation of CO_2 from flue gas: a review, *Separation Science and Technology*, **40**, 321-348.

Akinola T. E., Oko E., Wang M. (2019a), Study of CO_2 removal in natural gas process using mixture of ionic liquid and MEA through process simulation, *Fuel*, **236**, 135-146.

Akinola T.E., Oko E., Gu, Y., Wei H.L., Wang M., (2019b), Non-linear system identification of solvent-based post-combustion CO_2 capture process, *Fuel*, **239**, 1213-1223.

Altway A., Susianto S., Suprapto S., Nurkhamidah S., Nisa N.I.F., Hardiyanto F., Mulya H.R., Altway S., (2015), Modeling and simulation of CO_2 absorption into promoted aqueous potassium carbonate solution in industrial scale packed column, *Bulletin of Chemical Reaction Engineering & Catalysis*, **10**, 111-124.

Aroonwilas A., Chakma A., Tontiwachwuthikul P., Veawab A., Austgen D.M., Rochelle G.T., Peng X., Chen C.C., (2003), Mathematical modelling of mass transfer and hydrodynamics in CO_2 absorbers packed with structured packings, *Chemical Engineering Science*, **58**, 4037-4053.

Behr P., Maun A., Deutgen K., Tunnat A., Oeljeklaus G., Görner K., (2011), Kinetic study on promoted potassium carbonate solutions for CO_2 capture from flue gas, *Energy Procedia*, **4**, 85–92.

Berechet M., Mirel I., Staniloiu C., Fischer K., (2019), Carbon footprint of waste management in Romania in the context of circular economy, *Environmental Engineering Management Journal*, **18**, 1289-1295.

Bui M., Gunawan I., Verheyen V., Feron P., Meuleman E., Adeloju S., (2014), Dynamic modelling and optimisation of flexible operation in post-combustion CO_2 capture plants: A review, *Computer & Chemical Engineering*, **61**, 245-265.

Cai B., Yang W., Zhang L., Feng Y., (2019), Analysis of CO_2 emissions management performance in China at sub-province level, *Environmental Engineering and Management Journal*, **18**, 203-212.

Chisalita D.A., Petrescu L., Cobden P., van Dijk H.E., Cormos A.M., Cormos C.C., (2019), Assessing the environmental impact of an integrated steel mill with post-combustion CO_2 capture and storage using the LCA methodology, *Journal of Cleaner Production*, **211**, 1015-1025.

Choi J.H., Kim Y.E., Nam S.C., Park S.Y., Chun I.S., Yoon Y.I., Lee J.H., (2017), Promoter characteristic study on the K_2CO_3 absorbents for CO_2 capture: Mass transfer according to functional group and chain length of promoter, *Energy Procedia*, **114**, 898-905.

Cowan R.M., Jensen M.D., Pei P., Steadman E.N., Harju J.A., (2011), *Current status of CO_2 capture technology development and application*, National Energy Technology Laboratory US Department of Energy.

Das B., Deogam B., Mandal B., (2017), Experimental and theoretical studies on efficient carbon dioxide capture using novel bis (3-aminopropyl) amine (APA)-activated aqueous 2-amino-2-methyl-1-propanol (AMP) solutions, *RSC Advances*, **7**, 21518-21530.

Devries N.P., (2014), *CO_2 absorption into concentrated carbonate solutions with promoters at elevated temperatures*, MSc Thesis, University of Illinois at Urbana-Champaign, USA.

Dincă C., Badea A., (2019), Influence of desulphurization in the carbon dioxide absorption process using monoethanolamine, *Environmental Engineering and Management Journal*, **18**, 47-58.

EPA, (2019), *Climate Change Indicators in the United States*, On line at: https://www.epa.gov/climate-indicators.

Fărmuș R.E., Harja M., (2017), Experimental equipment used in the study of carbon dioxide absorption (I), *The Bulletin of the Polytechnic Institute from Iaşi - Chemistry and Chemical Engineering Section,* **63**, 23-33.

Hagiu C., Harja (Ivaniciuc) M., (1997), Determination of the enhancement factor for CO_2 Absorption in activated potassium carbonate solution, *Revista de Chimie*, **10-11**, 856-862.

Harja (Ivaniciuc) M., Siminiceanu I., (2000), Modelling and simulation of the industrial reactor for carbon dioxide absorption into activated potassium carbonate aqueous solution, *Ovidius University Annals Chemistry*, **XI**, 135-139.

Harja M., (1999), *Contributions to the modeling of gas – liquid absorption with chemical reaction*, PhD Thesis, "Gheorghe Asachi" Technical University, Iasi, Romania.

Harja M., Ciobanu G., Juzsakova T., Cretescu I., (2019), New approaches in modeling and simulation of CO_2 absorption reactor by activated potassium carbonate solution, *Processes*, **7**, 78-97.

Harja M., Ciobanu G., Rusu L., Lazar L., (2018), The enhancement factor approach for chemisorption process, *Environmental Engineering and Management Journal*, **17**, 813-820.

Harja M., Rusu L., Barbuta M., (2008), The viscosity and density of the aqueous solutions used for the absorption accompanied by chemical reaction, *The Bulletin of the Polytechnic Institute from Iaşi - Chemistry and Chemical Engineering Section*, **9**, 55-62.

IEA, (2019), Climate change. The energy sector is central to efforts to combat climate change, On line at: http://www.iea.org/topics/climatechange.

Hu G., Smith K., Wu Y., Kentish S., Stevens G., (2017), Recent progress on the performance of different rate promoters in potassium carbonate solvents for CO_2 capture, *Energy Procedia*, **114**, 2279-2286.

Hultuana E., Ciobanu G., Cretescu I., Lazar L., Tataru-Farmus R.E., Harja M., (2018), *Modeling of CO_2 Absorption Process in Activated Solutions*, European exhibition of creativity and innovation - Euroinvent, Iasi, Romania, 53-54.

Isa F., Suleman H., Zabiri H., Maulud A.S., Ramasamy M., Tufa L.D., Shariff A.M., (2016), An overview on CO_2 removal via absorption: Effect of elevated pressures in counter-current packed column, *Journal of Natural Gas Science and Engineering,* **33**, 666-677.

Khan A.A., Halder G.N., Saha A.K., (2017), Experimental investigation on efficient carbon dioxide capture using piperazine (PZ) activated aqueous methyldiethanolamine (MDEA) solution in a packed column, *International Journal of Greenhouse Gas Control*, **64**, 163-173.

Koronaki I.P., Prentza L., Papaefthimiou V., (2015), Modeling of CO_2 capture via chemical absorption processes - an extensive literature review, *Renewable and Sustainable Energy Reviews*, **50**, 547-566.

Ma'mun S., Svendsen H.F., (2018), Absorption of carbon dioxide in aqueous solutions of n-methyldiethanolamine mixtures, *IOP Conference Series: Materials Science and Engineering*, **358**, 12-19.

Năstase G., Șerban A., (2019), Experimental study on CO_2 capture in a residential space, *Environmental Engineering and Management Journal*, **18**, 1001-1011.

Petrescu S., Harja M., (2006), *Chemical Reactor for Heterogen Systems*, Venus Publishing House, 294.

Petrescu S., Mămăligă I., Ivaniciuc M., (1998), Enhancement factor of the mass transfer for chemisorption process, *Revista de Chimie*, **1**, 64-67.

Qin J.Y., Xie J.L., Fu D., (2016), *Absorption Rate of CO_2 in DEA Promoted K_2CO_3 Solution at High Temperatures*, Proc. Int. Conf. on Civil, Transportation and Environment, Guangzhou, 1160-1164.

Ramazani R., Mazinani S., Hafizi A., Jahanmiri A., Van der Bruggen B., Darvishmanesh S., (2016), Solubility and absorption rate enhancement of CO_2 in K_2CO_3, *Separation Science and Technology,* **51**, 327-338.

Rotaru C.S., Manciulea I., Draghici C., (2019), Effect of environmental monitoring on the environmental legislative process, *Environmental Engineering and Management Journal*, **18**, 1843-1847.

Sivtsova O.N., Eremenko S.I., Derevschikov V.S., Veselovskaya J.V., (2017), Kinetics of carbon dioxide absorption from air in a flow reactor with a fixed bed of K_2CO_3-based sorbent, *Russian Journal of Physical Chemistry A*, **91**, 850-855.

Tan L.S., Lau K.K., Bustam M.A., Shariff A.M., (2012), Removal of high concentration CO_2 from natural gas at elevated pressure via absorption process in packed column, *Journal of Natural Gas Chemistry*, **21**, 7-10.

Tay W.H., Lau K.K., Shariff A.M., (2017), High performance promoter-free CO_2 absorption using potassium carbonate solution in an ultrasonic irradiation system, *Journal of CO_2 Utilization*, **21**, 383-394.

Todinca T., Tănasie C., Pröll T., Căta A., (2007), Absorption with chemical reaction: evaluation of rate promoters effect on CO_2 absorption in hot potassium carbonate solutions, *Computer Aided Chemical Engineering*, **24**, 1065-1070.

Wang G., Yuan X., Yu K., (2005), Review of mass-transfer correlations for packed columns, *Industrial & Engineering Chemistry Research*, **44**, 8715-8729.

Wu Y., Mirza N.R., Hu G., Smith K.H., Stevens G.W., Mumford K.A., (2017), Precipitating characteristics of potassium bicarbonate using concentrated potassium carbonate solvent for carbon dioxide capture. Part I: Nucleation, *Industrial & Engineering Chemistry Research,* **56,** 6764-6774.

Xu Z., Afacan A., Chuang K., (2000), Predicting mass transfer in packed columns containing structured packing, *Chemical Engineering Research and Design*, **78**, 91-98.

Yasari E., (2017), A green industrial scale di-methyl ether reactor with aiming to CO_2 reduction: staging and multi-objective optimization approach, *Journal of the Taiwan Institute of Chemical Engineers*, **81**, 110-118.

Yildirim Ö., Kiss A.A., Hüser N., Leßmann K., Kenig E.Y., (2012), Reactive absorption in chemical process industry: A review on current activities, *Chemical Engineering Journal*, **213**, 371-391.

Zeng Q., Guo Y., Niu Z., Lin W., (2013), The absorption rate of CO_2 by aqueous ammonia in a packed column, *Fuel Processing Technology*, **108**, 76-81.

Environmental Engineering and Management Journal February 2020, Vol. 19, No. 2, 335-343
http://www.eemj.icpm.tuiasi.ro/; http://www.eemj.eu

"Gheorghe Asachi" Technical University of Iasi, Romania

AGRI-WASTES AS A LOW-COST ADSORBENT FOR NICOSULFURON HERBICIDE

Irina Gabriela Cara[1], Denis Topa[3], Anca Elena Calistru[3], Iuliana Motrescu[3], Laura Bulgariu[2], Gerard Jităreanu[3]*

[1] "Ion Ionescu de la Brad" University of Agricultural Sciences and Veterinary Medicine,
Research Institute for Agriculture and Environment, Aleea M. Sadoveanu Street, No. 3, 700490 Iasi, Romania
[2] "Gheorghe Asachi" Technical University, Faculty of Chemical Engineering and Environmental Protection,
D. Mangeron Street, 71A, 700050 Iasi, Romania
[3] "Ion Ionescu de la Brad" University of Agricultural Sciences and Veterinary Medicine, Faculty of Agriculture,
Aleea M. Sadoveanu Street, No. 3, 700490 Iasi, Romania

Abstract

The contamination of aquatic and terrestrial environments by pesticides is highlighted by their possible toxic properties and poor biodegradability on the environment. The development of low cost by products from agricultural sectors as a suitable solution for contaminated areas remediation is of great environmental interest. Straw wastes can be considered as a promising alternative to remove different chemical compound that are environmentally toxic.

In this study, some materials derived from agricultural (agri)-wastes (wheat and corn straw) in mixture with soil, were investigates as potential adsorbents for nicosulfuron removal. After mineralization (850°C) and KOH activation to obtain the biochars, the samples were structurally characterized by scanning electron microscopy and Fourier transform infrared spectroscopy. Interaction studies between nicosulfuron - biochars and soil were performed at various concentrations and pH of 7. The adsorbent capacity was evaluated using batch sorption test and liquid chromatography coupled with mass spectrometry. The characterization results showed different functional groups present in the structure of these biochars while surface analysis showed an increase of surface roughness. The Langmuir isotherm and pseudo second order mechanism describes the kinetics of nicosulfuron herbicide. The results obtained highlight the importance of agri-waste as a natural adsorbent, being a solution for the removal of nicosulfuron from contaminated environments.

Key words: adsorption, agri-wastes, nicosulfuron, soil, straw

Received: January, 2019; Revised final: February, 2020; Accepted: February, 2020; Published in final edited form: February, 2020

1. Introduction

Nicosulfuron (2-[(4, 6-dimethoxypyrimidin-2-ylcarbamoyl) sulfamoyl]-N, N-dimethylnicotinamide) is a selective herbicide adopted by Integrated Pest Management to advocate growth of healthy crops and minimize pesticide use. This management practices have engendered the use of new-generation pesticides applied at lower doses (but often in mixture), in order to improve their efficiency in the range of weeds treated (Carles et al., 2018). Despite their low application rate (60 g a.i. ha^{-1}) on soil surface, this herbicide is persistent and do not degrade into less harmful components. Their metabolites present significant ecological and health risks in biotic and abiotic matrices (Petric et al., 2016; Hlihor et al., 2019). Therefore, the efficient removal and recycling of nicosulfuron from environment have become a significant issue from economical and health perspectives.

Different types of methods such as photocatalytic degradation, advanced oxidation

---

* Author to whom all correspondence should be addressed: e-mail: gerardj@uaiasi.ro; Phone: +40 232407401; Fax: +40 232260650

processes, enzymatic biodegradation and adsorption are available to treat pesticides. Among these methods, adsorption is found to be promising technique due to its low operation cost, high attraction performance, and relatively low environmental impact (Ahmed and Hameed, 2018). Activated carbon (Suo et al., 2019), magnetic nanoparticles (Wang et al., 2017), silica nanomaterials (Kalhor et al., 2018) and graphene (Wanjeri et al., 2018) have been successfully utilized to treat various pesticide due to their high surface area and adsorption capacity. In terms of raw materials and preparation methods, these adsorbents are costly. For instance, the cost of activated carbon ranges between 1650 USD tons^{-1} to 9900 USD tons^{-1}, whereas that of carbon nanotubes is in the range of 20,000 - 80,000 USD tons^{-1} (Liu et al., 2018). Furthermore, the high cost of this approach has prompted the search for alternative that do not increases the operational price of treatment technique.

Recent findings have concentered on highly selective adsorbents of agriculture origin, as an efficient adsorbent in the field of land remediation, which can not only reduce the environmental charge but also achieve the effect of treating „waste by waste'' (Chesca et al., 2018; Huang, 2017; Periyaraman et al., 2019). Generally, the goal is to replace activated carbons - representing the state-of-the-art - by means of a byproduct coming from various activities such as agriculture and industry (De Gisi et al., 2016).

Straw biomass (wheat, corn, soybean, barley, rice, etc.) is a renewable energy source and very common all over the world. However, most straw biomass is incinerated and discarded, which has caused serious environmental pollution (Li et al., 2017). At present, modified biomass adsorption contaminants have been extensively studied, being reported to have potential for heavy metal and pesticides sorption (Bulgariu et al., 2018; Cara et al., 2015; Khambhaty et al., 2016; Tounsadi et al., 2019). Rojas et al., (2014) reported that atrazine, alachlor, endosulfan sulfate and trifluraline were efficiently removed by three adsorbents, sunflower seeds shells, rice husk and composted sewage sludge. Mandal et al. (2017) showed that rice straw biochar could effectively adsorb pesticides from water. Cara et al. (2017) investigated the potential of alkaline treated straw (wheat and corn) in mixture with soil, for the removal of sulfonylurea molecules from an aqueous solution. The results sustained that the alkaline treated straw have biosorption characteristics, being suitable adsorbent materials.

In this work, an attempt was made to investigate two modified agri-wastes (wheat and corn straw) as a low - cost adsorbent for the removal of nicosulfuron herbicide from aqueous solution. Due to the fact that nicosulfuron is a sulfonylurea herbicide which has high solubility in water, high mobility and slow degradation, there are definite concerns about environmental risk. For this, the specific parameters associated with adsorptive capacity of agri-waste-soil mixture for nicosulfuron herbicide, as well as Langmuir and pseudo-second order models were used to identify the mechanisms involved in adsorption process.

2. Experimental

2.1. Materials

The soil and straw material (wheat and corn type) were collected from Ezăreni - the Experimental Farm of the Agricultural University Iasi Romania (47°07′ N latitude, 27°30′ E longitude). The agri-straws were washed several times with ultrapure water and cut into small pieces. The samples were dehydrated at 70°C for 24h, grinded, and sieved to obtained particle with a size of 500 -700 μm. Then they were subject to KOH activation in the ratio of 1:1 (w/w) at 100°C for 2 h. After that, the samples were transferred to furnace - 3 h at a heating rate of 10 C min^{-1}, 450 C + 2h at a heating rate of 10 C min^{-1}, 850°C. The samples were cooled at room temperature and washed with ultrapure water until a pH of ~7 was reached (almost the same pH as the soil). Then, they were dried at 105 C for 24 h and stored in desiccators for further use. The agri-wastes samples acquired after KOH activation and 850°C mineralization were assigned as Cs-850°C and Ws-850°C.

To provide information on the physical and chemical nature of the soil, standard characterization methods were used. The soil of the study area is mainly characterized by clay-loamy texture (cambic chernozem - SRTS, 2012, haplic chernozem - WRB-SR, 2006) with 3.06% humus content and 21.22 me 100 g^{-1} soil cationic exchange capacity (Cara et al., 2017). The soil pH was measured in a 1/2.5(w/w) soil/ultrapure water mixture, using a direct-reading pH meter, while total organic carbon content (1.39% C org) was determined by dichromate oxidation.

Nicosulfuron with a purity of 95%, chemical formula of $C_{15}H_{18}N_6O_6S$ and molecular weight of 410.405 g mol^{-1} was obtained from Dr. Ehrenstorfer GmbH (Augsburg, Germany). All other compounds were commercially available and of high-performance liquid chromatography grade.

2.2. Instrumentation

All adsorption measurements were performed at room temperature on a Thermo Scientific LC-MS coupled with an Orbitrap Q-Exactive analyser. The retention time of nicosulfuron was 5.38 min using methanol/water (60:40 v/v) as liquid phase, at a flow rate of 1 mL min^{-1}. A pH meter combined with glass electrode was employed to measure pH of all the solutions. Orbital shaker was used for shaking of solution during adsorption study. Scanning Electron microscopy (SEM) (FEI - Field Electron and Ion Company) was used to analyze surface morphology and structural images of each material. The functional groups and any chemical changes that may have occurred after activation and mineralization of the agri - wastes were obtained using KBr pellets (1:100

sample/KBr), and the spectra were acquired on a FT-IR spectrometer in the region of 400-4000 cm^{-1} in transmission mode with 4 cm^{-1} resolution and the average of 100 scans.

2.3. Adsorption performance

The performance of the agri-wastes for retaining nicosulfuron molecules was evaluated under initial nicosulfuron concentrations, contact time and solution pH of 7. 2 g of soil and 0.01 g of agri-waste was added to a set of 100 mL Erlenmeyer flasks containing 20 mL of solution with the required initial concentration. The content of the flasks was shacked on an orbital shaker at 350 rpm, at room temperature. The influence of initial concentration on agri-wastes performance was study at a pH=7, the pH value of the soil. The solution pH was adjusted using either 0.1 M NaOH or 0.1M HCl. The influence of contact time (0 -24 h) was explored at various initial concentrations (1 – 100 mg L^{-1}). The removal efficiency and the adsorbed amount q (mg g^{-1}) were evaluated by Eq. (1):

$$q = \frac{(C_0 - C)}{W} V \qquad (1)$$

where: C (mg L^{-1}) and C_o (mg L^{-1}) are the residual and initial concentration of nicosulfuron, respectively. The soil and agri-waste mass and the volume solution are W (g) and V (L), respectively.

2. 4. Adsorption studies

The adsorption isotherms and kinetics of the soil-agri-waste system were obtained under the same procedure as that for adsorption performance. Isotherm study was performed until an equilibrium state was reached, and the equilibrium uptake, q_e (mg g^{-1}) was determined by applying Eq. 1 at the equilibrium concentration, C_e (mg L^{-1}).

The adsorption studies were performed by adding 2 g of soil and 0.01 g of agri-waste to 20 mL of nicosulfuron solution at different concentrations (1-100 mg L^{-1}) at pH 7.0 for 120 min. the experimental data were analyzed by Langmuir and Freundlich models as follow:

$$\text{Langmuir isotherm: } q_e = q_{max} \frac{K_L C_e}{1 + K_L C_e} \qquad (2)$$

$$\text{Freundlich isotherm: } q_e = K_F C_e^{1/n} \qquad (3)$$

where: q_{max} is the maximum adsorption capacity (mg g^{-1}); C_e is the concentration of nicosulfuron at equilibrium (mg L^{-1}); K_L (mg g^{-1}), K_F (L g^{-1}) and n are the Langmuir and Freundlich constants.

The kinetic study was conducted for the time range of 0 - 24 h; using the residual concentration at time t, C_t (mg L^{-1}), the adsorbed amount at time t, q_t (mg g^{-1}) was also evaluated from Eq. (1). Pseudo-first order (Langergren, 1898) and pseudo-second order (Ho and McKay, 1999) models were adopted for the analysis of kinetic data, as follows:

$$\text{Pseudo-first order: } q_t = q_e (1 - e^{-k_1 t}) \qquad (4)$$

$$\text{Pseudo-second order: } q_t = \frac{q_e^2 k_2}{1 + K2qet} \qquad (5)$$

where: q_e (mg g^{-1}) and q_t (mg g^{-1}) are the nicosulfuron adsorbed at equilibrium and time t, respectively; k_1 and k_2 (mg $g^{-1}min^{-1}$) are the rate parameters of both models.

3. Results and discussions

3.1. Characterization of the adsorbents

The basic and consequent analysis of the Cs, Ws, Cs-850°C and Ws-850°C are presented in Table 1. The results reveal that the H and O content of the obtained Ws and Cs-850°C, were 1.13-1.94% and 16.46 - 20.42%, and those of agri-waste (Cs and Ws) were 5.23 - 7.13% and 41.75 - 45.86%, respectively.

Analytical elements likewise the atomic H/C and O/C ratio are relevant indicators of biochar characteristics. Generally, the changes in oxygen and hydrogen content and the low (H and O) percentages denote an intense deoxygenation and dehydrogenation reaction through the mineralization process (Manya et al., 2014). Oxygen content and its close relationship with composition of functional groups substituted, plays an important role in surface chemistry of biochars. Therefore, the higher C content in Ws-850°C facilitated the formation of structures which can improve the adsorption of nicosulfuron and another aqueous contaminant (Yi et al., 2016). These results are in agreement with the results described by Peng et al., (2016) where they explored reed biochars, by pyrolysis temperatures ranging from 300°C to 600°C.

The molar ratios O/C and H/C of the Cs and Ws-850°C were lower than those of the raw agri-wastes. As well, the lower polarity index (O+N)/C suggest the same enhancement in hydrophobicity and reduction of surface polar functional groups. This finding confirmed the high mineralization of the wheat straw, which can provide favorable and hydrophobic adsorption sites for nicosulfuron (Sun et al., 2014). The high temperature involved in mineralization process, minimize the H/C and O/C ratios which reflects the loss of easily degradable carbon compounds (Manya et al., 2014). Similar results were found by Ahmed et al., (2018) who utilized barley straw as precursor to prepare biochar adsorbent through thermal pyrolysis. Important properties of adsorbents e.g. surface area, volatiles, ash and water holding capacity are susceptible functions of agri-wastes mineralization and process conditions (Chen et al., 2014; Varjani et al., 2019). Agri-wastes with high moisture content had the drawback of more energy input during water evaporation (Wang et al., 2017). Based on low moisture (2.56 - 4.58%) and ash percentages of Cs and Ws-950°C, and corroborated with high carbon content 76.48%, these results indicated that Ws and Cs are effective raw material for the preparation of adsorbents with highly reactive surfaces.

Table 1. Basic and consequent analysis of Cs, Ws, Cs-850°C and Ws-850°C

Material	*Basic analysis (wt %)*		*Consequent analysis (wt %)*					*Atomic ratios (wt %)*	
	Ash	*Moisture*	*C*	*H*	*O*	*N*	*H/C*	*O/C*	*(O+N)/C*
Ws	8.72	2.56	48.29	7.13	41.75	2.83	0.147	0.864	0.923
Cs	5.23	2.87	47.62	5.23	45.86	1.29	0.109	0.963	0.990
Ws-850ºC	6.77	4.32	76.48	1.94	16.46	5.12	0.025	0.215	0.282
Cs-850ºC	3.28	4.58	71.76	1.13	20.42	6.7	0.015	0.284	0.377

Morphology analysis

Scanning electron microscopy (SEM) was used to examine the morphological features of agri-waste before and after mineralization. The SEM images of the Cs, Ws, Cs-850°C and Ws-850°C structures are presented in Fig. 1.

Were numerous well-ordered parallel textures on the surface of Ws and Cs previous to treatments (Fig. 1 a_1 and a_2). After mineralization and activated by KOH, the parallel structures were broken and with the release of the gases produced by high temperatures, the surface of the Ws and Cs presents different dimensions in the form of spherical agglomerates that are intersecting and interconnecting (Fig. 1 b_1 and b_2). Suo et al (2019) prepared activated carbon from starch by KOH activation and found that the porosity is created by KOH remaining intercalated in the lignocellulosic structure of the straw (Danish and Ahmad, 2018). Therefore, mineralization and KOH solution modified the morphology by destroying cell tissues and reduction the connection between the cells. The Cs-850°C and Ws-850°C were found to have rougher surfaces with increased specific area, which would strongly affect their adsorption properties.

FT-IR spectra of agri-waste (Cs and Ws) before and after mineralization (Cs-850°C and Ws 850°C) were used to characterize the adsorbents. The spectra consist of similar characteristics peaks, with a predominant analogous structure and bands typically assigned to cellulose and hemicellulose (Fig. 2).

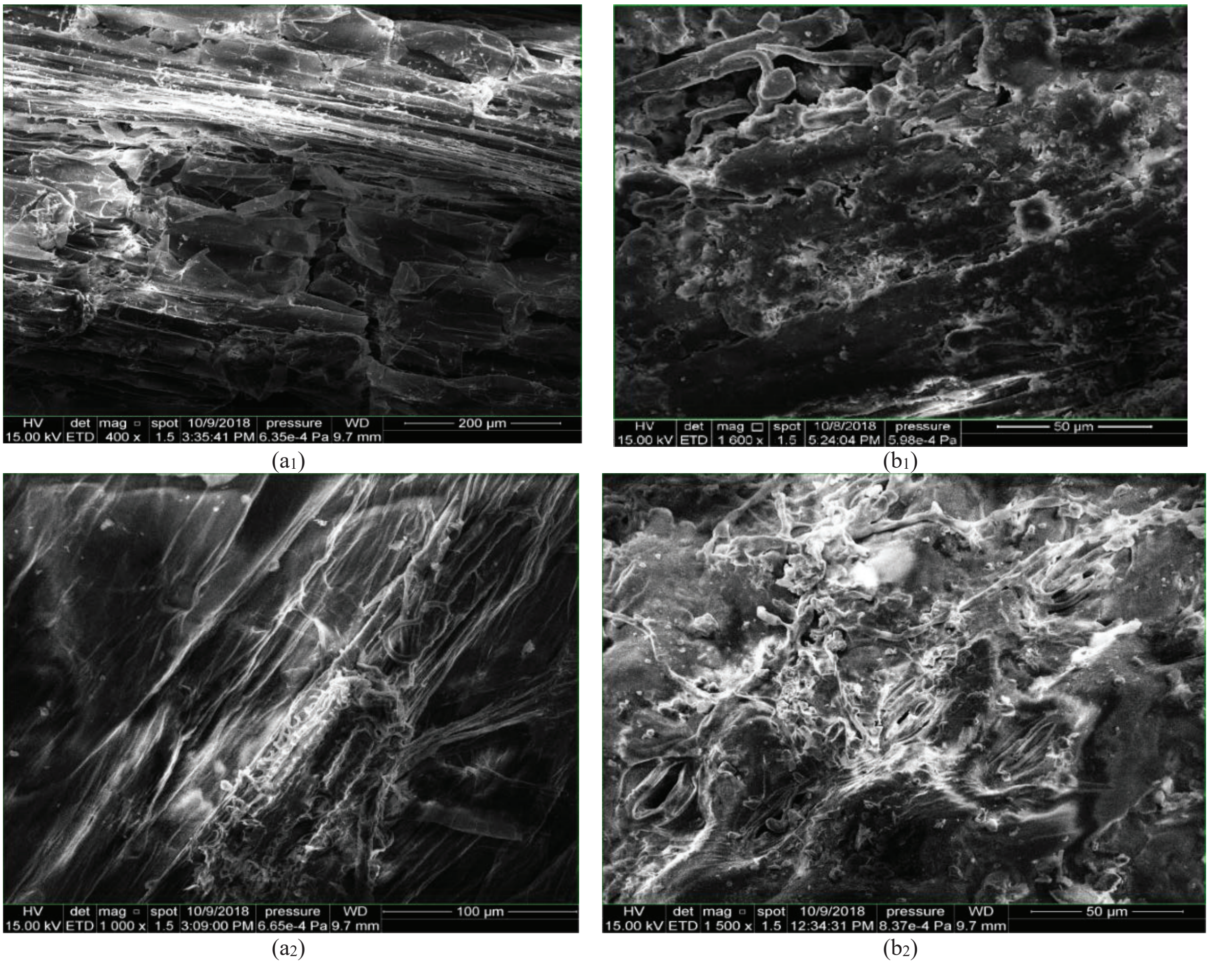

(a_1) (b_1)

(a_2) (b_2)

Fig. 1. SEM morphology for untreated wheat (a_1) and corn straw (a_2) and (b_1) treated wheat and corn straw (b_2)

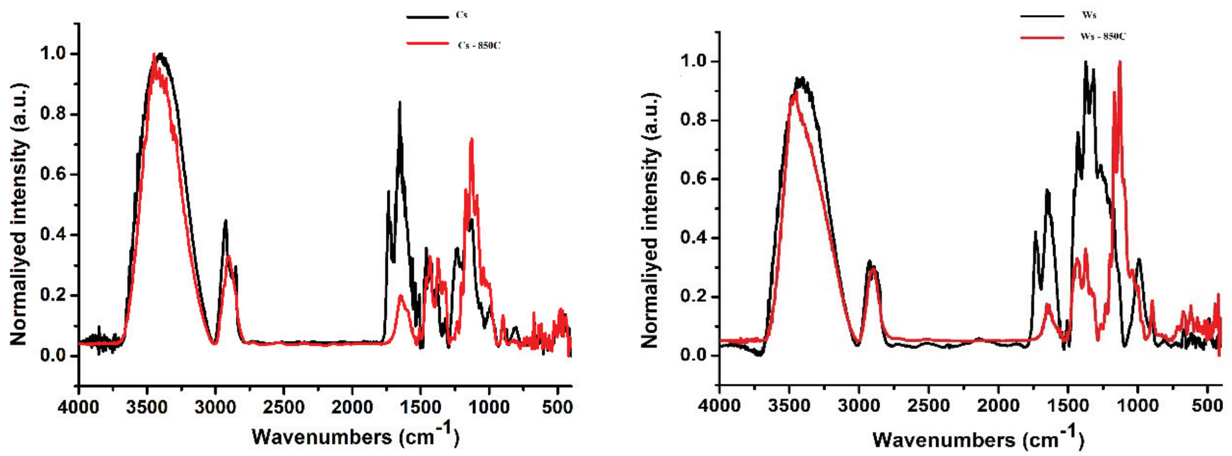

(a)

(b)

Fig. 2. FTIR analysis spectra of (a) corn straw and (b) wheat straw

A dominating band centered at 3398.1 cm^{-1} representing O-H and N-H stretching vibration, which is common in hydrophilic materials. The peak at 2990.63 cm^{-1}, represented C-H bonds in aliphatic radicals (Andrade-Mahecha et al., 2015; Martelli-Tosi et al., 2017). Moreover, the band at 1734.63 cm^{-1}, was attributed to the carbonyl groups present in carboxylic compounds (such as: uronic acids, hemicelluloses, etc). It may also be attributed to ester linkage of carboxylic groups of the ferulic and p-coumaric acids of lignin (Andrade-Mahecha et al., 2015). For example, this peak intensity significantly changed through the chemical treatment, due to lignin and hemicelluloses thermal degradation. The peak at 1458.39 cm^{-1} correspond to the aromatic skeleton of materials.

A minimization in its intensity and/or its shift to higher wavelengths was associated with modification of the aromatic radicals. The band at 1234.75 cm^{-1} was attributed to the C-N stretching vibration, while the band at 803.64 cm^{-1} is the fingerprint band. Based on these remarks, the hydroxyl, amine, carbonyl, carboxylic groups, etc. from the structure of agri-waste may interact with nicosulfuron molecules during the adsorption process.

The greatly distinctions through the new agri-waste (after KOH treatment), were in the region of 1641.95 cm^{-1} and 1127.12 cm^{-1} corresponding to the carbonyl C=O groups and C-O/O-C-O stretching vibrations respectively. The small bands at 1429.04 cm^{-1} and 1374.67 cm^{-1} proves the aromatic structure of materials. Due to the dominant C-C and C-H groups, a hydrophobic structure was established, with low oxygenated functional groups, which enhanced the adsorption process (Ahmed et al., 2018).

The mechanism revealed by FT-IR spectra, is proposed as follows (Bulgariu et al., 2011): neutralization of free carboxylic groups and/or alkaline hydrolysis of esters and others carboxylic acid derivates.

3.2. Adsorption performance

3.2.1. Influence of nicosulfuron concentration and time

Fig. 3 shows the time – dependent effectiveness of nicosulfuron – agri-waste – soil mixture, at different initial nicosulfuron concentration (10, 20 and 100 mg L^{-1}). A decrease in the amount of nicosulfuron adsorbed was noticed with time, until equilibrium was reached within 7 and 11 h for initial nicosulfuron concentration of 10 and 100 mg L$^{-1,}$ respectively. For all studied initial concentrations, the adsorption of nicosulfuron proved to be at an initial stage, fast and then slowed down gradually. Further increase of contact time showed negligible changes to the rate of adsorption, thereby confirming the equilibrium state. The preliminary high adsorption of nicosulfuron was due to the existence of available binding sites on the Ws and Cs - 850^{o}C surface which accelerated the adsorption rate. The subsequent lower adsorption rate could be due to the cluster of nicosulfuron molecules onto the surface particles which delay the diffusion of nicosulfuron molecules towards the agri-wastes surfaces (Arshadi et al., 2017).

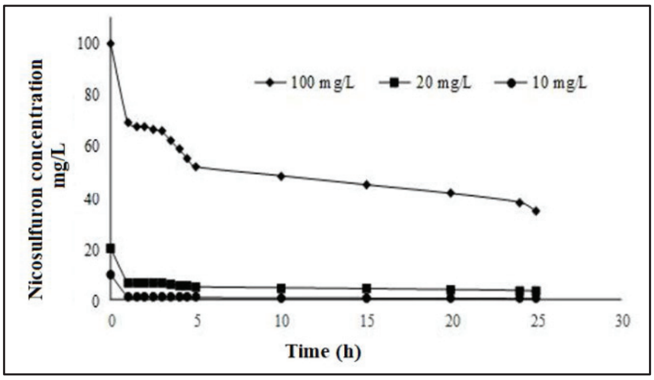

Fig. 3. Influence of initial nicosulfuron concentration on nicosulfuron adsorption by Ws - 850^{o}C

After 24 h contact time, a decline around 89% and 84.37% in nicosulfuron concentration is related with low initial concentration of 10 and 20 mg L^{-1}, respectively. For concentrated nicosulfuron solution this reduction decreased to 69.87% due to the high percentage of nicosulfuron molecules compared to the available active sites from the surface of Ws and Wc – 850^{o}C. Based on Mohammed et al., (2018) and Chen et al., (2016) the large amount of solute led to a competition between the molecules of solute towards the pores from the structure of the low-cost adsorbent and consequently reduces the adsorption extent. The obtained equilibrium time of 11 h, is in accordance with the results reported by Ogunah et al., (2016) where chlorsulfuron equilibrium was established in a period of 12h and no changes in concentration after 24h on different types of soil. Cara et al., (2017) studied the adsorption of chlorsulfuron on alkaline treated straw and found that equilibrium was reached after 12 h, while Otero et al., (2013) established a 4 h state of equilibrium for nicosulfuron on a calcinated Mg - Al hydrocalcite.

3.2.2. Adsorption isotherm

The study of adsorption equilibrium data by applying different isotherm models are used to express both the adsorption mechanism (surface properties) and the maximum adsorption extent. The analysis shows better fitting of data by the Langmuir model with R^2 values (0.968 - 0.997) relative to the R^2 values (0.8480 - 978) for the Freundlich model (Table 2). The analysis of experimental equilibrium data, reveals the monolayer coverage of nicosulfuron molecules may occur onto the homogeneous surface of Cs and Ws-850^{o}C.

According to the parameters of the Langmuir model, the maximum uptake which is a measure of the adsorption capacity to form a monolayer, increases in the order Ws-850^{o}C > Cs- 850^{o}C under tested conditions. Moreover, the differences in adsorption capacity depends on the nature of the material (Fig. 4). Nicosulfuron adsorption on soil gave the lowest Langmuir sorption capacity (q_m). Thus, the sorption capacity and the q_m values increased with the addition of exogenous organic carbon. Adsorption being the main process, which reduces the mobility of pesticides in soil, the addition of exogenous organic carbon has been suggested as a method to reduce nicosulfuron leaching (Rojas et al., 2014). Fig. 5 presents the adsorption data and their correlation by Langmuir isotherm. Similar results were found on various adsorbents derived from rice straw, corn straw and wheat straw (Tartakova et al., 2013; Zhao et al., 2013).

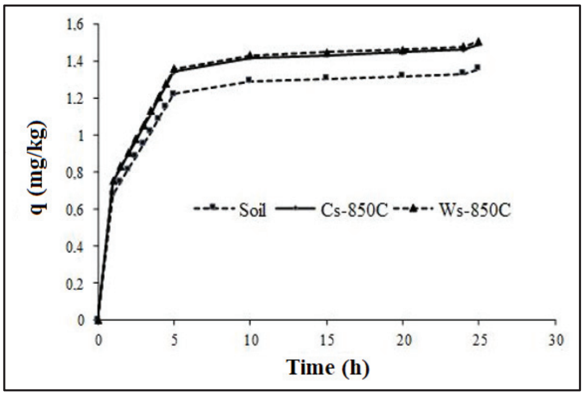

Fig. 4. Influence of the agri-waste and concentration on nicosulfuron adsorption

Additionally, the high values of adsorption equilibrium constant (K_L) confirmed strong chemical interaction between superficial groups of the Cs and Ws - 850^{o}C and chlorsulfuron molecules, which enhance the adsorption process. The differences of the adsorption capacity among materials were caused by the raw material, H-bonding interaction between nicosulfuron and polar groups on the straw surface, π - π electron donor-acceptor interactions, and hydrophobic moieties from the straw surface (Liu et al., 2015). According to Ji et al., (2011) and Zhang et al., (2011), a larger surface area with more porous sites which favors the pore filling mechanism is due to the high temperature. These suggest the different mechanisms that might control the adsorption of nicosulfuron.

For nicosulfuron-agri-waste-soil mixture, the Freundlich isotherm is related to multilayer sorption and associated with heterogeneous systems (Freundlich, 1906). According to the parameters of Freundlich isotherm, the sorption is not linear due to the greater degree of heterogeneity on the surface of Ws and Cs-850^{o}C which can influence the adsorption process (Rosa et al., 2018).

The fitted parameters of the isotherm models, suggested that the adsorption of nicosulfuron on Cs and Ws – 850^{o}C was not govern by a strict monolayer adsorption process and heterogeneous surface adsorption and chemical adsorption might also be involved (Yi et al., 2016).

Table 2. Adsorption isotherm parameters for nicosulfuron on soil and treated straw

Isotherm	*Constants*	*Soil*	*Ws – 850^{o}C*	*Cs – 850^{o}C*
Langmuir	R^2	0.997	0.968	0.977
	q_L (mg g^{-1})	166.6	431.03	348.43
	K_L (L g^{-1})	0.50	0.53	0.174
	R_L	0.019	0.018	0.054
Freundlich	R^2	0.978	0.848	0.900
	n	0.7	0.6	0.67
	K_F (L g^{-1})	79.43	141.25	126.18

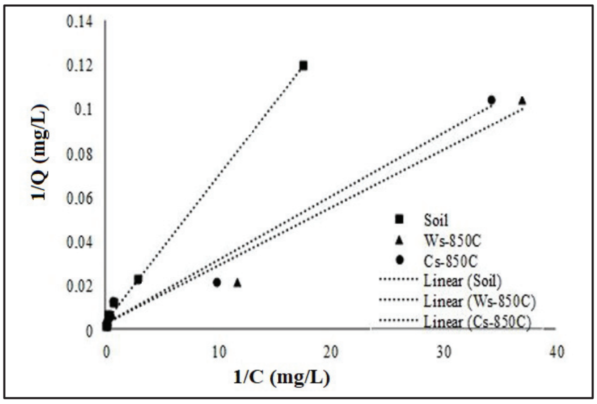

Fig. 5. Langmuir sorption isotherm of nicosulfuron

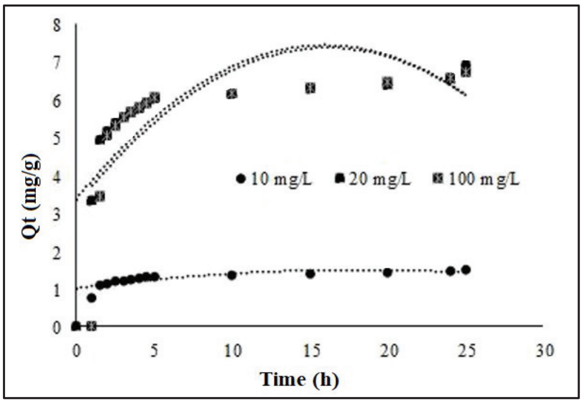

Fig. 6. Kinetic model of nicosulfuron

Compared with low cost adsorbents from other wastes, the data provides an intuitive adsorption performance towards nicosulfuron molecules that competes with other expensive adsorbents. For example, the capacity of the Ws and Cs – 850°C was much higher than of the biochar from paper mill sludge (Devi and Saroha, 2015).

3.2.3. Adsorption kinetics

The experimentally kinetics data are widely applied to predict (identify) the mechanism and rate constant of the adsorption process. Fig. 6 presents the kinetics models based on the quantity of nicosulfuron adsorbed as a function of contact time. The pseudo-first-order kinetics model of Lagergren (1898) and the pseudo-second-order model of Ho and McKay (1999) were used to determine the rate of adsorption and to distinguish whether the adsorption was chemisorption or physisorption.

In terms of determination coefficient (R^2), the results showed that the pseudo-second-order type showed the successful fitting of the data, relative to the R^2 values of the pseudo-first-order kinetics model (Table 3). The results also showed good agreement between the experimental q_e values and calculated q_e values of the pseudo-second order model. The slight differences between the experimental q_e values and calculated q_e values may be due to the uncertainty inherent in obtaining the experimental q_e values (Kumar et al., 2012). The pseudo-second-order type suggests that the adsorption rate is controlled by the active sites, then the concentration of nicosulfuron, identifying adsorption under chemisorption type. Additionally, the second model, implies ion exchange or superficial complexation between the superficial groups of the Cs and Ws – 850°C and nicosulfuron molecules from soil solution.

According to this model, the increase in nicosulfuron concentration from 10 mg L^{-1} to 100 mg L^{-1} enhance the calculated q_e values from 1.253 mg g^{-1} to 1.324 mg g^{-1} at room temperature. Moreover, the same increase in nicosulfuron concentration, decrease the values of the rate constant, k_2 from 1.52 mg g^{-1} min^{-1} to 0.87 mg g^{-1} min^{-1}. This finding might be (inter)connected with the presence of more nicosulfuron molecules with high competition towards active sites, leading a slow uptake (Reguyal et al., 2017). The best correlation of experimental kinetic data with pseudo-second-order model was also reported for nicosulfuron adsorption on Mg - Al hydrocalcite and other low cost adsorbents.

4. Conclusions

Corn and wheat straw were utilized as raw material to remove nicosulfuron herbicide from and agricultural soil. The analysis confirmed the efficient mineralization and activation of agri-waste with adsorbents generation towards highly reactive surfaces, as confirmed by SEM and FT-IR. Langmuir model and pseudo-second order model were successfully applied for the analysis of adsorption equilibrium and kinetics data. The adsorption process was found to be complex, depending on both time and concentration.

Additionally, the adsorption of nicosulfuron molecules onto the Ws and Cs - 850 °C was not govern by a strict monolayer adsorption process; heterogeneous surface adsorption and chemical adsorption might also be involved. Thus, the agri-waste have great potential to be utilized as an effective low-cost adsorbent for the removal of contaminants such as nicosulfuron molecules from soil and aqueous solutions.

Table 3. Kinetic model parameters for nicosulfuron and soil-treated straw system

	Pseudo-first-order				***Pseudo-second-order***		
	$q_{e\,exp}$ (mg g^{-1})	**$q_{e\,est}$ (mg g^{-1})**	**K_1 (mg g^{-1} min^{-1})**	**R^2**	**$q_{e\,est}$ (mg g^{-1})**	**K_2 (mg g^{-1} min^{-1})**	**R^2**
Soil	1.3563	3.090	0.025	0.146	1.253	1.52	0.969
Ws – 850°C	1.5065	5.584	0.0097	0.02	1.351	0.865	0.958
Cs – 850°C	1.4905	5.714	0.009	0.02	1.324	0.87	0.963

Acknowledgements

This work was co-financed from Competitiveness Operational programme (COP) 2014 – 2020, under the project number 4/AXA1/1.2.3.G/05.06.2018, SMIS2014 +code 119611, with the title „Establishing and implementing knowledge transfer partnerships between the Institute of Research for Agriculture and Environment - Iasi and agricultural economic environment''.

References

Ahmed M.J., Hameeda B.H., (2018), Removal of emerging pharmaceutical contaminants by adsorption in a fixedbed column: A review, *Ecotoxicology and Environmental Safety,* **149**, 257–266.

Arshadi M., Mousavinia F., Abdolmaleki M.K., Amiri M.J., Khalafi-Nezhad A., (2017), Removal of salicylic acid as an emerging contaminant by a polar nano-dendritic adsorbent from aqueous media, *Journal of Colloid Interface Science*, **493**, 138-149.

Bulgariu L., Bulgariu D., Macoveanu M., (2011), Adsorptive performance of alkaline treated peat for heavy metal removal, *Separation Science Technology*, **46**, 1023-1033.

Bulgariu L., Bulgariu D., (2018), Functionalized soy waste biomass - A novel environmental-friendly biosorbent for the removal of heavy metals from aqueous solution, *Journal of Cleaner Production*, **197**, 875-885.

Cara I.G., Trinca L.C., Trofin A.E., Cazacu A., Topa D., Peptu C.A., Jitareanu G., (2015), Assessment of some straw derived materials for reducing the leaching potential of Metribuzin residues in the soil, *Applied Surface Science*, **358**, 586-594.

Cara I.G., Rusu B.G., Raus L., Jitareanu G., (2017), Sorption potential of alkaline treated straw and a soil for sulfonylurea herbicide removal from aqueous solutions: An environmental management strategy, *Chemosphere*, **186**, 360-366.

Carles L., Joly M., Bonnemoy F., Leremboure M., Donnadieu F., Batisson I., Besse-Hoggan P., (2018), Biodegradation and toxicity of a maize herbicide mixture: mesotrione, nicosulfuron and S-metolachlor, *Journal of Hazardous Materials,* **354**, 42-53.

Chen T., Zhang Y., Wang H., Lu W., Zhou Z., Zhang Y., Ren L., (2014), Influence of pyrolysis temperature on characteristics and heavy metal adsorptive performance of biochar derived from municipal sewage sludge, *Bioresource Technology*, **164**, 47-54.

Chesca A.M., Tofanica B.M., Puitel A.C., Nicu R., Gavrilescu D., (2018), Environmentally friendly cellulosic fibers from corn stalks, *Environmental Engineering and Management Journal*, **17**, 1765-1771.

Danish M., Ahmad T., (2018), A review on utilization of wood biomass as a sustainable precursor for activated carbon production and application, *Renewable and Sustainable Energy Reviews,* **87**, 1–21.

De Gisi S., Lofrano G., Grassi M., Notarnicola M., (2016), Characteristics and adsorption capacities of low-cost sorbents for wastewater treatment: A review, *Sustainable Materials and Technologies*, **9**, 10-40.

Devi P., Saroha AK., (2015), Simultaneous adsorption and dechlorination of pentachlorophenol from effluent by Ni-ZVI magnetic biochar composites synthesized from paper mill sludge, *Chemical Engineering Journal,* **271**, 195-203.

Giles C.H., MacEwan T.H., Nakhwa S.N., Smith D., (1960), Studies in adsorption. Part XI. A system of classification of solution adsorption isotherms, and its use in diagnosis of adsorption mechanisms and in measurement of specific surface area of solids, *Journal of the Chemical Society*, **786**, 3973-3993.

Harja M., Buema G., Bulgariu L., Bulgariu D., Sutiman D.M., Ciobanu G., (2015), Removal of cadmium (II) from aqueous solution by adsorption onto modified algae and ash, *Korean Journal of Chemical Engineering*, **32**, 1804-1811.

Huang Y.Y., (2017) Research progress of wastewater treatment by agricultural wastes as biological adsorbent, *Applied Chemical Industry Volume,* **46**, 372-638.

Hlihor R.M., Pogacean M.O., Rosca M., Cozma P., Gavrilescu M., (2019), Modelling the behavior of pesticide residues in tomatoes and their associated long-term exposure risks, *Journal of Environmental Management,* **233**, 523-529.

Ho Y.S., Mckay G., (1999), Pseudo-second-order model for sorption processes, *Process Biochemistry,* **34**, 451-465.

Khambhaty Y., Mody K., Basha S., Jha B., (2016), Biosorption of safranin onto chemically modified biomass of marine *Aspergillus wentii*: a kinetic study, *Environmental Engineering and Management Journal,* **15**, 61-73.

Kumar P.S., Gayathri R., Senthamarai C., Priyadharshini M., Fernando P.S.A., Srinath R., Kumar V.V., (2012), Kinetics, mechanism, isotherm and thermodynamic analysis of adsorption of cadmium ions by surface-modified strychnos potatorum seeds, *Korean Journal of Chemical Engineering*, **29**, 1752-1760.

Kalhor M.M., Rafati A.A., Rafati L., Rafati A.A., (2018), Synthesis, characterization and adsorption studies of amino functionalized silica nano hollow sphere as an efficient adsorbent for removal of imidacloprid pesticide, *Journal of Molecular Liquids*, **266**, 453-459.

Lagergren S., (1898), Lagergren Zur theorie der sogenannten adsorption gelöster stroffe, *Kungliga Svenska Vetenskapsakademiens handlingar*, **24**, 1-39.

Langmuir I., (1918), The adsorption of gases on plane surfaces of glass, mica and platinum, *Journal of the American Chemical Society,* **40**, 1361-1403.

Li B., Yang L., Wang C.Q., Zhang Q.P., Liu Q.C., Li Y.D., Xiao R., (2017), Adsorption of Cd(II) from aqueous solutions by rape straw biochar derived from different modification processes, *Chemosphere*, **175**, 332-340.

Liu G., Zheng H., Zhai X., Wang Z., (2018), Characteristics and mechanisms of microcystin-LR adsorption by giant reed-derived biochars: role of minerals, pores and functional groups, *Journal of Cleaner Production*, **176**, 463-473.

Manya J.J., Ortigosa M.A., Laguarta S., Manso J.A., (2014), Experimental study on the effect of pyrolysis pressure, peak temperature, and particle size on the potential stability of vine shoots-derived biochar, *Fuel*, **133**, 163-172.

Martelli-Tosi M., Assis O.B.G., Silva N.C., Esposto B., Martins M.A., Tapia-Blacio D.R., (2017), Chemical treatment and characterization of soybean straw and soybean protein isolate/straw composite films, *Carbohydrates Polymers*, **157**, 512-520.

Mandal A., Singh N., Purakayastha T.J., (2017), Characterization of pesticide sorption behaviour of slow pyrolysisbiochars as low cost adsorbent for atrazine and imidacloprid removal, *Science of Total Environment,* **577**, 376-385.

Mozhgan M.K., Rafati A.A., Rafati L., Rafati A.A., (2018), Synthesis, characterization and adsorption studies of amino functionalized silica nano hollow sphere as an efficient adsorbent for removal of imidacloprid pesticide, *Journal of Molecular Liquids,* **266**, 453-459.

Mahecha A., Pelissari M.M., Tapi-Blacido F.M., Menegalli D.R., (2015), Achira as a source of biodegradable materials: isolation and characterization of nanofibers, *Carbohydrates Polymers*, **123**, 406-415.

Mohammed Ali M.M., Ahmed M.J., Hameed B.H., (2018), NaY zeolite from wheat (*Triticum aestivum* L.) straw ash used for the adsorption of tetracycline, *Journal of Cleaner Production*, **172**, 602-608.

Ogunah J.A., Owuor P.O., Kowenje C.O., Lalah J.O., (2016), Adsorption and desorption of chlorsulfuron in agricultural soil of Mara River basin, Kenya, *American Journal of Experimental Agric*ulture, **12**, 1-10.

Petric I., Karpouzas D.G., Bru D., Udikovic-Kolic N., Kandeler E., Djuric S., Martin-Laurent F., (2016), Nicosulfuron application in agricultural soils drives these lection towards NS-tolerant microorganisms harboring various levels of sensitivity to nicosulfuron, *Environmental Science Pollution Research*, **23**, 4320-4333.

Peng P., Langa Y.H., Wang X.M., (2016), Adsorption behavior and mechanism of pentachlorophenol on reed biochars: pH effect, pyrolysis temperature, hydrochloric acid treatment and isotherms, *Ecological Engineering*, **90**, 225-233.

Periyaraman P.M., Karan S., Ponnusamy S.K., Vaidyanathan V., Vasanthakumar S., Dhanasekaran A., Subramanian S., (2019), Adsorption of an anionic dye onto native and chemically modified agricultural waste, *Environmental Engineering and Management Journal*, **18**, 257-270.

Rojas R., Vanderlinden E., Morillo J., Usero J., El Bakouri H., (2014), Characterization of sorption process for the development of low cost pesticide decontamination techniques, *Science of Total Environmental*, **488-489,** 124-135.

Reguyal F., Sarmah A.K., Gao W., (2017), Synthesis of magnetic biochar from pine sawdust via oxidative hydrolysis of $FeCl_2$ for the removal sulfamethoxazole from aqueous solution, *Journal of Hazard Material*, **321**, 868-878.

Suo F., Liu X., Li C., Yuan M., Zhang B., Wang J., Ma Y., Lai Z., Mingshan J., (2019), Mesoporous activated carbon from starch for superior rapid pesticides removal, *International Journal of Biological Macromolecules,* **121**, 806-813.

Sun Y., Gao B., Yao Y., Fang J., Zhang M., Zhou Y., Chen H., Yang L., (2014), Effects of feedstock type, production method, and pyrolysis temperature on biochar and hydrochar properties, *Chemical Engineering Journal,* **240**, 574-578.

Tartakova V., Hiller E., Vaculı´ık M., (2013), Impact of wheat straw biochar addition to soil on the sorption, leaching, dissipation of the herbicide(4-chloro-2-methylphenoxy) acetic acid and the growth of sunflower (*Helianthus annuus* L.), *Ecotoxicology and Environmental Safety,* **92**, 215–221.

Tounsadi H., Khalidi A., Farnane M., Machrouhi A., Elhalil A., Barka N., (2019), Efficient removal of heavy metals by KOH activated *Diplotaxis harra* biomass: Experimental design optimization, *Environmental Engineering and Management Journal*, **18**, 651-664.

Varjani S., Kumar G., Rene R., (2019), Developments in biochar application for pesticide remediation: Current knowledge and future research directions, *Journal of Environmental Management,* **232**, 505-513.

Zhang G., Zhang Q., Sun K., Liu X., Zheng W., Zhao Y., (2011), Sorption of simazine to corn straw biochars prepared at different pyrolytic temperatures, *Environmental Pollution*, **159**, 2594-2601.

Zhao X., Ouyang W., Hao F., Lin C., Wang F., Han S., Geng X., (2013), Properties comparison of biochars from corn straw with different pretreatment and sorption behaviour of atrazine, *Bioresource Technology*, **147**, 338-344.

Wang J., Jiao M., Li., Song C.Y., Wang C., Wu Q., Wang Z., (2017), Preparation of a magnetic porous organic polymer for the efficient extraction of phenyl urea herbicides, *Journal of Chromatography*, **1519**, 19-25.

Wanjeri V.W.O., Sheppard C.J., Prinsloo A.R.E., Ngila J.C., Ndungu P.G., (2018), Isotherm and kinetic investigations on the adsorption of organophosphorus pesticides on graphene oxide based silica coated magnetic nanoparticles functionalized with 2-phenylethylamine, *Journal of Environmental Chemical Engineering*, **6**, 1333-1346.

Yi S., Gao B., Sun Y., Wu J., Shi X., Wu B., Hu X., (2016), Removal of levofloxacin from aqueous solution using rice-husk and wood-chip biochars, *Chemosphere*, **150**, 694-701.

Environmental Engineering and Management Journal

February 2020, Vol. 19, No. 2, 345-352
http://www.eemj.icpm.tuiasi.ro/; http://www.eemj.eu

"Gheorghe Asachi" Technical University of Iasi, Romania

OLEFINS AND FUELS FROM FRYING PALM OIL THROUGH PYROLYSIS

Ana Maria Sivriu[1]*, Claudia-Irina Koncsag[2], Alina-Monica Mares[1], Roxana Tirpan[2], Olga Sapunaru[2], Gheorghita Jinescu[3]

[1]*University Politehnica of Bucharest, Faculty of Applied Chemistry and Materials Science*
[2]*University Ovidius of Constanta, Faculty of Applied Science and Engineering, 124, Bld. Mamaia, 900527, Constanta, Romania*
[3]*Romanian Academy of Technical Sciences, Bucuresti, Romania*

Abstract

The pyrolysis of frying palm oil was studied in continuous stationary process, in a micropilot plant. The main factors affecting the products yields are temperature and residence time. For the studied parameters range (temperature: 475°C - 630°C and residence time: 120 s- 240 s), the gas yield varied between 7.9% (w/w) and 63.3% (w/w), related to feed. Unsaturated hydrocarbon yields (olefins) can reach 24-29% (w/w) related to feed, at the right processing parameters, the main products having good yields: up to 10% w/w for ethylene and 10.5% (w/w) for propylene. Also, the liquid fractions produced in the experiment were characterized having in view the use as fuel oils. The low viscosity (4.4-8.3 cSt at 20°C) and high heat of combustion value (9225-9260 kcal/kg) demonstrated that liquids are fit for use as fuel oil. These results are encouraging for industrial applications consideration. For this reason, mathematical modeling for the prediction of products yields was performed. The individual models for the main compounds (ethylene, propylene, methane, ethane, propane, carbon oxides) are in form of second degree polynomial equations; they are accurate as the statistical analysis proved.

Key words: biofuel, mathematical model; pyrolysis mechanism; renewable olefins; vegetable oil

Received: January, 2019; Revised final: February, 2020; Accepted: February, 2020; Published in final edited form: February, 2020

1. Introduction

Global polyethylene (PE) and polypropylene (PP) production grew in last decade (Esposito, 2019) but this growth is based on building new capacities based on petroleum and gas. Also, the fuels required in increasing quantity, for transportation and energy generation, are mainly produced from oil&gas. The deployment of fossil reserves leads to search for alternative resources such as recycling of plastics (Olugu et al., 2017) or producing monomers and fuels by pyrolysis of PE, PP waste (Kuncser et al., 2010) or tyres (Miandad et al., 2018; Neri et al., 2018; Osayi et al., 2018; Umeki et al., 2016).

Hydrocarbons can be also produced from renewable resources such as agricultural and forest waste or waste resulted in biomass processing (tall oil, lignin, glycerol) (Marton, 2013). Waste vegetable oils can also count for feedstock in valuable chemicals production (Wiggers et al., 2017). Best known for their use as fuels, either directly or after conversion into biodiesel by transesterification, or into Diesel-like oil by thermocatalytical processes (Xu et al, 2016), waste vegetable oils are also prone for olefins production with good yields (Kubatova et al., 2011).

There are three ways in olefins production from vegetable oils: the thermal cracking in presence or in absence of steam or another inert gas, the thermal cracking over an inert solid material also with and without steam, and thermal catalytic cracking over a large variety of catalysts: zeolites (Biswas and Sharma, 2014), mesoporous metallic catalysts (Yu et

---

[*] Author to whom all correspondence should be addressed: e-mail: sivriu_ana@yahoo.com

al., 2013), sodium carbonate (Zaher et al., 2017), vanadium pentoxide (Yigezu and Muthukumar, 2015), biomass derived heterogeneous catalysts (Aslam et al., 2015) etc.

The thermal cracking over an inert solid material and catalytic cracking are intended for Diesel-like fuels production, so gaseous products are considered as by-products. Liquid products yield are in range 62.3-73.9% (w/w) when using ZSM-5 (Biswas and Sharma, 2014). In other catalysts case, such as sodium carbonate (Dandik and Aksoy, 1998) and mesoporous Ni-Al-MCM-41 (Zaher et al., 2017), the liquid yields range from 51.6 to 57.9 % (w/w) (Zandonai et al., 2015).

Pyrolysis is a thermal cracking occurring in inert environment (in absence of oxygen) and in absence of a catalyst, at high temperature (300-1000^{o}C). Unlike the thermal cracking over an inert solid material or the catalytic cracking, the pyrolysis is a process intended for high gaseous products yields. The gaseous products yield and distribution depend on temperature, residence time and presence of other gas in the system (inert gas, steam, hydrogen). The literature data indicated the thermal cracking of the vegetable oils as an effective way to obtain olefins. With pyrolysis performed in a tubular reactor, at 400^{o}C, Sadrameli and Green (2007) obtained 55.5% (w/w) gaseous product from canola oil, with 28.1% (w/w) unsaturated hydrocarbons. Idem et al. (1996) obtained similar results in similar conditions. In fast pyrolysis of soybean, palm and rapeseed oils (residence time 0.3 s) and at high temperature (820^{o}C) (Zamostny et al., 2012), the product yields and distribution was very close to that in case of hydrocarbon steam cracking, and good ethylene and propylene yields were reached: 28% (w/w) and 12% (w/w), respectively.

The more saturated vegetable oil produced more ethylene and propylene. The propylene and propane yield is an indicator of triglycerides conversion (Zandonai et al., 2015).

Taking into account the waste frying palm oil as a raw material, the present study is focused on olefins and fuels production by thermal cracking, since large amounts of waste cooking oils are generated worldwide, some countries (e.g. Mexico, Malaysia, Japan, USA) producing between 450,000-1,000,000 tons/year (Owolabi et al., 2011), and making this resource economically attractive for industrial processing.

2. Experimental

2.1. Reagents and materials

The raw material for this study was a waste palm oil supplied by a restaurant in Bucharest; it resulted from frying of potatoes chips and was passed in our laboratory through a metallic sieve to retain grossly the mechanical impurities, then filtered through filtering paper for finer separation. Some characteristics were determined to observe the degradation level of the oil. The only indication of degradation was the small Iodine Number of 3.84 g I_2/100 g oil comparing with 44-51 in fresh oil (Thomas, 2002), indicating that double bonds were oxidized during cooking, so they were not available for further iodine oxidation. High kinematic viscosity (47.3 cSt at 40^{o}C) and high flash point (240^{o}C) indicate that thermal cracking of the oil during cooking was moderate. The oil density at 20^{o}C was 924 kg m^{-3}.

The elementary analysis of the raw material oil lead to the following composition: C=75,7% wt; H=11,9% wt; O=12.4% wt which compares with data in literature (Xu et al., 2016) of fresh palm oil: C= 76,7% wt., H=11,5% wt., O=11,8% wt. or of waste frying oil: C=76,9%, H=11,3%, O=11,8%. No big difference before frying and after can be noticed in the elementary composition of the oil, even though new compounds formed in thermolytic reactions (n-alkanes, alkenes, low molecular weight fat acids, symmetrical ketones, oxo-propyl esters, CO and CO_2) oxidation (hydroperoxydes, aldehydes and acids) and hydrolysis (free fat acids, glycerol, mono- and di-glicerides). The loss of oxygen with CO and CO_2 produced in thermolytic reactions must have been compensated by molecular oxygen included in oxidation reactions.

2.2. Experimental set-up and procedure

The thermal cracking runs took place in a micropilot plant presented in Fig.1. The main equipment consists in a tubular reactor with electrical heating, temperature control and temperature digital monitoring.

The oil is fed by a reciprocating pump with adjustable flow rate 0-4 L/h, in order to perform the experiment at different residence times (120 s, 180s and 240 s respectively).

The internal diameter of the reactor is 0.019 m and its length is 0.47 m. The heating is made with three electrical coils placed in a ceramic shell around the metallic reactor, in three zones: up, middle and bottom, with thermostats, so the temperature profile can be established. We chose to have a uniform temperature profile along the reactor shell. The temperature inside the reactor can be monitored in one point at choice (T_1, T_2 or T_3), and we chose to have it registered in the middle (T2). During this experiment, temperature was in range of 475 ^{o}C - 630 ^{o}C; running over 630^{o}C was avoided due to the limitations of the heating system. Since the temperature in the heating shell can be established (with variance ±5^{o}C), the temperature in the reactor was influenced by the feed rate, so small variations in temperature from one set of data to the other occurred, without influencing the conclusions of the work. Pressure in the effluent was 2 barg, needed to fill the gas sample bags. The pressure also corresponds to industrial systems working at “atmospheric pressure”, in order to compensate the pressure drop downstream. Pressure is measured with a Bourdon manometer, calibrated in the range 1 - 40 barg. The thermal cracking takes place in a continuous stationary regime, and the effluent is cooled and condensed at 30ºC, with running water at 15ºC. During the experimental runs, the valve between the manometer and the cooler was shut up, so all effluent passed out at the bottom of the reactor. The vapor condensation system (a coil exchanger) is 0.4 m long. The transfer line from the reactor to the cooler is 0.31 m in length and has a 0.004 m internal diameter. In the separator, a liquid and a gaseous phase are separated; the separator provided with a cooling mantle itself is 0.4 m long and 0.1 m external diameter. The temperature in the liquid-gas separator is approx.30ºC. Samples of gas product are collected at the separator for gas-chromatographic analysis in special aluminum foil bags (5L) and liquid samples are collected in glass containers sealed to the gas-liquid separator.

2.3. Samples characterization procedure

The composition of the cracked gas was determined by a gas chromatography method developed by Wasson ECE for extended analysis of gases, using an equipment with a complex configuration produced by Agilent - USA: one FID detector, two thermoconductivity detectors, capillary and packed columns depending on applications, injector split/splitless with EPC, and an auxiliary isothermal oven automatically controlled. The working parameters for hydrocarbons and permanent gases determination are presented in Table 1.

The yields of different gaseous compounds were calculated from the chromatographic composition % (v/v), transformed into % (w/w) through the average molecular weight of the effluent, also taking into account the total gas yield.

Liquid samples were summary characterized: density by pycnometer (method ASTM D1298-99), kinematic viscosity at 20ºC by Ubbelohde viscometer (method ISO 3104-02) and Iodine Number (STAS 315-74, in use, for mineral oils, adapted to vegetable oils). Three composite samples were characterized for the heat of combustion with method ASTM D240-14, in order to find their suitability as fuel oils. A short description of the analysis methods is given further on:

Density by pycnometer serves to establish in first instance the relative density of the oil towards water as reference liquid. The method was chosen in detriment of a modern method (by digital density analyzer) because of the fouling caused by the oil in the capillary tube of the apparatus. The density of the oil at 20ºC relative to water at 20ºC, d_{20}^{20}, is calculated with Eq.(1):

$$d_{20}^{20} = \frac{m_{oil} - m_{empty}}{m_{water} - m_{empty}} \qquad (1)$$

where: m_{oil} and m_{water} is the weight of picnometer filled with oil and water respectively, and m_{empty} is the weight of empty pycnometer, all measured at 20ºC; then, the density of the oil at 20ºC is calculated with Eq. (2):

$$\rho_{oil}^{20} = \rho_{water}^{20} \cdot d_{20}^{20} = 998.2 \cdot d_{20}^{20}, \text{kgm}^{-3} \qquad (2)$$

Kinematic viscosity at 20ºC was measured with an Ubbelohde viscometer, by clocking (t) the flowing of the oil in the capillary between two marks, and calculating with Eq.3:

$$\gamma = k \cdot t, \text{cSt} \qquad (3)$$

where, k is the constant of the apparatus, in this case k=0.05113.

Iodine number gives an indication of the amount of unsaturation either in the original oil formula or as the result of dehydrogenation reaction during thermal decomposition process; the double bonds react with alcoholic solution of iodine in an alcoholic anhydrous medium, and the excess iodine is consumed in titration with sodium thiosulfate, in presence of starch:

$$2Na_2S_2O_3 + I_2 \longrightarrow 2NaI + Na_2S_4O_6$$

Then, the iodine number (IN) is calculated with Eq.4:

$$IN = \frac{(V - V_1) \cdot 0.01269 \cdot F}{m} \times 100, \text{ g } I_2/100 \text{ g oil} \qquad (4)$$

where: V is the volume of $Na_2S_2O_3$ 0.1N sol. consumed in titration of blank essay (all components included but oil), ml; V_1 – the volume of $Na_2S_2O_3$ 0.1N sol. consumed in titration of essay with oil, ml; F – the factor of $Na_2S_2O_3$ 0.1N sol.; 0.01269 – grams of iodine stoichiometric corresponding to 1 ml $Na_2S_2O_3$ 0.1N sol., g; m – the quantity of oil taken into analysis, (cca. 1g).

Heat of combustion was measured in bomb calorimeter Parr Instruments, model 1261. The principle of the method is to measure the heat released at the combustion of 0.5-1 g of fuel, transferred to a known quantity of water, increasing the temperature.

3. Results and discussions

The yields of products obtained in nine runs of thermal cracking experiment are presented in Table 2.

3.1. Total gas yields

Since a large part of gas produced was collected for analyses purposes, the direct measurement of the quantities was difficult to perform. The total gas yield is usually calculated from the material balance with Eq. (5):

$$y_{gas} = \frac{m_{raw} - (m_{liquid} + m_{coke})}{m_{raw}} \cdot 100, \% \qquad (5)$$

The quantity of raw material (m_{raw}) and that of the liquid - pyrolis oil (m_{liquid}) can be precisely determined but coke formation is difficult to measure in a continuous system like this; the quantity of raw was calculated from the pump flowrate and the measured time of the run; the liquid product accumulated in one run was weighed.

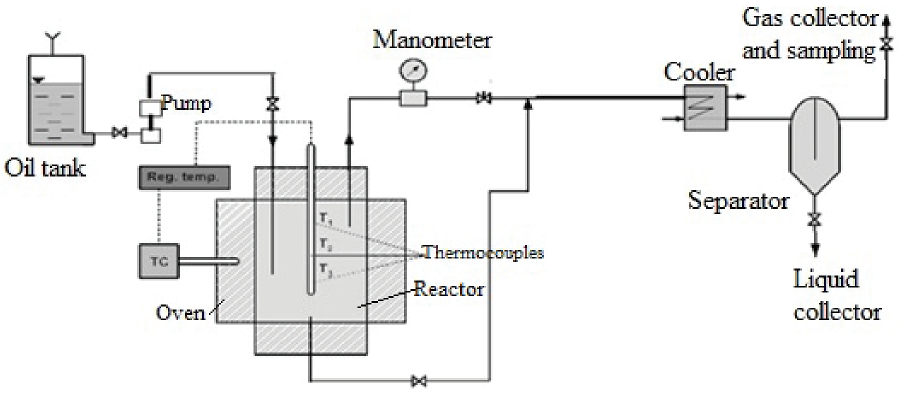

Fig. 1. Micropilot plant for thermal cracking of waste palm oil (Sivriu et al., 2017)

Table 1. Working parameters for hydrocarbons and permanent gases determination with the gas-chromatograph 6890N-Wasson ECE

	Initial temperature, ^{o}C	***Temperature ramp, ^{0}C/min***	***Flow, mL/min***	***Split ratio***	***Pressure, psig***
Inlet mode: split	150	-	He: 32.5	5:1	7.35
Oven	75	15, up to 165^{0}C 30, up to 175^{0}C			
Auxiliary oven	90	-	-		
Detector TCD B	50		He: 30		
Detector TCD C	50		N_2: 40		
Detector FID	250		H_2: 30; Air:300; Makeup He: 30		
Capilary columns			He - 5		7.35
Packed columns			He – 40		

The coke is deposed and accumulated on the reactor coil during the entire experiment, including the intermediary periods between two runs. Even weighing it at the end of the experiment is useless for balance purposes. In other articles describing vegetable oil pyrolysis experiments in continuous systems, the coke yields are not reported (Kozliak et al, 2013, Wiggers et al., 2009, Zamostny et al, 2012,). Unlike the mineral oil, plastic (Kuncser et al., 2010) or tires pyrolysis (Andreola et al., 2016), the formation of coke is much reduced in case of vegetable oils because of the high content of oxygen in molecules (12.3 % wt) reacting with carbon to result carbon oxides which are found in high yields in the pyrolysis gas (as seen in Table 2). In this case, the coke yield is charged to the total gas yield.

Comparing the total gas yields obtained in this study with other authors findings is not easy task since the reaction conditions are different.

For example, in a review from 2017, Wiggers et al., acquired and synthesized a large amount of data between 1996-2016, for all kind of vegetable oils, in very different reaction systems. The pyrolysis temperatures were between 300^{o}C-600^{o}C, the residence time between 1 min-1800 min. The average gas yield was 28.77±21.06%. At the pyrolysis of canola oil, Sadramelli and Green (2007) reported, in range of 300-500^{o}C, in a very slow process (residence time 90 min - 360 min) gas yields of 15-75% w/w. Experimental data for temperature over 600^{o}C, are found rarely. Zamostny et al. (2012) pyrolysed different vegetable oils at 800^{o}C, in the oven of a gas chromatograph, in presence of nitrogen, but they only reported yields of the main compounds; however, one can calculate that the gas yield is over 80%. In conditions closed to the present study (residence time 3 min and temperature 470^{o}C), from Jojoba oil, Kozliak et al (2013) obtained a total gas yield of 23.5 ±3.5% wt/wt, comparing with ours 25.47% wt/wt, at the same temperature and 4 min time residence.

From our experimental results, it is obvious that the total gas yield increases with temperature and also it is strongly affected by the residence time. For example, the gas yield at 480^{o}C and 120 s residence time is barely 7.97% (w/w), since at 475^{o}C and 240 s, it was 25.47% (w/w).

The maximum gas yield was obtained at longer residence time: 63.31% (w/w) at 620^{o}C and 240 s, since at comparable temperature (630^{o}C) and 180 s, the gas yield was 51.51% (w/w).

3.2. Gaseous products

As the feedstock contains C, H and O, the pyrolysis gas contains hydrogen, hydrocarbons and carbon oxides. Based on gaseous compounds obtained in this experiment, and in accordance with mechanisms presented in Maher and Bressler's (2007) work, the pathway to the products starts with triglycerides decomposition into fat acids, acroleine and ketenes, followed by the fat acids decomposition producing carbon dioxide and alkanes.

Table 2. Experimental data at the thermal cracking of waste palm oil in a continuous stationary regime (pressure: 2 barg; temperature range: 475 °C - 630 °C; residence time: 120 s - 240 s)

Sample #	***1***	***2***	***3***	***4***	***5***	***6***	***7***	***8***	***9***
Residence time, s	240	240	240	180	180	180	120	120	120
Temperature, °C	620	600	475	555	580	630	550	530	480
Average Molecular Weight, g/mol	29.0	29.6	33.1	31.6	30.6	29.9	30.6	31.4	32.6
Total gas yield, % (w/w) from which:	63.31	59.32	25.47	45.24	49.20	51.51	31.92	25.91	7.97
Hydrogen	0.37	0.25	0.04	0.09	0.14	0.15	0.05	0.04	0.01
CO	9.07	8.80	5.89	7.60	7.32	7.28	5.73	4.65	2.01
CO_2	8.20	8.05	7.06	8.56	9.03	7.21	5.94	4.82	2.29
Oxygen	0.10	0.10	0.04	0.09	0.13	0.15	0.08	0.07	0.11
Nitrogen	0.46	0.40	0.18	0.31	0.44	0.53	0.31	0.25	0.34
Methane	5.22	4.54	0.54	2.33	3.05	3.67	1.54	1.25	0.22
Ethane	5.69	5.27	1.48	3.47	3.97	4.40	2.37	1.92	0.38
Propane	2.36	2.15	1.18	2.02	1.90	1.76	1.35	1.09	0.32
Butanes	1.06	0.94	0.74	0.97	0.88	0.71	0.72	0.59	0.25
Pentanes	0.60	0.52	0.34	0.46	0.46	0.36	0.33	0.27	0.10
Alkanes C6+	0.44	0.15	0.19	0.37	0.17	0.19	0.08	0.06	0.06
Ethylene	9.88	9.98	2.61	7.62	8.47	10.00	5.66	4.60	0.73
Propylene	10.45	9.50	2.49	6.02	6.94	7.91	4.12	3.35	0.61
1-Butene	2.06	1.98	1.05	2.72	2.65	2.91	2.05	1.66	0.34
2-Butene	5.01	4.71	0.61	0.92	1.85	1.78	0.40	0.32	0.06
i-Butene	1.43	0.74	0.08	0.13	0.18	0.21	0.07	0.06	0.01
Butadiene	0.36	0.66	0.37	1.14	1.19	1.58	0.90	0.73	0.09
Cyclopentane+Cyclohexane	0.13	0.12	0.03	0.09	0.12	0.12	0.06	0.05	0.01
Benzene	0.42	0.45	0.07	0.33	0.32	0.58	0.15	0.12	0.04

Decomposition of acrolein and ketenes leads to carbon monoxide and alkenes. Hydrogen can proceed from dehydrogenation of alkans to alkenes, or even from hydrocarbon decomposition in elements. Long chains of paraffins are decomposed into shorter alkane chains and alkenes. Cyclopentane and cyclohexane are formed by cyclization of nC_5-C6 olefins. Benzene results from cyclohexane dehydrogenation. Of course, in the literature, the mechanism is more complex, explaining the presence of other compounds such as: aldehydes, ketones, alcohols, dimethyl ether, most of them in the liquid phase. We could add to this mechanism, the reaction between carbon (coke) with oxygen containing radicals (e.g. carboxylate) which could explain the high content of carbon oxides in gas (up to 17.27% wt.) very close to that of 18.5%, if all oxygen in the raw would transform in carbon oxides (1:1 CO/CO_2 mass ratio); this would be impossible because not all triglycerides decompose and if so, the oxygen is also found in other products: acrolein, ketenes, free carboxylic acids, ethers, aldehydes, ketones, etc.

Yields of the most interesting gaseous compounds are reported in literature but they are very different from an experiment to another, as the experimental conditions differ very much. For example, at relatively low temperature (400-500°C) and long residence time (90-360 min), Sadramelli and Green (2007) obtained from canola oil 17-23.7% w/w ethylene and 10.3-13.6% w/w propylene, since Zamostny and al.(2012), from the same oil obtained 28,5% w/w ethylene and 11.5% w/w propylene, at 800°C and short (unspecified) residence time; at temperature of 475-630°C, and residence time between 2 and 4 min, we obtained 0.73-9.88 %w/w ethylene and 0.61-10.45% propylene, from waste palm oil. In the present study, were obtained 4.39-17.27% w/w carbon oxides, which is much comparing with Sadrameli and Green (2007): 2,9-3.9% w/w, but close to 15.2% w/w obtained by Zamostny et al (2012): 15.2%.

Concerning the yield of gaseous products obtained in this study, the following are observed:

- The hydrogen is in concentration of little importance for recovery and purification, but hydrocarbons are predominantly olefins in good yields. As seen in Table 2, the olefins yields are highest at high temperature and residence time: 28.8% (w/w) at 620°C and 240 s. At 480°C and 120 s, the olefins yield is merely 1.75% (w/w). The carbon oxides yield also increases with temperature and residence time, having a maximum of 17.27% (w/w) at 620°C and 240 s. It is obvious that longer residence time and higher temperature favor the breaking of oil molecules into numerous smaller molecules.

-The olefins: alkanes ratio also increases with temperature and residence time from 1.58 at 480°C and 120 s to 2.76 at 620°C and 240 s. Correlated with hydrogen yield increasing at higher temperature and longer residence time, this is a proof of dehydrogenation being favored in such conditions.

3.3. Liquid products

In every run, a liquid product was obtained, with a yield varying between 26.69% w/w and 92.03% w/w, as seen in Table 3. The liquid yield was calculated as product weight percent from feed weight. In general, the pyrolytic oil yield is lower at higher temperature and shorter residence time.

Comparable results were obtained by Wiggers et al (2009) from soybean oil pyrolysis, in absence of water or inert gas at 450ºC (92% w/w) and at 600ºC (58% w/w) , but at shorter residence times (12 s and 36 s, respectively). Kozliak et al (2013) studied the pyrolysis of Jojoba oil and, at 180 s (like us) and temperatures between 430ºC-470ºC. They obtained a liquid yield of 95% w/w at 430ºC and 73% w/w at 470ºC. It is notable that reactors were different: Wiggers et al. (2009) worked on a similar tubular continuous reactor but with a bigger diameter (0.067 mm) and Kozliak et al. (2013) worked on a continuous stirred reactor. The type and geometry of the reactor affect the results. In general, to obtain large yields of liquid, the pyrolysis is recommended at temperature between 300ºC and 450ºC. Some characteristics of the liquid obtained in this study are shown in Table 3.

As seen in Table 3, the density of the liquid products, in range of 852- 879 kg m^{-3}, is sensibly under the density of feed oil (924 kg m^{-3}), this proving the breaking of large molecules during the process. Differences among the nine samples are small, noting lower values for higher process temperature. The flash points are in range of 45-50ºC, due to volatile compounds in the samples (light hydrocarbon, aldehydes, alcohols). The kinematic viscosity is much lower (4.4 - 8.3 cSt at 20ºC) than that of the feed, as a result of cracking reactions. The Iodine numbers, as an indicative of the unsaturated character, is sensibly higher than the oil's, noting highest values at process temperature over 600 ºC, showing that the influence of temperature is greater than of residence time.

All these characteristics indicate the opportunity for the use of the pyrolysis oil as it is or as a component of fuel oil, but the main characteristic counting for such use is the calorific power. Three composite samples were made-up, one for each residence time runs, and the heat of combustion (the lower calorific power) was determined. All samples had very close calorific power: 9225, 9253, and 9260 kcal/kg, respectively (1 kcal = 4.184 kJ). These are considered good values for fuel oils and are in range of other experimental data. For example, in their review from 2017, Wiggers et al. reported a calorific power of 8015 ±3670 kcal/kg.

3.4. Mathematical modelling

Since the internal diameter of the reactor (0.019 m) in this study is of the same size grade as the industrial tubes (0.07-0.08 m), the experimental data could be processed for drawing-up mathematical models serving to scale-up the process for industrial applications.

Firstly, the total gas yield was modelled. The experimental results for the dependency of total gas yield on the process factors (temperature and residence time) suggest that a polynomial equation of second order (Eq.6) should describe the process:

$$y = a_0 + a_1 \cdot x_1 + a_2 \cdot x_2 + a_3 \cdot x_1 \cdot x_2 + a_4 \cdot x_1^2 + a_5 \cdot x_2^2 \qquad (6)$$

where: y is the total gas yield, (%) (w/w); x_1 - the residence time, (s); x_2 - the temperature, (ºC); $a_0 ... a_5$ - the model coefficients.

The model's coefficients were calculated by linear regression and statistically explored with "Data analysis" facility of Microsoft Excel. The regression statistics shows apparently a good fitting of the model's coefficients to the experimental data, since the correlation coefficient r^2 and adjusted r^2 are very high: 0.9995 and 0.9987, respectively. The analysis of variance (ANOVA), presented in Table 4 shows that most of coefficients in (Eq.1) are significant ($p < 0.05$), except the coefficient for the term x_1x_2, where p=0.204953; also, the standard error for this coefficient, 0.00012, is too high comparing with its value: 0.00019. As a consequence, this coefficient is not significant for the model, so it was discarded from (Eq.6), and the other coefficients were re-estimated.

The resulted model is presented in Eq.7:

$$y = -458.459 + 0.501 \cdot x_1 + 1.374 \cdot x_2 - 0.00084 \cdot x_1^2 - 0.00102 \cdot x_2^2 \qquad (7)$$

Table 3. Physico-chemical characteristics of liquid products at the thermal cracking of waste palm oil

Sample #	***1***	***2***	***3***	***4***	***5***	***6***	***7***	***8***	***9***
Residence time, s	240	240	240	180	180	180	120	120	120
Temperature, °C	620	600	475	555	580	630	550	530	480
Liquid yield, %w/w from which:	26.69	40.68	74.53	54.76	50.8	48.49	68.08	74.09	92.03
Density , kg m^{-3}	852	860	873	870	860	856	875	866	879
Flash point, ºC	45	47	50	48	47	46	48	47	49
Kinematic viscosity at 20ºC, cSt	5.4	5.6	6.3	5.2	4.9	4.4	5.9	4.4	8.3
Iodine number, g I_2/100 g oil	7.54	7.37	5.07	6.50	6.77	7.90	5.54	5.47	4.62

Table 4. Coefficients and ANOVA analysis for the model (Eq.6)

	Coefficients	***Standard Error***	***t Stat***	***P-value***
Intercept	-465.89	30.39789	-15.3264	0.000603
x1	0.501362	0.061947	8.093407	0.003942
x2	1.379573	0.110445	12.49109	0.001106
x1x1	-0.00069	0.000177	-3.90159	0.029889
x1x2	-0.00019	0.000118	-1.6139	0.204953
x2x2	-0.00099	0.000102	-9.6741	0.002345

This time, the statistical analysis proved that the model has a good fitting (adjusted r^2=0.9981) and all coefficients are significant ($p<0.05$), so it can be considered as reliable.

For the main products in gas, a polynomial model of second degree was also preferred because it seems more appropriate for the results obtained in the experiment. The complete model is in Eq.6 form, but after many trials, only the significant coefficients were taken into account and only the models with good fitting remained. In Table 5, the model's parameters are presented succinctly, for the main products in the pyrolysis gas.

Even though butenes and butadiene are also important, the modeling lead to nothing and there is an explanation: due to the final condensation conditions (cca. 30ºC; 2 barg), an important part of these compounds can be found in the liquid product and so, not all the produced C_4 was quantified in gas.

As seen in Table 5, the gaseous products yields are predicted with good fitness by a second degree polynomial but propane's yield by a first degree polynomial equation, describing correctly the tendency of linear increasing with temperature and residence time; the model's accuracy is not so high in case of propane. The models are valid in the studied temperature range (475ºC-630ºC) and residence time (120-240 s).

4. Conclusions

This work investigated the obtaining of olefins and other valuable products from waste cooking palm oil through pyrolysis, in continuous stationary regime. The effect of process temperature (475ºC - 630ºC) and residence time (120 s- 240 s) on gaseous products was observed and quantified. Higher temperature (620-630ºC) and longer residence time (240 s) lead to highest gas yield and olefins. Yields could be even higher at temperature over 630ºC, but the experimental set is limited to this. However, olefins yield between 24% and 29% w/w, and particularly good yield of ethylene (up to 10% w/w) and propylene (up to 10.5% w/w) are significant even in these experimental conditions. Also, liquid product obtained in the process, with yields varying between 26.69% w/w and 92.03% w/w, had good heat of combustion value and physical characteristics fit for use as fuel oil itself or as a component.

For total gas and separately for ethylene, propylene, methane, ethane, propane, and carbon oxides, polynomial models were developed predicting yields as a function of temperature and residence time. The models have good accuracy and analysis of variance proved that models are good at 5% significance level. The olefins yield, good quality of pyrolysis oil as liquid fuel and the possibility to predict their yields with accuracy, recommend the results of this study as a step in scaling up for industrial applications.

Acknowledgements

Many thanks to the analytical laboratory of Rompetrol Quality Control, Năvodari, Romania, where the chromatographic analyses and heat of combustion determinations were performed.

Table 5. Summary of models for predicting the main products yields at the pyrolysis of waste palm oil

Product	***Model***	***Analysis of variance for the Eq.6 coefficients, p values***	***Adjusted correlation coefficient, r^2***	***Standard error***
Ethylene	$y=-105.16+0.0174\cdot x_1+0.3425\cdot x_2-0.00026\cdot x_2^2$	a_0:0.0024 a_1:0.0033 a_2:0.0038 a_5:0.0079	0.9858	0.408
Propylene	$y=-70.58-0.0551\cdot x_1+0.2429\cdot x_2+0.00015\cdot x_1x_2-0.00021\cdot x_2^2$	a_0:0.0007 a_1:0.0364 a_2:0.0009 a_3: 0.0071 a_5:0.0012	0.9980	0.150
Methane	$y=-16.66-0.0685\cdot x_1+0.00015\cdot x_2+0.000151\cdot x_1x_2-0.000063\cdot x_2^2$	a_0:0.0399 a_1:0.0018 a_2:0.0312 a_3: 0.0010 a_5:0.0263	0.9954	0.120
Ethane	$y=-44.0014-0.0222\cdot x_1+0.1504\cdot x_2+0.00007\cdot x_1x_2-0.00026\cdot x_2^2$	a_0:0.0001 a_1:0.0123 a_2:0.0002 a_3: 0.0020 a_5:0.0002	0.9987	0.066
Propane	$y=-3.72+0.0052\cdot x_1+0.0020\cdot x_2$	a_0:0.0121 a_1:0.0520 a_2:0.0079	0.7878	0.297
$CO+CO_2$	$y=-225.904+0.0612\cdot x_1+0.7992\cdot x_2-0.00069\cdot x_2^2$	a_0:0.0156 a_1:0.0028 a_2:0.0173 a_5:0.0209	0.8951	1.38

References

Andreola F., Barbieri L, Lancellotti I., (2016), Valorization of tyres waste pyrolysis residue in lightweight materials, *Environmental Engineering and Management Journal*, **15** ,1907-1914.

Aslam M., Konwar L.J., Sarma A.K.R, Kothiyal N.C., (2015), An investigation of catalytic hydrocracking of high FFA vegetable oils to liquid hydrocarbons using biomass derived heterogeneous catalysts, *Journal of Analytical and Applied Pyrolysis*, **115**, 401–409.

Biswas Sh., Sharma D.K., (2014), Effect of different catalysts on the cracking of Jatropha oil, *Journal of Analytical and Applied Pyrolysis,* **110**, 346–352.

Dandik L., Aksoy H.A., (1998), Pyrolysis of used sunflower oil in the presence of sodium carbonate by using fractionating pyrolysis reactor, *Fuel Processing Technology,* **57**, 81–92.

Kozliak E., Mota R. , Rodriguez D., Overby P., Kubatova A, Stahl D, Niri, V, Ogden G., Seames W.S., (2013), Non-catalytic cracking of jojoba oil to produce fuel and chemical by-products, *Industrial Crops and Products*, **43**, 386-392.

Kubatova A., Luo Y., Stavova J., Sadrameli S.M., Aulich T., Kozliak E., Seames W., (2011), New path in the thermal cracking of triacylglycerols (canola and soybean oil), *Fuel*, **90,** 2598–2608.

Kuncser R., Paraschiv M., Tazerout M., Bellettre J., (2010), Liquid fuel recovery through pyrolysis of polyethylene waste, *Environmental Engineering and Management Journal*, **10**, 1371-1374

Maher K.D., Bressler D.C., (2007), Pyrolysis of triglyceride materials for the production of renewable fuels and chemicals*, Bioresource Technology*, **98**, 2352-2358.

Marton S., (2013), *Renewable Ethylene. A review of options for renewable steam cracker feedstocks*, MSc Thesis, Chalmers University of Technology, Gothenburg, Sweeden.

Miandad R., Barakat M.A., Rehan M., Aburiazaiza A.S., Gardy J., Nizami A.S., (2018), Effect of advanced catalysts on tire waste pyrolysis oil, *Process Safety and Environmental Protection,* **116**, 542-552.

Neri E., Berti B., Passarini F., Vassura I., Giorgini L., Zattini G., Tosi C., Cavazzoni M., (2018), Application of LCA methodology in the assessment of a pyrolysis process for tyres recycling, *Environmental Engineering and Management Journal*, **17**, 2437-2445.

Olugu E.U., Wong K.Y., Awaluddin M.Sh., Abdul-Rashid S.H., Bin Raja Ghazilla R.A., (2017), Sustainable supply chain management in Malaysian SMEs: perspectives from practitioners, *Environmental Engineering and Management Journal*, **16**, 2123-2132.

Osayi J.I., Iyuke S., Daramola M.O., Osifo P., Van Der Walt I.J., Ogbeide S.E., (2018), Pyrolytic conversion of used tyres to liquid fuel: characterization and effect of operating conditions, *Journal of Material Cycles and Waste Management*, **20**, 1273-1285.

Owolabi R.U., Osiyemi N.A., Amosa M.K., Ojewumi M.E., (2011), Biodiesel from Household/Restaurant Waste Cooking Oil (WCO), *Journal of Chemical Engineering & Process Technology*, **2**, 1-4.

Sadrameli S.M., Green A.E.S., (2007)**,** Systematics of renewable olefins from thermal cracking of canola oils, *Journal of Analytical and Applied Pyrolysis*, **78**, 445-451.

Sivriu A.M., Koncsag C.I., Jinescu G., Mares A.M, (2017), Thermal cracking of waste vegetable oil- A preliminary research, *UPB Scientific Bulletin*, **79**, 67-74.

Thomas A., (2002), *Fats and Fatty Oils*, In: *Ullmann's Encyclopedia of Industrial Chemistry*, Weinheim: Wiley-VCH, On line at: https://doi:10.1002/14356007.a10_173.

Umeki E.R, Fernandes de Oliveira C, Torres R.B., Gonçalves dos Santos R., (2016), Physico-chemistry properties of fuel blends composed of diesel and tire pyrolysis oil, *Fuel*, **185**, 236-242

Wiggers V.R., Meier H.F., Wisniewski Jr.A., Chivanga Barros A.A., Wolf Maciel M.R., (2009), Biofuels from continuous fast pyrolysis of soybean oil: A pilot plant study, *Bioresource Technology*, **100**, 6570–6577.

Wiggers V.R., Beims R.F., Ender L., Simionatto E.L., Meier H.F., (2017), *Renewable Hydrocarbons from Trigliceride's Thermal Cracking*, In: *Frontiers in Bioenergy and Biofuels*, Jacob-Lopes E., Queiroz-Zepka L. (Eds.), Inech Open Ltd., London, 407-424.

Xu J., Jiang J., Zhao J., (2016),Thermochemical conversion of triglycerides for production of drop-in liquid fuels, *Renewable and Sustainable Energy Reviews*,**58**, 331-335.

Yigezu Z.D., Muthukumar K., (2015), Biofuel production by catalytic cracking of sunflower oil using vanadium pentoxide, *Journal of Analytical and Applied Pyrolysis*, **112**, 341–347.

Yu F., Gao L., Wang W., Zhang G., Ji J., (2013), Bio-fuel production from the catalytic pyrolysis of soybean oil over Me-Al-MCM-41 (Me=La, Ni or Fe) mesoporousmaterials, *Journal of Analytical and Applied Pyrolysis*, **104**, 325-329.

Zaher F., Gad M.S., Aly S.M., Hamed S.F., Abo-Elwafa G., Zahran H.,(2017), Catalytic cracking of vegetable oils for producing biofuel, *Egyptian Journal of Chemistry*, **60**, 291-300.

Zamostny P., Belohlav Z., Smidrkal J., (2012), Production of olefins via steam cracking of vegetable oils, *Resources, Conservation and Recycling*, **59**, 47-51.

Zandonai C.H., Ortiz Bravo C.A., Fernandes-Machado R. C., (2015), Biofuel production from thermocatalytic processing of vegetable oils: a review, *Revista Fuentes: El Reventon Energetico*, **13**, 84-89.

Environmental Engineering and Management Journal
February 2020, Vol.19, No. 2, 353-358
http://www.eemj.icpm.tuiasi.ro/; http://www.eemj.eu

"Gheorghe Asachi" Technical University of Iasi, Romania

STUDY OF DIFFERENT LIQUID MEDIA INFLUENCE ON *Arthrospira platensis* MICROALGAE CULTIVATION FOR ENVIRONMENTAL APPLICATIONS

Mariana Diaconu, Irina Volf, Igor Crețescu, Gabriela Șoreanu[*]

"Gheorghe Asachi" Technical University of Iasi, "Cristofor Simionescu" Faculty of Chemical Engineering and Environmental Protection, Department of Environmental Engineering and Management, 73 D. Mangeron Blvd., Iasi 700050, Romania

Abstract

Growth rate and biomass yield in the case of *Arthrospira platensis* depend on nutrient availability, temperature and light, which can determine changes in the metabolism and therefore in the biomass composition. The aim of this study is to evaluate the behavior of *A. platensis* during the growing time in several liquid culture media and their influence on the yield of biomass production. The following culture media have been investigated in this sense: ARS, Zarrouk (Z), modified Zarrouk (MZ), economic (EM) and UTEX media. Experiments have been carried out by using Erlenmeyer flasks containing 100 mL medium inoculated with 5% cellular suspension of *A. platensis*. Monitoring of microalgae development has been performed for 30 days at room temperature, 12/12 light/dark alternation regime and daily intermittent shaking. Optical density (OD) has been measured every three days. Dry substance, protein and antioxidant enzymes (catalase and dehydrogenase) were determined at the end of the cultivation period. Results of OD monitoring relieved a very fast acclimatization and exponential growth of *A. platensis* on UTEX, ARS and Zarrouk media, while a higher lag period and a slower growth have been observed on MZ and EM. The algal dry weight (DW) was greatly enhanced on UTEX, ARS and Z media, where the highest amounts of protein were recorded. The lack of carbon source in EM and MZ media has increased the activity of antioxidant enzymes, which suggests that these conditions could be considered in further investigations related to the antioxidants harvesting from *A. platensis*. Overall, economic media in the microalgae-based systems used in environmental applications can sustain biomass development and the increase of the enzymatic activity, at a reasonable yield and lower costs.

Key words: Arthrospira platensis, catalase, culture media, dehydrogenase, dry mass, protein

Received: January, 2019; Revised final: February, 2020; Accepted: February, 2020; Published in final edited form: February, 2020

1. Introduction

Of all cyanobacteria, *Arthrospira platensis* is most often used for biomass production, because of its high cell growth rate, easy process control and biomass recovery, ability to grow on alkaline and high-salt media, reduced risks of contamination and flexibility and resistance to adverse or suboptimal conditions (Vonshak, 1997). *Arthrospira (spirulina) platensis* is a mesophilic microalga that grows naturally in many places, including freshwater, saltwater lakes and marine environments. It usually develops under photoautotrophic conditions, but can also adapt to mixotrophic and heterotrophic conditions (Chen and Zhang, 1997). Undoubtedly, *A. platensis* is one of the most cultivated microalgae in the world. Overall, cultivation conditions dictate the biomass yield, quality and production costs, with a significant impact on the *A. platensis* industry (Delrue et al., 2017) and related applications. The growth of *such microalgae* and the composition of the produced biomass depend on several key factors, such as the availability of nutrients, temperature, light and pH (Fagiri et al., 2013). Particularly, *A. platensis* growth

---

[*] Author to whom all correspondence should be addressed: e-mail: gsor@tuiasi.ro

is favored at relatively high pH values e.g. between 9.5 and 11.0 with an optimum at 10.5, which also inhibits the culture contamination (Delrue et al., 2017; Madkour et al., 2012). Therefore, high amounts of sodium bicarbonate must always be present in the culture medium to sustain the high pH and prevent fluctuation. The composition of the culture medium plays an important role when referring to biomass yield and other compounds of interest such as protein content, antioxidant enzymes, pigments etc. (Marrez et al., 2013). In biotechnological processes, the components of culture media are responsible for high costs and exert a strong influence on the behavior of microorganisms. Several studies have been conducted to reduce these costs by using alternative components or by changing their concentration (Pandey and Tiwari, 2010). Zarrouk medium is a standard culture medium used for the development of *A. platensis* (de Castro et al., 2015). Manipulation of cultivation conditions can promote the biosynthesis of various compounds and, in addition, these variables can be controlled to reduce the cost of the production process.

Particularly, cultivation aspects play an important role for further tailoring of appropriate conditions in the perspective of involving *A. platensis* in environmental applications (e.g. wastewater or air treatment). In fact, using microalgae for the decontamination of gaseous or aqueous streams is a very promising trend in the field of environmental biotechnology (Markou et al., 2012; Șoreanu et al., 2018; Zinicovscaia et al. 2013). Despite this potential, such microalgae-based environmental applications are in the early stage of development (Șoreanu et al., 2018). In a sustainable process, biomass production should be correlated with the economical and the environmental benefits. Thus, *A. platensis* cultivation can be improved taking into account three criteria: productivity, quality and cost. The productivity of spirulina biomass can be significantly improved by using the suitable medium.

Therefore, the present study has been conducted to assess the growth of *A. platensis* on different culture media and to compare the growth characteristics, productivity and biochemical composition of the organism developed on these nutrient substrates, while depicting their implication from the environmental application perspective.

2. Materials and methods

2.1. Microorganism and inoculum preparation

The strain *A. platensis* (Algae Research Supply) was supplied as kit culture comprising the 1.7 mL algae and the standard culture medium (ARS) required for obtaining the inoculum used in the experiments.

An axenic stock culture of 50 mL standard medium (ARS) and 1.7 mL algae was maintained in 250 mL sterilized Erlenmeyer flask at room temperature, pH 10.1± 0.2 with 12/12 light/dark alternation regime and daily intermittent shaking. Thus, the inoculum used in the subsequent experiments was obtained.

2.2. Culture media and experiments

Batch experiments were conducted in 300 mL Erlenmeyer flasks containing 100 mL medium inoculated with 5% cellular suspension of *A. platensis*, to evaluate the effects of media composition on the growth profile, productivity and biochemical composition of the *A. platensis*. The following culture media have been investigated in this sense: ARS (available from Algae Research Supply), Zarrouk (Z) (adapted from Nyabuto et al., 2015), modified Zarrouk (MZ), economic (EM) and UTEX media (available from UTEX Culture Collection of Algae). The chemical composition of these media is presented in Table 1.

Table 1. Ingredients of synthetic media used in experiments

No.	***Ingredients***	***Culture media***				
		ARS	***Zarrouk***	***MZ***	***EM***	***UTEX***
		Amount (g/L)				
1	$NaHCO_3$	13.61	18.00	-	4.50	13.61
2	Na_2CO_3	4.03	-	-	-	4.03
3	Sodium bicarbonate food	-	-	18.0	5.00	-
4	$NaNO_3$	2.50	2.50	2.50	1.50	2.50
5	K_2HPO_4	0.50	0.50	0.50	0.05	0.50
6	K_2SO_4	1.00	1.00	1.00	1.00	1.00
7	NaCl	1.00	1.00	1.00	1.00	1.00
8	$CaCl_2 \cdot 2H_2O$	0.04	0.04	0.04	0.04	0.04
9	$MgSO_4 \cdot 7H_2O$	0.20	0.20	0.20	0.20	0.20
10	$FeSO_4 \cdot 7H_2O$	0.0007	0.01	0.01	0.015	-
11	$FeCl_3 \cdot 6H_2O$	-	-	-	-	0.00058
12	Na_2- EDTA$\cdot 2H_2O$	0.0008	0.08	0.08	-	0.00450
13	**Micronutrients***	***a***	***b***	***b***	***b***	***c***
14	Vitamin B12	0.0005 mg/L	-	-	-	0.135 mg/L
15	**Other adjuvants****	-	-	-	-	d
16	Distilled water	1000 mL	1000 mL	1000 mL	1000 mL	1000 mL

***Micronutrients**

No.	Ingredients	a	b	c
		(mg/L)		
1	H_3BO_3	0.010	2.860	0.620
2	$MnCl_2 \bullet 4H_2O$	-	1.810	0.012
3	$MnSO_4 \bullet 7H_2O$	0.002	-	-
4	$ZnSO_4 \bullet 7H_2O$	0.001	0.222	0.044
5	$CuSO_4 \bullet 5H_2O$	0.000005	0.079	0.020
6	$Na_2MoO_4 \bullet 2H_2O$	0.001	0.390	0.012
7	Na_2- EDTA • $2H_2O$	-	-	0.050
8	$CoCl_2 \bullet 6H_20$	-	-	0.020
9	$Co(NO_3)_2 \bullet 6(H_2O)$	0.001	-	-

*****Other adjuvants (d)**: $MnCl_2 \bullet 4H_2O$ - 0.246 mg/L; $ZnCl_2$ - 0.030 mg/L; $CoCl_2 \bullet 6H_2O$ - 0.012 mg/L; $Na_2MoO_4 \bullet 2H_2O$ - 0.024 mg/L; HEPES buffer pH 7.8 – 0.012 g/L.*

2.3. Growth, biomass and biochemical analysis

Monitoring of microalgae development has been performed for 30 days at room temperature, 12/12 light/dark alternation regime and daily intermittent shaking. The development of submerged microalgae cultures was determined every three days by measuring the optical density at λ 600 nm, using a UV- VIS spectrophotometer "Helyos ε" (Thermo Electron Corporation).

Cell productivity (CP_x) of *A. platensis* was evaluated using the equation:

$$CP_x(mg/L/day)= (X_m– X_i/t_m), \quad (1)$$

where: X_i = initial cell concentration (mg/L); X_m = maximum cell concentration (mg/L); t_m = cultivation time related to maximum cell concentration (days).

After the incubation period, *A. platensis* cultures were harvested by centrifugation at 7000 rpm for 15 min at 4°C, and the cell mass obtained were washed with 10 mM Na_2-EDTA and then twice with distilled water. The algal pellets were homogenized with an equal volume of glass beads at 4°C in 2 mL of extraction buffer containing 50 mM of phosphate buffer (pH 7.0). A further centrifugation is performed under the same conditions. The supernatant was used to measure the protein content according to Lowry et al. (1951) and modified by Clayton et al. (1988). A calibration curve was prepared using bovine standard albumin at a concentration range of 0 to 1500 μg mL^{-1}. In order to measure the protein content, 0.2 mL of each standard or samples containing the crude protein extract was withdrawn and then 1 mL of modified Lowry reagent was added to each sample. Each sample was then vortexed and incubated for 10 min. After incubation, 100 μL of Folin-Ciocalteu Reagent (1 N) was added and again vortexed and incubated for 30 min. The blue color solution was then measured at 750 nm with a UV-VIS Helyos ε spectrophotometer.

Also, the activity of the antioxidant enzymes (catalase and dehydrogenase) was determined. The activity of the catalase was assayed according to the method of Kar and Mishra (1976). One unit of catalase activity is defined as the amount of enzyme that decomposes 1 mmol of H_2O_2 in 1 min under the assay conditions described. The activity was expressed in U/mg protein.

Dehydrogenase activity was determined based on the reduction of 2,3,5-triphenyltetrazolium (TTC) chloride to triphenylformazan (TPF) colored in red. The amount of formazan formed was determined spectrophotometrically at 480 nm. Dehydrogenase activity was expressed in micrograms of TPF formed on one milligram of dry biomass (Kar and Mishra, 1976). To estimate the dry biomass a known volume of culture was sampled and weighed. Then it was centrifuged at 7000 rpm for 10 minutes. The supernatant was discarded and the pellets were washed three times with sterile distilled water, dried in oven at 50-60^{0}C and weighed. The difference in weight before and after drying represented the biomass and was expressed as mg/L.

3. Results and discussions

In experiments conducted to evaluate *A. platensis* growth and biomass production, five culture media (ARS, Z, MZ, EM, UTEX) with different chemical composition were used. All trials have been performed in triplicates. The presented results represent the average values. The other parameters (pH, temperature, light) were kept constant during the cultivation period so that growth differences and active metabolic products (protein, enzymes) were due exclusively to the composition of the culture medium. Growth performance of *A. platensis* under different culture media was measured in terms of optical density. The results are shown in Fig. 1.

The growth curves lacked a lag phase for ARS, UTEX and Z media. In contrast the lag phase on the EM and MZ media keep up to three days. On these media, culture grows exponentially until 24 days, after which the stationary phase is established, due to the lack of nutrients. A rapid increase in biomass values was observed in UTEX, ARS and Z media, giving the maximum biomass values at the end of the cultivation period, which indicates that culture is still in the exponential growth phase due to the availability of nutrients. The maximum growth belongs to the UTEX media. The OD of these cultures was 1.821 after 30 days, but close values were also recorded on ARS (1.728) and Z (1.711), respectively. It might be possible that the higher content of vitamin B12 in UTEX medium contributed to its superior performances among these performant mediums, otherwise their composition is quite equilibrated (Table 1) and could explain the close values.

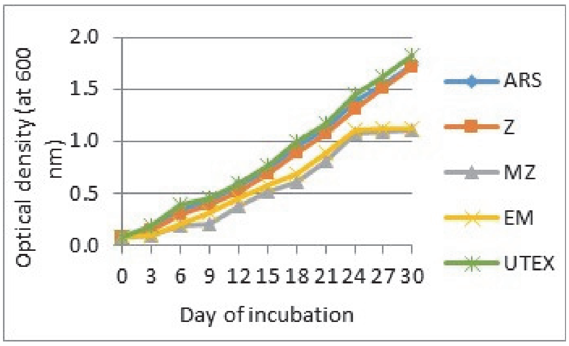

Fig. 1. The growth pattern of *A. platensis* in different liquid media by measured optical density

In a study conducted by Murugan and Radhamadhavan (2010) using Zarrouk medium with four different supplements and four different concentrations to increase *A. platensis* growth, an exponential increase in OD (0.6 -0.7 maximum) was recorded throughout the cultivation period (20 days) at optimal nutrient concentrations. These values were lower than the maximum OD observed in the present study, which is comparable to those obtained by Soni et al., (2012) that cultivated *A. platensis* under three different conditions i.e. F.G.C. (Fibre Glass Chamber), outdoor conditions and lab conditions.

Table 2 shows the cell productivity, protein and dry mass found for the five experimental variants. The biochemical composition of the microalgae greatly depends on the type and amount of nutrients present in the culture medium, especially the carbon and nitrogen sources. Cellular productivity reflects the daily growth rate of *A. platensis* culture, which is much more intense in UTEX, ARS and Z media compared to EM and MZ, which also led to different biomass (Fig. 2). The values of proteins varied from 46.07% dw^{-1} (MZ) to 52.31 % dw^{-1} (UTEX), depending on the composition of the culture media. Higher levels of protein content (60-67%) were reported by other authors (Danesi et al., 2002), but in other experimental conditions in which the nitrogen source increased. El-Baky et al., (2008) reported that the use of 1.875 g/L sodium nitrite, maintaining the culture at 35° C, decreases biomass production but results in higher protein, lipid and phenolic compounds. However, these results were obtained varying the concentration of nitrates without simultaneous variation of bicarbonate, a factor of particular importance in the process of cyanobacterial development. Also, the amount of protein varies from one experimental variation to another and is in direct correlation with the determined biomass.

The obtained biomass concentration was 2.8932 g/L (UTEX), 2.6827 g/L (ARS) and 2.4911g/L (Z). For EM and MZ, the recorded biomass values were 2.0372 g/L and 1.9553 g/L. The reduction of algae production in EM and MZ can be explained by the existence of an insufficient amount of CO_2 due to a small contribution of bicarbonate as a carbon source.

Fig. 2. General aspect of the *A. platensis* culture growing on liquid media

Because of the stress from carbon dioxide deficiency, the free radicals or ROS (reactive oxygen species) levels in algal cells may increase, which causes the algal cells to undergo oxidative stress (Choo et al., 2004; Ismaiel et al., 2016). The source of carbon is the main nutrient needed for *A. platensis* growth. Vonshak et al. (1982) have shown that, apart from the biotechnological process, the second major cost of biomass production of *A. platensis* is the cost of nutrients, mainly the carbon source. Experimental results showed that when higher concentrations of sodium bicarbonate were used, even at a lower luminous intensity, there was an increase in the amount of biomass, confirming that $NaHCO_3$ is the most influential factor in obtaining a large amount of biomass.

Cyanobacterial cells prefer to capture HCO_3^- rather than CO_2, although this is a poorer carbon source when it is quantitatively limited in the culture medium. Biomass productivity increases with the concentration of CO_2 in the gas mixture to a certain percentage, after which productivity decreases (Kumar et al., 2011). This preference for bicarbonate favors the continuous growth of cyanobacteria, fact demonstrated by the existence of culture in the exponential phase, even after 30 days of cultivation on the UTEX, Z and ARS media (Fig. 1).

Table 2. Cell productivity (CP_x), protein and dry mass of *A. platensis* grown on different media

No.	*Culture media*	*CP_x (mg/L/day)*	*Protein (%dw^{-1})*	*Dry mass (g/L)*
1	ARS	0.0655 ± 0.0025	51.72 ± 1.33	2.6827 ± 0.0257
2	Z	0.0648 ± 0.0013	51.7 ± 1.50	2.4911 ± 0.0189
3	MZ	0.0418 ± 0.0009	46.07 ± 1.02	1.9553 ± 0.0292
4	EM	0.0427 ± 0.0009	47.62 ± 1.02	2.0372 ± 0.0264
5	UTEX	0.0690 ± 0.0008	52.31 ± 1.00	2.8932 ± 0.0192

Madkour et al. (2012) conducted a study to assess the production of *A. platensis* biomass under different nutritive conditions, with comparable behaviour to that in the present study. Data obtained in this study shows that the growth and biomass yield of *A. platensis* were clearly affected by the composition of the culture medium, especially the carbon source, which is a limiting factor in the EM and MZ media, becoming a stress factor for the development of cyanobacteria. As a result, it can increase the enzymatic activity, especially antioxidant enzymes such as catalase and dehydrogenase.

The values obtained by the determination of catalase and dehydrogenase (Figs. 3-4) reveal the existence of oxidative stress in the cultures of EM and MZ media, where the largest activities were recorded. In this case, the relative reduction of *A. platensis* growth on EM and MZ culture media could be compensated by the higher antioxidant content, which is beneficial for the growth of microalgae in the presence of toxic compounds. Thus, the antioxidant enzyme activity will accelerate the detoxification and removal of contaminants (El-Baky et al., 2007).

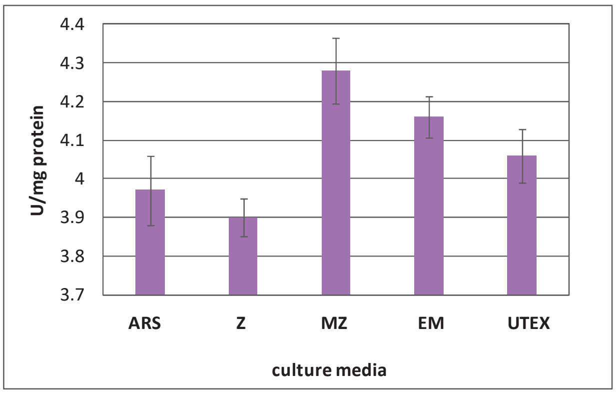

Fig. 3. Catalase activity of *A. platensis* grown on different liquid media

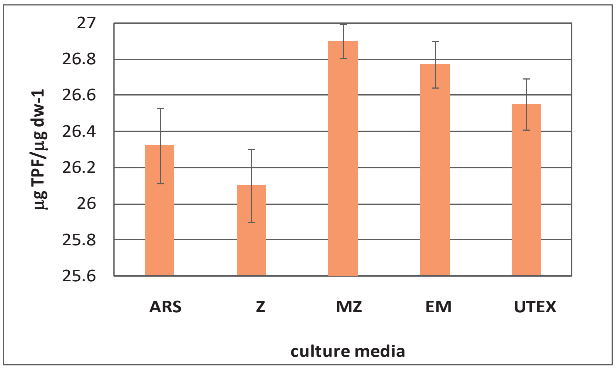

Fig. 4. Dehydrogenase activity of *A. platensis* grown on different liquid media

Environmental application perspectives

The obtained results in this study show that a low cost media can sustain a reasonable biomass development and favors the increase of the enzymatic activity. These aspects can be thus considered when developing sustainable microalgae-based biosystems for environmental applications. Soreanu et al. (2018) investigated CO_2 uptake from indoor air by microalgae in a sparged photobioreactor and shown that using nutrient/substrate - limiting culture can favor the contaminant uptake from the gas phase, thus creating perspectives for developing a cost-effective and environmental-friendly process. Under non-limiting conditions, microalgae tend to use the substrate readily available in the culture, rather than from the gas phase, which is in a good agreement with the results of the present study.

4. Conclusions

In order to optimize *A. platensis* cultivation conditions, it must be taken into account three criteria: quality, productivity and cost. The productivity of biomass can be significantly improved by using the suitable medium.

Although the highest biomass yield and dry substance, respectively, are obtained on the UTEX medium, the ARS and Zarrouk medium lead to good development performances of *A. platensis*. It should be also noted that the other alternative screened options (EM and MZ) allow a reasonable yield of biomass production at lower costs. Protein content in biomass developed on UTEX, ARS and Z medium was higher than in the case of EM and MZ medium, while an increased enzymatic activity was noticed for these last two medium.

Such information contributes to the development of cost-effective methods for biomass production based on *A. platensis*, with benefits for many practical applications, including those related to environmental biotechnology.

Acknowledgments

This work is supported by ROSA (Romanian Space Agency) - RDI Program for Space Technology and Advanced Research - STAR, project no. 157/2017.

References

Chen F., Zhang Y., (1997), High cell density mixotrophic culture of *Spirulina platensis* on glucose for phycocyanin production using a fed-batch system, *Enzyme and Microbial Technology*, **20**, 221-224.

Choo K.S., Snoeijs P., Pedersén M., (2004), Oxidative stress tolerance in the filamentous green algae *Chladophora glomerata* and *Enteromorpha ahlneriana*, *Journal of Experimental Marine Biology and Ecology*, **298**, 111-123.

Clayton J.R., Dortch Q., Thorensen S.S., Ahmed S.I., (1988), Evaluation of methods for the separation and analysis of proteins and free amino acids in phytoplankton samples, *Journal of Plankton Research*, **10**, 341-358.

Danesi E.D.G., Rangel-Yagui C.O., Carvalho J.C.M., Sato S., (2002), An investigation of effect of replacing nitrate by urea in the growth and production of chlorophyll by *Spirulina platensis*, *Biomass Bioenergy,* **23**, 261-269.

de Castro G.F.P.S., Rizzo R.F., Passos T.S., dos Santos B.N.C., Dias D.S., Domingues J.R., Araujo K.G.L., (2015), Biomass production by *Arthrospira platensis* under different culture conditions, *Food Science and Technolology (Campinas)*, **35**, 18-24.

Delrue F., Alaux E., Moudjaoui L., Gaignard C., Fleury G., Perilhou A., Richaud P., Petitjean M., Sassi J.F., (2017), Optimization of *Arthrospira platensis* (*Spirulina*) growth: from laboratory scale to pilot scale, *Fermentation*, **3**, doi:10.3390/fermentation3040059.

El-Baky H.H.A., El Baz F.K., El-Baroty G.S., (2007), Enhancement of antioxidant production in *Spirulina plantensis* under oxidative stress, *American-Eurasian Journal of Scientific Research*, **2**, 170-179.

El-Baky H.H.A., El-Baz F.K., El-Baroty G.S., (2008), Characterization of nutraceutical compounds in blue green alga *Spirulina maxima*, *Journal of Medicinal Plants Research*, **2**, 292-300.

Fagiri Y.M.A., Salleh A., El-Nagerabi S.A.F., (2013), Influence of chemical and environmental factors on the growth performance of *Spirulina platensis* strain SZ100, *Journal of Algal Biomass Utilization,* **4**, 7-15.

Ismaiel M.M.S., El-Ayouty Y.M., Piercey-Normore M., (2016), Role of pH on antioxidants production by *Spirulina (Arthrospira) platensis*, *Brazilian Journal of Microbiology*, **47**, 298-304.

Kar M., Mishra D., (1976), Catalase, peroxidase and polyphenol oxidase activities during rice leaf senescence, *Plant Physiology*, **57**, 315-319.

Kumar K., Dasgupta C.N., Nayak B., Lindblad P., Das D., (2011), Development of suitable photobioreactors for CO_2 sequestration addressing global warming using green algae and cyanobacteria, *Bioresource Technology*, **102**, 4945-4953.

Lowry O.H., Rosebrough N.J., Farr A.L., Randall R.J., (1951), Protein measurement with the Folin phenol reagent, *Journal of Biological Chemistry*, **193**, 265-275.

Madkour F.F., El-Wahab Kamil A., Nasr H.S., (2012), Production and nutritive value of *Spirulina platensis* in reduced cost media, *Egyptian Journal of Aquatic Research*, **38**, 51-57.

Markou G., Chatzipavlidis I., Georgakakis D., (2012), Effects of phosphorus concentration and light intensity on the biomass composition of *Arthrospira (Spirulina) platensis*, *World Journal of Microbiology and Biotechnology*, **28**, 2661-2670.

Marrez D.A., Naguib M.M., Sultan Y.Y., Daw Z.Y., Higazy A.M., (2013), Impact of culturing media on biomass production and pigments content of *Spirulina platensis*, *International Journal of Advanced Research*, **1**, 951-961.

Murugan T., Radhamadhavan I., (2010), Media optimization for the enhanced growth and yield of *Spirulina platensis* biomass and determination of generation time, *International Journal of Medical Sciences*, **3**, 34-39.

Nyabuto D.K., Cao K., Mariga A.M., Kibue G.W., He M., Wang C., (2015), Growth performance and biochemical analysis of the genus *Spirulina* under different physical and chemical environmental factors, *African Journal of Agricultural Research*, **10**, 3614-3624.

Pandey J.P., Tiwari A., (2010), Optimization of biomass production of *Spirulina maxima*, *Journal of Algal Biomass Utilization,* **1**, 20–32.

Soni S.K., Agrawal K., Srivastava S.K., Gupta S., Pankaj C.K., (2012), Growth performance and biochemical analysis of *Spirulina platensis* under different culture conditions, *Journal of Algal Biomass Utilization*, **3**, 55-58.

Soreanu G., Cretescu I., Diaconu M., Ignat M., Harabagiu V., Cojocaru C., Samoila P., (2018), *Monitoring of CO_2 uptake by microalgae in indoor environment*, Proc. GLOREP 15-17 November, Timisoara, Romania, 255-259.

Vonshak A., (1997), *Spirulina Platensis (Arthrospira): Physiology, Cell Biology and Biotechnology*, Taylor & Francis Ltd., London.

Vonshak A., Abeliovich A., Boussiba S., Arad S., Richmond A., (1982), Production of Spirulina biomass: effects of environmental factors and population density, *Biomass*, **2**, 175-185.

Zinicovscaia I., Duca G., Rudic V., Cepoi L., Chiriac T., Frontasyeva M.V., Pavlov S.S., Gundorina S.F., (2013), *Spirulina platensis* as biosorbent of zinc in water, *Environmental Engineering and Management Journal*, **12**, 1079-1084.

Websites

https://algaeresearchsupply.com/pages/spirulina-media
https://utex.org/products/spirulina-medium

Environmental Engineering and Management Journal

February 2020, Vol. 19, No. 2, 359-367
http://www.eemj.icpm.tuiasi.ro/; http://www.eemj.eu

"Gheorghe Asachi" Technical University of Iasi, Romania

STUDY OF HEAVY METAL DYNAMICS IN SOIL

Georgiana Cezarina Bartic Lazăr*, Florian Stătescu, Daniel Toma

"Gheorghe Asachi" Technical University of Iasi, Faculty of Hydrotechnical Engineering, Geodesy and Environmental Engineering, Department of Hydroamelioration and Environmental Protection,
65 Prof. Dr. docent D. Mangeron Blvd., 700050, Iasi, Romania

Abstract

The paper covers the results of a study, carried out during 2005 and 2018, regarding the impact of sludge dump of a wastewater treatment plant from Iasi city, Romania, on the soil characteristics. Experimental research was conducted to highlight the evolution of the heavy metal content of both the material in the storage site and the soil in its proximity. The following heavy metal concentrations were analyzed with atomic adsorption spectrometry method: Zn, Ni, Cr, Pb, Co, Cu and Cd. Research has also addressed other physical (particle size composition and soil moisture) and chemical (pH, sludge and soil reaction, organic carbon content, nitric nitrogen concentration, total nitrogen, mobile phosphorus and potassium content) properties that influence the mobility and retention of chemical compounds in the soil.

The results of this study showed that the material consisting of sludge, on the depth of 0-20 cm, shows well-developed structural aggregates, with a structure between granules and subangular polyhedra, with a medium level of development. The analyzed material has good hydrophysical properties that give it mechanical and hydronic stability. Following the analyzes carried out during 2005 to 2018, we can say that there has been an increase in the humidity and the zinc content in the soil due to the sludge dump from the wastewater treatment plant in Iasi.

Research results can be used as a scientific basis for developing an appropriate soil management system in the study area.

Key words: concentration, effects, evolution, heavy metals, soil

Received: January, 2019; Revised final: February, 2020; Accepted: February, 2020; Published in final edited form: February, 2020

1. Introduction

The application on soil of treated sludge has been adopted worldwide as a sustainable economic option for sludge management. At European Union (EU) level, there are countries where the greatest percent of sludge disposal is for agricultural use. For example, in 2012, Spain, Germany and United Kingdom were the largest sludge producers (2577.2, 1844.4, 1078.4 thousand tones dry matter, respectively, of which 74.5%, 29.3% and 78.2% were used in agriculture) (Smith, 2005). In other countries such as Hungary, Greece and Romania, despite the fact that they produce considerably amounts of sludge, its utilization in agriculture is limited (157.7, 118.6, 48.4, thousand tones dry matter total production of which 9.5%, 11.8% and 4.1% are used in agriculture). Even though in 2013 the total production of sludge increased in Romania to 172400 tones dry matter, only 8000 tones (4.65%) dry matter was used in agriculture (Eurostat, 2016).

The reasons why in some countries of the European Union the agricultural use of sludge is limited are the lack of awareness about the benefits of using it agricultural, fear of contaminating the land with heavy metals, the costs of sludge transportation on agricultural land and costs of monitoring the quality of sludge and of the land on which it is used.

Most scientific papers show positive effects of sludge on improving plant yield because of the macro nutrient content in the sludge (Chrysargyris and Tzortzakis, 2015; Cornfield et al., 1976; Özyazıcı,

---

* Author to whom all correspondence should be addressed: e-mail: bartic.georgiana91@gmail.com; Phone: 0040754635369

2013; Vaca et al., 2011), but also of the better physico-chemical properties of soils on which they are used, by altering the bulk density of the soil, aeration and stabilization of eroded soils (Gu et al., 2013; Holz et al., 2000; Mihalache et al., 2014; Ros et al., 2003). There are also articles that show some negative effects, concerning the increase in heavy metals in plants and soils, pathogens and esthetic alteration of the environment through smell (Collivignarelli et al., 2015; Mazen et al., 2010; Singh and Agrawal, 2007; Vaitkute et al., 2010).

The study area is a sludge dump in Tomești, where the sludge comes from the wastewater treatment plant, Iasi. It was built in 1994 by removing the fertile soil layer from an area of 9.1 hectares of land and building contour dams and subdivisions. The dump is surrounded by a draining channel, which ensures its drainage (Lăcătușu et al., 2012). The dump is located in the major river bed of the Bahlui River, on its right side. The straight line distance to Iaşi wastewater treatment plant is about 2000 m (Cojocaru et al., 2010). The dump (Fig. 1a, b) was divided into 11 compartments, with variable areas delimited by the partition dams. Between the compartments there were breaches of water and sludge circulation. The height of the sludge dumping layer is 1.5-1.8 m. The total volume of the dump is 225.000 m^3 (Neagu, 2007).

The research carried out in the study area involved the concentration of the following heavy metals: Zn, Ni, Cu, Co, Cr and Pb. The total concentration of heavy metals in the soil is a relevant indicator of the risk to human health and the environment (David and Janez, 2018). The knowledge of the total load of the soil with heavy metals is the basis to justify the remediation of the contaminated soil. In an attempt to minimize uncertainty in the decision-making process, this has gone from the total heavy metal loading to the bioavailable fraction (Lăcătușu et. al., 2017). The metals present in the soil are generally mobile and present higher potential risks to potential receptors. Therefore, the research of the free metal ions together with the soil properties is vital for understanding the mechanisms of their absorption by the roots of the plants (Lăcătușu, 2017).

The physical and chemical properties of the soil, which have been determined in this work are: pH, humidity, sludge and soil reaction, organic carbon content, nitric nitrogen concentration, total nitrogen content, mobile phosphorus and mobile potassium, these can influence the mobility and retention of chemical compounds in soil. Soils are influenced by stand composition and hydrological regime as well as by abiotic stress factors (Onet et al., 2019).

Growing plants in polluted areas can be a remedial solution and serve as an alternative tool in sustainable agriculture. Plants can influence the accumulation of heavy metals in soils, either by decreasing or increasing their accumulation (Boglárka et al., 2018).

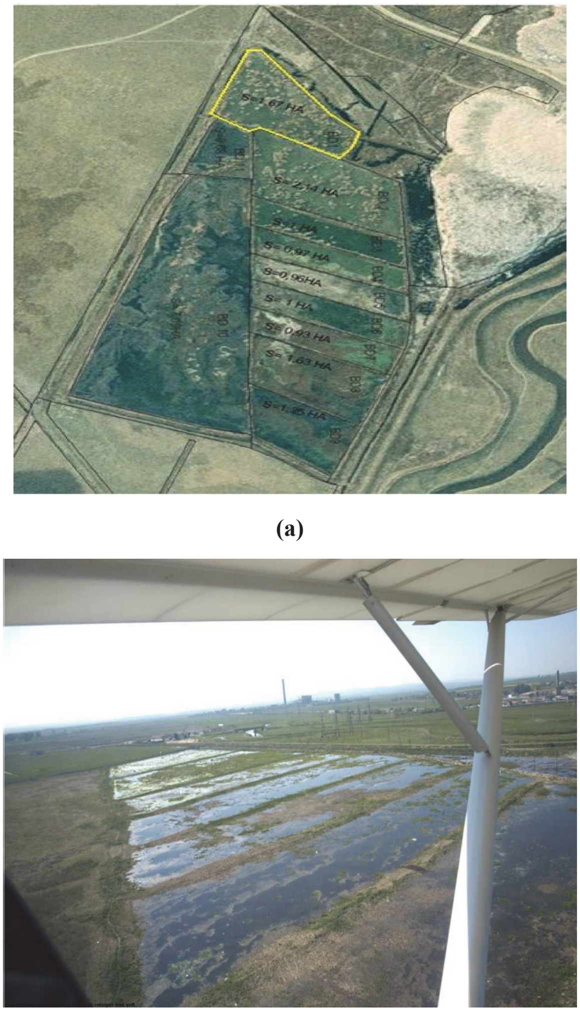

(a)

(b)

Fig. 1. Sludge storage in Tomești (a) and the dump divided into 11 compartments (b)

2. Case studies

2.1. Objectives of research

The studies were conducted in order to highlight heavy metal content, both of the material within the dump and of the soil in its vicinity during the period of 2005-2018.

The physical and chemical properties of the soil and the content of the heavy metals were analyzed: Zn, Ni, Cr, Pb, Co, Cu and also the influence of the sludge dump on the soil.

2.2. Sampling

The distribution of soil sampling zones, harvesting technique and field practice are presented in Figs 2a-2b and 3. In the dump there were placed 5 collecting spots (named S1, S2, ..., S5) and a drilling spot (named F1 - control drill, located outside the battlefield but close to it).

Fig. 2a. Harvesting soil samples

Fig. 2b. Soil samples from land

Fig. 3. Distribution of soil sampling points

The sample collection, of the 5 collecting spots, was done on three standardized depths (0-20, 20-40, 40-60), while the drilling sample was from 20 cm to 20 cm to a depth of 140 cm. Nearly 5 polls were encoded in the vicinity (named SE1, SE2, ..., SE5), plus a drill (named F2 – dump drilling, carried out in the 8th compartment of the sludge dump, to which the infiltration water flows from compartment 1 to 8, so that the samples from this drilling characterize the sludge).

The sampling of the outdoor collecting spots was carried out in the same way as those in the dump, on three standardized depths (0-20, 20-40, 40-60), and in the case of drilling, the same as in the dump drill starting from 0 cm (20 cm distance from each other) to 140 cm deep.

2.3. Experimental technique

Soil physical and chemical properties were analyzed. For the characterization of the physical properties, the granulometric composition and humidity was determined by laboratory analysis, (determined gravimetrically, by drying the samples in the laboratory oven, at 105°C and then cut down în mortar and pestle) and observations were made in the field. For chemical analyzes they were determined by the Walkley-Black and Kjeldahl method, with atomic absorption spectrometry (Sudip et al., 2018), the total content of heavy metals (Zn, Ni, Cr, Pb, Co, Cu) was determined in the solution obtained by disaggregating soil samples with a mixture of perchloric acid, nitric acid and sulfuric acid.

The research would also target other physical and chemical soil properties (humidity, pH and heavy metal content) that influence the mobility and retention of chemical compounds in the soil. For the physical parameters the particle size and soil moisture were determined, which was determined gravimetrically, by drying the samples in the oven, at 105℃.

Phosporus, calcium and heavy metals (Zn, Ni, Cr, Pb, Co, Cu) were determined in the solution obtained by disaggregating soil samples with a mixture of perchloric acid, nitric acid and sulfuric acid in the laboratory located within the Faculty of Hydrotechnics, Geodesy and Environmental Engineering of the ”Gheorghe Asachi” Technical University of Iasi, Romania, using an Atomic Absorbtion Spectometer (AAS ZEEnit 700) (Fig. 4).

The research aimed at determining other physical and chemical properties of the soil that influence the mobility and retention of chemical compounds in the soil:

- the reaction of sludge and soil, evidenced by the pH value, was potentiometrically determined in aqueous suspension, at a sludge-water ratio of 1: 2.5, using a combined glass-calomel electrode;
- the organic carbon content was determined according to the Walkley-Black method (FAO, 2019), with the Gogoasa modification (Edu et al., 2013);
- the mobile form of nitric nitrogen ($N-NO_3$) was determined potentiometrically, with an ion selective electrode for $N-NO_3$. The determination of total nitrogen content was performed by the Kjeldahl method.
- the content of mobile phosphorus (P_{AL}) and mobile potassium (K_{AL}) were determined in ammonium acetate-lactate solution at pH - 3.7 (Domingo et al., 2015) and the dosage by spectrophotometry and photometry in flame.

3. Results and discussions

The samples (S1, S2, S3, S4, S5, FD) consisting of soil and sludge, sampled at the 0-20 cm depth, showed well-developed structural aggregates with a structure ranging from grain to subangular, polyhedron, with an average development level. The analyzed material has good hydrophysical properties which give it mechanical and hydraulic stability, moderate dry, moderate adhesive, loose, medium-sized and large macroporous medium.

These physical and mechanical properties determine good aeration porosity and optimum aerohydricity. In the case of the S2 and S4 surveys, where the material layer consisting of municipal sludge is well drained and without groundwater entrainment between it and the upper horizon of the soil prior to dumping. Also, the FD drilling (where groundwater occurs at approximately 70 cm) identified traces of intense meso-faunistic activity, especially an intense activity of earthworms. In the range of 0-20 cm and even below this depth, the soil material is relatively well structured, with smaller structural aggregates, lack of groundwater causing an increase in consistency, plasticity and reduction of aggregate interstices.

At the bottom of the last sampling segment (40-60 cm), but also in the case of drilling (which continues to a depth of 140 cm), the soil material is still under the influence of water, the hydromorphism influencing the degree of aggregation and structure of elementary particles. The plasticity is reduced and gleization characteristics appear on the surface.

Fig. 4. Atomic Absorbtion Spectometer (AAS ZEEnit 700)

In the rest of the samples collected from the dump (S1, S3 and S5) the presence of water at approximately 25-30 cm from the surface and in the second half of the FD drilling (from 70 cm) determines a relatively structured soil material, but once with the appearance of water, it becomes from very poor cohesive to noncoating, sometimes non-plastic, very adherent to the depth of water harvesting.

Samples collected from the landfill (FM, SE1, SE2, SE3, SE4, SE5) did not show water in the control section, with visible gleyzation traces being identified at the base (40-60 cm). The soil is well-structured, with medium-sized aggregates, with a grainy structure in the first part, sub-angled polyhedral in the sub-surface. The humidity parameters, the reaction and the content of macroelements from 0-60 cm layer of the sewage sludge from the Tomești basin are presented in table no. 1.

Laboratory analyzes determined heavy metal concentrations in soil samples. For the sampling depth of 0-20 cm, the values corresponding to the 2 drillings are shown in the diagrams of Figs 5 to 10. In graphical representations, the alert threshold values for less sensitive soils (P.A. SMP) were used as comparative limits according to MAPPM Order 756/1997.

Following the data presented graphically, it can be noticed that since 2010 the heavy metals: Ni, recorded small concentrations close to the normal ones in the soils while for Zn, Cr, and Pb the concentrations varied from one analysis period to another, but remained above the normal soil value. The 2018 drought conditions have led to the preservation of a high content of soluble salts in the upper horizons, both at the level of the dump and the alluvial soil around them. Research has shown that some physical and chemical properties of the sludge have been transmitted to the soil that it stagnates. Thus, soil moisture under the sludge layer increased by up to 20% relative to the moisture content of the neighboring soil, which was not influenced by the presence of sludge.

The advanced clayiness of up to 83% of colloidal clay below 2 μ, constituted a geochemical barrier to the leaching of the chemical elements in the sludge with the liquid sludge phase. At the same time, it also constituted an absorption medium for many cations and anions.

The sludge liquid phase contributed on one hand to the washing of salts from the first two horizons of the soil on which the sludge stagnated and on the other hand to the pH decrease by up to 0.61 pH units but the reaction field remained the same: weak-alkaline. Natural salt washes to about 1000 mg / 100g of soil, but the level of salinization remained the same, namely strong and very strong salinization.

From the group of heavy metals analyzed (Zn, Ni, Cr, Pb, Co), the only chemical element present at the pollutant was zinc. In the harvested samples, the total Zn content varies between 49 and 127 ppm with an average of 91 ± 23 ppm, while the zinc content range in the soil under the sludge dump varies between 3236 ppm in the horizon of contact with sludge and 78 ppm in the horizon of 280-300 cm. Therefore, a Zn load of the soil under the sludge layer was produced 7.7 times against the control soil.

Other chemical elements of metallic character, which exhibit a certain degree of load without reaching the maximum admissible limit values, are Pb, Ni and Cr. They have slightly increased content levels in the first soil horizon beneath the sludge layer. The high clay content did not allow them to migrate, resulting in reduced content levels, on a 20 cm thickness, from 100 to 120 cm. The only heavy metal polluting in the sludge of the Iasi wastewater treatment plant is zinc. The zinc pollution level is maintained at a thickness of 40 cm, from 100 to 140 cm. In the first horizon, the Zn content exceeds the LMA value by 10.8 times and in the second horizon by 1.6 times.

Table 1. Statistical parameters of the moisture, the reaction and the content of macroelements in the 0-60 cm layer of the sewage sludge from the Tomești basin, Iasi county

Statistical parameters	***Humidity (%)***	***pH***	***$C_{organic}$***	***N_t***	***C/N***	***$N\text{-}NO_3$***	***P_{AL}***	***K_{AL}***
		unit. pH	%	%		mg/kg	mg/kg	mg/kg
Min. value	19	6.55	1.17	0.229	1.6	19	333	356
Max. value	85	7.95	18.00	1.460	38.6	792	1.777	1.982
Arithmetic mean	58	7.20	8.33	0.641	16.0	275	1.087	849
Standard deviations	19	0.37	5.75	0.279	10.9	213	377	440
Geometric Mean	56	7.20	5.79	0.590	11.5	186	1.013	757
Coefficient of variation (%)	33	5.08	69.04	43.51	68.18	77.57	34.67	51.82
Median values	60	7.26	8.59	0.610	13.6	232	1.107	771
Module values	63	7.29	3.12	0.555	7.5	147	1.099	533

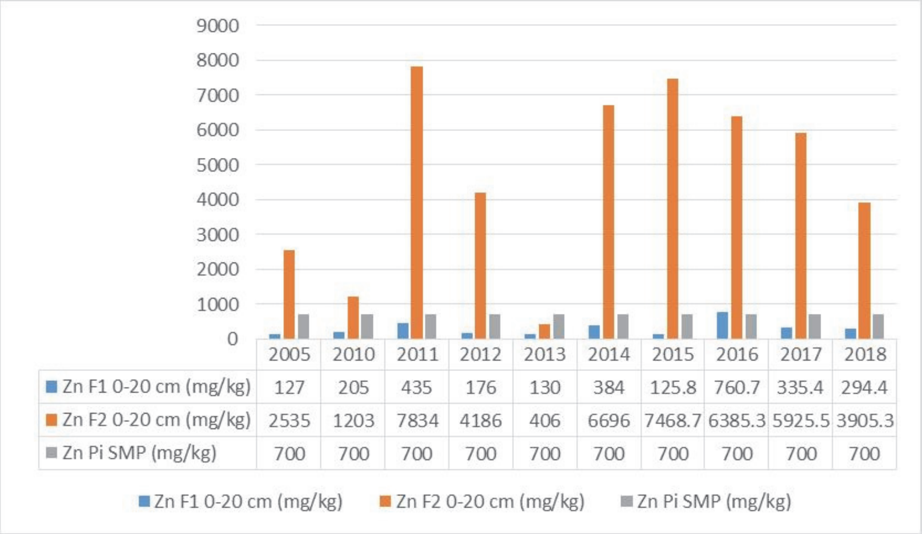

	2005	2010	2011	2012	2013	2014	2015	2016	2017	2018
■ Zn F1 0-20 cm (mg/kg)	127	205	435	176	130	384	125.8	760.7	335.4	294.4
■ Zn F2 0-20 cm (mg/kg)	2535	1203	7834	4186	406	6696	7468.7	6385.3	5925.5	3905.3
■ Zn Pi SMP (mg/kg)	700	700	700	700	700	700	700	700	700	700

Fig. 5. Dynamics of Zn content in soil

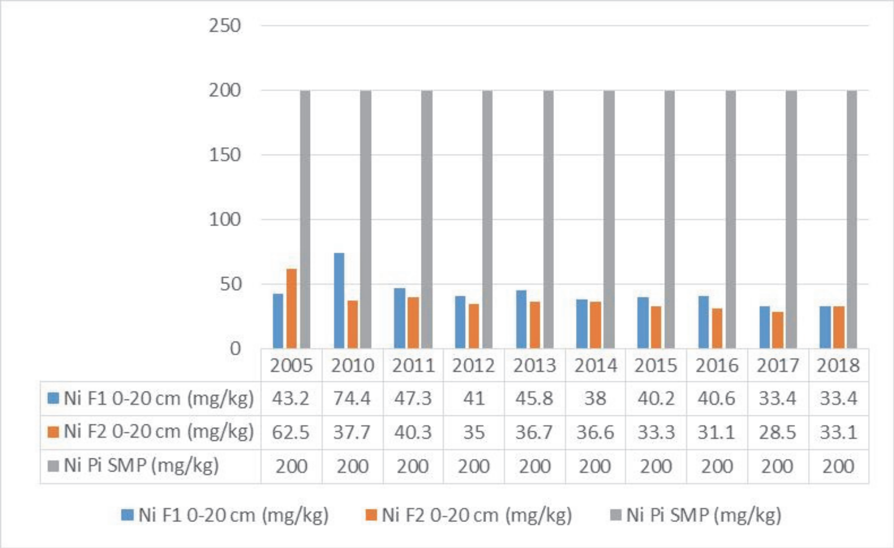

	2005	2010	2011	2012	2013	2014	2015	2016	2017	2018
■ Ni F1 0-20 cm (mg/kg)	43.2	74.4	47.3	41	45.8	38	40.2	40.6	33.4	33.4
■ Ni F2 0-20 cm (mg/kg)	62.5	37.7	40.3	35	36.7	36.6	33.3	31.1	28.5	33.1
■ Ni Pi SMP (mg/kg)	200	200	200	200	200	200	200	200	200	200

Fig. 6. Dynamics of Ni content in soil

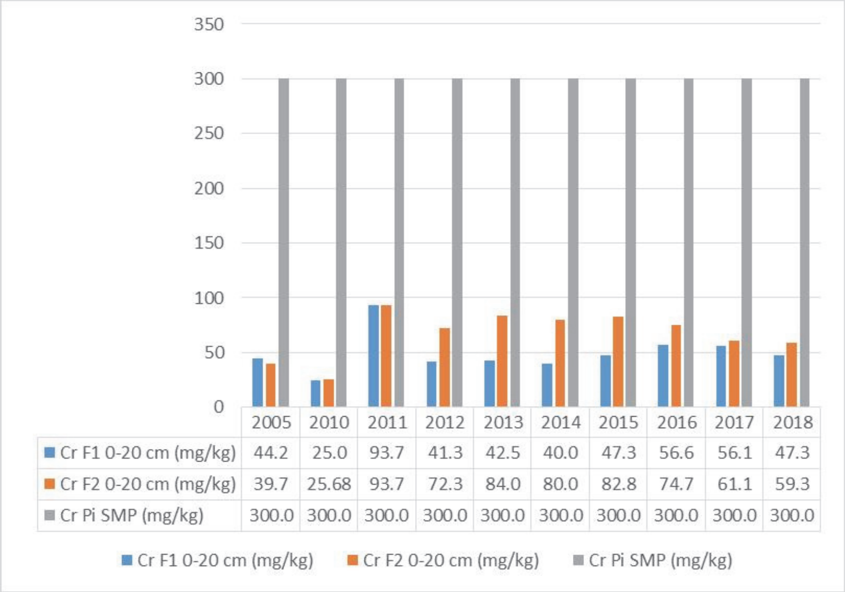

	2005	2010	2011	2012	2013	2014	2015	2016	2017	2018
■ Cr F1 0-20 cm (mg/kg)	44.2	25.0	93.7	41.3	42.5	40.0	47.3	56.6	56.1	47.3
■ Cr F2 0-20 cm (mg/kg)	39.7	25.68	93.7	72.3	84.0	80.0	82.8	74.7	61.1	59.3
■ Cr Pi SMP (mg/kg)	300.0	300.0	300.0	300.0	300.0	300.0	300.0	300.0	300.0	300.0

Fig. 7. Dynamics of Cr content in soil

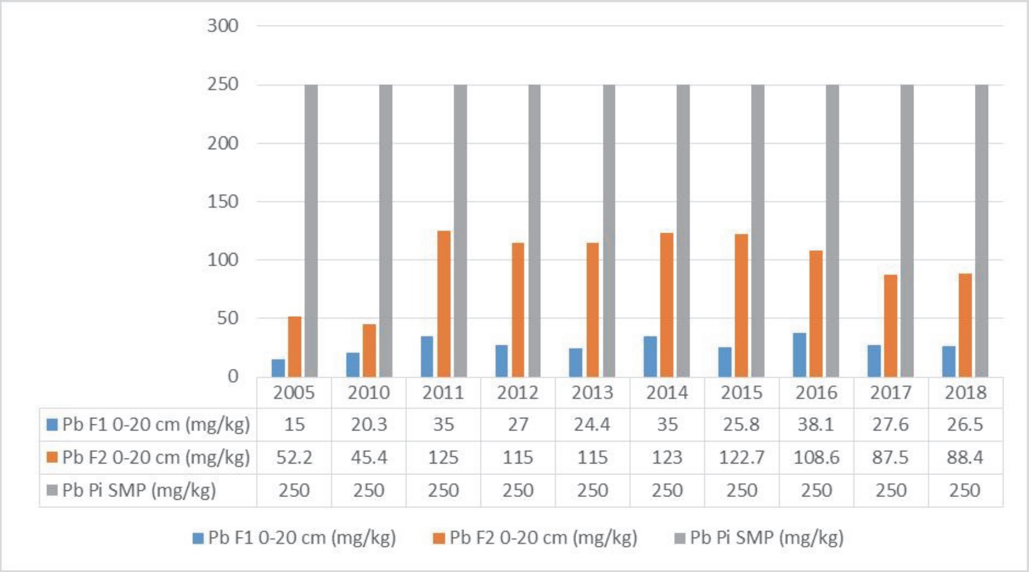

	2005	2010	2011	2012	2013	2014	2015	2016	2017	2018
■ Pb F1 0-20 cm (mg/kg)	15	20.3	35	27	24.4	35	25.8	38.1	27.6	26.5
■ Pb F2 0-20 cm (mg/kg)	52.2	45.4	125	115	115	123	122.7	108.6	87.5	88.4
■ Pb Pi SMP (mg/kg)	250	250	250	250	250	250	250	250	250	250

Fig. 8. Dynamics of Pb content in soil

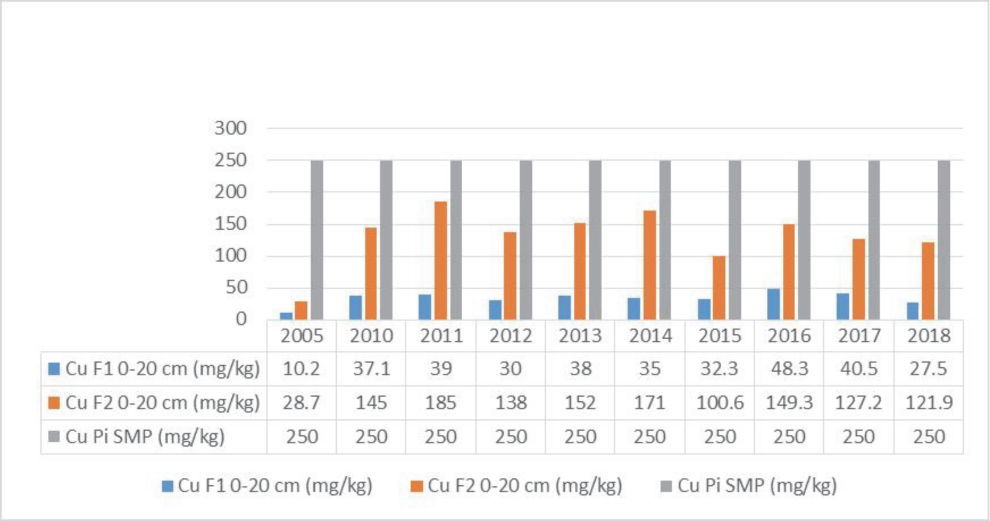

	2005	2010	2011	2012	2013	2014	2015	2016	2017	2018
■ Cu F1 0-20 cm (mg/kg)	10.2	37.1	39	30	38	35	32.3	48.3	40.5	27.5
■ Cu F2 0-20 cm (mg/kg)	28.7	145	185	138	152	171	100.6	149.3	127.2	121.9
■ Cu Pi SMP (mg/kg)	250	250	250	250	250	250	250	250	250	250

Fig. 9. Dynamics of Cu content in soil

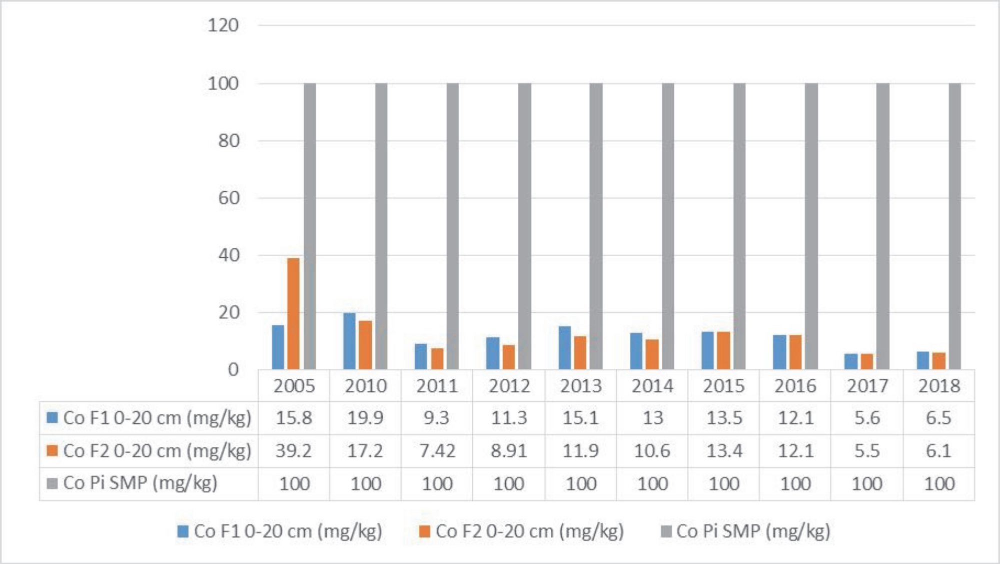

	2005	2010	2011	2012	2013	2014	2015	2016	2017	2018
■ Co F1 0-20 cm (mg/kg)	15.8	19.9	9.3	11.3	15.1	13	13.5	12.1	5.6	6.5
■ Co F2 0-20 cm (mg/kg)	39.2	17.2	7.42	8.91	11.9	10.6	13.4	12.1	5.5	6.1
■ Co Pi SMP (mg/kg)	100	100	100	100	100	100	100	100	100	100

Fig. 10. Dynamics of Co content in soil

4. Conclusions

The extensive study to highlight the impact of sludge storage at the Iasi wastewater treatment plant is a necessary and useful material for risk analysis.

The results of this study showed that the soil material, consisting of sludge, on 0-20 cm depth, presents well-developed structural aggregates, with a structure between granules and subangular polyhedral, with a medium level of development. The analyzed material has good hydrophysical properties that give it mechanical and hydronic stability.

The chemical analyzes showed a neutral low alkaline reaction accompanied by high contents of organic Carbon, mobile phosphorus and mobile potassium. Also, there were high concentrations of mineral forms of nitrogen (N-NO_3 and N-NH_4) and high concentrations of total N.

The results showed that the increase in humidity, and some degree of loading is noted, without reaching the maximum limit values allowed for Pb, Ni, and Cr, but the Zn content exceeds the LMA value by 10.8 times, and in the second 1.6 times.

As a result of the analyzes carried out, we can say that the sludge storage at the Wastewater Treatment Plant in Iasi has a minor impact on the soil.

The surface area occupied by the dump can be introduced into the natural circuit by using a technological solution, namely the planting of rapidly growing trees of Populus, Salix or Paulownia species. They will also solve the problem of excess moisture, which still exists at depths greater than 60 cm or more, and at the same time it will decrease the zinc content of the sludge, by absorbing it and removing it from the system by cutting of the trees to be used for other purposes.

The results of this research can be used as a scientific basis for developing an appropriate soil management system in the study area.

References

Boglárka V., Salamon R., Kovács E., Gyöngyvér M., (2018), Effect of metal tolerant plant growth promoting Rhizobacteria on bean growth, cadmium and zinc uptake and stress responses, *Environmental Engineering and Management Journal*, **17**, 803-811.

Chrysargyris P., Tzortzakis A., (2015), Municipal solid wastes and mineral fertilizer as an eggplant transplant medium, *Journal of Soil Science and Plant Nutrition*, **15**, 163-172.

Cojocaru P., Macoveanu M, Cojocaru I., (2010), Studies to determine the level of contamination with heavy metals of a situ located in Iasi, *Scientific Works, Agronomy Iaşi*, **53**, 36-47.

Collivignarelli M., Bertanza G., Sordi M., Pedrazzani R., (2015), High-strength wastewater treatment in a pure oxygen thermophilic process: 11-year operation and monitoring of different plant configurations, *Water Science and Technology*, **71**, 79-91.

Cornfield A., Beckett P., Davis R., (1976), Effect of sewage sludge on mineralisation of organic carbon in soil, *Nature*, **20**, 518-260.

David E., Janez K., (2018), Toxic compounds generated by metalworking fluids and aluminum slag landfill and their effects on environment and people, *Environmental Engineering and Management Journal*, **17**, 739-748.

Domingo W., Egnér H., Riehm H., (2015), Studies on chemical soil analysis as the basis for assessing the nutrient status of the soil. II. Chemical extraction methods for the determination of phosphorus and potassium, *Kungliga Lantbrukshögskolans Annaler*, **26**, 199-215.

Edu E.M., Mihalache M., Ionescu M., (2013), Determination of organic carbon in forest soils by comparative analysis of methods: Walkley Black method with the Gogoasa modification versus dry combustion Dumars method, *Research Journal of Agricultural Science*, 45, 13-20.

Eurostat, (2016), Sewage sludge production and disposal, On line at: http://ec.europa.eu/eurostat/web/ products-datasets/-/env_ww_spd.

FAO, (2019), Standard operating procedure for soil organic carbon. Walkley-Black method. Titration and colorimetric method, GLOSOLAN-SOP-02, Food and Agriculture Organization of the United Nations, On line at: http://www.fao.org/3/ca7471en/CA7471EN.pdf

Gu C., Bai Y., Tao T., Chen G., Shan Y., (2013), Effect of sewage sludge amendment on heavy metal uptake and yield of ryegrass seedling in a mudflat soil, *Journal of Environmental Quality,* **42**, 421-428.

Holz M., Heil S., Sacco A., (2000), Temperature-dependent self-diffusion coefficients of water and six selected molecular liquids for calibration in accurate ^{1}H NMRPFG measurements, *Physical Chemistry Chemical Physics,* **20***,* 63-78.

Lăcătuşu R., Lăcătuşu A., Vrînceanu A., Lungu M., Rizea N., Lazăr D., Trofin O., Catrina V., (2017), *Evolution of the Chemical Properties of the Alluvial Soil of Tomeşti (Iaşi County) under Sludge Dumping of Wastewater from Iaşi Municipality*, Proc. of the Nat. Conf. of Soil Science, Chişinău, Moldova, 54-64.

Lăcătuşu R., (2017), *Agrochemistry (in Romanian)*, 3rd Edition, Publishing House Terra Nostra, Iaşi, Romania.

Lăcăuşu R., Stanciu B., Lazăr D, Lungu M., Rizea N., Catrina V., (2012), Phytoremediation of a sludge dump proceeding from a city wastewater treatment plant, *Carpathian Journal of Earth and Environmental Sciences*, **7**, 71-79.

Mazen A., Faheed A.F., Ahmed F.A., (2010), Study of potential impacts of using sewage sludge in the amendment of desert reclaimed soil on wheat and jews mallow plants, *Brazilian Archives of Biology and Technology*, **53**, 917-930.

Mihalache R., Justin J., Frans A., Henk W., (2014), Top management team shared leadership and organizational ambidexterity: a moderated mediation framework, *Strategic Entrepreneurship Journal*, **8**, 128-148.

Neagu G., (2007), *Decontamination of Soils and Groundwaters*, Publishing House of Science Book, Cluj-Napoca, Romania.

Onet A., Dinca L., Teusdea A., Crisan V., Braga C., Enescu R, Onet C., (2019), The influence of fires on the biological activity of forest soils in Vrancea, Romania, *Environmental Engineering and Management Journal*, **18**, 64-76.

Özyazıcı M., (2013), Effects of sewage sludge on the yield of plants in the rotation system of wheat-white head cabbage-tomato, *Eurasian Journal of Soil Science*, **2**, 35-44.

Ros M., Hernandez M., García C., (2003), Bioremediation of soil degraded by sewage sludge: effects on soil properties and erosion losses, *Environmental Management*, **31**, 741-747.

Singh R., Agrawal M., (2010), Effect of different sewage sludge applications on growth and yield of *Vigna radiata* L. field crop: Metal uptake by plant*, Ecological Engineering*, **36**, 969-972.

Smith S., (2005), Are organic contaminants necessary to protect the environment when sewage sludge is used in agriculture, *Program Environmental Science,* **2**, 129-146.

Sudip K., Steve G., Scott A., (2018), Spatial variability of heavy metal pollution potential from an urban road network, *Environmental Engineering and Management Journal*, **17**, 2097-2102.

Vaca R., Lugo J., Martínez R., Esteller M.V., Zavaleta H., (2011), Effects of sewage sludge and sewage sludge compost amendment on soil properties and *Zea mays* plants, *Revista Internacional de Contaminación Ambiental,* **27**, 303-311.

Vaitkutė D., Baltrėnaitė E., Booth C.A., Fullen M.A., (2010), Does sewage sludge amendment to soil enhance the development of Silver birch and Scots pine? *Hungarian Geographical Bulletin*, **59**, 393-410.

Environmental Engineering and Management Journal

"Gheorghe Asachi" Technical University of Iasi, Romania

73 Mangeron Blvd., 700050, Iasi, Romania
Tel./Fax. +40-232-271759, PO 10, BOX 2111,
URL: *http://omicron.ch.tuiasi.ro/EEMJ/*
e-mail: *eemjournal@yahoo.com*, *eemj.office@gmail.com*

INSTRUCTIONS FOR AUTHORS

1. Introduction

Environmental Engineering and Management Journal (EEMJ) is an international medium for publication of Original Papers, Reviews, Case Studies, Book Reviews on the fundamentals, applications in environmental engineering and technologies, applied environmental sciences, environmental health, management, sustainable development, education for sustainability. Advertising is also accepted with contractual payment forms.

Submission of a manuscript implies that the work described has not been published before (except in the form of an abstract or as part of a published lecture, or thesis); that it is not under consideration for publication elsewhere; that its publication has been approved by all coauthors, if any, as well.
Papers, books for review, offers to review, suggestions and commercials (advertising) should be submitted to the *Editor-in-Chief* All papers will be published in English. Non-English speaking authors should seek the advice of a professional language expert or an English speaker to help translate the paper.

2. Legal requirements

The author(s) guarantee(s) that the manuscript is/will not be published elsewhere in any language without the consent of the copyright holders, that the rights of third parties will not be violated, and that the publisher will not be held legally responsible should there be any claims for compensation.
Authors wishing to include figures or text passages that have already been published elsewhere are required to obtain permission from the copyright holder(s) and to include evidence that such permission has been granted when submitting their papers. Any material received without such evidence will be assumed to originate from the authors.
The author(s) are encouraged to transfer the copyright of the article to the publisher upon acceptance of an article by the journal, using the Authors' Warranty and Assignment of Copyright agreement. This transfer enables the Editor to protect the copyrighted material for the authors, but does not relinquish the author's proprietary rights. The publication of an article is conditioned by the signature of the author to whom correspondence should be addressed on this Authors' Warranty and Assignment of Copyright that is provided by the Editor.

Ethics in Publishing

For information on ethics in publishing for journal publication see http://omicron.ch.tuiasi.ro/EEMJ/plagiarism.htm

Conflict of interest

All authors are requested to disclose any actual or potential conflict of interest such as any financial, personal or other relationships with other people or organizations concerning the submitted work that could inappropriately influence, or be perceived to influence, their work.

3. Editorial procedure

For original papers, an upper limit of 7000 words is recommended (including Abstract, Keywords, References, Figures and Tables), processed with MS editing facilities.

For review papers (critical evaluation of existing data, defined topics or emerging fields of investigation, critical issues of public concern), an upper limit of 15000 words is recommended (including Abstract, Keywords, References, Figures and Tables).

Manuscripts should be written in English (American or British usage is accepted, but not a mixture of these) and submitted **electronically**, in .doc format (please do not use .docx) to the *Editor-in-Chief*, at one (and only one) of the following e-mail addresses: **eemjournal at yahoo dot com**; **eem_journal at yahoo dot com**; **eemjeditor at yahoo dot com**; **eemj_editor at yahoo dot com**; **eemjournal at gmail dot com**; **eemjeditor at gmail dot com; eemjoffice at gmail dot com.**
Please be sure to include your full affiliation and e-mail address (see Sample manuscript).

When submitting the manuscript, it is mandatory to include a cover letter to the editor. The cover letter must state:

- that all authors mutually agree that the manuscript can be submitted to EEMJ;
- that the manuscript contains the original work of the authors;

- the novelty in results/findings, or significance of results;
- that the manuscript has not already been published, or is not under consideration for publication elsewhere.

Manuscripts are evaluated first in the Editorial Office (as a preliminary condition for acceptance) in terms of meeting the requirements of the journal, including attempts of plagiarism. The authors are responsible for the accuracy of the whole paper and references. Authors will be notified about the registration of their contribution. Only those contributions, which conform to the following instructions, can be considered for the peer-review process. Otherwise, the manuscripts are returned to the authors, with observations, comments and annotations.

The peer review process is decisive for paper acceptance. It could be done in several stages, depending on the revision quality of the manuscript in accordance with the requirements of paper evaluators.

Please do not transmit electronic data or requirements to the publisher until your manuscript has been reviewed and accepted for publication. Please follow the instructions below.

A minimum of four suitable *potential reviewers* should be provided by the authors. Please provide their name, email addresses, and institutional affiliation. When compiling this list of potential reviewers please consider the following important criteria: they must be knowledgeable about the manuscript subject area of the manuscript; they must not be from the authors' own institution or country; they should not have recent (less than five years) joint publications with any of the authors. However, the final choice of reviewers is at the editors' discretion.

4. Manuscript preparation

General:

Authors must follow the Instructions for authors strictly, failing which the manuscripts would be rejected without review. Editors reserve the right to adjust the formatting style to conform to the standards of the journal.

Manuscripts should be concise, in 1.5 line spacing, and should have 2 cm all over margins. The font should be Times New Roman of size 12 points. The numbering of chapters should be in decimal form. Ensure that each new paragraph is clearly indicated, using TAB at 1.25 pts.

The text layout should be in single-column format. Keep the layout of the text as simple as possible. Most formatting codes will be removed and replaced on processing the manuscript. However, do use bold face, italics, subscripts, superscripts etc. Add line numbering and page numbers. To avoid unnecessary errors it is strongly advised to use the 'spell-check' and 'grammar-check' functions of your word processor.

Title page will contain:

- A concise and informative title (Times New Roman bold, all caps of size 14 points); the maximum length of the title should be maximum 100 letters and spaces; The full name(s) of the author(s) (first name, then last name, with Times New Roman bold 12 points) should be written below the title. The affiliation(s) and complete postal address(es) of the author(s) will be provided immediately after the full name of the authors and will be written with Times New Roman 12 points. When the paper has more than one author, their name will be followed by a mark (Arabic numeral) as superscript; for the corresponding author, an asterix will be added using *Word_Insert_Reference_Footnote_Symbol* sequence. Also, the full and e-mail addresses, telephone and fax numbers of the corresponding author will be provided in the footer of the first page, as: Author to whom all correspondence should be addressed: email….., Phone…….., Fax…………
- **Abstract:** each paper must be preceded by an abstract presenting the most important results and conclusions in no more than 250 words. Do not include citations in the Abstract.
- **Keywords:** three to five keywords should be supplied after the Abstract for indexing purposes, separated by comma, **ordered alphabetically,** using American spelling and avoiding general and plural terms and multiple concepts (avoid, for example, "and", "of"). Be sparing with abbreviations: only abbreviations firmly established in the field may be eligible.
- The text of the paper should be divided into **Introduction, Materials and methods (**or **Experimental), Results and discussion, Conclusions, References** (for papers dealing with environmental management, policy, education etc., the Experimental part can be replaced by case-studies presentation).

1. Introduction

State the objectives of the work and provide an adequate background, avoiding a detailed literature survey or a summary of the results.

2. Material and methods (or 2. Experimental)

Provide sufficient detail to allow the work to be reproduced. Methods already published should be indicated by a reference: only relevant modifications should be described.

3. Results and discussion

Results should be clear and concise. Discussion should explore the significance of the results of the work, not repeat them. Avoid extensive citations and discussion of published literature.

4. Conclusions

The main conclusions drawn from results should be presented in a short Conclusions section. Do not include citations in this section.

Formulae, symbols and abbreviations: Formulae will be typeset in Italics (preferable with the Equation Editor of Microsoft Office 2003) and should be written or marked as such in the manuscript, unless they require a different styling. The formulae should be numbered on the right side, between brackets:

$$a^3 = 3M / 4N \qquad (1)$$

Always refer in the text to Equations as (Eq. 1), Eqs. (1-4) etc.
The more complex Chemical Formulae should be presented as Figures.
Abbreviations should be defined when first mentioned in the abstract and again in the main body of the text and used consistently thereafter.

SI units must be used throughout.

Footnotes should be avoided.

References:
The list of References should only include works that are cited in the text and that have been published. References should be cited in the text in brackets ***(Harvard style)*** as in the following examples:

(Chisti, 1989), (Gavrilescu and Roman, 1996), (Moo-Young et al., 1999).
References should be alphabetically listed at the end of paper, with complete details, as follows:

Books: Names and initials of authors, year (between brackets), chapter title, title of the book (italic), editors, edition, volume number, publisher, place, page number:

Mauch K., Vaseghi S., Reuss M., (2000), *Quantitative Analysis of Metabolic and Signaling Pathways in Saccharomyces cerevisiae*, In: *Bioreaction Engineering*, Schügerl K., Bellgardt K.H. (Eds.), Springer, Berlin Heidelberg New York, 435-477.

Faber K., (2000), *Biotransformations in Organic Chemistry – A Textbook*, vol. VIII, 4th Edition, Springer, Berlin-Heidelberg-New York.

Handbook, (1951), *Handbook of Chemical Engineer*, vol. II, (in Romanian), Technical Press, Bucharest, Romania.

Symposia volumes: Names and initials of authors, year (between brackets), paper title, symposium name, volume number, place, date, page numbers:

Clark T.A., Steward D., (1991), *Wood and Environment*, Proc. 6th Int. Symp. on Wood and Pulping Chemistry, Melbourne, vol. 1, 493-498.

Journal papers: Names and initials of authors, year (between brackets), full title of the paper, full name of the journal (italic), volume number (bold), first and last page numbers:

Tanabe S., Iwata H., Tatsukawa R., (1994), Global contamination by persistent organochlorines and their ecotoxicologcial impact on marine mammals, *Science of the Total Environment*, **154**, 163-177.

Patents: Names and initials of authors, year (between brackets), patent title, country, patent number (italic):

Grant P., (1989), Device for Elementary Analyses. USA Patent, No. *123456*.

Dissertations: Names and initials of authors, year (between brackets), title, specification (PhD Thesis, MSc Thesis), institution, place:

Aelenei N., (1982), *Thermodynamic study of polymer solutions*, PhD Thesis, Institute of Macromolecular Chemistry Petru Poni, Iasi, Romania.

Star K., (2008), *Environmental risk assessment generated by natural hazards*, MSc Thesis, Institute of Hazard Research, Town, Country.

Legal regulations and laws, organizations: Abbreviated name, year (between brackets), full name of the referred text, document type, author, URL address:

ESC, (2007), Improving access to modern energy services for all fundamental challenge, Economic and Social Council, ENV/DEV/927, On line at: http://www.un.org/News/Press/docs/2007/envdev927.doc.htm.

EPA, (2007), Biomass Conversion: Emerging Technologies, Feedstocks, and Products, Sustainability Program, Office of Research and Development, EPA/600/R-07/144, U.S. Environmental Protection Agency, Washington, D.C., On line at: http://www.epa.gov/Sustainability/pdfs/Biomass%20Conversion.pdf.

EC Directive, (2000), Directive 2000/76/EC of the European Parliament and of the Council of 4 December 2000, on the incineration of waste, Annex V, *Official Journal of the European Communities*, L 332/91, 28.12.2000, Brussels.

GD, (2004), Governmental Decision No. 1076/2004 surnamed SEA Governmental Decision, regarding the procedure for strategic environmental impact assessment for plans or programs, *Romanian Official Monitor*, Part I, No. 707 from 5th of August, 2004.

Web references
The full URL should be given in text as a citation, if no other data are known. If the authors, year, title of the documents are known and the reference is taken from a website, the URL address has to be mentioned after these data:

Burja C., Burja V., (2008), Adapting the Romanian rural economy to the European agricultural policy from the perspective of sustainable development, MPRA, Munich Personal RePEc Archive, On line at: http://mpra.ub.uni-muenchen.de/7989/1/MPRA_paper_7989.pdf

Web references must not be listed separately, after the reference list.

All references must be provided in English with a specification of original language in round brackets.

Citation in text
Please ensure that every reference cited in the text is also present in the reference list (and vice versa). Do not cite references in the abstract and conclusions.
Unpublished results, personal communications as well as URL addresses are not recommended in the references list..
Citation of a reference as "in press" implies that the item has been accepted for publication.

Papers which have been accepted for publication should be included in the list of references with the name of the journal and the specification "in press".

References style

Text: All citations in the text may be made directly (or parenthetically) and should refer to:
- *single author:* the author's name (without initials, unless there is ambiguity) and the year of publication: “as previously demonstrated (Smith, 2007)”; “as Smith (2007) demonstrated”
- *two authors:* both authors' names and the year of publication: (Arnold and Sebastian, 2008; Smith and Hansel, 2006; Stern and Lars, 2009)
- *three or more authors:* first author's name followed by "et al." and the year of publication: “As has recently been shown (Werner et al., 2005)…”, “Kramer et al. (2000) have recently shown ...."

Citations of groups of references should be listed first alphabetically, then chronologically.

Examples: ".….as demonstrated (Aden, 1996a, 1996b, 1999; Allan and Jones, 1995; Han et al., 2007; Weiss and Schmidt, 1988)”.

Abbreviations

Define all abbreviations at their first mention in the text. Ensure consistency of abbreviations throughout the article.

Acknowledgements

Include acknowledgements in a separate section at the end of the article before the references and do not, therefore, include them on the title page, as a footnote to the title or otherwise. List here those individuals who provided help during the research (e.g., providing language help, writing assistance or proof reading the article, funding supports etc.).

Footnotes

Footnotes must be avoided. Do not include footnotes in the Reference list.

Table footnotes

Indicate each footnote in a table with a superscript lowercase letter.

Tables

Draw the Tables in grid format using a basic, solid line style without shadows.
Ensure that the data presented in Tables do not duplicate results described in Figures or elsewhere in the paper.

Figures

Number Figures consecutively in accordance with their appearance in the text. All illustrations should be provided in camera-ready form, suitable for reproduction, which may include reduction without retouching. Photographs, charts and diagrams are all to be referred to as Figure(s) and should be numbered consecutively, in the order to which they are referred.

Figures may be inserted preferably as black line drawings. They should be pasted on, rather than taped, since the latter results in unclear edges upon reproduction.
Ensure that each illustration has a caption, placed below the Figure. Supply also captions separately, not attached to the figure. A maximum limit of 8 Figures are allowed per manuscript.

A caption should comprise a brief title (**not** on the Figure itself) and a description of the illustration. Keep text in the illustrations themselves to a minimum but explain all symbols and abbreviations used. Multiple Figures can be expressed as one Figure (for e.g. 1a, 1b, 1c etc...), while retaining the maximum limit of 6.

ALL Figures must be submitted in either .jpg or .tiff format with a very good resolution (but do not submit graphics that are disproportionately large for the content).

Figures and Tables must be embedded in the text.

Proofs

Proofs will be sent to the corresponding author (by e-mail) and should be returned within 72 hours of receipt. Corrections should be restricted to typesetting errors; any other changes may be charged to the authors.

Paper in Electronic Format:

Authors are asked to submit their final and accepted manuscript as an attachment to one of the above-mentioned e-mail addresses. Use the **.doc** format (not .docx !).

5. Page charge

There is no charge per printed page for regular papers.

6. Reprints

The corresponding author will be provided with a .pdf file of the paper via e-mail, free of charge. A hard copy Of the issue containing the paper can be provided on request, for a fee. This request will be formulated when the final form of the manuscript (the electronic one) is provided.

7. Additional procedures for the editorial management of *Environmental Engineering and Management Journal*

Starting with volume 13/2014, the members of the Scientific Advisory Board and the Corresponding authors will receive each issue of the journal in electronic .pdf format. Printed copies can be delivered on request.
An author cannot appear on more than two papers per regular issue. An author cannot appear on more than three papers in a Guest Editor/ Conference issue.
The evaluation/peer-review process of manuscripts submitted for Guest Editor / Conference issues published according to journal *Editorial Procedure and Policy* will be handled and evaluated as with regular manuscripts, so that only consistent papers will be published. The manuscripts must be sent at least six months before the presumed data of publication. Those manuscripts which do not fulfill the journal requirements

will be rejected. This is to discourage superficiality in the development of the manuscript, from formal and scientific points of view. No amount of money will be refunded following the rejection of manuscripts.

No more than 160 pages and no more than 20 papers are acceptable for regular issues. No more than 180 pages and no more than 25 papers are opportune for special issues. The number of pages is based on the published version of an article, not on the submitted version (for instance, when page breaks are changed and when images are enlarged for easier viewing).

An issue can include, as an exception, a number of 25-30 papers as a maximum. This situation could appear when the authors of an already accepted paper need and ask for early publication, from the position in the list of accepted papers. In this circumstance, a yearly submission to our journal (500 Euro) will be asked for each already accepted paper, for its publication in advance.

A newly-received manuscript can be evaluated by priority, when a deposit of 200 Euro shall be paid by authors in advance. If the manuscript is deemed unsuitable for publication, the authors will not be eligible for a refund.

Failure to pay mandatory charges may result in the paper being withheld from early publication.

In all cases, the corresponding author will sign an agreement with the *Editor-in-Chief*, and the *Director* of the *EcoZone* Publishing House according to journal *Editorial Procedure and Policy.*

Automated software is used for checking against plagiarism. In order to avoid false results, the generated reports are cautiously checked and confirmed by journal staff. We do not send plagiarism reports to authors. Any manuscripts which do not prove to be at least 90% original will be rejected. The rejection for plagiarism may arise at any phase of the editorial / review process, even if the manuscript was accepted for publication. The authors are solely responsible for the originality of their submission. Therefore, any manuscript should be carefully checked for such inconsistencies before submitting to EEMJ.

The authors are required to follow academic publishing rules, to adhere to the principles of scientific ethics and to sign the Authors’ warranty and Copyright transfer.

Detailed information concerning these issues may be found of the EEMJ website, under *Editorial Procedure and Policy.*

ISSN: 1582-9596

Environmental Engineering and Management Journal is edited by the
Publishing House ***ECOZONE*** of the
Academic Organization for Environmental Engineering and Sustainable Development **(OAIMDD)**
within the ***Department of Environmental Engineering and Management – Faculty of Chemical Engineering and Environmental Protection under the aegis of "Gheorghe Asachi" Technical University of Iasi***
73 *Prof.Dr.docent Dimitrie Mangeron* Street, 700050-Iasi, Romania

"Gheorghe Asachi" Technical University of Iasi

Printed in Romania by ***POLITEHNIUM Iasi***